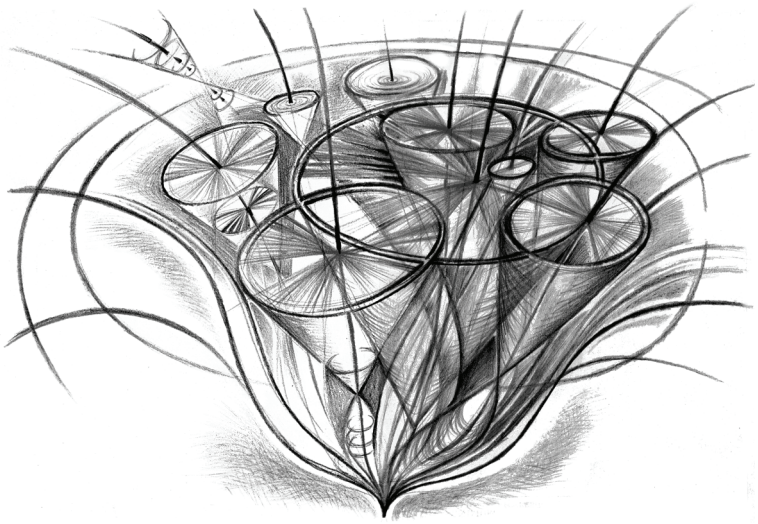
SELECTED TOPICS IN THEORETICAL PHYSICS III



Petr Kulhánek

Plasma Theory
Numerical Simulations

AGA 2026

Text © Petr Kulhánek
ISBN: 978-80-906638-4-8

Contents

FOREWORD **8**

1. PLASMA THEORY **11**

1.1 WHAT IS PLASMA? **12**

1.2 CHARGED PARTICLE MOTION **16**
1.2.1 Non-Relativistic Motion 16
Lagrangian and Hamiltonian 16
Motion in an Electric Field and the Optical Analogy 18
Motion in a Homogeneous Magnetic Field 19
Motion in Crossed Fields 22
1.2.2 Relativistic Motion 25
Lagrangian and Hamiltonian 25
Relativistic Equation of Motion 26
Motion in a Homogeneous Electric Field 28
Collinear Magnetic and Electric Fields 30
1.2.3 Adiabatic Approximation 34
First Adiabatic Invariant 34
Motion of the Guiding Center 36
Force $-\mu$ grad B 38
Drift Equation 39
Drifts 40
1.2.4 Motion in Special Configurations 43
Magnetic Mirror 43
Second Adiabatic Invariant and Fermi Mechanism 44
Magnetic Dipole and Third Adiabatic Invariant 45
Electric and Magnetic Monopole 48
Tokamaks 49
Drifts and Currents in Plasma Filaments 54

1. 3 MAGNETOHYDRODYNAMICS **57**
1.3.1 Minimal Model 57
Basic Concepts 57
Assumptions of the Minimal Model 60
Equations for Magnetic Field 62
Equation for Density 68
Equation for Velocity 69
MHD Equations Closure 73
1.3.2 Exact MHD Solutions 75
Hartmann Solution 75
Waves of Finite Amplitude 78
Helicity 80
Fluid Dynamo 85
Reconnection of Magnetic Field Lines 92

1.3.3 Some Equilibrium Configurations in Plasma 100
Equilibrium in Plasma 100
Current Filament (Pinch) 102
Current Sheet 107
Electrical Double Layer 108
Shock Waves 113

1.4 LINEAR WAVES IN PLASMA 116
1.4.1 Basic Concepts 116
Superposition of Plane Waves 116
Nonlinear System of Equations 118
1.4.2 Sound Waves in Gases 119
Static Medium 119
Moving Medium 121
Jeans Criterion 122
1.4.3 Plasma Oscillations and Waves 125
Derivation of the Dispersion Relation 125
Plasma Oscillations 127
Plasma Waves 128
Ion Waves 129
Other Factors 131
1.4.4 Magnetoacoustic Waves 132
Derivation of the Dispersion Relation 132
Wavefronts of Magnetoacoustic Waves 134
Directions of Vectors in Magnetoacoustic Waves 135
1.4.5 Electromagnetic Waves 137
Dispersion Relations of the Electromagnetic Complex 137
Parallel Propagation: R and L Waves 140
Perpendicular Propagation: O and X Waves 141
Stix Coefficients and the CMA Diagram 145
Faraday Rotation 148
Whistlers 150
Permittivity Tensor for Electromagnetic Waves in Plasma 153
Schlieren Photography 154

1.5 INSTABILITIES IN PLASMA 156
1.5.1 Unbounded Cold Plasma 156
Basic Concepts 156
Multistream Instability 159
Two Symmetrical Beams 160
Beam-Plasma Instability 162
Other Instabilities (Drift and Weibel) 163
1.5.2 Boundary and Interchange Instabilities 164
Governing Equations and the Displacement Vector 164
Displacement Vector 166
Governing Equations for the Displacement Vector 167
Matching Fields at a Boundary 169
Plasma Filament Instabilities 170
Rayleigh–Taylor Instability 177
Kelvin–Helmholtz Instability 181

Other Instabilities (Richtmyer–Meshkov and Diocotron) 184
Interchange Instabilities 186
Schwarzschild Convection Criterion 190
1.5.3 Resistive Instabilities 193
Governing Equations 193
Tearing Instability 196
Driven Resistive Instabilities 198
Tokamak Instabilities 198

1.6 Statistical Description of Plasma 200
1.6.1 Boltzmann Equation 200
Various Forms of the Boltzmann Equation 201
Relativistic Boltzmann Equation 204
Boltzmann Collision Term 206
Transport Equation 209
1.6.2 Transition from Kinetics to Continuum 212
Zeroth-Order Moment and Charge Conservation for Particles 212
Zeroth-Order Moment and Charge Conservation for Fields 213
First-Order Moment and Momentum Conservation for Particles 214
First-Order Moment and Momentum Conservation for Fields 216
Second-Order Moment and Energy Conservation for Particles 218
Second-Order Moment and Energy Conservation for Fields 219
1.6.3 Simple Transport Phenomena 220
Charge Transport and Ohm Law 221
Particle Transport and Fick Law 222
Ambipolar Diffusion 223
Diffusion in a Magnetic Field 225
Heat Transport and Fourier Law 228
Entropy Production and Onsager Relations 229
1.6.4 Coulomb Interaction 231
Debye Shielding 231
Coulomb Scattering and Rutherford Formula 232
Fokker–Planck Equation 235
Rosenbluth Potentials 237
Error Function and Chandrasekhar Function 244
Rosenbluth Potentials for a Maxwellian Target 245
Decelerated and Runaway Test Particles 247
Relaxation Times and Collision Frequencies 250
1.6.5 Microinstabilities 251
Governing Relations 251
Electron Landau Damping 252
Physical Interpretation of Landau Damping 256
Laser Wake Field Accelerators (LWFA) 257
Ion Landau Damping 258
Bernstein Modes 260

1.7 Topics in Nonlinear Phenomena 261
1.7.1 Equation of Motion of a Radiating Particle 261
Potentials Generated in the Vicinity of a Particle 261
Abraham–Lorentz Equation of Motion 263

Lorentz–Dirac Equation of Motion 265
Pauli Representation of Radiation Reaction 266
Iterative Solution: Landau–Lifshitz Equation 268
Avenues for Resolving Pathologies 269
1.7.2 Runaway Electrons 270
Historical Background 271
Frictional Collisional Drag Force 272
Radiation Reaction 274
Key Parameters of the Runaway Regime 275
1.7.3 Solitons 277
From the Union Canal to Solitons 277
Solitons vs. Solitary Waves 279
Sine-Gordon Solitary Wave 281
KdV and NLS Solitons 285
Solitons in Plasma Environments 290
1.7.4 Turbulence 293
Turbulent Structures 293
Kolmogorov Turbulence Model 294
Turbulence in Magnetohydrodynamics 295
Elsässer Variables 296
Strong Anisotropic Turbulence 299

2. NUMERICAL SIMULATIONS 301

2.1 PARTICLE MOTION SIMULATIONS 302
2.1.1 Newton-Euler Scheme (NE) 302
Order of the Scheme 304
Stability of the Scheme 304
2.1.2 Leap-Frog Scheme (LF) 305
2.1.3 Higher-Accuracy Schemes (RK, BB) 306
Runge-Kutta Scheme (RK)a 306
Boris-Buneman Scheme (BB) 307
2.1.4 Relativistic Schemes 308

2.2 DIFFERENCE SCHEMES IN MAGNETOHYDRODYNAMICS 310
2.2.1 Partial Differential Equations 310
Classification of the Equations 310
Initial and Boundary Conditions 312
2.2.2 Designing Differential Schemes 313
Simple Explicit Scheme for the Diffusion Equation 314
Du Fort-Frankel Scheme for the Diffusion Equation 315
Lax-Wendroff Scheme 315
Crank-Nicolson Scheme 316
Richtmyer-Morton Scheme 316
Tridiagonal Matrices 317
2.2.3 Assessment of Scheme Stability 318

2.3 NUMERICAL ROOT-FINDING FOR POLYNOMIAL EQUATIONS 321
2.3.1 Weyl Algorithm 321
2.3.2 Newton Algorithm 323
2.3.3 Generalized Newton Algorithm 324

2.4 PIC SIMULATIONS 326
2.4.1 Weighting 328
2.4.2 Field Solvers 329
2.4.3 Particle Motion Solvers 330

2.5 MONTE CARLO SIMULATIONS 331
2.5.1 Random Number Generators 332
Linear Multiplicative Congruential Generator (LCG) 333
Fibonacci Generators 333
2.5.2 Implementation of Probability Distributions 334
Rejection Method 334
Von Neumann Method 337
Superposition Method 338
Useful Realizations of Specific Distributions 339
2.5.3 Metropolis Method 340
2.5.4 Monte Carlo Simulation of Binary Collisions 342

LIST OF SYMBOLS 345

BIOGRAPHICAL INDEX 351
Plasma Theory 352
Numerical Simulations 365

SUBJECT INDEX 369

REFERENCES 374

INSIDE OTHER VOLUMES 379
Selected Topics in Theoretical Physics I 381
Selected Topics in Theoretical Physics II 383



Foreword

Dear Readers,

You are holding the third and final volume of *Selected Topics*. Its structure is the same as that of the first and second volumes. The only difference is that all the mathematics necessary for studying the material has been deliberately concentrated in the first volume. You do not need to search for the mathematical basics scattered throughout various appendices, but will find them all in one place.

The third volume of "*Selected Topics*" is devoted primarily to plasma theory. The only exception is the radiation of charged particles, which is discussed in the second volume of Selected Topics under the section *Electromagnetic Fields*. The section on numerical simulations in the second part of this book is by no means a coherent textbook. They serve a single purpose: to enable an interested student to directly simulate some of the described phenomena on a computer. That is why, in most cases, only one solution option is presented – one of the basic algorithms. In textbooks on numerical simulations, the reader will find a whole range of other algorithms that may be just as good, if not better, for a given task.

This text on plasma physics was compiled over many years from lectures I initially gave at the Faculty of Electrical Engineering and later at the Faculty of Nuclear and Physical Engineering at the Czech Technical University in Prague. My first encounter with plasma, however, occurred much earlier, during my studies at the Faculty of Mathematics and Physics at Charles University, where, in my fourth year, I attended an excellent lecture titled "Introduction to Plasma Physics" by Professor Jozef Kvasnica. After graduation, I joined the Department of Physics at the FEE CTU, which was then headed by Professor Jiří Kracík, a man who dedicated most of his life to plasma physics. I would also like to take this opportunity to remember the supervisor of my doctoral thesis, Associate Professor Josef Maloch, who was both an excellent mentor and manager, especially during an exceptionally difficult time. Unfortunately, none of those who once influenced and shaped my relationship with plasma physics are still with us. Without their efforts, the third volume of *Selected Topics* would never have been written.

Before you begin studying this material, you should have a basic understanding of theoretical mechanics, particularly the ability to apply Lagrange and Hamilton equations. Knowledge of the Einstein summation convention is assumed. A basic understanding of equilibrium statistical physics would also be helpful, though it is not essential for understanding the text. As for mathematics, you should be familiar with the basics of differential and integral calculus at the level of a standard undergraduate mathematics course. At least a cursory knowledge of partial differential equations and complex analysis is also recommended. All the necessary mathematics is presented in the first volume of *Selected Topics* in the section *Mathematics for Physics*. The reader does not need to study the mathematics in advance; it is sufficient to return to this chapter only when necessary.

In a brief introduction, you will learn about plasma as the fourth state of matter, as well as its various types and forms. The first part of the book addresses the motion of charged particles in given electric and magnetic fields. The second part of the book is devoted to the fundamentals of magnetohydrodynamics, which views plasma as a conductive fluid. The following chapters are devoted to the basic types of waves and instabilities in plasma. The fifth part will likely be the most challenging for readers; it involves a statistical description of plasma, in which we focus primarily on the collective behavior of a large number of charged particles in phase space (we are interested in the information contained in the statistical distribution of particle positions and velocities). This approach is useful, for example, for understanding transport phenomena, collisions, and certain types of instabilities in plasma. In this second edition, a chapter devoted to selected nonlinear phenomena in plasma has been added.

Variables are always typeset in italics, and vectors in boldface. In rare cases where ambiguity or confusion might arise, arrows are placed above vectors and tensors. Functions, abbreviations, digits, and various mathematical operations are displayed in regular typeface. Latin indices denote components of a quantity, coordinate axes, etc. Greek letters are used as indices for particle types (electrons and ions of various charges) or components of four-vectors (0 – time component, 1, 2, 3 – spatial components). Subscripts are usually placed at the bottom right of the base symbol. For clarity, a superscript is used in some cases. If there is a risk of confusion with an exponent, such a superscript is placed in parentheses:

$$F_n,\ F_{\mathrm{EM}}^{(n)}.$$

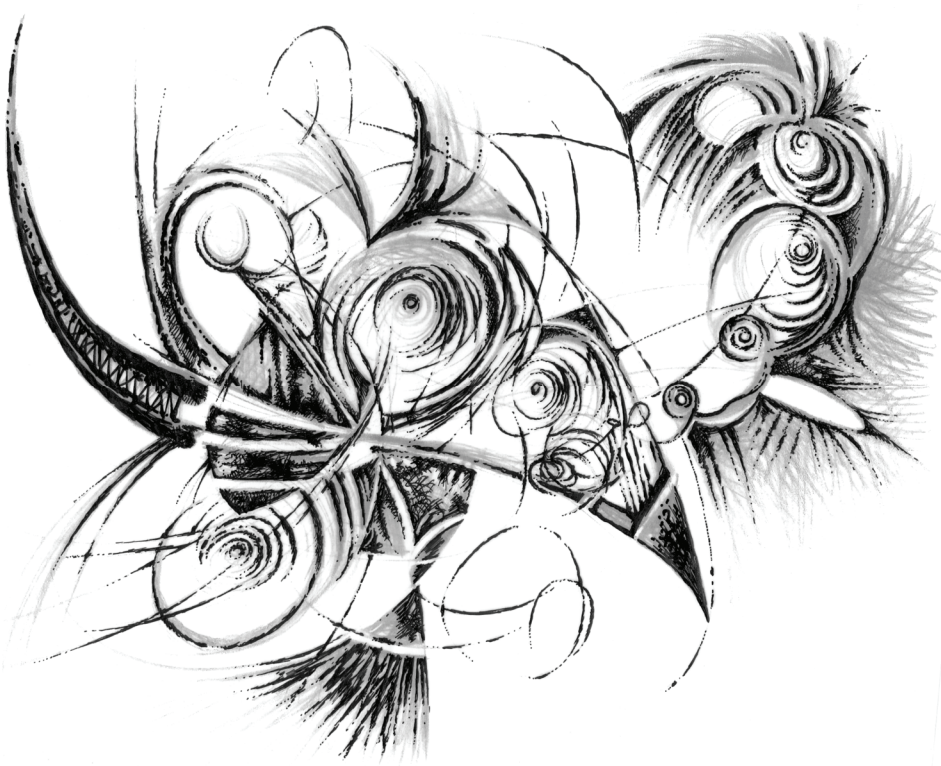
Since the number of letters in the alphabet is limited, some quantities are denoted by the same symbol. However, their meaning can be easily inferred from the context. The list of symbols included at the end of the book can also be helpful. When reading, do not skip the notes; they often contain important insights necessary for understanding the phenomenon being discussed. In the book, you will find them on a gray background. Illustrative examples are separated from the rest of the text at the beginning and end by a crescent moon symbol. Important relations are marked on the left side with a black triangle. Hopefully, these markings will help the reader navigate this challenging academic text more easily.

What can I say in conclusion? I would like to thank many of my students, who studied the texts on which this book is based and carefully identified typos and ambiguities. My thanks also go to Ing. arch. Ivan Havlíček, who handled the graphics for all three volumes of *Selected Topics*. To future students, I would like to wish that they experience the unique and indescribable joy of grasping and understanding the laws that describe the processes taking place in nature around us.

Petr Kulhánek, 2026, Prague

On the aldebaran.cz website, under the Study section, you can download an electronic version of this textbook and other supplementary materials for the lectures.

1. Plasma Theory



1.1 What is Plasma?

Plasma is often referred to as the fourth state of matter. It naturally complements the sequence of solid–liquid–gas. If additional thermal energy is supplied to a gas, it undergoes partial and eventually complete ionization. The substance becomes plasma, containing free charge carriers, which gives this state entirely new properties; it is unique in its collective response to electric and magnetic fields, which it also generates. The properties of plasma differ significantly from those of gases and liquids.

The term "plasma" for ionized gas was first used by Irving Langmuir in 1928, likely because the behavior of this state of matter reminded him of blood plasma. Langmuir understood plasma to be the region of a gas discharge that is not influenced by walls or electrodes and has the following three properties:

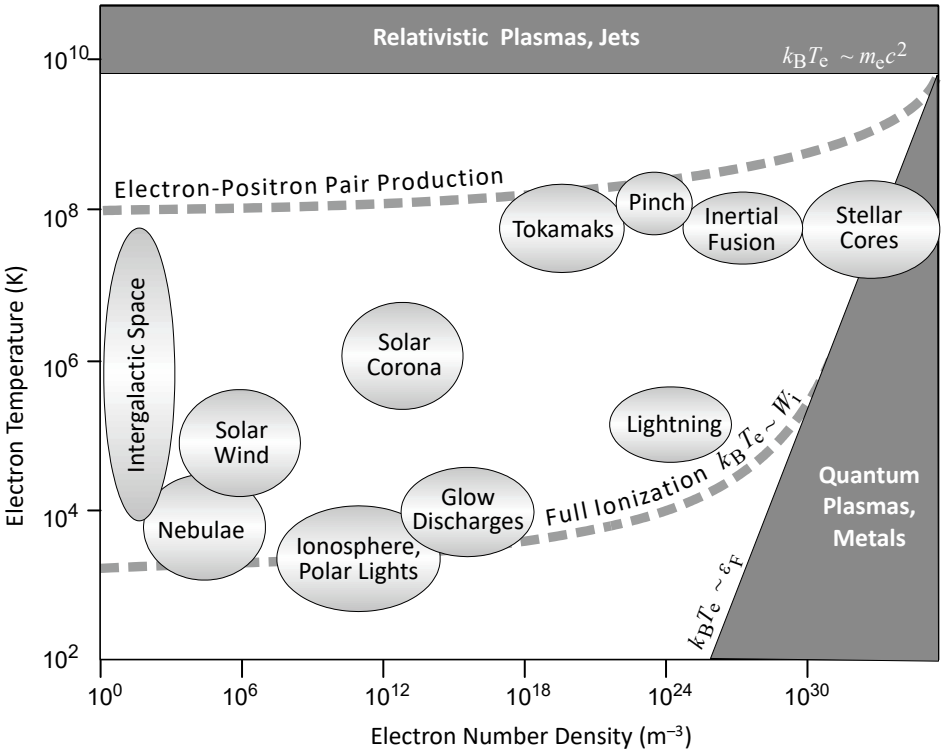
1. Plasma contains free charge carriers.
2. Plasma exhibits collective behavior, i.e., as a whole it responds to electric and magnetic fields and also generates them.
3. Plasma is quasi-neutral, i.e., within a macroscopic volume, there is an equal amount of positive and negative charges.

In space, most baryonic matter is ionized and exists in the form of plasma. Plasma makes up the interiors and outer layers of stars, nebulae, jets, our Sun, and its vast corona. Our entire solar system is flooded with solar wind plasma, and Earth forms a small, neutral oasis within it. On Earth, plasma is encounter only rarely; natural plasma can be found in lightning channels, in the ionosphere, and in auroras. Plasma in lightning channels is under high pressure and is localized within a narrow, sharply defined luminous channel. In contrast, the plasma of an aurora has low pressure and consists of extensive, sheet-like formations with a diffuse glow. Plasma can also be found in research laboratories and in many industrial facilities utilizing various plasma technologies (cutting, machining, coating, etc.).

Plasma is characterized by linear and two-dimensional structures (filaments and walls) held in place by its own magnetic field, which is generated by the flowing current. Charged particles can both gyrate around magnetic field lines and drift across the magnetic field and additional external fields. In regions of a stronger magnetic field, they can be reflected; this phenomenon is called a *magnetic mirror*. A vast number of low-frequency and high-frequency wave modes exist in plasma. The presence of plasma significantly affects the propagation of both acoustic and electromagnetic waves. Plasma is characterized by numerous instabilities that thermonuclear reactor engineers have been grappling with for many years. No less interesting are nonlinear phenomena in plasma or plasma radiation. Some of these phenomena are explored in this textbook.

The electronvolt is a very popular unit among plasma physicists. Electronvolts can be used to express not only energy ($1\ \text{eV} \approx 1.6\times10^{-19}$ J), but also temperature ($E = k_\text{B}T$, $1\ \text{eV} \approx 11{,}600$ K) or particle mass (via the relation $E = mc^2$). SI units are predominantly used in this textbook.

Plasma can be classified from many perspectives. Its properties depend primarily on temperature, number density, and magnetic field. The following diagram shows some typical types of plasma as a function of electron number density and temperature:



The diagram is plotted for hydrogen plasma, but a similar diagram applies to any other plasma. Moving along the temperature axis (vertically) reveals a total of four plasma regimes. At the lowest temperatures, the plasma is only partially ionized. Beyond the curve labeled "full ionization," the plasma is *fully ionized* (which occurs once for hydrogen). The boundary of this region can be expressed as $k_B T_e \approx W_i$, where W_i is the ionization energy. At even higher temperatures (approximately above 10^8 K), spontaneous electron-positron *pair production* occurs. Above a temperature of 6×10^9 K, the thermal energy of the electrons exceeds their rest mass energy, i.e., the inequality $k_B T_e > m_e c^2$ holds, and the plasma is considered *relativistic*. This yields the first criterion for plasma classification:

- Partially ionized plasma / Fully ionized plasma;
- Plasma without / with electron-positron pair production;
- Non-relativistic plasma / Relativistic plasma.

The lower right section of the diagram (dense and cold plasmas) contains the region of quantum plasma. Here, the electron gas is degenerate, i.e., its occupation numbers in phase space are not small. Within the phase volume $\Delta\phi = \Delta^3 x \Delta^3 p$, the number of available quantum states is equal to $\Delta\phi/(2\pi\hbar)^3$, see [2]. If the number of electrons per state is negligible, the electron gas exhibits classical behavior and is described by the Boltzmann distribution. If this is not the case, the Fermi-Dirac distribution must be applied, and the electron gas *behaves quantum mechanically*. This occurs in stellar cores, throughout the entire volume of a white dwarf, or in a neutron star (where the system

consists of neutrons rather than electrons). The boundary equation for this region can be expressed using the Fermi energy of electrons ε_F as $k_B T_e \approx \varepsilon_F$. Another possible classification of plasma is therefore

- Classical plasma / Quantum plasma.

Plasma is capable of conducting electric current. It is often a better conductor than gold or copper. Its conductivity is proportional to $T_e^{3/2}$ and depends only slightly on the plasma density. In calculations, plasma is often replaced by a perfectly conducting fluid. In this limit, no diffusion processes occur in the plasma, and the magnetic field is perfectly "*frozen*" into the plasma, i.e., it follows all its movements. If the conductivity is finite, the magnetic field is partially frozen and partially diffuses into the surroundings. This allows us to further classify plasma:

- Plasmas with a frozen magnetic field / Plasmas with a diffusing field.

The temperature of a plasma is determined by the chaotic motion of its individual components. External stimuli are first responded to by the low-mass electrons; the electron fluid heats up and then transfers its thermal energy to the ions during collisions. It is therefore possible for the electrons to have a different temperature than the ions. If both temperatures are equalized and all macroscopic flows cease, the plasma is considered to be in *thermodynamic equilibrium*. Otherwise, it is classified as a *non-equilibrium plasma*, leading to a further distinction:

- Equilibrium plasma / Non-equilibrium plasma.

In the presence of a magnetic field, the definition of temperature becomes even more complex. The motions of charged particles along magnetic field lines differ from those across the field lines, allowing the definition of two temperatures – parallel and perpendicular. In addition to the equilibrium or non-equilibrium classification, plasma can also be categorized based on ion temperature into *high-temperature* (fusion, $T_i > 10^6$ K) and *low-temperature* ($T_i < 10^5$ K):

- Low-temperature plasma – High-temperature plasma.

Sometimes, however, low-temperature plasma is defined as partially ionized plasma and high-temperature plasma as fully ionized plasma.
In a neutral gas, collisions are characterized by a sudden change in the direction of motion; the path of atoms or molecules resembles a jagged "zigzag" line. In a fully ionized plasma, collisions are governed by Coulomb interactions (electrical attraction or repulsion), and particles change direction only gradually. The mean free path is defined as the average distance over which the direction of a particle's motion changes by 90°.

In partially ionized plasma, both types of collisions occur – Coulomb collisions between charged particles and "zigzag" collisions between a charged and a neutral particle or between two neutral particles. Plasma is considered collisionless if the mean free path between collisions is greater than the dimensions of the plasma ($\lambda_{e,i} > L$). In such a case, the particles either do not interact or interact with each other via self-generated collective fields. In *collisionless* plasma, regions that are not quasi-neutral can easily form. Plasma can therefore also be divided into

- Collisionless plasma – Collisional plasma.

A very important parameter for assessing the properties of plasma is the Debye length λ_D. If a charged particle is in a vacuum, its potential decreases with distance as $1/r$. In plasma, the particle is shielded, and its electric potential decreases as $\exp(-r/\lambda_D)/r$. Up to a distance of λ_D from the charged particle, other particles feel its individual presence; at greater distances, its potential is shielded. This region is referred to as the Debye sphere, where the key parameter is the number of particles within this volume, $N_D = (4/3)\pi n\lambda_D^3$. If $N_D >> 1$, the total average force from individual particles cancels out, and collective processes prevail over collisions – a regime known as an *ideal plasma*, for which the ideal gas equation of state applies to all components.. Typically, this involves hot (high-conductivity) and/or tenuous plasma. Another possible classification is therefore:

- Ideal plasma / Non-ideal plasma.

In astrophysical applications, as well as in laboratory plasmas, plasmas containing dust are frequently encountered. Such plasma possesses specific properties; it is necessary to consider the charging of dust grains, ultra-low-frequency wave modes associated with their motion, and in the case of large clouds, the inclusion of the gravitational interaction of dust grains is indispensable. For this reason, plasma is often classified into:

- Dusty plasma / Dust-free plasma.

Of course, there are other classifications of plasmas; different aspects are important in each field. The overview provided above is sufficient for a basic understanding of the types of plasma.



1.2 Charged Particle Motion

Throughout the first chapter, the motion of particles is calculated in external, known (given) fields under the assumptions that:

1. Particles do not interact with one another.
2. Particles' own fields are negligible.

To describe the electric field, the electric field **E** is used; to describe the magnetic field, the magnetic flux density **B** is used. Alternatively, the electric and magnetic fields can be described using scalar and vector potentials (ϕ, **A**). The relations between fields and potentials are:

$$\mathbf{E} = -\frac{\partial \mathbf{A}}{\partial t} - \frac{\partial \phi}{\partial \mathbf{x}}, \tag{1.1}$$

$$\mathbf{B} = \nabla \times \mathbf{A}. \tag{1.2}$$

The reader can find the derivations of these relations in any textbook on electromagnetic fields, for example in [2]. When calculating the motion of charged particles, we will assume that the potentials $\phi(t, \mathbf{x})$ and $\mathbf{A}(t, \mathbf{x})$ are given functions. Note that they form a relativistic four-vector and can be transformed from one coordinate system to another using the Lorentz transformation.

1.2.1 Non-Relativistic Motion

The motion of charged particles is considered non-relativistic if their velocity is negligible compared to the speed of light, i.e., $v \ll c$. Such particles can be found, for example, in the solar wind or in the plasma of an arc discharge.

Lagrangian and Hamiltonian

The problem of the motion of charged particles in electromagnetic fields is described by the Lagrangian

$$L = L_{\text{part}} + L_{\text{int}}, \tag{1.3}$$

where L_{part} is the particle's Lagrangian, and L_{int} describes the interaction between the particle and the field. If the particle itself generated an electromagnetic field, the field term of the Lagrangian would have to be added. In such a case, however, the Lagrangian density would be required (as this would be a continuous medium). In this approximation, the fields are fixed and are not calculated, meaning the field part of the Lagrangian is zero. For a conservative electric field, the Lagrangian is given by the relation:

$$L = \frac{1}{2} m \mathbf{v}^2 - Q\phi. \tag{1.4}$$

The form is identical to that in classical mechanics [1], where the Lagrangian is given by the difference between kinetic and potential energy: $L = T - V$. The kinetic energy

corresponds to the Lagrangian of a free particle, L_{part}, and the potential energy corresponds to the interaction with the electric field, L_{int}. In the presence of a non-conservative magnetic field, the interaction part must include an additional term. This term is a function of the four-vector of the particle's charge flux (characterizing the particle) and the four-vector of the field potentials (characterizing the field):

$$\mathbf{J} = \begin{pmatrix} c\rho_Q \\ \mathbf{j} \end{pmatrix} = \begin{pmatrix} cQ\delta(\mathbf{x}' - \mathbf{x}) \\ Q\mathbf{v}\delta(\mathbf{x}' - \mathbf{x}) \end{pmatrix}; \qquad \mathbf{A} = \begin{pmatrix} \phi/c \\ \mathbf{A} \end{pmatrix},$$

where $\mathbf{x}'$ is the position of the particle and $\mathbf{x}$ is the position of the observer. The Lagrangian must be a scalar; therefore, the only reasonable combination is a quantity proportional to the scalar product of both four-vectors integrated over the volume (without integration, a quantity proportional to the Lagrangian density is obtained):

$$\int (\mathbf{J} \cdot \mathbf{A})\, \mathrm{d}^3\mathbf{x}' = \int (-Q\phi + Q\mathbf{A} \cdot \mathbf{v})\, \delta(\mathbf{x}' - \mathbf{x})\ \mathrm{d}^3\mathbf{x}' = -Q\phi + Q\mathbf{A} \cdot \mathbf{v}\,.$$

From the above relation, the missing term in (1.4) is now apparent; the correct Lagrangian for the non-relativistic motion of particles in an electric and magnetic fields is:

$$L = \frac{1}{2} m\mathbf{v}^2 - Q\phi + Q\mathbf{A} \cdot \mathbf{v}\,. \tag{1.5}$$

Following standard procedures, the generalized momentum, the generalized energy, and, after eliminating velocity from both relations, the Hamiltonian are determined:

$$\mathbf{p} \equiv \frac{\partial L}{\partial \mathbf{v}} = m\mathbf{v} + Q\mathbf{A}\,, \tag{1.6}$$

$$\mathscr{E} = \frac{\partial L}{\partial \mathbf{v}} \cdot \mathbf{v} - L = \frac{1}{2} m\mathbf{v}^2 + Q\phi\,, \tag{1.7}$$

$$H = \frac{(\mathbf{p} - Q\mathbf{A})^2}{2m} + Q\phi\,. \tag{1.8}$$

Note 1: In this chapter, energy is denoted by the symbol $\mathscr{E}$ to distinguish it from the electric field **E**.

Note 2: Unlike in classical mechanics, the generalized momentum is not simply the product of mass and velocity, but also includes the vector potential.

Note 3: Energy does not depend on the magnetic field (**A**), since the magnetic field does not alter the particle's energy, but only changes the direction of its velocity.

The corresponding Lagrange equations are identical to the Lorentz equation of motion for a charged particle. In component form, the relations are:

$$L = \frac{1}{2} m v_l v_l - Q\phi(t, \mathbf{x}) + QA_l(t, \mathbf{x}) v_l\,;$$

$$\frac{\mathrm{d}}{\mathrm{d}t} \frac{\partial L}{\partial v_k} - \frac{\partial L}{\partial x_k} = 0\,,$$

$$\frac{\mathrm{d}}{\mathrm{d}t}(mv_k + QA_k) + Q\frac{\partial\phi}{\partial x_k} - Q\frac{\partial A_l}{\partial x_k}v_l = 0,$$

$$\frac{\mathrm{d}}{\mathrm{d}t}(mv_k) + Q\frac{\partial A_k}{\partial t} + Q\frac{\partial A_k}{\partial x_l}\frac{\mathrm{d}x_l}{\mathrm{d}t} + Q\frac{\partial\phi}{\partial x_k} - Q\frac{\partial A_l}{\partial x_k}v_l = 0,$$

$$\frac{\mathrm{d}}{\mathrm{d}t}(mv_k) = Q\left[-\frac{\partial A_k}{\partial t} - \frac{\partial\phi}{\partial x_k} + v_l\left(\frac{\partial A_l}{\partial x_k} - \frac{\partial A_k}{\partial x_l}\right)\right].$$

Using the Levi-Civita tensor, the last expression in square brackets can be transformed into the form (for the complete derivation, see *Selected Topics, Volume I*, Section I.3.3.4, Vector Identities):

$$\frac{\mathrm{d}}{\mathrm{d}t}(m\mathbf{v}) = Q\left[-\frac{\partial\mathbf{A}}{\partial t} - \frac{\partial\phi}{\partial\mathbf{x}} + \mathbf{v}\times\operatorname{curl}\mathbf{A}\right] \quad \Rightarrow \quad \frac{\mathrm{d}}{\mathrm{d}t}(m\mathbf{v}) = Q\left[\mathbf{E} + \mathbf{v}\times\mathbf{B}\right], \tag{1.9}$$

which represents the well-known Lorentz force equation.

Motion in an Electric Field and the Optical Analogy

If a charged particle moves for a sufficiently long time in a homogeneous electric field, the problem cannot be solved non-relativistically, as the electric field would accelerate the particle beyond the speed of light, contradicting special relativity. However, it is possible to analyze scenarios where the electric field is confined to a localized region, such as a plasma layer. An idealized example is a shock wave featuring an electric potential jump (a double layer, examined in more detail in Section 1.3.3).

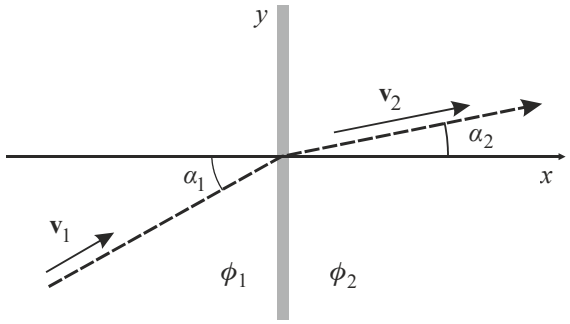


Fig. 1.1: Jump in electrical potential.

It is assumed that the potential is constant in both half-spaces shown in the figure, meaning the electric field vanishes there. Consequently, a charged particle moves at a constant velocity in these regions. Within the thin transition layer (shaded gray) at the interface, the potential changes; here, the electric field is non-zero and points along the *x*-axis. If this transition layer is infinitesimally thin, the potential change becomes step-like. Since no field acts along the *y*-axis, the *y*-component of the particle's velocity remains unchanged and is therefore continuous:

$$v_1 \sin\alpha_1 = v_2 \sin\alpha_2 \,. \tag{1.10}$$

The total energy of the charged particle is conserved during its motion, see (1.7):

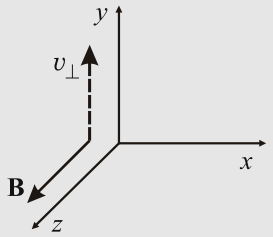
$$\frac{1}{2} m v_1^2 + Q\phi_1 \;=\; \frac{1}{2} m v_2^2 + Q\phi_2 = \mathscr{E}\,. \tag{1.11}$$

Substituting the velocities from (1.11) into (1.10) yields:

$$\frac{\sin\alpha_1}{\sin\alpha_2} = \frac{v_2}{v_1} = \sqrt{\frac{\mathscr{E} - Q\phi_2}{\mathscr{E} - Q\phi_1}} = \sqrt{\frac{C - \phi_2}{C - \phi_1}} = \sqrt{\frac{U_2}{U_1}}\,. \tag{1.12}$$

This relation represents the *optical analogy* of particle motion in an electric field. While its form resembles the law of refraction, the velocity ratio is inverted. A similar approach was adopted by René Descartes when deriving the refractive index; he modeled light as particles that lose energy at the interface between two media, as if penetrating a barrier. The inverted velocity ratio did not concern him, as he interpreted it as an intrinsic property of the medium (the refractive index). The law of refraction was correctly derived by the Dutch mathematician and astronomer Willebrord Snellius, which is why it is known as Snell law.

Motion in a Homogeneous Magnetic Field



Electromagnetic field:
$\mathbf{E} = (0,0,0)$,
$\mathbf{B} = (0,0,B)$;

Initial conditions:
$\mathbf{x}(0) = (0,0,0)$,
$\mathbf{p}(0) = (0, m v_\perp, 0)$.

Consider a homogeneous magnetic field; where the coordinate system is chosen with the *z*-axis pointing in the direction of the field. A charged particle is injected perpendicular to the magnetic field lines in the direction of the *y*-axis. The motion is determined using Hamilton equations. To construct the Hamiltonian, the field potentials must first be found. They are not uniquely determined (different potentials yield the same fields). For example, for the magnetic potential, the expressions $\mathbf{A} = (-yB, 0, 0)$, $\mathbf{A} = (0, xB, 0)$, or $\mathbf{A} = ½\,(-yB, xB, 0)$ can be used. Verify that the curl of $\mathbf{A}$ always yields the field $\mathbf{B} = (0, 0, B)$. Here, potentials of the following form are selected:

$$\phi = 0\,,$$

$$\mathbf{A} = (0, xB, 0)\,.$$

The potentials of electric and magnetic fields for typical configurations can be found in *Selected Topics*, *Volume II*, on p. 172. The generalized momentum is given in our case by the relation $\mathbf{p} = m\mathbf{v} + Q\mathbf{A}$. For the Hamiltonian, we have

$$H = \frac{(\mathbf{p} - Q\mathbf{A})^2}{2m} + Q\phi \;=\; \frac{p_x^2 + (p_y - QBx)^2 + p_z^2}{2m}$$

and the Hamiltonian equations are

$$\dot{x} = \frac{\partial H}{\partial p_x} = \frac{p_x}{m}, \tag{1.13}$$

$$\dot{y} = \frac{\partial H}{\partial p_y} = \frac{p_y - QBx}{m}, \tag{1.14}$$

$$\dot{z} = \frac{\partial H}{\partial p_z} = \frac{p_z}{m}, \tag{1.15}$$

$$\dot{p}_x = -\frac{\partial H}{\partial x} = \frac{QB(p_y - QBx)}{m}, \tag{1.16}$$

$$\dot{p}_y = -\frac{\partial H}{\partial y} = 0, \tag{1.17}$$

$$\dot{p}_z = -\frac{\partial H}{\partial z} = 0. \tag{1.18}$$

From equations (1.17) and (1.18), we immediately obtain

$$p_y(t) = p_y(0) = m v_\perp ,$$

$$p_z(t) = p_z(0) = 0 .$$

Substituting these expressions, along with p_x as expressed in (1.13), into (1.16) yields

$$\ddot{x} + \left(\frac{QB}{m}\right)^2 x = \frac{QB v_\perp}{m}.$$

This is the equation for the variable x. After solving it (the general solution is composed of the complementary and particular solutions), the time dependence $x(t)$ is established, allowing for the direct integration of equations (1.14) and (1.15). The result is

$$\begin{aligned} x(t) &= R_\mathrm{L} - R_\mathrm{L} \cos \omega_\mathrm{c} t, \\ y(t) &= R_\mathrm{L} \sin \omega_\mathrm{c} t, \\ z(t) &= 0, \end{aligned} \tag{1.19}$$

where R_L denotes the so-called Larmor radius and ω_c the cyclotron frequency:

$$R_\mathrm{L} \equiv \frac{m v_\perp}{QB}; \qquad \omega_\mathrm{c} \equiv \frac{QB}{m} \tag{1.20}$$

The trajectory is obtained by eliminating time from (1.19):

$$\left(x - R_\mathrm{L}\right)^2 + y^2 = R_\mathrm{L}^2 . \tag{1.21}$$

The motion occurs along a circle with radius R_L and center $S = [\, R_\mathrm{L}, 0\,]$. The position of the center depends on the sign of the particle's charge.

The magnetic field does not affect the particle's motion parallel to the field lines. Perpendicular to the direction of the field, the Lorentz force acts, forcing the particle into a circular trajectory. For a non-zero initial velocity $v_z(0)$, the particle's motion consists of uniform linear motion along the field and Larmor rotation (so-called *gyration*) in a plane perpendicular to the field – resulting in helical motion.

An electric field, on the other hand, does not affect the motion perpendicular to its lines of force (in the non-relativistic case), or does so only negligibly (in the relativistic case). Acceleration occurs exclusively in the direction of the electric field.

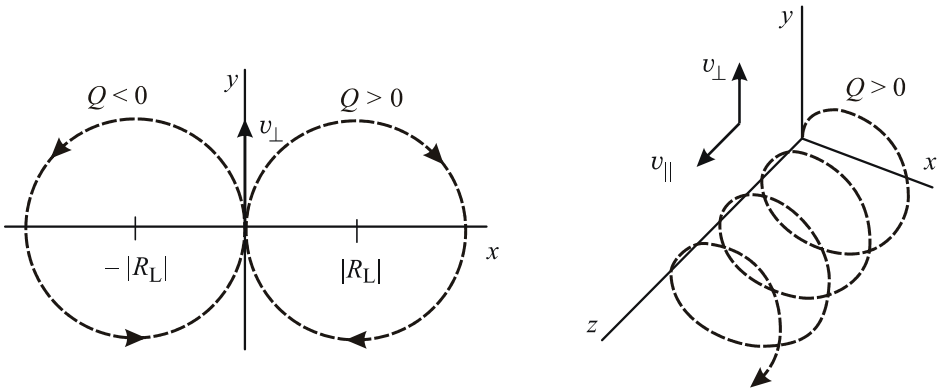


Fig. 1.3: Motions of a charged particle in a homogeneous magnetic field.

Note: The Larmor motion can also be calculated directly from the Lorentz equation of motion $m\ddot{\mathbf{r}} = Q\,\dot{\mathbf{r}} \times \mathbf{B}$. The z-component again leads to uniform linear motion. For the x and y components, we obtain

$$\ddot{x} = \frac{QB}{m}\,\dot{y}\,, \tag{1.22}$$

$$\ddot{y} = -\frac{QB}{m}\,\dot{x}\,. \tag{1.23}$$

Both equations can be solved in several ways. Landau method is probably the most efficient approach: the second equation is multiplied by the imaginary unit and added to the first. The ratio QB/m is denoted as the cyclotron frequency:

$$\ddot{x} + \mathrm{i}\,\ddot{y} = -\mathrm{i}\,\omega_\mathrm{c}\,(\dot{x} + \mathrm{i}\,\dot{y}) \tag{1.24}$$

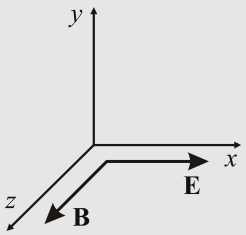
Now, the complex variable $\xi = x + \mathrm{i}y$ can be introduced to solve a simple equation

$$\ddot{\xi} = -\mathrm{i}\,\omega_\mathrm{c}\,\dot{\xi} \tag{1.25}$$

in the complex plane. After determining the integration constants, the desired particle positions x and y are obtained by separating the real and imaginary parts of the solution. This procedure is discussed in detail in the *Selected Topics*, *Volume II*; see Example 3.1 on page 255, where this solution is presented as an application of complex numbers.

Motion in Crossed Fields

Consider now motion in a homogeneous magnetic field and a homogeneous electric field perpendicular to it:



Electromagnetic field

$\mathbf{E} = (E, 0, 0)$,

$\mathbf{B} = (0, 0, B)$;

Initial conditions:

$\mathbf{x}(0) = (0, 0, 0)$,

$\mathbf{p}(0) = (0, 0, 0)$.

The choice of the coordinate system is illustrated in the figure. A charged particle is assumed to be initially at rest at the origin. The field potentials are chosen in the form

$$\phi = -Ex\,,$$

$$\mathbf{A} = (0, Bx, 0)\,.$$

The generalized momentum is again $\mathbf{p} = m\mathbf{v} + Q\mathbf{A}$. The Hamiltonian is given by

$$H = \frac{(\mathbf{p} - Q\mathbf{A})^2}{2m} + Q\phi = \frac{p_x^2 + (p_y - QBx)^2 + p_z^2}{2m} - QEx$$

and the Hamiltonian equations for our problem are

$$\dot{x} = \frac{\partial H}{\partial p_x} = \frac{p_x}{m}\,, \tag{1.26}$$

$$\dot{y} = \frac{\partial H}{\partial p_y} = \frac{p_y - QBx}{m}\,, \tag{1.27}$$

$$\dot{z} = \frac{\partial H}{\partial p_z} = \frac{p_z}{m}\,, \tag{1.28}$$

$$\dot{p}_x = -\frac{\partial H}{\partial x} = \frac{QB(p_y - QBx)}{m} + QE\,, \tag{1.29}$$

$$\dot{p}_y = -\frac{\partial H}{\partial y} = 0\,, \tag{1.30}$$

$$\dot{p}_z = -\frac{\partial H}{\partial z} = 0\,. \tag{1.31}$$

Following a procedure completely analogous to the previous example, the solution

$$x(t) = R_D - R_D \cos \omega_c t \,,$$
$$y(t) = R_D \sin \omega_c t \; - \; v_D t \,, \tag{1.32}$$
$$z(t) = 0 \,,$$

is obtained

$$\omega_c \equiv \frac{QB}{m}; \qquad v_D \equiv \frac{E}{B}; \qquad R_D \equiv \frac{m v_D}{QB}, \tag{1.33}$$

where ω_c denotes the cyclotron frequency, v_D the drift velocity, and R_D the drift radius. After partially eliminating time from the equations (1.32), the trajectory takes the form

$$\left(x - R_D\right)^2 \; + \; \left(y + v_D t\right)^2 \; = \; R_D^2 \,. \tag{1.34}$$

This represents motion along a circle of radius R_D, whose center $S = [R_D \,, -v_D t]$ moves at with drift velocity v_D perpendicular to both the electric and magnetic fields. For zero initial velocity, the relation directly following from the definitions (1.33) holds:

$$v_D = \omega_c R_D \tag{1.35}$$

and the resulting curve (1.34) is called a *cycloid*. This is the same curve traced by point on the rim of a rolling car wheel. For a non-zero initial velocity, relation (1.35) no longer holds, and the motion follows a so-called *trochoid*:

$$x(t) = R_D - R_D \cos \omega_c t \,,$$
$$y(t) = R_D \sin \omega_c t \; - \; v_D t \,, \tag{1.36}$$
$$z(t) = v_{0z}\, t \,,$$

where the drift radius has changed to

$$R_D = \frac{m}{QB} \sqrt{v_{0x}^2 + \left(v_{0y} + v_D\right)^2} \,. \tag{1.37}$$

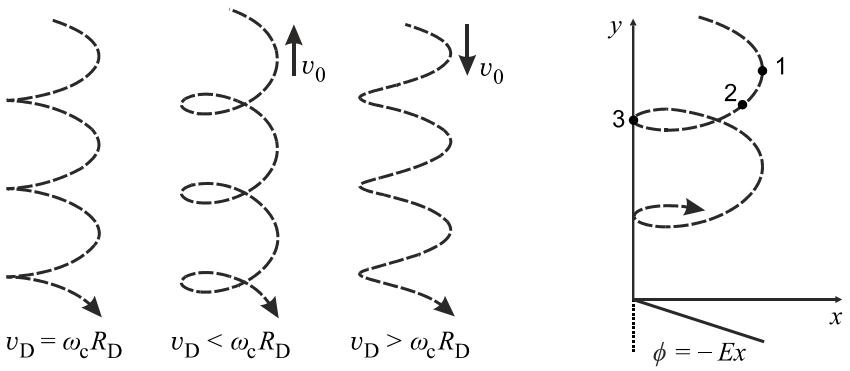


Fig. 1.5: Motions of a charged particle in crossed fields.

For $v_{0z} = 0$, the resulting trochoid is a superposition of a circular motion and a moving center $S = [R_D\,, -v_D t]$. The trochoid can again be visualized using the analogy of a moving car. However, the car is skidding on ice while accelerating or braking. The wheels are partially spinning, meaning that the tangential velocity of the tire differs from the vehicle's forward speed. In this case a point on the wheel traces a trochoid. For $Q > 0$, the trochoids take the shapes shown in Figure 1.5 (a cycloid is a special case of a trochoid and is shown on the left in the figure). At points 1, 2, and 3 on the trajectory, the electric potential is different

$$\phi = -Ex \qquad \Rightarrow \qquad \phi_1 < \phi_2 < \phi_3\,.$$

and, due to the law of conservation of energy, the particle has a different velocity

$$\frac{1}{2}mv^2 + Q\phi = \text{const} \qquad \Rightarrow \qquad v_1 > v_2 > v_3$$

and thus a different Larmor radius:

$$R_L = \frac{m\,v}{QB} \qquad \Rightarrow \qquad R_{L_1} > R_{L_2} > R_{L_3}\,.$$

The trochoidal trajectory of the particle can therefore be interpreted as motion along a circle with a variable radius. The following Figure shows typical tracks of charged particles in a cloud chamber. The influence of the magnetic field is very clearly visible.

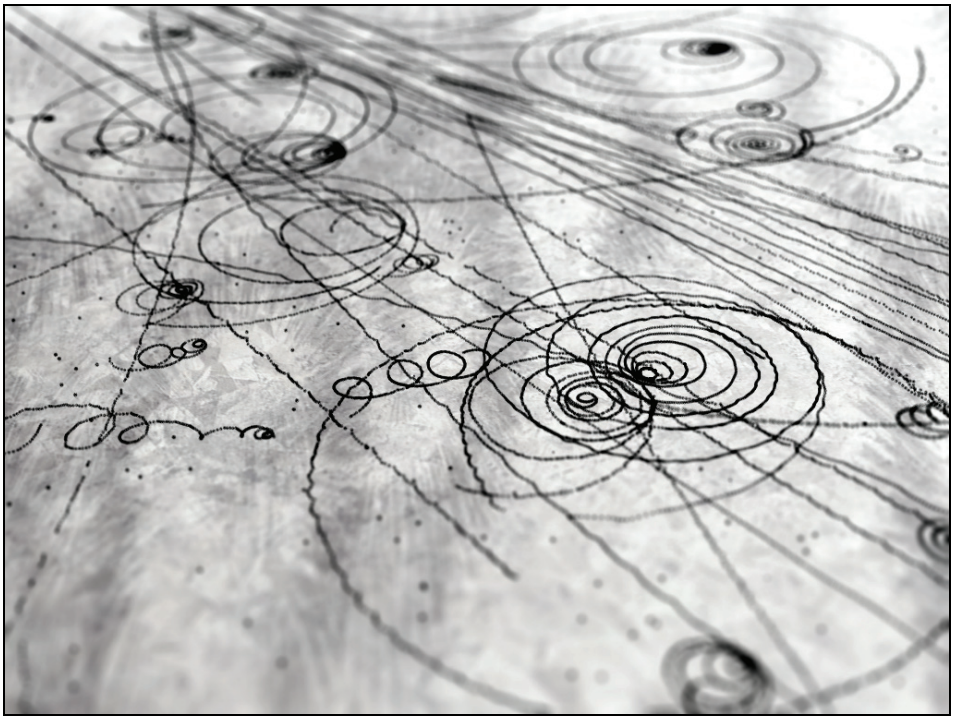


Fig. 1.6: Particle tracks in a cloud chamber. Source: Christian Parsons, Argentina.

1.2.2 Relativistic Motion

Lagrangian and Hamiltonian

In the Lagrangian (1.5), only the interaction term is expressed in relativistic form, since it arises as the scalar product of two four-vectors. The action $\mathrm{d}S = L\mathrm{d}t$ for a free particle must be an invariant of the theory. In non-relativistic physics, where time is absolute, the invariance of the Lagrangian function L suffices. In relativity, the invariance of the entire $L\mathrm{d}t$ term is required. The only invariant is the interval $\mathrm{d}s^2 = -c^2\mathrm{d}t^2 + \mathrm{d}l^2$. In the particle's proper frame, $\mathrm{d}s^2 = -c^2\mathrm{d}\tau^2$, where τ is the particle's proper time. From the last

$$\mathrm{d}\tau \equiv \mathrm{d}t\sqrt{1-\mathbf{v}^2/c^2}\,, \tag{1.38}$$

The term $L\mathrm{d}t$ should be a function of this invariant; the simplest choice is $L\mathrm{d}t = \alpha\,\mathrm{d}\tau$, i.e.,

$$L_{\text{part}} = \alpha\sqrt{1-\mathbf{v}^2/c^2}\,.$$

The proportionality coefficient α is determined such that, in the limit of low velocities, the expression reduces to the Lagrangian function $m_0\mathbf{v}^2/2$ for a non-relativistic particle (where m_0 is the rest mass of the particle):

$$L_{\text{part}} = \alpha\sqrt{1-\mathbf{v}^2/c^2} \approx \alpha\left(1-\frac{\mathbf{v}^2}{2c^2}\right) = \alpha - \alpha\frac{\mathbf{v}^2}{2c^2} \qquad \Rightarrow \qquad \alpha = -m_0c^2.$$

The square root was expanded to first order using the relation $(1+x)^n \approx 1+nx$, which holds for $x \ll 1$. The shift by a constant is negligible. The resulting Lagrangian for the relativistic motion of charged particles in electric and magnetic fields is therefore

► $$L = -m_0c^2\sqrt{1-\mathbf{v}^2/c^2} \;-\; Q\phi \;+\; Q\,\mathbf{A}\cdot\mathbf{v}\,. \tag{1.39}$$

Momentum and energy are determined in the standard way:

$$\mathbf{p} \equiv \frac{\partial L}{\partial \mathbf{v}} = \frac{m_0\,\mathbf{v}}{\sqrt{1-\mathbf{v}^2/c^2}} + Q\,\mathbf{A}\,, \tag{1.40}$$

$$\mathscr{E} = \frac{\partial L}{\partial\,\mathbf{v}}\cdot\mathbf{v} - L \;=\; \frac{m_0c^2}{\sqrt{1-\mathbf{v}^2/c^2}} + Q\phi\,, \tag{1.41}$$

If the Lorentz factor from special relativity is introduced in the standard way

$$\gamma \equiv \frac{1}{\sqrt{1-\mathbf{v}^2/c^2}}\,,$$

the relations for energy and momentum take on a simple form

► $$\mathbf{p} \equiv \gamma m_0\mathbf{v} + Q\mathbf{A}\,, \tag{1.42}$$

► $$\mathscr{E} = \gamma m_0c^2 + Q\phi\,. \tag{1.43}$$

Introducing the so-called "relativistic" mass (which is not the most suitable designation)

$$m \equiv \gamma m_0 \,, \tag{1.44}$$

the relations for momentum and energy take on a simple and intuitive form

$$\mathbf{p} = m\mathbf{v} + Q\,\mathbf{A}\,; \qquad \mathscr{E} = mc^2 + Q\phi\,. \tag{1.45}$$

The final step will be to derive the Hamiltonian. From classical mechanics, it is known that it is always possible to find a Legendre dual transformation, i.e., to eliminate velocity from expressions (1.40) and (1.41). The most straightforward procedure is to isolate the square roots on the right hand side and square the equations:

$$\left(\mathbf{p} - Q\mathbf{A}\right)^2 = \frac{m_0^2\mathbf{v}^2}{1 - \mathbf{v}^2/c^2}\,;$$

$$\frac{1}{c^2}\left(\mathscr{E} - Q\phi\right)^2 = \frac{m_0^2 c^2}{1 - \mathbf{v}^2/c^2}\,.$$

If the two equations are now subtracted from each other, the numerator and denominator on the right-hand side cancel out, and the velocity dependence is eliminated:

$$\frac{1}{c^2}\left(\mathscr{E} - Q\phi\right)^2 - \left(\mathbf{p} - Q\mathbf{A}\right)^2 = m_0^2 c^2\,.$$

Finally, the energy is calculated and defined as the Hamiltonian:

$$H = c\sqrt{m_0^2 c^2 + \left(\mathbf{p} - Q\mathbf{A}\right)^2} + Q\phi\,. \tag{1.46}$$

Relativistic Equation of Motion

When deriving the relativistic equation of motion, the procedure is similar to that of its non-relativistic version (1.9). All modifications are completely identical; the momentum $\gamma m_0 v_k + Q\mathbf{A}$ from (1.40) is simply substituted for $\partial L/\partial v_k$, yielding

► $$\frac{\mathrm{d}}{\mathrm{d}t}\left(m_0\gamma\mathbf{v}\right) = Q\,\mathbf{E} + Q\,\mathbf{v}\times\mathbf{B}\,, \tag{1.47}$$

which is the well-known Lorentz equation of motion. Its left-hand side contains the additional Lorentz factor γ, which depends on velocity and is embedded inside a square root. This complicates numerical simulations, making Hamilton equations more advantageous due to their explicit first-order form. To use the Lorentz equation effectively, the following substitution is appropriate

$$\mathbf{u} = \frac{\mathbf{v}}{\sqrt{1 - \mathbf{v}^2/c^2}}\,, \tag{1.48}$$

which transforms the equation into a form more suitable for numerical integration

$$\frac{\mathrm{d}}{\mathrm{d}t}\left(m_0\mathbf{u}\right) = Q\,\mathbf{E} + \frac{Q\,\mathbf{u}\times\mathbf{B}}{\sqrt{1 + \mathbf{u}^2/c^2}}\,. \tag{1.49}$$

The equation of motion can now be rewritten in its Lorentz-covariant form. To understand these derivations, the reader should be familiar with the basics of special relativity, particularly four-vectors and the electromagnetic field tensor. Both can be found in *Selected Topics II*, which is available in both online and print versions. The reader may also skip the remainder of this section without loss of continuity. The field itself is described using the four-potential and the electromagnetic field tensor:

► $$A^{\alpha} \equiv \begin{pmatrix} \phi/c \\ \mathbf{A} \end{pmatrix}, \tag{1.50}$$

► $$F^{\mu\nu} \equiv \partial^{\mu} A^{\nu} - \partial^{\nu} A^{\mu} = \begin{pmatrix} 0 & E^x/c & E^y/c & E^z/c \\ -E^x/c & 0 & B^z & -B^y \\ -E^y/c & -B^z & 0 & B^x \\ -E^z/c & B^y & -B^x & 0 \end{pmatrix}. \tag{1.51}$$

To describe a particle, the four-velocity is introduced as:

► $$U^{\alpha} \equiv \frac{\mathrm{d}x^{\alpha}}{\mathrm{d}\tau}. \tag{1.52}$$

The time derivative must be taken with respect to proper time; otherwise, the transformation properties of the four-vector would be altered. Using relation (1.38), the four-velocity is expressed in terms of the ordinary velocity $\mathbf{v} = \mathrm{d}\mathbf{r}/\mathrm{d}t$ as

$$U^{\alpha} \equiv \frac{\mathrm{d}x^{\alpha}}{\mathrm{d}\tau} = \frac{\mathrm{d}x^{\alpha}}{\mathrm{d}t}\frac{\mathrm{d}t}{\mathrm{d}\tau} = \begin{pmatrix} \gamma c \\ \gamma \mathbf{v} \end{pmatrix}. \tag{1.53}$$

The square of the magnitude of the four-vector velocity is given by:

$$U^{\alpha}U_{\alpha} \equiv \frac{\mathrm{d}x^{\alpha}}{\mathrm{d}\tau}\frac{\mathrm{d}x_{\alpha}}{\mathrm{d}\tau} = \frac{\mathrm{d}s^2}{\mathrm{d}\tau^2} = \frac{-c^2\mathrm{d}\tau^2}{\mathrm{d}\tau^2} = -c^2. \tag{1.54}$$

The scalar product of the four-velocity with itself is invariant and independent of the coordinate system. Similarly, the particle's four-acceleration is defined as:

$$a^{\alpha} = \frac{\mathrm{d}U^{\alpha}}{\mathrm{d}\tau} \tag{1.55}$$

Differentiating (1.54) proves the four-acceleration is perpendicular to the four-velocity:

$$\frac{\mathrm{d}}{\mathrm{d}\tau}\left(U^{\alpha}U_{\alpha}\right) = 0,$$

$$\frac{\mathrm{d}U^{\alpha}}{\mathrm{d}\tau}U_{\alpha} + U^{\alpha}\frac{\mathrm{d}U_{\alpha}}{\mathrm{d}\tau} = 0,$$

$$2\frac{\mathrm{d}U^{\alpha}}{\mathrm{d}\tau}U_{\alpha} = 0,$$

From this, it immediately follows

$$a^{\alpha}U_{\alpha} = 0\,. \tag{1.56}$$

The final required quantity is the four-momentum, defined as:

$$p^{\alpha} \equiv m_0 U^{\alpha} + QA^{\alpha} = \begin{pmatrix} \gamma m_0 c + Q\phi/c \\ \gamma m_0 \mathbf{v} + Q\mathbf{A} \end{pmatrix}. \tag{1.57}$$

The time component of the four-momentum represents energy, and the spatial components represent the momentum vector, leading to:

$$\begin{pmatrix} \mathscr{E}/c \\ \mathbf{p} \end{pmatrix} = \begin{pmatrix} \gamma m_0 c + Q\phi/c \\ \gamma m_0 \mathbf{v} + Q\mathbf{A} \end{pmatrix} \tag{1.58}$$

This directly yields the well-known relations:

$$\mathscr{E} = \gamma m_0 c^2 + Q\phi = mc^2 + Q\phi\,, \tag{1.59}$$

$$\mathbf{p} = \gamma m_0 \mathbf{v} + Q\mathbf{A} = m\,\mathbf{v} + Q\mathbf{A}\,. \tag{1.60}$$

Using the four-velocity (1.53) and the field tensor (1.51), the equation of motion (1.47) is elegantly expressed as:

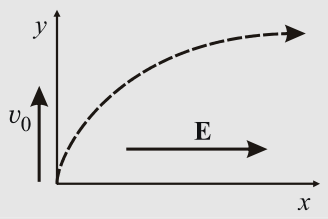
$$m_0 \frac{\mathrm{d}U^{\alpha}}{\mathrm{d}\tau} = QF^{\alpha\beta}U_{\beta}\,. \tag{1.61}$$

This transformation utilizes the identity $\mathrm{d}/\mathrm{d}\tau = \gamma\,\mathrm{d}/\mathrm{d}t$ and the definition of the four-velocity (1.53). The spatial component yields the Lorentz equation of motion, while the temporal component provides the energy balance:

$$\frac{\mathrm{d}\,mc^2}{\mathrm{d}t} = Q\,\mathbf{E}\cdot\mathbf{v}\,, \tag{1.62}$$

which represents the power supplied by the electric field (force multiplied by velocity).

Motion in a Homogeneous Electric Field



Electromagnetic field:

$\mathbf{E} = (E,0,0)$,

$\mathbf{B} = (0,0,0)$;

Initial conditions:

$\mathbf{x}(0) = (0,0,0)$,

$\mathbf{p}(0) = (0,p_0,0)$, kde $p_0 \equiv \dfrac{m_0 v_0}{\sqrt{1 - v_0^2/c^2}}$.

The problem is solved as a planar (2D) problem, with the coordinate system chosen according to the figure. The particle's initial velocity is assumed to be perpendicular to the electric field. The field potentials are chosen in the form:

$$\phi = -Ex\,,$$

$$\mathbf{A} = 0\,.$$

The value of the potential ϕ follows from equation (1.1) for $\mathbf{A} = 0$. The Hamiltonian is

$$H = c\sqrt{m_0^2c^2 + (\mathbf{p} - Q\mathbf{A})^2} + Q\phi = c\sqrt{m_0^2c^2 + p_x^2 + p_y^2} - QEx$$

and the corresponding Hamiltonian equations take the form

$$\dot{x} = \frac{\partial H}{\partial p_x} = \frac{cp_x}{\sqrt{m_0^2c^2 + p_x^2 + p_y^2}}, \tag{1.63}$$

$$\dot{y} = \frac{\partial H}{\partial p_y} = \frac{cp_y}{\sqrt{m_0^2c^2 + p_x^2 + p_y^2}}, \tag{1.64}$$

$$\dot{p}_x = -\frac{\partial H}{\partial x} = QE, \tag{1.65}$$

$$\dot{p}_y = -\frac{\partial H}{\partial y} = 0. \tag{1.66}$$

By integrating equations (1.65) and (1.66), the following relations are obtained:

$$p_x(t) = QEt,$$
$$p_y(t) = p_y(0) = \text{const} = p_0.$$

This solution is substituted into equations (1.63), and (1.64), and integrated (a table of the necessary integrals can be found in *Selected Topics I*, Section I.3.10.4, p. 369):

$$x(t) = \int_0^t \frac{cp_x}{\sqrt{m_0^2c^2 + p_x^2 + p_y^2}}\,\mathrm{d}t' = c\int_0^t \frac{QEt'}{\sqrt{\pi_0^2 + (QEt')^2}}\,\mathrm{d}t' = \frac{c}{QE}\left(\sqrt{\pi_0^2 + (QEt)^2} - \pi_0\right),$$

$$y(t) = \int_0^t \frac{cp_y}{\sqrt{m_0^2c^2 + p_x^2 + p_y^2}}\,\mathrm{d}t' = c\int_0^t \frac{p_0}{\sqrt{\pi_0^2 + (QEt')^2}}\,\mathrm{d}t' = \frac{p_0 c}{QE}\ \operatorname{argsh}\left(\frac{QEt}{\pi_0}\right).$$

The resulting solution is therefore given by the relations

► $$\begin{aligned} x(t) &= \frac{\pi_0 c}{QE}\left(\sqrt{1 + \left(QEt/\pi_0\right)^2} - 1\right), \\ y(t) &= \frac{p_0 c}{QE}\operatorname{argsh}\left(QEt/\pi_0\right), \end{aligned} \tag{1.67}$$

where the following notation has been introduced:

$$\begin{aligned} p_0 &\equiv m_0 v_0 \Big/ \sqrt{1 - v_0^2/c^2}, \\ \pi_0 &\equiv \sqrt{m_0^2c^2 + p_0^2}. \end{aligned} \tag{1.68}$$

For short time intervals, the expressions reduce to their non-relativistic forms:

$$v \ll c \ \ (\text{tj. } p_0 \ll m_0 c) \ \Rightarrow \ \pi_0 \approx m_0 c; \quad p_0 = m_0 v_0, \text{ i.e.}$$

$$x(t) = \frac{m_0c^2}{QE}\left(\sqrt{1+\left(\frac{QEt}{m_0c}\right)^2} - 1\right) \approx \frac{m_0c^2}{QE}\left(1+\frac{1}{2}\left(\frac{QEt}{m_0c}\right)^2 - 1\right) = \frac{QE}{2m_0}t^2,$$

$$y(t) = \frac{cm_0v_0}{QE}\operatorname{argsh}\left(\frac{QEt}{m_0c}\right) \approx \frac{cm_0v_0}{QE}\cdot\frac{QEt}{m_0c} = v_0t.$$

The expressions clearly reduce to the familiar classical relations – uniformly accelerated motion in the direction of the field and uniform motion perpendicular to the field. Unlike in the classical case, the velocity in the direction of the field, v_x, does not increase indefinitely during acceleration in a homogeneous electric field:

$$\lim_{t\to\infty} v_x(t) = \lim_{t\to\infty}\frac{\mathrm{d}x}{\mathrm{d}t} = \lim_{t\to\infty}\frac{c}{QE}\cdot(QE)^2\cdot\frac{t}{\sqrt{\pi_0^2+(QEt)^2}} = c.$$

At any finite time t, v_x remains strictly less than c. Eliminating time from (1.67) by substitution yields the particle's trajectory:

► $$x = \frac{\pi_0 c}{QE}\left[\cosh\left(\frac{QE}{p_0c}y\right) - 1\right]. \qquad (1.69)$$

The figure below plots the classical $x = y^2/2$ and relativistic $x = \cosh(y) - 1$ functions.

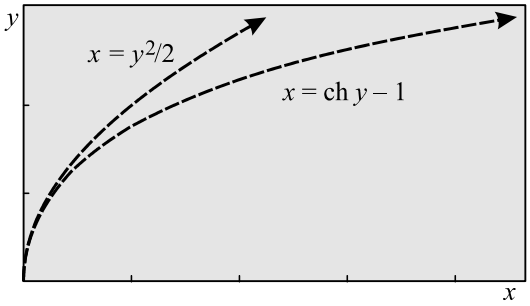


Fig. 1.8: Difference between the relativistic (actual) and non-relativistic trajectories.

Collinear Magnetic and Electric Fields

The magnetic field alters the velocity direction, not its magnitude. An interesting scenario arises when the magnetic and electric fields are parallel. In this case, there is no **E**×**B** drift; the particle gyrates around the magnetic field lines and accelerates along them, asymptotically approaching the speed of light. Even in this situation, the Larmor radius remains unchanged, while its gyrofrequency varies.

Invariance of the Gyration Radius

If the technical details are not required, the invariance of the gyration radius can be accepted without proof, and this entire section, "Collinear Magnetic and Electric Fields," may be skipped. In Cartesian coordinates, both fields are oriented along the z-axis, i.e.

$$\begin{aligned}\mathbf{B} &= (0,0,B)\,,\\ \mathbf{E} &= (0,0,E)\,.\end{aligned} \tag{1.70}$$

The Lorentz equation of motion

$$\frac{\mathrm{d}}{\mathrm{d}t}\left(\gamma m_0 \mathbf{v}\right) = Q\left(\mathbf{E} + \mathbf{v}\times\mathbf{B}\right) \tag{1.71}$$

leads to the system

$$\begin{aligned}\frac{\mathrm{d}}{\mathrm{d}t}\left(\gamma v_x\right) &= \omega_{\mathrm{c}0} v_y\ ;\\ \frac{\mathrm{d}}{\mathrm{d}t}\left(\gamma v_y\right) &= -\omega_{\mathrm{c}0} v_x\ ;\\ \frac{\mathrm{d}}{\mathrm{d}t}\left(\gamma v_z\right) &= \frac{QE}{m_0}\,,\end{aligned} \tag{1.72}$$

where $\omega_{\mathrm{c}0}$ denotes the non-relativistic cyclotron frequency:

$$\omega_{c0} \equiv QB/m_0\,. \tag{1.73}$$

The first two equations are coupled to the third via the Lorentz factor:

$$\gamma = \frac{1}{\sqrt{1-(v_x^2+v_y^2+v_z^2)/c^2}} \tag{1.74}$$

For now, only the first two equations are considered, representing the projection of the motion onto the (x, y) plane perpendicular ($\perp$) to both fields. Let the vector

$$\mathbf{K}_\perp \equiv \frac{\mathrm{d}}{\mathrm{d}t}\left(\gamma \mathbf{v}_\perp\right) = \left(\omega_{\mathrm{c}0} v_y, -\omega_{\mathrm{c}0} v_x\right). \tag{1.75}$$

be introduced. By differentiation, it follows that

$$\mathbf{K}_\perp \equiv \dot{\gamma}\mathbf{v}_\perp + \gamma \mathbf{a}_\perp\,, \tag{1.76}$$

from which the acceleration in the perpendicular plane is calculated:

$$\mathbf{a}_\perp = \frac{\mathbf{K}_\perp}{\gamma} - \frac{\dot{\gamma}}{\gamma}\mathbf{v}_\perp\,, \tag{1.77}$$

which represents the superposition of two vectors:

$$\mathbf{a}_1 = -\frac{\dot{\gamma}}{\gamma}\mathbf{v}_\perp\ ; \qquad \mathbf{a}_2 = \frac{\mathbf{K}_\perp}{\gamma}\,. \tag{1.78}$$

The first vector points in the direction of $\mathbf{v}_\perp$ and the second vector is perpendicular to the first, because

$$\mathbf{a}_1 \cdot \mathbf{a}_2 \propto \mathbf{v}_\perp \cdot \mathbf{K}_\perp = v_x \cdot \omega_{\mathrm{c}0} v_y - v_y \cdot \omega_{\mathrm{c}0} v_x = 0\,. \tag{1.79}$$

The second vector is normal to the trajectory's projection onto the perpendicular plane, representing the normal acceleration. This allows the calculation of the curvature radius:

$$R = \frac{v_\perp^2}{|\,\mathbf{a}_2\,|} = \frac{v_\perp^2}{\frac{|\,\omega_{c0}\,|}{\gamma}\sqrt{v_x^2+v_y^2}} = \frac{\gamma v_\perp}{|\,\omega_{c0}\,|}. \tag{1.80}$$

This constant radius of curvature implies that the perpendicular motion is circular. To demonstrate this, it is sufficient to prove that

$$\frac{\mathrm{d}}{\mathrm{d}t}(\gamma v_\perp) = 0. \tag{1.81}$$

Let the vector

$$\mathbf{u}_\perp \equiv \gamma \mathbf{v}_\perp. \tag{1.82}$$

be introduced. The proof of the above statement is then relatively straightforward:

$$\frac{\mathrm{d}}{\mathrm{d}t}(\gamma v_\perp) = \frac{\mathrm{d}}{\mathrm{d}t}u_\perp = \frac{\mathrm{d}}{\mathrm{d}t}\sqrt{u_x^2+u_y^2} \;=\; \frac{\mathbf{u}_\perp \cdot \dot{\mathbf{u}}_\perp}{u_\perp}.$$

From the relation (1.75), it is clear that

$$\frac{\mathrm{d}\mathbf{u}_\perp}{\mathrm{d}t} = \mathbf{K}_\perp, \tag{1.83}$$

and therefore

$$\frac{\mathrm{d}}{\mathrm{d}t}(\gamma v_\perp) \;\propto\; \mathbf{u}_\perp \cdot \mathbf{K}_\perp = (\gamma v_x, \gamma v_y)\cdot(\omega_{c0} v_y, -\omega_{c0} v_x) = 0. \tag{1.84}$$

This proves that the motion is circular with a Larmor radius given by (1.80)

► $$R_\mathrm{L} = \frac{\gamma v_\perp}{|\,\omega_{c0}\,|} = \text{const}, \tag{1.85}$$

which remains constant during the motion. An increase in the longitudinal component of velocity leads to an increase in γ, which is compensated by a decrease in the azimuthal component of velocity. This expression can be rewritten using individual velocity components in cylindrical coordinates, $v_r = 0$ and $v_\perp = v_\varphi$:

$$R_\mathrm{L} = \frac{v_\varphi}{|\,\omega_{c0}\,|\sqrt{1-(v_\varphi^2+v_z^2)/c^2}}. \tag{1.86}$$

The increase in the longitudinal velocity component caused by the acceleration from the electric field is compensated by a decrease in the azimuthal velocity component, keeping the Larmor radius constant. The Larmor radius (1.85) can be recorded for further use using the initial values:

$$R_\mathrm{L} = \frac{u_0}{|\,\omega_{c0}\,|}; \qquad u_0 \equiv \frac{v_{\varphi 0}}{\sqrt{1-(v_{\varphi 0}^2+v_{z0}^2)/c^2}}. \tag{1.87}$$

Time Dependence of the Velocity Components

From the remaining component of the equation of motion (1.72), it follows that

$$\gamma v_z = \frac{QE}{m_0}(t - t_0), \tag{1.88}$$

where t_0 is the time at which the longitudinal velocity component was zero. For a trajectory with a fixed Larmor radius ($v_r = 0$):

$$\gamma = \frac{1}{\sqrt{1-(v_\varphi^2 + v_z^2)/c^2}}. \tag{1.89}$$

From equations (1.86), (1.88), and (1.89), the time dependencies are readily obtained:

$$v_\varphi(\tau) = \frac{u_0}{\sqrt{\left(1+u_0^2/c^2\right)\left(1+\tau^2\right)}}; \qquad v_z(\tau) = \frac{c\,\tau}{\sqrt{1+\tau^2}}; \tag{1.90}$$

$$\gamma(\tau) = \sqrt{\left(1+u_0^2/c^2\right)\left(1+\tau^2\right)}, \tag{1.91}$$

where the Larmor radius is expressed from (1.87), and τ denotes the dimensionless time measured from the moment when the longitudinal (z) velocity component is zero:

$$\tau \equiv \frac{QE}{m_0 c}\frac{t - t_0}{\sqrt{1+u_0^2/c^2}}, \tag{1.92}$$

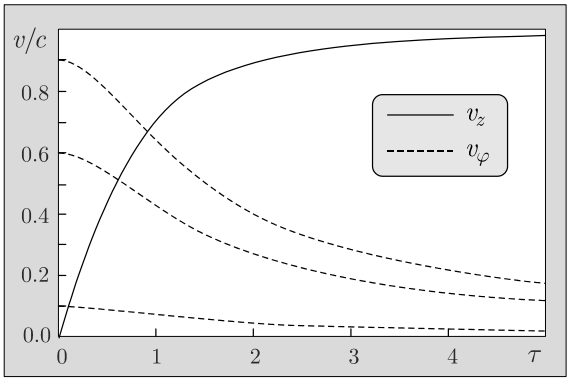


Fig. 1.9: Longitudinal velocity component increases with time, asymptotically approaching c. The transverse (azimuthal) component decreases (the curves correspond to different initial values). The radial component is zero. The dimensionless time τ is defined by (1.92).

As the azimuthal velocity decreases, the gyration frequency also drops:

► $$\omega_c(\tau) = \dot{\varphi} = \frac{v_\varphi}{R_L} = \frac{\omega_{c0}}{\gamma} = \frac{\omega_{c0}}{\sqrt{\left(1+u_0^2/c^2\right)\left(1+\tau^2\right)}}. \tag{1.93}$$

1.2.3 Adiabatic Approximation

In theoretical mechanics, fundamental conservation laws are associated with symmetries in nature (conservation of energy, momentum, angular momentum, and other quantities), alongside so-called *adiabatic invariants*. Consider an arbitrary periodic motion described by a variable q (such as an angle or distance). If external fields change only slightly over a single period of motion (an adiabatic process), it can be demonstrated that the quantity

► $$I \equiv \oint p_q \, \mathrm{d}q = \text{const} \tag{1.94}$$

remains constant, p_q is the generalized momentum with respect to the variable q. Such a quantity is termed an adiabatic invariant. A detailed derivation is provided in *Selected Topics* , *Volume I*.

In plasma physics, the magnetic field is assumed to dominantly influence the motion of charged particles, making the Larmor rotation (gyration around magnetic field lines) the fundamental periodic motion. Other fields, such as electric and gravitational fields, may also be present. Under the assumption that all fields change only slightly during one Larmor rotation, this condition implies a small temporal change in the fields over one particle rotation. Spatially, it states that the fields vary minimally over the scale of the Larmor radius. Mathematically, both assumptions are expressed as follows:

$$\left|\frac{\partial F_k}{\partial t}\right| \ll \frac{F}{T}; \qquad \left|\frac{\partial F_k}{\partial x_l}\right| \ll \frac{F}{R_\mathrm{L}} \qquad \text{for } \forall k,l\,, \tag{1.95}$$

where **F** represents any field affecting the particle motion. Fields may vary in both time and space, but only to a small extent. Under this assumption, a quantity called the *first adiabatic invariant* is conserved. Subsequent calculations frequently require the projection of the particle's velocity parallel to the magnetic field (where motion is force-free and follows the field lines) and the projection perpendicular to the field lines (corresponding to the Larmor rotation):

► $$\mathbf{v}_{\parallel} = \text{ magnitude} \times \text{direction} = \left(\mathbf{v}\cdot\frac{\mathbf{B}}{B}\right)\frac{\mathbf{B}}{B} = (\mathbf{v}\cdot\mathbf{e}_B)\mathbf{e}_B\,, \tag{1.96}$$

► $$\mathbf{v}_{\perp} = \mathbf{v} - \mathbf{v}_{\parallel} = \mathbf{v} - (\mathbf{v}\cdot\mathbf{e}_B)\mathbf{e}_B = \mathbf{v}(\mathbf{e}_B\cdot\mathbf{e}_B) - \mathbf{e}_B(\mathbf{v}\cdot\mathbf{e}_B) = \mathbf{e}_B\times(\mathbf{v}\times\mathbf{e}_B)\,. \tag{1.97}$$

First Adiabatic Invariant

In gyration, the generalized coordinate describing the periodic motion is the rotation angle. The particle's generalized angular momentum corresponds to the axis of gyration. If the other fields vary only slightly, the quantity

$$I \equiv \oint p_q \, \mathrm{d}q = mR_\mathrm{L}v_{\perp}\cdot 2\pi \tag{1.98}$$

is conserved. Substituting the Larmor radius from the relation (1.20) yields

$$\frac{v_{\perp}^2}{B} = \text{const} \tag{1.99}$$

Consequently, a stronger magnetic field grows the perpendicular velocity component, increasing the pitch angle between the trajectory and the field. This quantity is the *first adiabatic invariant*, conventionally scaled to represent the ratio of perpendicular kinetic energy to the magnetic field:

► $$\mu \equiv \frac{m v_\perp^2}{2B} = \text{const} \tag{1.100}$$

The conservation of this quantity can be demonstrated through a simple example. Consider a homogeneous magnetic field whose magnitude increases over time (causing the field lines to tighten). The non-zero change in the field $\partial\mathbf{B}/\partial t$ points in its own direction. According to Maxwell equation $\nabla\times\mathbf{E} = -\partial\mathbf{B}/\partial t$, an induced non-conservative (rotational) electric field arises, accelerating the gyrating particle. The increase in the perpendicular component of the kinetic energy during one period is given by

$$\Delta W_\perp = \oint\limits_{\gamma=\partial S} \mathbf{F}\cdot\mathrm{d}\mathbf{l} = \oint\limits_{\gamma=\partial S} Q\mathbf{E}\cdot\mathrm{d}\mathbf{l} =$$

$$= Q\int\limits_S (\nabla\times\mathbf{E})\cdot\mathrm{d}\mathbf{S} = -\,Q\int\limits_S \frac{\partial\mathbf{B}}{\partial t}\cdot\mathrm{d}\mathbf{S}\,.$$

The derivation utilizes the Stokes theorem and the Faraday law of induction. In this example the time variation of the magnetic field is considered constant, allowing it to be extracted from the integration and replaced by the field variation over a single gyration period. Under the adiabatic approximation, the area of the Larmor rotation remains unchanged over one turn and equals the area of the gyration circle. The sign is positive because, in a strengthening magnetic field, the electric field is oriented such that it accelerates the particle (the increasing magnetic energy is transferred to the particle):

$$\Delta W_\perp \cong Q\frac{\partial B}{\partial t}\pi R_\mathrm{L}^2 = Q\frac{\Delta B}{T}\pi R_\mathrm{L}^2 = Q\frac{\Delta B}{2\pi/\omega_\mathrm{c}}\pi R_\mathrm{L}^2\,.$$

Substituting the previously derived relations for the Larmor radius $R_\mathrm{L} = mv_\perp/QB$ and the cyclotron frequency $\omega_\mathrm{c} = QB/m$ yields the relation

$$\Delta W_\perp = \frac{m v_\perp^2}{2}\frac{\Delta B}{B} = W_\perp\frac{\Delta B}{B} \quad \Rightarrow$$

$$\frac{\Delta W_\perp}{W_\perp} = \frac{\Delta B}{B} \quad \Rightarrow \quad \int\frac{\mathrm{d}W_\perp}{W_\perp} = \int\frac{\mathrm{d}B}{B} \quad \Rightarrow$$

$$\ln\frac{W_\perp}{W_{\perp 0}} = \ln\frac{B}{B_0} \quad \Rightarrow \quad \frac{W_\perp}{W_{\perp 0}} = \frac{B}{B_0} \quad \Rightarrow$$

$$\frac{W_\perp}{B} = \frac{W_{\perp 0}}{B_0} = \text{const} \quad \Rightarrow$$

$$\mu \equiv \frac{W_\perp}{B} = \frac{m v_\perp^2}{2B} = \text{const}\,. \tag{1.101}$$

Thus, this specific example validates the general formula (1.100).

Note: The first adiabatic invariant has several physical interpretations:

$$\begin{aligned} &1) \quad \mu = \frac{m v_\perp^2}{2B} = \frac{W_\perp}{B}; \\ &2) \quad \mu = IS; \\ &3) \quad \mu = \left| \frac{1}{2} Q \mathbf{r} \times \mathbf{v} \right|. \end{aligned} \tag{1.102}$$

The second and third expressions represent the magnitude of the magnetic moment of a gyrating particle. The equivalence of all expressions can be verified by direct substitution (where I is the electric current generated by the particle)

$$IS = \frac{Q}{T} \pi R_\mathrm{L}^2 = \cdots = \frac{m v_\perp^2}{2B};$$

$$\left| \frac{1}{2} Q \mathbf{r} \times \mathbf{v} \right| = \frac{1}{2} Q R_\mathrm{L} v_\perp = \cdots = \frac{m v_\perp^2}{2B}.$$

Motion of the Guiding Center

In many cases, knowledge of the detailed motion of a particle in a magnetic field is not required. By centering the problem around a known gyration motion, the focus can be shifted solely to the motion of the guiding center itself. The derivation utilizes a small parameter ε, which determines the significance of individual terms. After centering, the limit $\varepsilon \to 1$ is taken. Prior to centering, two distinct timescales are utilized:

- t a slowly varying time in accordance with the adiabatic approximation (describing changes in the fields)
- τ a rapidly varying time describing the individual phases of gyration, used for averaging, assuming that $\tau \sim t/\varepsilon$.

Let $\mathbf{R}(t)$ be the guiding center (see figure), $\mathbf{r}(t, \tau)$ the actual position of the particle, and $\boldsymbol{\rho}(t, \tau)$ the gyration vector, over which the values are averaged:

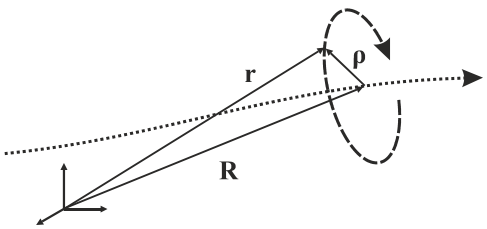


Fig. 1.10: Motion of the guiding center (dotted) and motion of the particle (dashed).

A coordinate system is introduced such that the third axis locally points in the direction of the magnetic field, so that:

$$\mathbf{e}_3(t) = \mathbf{B}/B. \tag{1.103}$$

According to the figure, the position vector of the particle is:

$$\mathbf{r}(t,\tau) = \mathbf{R}(t) + \varepsilon\,\boldsymbol{\rho}(t,\tau)\,. \tag{1.104}$$

The parameter ε is used to indicate that gyration is less significant than the motion of the guiding center. According to (1.19), gyration in this coordinate system yields:

$$\boldsymbol{\rho}(t,\tau) = -\mathbf{e}_1(t)R_{\mathrm{L}}(t)\cos\left(\omega_{\mathrm{c}}(t)\,\tau\right) + \mathbf{e}_2(t)R_{\mathrm{L}}(t)\sin\left(\omega_{\mathrm{c}}(t)\,\tau\right). \tag{1.105}$$

Note that rapid changes related to gyration are denoted by the time τ, over which the averaging is performed. The equation of motion for the particle is written in the form:

$$m\frac{\mathrm{d}^2\mathbf{r}}{\mathrm{d}t^2} = \mathbf{F}_{\mathrm{ext}} + Q\,\frac{\mathrm{d}\mathbf{r}}{\mathrm{d}t}\times\mathbf{B}\,. \tag{1.106}$$

The parameter ε could also distinguish between important and less important terms in the equation of motion, but this is non-essential here. The fields are calculated at the particle's position, i.e., in coordinates (t, $\mathbf{r}$):

$$m\frac{\mathrm{d}^2\mathbf{r}}{\mathrm{d}t^2} = \mathbf{F}_{\mathrm{ext}}(t,\mathbf{r}) + Q\,\frac{\mathrm{d}\mathbf{r}}{\mathrm{d}t}\times\mathbf{B}(t,\mathbf{r})\,, \tag{1.107}$$

The individual terms are now calculated in accordance with (1.104). The derivative with respect to time t is denoted by a dot, and the derivative with respect to the rapid time $\tau \sim t/\varepsilon$ by a prime, i.e., $\partial/\partial t \to \cdot$, $\partial/\partial\tau \to '$. Furthermore, $\mathrm{d}\tau/\mathrm{d}t \sim 1/\varepsilon$. Expressing both fields ($\mathbf{F}$, $\mathbf{B}$) in the argument and performing a first-order Taylor expansion yields:

$$\mathbf{r}(t) = \mathbf{R}(t) + \varepsilon\,\boldsymbol{\rho}(t,\tau)\,;$$

$$\frac{\mathrm{d}\mathbf{r}}{\mathrm{d}t} = \dot{\mathbf{R}} + \varepsilon\,\dot{\boldsymbol{\rho}} + \boldsymbol{\rho}'\,;$$

$$\frac{\mathrm{d}^2\mathbf{r}}{\mathrm{d}t^2} = \ddot{\mathbf{R}} + \varepsilon\,\ddot{\boldsymbol{\rho}} + 2\dot{\boldsymbol{\rho}}' + \frac{1}{\varepsilon}\boldsymbol{\rho}''\,;$$

$$\mathbf{F}_{\mathrm{ext}}(t,\mathbf{r}) \approx \mathbf{F}_{\mathrm{ext}}(t,\mathbf{R}) + \varepsilon(\boldsymbol{\rho}\cdot\nabla)\mathbf{F}_{\mathrm{ext}}\,;$$

$$\mathbf{B}(t,\mathbf{r}) \approx \mathbf{B}(t,\mathbf{R}) + \varepsilon(\boldsymbol{\rho}\cdot\nabla)\mathbf{B}\,.$$

After substitution, the equation of motion takes the form:

$$m\left[\ddot{\mathbf{R}} + \varepsilon\,\ddot{\boldsymbol{\rho}} + 2\dot{\boldsymbol{\rho}}' + \frac{1}{\varepsilon}\boldsymbol{\rho}''\right] =$$

$$= \mathbf{F}_{\mathrm{ext}}(\mathbf{R}) + \varepsilon(\boldsymbol{\rho}\cdot\nabla)\mathbf{F}_{\mathrm{ext}} + Q\left[\dot{\mathbf{R}} + \varepsilon\,\dot{\boldsymbol{\rho}} + \boldsymbol{\rho}'\right]\times\left[\mathbf{B}(\mathbf{R}) + \varepsilon(\boldsymbol{\rho}\cdot\nabla)\mathbf{B}\right].$$

Averaging over the rapidly changing time τ reveals from (1.105) that:

$$\langle\boldsymbol{\rho}\rangle_\tau = \langle\dot{\boldsymbol{\rho}}\rangle_\tau = \langle\boldsymbol{\rho}'\rangle_\tau = \langle\dot{\boldsymbol{\rho}}'\rangle_\tau = \langle\ddot{\boldsymbol{\rho}}\rangle_\tau = \langle\boldsymbol{\rho}''\rangle_\tau = 0\,. \tag{1.108}$$

Only the mean values of the square of the gyration vector $\boldsymbol{\rho}$ will remain non-zero. In the equation of motion, only terms up to the first order in ε are retained:

$$m\ddot{\mathbf{R}} = \mathbf{F}_{\mathrm{ext}}(\mathbf{R}) + Q\dot{\mathbf{R}}\times\mathbf{B}(\mathbf{R}) + \varepsilon Q\left\langle\boldsymbol{\rho}'\times(\boldsymbol{\rho}\cdot\nabla)\mathbf{B}\right\rangle_\tau.$$

All that remains is to perform the averaging of the last term. Substituting the gyration vector from (1.105) and the gradient $\mathbf{e}_1\partial_x + \mathbf{e}_2\partial_y + \mathbf{e}_3\partial_z$, and the relations

$$\mathbf{e}_1\times\mathbf{e}_2 = \mathbf{e}_3\,; \qquad \mathbf{e}_2\times\mathbf{e}_3 = \mathbf{e}_1\,; \qquad \mathbf{e}_3\times\mathbf{e}_1 = \mathbf{e}_2\,; \qquad \mathbf{B} = B\,\mathbf{e}_3\,;$$

$$\langle\cos\omega_c\tau\rangle_\tau = \langle\sin\omega_c\tau\rangle_\tau = \langle\sin\omega_c\tau\cos\omega_c\tau\rangle_\tau = 0\,; \qquad \left\langle\cos^2\omega_c\tau\right\rangle_\tau = \left\langle\sin^2\omega_c\tau\right\rangle_\tau = \frac{1}{2}.$$

is utilized. The averaging does not apply to the vectors $\mathbf{e}_k$, which vary with slow time t. During averaging, the third component of the gradient vanishes, assuming that the particle moves only in the (xy) plane. The result of the averaging is:

$$m\ddot{\mathbf{R}} = \mathbf{F}_{\text{ext}}(\mathbf{R}) + Q\dot{\mathbf{R}}\times\mathbf{B}(\mathbf{R}) - \varepsilon\frac{m v_\perp^2}{2B}\nabla B\,.$$

Taking the limit $\varepsilon \to 1$, the desired equation of motion for the gyrocenter is obtained:

$$m\ddot{\mathbf{R}} = \mathbf{F}_{\text{ext}} + Q\dot{\mathbf{R}}\times\mathbf{B} - \mu\nabla B\,;$$

$$\mu \equiv \frac{m v_\perp^2}{2B}\,. \tag{1.109}$$

Note: All forces in the equation are fictitious; they act at the gyrocenter, where in reality no particle is present.

Force –μ grad B

The effective force $-\mu\nabla B$ repels particles from regions of stronger magnetic fields. It depends solely on the field magnitude B, not its direction, pointing from stronger to weaker field regions. Its coefficient is the first adiabatic invariant. This force acts at the guiding center and results from gyration averaging, as illustrated for converging field lines in Figure 1.11. Since the Lorentz force is perpendicular to the field lines, a non-zero parallel component arises during averaging, pushing the particle out of the strong field. The original unperturbed field is assumed to point along the z-axis:

$$\mathbf{B} = (0, 0, B)\,.$$

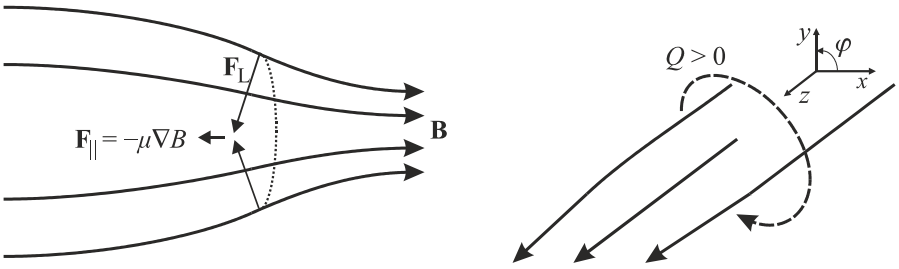


Fig. 1.11: Gradient B force acting due to converging magnetic field lines.

A small field variation $\partial B/\partial z > 0$ is introduced, as shown in the figure on the right. Consequently, a non-zero radial field component B_r (in cylindrical coordinates) and a force F_z pushing the particle out of the region of field compression arise. This is best demonstrated by rewriting the equation div **B** = 0 in cylindrical coordinates ($B_\varphi = 0$):

$$\frac{1}{r}\frac{\partial}{\partial r}(rB_r)+\frac{\partial B_z}{\partial z}=0\,,$$

$$\frac{\partial}{\partial r}(rB_r)=-r\frac{\partial B_z}{\partial z}\,, \qquad /\int$$

$$rB_r=-\frac{r^2}{2}\frac{\partial B_z}{\partial z}\,,$$

$$B_r=-\frac{r}{2}\frac{\partial B_z}{\partial z}\cong-\frac{r}{2}\frac{\partial B}{\partial z}.$$

This radial field component ($B_r \ll B_z \cong B$) causes a force along the z axis:

$$F_z=-Qv_\varphi B_r=-Q(-\omega_c R_L)\left(-\frac{R_L}{2}\frac{\partial B}{\partial z}\right)=-\frac{Q\omega_c R_L^2}{2}\frac{\partial B}{\partial z}\,.$$

According to Fig. 1.11, the angular velocity component for a positive charge is negative. Substituting the angular frequency and the Larmor radius from (1.20) yields

$$F_z=-\frac{mv_\perp^2}{2B}\frac{\partial B}{\partial z}=-\mu\frac{\partial B}{\partial z}.$$

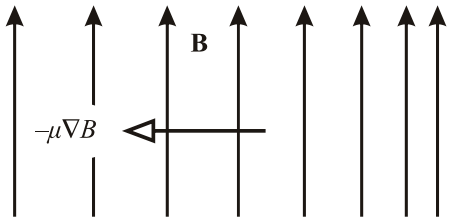


Fig. 1.12: Gradient B force acting during spatial magnetic field compression.

The $-\mu\nabla B$ force can therefore be derived without averaging over the gyration. However, the averaging method is more general, as it yields this force even for transverse field convergence where $\partial B/\partial x \neq 0$.

Drift Equation

The equation (1.109) describing the motion of the guiding center is multiplied by the magnetic field vector. Following a standard vector triple product manipulation and dividing the entire equation by QB^2, it follows that

$$\dot{\mathbf{R}}-\left(\dot{\mathbf{R}}\cdot\frac{\mathbf{B}}{B}\right)\frac{\mathbf{B}}{B}=\frac{\mathbf{F}_{\text{ext}}\times\mathbf{B}-\mu\nabla B\times\mathbf{B}-m\ddot{\mathbf{R}}\times\mathbf{B}}{QB^2}\,.$$

The second term on the left is the parallel velocity of the guiding center. The left-hand side then becomes $\dot{\mathbf{R}} - \dot{\mathbf{R}}_{||}$, yielding the perpendicular projection:

$$\dot{\mathbf{R}}_{\perp} = \frac{\mathbf{F}_{\text{ext}} \times \mathbf{B} - \mu \nabla B \times \mathbf{B} - m\ddot{\mathbf{R}} \times \mathbf{B}}{QB^2} \,. \tag{1.110}$$

The derived relation is called the *drift equation*. The guiding center can move at a non-zero velocity $\dot{\mathbf{R}}_{\perp}$ perpendicular to the field lines. This drift arises from three factors corresponding to the three terms on the right-hand side. The first term represents external forces, such as electric or gravitational fields. The second term stems from magnetic field inhomogeneities, causing the gradient drift. The final term is driven by non-uniform motion of the guiding center, caused either by velocity direction changes due to field line curvature (*curvature drift*) or velocity magnitude changes (*inertial drift*).

The drift of charged particles perpendicular to the magnetic field is a very common phenomenon in plasma. It usually involves a combination of several simultaneous drifts, as certain drifts cause charge separation and induce an electric field, subsequently leading to an **E**×**B** drift. If the conditions vary slowly, the drift velocity of the guiding center follows these changes, making the last term in the drift equation non-zero. For example, an inertial drift arises from variations in the magnitude of the guiding center's velocity.

Drifts

E×B drift

This drift occurs for a charged particle in crossed electric and magnetic fields (see also Section 1.2.1). Substituting $\mathbf{F} = Q\mathbf{E}$ into the drift equation (1.110) yields

$$\mathbf{v}_E = \frac{\mathbf{E} \times \mathbf{B}}{\mathbf{B}^2} \,. \tag{1.111}$$

The drift velocity is perpendicular to both fields, with a magnitude of

$$v_E = \frac{E}{B} \sin \alpha, \tag{1.112}$$

where α is the angle between the two fields. The previously derived relation (1.33) for the drift velocity represents a special case of equation (1.111). Notably, is independent of the particle's mass and charge; electrons and ions drift in the same direction. Consequently, this drift does not generate an electric current.

Gravitational Drift

In a gravity field $\mathbf{F} = m\,\mathbf{g}$ and a magnetic field **B**, drift velocity is given by

$$\mathbf{v}_g = \frac{m\,\mathbf{g} \times \mathbf{B}}{Q\,\mathbf{B}^2}, \tag{1.113}$$

which is perpendicular to both the gravitational and magnetic fields. Its direction depends on the particle's charge, being opposite for electrons and ions. Since the force magnitude depends on the particle mass, this drift can act as a source of electric currents. It leads to charge separation, which subsequently induces a secondary **E**×**B** drift.

Grad |B| Drift

This drift is caused by spatial variations in the magnitude of the magnetic field. The corresponding drift velocity is given by

$$\mathbf{v}_{\nabla B} = \frac{-\mu \nabla B \times \mathbf{B}}{QB^2} = \frac{m v_\perp^2}{2Q} \frac{\mathbf{B} \times \nabla B}{B^3} \ . \tag{1.114}$$

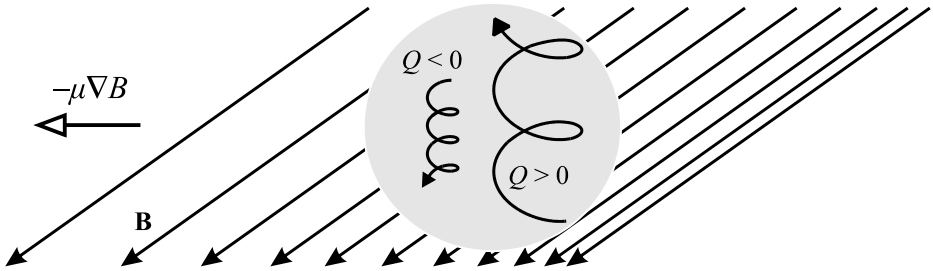


Fig. 1.13: Gradient *B* drift.

The gradient *B* drift depends on particles' *perpendicular velocity*, mass, and charge. It drives electrons and ions in opposite directions, generating an electric current in the plasma. This drift subsequently causes charge separation and a secondary **E**×**B** drift.

Curvature Drift

During motion along a curved field line, a centrifugal force acts on the particle:

$$\mathbf{F} = -m\ddot{\mathbf{R}} = \frac{m v_\parallel^2}{R_\mathrm{k}} \frac{\mathbf{R}_\mathrm{k}}{R_\mathrm{k}} , \tag{1.115}$$

where $\mathbf{R}_\mathrm{k}$ is the radius of curvature of the field line.

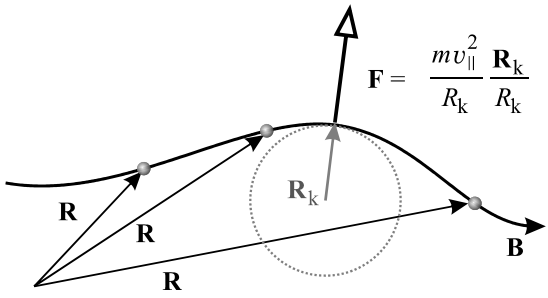


Fig. 1.14: Curvature drift.

The curvature drift velocity is expressed as

$$\mathbf{v}_R = \frac{m v_\parallel^2}{Q B^2} \frac{\mathbf{R}_\mathrm{k} \times \mathbf{B}}{R_\mathrm{k}^2} \ . \tag{1.116}$$

Unlike the gradient B drift, the curvature drift depends on the parallel velocity component. It similarly generates a current in the plasma, leading to charge separation. The radius of curvature for a parametrically defined curve $\mathbf{r} = \mathbf{r}(t)$ can be determined from the relation:

$$\frac{1}{R_\mathrm{k}} = \left\| \mathrm{d}^2\mathbf{r} \big/ \mathrm{d}s^2 \right\|; \qquad \mathrm{d}s = \sqrt{\mathrm{d}x^2 + \mathrm{d}y^2 + \mathrm{d}z^2} = \sqrt{\dot{x}^2 + \dot{y}^2 + \dot{z}^2}\ \mathrm{d}t\ . \quad (1.117)$$

Alternatively, another expression for the radius of curvature may be more suitable for direct substitution into equation (1.116):

$$\frac{1}{R_\mathrm{k}} \frac{\mathbf{R}_\mathrm{k}}{R_\mathrm{k}} = \frac{\mathbf{R}_\mathrm{k}}{R_\mathrm{k}^2} \cong \left(\frac{\mathbf{B}}{B} \cdot \boldsymbol{\nabla} \right) \frac{\mathbf{B}}{B}\,. \quad (1.118)$$

Polarization Drift

If the electric field magnitude varies slowly over time, the guiding center's drift velocity $\mathbf{v}_\mathrm{E}(t)$ changes accordingly. This non-uniform motion induces an inertial drift corresponding to the inertial force

$$-m\ddot{\mathbf{R}} = -m \frac{\mathrm{d}\,\mathbf{v}_\mathrm{E}\,(t)}{\mathrm{d}t} = -m \frac{\mathrm{d}\mathbf{E}/\mathrm{d}t \times \mathbf{B}}{B^2}$$

and results in the polarization drift velocity

► $$\mathbf{v}_\mathrm{P} = \frac{m}{QB^4} \left[\mathbf{B} \times \left(\mathrm{d}\mathbf{E}/\mathrm{d}t \times \mathbf{B} \right) \right]. \quad (1.119)$$

This polarization drift generates a current in the plasma and leads to charge separation, which subsequently triggers a secondary $\mathbf{E}\times\mathbf{B}$ drift. It is thus common for a primary drift to induce subsequent secondary drifts.



1.2.4 Motion in Special Configurations

Magnetic Mirror

If a particle moves through a slowly varying magnetic field, the orientation of its velocity vector relative to the magnetic field lines changes. Let α denote the angle between the particle's velocity and the field lines (the pitch angle):

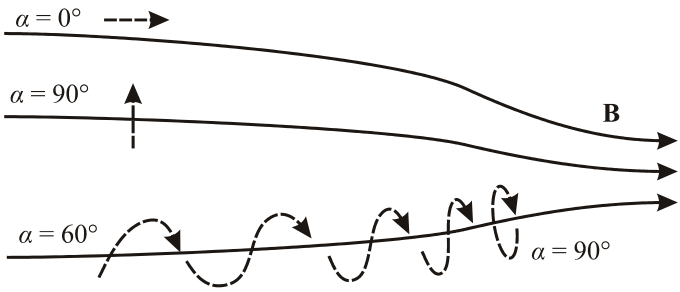


Fig. 1.15: Magnetic mirror.

The parallel and perpendicular velocity components are given by:

$$v_{||} = v\cos\alpha \quad ; \quad v_{\perp} = v\sin\alpha\,. \tag{1.120}$$

From the law of conservation of energy $\mathscr{E}$ and the adiabatic invariant μ

$$\begin{gathered}\mathscr{E} = \frac{1}{2}mv^2 + Q\phi = \frac{1}{2}mv_{\perp}^2 + \frac{1}{2}mv_{||}^2 = \text{const}\,; \\ \mu = \frac{mv_{\perp}^2}{2B} = \text{const}\end{gathered} \tag{1.121}$$

the so-called mirror equation is derived:

► $$\frac{\sin^2\alpha}{B} = \text{const} \quad ; \quad \text{i.e.} \quad \frac{\sin^2\alpha}{B} = \frac{\sin^2\alpha_0}{B_0}\,. \tag{1.122}$$

The subscript 0 denotes initial values of the field and the pitch angle. As the particle enters a stronger magnetic field, its pitch angle increases, making the gyration plane more perpendicular to the field lines. pitch angle reaches $\alpha = 90°$, the particle is reflected. From (1.122), it follows that a particle starting with an initial pitch angle α_0 at a point with a field B_0 is reversed if the magnetic field increases to a critical value:

$$B_c = \frac{B_0}{\sin^2\alpha_0}\,. \tag{1.123}$$

If the magnetic field does not reach this value, the particle passes through the region of converging field lines. Conversely, if a maximum field B_{max} is specified, particles entering from a region with field B_0 is specified, particles entering from a region with field

B_0 will pass through the mirror without reflection if their initial pitch angle satisfies the following condition (placing them inside the so-called loss cone):

$$\alpha < \alpha_c ; \qquad \sin^2 \alpha_c = \frac{B_0}{B_{\max}} . \tag{1.124}$$

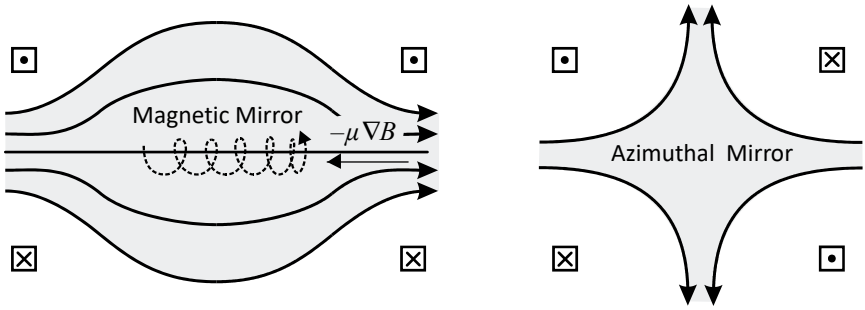


Fig. 1.16: Magnetic mirrors formed by coils (left) and a cusp configuration (right).

The simplest magnetic mirror is created using two coaxially aligned coils with identical current orientations, as shown in the figure on the left. Reversing the current direction in one of the coils creates a so-called cusp configuration (figure on the right). In a cusp field, $B = |\mathbf{B}| = 0$ at the exact center, meaning the Larmor radius becomes infinite, the cyclotron frequency drops to zero, and the spatial field variations are no longer small compared to the Larmor scale. Consequently, the adiabatic invariant μ is not conserved, allowing particles that pass through the central region to easily enter the loss cone. Particle motion within a cusp configuration cannot be resolved using the adiabatic approximation; instead, the full Lorentz equation of motion must be applied.

Second Adiabatic Invariant and Fermi Mechanism

Consider a particle trapped between two magnetic mirrors, a scenario typical for dipole fields (such as Earth's Van Allen belts) or tokamaks (banana orbits).

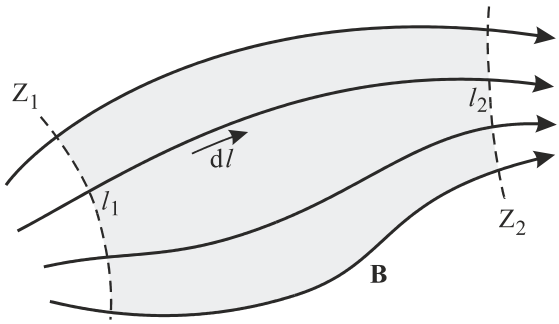


Fig. 1.17: Second adiabatic invariant. Particles move within the gray region.

The particle undergoes two distinct periodic motions:

1) Larmor gyration, associated with the first adiabatic invariant μ.
2) Bouncing back and forth between the two mirrors (longitudinal oscillation).

Assume that the magnetic field varies slowly over time compared to the period of oscillation between the mirrors. Such variations naturally shift the mirror positions Z_1 and Z_2. Under these conditions, the so-called *second adiabatic invariant*,

$$I_2 \equiv \oint v_{\parallel} \, \mathrm{d}l \,, \tag{1.125}$$

is conserved.

First-Order Fermi Acceleration
Consider a strengthening magnetic field with two slowly approaching mirrors. Assuming the region of field variation is small compared to the distance between them, the second adiabatic invariant can be approximately written as:

► $$2L \, v_{\parallel} \approx \text{const} \,, \tag{1.126}$$

where L is the distance between the mirrors. As the distance L decreases, the parallel component of the velocity must increase, thereby raising the total kinetic energy of the particle. Upon reflection, the particle absorbs energy from the oncoming mirror and accelerates. This process is known as *first-order Fermi acceleration*. If a mirror moves toward the particle at a speed v_Z, the particle's parallel velocity after reflection becomes $v_{\parallel} + 2v_Z$.

Second-Order Fermi Acceleration
Consider charged particles moving through randomly varying magnetic fields and reflecting off moving magnetic mirrors moving in random directions. Through this Fermi mechanism, they statistically accelerate or decelerate. This process broadens the velocity distribution, allowing a fraction of fast particles to gain significant energy from energetically favorable reflections. Enrico Fermi utilized this *second-order Fermi acceleration* mechanism to explain the origin of high-energy cosmic rays.

Magnetic Dipole and Third Adiabatic Invariant

A magnetic dipole represents the lowest-order multipole expansion of a magnetic field. Its source can be, for example, a current flowing along a small circular loop. The magnitude of the dipole is determined by the magnetic dipole moment $\mathbf{p}_\mathrm{M}$. For a system of charged particles, the magnetic moment is given by the relation (see [2]):

$$\mathbf{p}_\mathrm{M} = \sum_a \frac{1}{2} Q_a \left(\mathbf{r}_a \times \mathbf{v}_a \right) . \tag{1.127}$$

The sum is performed over all particles within the system. For a single particle moving in a circular orbit, the magnetic moment corresponds to the first adiabatic invariant of the particle; according to (1.102), the following holds

$$\mathbf{p}_\mathrm{M} = \left| \frac{1}{2} Q \left(\mathbf{r} \times \mathbf{v} \right) \right| = \frac{m v_\perp^2}{2B} = IS \,, \tag{1.128}$$

where I is the electric current flowing along the circumference of a loop with area S, induced by the motion of the charged particle. The volume density of the magnetic moment is termed magnetization and is defined as:

$$\mathbf{M} \equiv \lim_{\Delta V \to 0} \frac{1}{\Delta V} \sum_a \frac{1}{2} Q_a \left(\mathbf{r}_a \times \mathbf{v}_a \right). \tag{1.129}$$

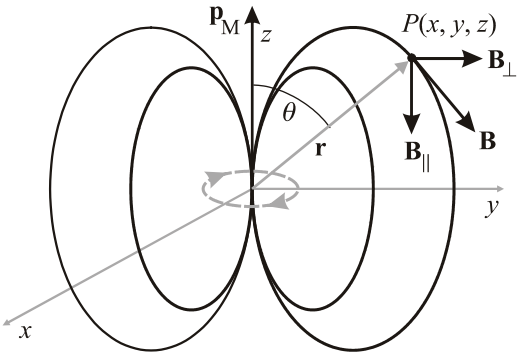


Fig. 1.18: Magnetic dipole. The current loop generating the dipole field is shown as a dashed line.

The vector potential can be determined from the magnetic moment (see [2], chapter *Electromagnetic Field*), yielding the magnetic field::

$$\mathbf{A} = \frac{\mu_0}{4\pi} \frac{\mathbf{p}_\mathrm{M} \times \mathbf{r}}{r^3}, \tag{1.130}$$

$$\mathbf{B} = \nabla \times \mathbf{A} = \frac{\mu_0}{4\pi} \frac{3(\mathbf{p}_\mathrm{M} \cdot \mathbf{r})\mathbf{r} - r^2 \mathbf{p}_\mathrm{M}}{r^5}. \tag{1.131}$$

For a magnetic dipole moment oriented along the z-axis, the components are:

$$\mathbf{B} = \frac{\mu_0}{4\pi} p_\mathrm{M} \left(\frac{3zx}{r^5}, \frac{3zy}{r^5}, \frac{3z^2}{r^5} - \frac{1}{r^3} \right), \tag{1.132}$$

$$\mathbf{B} = (B_\perp, B_\parallel) = \frac{\mu_0}{4\pi r^3} p_\mathrm{M} \left(3\cos\theta \sin\theta,\ 3\cos^2\theta - 1 \right). \tag{1.133}$$

These explicit formulas enable the analysis of charged particle motion, for example, through numerical simulations. Given the particle's initial pitch angle and position, the mirror equation determines the critical field strength required for reflection along a given field line. If the dipole field remains stationary between reflections, both the first and second adiabatic invariants are conserved. Due to curvature drift, the particle also moves azimuthally around the dipole, performing three distinct quasi-periodic motions: 1) Larmor gyration, 2) bounce oscillation between mirrors, and 3) azimuthal curvature drift. This third motion is associated with the *third adiabatic invariant*, which is proportional to the magnetic flux through the surface bounded by the guiding center's trajectory.

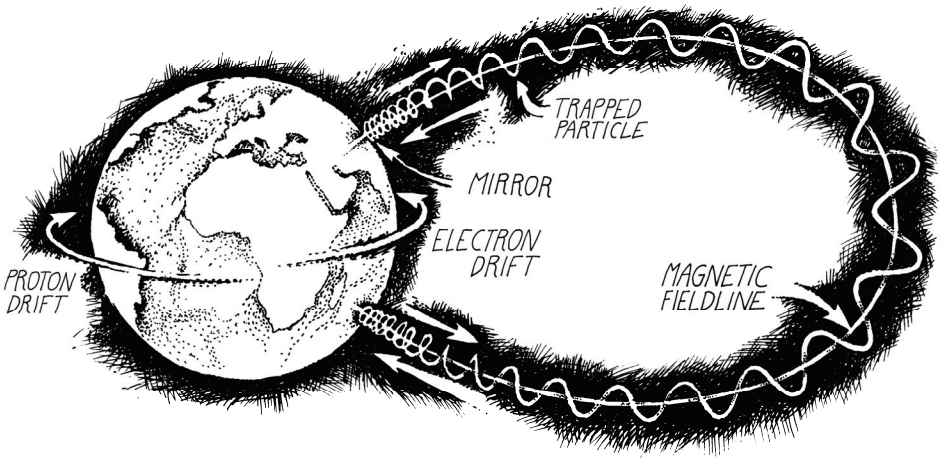


Fig. 1.19: Quasi-periodic motions of a charged particle in a magnetic dipole field.

In the Earth's dipole field, typical periods for these individual processes (for a particle energy of 1 keV on a field line at an equatorial distance of four Earth radii), see [12]:

Particle	1 – gyration	2 – between mirrors	3 – drift
Electron 1 keV	10^{-4} s	4 s	180 h
Proton 1 keV	0.14 s	170 s	180 h

The drift velocity of electrons and ions is identical; this constitutes a curvature drift, the value of which depends on the parallel component of the particle's kinetic energy.

Note: Since a dipole field decreases with the cube of the distance, the dipole moment of celestial bodies is often expressed as the product of the equatorial field strength and the cube of the radius, with the unit Tm^3. This quantity is proportional to the actual dipole moment (1.127).

Most Solar System planets possess a magnetic moment, except Mars and Venus. On Mars, the *Mars Global Surveyor* spacecraft localized crustal magnetic fields indicating that the planet once had a global magnetic field but subsequently lost it. On Venus, the surface temperature reaches approximately 460 °C, exceeding the Curie temperature at which magnetic signatures in rocks are erased. Consequently, it is impossible to determine Venus's past magnetic field using paleomagnetic methods.

Planet magnetospheres are characteristically deformed by the solar wind: a *bow shock* forms on the day side, while a long *magnetotail* develops on the night side. Near the planet, the field retains an approximately dipolar character. In the polar regions, *polar cusps* – funnel-shaped structures – allow charged particles from the solar wind to enter the upper atmosphere. The trapped charged particles form *radiation belts*, where orbiting particles emit electromagnetic radiation (referred to as the *Van Allen radiation belts* on Earth). Mercury's magnetosphere is particularly valuable for studying the inter-

action between the solar wind and planetary magnetic fields; the solar wind is strongest at Mercury's orbit, and the interaction is minimally affected by an atmosphere, which is extremely thin.

The gas and ice giants (Jupiter, Saturn, Uranus, and Neptune) possess the most extensive *magnetospheres*. Lacking a solid surface, their conductive liquid interiors generate exceptionally strong magnetic fields. Jupiter's magnetosphere is unique, featuring a tail that extends up to 5 astronomical units, thereby reaching the orbit of Saturn. Its total volume is many times greater than that of the Sun and its corona combined. Jupiter also features intense radiation belts whose decametric and kilometric radio emissions serve as a standard reference source for calibrating spacecraft instruments.

Planet	Dipole moment ($T\ m^3$)	Equator field (μT)	Dipole offset (% radius)	Dipole-tilt angle (°)
Mercury	5×10^{12}	0.33	17	169
Venus	–	–	–	–
Earth	8×10^{15}	31	7.25	11.4
Mars	–	Remanent	–	–
Jupiter	160×10^{18}	430	13	9.6
Saturn	5×10^{18}	21	5	<1
Uranus	0.4×10^{18}	23	30	59
Neptune	0.2×10^{18}	14	55	47

Electric and Magnetic Monopole

Although magnetic monopoles have not been experimentally observed, it is instructive to theoretically analyze particle motion in the combined fields of electric and magnetic monopoles, given by the relations:

$$\mathbf{E} = \frac{Q_\mathrm{E}}{4\pi\varepsilon_0}\frac{\mathbf{r}}{r^3}; \qquad \mathbf{B} = Q_\mathrm{M}\frac{\mathbf{r}}{r^3}. \tag{1.134}$$

It is straightforward to demonstrate that during the motion of a test particle with charge q, the standard angular momentum is not conserved, whereas the modified vector

$$\mathbf{N} \equiv \mathbf{r}\times m\mathbf{v} - qQ_\mathrm{M}\frac{\mathbf{r}}{r} \tag{1.135}$$

remains an invariant of the motion. The proof of this statement is as follows:

$$\frac{\mathrm{d}\mathbf{N}}{\mathrm{d}t} = \frac{\mathrm{d}}{\mathrm{d}t}\left(\mathbf{r}\times m\mathbf{v} - qQ_\mathrm{M}\frac{\mathbf{r}}{r}\right) = \mathbf{v}\times m\mathbf{v} + \mathbf{r}\times\mathbf{F} - qQ_\mathrm{M}\frac{r\mathbf{v} - (\mathbf{r}\cdot\mathbf{v})\dfrac{\mathbf{r}}{r}}{r^2} =$$

$$= 0 + \mathbf{r}\times\left(q\mathbf{E} + q\mathbf{v}\times\mathbf{B}\right) - qQ_\mathrm{M}\frac{\mathbf{v}}{r} + qQ_\mathrm{M}\frac{(\mathbf{r}\cdot\mathbf{v})\mathbf{r}}{r^3} =$$

$$= q\mathbf{r}\times\left(\frac{Q_\mathrm{E}}{4\pi\varepsilon_0}\frac{\mathbf{r}}{r^3}+\mathbf{v}\times Q_\mathrm{M}\frac{\mathbf{r}}{r^3}\right)-qQ_\mathrm{M}\frac{\mathbf{v}}{r}+qQ_\mathrm{M}\frac{(\mathbf{r}\cdot\mathbf{v})\mathbf{r}}{r^3}=$$

$$= 0+\frac{qQ_\mathrm{M}}{r^3}\mathbf{r}\times(\mathbf{v}\times\mathbf{r})-qQ_\mathrm{M}\frac{\mathbf{v}}{r}+qQ_\mathrm{M}\frac{(\mathbf{r}\cdot\mathbf{v})\mathbf{r}}{r^3}=0\,.$$

The vector **N** is conserved during the motion, which is confined to a conical surface around the **N** axis. The increasing magnetic field near the origin reflects the charge via the $-\mu\nabla B$ force at a minimum distance r_min. For like signs of q and Q_E, the particle is repelled, resulting in unbound motion with $r \in (r_\mathrm{min}, \infty)$. For opposite signs, the motion is bound within $r \in (r_\mathrm{min}, r_\mathrm{max})$, where the turning point r_max follows from energy conservation.

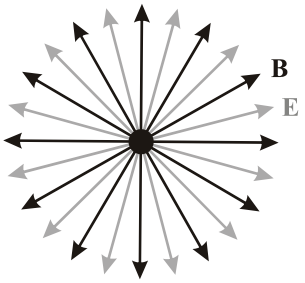


Fig. 1.20: Electric and magnetic monopole configuration.

Tokamaks

In a tokamak (an acronym from the Russian *TOroidnaya KAmera v MAgnitnykh Katushkakh*), the plasma filament is confined within a *toroidal* geometry. The primary toroidal magnetic field lines follow the filament and are generated by external coils wound around the shell of the torus. The tokamak configuration was originally proposed in the 1950s in the Soviet Union by Igor Tamm and Andrei Sakharov. However, a purely toroidal magnetic field induces drifts that inevitably lead to particle escape.

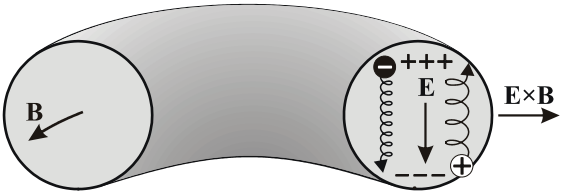


Fig. 1.21: Particle drifts in a purely toroidal geometry.

Within a toroidal geometry, the curvature and gradient drifts cause charge separation, which induces a vertical electric field and subsequently triggers a rapid **E**×**B** drift that forces particles outward. This loss mechanism can be mitigated by twisting the magnetic field lines, thereby introducing an additional poloidal field component. Particle transport along these helical field lines connects the regions of positive and negative charge, effectively neutralizing the charge separation. This essential poloidal field can be generated through several distinct methods, such as:

1) *Stellarator*: The poloidal field is generated externally by helical coils wound around the vacuum vessel.
2) *Tokamak*: The plasma torus acts as a transformer secondary. An induced longitudinal current flows through the plasma, generating the poloidal field.

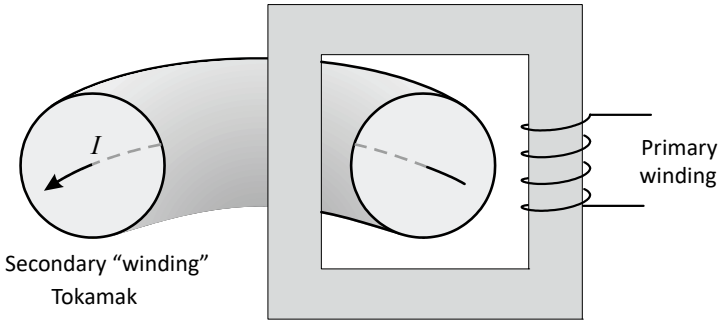


Fig. 1.22: Schematic diagram of a tokamak configuration.

3) *Multipoles*: External conductors placed within or around the confinement region generate the poloidal field configuration.

Approximate analytical expressions for fields in toroidal geometry enable estimating particle motion and calculating trajectories numerically. Realistic field configurations are typically computed using simulation codes.

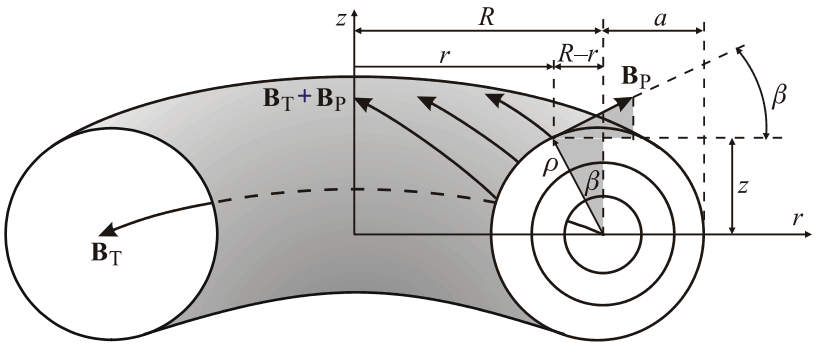


Fig. 1.23: Magnetic field structure inside a tokamak.

According to Ampère law, the toroidal magnetic field strength decreases as $1/r$:

$$B_{\mathrm{T}}(r) = B_{\mathrm{T0}}\frac{R}{r}; \qquad B_{\mathrm{T0}} \equiv B_{\mathrm{T}}(R). \tag{1.136}$$

The poloidal field varies across each magnetic surface of minor radius ρ (see figure) and decreases with the major radius like the toroidal field:

$$B_{\mathrm{P}}(\rho, r) = B_{\mathrm{P0}}(\rho)\frac{R}{r}; \qquad B_{\mathrm{P0}}(\rho) \equiv B_{\mathrm{P}}(\rho, R). \tag{1.137}$$

The radial and vertical (z-axis) projections of the poloidal field can be determined by utilizing the geometric similarity of the triangles highlighted on the right of the figure:

$$B_{\mathrm{P}\,r}(\rho,r) = B_{\mathrm{P}} \cos\beta = B_{\mathrm{P0}}(\rho)\,\frac{R}{r}\,\frac{z}{\rho}, \tag{1.138}$$

$$B_{\mathrm{P}\,z}(\rho,r) = B_{\mathrm{P}} \sin\beta = B_{\mathrm{P0}}(\rho)\,\frac{R}{r}\,\frac{R-r}{\rho}. \tag{1.139}$$

It follows that

$$B_{\mathrm{P}}^2 = B_{\mathrm{P}r}^2 + B_{\mathrm{P}z}^2\ ; \qquad \rho^2 = (R-r)^2 + z^2\ . \tag{1.140}$$

Assume a particle is introduced at an angle α_0 at the outer edge of the magnetic surface, where the total magnetic field strength reaches its minimum across the entire surface:

$$B_{\min} = \sqrt{B_{\mathrm{T0}}^2 + B_{\mathrm{P0}}^2(\rho)}\ \frac{R}{R+\rho}\,. \tag{1.141}$$

The particle follows the field line toward smaller r values, where the field strength increases. Reflection occurs according to the mirror equation at a critical field (1.123):

$$B_{\mathrm{c}} = \frac{B_{\min}}{\sin^2\alpha_0}\,. \tag{1.142}$$

Reflection occurs only if the critical field is smaller than the maximum field at the inner edge, i.e., the particle encounters a magnetic mirror strong enough to reverse its motion:

$$B_{\mathrm{c}} < B_{\max} = \sqrt{B_{\mathrm{T0}}^2 + B_{\mathrm{P0}}^2(\rho)}\ \frac{R}{R-\rho}\,. \tag{1.143}$$

Combining the last three equations yields the necessary condition for particle reflection:

$$\sin^2\alpha_0 > \frac{R-\rho}{R+\rho}\ . \tag{1.144}$$

If this condition is not met, the particle continues along the helical field line. If met, the particle reflects at a turning point. Due to drifts, a characteristic *banana orbit* forms in the poloidal cross-section, named after the shape of the guiding center's trajectory.

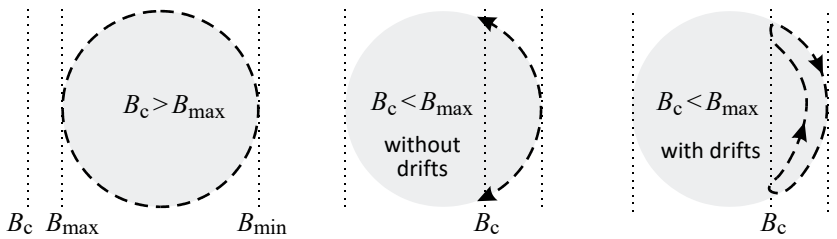


Fig. 1.24: Formation of a banana orbit in a tokamak cross-section.

In addition, tokamaks utilize a vertical magnetic field generated by external coils. This field induces an inward radial force toward the major axis, preventing the plasma torus from expanding due to internal pressure.

The tokamak plasma is not perfectly isolated from the wall, whose inner surface must withstand extreme heat fluxes. This flux is directed toward a chamber region covered with heat-resistant materials (tungsten, graphite) for cooling. In older designs, a material *limiter* at the chamber bottom served as the contact point, introducing impurities and preventing product removal. Since the 1980s, a contactless *divertor* has been implemented instead. Divertor coils generate a magnetic field that creates an X-point at the bottom of the plasma's outer magnetic surface, guiding escaping plasma to cooled plates outside the active region.

The primary heating of tokamak plasma is provided by the induced longitudinal plasma current. In most modern tokamaks, auxiliary plasma heating systems are also deployed, utilizing either neutral beam injection (NBI) or electromagnetic radiation tuned to suitable resonant frequencies, such as cyclotron heating or lower hybrid heating (LHH). Experiments have demonstrated that when the auxiliary heating power exceeds a certain threshold, plasma turbulence drops significantly, and particle confinement improves substantially. This operational regime is referred to as the *High-confinement mode* (H-mode). This phenomenon was first observed on the ASDEX tokamak in 1982, and today, the vast majority of large tokamaks operate routinely in the H-mode.

The following table compares the large tokamaks WEST and JET with the giant international experimental reactor ITER and the Czech tokamak COMPASS. Tore Supra was constructed at the Cadarache center in France, generating its first plasma in 1988 and achieving a record 6.5-minute plasma sustainment in 2003. Following an extensive upgrade between 2010 and 2016, it operates under the name WEST (*W Environment in Steady-state Tokamak*). The JET (*Joint European Torus*) tokamak in Culham, England, operated from 1983 until its final shutdown in December 2023, setting a final world fusion energy record of 69 MJ. Initially managed by the JET Joint Undertaking until 1999, its operation was subsequently overseen by the UKAEA. The Czech tokamak COMPASS ceased operations in 2021 to clear the way for the new COMPASS-U device. Finally, the international ITER reactor, designed to produce 500 MW of fusion power, is under construction in Cadarache, France, with its first plasma phase now officially rescheduled for 2034.

COMPASS-U, under construction at the Institute of Plasma Physics of the Czech Academy of Sciences (IPP CAS), will feature a major radius of 0.894 m, a magnetic field of up to 5 T, and a 2 MA plasma current. Experimental operation is scheduled for approximately 2027. The original COMPASS-D tokamak was relocated to Prague in 2006 from Culham, England, where it had been replaced by the larger MAST tokamak. In terms of plasma geometry, COMPASS-D was similar to the proposed ITER configuration; both vacuum vessels featured a cross-section resembling the letter D. However, COMPASS-D was not the first Czech tokamak. It succeeded the small CASTOR (*Czech Academy of Sciences TORus*) tokamak, which was originally built at the Kurchatov Institute in the USSR in 1958. From 1977, it was located in Prague and served the scientific and educational goals of the IPP CAS. In 1983, it underwent a major reconstruction and received a new vacuum chamber, with operations eventually terminating in 2006. The CASTOR tokamak had a major radius of 0.4 m and a maximum magnetic field of 1.5 T. Following its decommissioning, it was transported to the Faculty of Nuclear Sciences and Physical Engineering at the Czech Technical University in Prague, where it was recommissioned in 2009 for educational purposes under the name Golem.

Tokamak	WEST	JET	ITER	Compass D
Major radius (m)	2.5	3	6.2	0.56
Minor radius (m)	0.5	1.25	2.0	0.23
Plasma volume (m^3)	25	155	837	0.5
Plasma current (MA)	1.7	5÷7	15	0.4
Electron temperature (eV)	5 000	3 000	8 800	500
Electron density (m^{-3})	3.5×10^{19}	4×10^{19}	10^{20}	10^{19}
Magnetic field (T)	3.7	3.4	5.3	1.15
Confinement time (s)	~ 400	10	> 300	2
Thermonuclear power	~ 1 kW	16 MW	500 MW	–

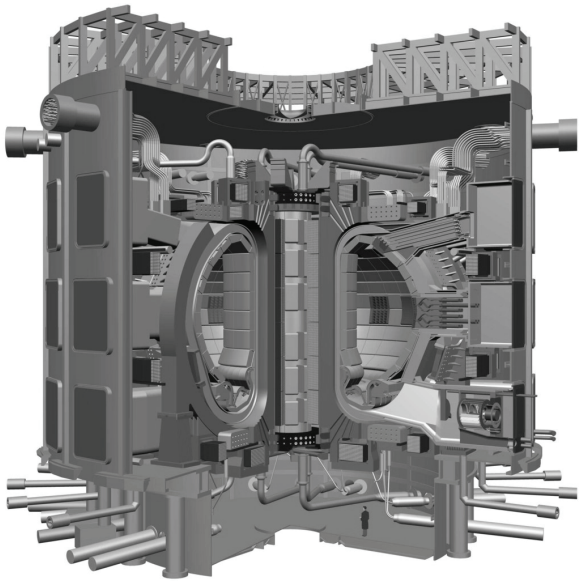


Fig. 1.25: Schematic diagram of the ITER tokamak featuring a D-shaped vacuum chamber.

Note: Fusion research is not limited to tokamaks; numerous alternate configurations explore inertial confinement fusion (laser-initiated fusion) and other innovative concepts. The primary objective is to satisfy the Lawson criterion, ensuring that the generated fusion power exceeds the sum of plasma heating requirements and radiation losses. Physicist John Lawson demonstrated that the product of electron density and energy confinement time must exceed a temperature-dependent function: $n_e\tau > f(T)$. Evaluating the minimum of this function for the deuterium–tritium (D-T) reaction at an optimal temperature of 25 keV (290×10^6 K) yields a minimum required value of $n_e\tau = 1.5\times10^{20}$ s/m^3.

Drifts and Currents in Plasma Filaments

In gravitational interactions, a sphere is the typical equilibrium configuration, as seen in stars and massive planets. Electromagnetic interactions, however, primarily generate linear plasma structures – filaments often twisted into helices or more complex geometries. These are sustained by self-generated magnetic fields. Later chapters demonstrate that only helical filaments, possessing both azimuthal and axial magnetic components, achieve macroscopically stable configurations.

Consider the simplest case of an equilibrium plasma filament carrying an axial electric current, as illustrated in the figure. The associated magnetic field is strictly azimuthal, with its only non-zero component being B_φ. Inside the filament, the magnetic field strength increases with radial distance from the center, a direct consequence of Ampère law: a larger contours encloses a greater cross-sectional area and thus encompasses a larger total enclosed current. Outside the filament, the magnetic field decreases inversely with radius $1/r$.

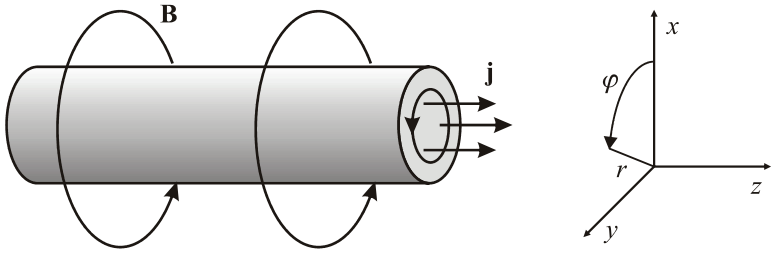


Fig. 1.26: Plasma filament carrying a purely axial current (*z*-pinch configuration).

The motion of charged particles outside the filament is straightforward, consisting of curvature drift and gradient B drift, both acting along the z-axis. This results in net particle drift along the length of the filament. Inside the filament, the analysis focuses on particle dynamics. The curl of the magnetic field $\mathbf{B}$ is given by:

$$\nabla\times\mathbf{B} = \mu_0\,\nabla\times(\mathbf{H}+\mathbf{M}) = \mu_0\left(\mathbf{j}_\mathrm{C} + \frac{\partial\mathbf{D}}{\partial t} + \mathbf{j}_\mathrm{M}\right). \tag{1.145}$$

The total current flowing through the filament is represented in the parentheses. The first term corresponds to the conduction current, which comprises the curvature drift and gradient B drift of the particles inside the filament. The second term vanishes in this static equilibrium case (under time-varying conditions, it would correspond to the polarization drift). The final term represents the magnetization current density $\mathbf{j}_\mathrm{M} = \nabla\times\mathbf{M}$, which arises from the Larmor gyration of particles that is not perfectly compensated by neighboring particle orbits. The relations for the individual current densities inside the filament can now be explicitly derived.

Gradient *B* current Density

The mean current density is expressed using the particle number density and the average velocity of the charge carriers as:

$$\mathbf{j}_{\nabla B} = \left\langle \sum_\alpha Q_\alpha n_\alpha \mathbf{v}_\alpha \right\rangle.$$

The sum is performed over electrons and ions, and the angle brackets denote velocity averaging. Substituting the drift velocity from equation (1.114) and utilizing the cylindrical symmetry of the current filament yields:

$$\mathbf{j}_{\nabla B} = -\frac{1}{B^2}\left\langle n_\mathrm{e}\frac{m_\mathrm{e}\,v_{\mathrm{e}\perp}^2}{2} + n_\mathrm{i}\frac{m_\mathrm{i}\,v_{\mathrm{i}\perp}^2}{2}\right\rangle \frac{\partial B}{\partial r}\,\mathbf{e}_z\,.$$

Since the magnetic field inside the filament increases with radial distance r, the derivative satisfies $\partial B/\partial r > 0$. The geometry of the problem dictates that the gradient B drift points in the negative z-direction. Averaging the perpendicular component of the kinetic energy, which possesses two degrees of freedom, yields:

$$\left\langle \frac{m v_\perp^2}{2}\right\rangle = 2\cdot\frac{1}{2}k_\mathrm{B}T = k_\mathrm{B}T$$

and thus:

$$\mathbf{j}_{\nabla B} = -\frac{1}{B^2}\left(n_\mathrm{e}k_\mathrm{B}T_\mathrm{e} + n_\mathrm{i}k_\mathrm{B}T_\mathrm{i}\right)\frac{\partial B}{\partial r}\,\mathbf{e}_z \;=\; -\frac{p}{B^2}\frac{\partial B}{\partial r}\,\mathbf{e}_z\,. \tag{1.146}$$

Curvature Drift Current Density

Analogous to the gradient B case, the current density arising from the curvature drift (1.116) is determined by:

$$\mathbf{j}_\mathrm{R} = \frac{1}{rB}\left\langle n_\mathrm{e}m_\mathrm{e}\,v_{\mathrm{e}\|}^2 + n_\mathrm{i}m_\mathrm{i}\,v_{\mathrm{i}\|}^2\right\rangle \mathbf{e}_z.$$

Evaluating the average value of the parallel kinetic energy component (where the particle possesses one degree of freedom along the magnetic field line) gives:

$$\left\langle \frac{m v_\|^2}{2}\right\rangle = 1\cdot\frac{1}{2}k_\mathrm{B}T = \frac{1}{2}k_\mathrm{B}T\,,$$

which leads to the final relation for the curvature drift current density:

$$\mathbf{j}_\mathrm{R} = \frac{1}{rB}\left(n_\mathrm{e}k_\mathrm{B}T_\mathrm{e} + n_\mathrm{i}k_\mathrm{B}T_\mathrm{i}\right)\mathbf{e}_z \;=\; \frac{p}{rB}\,\mathbf{e}_z\;. \tag{1.147}$$

Magnetization Current Density

In a homogeneous plasma with a constant magnetic field, the net current contribution from the system of gyrating particles vanishes. However, if the magnetic field is inhomogeneous, the Larmor orbits vary spatially, and the average contribution to the current can be non-zero. Similarly, in a non-homogeneous plasma, the particle number density increases in a particular direction, and velocity averaging yields a non-zero net current. The magnetic moment of a single particle is given by:

$$\boldsymbol{\mu} = \frac{m v_\perp^2}{2B}\,\mathbf{e}_\varphi\,. \tag{1.148}$$

Note: A gyrating charged particle generates a self-magnetic field that is antiparallel to the background magnetic field. This property is referred to as plasma diamagnetism. In the coordinate system illustrated in the figure 1.26, the background magnetic field points along $-\mathbf{e}_\varphi$, whereas the particle's magnetic moment points along $+\mathbf{e}_\varphi$.

The total magnetization is determined by averaging over the velocity distribution:

$$\mathbf{M} = \left\langle \sum_\alpha n_\alpha \boldsymbol{\mu}_\alpha \right\rangle = \frac{\left\langle n_\mathrm{e} m_\mathrm{e} v_{\mathrm{e}\perp}^2 + n_\mathrm{i} m_\mathrm{i} v_{\mathrm{i}\perp}^2 \right\rangle}{2B} \mathbf{e}_\varphi = \frac{\left(n_\mathrm{e} k_\mathrm{B} T_\mathrm{e} + n_\mathrm{i} k_\mathrm{B} T_\mathrm{i} \right)}{B} \mathbf{e}_\varphi = \frac{p}{B} \mathbf{e}_\varphi .$$

The magnetization current density in this geometry is evaluated as:

$$\mathbf{j}_\mathrm{M} = \boldsymbol{\nabla} \times \mathbf{M} = -\frac{1}{r} \frac{\partial}{\partial r} \left(r \frac{p}{B} \right) \mathbf{e}_z . \tag{1.149}$$

Finally, it can be demonstrated that the sum of the three derived current densities yields the total current flowing through the plasma:

$$j_{\nabla B} + j_\mathrm{R} + j_\mathrm{M} = -\frac{p}{B^2} \frac{\partial B}{\partial r} + \frac{p}{rB} - \frac{1}{r} \frac{\partial}{\partial r} \left(r \frac{p}{B} \right) = -\frac{1}{B} \frac{\partial p}{\partial r} .$$

It follows that:

$$\left(j_{\nabla B} + j_\mathrm{R} + j_\mathrm{M} \right) B = -\frac{\partial p}{\partial r} , \tag{1.150}$$

which represents the fundamental macroscopic magnetohydrodynamic fluid equilibrium condition $\mathbf{j} \times \mathbf{B} = -\boldsymbol{\nabla} p$, where the total current density appears. Microscopic particle drifts are thus naturally linked to macroscopic currents within a conductive continuum.

1. 3 Magnetohydrodynamics

1.3.1 Minimal Model

The Swedish physicist Hannes Alfvén first described plasma using continuum theory, receiving the 1970 Nobel Prize in Physics for his pioneering work in magnetohydrodynamics (MHD). The MHD equations generalize standard hydrodynamics to a conductive fluid, or a system of multiple fluids, whose macroscopic behavior is dominantly influenced by a magnetic field. In this framework, the plasma is described by macroscopic quantities varying in time and space, such as mass density $\rho(t, \mathbf{x})$, magnetic field $\mathbf{B}(t, \mathbf{x})$, temperature $T(t, \mathbf{x})$, and the velocity field $\mathbf{u}(t, \mathbf{x})$. The velocity field is deliberately denoted by the symbol $\mathbf{u}$ to avoid confusion with the velocities of individual particles, $\mathbf{v}$. While several alternative sets of initial assumptions exist, this section focuses on the minimal model incorporating the simplest formulations. First, the basic continuum concepts necessary to understand magnetohydrodynamics are introduced.

Basic Concepts

Material Derivative

The total time derivative of a vector field $\mathbf{A}(t, \mathbf{x})$ is given by:

$$\frac{\mathrm{d}}{\mathrm{d}t} A_k(t,\mathbf{x}) = \frac{\partial A_k}{\partial t} + \frac{\partial A_k}{\partial x_l}\frac{\mathrm{d}x_l}{\mathrm{d}t} =$$

$$= \frac{\partial A_k}{\partial t} + u_l \frac{\partial A_k}{\partial x_l} = \frac{\partial A_k}{\partial t} + (\mathbf{u}\cdot\boldsymbol{\nabla}) A_k \,.$$

The total (or material) derivative of a vector field consists of two distinct parts:

$$\frac{\mathrm{d}}{\mathrm{d}t}\mathbf{A} = \frac{\partial \mathbf{A}}{\partial t} + (\mathbf{u}\cdot\boldsymbol{\nabla})\mathbf{A} \,. \tag{1.151}$$

The first part (the local derivative) corresponds to explicit temporal changes in the fields, while the second part (the convective derivative) is related to the fluid flow. The material derivative can be written in operator form as:

► $$\frac{\mathrm{d}}{\mathrm{d}t} = \frac{\partial}{\partial t} + \mathbf{u}\cdot\boldsymbol{\nabla} \,. \tag{1.152}$$

Streamline Equation

The time derivative of a streamline element $\delta\mathbf{l}$ caused by a spatial variation in the velocity field is determined by:

$$\frac{\mathrm{d}\,\delta\mathbf{l}}{\mathrm{d}t} = \delta\mathbf{u} = \mathbf{u}(\mathbf{r}+\delta\mathbf{l}) - \mathbf{u}(\mathbf{r}) = (\delta\mathbf{l}\cdot\boldsymbol{\nabla})\mathbf{u} \,,$$

$$\frac{\mathrm{d}\,\delta\mathbf{l}}{\mathrm{d}t} = (\delta\mathbf{l}\cdot\nabla)\mathbf{u}\,. \tag{1.153}$$

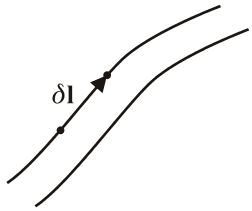


Fig. 1.27: Streamline element within a velocity field.

Fluid Flow and the Continuity Equation

The continuity equation was introduced in *Selected Topics*, *Volume II*, Section II.3.4.2. Since it represents a key concept in magnetohydrodynamics, its derivation is reviewed here. Consider the flux of an extensive (additive) quantity A that scales linearly with the particle number (e.g., mass, charge, energy, momentum). Conversely, intensive quantities are independent of the particle number (e.g., temperature, velocity field, electric field intensity). The flux of an additive quantity is described using four variables, the first being its *volume density*, defined by the relation:

$$\rho_A \equiv \lim_{\Delta V\to 0}\frac{\Delta A}{\Delta V}\,. \tag{1.154}$$

Examples include mass density (kg/m^3), charge density (C/m^3), energy density (J/m^3), power density (W/m^3), or momentum density (kg·m·s^{-1}/m^3); in general, the density of an additive quantity has the dimension

$$[\rho_A] = \frac{[A]}{\mathrm{m}^3}\,. \tag{1.155}$$

The second quantity is a vector; termed the flux density of the quantity A, defined by:

$$\mathbf{j}_A \equiv \rho_A\mathbf{u}\,. \tag{1.156}$$

Like any vector field, the flux density possesses both magnitude and direction. Its direction follows the velocity field describing the fluid flow. The magnitude of the flux density can be determined by observing the flow through a normal surface. Over a time interval dt, particles traverse a distance d$l = u\,$dt toward another imaginary surface.

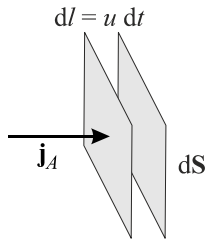


Fig. 1.28: Flux density of an extensive quantity through a surface element.

The following relation applies to the flux magnitude:

$$j_A = \rho_A u = \frac{\mathrm{d}A}{\mathrm{d}V}\frac{\mathrm{d}l}{\mathrm{d}t} = \frac{\mathrm{d}A}{\mathrm{d}S\,\mathrm{d}l}\frac{\mathrm{d}l}{\mathrm{d}t} = \frac{\mathrm{d}A}{\mathrm{d}S\,\mathrm{d}t}. \tag{1.157}$$

The flux density of a quantity is therefore defined as the amount of that quantity passing through a normal unit area per unit time, with the dimension:

$$[j_A] = \frac{[A]}{\mathrm{m}^2\,\mathrm{s}}. \tag{1.158}$$

Examples include energy flux density ($\mathrm{J{\cdot}m^{-2}{\cdot}s^{-1}}$), charge flux density ($\mathrm{C{\cdot}m^{-2}{\cdot}s^{-1}}$), or mass flux density ($\mathrm{kg{\cdot}m^{-2}{\cdot}s^{-1}}$). If the quantity A is neither created nor destroyed during the fluid flow, its rate of decrease within any arbitrary volume must equal the net flux of the quantity out of the enclosing surface:

$$-\frac{\mathrm{d}}{\mathrm{d}t}\int_V \rho_A\,\mathrm{d}V = \int_{\partial V} \mathbf{j}_A \cdot \mathrm{d}\mathbf{S}. \tag{1.159}$$

The boundary of V is denoted by ∂V. Moving the time derivative inside the integral yields a partial derivative, since $\rho_A(t, \mathbf{x})$ depends on space. On the right-hand side, Gauss theorem converts the surface integral into a volume integral:

$$-\int_V \frac{\partial \rho_A}{\partial t}\,\mathrm{d}V = \int_V \operatorname{div}\mathbf{j}_A\,\mathrm{d}V. \tag{1.160}$$

Combining both integrals yields:

$$\int_V \left(\frac{\partial \rho_A}{\partial t} + \operatorname{div}\mathbf{j}_A\right)\mathrm{d}V = 0. \tag{1.161}$$

This relation must hold for any arbitrary volume during the flow, which is possible only if the integrand itself vanishes identically (in principle, it could be non-zero only at isolated points or surfaces, generally on a set of lower dimension than the integration domain):

► $$\frac{\partial \rho_A}{\partial t} + \operatorname{div}\mathbf{j}_A = 0. \tag{1.162}$$

The derived relation is called the *continuity equation*. The right-hand side vanishes if the quantity A is strictly conserved during the flow. If it is not conserved, the right-hand side is non-zero, allowing the continuity equation to be written in the general form:

► $$\frac{\partial \rho_A}{\partial t} + \operatorname{div}\mathbf{j}_A = \mathscr{S} + \mathscr{F}, \tag{1.163}$$

where $\mathscr{S}$ describes collision processes and $\mathscr{F}$ describes the influence of force fields. The separation of temporal and spatial variables is merely formal; the continuity equation can also be expressed compactly as a four-dimensional divergence:

$$\frac{\partial j_0}{\partial x_0} + \frac{\partial j_1}{\partial x_1} + \frac{\partial j_2}{\partial x_2} + \frac{\partial j_3}{\partial x_3} = 0, \tag{1.164}$$

where the following four-vectors are defined:

$$j_0 = \rho_A c\,; \quad j_1 = j_x\,; \quad j_2 = j_y\,; \quad j_3 = j_z\,, \tag{1.165}$$

$$x_0 = ct\,; \quad x_1 = x\,; \quad x_2 = y\,; \quad x_3 = z\,. \tag{1.166}$$

The index A has been omitted for simplicity. The speed of light c in the zero components of the four-vectors ensures that all four components possess identical dimensions. In special relativity, both of these four-vectors transform in the same manner under Lorentz transformations, representing typical four-vectors.

Assumptions of the Minimal Model

1) Plasma as a Continuum

Plasma is collision-dominated, making collisions a significant phenomenon on both spatial and temporal scales. The mean free paths of particles are much shorter than the dimensions L of the plasma under consideration, and the mean collision time for individual particles is much shorter than the time T of observation:

$$\lambda_\mathrm{e}, \lambda_\mathrm{i}, \lambda_\mathrm{n} \ll L\,; \qquad \tau_\mathrm{e}, \tau_\mathrm{i}, \tau_\mathrm{n} \ll T\,. \tag{1.167}$$

2) Quasi-Neutrality of Plasma

Free charge carriers are present in the plasma, but every macroscopic volume contains an equal number of positive and negative charges. The spatial charge density is zero:

$$\rho_Q = 0 \qquad \Rightarrow \qquad \sum Q_\alpha n_\alpha = 0\,, \tag{1.168}$$

where n is the number density (the number of particles per unit volume). In some variants of magnetohydrodynamics, this assumption is not satisfied.

3) Single-Fluid Model

In the first approximation, plasma can be treated as a single fluid. In this model, instead of the velocities of the various individual components, only the center-of-mass velocity $\mathbf{u}$ of all components and the current density $\mathbf{j} = \rho_Q \mathbf{u} = nQ\mathbf{u}$ are utilized, where n is the number density:

► $$\mathbf{u} = \frac{\sum m_\alpha \mathbf{u}_\alpha}{\sum m_\alpha}\,, \tag{1.169}$$

► $$\mathbf{j} = \sum Q_\alpha n_\alpha \mathbf{u}_\alpha\,. \tag{1.170}$$

If the plasma consists solely of electrons and ions, ambipolar diffusion occurs; if the lighter electrons escape from the system, they pull the heavier ions along with them via the Coulomb field. The velocities of the electron and ion components are roughly balanced and equal to the center-of-mass velocity:

$$\mathbf{u}_\mathrm{e} \approx \mathbf{u}_\mathrm{i} \approx \mathbf{u}\,. \tag{1.171}$$

The slight difference in the velocities of electrons and ions determines the current density. For example, for a singly ionized plasma: $n_\mathrm{e} = n_\mathrm{i} = n$, $\mathbf{j} = en(\mathbf{u}_\mathrm{i} - \mathbf{u}_\mathrm{e})$.

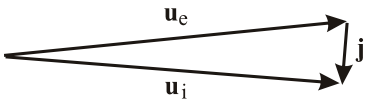


Fig. 1.29: Direction of the current density.

Of course, magnetohydrodynamic descriptions based on multi-fluid models also exist. The Lorentz force density in the single-fluid model is derived as follows:

$$\mathbf{F}_\alpha = Q_\alpha \mathbf{E} + Q_\alpha \mathbf{v}_\alpha \times \mathbf{B} ;$$

$$\mathbf{f}_\alpha = Q_\alpha n_\alpha \mathbf{E} + Q_\alpha n_\alpha \mathbf{u}_\alpha \times \mathbf{B} ;$$

$$\mathbf{f} = \sum (Q_\alpha n_\alpha \mathbf{E} + Q_\alpha n_\alpha \mathbf{u}_\alpha \times \mathbf{B}) = \left(\sum Q_\alpha n_\alpha\right)\mathbf{E} + \left(\sum Q_\alpha n_\alpha \mathbf{u}_\alpha\right)\times \mathbf{B} = \mathbf{j}\times\mathbf{B} .$$

The first term on the right vanishes due to quasi-neutrality. In the continuum limit, the velocity **v** of a single particle becomes the mean flow velocity **u**. In the minimal version of magnetohydrodynamics, the following relation for the force density is therefore used:

► $$\mathbf{f} = \mathbf{j}\times\mathbf{B}. \tag{1.172}$$

4) Non-Relativistic Plasma

The minimal MHD model requires non-relativistic velocities for all particles, i.e.,

$$\frac{u_\alpha}{c} \ll 1 . \tag{1.173}$$

This implies a relatively simple form of Ohm law. In a moving plasma, the electric field **E** must be transformed from the laboratory frame to the field $\tilde{\mathbf{E}}$ in the frame moving with the plasma, where Ohm law $\mathbf{j} = \sigma\,\tilde{\mathbf{E}}$ holds:

$$\mathbf{j} = \sigma\tilde{\mathbf{E}} = \sigma\frac{\mathbf{E} + \mathbf{u}\times\mathbf{B}}{\sqrt{1 - u^2/c^2}} \doteq \sigma(\mathbf{E} + \mathbf{u}\times\mathbf{B}) . \tag{1.174}$$

For the complex relativistic case, see Volume II, section *General Transformation of the Electromagnetic Field*, p. 229.

5) Negligible Displacement Current

In Maxwell equation curl $\mathbf{H} = \mathbf{j} + \partial\mathbf{D}/\partial t$, the displacement current is neglected compared to the current density. This holds only for low-frequency phenomena; specifically, for a time dependence $\exp[\mathrm{i}\omega t]$, the frequency is limited by:

$$\left|\partial\mathbf{D}/\partial t\right| \ll \left|\mathbf{j}\right| \quad \Rightarrow$$

$$\left|\mathrm{i}\,\omega\varepsilon\mathbf{E}\right| \ll \sigma E \quad \Rightarrow$$

► $$\omega \ll \sigma/\varepsilon . \tag{1.175}$$

This condition is satisfied for highly conductive plasmas or low-frequency phenomena. If this condition is violated, time-varying electric fields must also be taken into account.

Equations for Magnetic Field

The time evolution of the magnetic field is determined from Maxwell equations supplemented by Ohm law (1.174) in a moving medium:

$$\begin{aligned} &\nabla\times\mathbf{E} = -\frac{\partial\mathbf{B}}{\partial t}; && \rho_Q = 0; \\ &\nabla\times\mathbf{H} = \mathbf{j}; && \mathbf{j} = \sigma(\mathbf{E}+\mathbf{u}\times\mathbf{B}); \\ &\nabla\cdot\mathbf{B} = 0; && \mathbf{D} = \varepsilon\mathbf{E}; \\ &\nabla\cdot\mathbf{D} = \rho_Q; && \mathbf{H} = \mathbf{B}/\mu. \end{aligned} \tag{1.176}$$

The first equation yields the time derivative of the magnetic field; the electric field is substituted from Ohm law and the current density from the second Maxwell equation:

$$\frac{\partial\mathbf{B}}{\partial t} = -\nabla\times\mathbf{E} = -\nabla\times\left(\frac{\mathbf{j}}{\sigma} - \mathbf{u}\times\mathbf{B}\right) = -\frac{1}{\sigma\mu}\nabla\times(\nabla\times\mathbf{B}) + \nabla\times(\mathbf{u}\times\mathbf{B}).$$

Rewriting the double curl using relation I.3.218 (*Selected Topics*, *Volume I*, Section Mathematics for Physics) yields the resulting equation:

► $$\frac{\partial\mathbf{B}}{\partial t} = \frac{1}{\sigma\mu}\nabla^2\mathbf{B} + \nabla\times(\mathbf{u}\times\mathbf{B}). \tag{1.177}$$

The equation for the $\partial\mathbf{B}/\partial t$ can be rearranged into a form with a material derivative by rewriting the second term using expression I.3.219

$$\frac{\partial\mathbf{B}}{\partial t} = \frac{1}{\sigma\mu}\nabla^2\mathbf{B} + (\mathbf{B}\cdot\nabla)\mathbf{u} - \mathbf{B}\,\mathrm{div}\,\mathbf{u} - (\mathbf{u}\cdot\nabla)\mathbf{B},$$

$$\frac{\partial\mathbf{B}}{\partial t} + (\mathbf{u}\cdot\nabla)\mathbf{B} = \frac{1}{\sigma\mu}\nabla^2\mathbf{B} + (\mathbf{B}\cdot\nabla)\mathbf{u} - \mathbf{B}\,\mathrm{div}\,\mathbf{u}.$$

An alternative equation for the time evolution of the magnetic field is therefore:

$$\frac{\mathrm{d}\mathbf{B}}{\mathrm{d}t} = \frac{1}{\sigma\mu}\nabla^2\mathbf{B} + (\mathbf{B}\cdot\nabla)\mathbf{u} - \mathbf{B}\,\mathrm{div}\,\mathbf{u}. \tag{1.178}$$

According to (1.177), the magnetic field changes in two ways. The first term on the right-hand side represents classical diffusion – the slow penetration of the magnetic field into the plasma. The second term, related to plasma motion, is the frozen-in term. Magnetic field lines follow the plasma fluid. A rough estimation of their ratio (the magnetic Reynolds number) is performed by approximating vectors by their magnitudes and their derivatives by the inverse of the system dimension:

► $$\#_{\mathrm{Re,M}} = \frac{\text{Frozen-in term}}{\text{Diffusion term}} \approx \frac{\frac{1}{L}uB}{\frac{1}{\sigma\mu}\frac{1}{L^2}B} = \sigma\mu\,u\,L. \tag{1.179}$$



Fig. 1.30: Diffusion and a frozen field in plasma.

For an ideal plasma ($\sigma \to \infty$), freezing dominates ($\#_{\mathrm{Re,M}} >> 1$). Conversely, for slow plasma motions, the diffusion dominates ($\#_{\mathrm{Re,M}} << 1$). The limiting cases take the form

$$\begin{aligned} \sigma \to \infty: &\qquad \frac{\partial \mathbf{B}}{\partial t} = \nabla \times (\mathbf{u} \times \mathbf{B}); \\ \mathbf{u} \to 0: &\qquad \frac{\partial \mathbf{B}}{\partial t} = \eta_{\mathrm{M}} \nabla^2 \mathbf{B}; \qquad \eta_{\mathrm{M}} \equiv \frac{1}{\sigma \mu}. \end{aligned} \tag{1.180}$$

Frozen-in Term

Considering only the frozen-in term

$$\frac{\partial \mathbf{B}}{\partial t} = \nabla \times (\mathbf{u} \times \mathbf{B}),$$

the curl on the right is adjusted using the vector triple product – see I.3.219:

$$\frac{\partial \mathbf{B}}{\partial t} = (\mathbf{B} \cdot \nabla)\mathbf{u} - (\mathbf{u} \cdot \nabla)\mathbf{B} - \mathbf{B} \operatorname{div} \mathbf{u}.$$

Substituting div **u** from the continuity equation yields:

$$\frac{\partial \rho}{\partial t} + \operatorname{div} \rho \mathbf{u} = 0 \qquad \Rightarrow \qquad \frac{\partial \rho}{\partial t} + (\mathbf{u} \cdot \nabla)\rho + \rho \operatorname{div} \mathbf{u} = 0 \qquad \Rightarrow$$

$$\Rightarrow \quad \operatorname{div} \mathbf{u} = -\frac{1}{\rho}\frac{\partial \rho}{\partial t} - \frac{1}{\rho}(\mathbf{u} \cdot \nabla)\rho.$$

Elementary manipulations (neglecting the diffusion term) yield:

$$\frac{\partial \mathbf{B}}{\partial t} = (\mathbf{B} \cdot \nabla)\mathbf{u} - (\mathbf{u} \cdot \nabla)\mathbf{B} + \frac{\mathbf{B}}{\rho}\frac{\partial \rho}{\partial t} + \frac{\mathbf{B}}{\rho}(\mathbf{u} \cdot \nabla)\rho.$$

Dividing the entire equation by density and rearranging the individual terms yields:

$$\frac{1}{\rho}\frac{\partial \mathbf{B}}{\partial t} - \frac{\mathbf{B}}{\rho^2}\frac{\partial \rho}{\partial t} = \left(\frac{\mathbf{B}}{\rho} \cdot \nabla\right)\mathbf{u} - \frac{1}{\rho}(\mathbf{u} \cdot \nabla)\mathbf{B} + \frac{\mathbf{B}}{\rho^2}(\mathbf{u} \cdot \nabla)\rho.$$

Combining the first two terms on the left-hand side, as well as the last two terms on the right-hand side, leads to:

$$\frac{\partial}{\partial t}\left(\frac{\mathbf{B}}{\rho}\right) = \left(\frac{\mathbf{B}}{\rho}\cdot\boldsymbol{\nabla}\right)\mathbf{u} - (\mathbf{u}\cdot\boldsymbol{\nabla})\frac{\mathbf{B}}{\rho} .$$

Substituting $\mathbf{b} \equiv \mathbf{B}/\rho$ the equation becomes

$$\frac{\partial \mathbf{b}}{\partial t} + (\mathbf{u}\cdot\boldsymbol{\nabla})\mathbf{b} = (\mathbf{b}\cdot\boldsymbol{\nabla})\mathbf{u} .$$

Introducing the material derivative, the streamline equation (1.153) for $\mathbf{b}$ is obtained

$$\frac{\mathrm{d}\mathbf{b}}{\mathrm{d}t} = (\mathbf{b}\cdot\boldsymbol{\nabla})\mathbf{u} . \tag{1.181}$$

Consequently, the *magnetic field follows the streamlines* and is *frozen into the plasma*. The concept of freezing can also be formulated differently: The magnetic flux through a closed loop moving with the plasma is constant.

Diffusion Term

The second alternative, the diffusion term, is now considered. The coefficient η_M is called the magnetic diffusion coefficient. The diffusion equation can be rewritten as:

$$\hat{\mathcal{L}}\mathbf{B} = 0 ; \qquad \hat{\mathcal{L}} \equiv \frac{\partial}{\partial t} - \eta_\mathrm{M}\boldsymbol{\nabla}^2 . \tag{1.182}$$

The operator $\hat{\mathcal{L}}$ is linear. The solution is sought as a superposition of Fourier modes:

$$\mathbf{B}(t,\mathbf{x}) = \int \mathbf{B}_\mathbf{k}(t,\mathbf{x})\,\mathrm{d}^3\mathbf{k} = \int \mathbf{c}_\mathbf{k}(t)\mathrm{e}^{\mathrm{i}\mathbf{k}\cdot\mathbf{x}}\mathrm{d}^3\mathbf{k} . \tag{1.183}$$

Each of the Fourier modes $\mathbf{B}_\mathbf{k}$ must satisfy the diffusion equation:

$$\hat{\mathcal{L}}\mathbf{B}_\mathbf{k} = 0 ; \qquad \Rightarrow$$

$$\left(\frac{\partial}{\partial t} - \eta_\mathrm{M}\boldsymbol{\nabla}^2\right)\mathbf{c}_\mathbf{k}(t)\mathrm{e}^{\mathrm{i}\mathbf{k}\cdot\mathbf{x}} = 0 \qquad \Rightarrow$$

$$\frac{\mathrm{d}\mathbf{c}_\mathbf{k}}{\mathrm{d}t} + \eta_\mathrm{M}k^2\mathbf{c}_\mathbf{k} = 0 \qquad \Rightarrow$$

$$\mathbf{c}_\mathbf{k}(t) = \mathbf{c}_\mathbf{k}(0)\,\mathrm{e}^{-\eta_\mathrm{M}k^2 t} .$$

The total solution is therefore written in the form:

$$\mathbf{B}(t,\mathbf{x}) = \int \mathbf{c}_\mathbf{k}(0)\,\mathrm{e}^{-\eta_\mathrm{M}k^2 t}\,\mathrm{e}^{\mathrm{i}\mathbf{k}\cdot\mathbf{x}}\,\mathrm{d}^3\mathbf{k} . \tag{1.184}$$

Setting $t = 0$ and performing the inverse transform yields the initial value relation:

$$\mathbf{c}_\mathbf{k}(0) = \frac{1}{(2\pi)^3}\int \mathbf{B}(0,\mathbf{x})\,\mathrm{e}^{-\mathrm{i}\mathbf{k}\cdot\mathbf{x}}\,\mathrm{d}^3\mathbf{x} . \tag{1.185}$$

Relation (1.184) shows that each Fourier component $\exp(\mathrm{i}\mathbf{k}\cdot\mathbf{x})$ decays over time by a factor of $\exp(-\eta_\mathrm{M}k^2 t)$. Thus, small-scale fluctuations (large k) decay much faster than

large-scale fluctuations. This behavior is characteristic of diffusion, where small irregularities vanish first.

The Green function for the diffusion equation in an unbounded domain is found by choosing a Dirac delta distribution localized at the point **x'** as the initial impulse:

$$\mathbf{B}_0(\mathbf{x}) = \mathbf{B}(0,\mathbf{x}) = \boldsymbol{\beta}_0\,\delta(\mathbf{x}-\mathbf{x}')\,; \qquad \boldsymbol{\beta}_0 = (1,1,1).$$

The Green function can be calculated for each magnetic field component separately, as each satisfies the diffusion equation. Substituting the Dirac impulse into (1.185) and (1.184), and denoting the solution by **G** yields:

$$\mathbf{c}_\mathbf{k}(0) = \frac{\boldsymbol{\beta}_0}{(2\pi)^3}\int \delta(\mathbf{x}-\mathbf{x}')\,\mathrm{e}^{-\mathrm{i}\mathbf{k}\cdot\mathbf{x}}\,\mathrm{d}^3\mathbf{x} = \frac{\boldsymbol{\beta}_0}{(2\pi)^3}\mathrm{e}^{-\mathrm{i}\mathbf{k}\cdot\mathbf{x}'} \qquad \Rightarrow$$

$$\mathbf{G}(t,\mathbf{x},\mathbf{x}') = \frac{\boldsymbol{\beta}_0}{(2\pi)^3}\int \mathrm{e}^{-\eta_\mathrm{M}k^2 t}\,\mathrm{e}^{\mathrm{i}\mathbf{k}\cdot(\mathbf{x}-\mathbf{x}')}\,\mathrm{d}^3\mathbf{k}\,; \qquad \boldsymbol{\beta}_0 = (1,1,1)\ . \tag{1.186}$$

This represents the general form of the triplet of Green functions for the diffusion equation across all three coordinate axes. The result of the integration depends on the boundary conditions and the choice of coordinate system. The integration is performed for the simple case of an unbounded domain in the Cartesian coordinate system:

$$\mathbf{G}(t,\mathbf{x},\mathbf{x}') = \frac{\boldsymbol{\beta}_0}{(2\pi)^3}\int\limits_{\mathrm{R}^3} \mathrm{e}^{-\eta_\mathrm{M}k^2 t}\,\mathrm{e}^{\mathrm{i}\mathbf{k}\cdot(\mathbf{x}-\mathbf{x}')}\mathrm{d}^3\mathbf{k} = \qquad /\mathbf{x}-\mathbf{x}' \equiv \mathbf{a}$$

$$= \frac{\boldsymbol{\beta}_0}{(2\pi)^3}\int\limits_{\mathrm{R}^3} \mathrm{e}^{-\eta_\mathrm{M}\mathbf{k}^2 t}\,\mathrm{e}^{\mathrm{i}\mathbf{k}\cdot\mathbf{a}}\,\mathrm{d}^3\mathbf{k} = \frac{\boldsymbol{\beta}_0}{(2\pi)^3}\int\limits_{\mathrm{R}^3} \mathrm{e}^{-\eta_\mathrm{M}\mathbf{k}^2 t+\mathrm{i}\mathbf{k}\cdot\mathbf{a}}\,\mathrm{d}^3\mathbf{k} =$$

$$= \frac{\boldsymbol{\beta}_0}{(2\pi)^3}\int\limits_{\mathrm{R}^3} \exp\left[-\eta_\mathrm{M}t\left(\mathbf{k}^2 - \frac{\mathrm{i}\mathbf{k}\cdot\mathbf{a}}{\eta_\mathrm{M}t}\right)\right]\mathrm{d}^3\mathbf{k} =$$

$$= \frac{\boldsymbol{\beta}_0}{(2\pi)^3}\int\limits_{\mathrm{R}^3} \exp\left[-\eta_\mathrm{M}t\left(\mathbf{k} - \frac{\mathrm{i}\,\mathbf{a}}{2\eta_\mathrm{M}t}\right)^2 - \frac{\mathbf{a}^2}{4\eta_\mathrm{M}t}\right]\mathrm{d}^3\mathbf{k} =$$

$$= \frac{\boldsymbol{\beta}_0}{(2\pi)^3}\mathrm{e}^{-\frac{a^2}{4\eta_\mathrm{M}t}}\int\limits_{\mathrm{R}^3} \exp\left[-\eta_\mathrm{M}t\left(\mathbf{k} - \frac{\mathrm{i}\,\mathbf{a}}{2\eta_\mathrm{M}t}\right)^2\right]\mathrm{d}^3\mathbf{k} =$$

$$= \frac{\boldsymbol{\beta}_0}{(2\pi)^3}\mathrm{e}^{-\frac{a^2}{4\eta_\mathrm{M}t}}\left(\frac{\pi}{\eta_\mathrm{M}t}\right)^{3/2} = \frac{\boldsymbol{\beta}_0}{(4\pi\eta_\mathrm{M}t)^{3/2}}\mathrm{e}^{-\frac{a^2}{4\eta_\mathrm{M}t}}\ ,$$

where the argument in the wave vector **k** has been completed to the power of two. In an unbounded domain, the final result is:

$$\mathbf{G}(t,\mathbf{x},\mathbf{x}') = \frac{\boldsymbol{\beta}_0}{(4\pi\eta_\mathrm{M}t)^{3/2}}\mathrm{e}^{-\frac{|\mathbf{x}-\mathbf{x}'|^2}{4\eta_\mathrm{M}t}}\,; \qquad G(t,\mathbf{x},\mathbf{x}') = \frac{1}{(4\pi\eta_\mathrm{M}t)^{3/2}}\mathrm{e}^{-\frac{|\mathbf{x}-\mathbf{x}'|^2}{4\eta_\mathrm{M}t}}\ . \tag{1.187}$$

Consequently, the Dirac delta localized at **x'** is smoothed over time in a Gaussian manner. In the one-dimensional problem, this situation is illustrated in Figure 1.31. As time approaches zero, the Gaussian wave packet transforms back into a Dirac delta.

Decomposing the initial condition into individual Dirac impulses and summing the results (with the same Green function for all three field components) yields:

$$\mathbf{B}(t,\mathbf{x}) = G \underset{(\mathbf{x})}{*} \mathbf{B}_0 = \frac{1}{(4\pi\eta_{\mathrm{M}} t)^{3/2}} \int \mathrm{e}^{-\frac{|\mathbf{x}-\mathbf{x}'|^2}{4\eta_{\mathrm{M}} t}} \mathbf{B}(0,\mathbf{x}')\, \mathrm{d}^3\mathbf{x}' . \tag{1.188}$$

The field is thus the spatial convolution of the initial condition and the Green function. Direct substitution into the diffusion equation verifies that the relation (1.188) is its solution. The general derivation of the *N*-dimensional solution can be found in *Selected Topics I*, Section I.3.8.4 (*Green Function*).

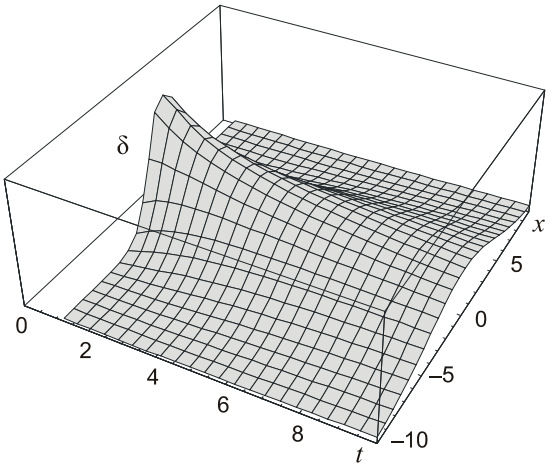


Fig. 1.31: Time evolution of the Dirac impulse.

Note 1: Alternatively, since the diffusion and Schrödinger equations share the same mathematical form, the solution can be written directly in operator form:

$$\left|\mathbf{B}(t)\right\rangle = \mathrm{e}^{\eta_{\mathrm{M}}\boldsymbol{\nabla}^2 (t-t_0)} \left|\mathbf{B}_0\right\rangle .$$

Substituting this into the diffusion equation verifies that the solution satisfies the initial condition. Following standard methods from *Selected Topics I*, Section I.3.4.5 (*Spectral Theory*), the spectrum of the Laplace operator $\boldsymbol{\nabla}^2$ is found, and the spectral expansion theorem is applied:

$$\left|\mathbf{B}(t)\right\rangle = \sum_k \mathrm{e}^{\eta_{\mathrm{M}}\lambda_k (t-t_0)} \left|k\right\rangle\left\langle k\middle|\mathbf{B}_0\right\rangle ,$$

$$\boldsymbol{\nabla}^2 \left|k\right\rangle = \lambda_k \left|k\right\rangle .$$

Note 2: The equation for particle diffusion has the same solution:

$$\frac{\partial n}{\partial t} = D\nabla^2 n\,;$$

$$G(t,\mathbf{x},\mathbf{x}') = \frac{1}{(4\pi Dt)^{3/2}}\ \mathrm{e}^{-\frac{|\mathbf{x}-\mathbf{x}'|^2}{4Dt}}\ ; \tag{1.189}$$

$$n(t,\mathbf{x}) = \int G(t,\mathbf{x},\mathbf{x}')\, n(0,\mathbf{x}')\,\mathrm{d}^3\mathbf{x}'$$

Note 3: For a 1D particle source maintaining a constant *number density* n_0 at the origin, the solution to the diffusion equation (proven by substitution) is

$$n(t,x) = n_0\left[1-\phi\left(\frac{x}{\sqrt{4Dt}}\right)\right], \tag{1.190}$$

where ϕ is an error function defined by the relation

$$\phi(x) \equiv \frac{2}{\sqrt{\pi}}\int_0^x \mathrm{e}^{-\xi^2}\,\mathrm{d}\xi\,. \tag{1.191}$$

◖ **Example 1.1:** Find the mean position and the mean square fluctuation of the particle positions for the diffusion of a Dirac delta function, i.e., for the Green function (1.189) with a source located at the origin of the coordinates (**x**' = 0).

Solution: Determining,, for example, $\langle x \rangle$ a $\langle x^2 \rangle$:

$$\langle x \rangle = \int G(t,\mathbf{x},\mathbf{x}')\, x\,\mathrm{d}^3\mathbf{x} = \int \frac{1}{(4\pi Dt)^{3/2}}\mathrm{e}^{-\frac{x^2+y^2+z^2}{4Dt}}\ x\,\mathrm{d}x\,\mathrm{d}y\,\mathrm{d}z = 0\,,$$

$$\langle x^2 \rangle = \int G(t,\mathbf{x},\mathbf{x}')\, x^2\,\mathrm{d}^3\mathbf{x} = \int \frac{1}{(4\pi Dt)^{3/2}}\mathrm{e}^{-\frac{x^2+y^2+z^2}{4Dt}}\ x^2\,\mathrm{d}x\,\mathrm{d}y\,\mathrm{d}z = 2Dt\,.$$

The integrals are split into individual integrations determined from relations I.3.574 to I.3.576. The mean position remains at the origin (where the Dirac impulse was localized), and the following holds:

$$\langle \mathbf{x} \rangle = (0,0,0)\,,$$

$$\langle \mathbf{x}\cdot\mathbf{x} \rangle = \left\langle x^2+y^2+z^2 \right\rangle = 6Dt\,,$$

$$l_{\mathrm{kv}} \equiv \sqrt{\langle \mathbf{x}\cdot\mathbf{x} \rangle - \langle \mathbf{x} \rangle\cdot\langle \mathbf{x} \rangle} = \sqrt{6Dt}\,.$$

For diffusion, it is typical that the mean square fluctuations grow with time as $t^{1/2}$. ◗

Equation for Vector Potential

Sometimes it is more convenient to use a vector potential satisfying the wave equation and the Lorentz calibration condition instead of the magnetic field directly:

$$\begin{aligned} \nabla^2 \mathbf{A} - \frac{1}{c^2}\frac{\partial^2}{\partial t^2}\mathbf{A} &= -\mu_0 \mathbf{j}\,, \\ \frac{\partial \phi}{c^2 \partial t} + \operatorname{div} \mathbf{A} &= 0\,. \end{aligned} \tag{1.192}$$

In magnetohydrodynamics, the Maxwell displacement current is neglected, which is equivalent to restricting the analysis to low-frequency phenomena, see (1.175). From the equation for the vector potential, only the following terms remain:

$$\nabla^2 \mathbf{A} = -\mu_0 \mathbf{j}\,.$$

The current density from the Ohm law (1.174) is substituted:

$$\nabla^2 \mathbf{A} = -\mu_0 \sigma \left(\mathbf{E} + \mathbf{u} \times \mathbf{B} \right).$$

In MHD, the electric and magnetic fields are determined solely by the vector potential:

$$\mathbf{E} = -\frac{\partial \mathbf{A}}{\partial t}\,; \qquad \mathbf{B} = \nabla \times \mathbf{A}\,.$$

Substituting these into the previous relation yields the vector potential equation

► $$\frac{\partial \mathbf{A}}{\partial t} = \frac{1}{\mu_0 \sigma} \nabla^2 \mathbf{A} + \mathbf{u} \times (\nabla \times \mathbf{A})\,. \tag{1.193}$$

The vector potential equation has a convective (frozen-in) and a diffusion term. Expanding the triple product on the right readily yields the material derivative form:

$$\frac{\mathrm{d} A_i}{\mathrm{d} t} = \frac{1}{\sigma \mu_0} \nabla^2 A_i + u_k \frac{\partial A_k}{\partial x_i}\,. \tag{1.194}$$

Equation for Density

The continuity equation (1.162) serves as the equation for the time evolution of plasma density, written in the form:

► $$\frac{\partial \rho}{\partial t} + \operatorname{div} \rho \mathbf{u} \;=\; 0\,. \tag{1.195}$$

This can be transformed into a form utilizing the material derivative:

$$\frac{\partial \rho}{\partial t} \;+\; \partial_k (\rho u_k) \;=\; 0 \qquad \Rightarrow$$

$$\frac{\partial \rho}{\partial t} \;+\; \frac{\partial \rho}{\partial x_k} u_k \;+\; \rho \frac{\partial u_k}{\partial x_k} \;=\; 0 \qquad \Rightarrow$$

$$\frac{\partial \rho}{\partial t} + (\mathbf{u} \cdot \nabla)\rho + \rho \operatorname{div} \mathbf{u} = 0\,.$$

The resulting expression with the total time derivative is therefore:

$$\frac{\mathrm{d}\rho}{\mathrm{d}t} + \rho \operatorname{div} \mathbf{u} = 0 . \tag{1.196}$$

From the last expression, it is clear that an incompressible fluid satisfies the relations:

$$\rho = \text{const} \quad \Leftrightarrow \quad \mathrm{d}\rho/\mathrm{d}t = 0 \quad \Leftrightarrow \quad \operatorname{div} \mathbf{u} = 0 . \tag{1.197}$$

A similar continuity equation also applies to number density or charge density. These represent the same fundamental relation, since the mass density is obtained by multiplying the number density by the mass of a single particle. Similarly, the charge density is obtained by multiplying the number density by the charge of a single particle.

Equation for Velocity

The velocity equation is derived in three stages: first for ideal hydrodynamics, then for viscous flow, and finally for a conductive fluid with magnetic and gravitational fields. In all cases, both a conservative form (expressed as a continuity equation) and a form utilizing the material derivative are established. The results are compatible with the velocity averaging of the Boltzmann equation in statistical physics.

1) Ideal Hydrodynamics

For an object of mass m, the Newton equation of motion applies:

$$m \frac{\mathrm{d}\mathbf{v}}{\mathrm{d}t} = \mathbf{F} .$$

For a flowing medium, the force density is introduced as:

$$\mathbf{f} \equiv \lim_{\Delta V \to 0} \frac{\Delta \mathbf{F}}{\Delta V} . \tag{1.198}$$

In terms of densities, the Newton equation of motion takes the form (the velocity $\mathbf{v}$ of a single particle becomes the fluid flow velocity $\mathbf{u}$):

$$\rho \frac{\mathrm{d}\mathbf{u}}{\mathrm{d}t} = \mathbf{f} . \tag{1.199}$$

Expanding the material derivative yields the equation:

$$\rho \frac{\partial \mathbf{u}}{\partial t} + \rho (\mathbf{u} \cdot \nabla) \mathbf{u} = \mathbf{f} . \tag{1.200}$$

The force density varies depending on the specific processes. It may correspond to the Lorentz force density $\mathbf{j} \times \mathbf{B}$, or to the pressure force in the case of acoustic waves in gases. Typically, the force points toward the minimum of potential energy:

$$\mathbf{F} = -\nabla W_{\mathrm{P}} , \tag{1.201}$$

or in terms of densities:

$$\mathbf{f} = -\nabla w_{\mathrm{P}} . \tag{1.202}$$

The pressure energy is defined as $W_{\mathrm{p}} = \int p \, \mathrm{d}V$, making the pressure energy density $w_{\mathrm{p}} = p$. The density of the force caused by pressure is then given by:

$$\mathbf{f} = -\nabla p\,. \tag{1.203}$$

The equation of motion (1.200) with the pressure force density therefore takes the form:

$$\rho\frac{\partial \mathbf{u}}{\partial t} + \rho(\mathbf{u}\cdot\nabla)\mathbf{u} \;=\; -\nabla p\,. \tag{1.204}$$

This is the desired equation for the time evolution of the velocity field:

► $$\rho\frac{\mathrm{d}\mathbf{u}}{\mathrm{d}t} \;=\; -\nabla p\,, \qquad \text{or} \qquad \rho\frac{\partial \mathbf{u}}{\partial t} + \rho(\mathbf{u}\cdot\nabla)\mathbf{u} \;=\; -\nabla p\,. \tag{1.205}$$

This equation can be rewritten in a conservative form, i.e., as a continuity equation for momentum. The time evolution of the momentum density is given by:

$$\frac{\partial}{\partial t}(\rho u_k) = \frac{\partial \rho}{\partial t}u_k + \rho\frac{\partial u_k}{\partial t}\,.$$

The time derivative of the density from the continuity equation (1.195) and the time derivative of the velocity from the equation of motion (1.205) are substituted:

$$\frac{\partial}{\partial t}(\rho u_k) = -\partial_l(\rho u_l)\,u_k - \rho\,(u_l\partial_l)\,u_k \;\; -\partial_k p\,.$$

Moving all terms to the left-hand side and simplifying yields:

$$\frac{\partial}{\partial t}(\rho u_k) \;+\; \frac{\partial(\rho u_l)}{\partial x_l}u_k \;+\; (\rho u_l)\frac{\partial u_k}{\partial x_l} \;+\frac{\partial p}{\partial x_k} = 0 \qquad \Rightarrow$$

$$\frac{\partial}{\partial t}(\rho u_k) \;+\; \frac{\partial}{\partial x_l}\left(\rho u_l u_k\right) \;+\; \frac{\partial p}{\partial x_k} = 0 \qquad \Rightarrow$$

$$\frac{\partial}{\partial t}(\rho u_k) \;+\; \frac{\partial}{\partial x_l}\left(p\delta_{kl} + \rho u_k u_l\right) = 0\,.$$

The momentum conservation law is thus obtained. The expression in parentheses represents the momentum flux (pressure tensor). Since momentum is a vector, its flux is a second-order tensor, whose symmetry ensures angular momentum conservation. The pressure tensor consists of a scalar part (isotropic normal pressure) and a tensor part related to the fluid flow. This law can be written in component form as:

► $$\frac{\partial}{\partial t}(\rho u_k) \;+\; \frac{\partial}{\partial x_l}\left(T_{kl}^{(\mathrm{P})}\right) = 0\,; \qquad T_{kl}^{(\mathrm{P})} \equiv p\delta_{kl} + \rho u_k u_l\,, \tag{1.206}$$

or in invariant form as:

► $$\frac{\partial}{\partial t}(\rho\mathbf{u}) \;+\; \vec{\nabla}\cdot\vec{\mathbf{T}}_{\mathrm{P}} = 0\,; \qquad \vec{\mathbf{T}}_{\mathrm{P}} \equiv p\vec{\mathbf{1}} + \rho\mathbf{u}\otimes\mathbf{u}\,. \tag{1.207}$$

The superscript (P) or subscript P denotes pressure; later, the viscosity tensor and Maxwell stress tensor will be added.

2) Viscous Fluid

Viscous fluids are characterized by non-zero velocity gradients. For example, a fluid flowing between two parallel plates has zero velocity at the walls and a maximum value in between, making the perpendicular spatial derivative $\partial u_x/\partial y$ non-zero. Viscous momentum losses are therefore described using the viscosity tensor:

$$V_{kl} = f_{kl}(\partial u_i/\partial x_j)\,.$$

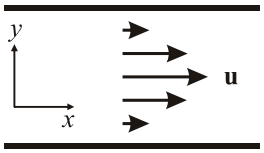


Fig. 1.32: Flow of a viscous fluid between two plates.

In the simplest approximation, the viscosity tensor is assumed to be linear in the velocity derivatives, alternatively, this corresponds to a first-order Taylor expansion in the velocity derivatives. It must be a symmetric second-order tensor to conserve angular momentum. Under these assumptions, its most general form is:

$$V_{kl} = a\left(\frac{\partial u_k}{\partial x_l} + \frac{\partial u_l}{\partial x_k}\right) + b\,\delta_{kl}\frac{\partial u_n}{\partial x_n} = a\left(\frac{\partial u_k}{\partial x_l} + \frac{\partial u_l}{\partial x_k}\right) + b\delta_{kl}\,\mathrm{div}\,\mathbf{u}\,.$$

This symmetric tensor is obtained by summing the derivatives in parentheses and all diagonal elements (the velocity divergence). In mathematics and physics, it is highly convenient to work with traceless tensors. Therefore, a portion of the second (scalar) term is combined with the first to ensure a zero trace:

$$V_{kl} = \eta\left(\frac{\partial u_k}{\partial x_l} + \frac{\partial u_l}{\partial x_k} - \frac{2}{3}\delta_{kl}\,\mathrm{div}\,\mathbf{u}\right) + \zeta\delta_{kl}\,\mathrm{div}\,\mathbf{u}\,. \tag{1.208}$$

The trace of the tensor part in parentheses is identical to zero:

$$\left(\frac{\partial u_k}{\partial x_k} + \frac{\partial u_k}{\partial x_k} - \frac{2}{3}\delta_{kk}\,\mathrm{div}\,\mathbf{u}\right) = \left(\mathrm{div}\,\mathbf{u} + \mathrm{div}\,\mathbf{u} - \frac{2}{3}\cdot 3\cdot \mathrm{div}\,\mathbf{u}\right) = 0.$$

The coefficients η and ζ are termed the *shear* and *bulk* viscosities, respectively. The conservative form of the law of conservation of momentum then takes the form

$$\frac{\partial}{\partial t}(\rho u_k) + \frac{\partial}{\partial x_l}T_{kl}^{(\mathrm{P})} = 0\,; \qquad T_{kl}^{(\mathrm{P})} \equiv p\delta_{kl} + \rho u_k u_l - V_{kl}\,. \tag{1.209}$$

The invariant form of this relation is

$$\frac{\partial}{\partial t}(\rho\,\mathbf{u}) + \vec{\nabla}\cdot\vec{\mathbf{T}}_{\mathrm{P}} = 0\,; \qquad \vec{\mathbf{T}}_{\mathrm{P}} \equiv p\vec{\mathbf{1}} + \rho\mathbf{u}\otimes\mathbf{u} - \vec{\mathbf{V}}\,. \tag{1.210}$$

A minus sign is introduced for the viscosity tensor because it represents losses within the momentum flux. Under this convention, both viscosity coefficients remain positive under normal physical conditions. The equation of motion is now derived by substituting both tensors into relation (1.209) and performing all required differentiations:

$$\frac{\partial}{\partial t}(\rho u_k) \; + \; \frac{\partial}{\partial x_l}\left[p\delta_{kl} + \rho u_k u_l - \eta\left(\frac{\partial u_k}{\partial x_l} + \frac{\partial u_l}{\partial x_k} - \frac{2}{3}\delta_{kl}\,\mathrm{div}\,\mathbf{u} \right) \; - \; \zeta\delta_{kl}\,\mathrm{div}\,\mathbf{u} \right] = 0\,.$$

Following a straightforward calculation, the equation of motion is established:

► $$\rho\frac{\partial \mathbf{u}}{\partial t} + \rho(\mathbf{u}\cdot\nabla)\mathbf{u} \; = \; -\nabla p \; + \; \eta\nabla^2\mathbf{u} \; + \; (\zeta + \eta/3)\,\nabla(\mathrm{div}\,\mathbf{u})\,. \qquad (1.211)$$

This is the famous *Navier-Stokes equation* for a viscous fluid. If the fluid is incompressible (i.e. liquid, div **u** = 0), the equation of motion reduces to a simple form:

► $$\rho\frac{\partial \mathbf{u}}{\partial t} + \rho(\mathbf{u}\cdot\nabla)\mathbf{u} \; = \; -\nabla p \; + \; \eta\nabla^2\mathbf{u}\,, \qquad (1.212)$$

where the fluid behavior can be described solely by the shear viscosity coefficient η.

3) Conductive Fluid

In magnetohydrodynamics, the Lorentz force density is introduced on the right-hand side of equation (1.211):

$$\rho\frac{\partial \mathbf{u}}{\partial t} + \rho(\mathbf{u}\cdot\nabla)\mathbf{u} \; = \; -\nabla p \; + \; \eta\nabla^2\mathbf{u} \; + \; (\zeta + \eta/3)\,\nabla(\mathrm{div}\,\mathbf{u}) + \mathbf{j}\times\mathbf{B}\,. \qquad (1.213)$$

To derive the conservative form, only the Lorentz force density requires modification, as the conservative forms of all other terms are already established:

$$(\mathbf{j}\times\mathbf{B})_k = (\mathrm{rot}\,\mathbf{H}\times\mathbf{B})_k = \varepsilon_{klm}\,(\mathrm{rot}\,\mathbf{H})_l\,B_m = \varepsilon_{klm}\varepsilon_{lno}\partial_n(H_o)B_m =$$

$$= -\varepsilon_{lkm}\varepsilon_{lno}\partial_n(H_o)B_m = (-\delta_{kn}\delta_{mo} + \delta_{ko}\delta_{mn})\,\frac{\partial H_o}{\partial x_n}\,B_m = -\frac{\partial H_m}{\partial x_k}\,B_m + \frac{\partial H_k}{\partial x_m}\,B_m =$$

$$= -\frac{\partial}{\partial x_k}\left(\frac{\mathbf{H}\cdot\mathbf{B}}{2}\right) + \frac{\partial}{\partial x_m}(H_k B_m) - H_k\,\frac{\partial B_m}{\partial x_m}\,.$$

The last term vanishes due to div **B** = 0, and the summation indices are swapped in the middle term:

$$(\mathbf{j}\times\mathbf{B})_k = -\frac{\partial}{\partial x_k}\left(\frac{\mathbf{H}\cdot\mathbf{B}}{2}\right) + \frac{\partial}{\partial x_l}(H_k B_l) = -\frac{\partial}{\partial x_l}\left[\frac{\mathbf{H}\cdot\mathbf{B}}{2}\delta_{kl} - H_k B_l\right].$$

The expression in square brackets represents the *Maxwell stress tensor* for the magnetic field. Similar to the pressure tensor, it consists of a scalar and a tensor component. Transferring this term to the left-hand side of the equation of motion yields the relation:

► $$\frac{\partial}{\partial t}(\rho u_k) \; + \; \frac{\partial}{\partial x_l}\left(T_{kl}^{(\mathrm{P})} + T_{kl}^{(\mathrm{M})}\right) = 0\,. \qquad (1.214)$$

The individual tensors possess the components:

$$T_{kl}^{(\mathrm{P})} \equiv p\delta_{kl} + \rho u_k u_l - V_{kl}\,, \qquad \ddot{\mathbf{T}}_{\mathrm{P}} \equiv p\,\ddot{\mathbf{1}} + \rho\mathbf{u}\otimes\mathbf{u} - \ddot{\mathbf{V}}\,;$$

$$\blacktriangleright \qquad T_{kl}^{(\mathrm{M})} \equiv \frac{\mathbf{H}\cdot\mathbf{B}}{2}\delta_{kl} - H_k B_l\,, \qquad \ddot{\mathbf{T}}_{\mathrm{M}} \equiv \frac{\mathbf{H}\cdot\mathbf{B}}{2}\,\ddot{\mathbf{1}} - \mathbf{H}\otimes\mathbf{B}\,; \tag{1.215}$$

$$V_{kl} \equiv \eta\left(\frac{\partial u_k}{\partial x_l} + \frac{\partial u_l}{\partial x_k} - \frac{2}{3}\delta_{kl}\,\mathrm{div}\,\mathbf{u}\right) + \zeta\delta_{kl}\,\mathrm{div}\,\mathbf{u}\,.$$

The scalar component of the Maxwell stress tensor is frequently termed *magnetic pressure* and corresponds to the energy density of the magnetic field:

$$\blacktriangleright \qquad p_{\mathrm{M}} = \frac{\mathbf{H}\cdot\mathbf{B}}{2} = \frac{B^2}{2\mu}\,. \tag{1.216}$$

Note 1: The magnetic field present within sunspots is partly responsible for their lower local temperature, since the total internal pressure is determined by both the magnetic and hydrodynamic components.

$$p_{\mathrm{out}} = p_{\mathrm{in}} \qquad \Rightarrow \qquad nkT_{\mathrm{out}} = B^2/2\mu + nkT_{\mathrm{in}}\,.$$

Note 2: The Lorentz force consists of two distinct components:

$$\mathbf{j}\times\mathbf{B} = -\ddot{\boldsymbol{\nabla}}\cdot\ddot{\mathbf{T}}_{\mathrm{M}} = -\boldsymbol{\nabla}p_{\mathrm{M}} + \frac{1}{\mu}(\mathbf{B}\cdot\boldsymbol{\nabla})\mathbf{B}\,. \tag{1.217}$$

The first term represents the magnetic pressure gradient, while the second is related to field line curvature. This force drives the plasma to either straighten the field lines or, if they are closed, force them into a circular geometry.

MHD Equations Closure

Velocity-space averaging of the Boltzmann equation leads to the continuity, velocity, energy, and heat flux equations. This infinite system of partial differential equations must be truncated at some stage by an algebraic relation. In this model, the system is closed at the pressure equation by assuming that the pressure satisfies an algebraic relation $p = p(\rho)$, such as a polytropic relation. Finally, the resulting set of MHD equations is written in conservative form:

$$\frac{\partial\mathbf{B}}{\partial t} = \frac{1}{\sigma\mu}\boldsymbol{\nabla}^2\mathbf{B} + \boldsymbol{\nabla}\times(\mathbf{u}\times\mathbf{B})\,,$$

$$\blacktriangleright \qquad \frac{\partial\rho}{\partial t} + \mathrm{div}\,\rho\mathbf{u} = 0\,, \tag{1.218}$$

$$\frac{\partial}{\partial t}(\rho u_k) + \frac{\partial}{\partial x_l}\left(T_{kl}^{(\mathrm{P})} + T_{kl}^{(\mathrm{M})}\right) = 0\,,$$

$$p = p(\rho)\,.$$

Explicit form utilizing the material time derivatives yields:

$$\frac{\mathrm{d}\mathbf{B}}{\mathrm{d}t} = \frac{1}{\sigma\mu}\nabla^2\mathbf{B} + (\mathbf{B}\cdot\nabla)\mathbf{u} - \mathbf{B}\,\mathrm{div}\,\mathbf{u}\,,$$

$$\frac{\mathrm{d}\rho}{\mathrm{d}t} + \rho\,\mathrm{div}\,\mathbf{u} = 0\,, \tag{1.219}$$

$$\rho\frac{\mathrm{d}\mathbf{u}}{\mathrm{d}t} = -\nabla p - \nabla p_{\mathrm{M}} + \frac{1}{\mu}(\mathbf{B}\cdot\nabla)\mathbf{B} + \eta\nabla^2\mathbf{u} + (\zeta+\eta/3)\,\nabla(\mathrm{div}\,\mathbf{u})\,,$$

$$p = p(\rho)\,.$$

Various alternative formulations exist; for example, considering separate continuity and momentum equations for electrons and ions, and closing the system after the energy equation using an algebraic heat conduction relation. The equations can also be generalized to include a dominant electric field influence. Common closures for the MHD system include:

Incompressible Fluid Closure

The mass density is assumed to be constant (ρ = const). The total time derivative of the density therefore vanishes:

$$\partial\rho/\partial t + (\mathbf{u}\cdot\nabla)\rho = 0 \tag{1.220}$$

and the continuity equation implies that div $\mathbf{u} = 0$.

Polytropic Closure

A polytropic relation between pressure and density is assumed:

$$p = K\rho^{\gamma}. \tag{1.221}$$

After rearrangement, it follows that:

$$\frac{\mathrm{d}}{\mathrm{d}t}\left(p\rho^{-\gamma}\right) = 0 \quad \Rightarrow \quad \frac{\partial}{\partial t}\left(p\rho^{-\gamma}\right) + u_k\frac{\partial}{\partial x_k}\left(p\rho^{-\gamma}\right) = 0\,.$$

Following straightforward manipulation, expanding both products and substituting the time derivative of the density from the continuity equation yields:

$$\frac{\partial p}{\partial t} + (\mathbf{u}\cdot\nabla)p + \gamma p\,\mathrm{div}\,\mathbf{u} = 0\,. \tag{1.222}$$

CGL Closure

This closure of magnetohydrodynamics accounts for the anisotropic behavior of plasma. It is named after its authors, Geoffrey Chew, Marvin Goldberger, and Francis Low, who as early as 1956 considered the pressure profile in the form

$$p\delta_{kl} \;\rightarrow\; p_{kl} = p_{\perp}\delta_{kl} + (p_{\parallel} - p_{\perp})\frac{B_k B_l}{B^2}\,. \tag{1.223}$$

1.3.2 Exact MHD Solutions

Hartmann Solution

In classical hydrodynamics, the behavior of an incompressible viscous fluid between horizontal plates is well established. A pressure difference drives a laminar flow governed by Poiseuille law, formulated by Jean Louis Marie Poiseuille. The velocity follows a parabolic profile – vanishing at the plates and reaching its maximum value in the center. Boundary effects at the edges of the plates are neglected.

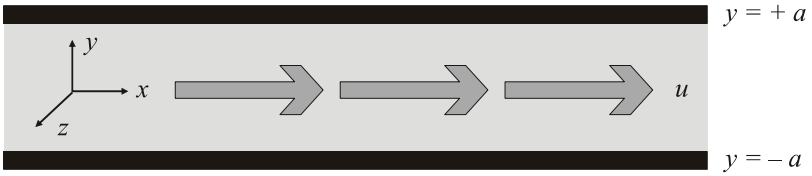


Fig. 1.33: Fluid flow between two flat parallel plates.

If the fluid is electrically conductive, a similar solution can be derived from the MHD equations, which were first formulated by Danish engineer Julian Hartmann in 1937. The fundamental system of magnetohydrodynamic equations is written as:

$$\begin{gathered} \operatorname{div}\mathbf{u} = 0\,, \\ \rho\frac{\partial\mathbf{u}}{\partial t} + \rho(\mathbf{u}\cdot\nabla)\mathbf{u} = -\nabla p + \eta\nabla^2\mathbf{u} + \left[\frac{\nabla\times\mathbf{B}}{\mu}\times\mathbf{B}\right], \\ \frac{\partial\mathbf{B}}{\partial t} = \frac{1}{\sigma\mu}\nabla^2\mathbf{B} + \nabla\times[\mathbf{u}\times\mathbf{B}]\,. \end{gathered} \tag{1.224}$$

The first relation represents the continuity equation for an incompressible fluid; the second is the equation of motion containing, in order on the right-hand side, the pressure force, the viscous force, and the Lorentz force. The final relation is the induction equation for the magnetic field, comprising a diffusion term and a frozen-in term.

Note 1: The equation of state cannot be utilized to close the system for an incompressible fluid because pressure is not a function of density. Instead, pressure decreases linearly in the flow direction while the density remains strictly constant. The system is closed by assuming a constant pressure gradient.

The coordinate system is chosen according to the figure to exploit the symmetry of the problem. Assuming a steady state, all temporal derivatives in (1.224) vanish. Fluid flow occurs exclusively parallel to the plates, meaning the velocity field possesses only the $u_x(y)$ component. At the walls ($y = \pm a$), the velocity vanishes, reaching its maximum in the center. A non-zero magnetic field with components $B_x(y)$ and $B_y(y)$ is assumed. From div $\mathbf{B} = 0$, it follows that B_y must be constant. Pressure decreases along the flow direction and may depend on y. The solution is sought in the form:

$$\mathbf{u} = [u(y), 0, 0]\,; \quad \mathbf{B} = \left[B(y),\, B_0\,,\, 0\right]; \quad p = p(x, y)\,. \tag{1.225}$$

The transverse field B_0 impedes the motion of the conductive fluid, while the field $B(y)$ is induced during this motion. Substituting these fields into the system (1.224) yields:

$$\begin{aligned} 0 &= -\frac{\partial p}{\partial x} + \eta \frac{\mathrm{d}^2 u}{\mathrm{d}y^2} + \frac{B_0}{\mu}\frac{\mathrm{d}B}{\mathrm{d}y}, \\ 0 &= -\frac{\partial p}{\partial y} - \frac{B}{\mu}\frac{\mathrm{d}B}{\mathrm{d}y}, \\ 0 &= \frac{1}{\sigma\mu}\frac{\mathrm{d}^2 B}{\mathrm{d}y^2} + B_0 \frac{\mathrm{d}u}{\mathrm{d}y}. \end{aligned} \tag{1.226}$$

Analogous to the Poiseuille law, a linear pressure drop $\partial p/\partial x$ = const. is assumed, which represents the only physically consistent behavior. The first and third equations then form a coupled system for the velocity and magnetic field, while the pressure profile is determined subsequently from the second equation. For u and B, the system reduces to:

$$\begin{aligned} \eta \frac{\mathrm{d}^2 u}{\mathrm{d}y^2} + \frac{B_0}{\mu}\frac{\mathrm{d}B}{\mathrm{d}y} &= \text{const}, \\ \frac{1}{\sigma\mu}\frac{\mathrm{d}^2 B}{\mathrm{d}y^2} + B_0 \frac{\mathrm{d}u}{\mathrm{d}y} &= 0. \end{aligned}$$

Differentiating the first equation with respect to y allows for the elimination of the second derivatives of the magnetic field from the equations:

$$\frac{\mathrm{d}^3 u}{\mathrm{d}y^3} - \frac{1}{D^2}\frac{\mathrm{d}u}{\mathrm{d}y} = 0; \qquad \text{kde} \quad \frac{1}{D^2} \equiv \frac{\sigma B_0^2}{\eta}, \ \text{tj.}$$

The first integration yields:

$$\frac{\mathrm{d}^2 u}{\mathrm{d}y^2} - \frac{1}{D^2} u = C_1.$$

This linear differential equation with a right-hand side has a general solution composed of a homogeneous solution and a constant particular integral:

$$u(y) = u_{\mathrm{H}}(y) + u_{\mathrm{P}}(y) \ = C_2 \cosh\left[\frac{y}{D}\right] + C_3 \sinh\left[\frac{y}{D}\right] - C_1 D^2.$$

Using a homogeneous solution basis of cosh and sinh functions, the integration constants are determined from the boundary conditions $u(\pm a) = 0$ and $u(0) = u_0$, yielding:

► $$u(y) = u_0 \frac{\cosh\left(\frac{a}{D}\right) - \cosh\left(\frac{y}{D}\right)}{\cosh\left(\frac{a}{D}\right) - 1}; \qquad D \equiv \sqrt{\frac{\eta}{\sigma B_0^2}}. \tag{1.227}$$

The magnetic field can be calculated from either the first or third equation in (1.226). The integration constants are determined from the continuity of the tangential **H** components at the interface, $B_{1\mathrm{t}}/\mu_1 = B_{2\mathrm{t}}/\mu_2$, from which follows $B(\pm a) = 0$. The result is:

► $$B(y) = \mu u_0 \sqrt{\sigma\eta}\, \frac{\sinh\left(\frac{y}{D}\right) - \frac{y}{a}\sinh\left(\frac{a}{D}\right)}{\cosh\left(\frac{a}{D}\right) - 1}; \qquad D \equiv \sqrt{\frac{\eta}{\sigma B_0^2}}. \tag{1.228}$$

The resulting velocity and magnetic field profiles are illustrated in Figure 1.34. The magnetic field flattens the velocity profile in the central region and causes a rapid velocity decrease near the plates. A constant transverse field component (B_y) thus induces a magnetic field component oriented in the flow direction.

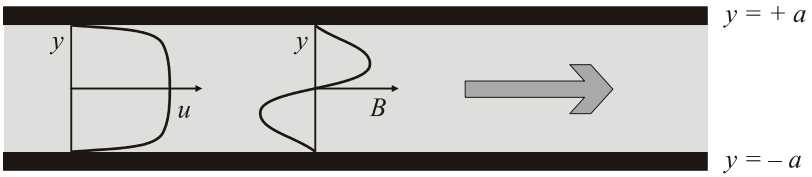


Fig. 1.34: Velocity and magnetic field profiles for the Hartmann solution.

The positions of the maximum and minimum of the magnetic profile can be obtained by differentiating the equation (1.228)

$$y_{1,2} = \pm D \operatorname{arcosh}\left[\frac{D}{a}\sinh\left(\frac{a}{D}\right)\right]. \tag{1.229}$$

Weak Fields

For weak magnetic fields ($a/D \ll 1$), expanding the hyperbolic functions to first order yields the well-known Poiseuille parabolic profile; the magnetic field exerts negligible influence on the fluid flow:

$$u \approx u_0\left[1 - \left(\frac{y}{a}\right)^2\right]. \tag{1.230}$$

Strong Fields

For strong magnetic fields ($a/D \gg 1$), the regions $y > 0$ and $y < 0$ must be analyzed separately. Consequently, only the positive exponential term is retained, yielding:

$$u \approx u_0\left[1 - \exp\left(\frac{|y| - a}{D}\right)\right]. \tag{1.231}$$

In this regime, the velocity field decreases exponentially near the walls. The characteristic length D determines the thickness of the boundary layer. A dimensionless quantity, termed the Hartmann number $\#_{\mathrm{Ha}}$, is introduced by the relation:

$$\#_{\mathrm{Ha}} \equiv \frac{a}{D} = B_0 a\sqrt{\frac{\sigma}{\eta}}. \tag{1.232}$$

The ratio of magnetic and viscous force equals to the square of the Hartmann number:

$$\frac{jB_0}{\eta\Delta u} \approx \frac{\sigma E B_0}{\eta u / a^2} \approx \frac{\sigma u B_0^2}{\eta u / a^2} = \frac{\sigma B_0^2 a^2}{\eta} = \#_{\mathrm{Ha}}^2. \tag{1.233}$$

Waves of Finite Amplitude

The nonlinear MHD equations are very complex. Linearization yields only infinitesimal amplitude waves, omitting many important solutions. In this section, it is demonstrated that special solutions satisfy the ordinary wave equation, allowing for traveling waves of arbitrary shape and amplitude. Consider the system for an incompressible, non-viscous, perfectly conductive fluid ($\eta = \zeta = 1/\sigma = 0$):

$$\begin{gathered}\rho\frac{\partial \mathbf{u}}{\partial t} + \rho(\mathbf{u}\cdot\nabla)\mathbf{u} = -\nabla p + \frac{1}{\mu}(\nabla\times\mathbf{B})\times\mathbf{B}\,; \\ \frac{\partial \mathbf{B}}{\partial t} = \nabla\times[\mathbf{u}\times\mathbf{B}]\,; \\ \operatorname{div}\mathbf{u} = 0\,; \\ \operatorname{div}\mathbf{B} = 0\,.\end{gathered} \tag{1.234}$$

These represent the equation for the velocity field (the equation of motion incorporating the pressure and Lorentz forces) and the induction equation for the magnetic field with a convective (frozen-in term). Supplementary equations include the incompressibility equations and Gauss law for the magnetic field.

Assume now that all quantities vary only in one direction. Let the z-axis of the coordinate system be chosen in this direction. A solution is then sought in the form:

$$\mathbf{u} = \mathbf{u}(t,z)\,; \quad \mathbf{B} = \mathbf{B}(t,z)\,; \quad p = p(t,z)\,. \tag{1.235}$$

From the supplementary divergence conditions in (1.234), it immediately follows that:

$$u_z = u_0(t)\,; \quad B_z = B_0(t)\,.$$

To find a solution in the form of a traveling wave packet that is localized in space, the plasma velocity must vanish at infinity, requiring $u_0 = 0$. In the given geometry, it follows that:

$$\mathbf{u} = (u_x, u_y, 0),\ \ \mathbf{B} = (B_x, B_y, B_0),\ \ \nabla \to (0,0,\partial/\partial z).$$

The more complex terms in the first two equations of (1.234) are expanded as follows:

$$\begin{gathered}(\mathbf{u}\cdot\nabla)\mathbf{u} = [0,\,0,\,0]\,; \\ (\nabla\times\mathbf{B})\times\mathbf{B} = \left[B_0\frac{\partial B_x}{\partial z}, B_0\frac{\partial B_y}{\partial z}, -\frac{\partial}{\partial z}\left(\frac{B_x^2 + B_y^2}{2}\right)\right]; \\ \nabla p = \left[0,0,\frac{\partial p}{\partial z}\right]; \\ \nabla\times(\mathbf{u}\times\mathbf{B}) = \left[B_0\frac{\partial u_x}{\partial z}, B_0\frac{\partial u_y}{\partial z}, 0\right].\end{gathered}$$

The expansions of the individual quantities differ along the z-axis and within the (x, y) plane. The governing equations yield:

Parallel Direction (along the *z*-axis)

$$0 = \frac{\partial}{\partial z}\left[p + \frac{B_x^2 + B_y^2}{2\mu} \right]; \quad \frac{\partial B_0}{\partial t} = 0 .$$

The first equation implies that the total pressure is independent of z; a constant field component $B_z = B_0$ can be added to the right-hand side. The second equation demonstrates that B_0 is a space-time constant. For the total pressure, the relation is:

$$\Pi \equiv p + \frac{\mathbf{B}^2}{2\mu} = \Pi(t) .$$

Perpendicular Direction (in the *xy*-plane)

$$\begin{aligned} \frac{\partial \mathbf{u}}{\partial t} &= \frac{1}{\mu\rho} B_0 \frac{\partial \mathbf{B}}{\partial z}; \\ \frac{\partial \mathbf{B}}{\partial t} &= B_0 \frac{\partial \mathbf{u}}{\partial z} . \end{aligned} \tag{1.236}$$

In the perpendicular direction, the system remains strictly linear even without requiring linearization. Furthermore, both equations are trivially satisfied along the z-axis, where all quantities are constant. They can thus be regarded as the fundamental system for waves propagating in both directions. Eliminating variables yields the wave equations for both the velocity and magnetic fields (differentiating one equation with respect to time and substituting the temporal derivative from the other suffices). The result is:

► $$\begin{aligned} \left(\frac{\partial^2}{\partial z^2} - \frac{1}{v_\mathrm{A}^2} \frac{\partial^2}{\partial t^2} \right) \mathbf{u} = 0 ; \\ \left(\frac{\partial^2}{\partial z^2} - \frac{1}{v_\mathrm{A}^2} \frac{\partial^2}{\partial t^2} \right) \mathbf{B} = 0 ; \end{aligned} \tag{1.237}$$

► $$v_\mathrm{A} \equiv \frac{B_0}{\sqrt{\mu\rho}} . \tag{1.238}$$

This wave equation features a characteristic propagation velocity equal to the Alfvén velocity. The nonlinear MHD system for an ideally conductive, incompressible fluid without viscosity yields a general wave solution of arbitrary amplitude. Notably, the Alfvén velocity can be determined directly from the equality between kinetic and magnetic energy densities:

$$\frac{\rho v_\mathrm{A}^2}{2} \approx \frac{B^2}{2\mu} \quad \Rightarrow \quad v_\mathrm{A} = \frac{B}{\sqrt{\mu\rho}} .$$

The plasma reaches the Alfvén speed when its entire magnetic energy is converted into kinetic energy, as observed during the reconnection of magnetic field lines. Several typical plasma wave modes also propagate at this speed.

Helicity

Typical helical structures are often observed in plasma filaments. They are found in both laboratory and interstellar plasmas, in pinch plasmas and in cometary tails. In mathematics, the term "helicity" is used to describe fields with similar structures.

Helicity and Beltrami Condition

The helicity density of a vector field **V** is defined as

$$\mathcal{H}(t,\mathbf{x}) \equiv \mathbf{V}\cdot\operatorname{curl}\mathbf{V} = \mathbf{V}\cdot(\nabla\times\mathbf{V})\,. \tag{1.239}$$

The total helicity is defined as the integral

$$K(t) = \int_V \mathcal{H}(t,\mathbf{x})\,\mathrm{d}^3\mathbf{x}\,. \tag{1.240}$$

Helicity is a scalar quantity characterizing the helical nature of field lines. It vanishes for all fields satisfying the irrotational condition ($\nabla\times\mathbf{V} = 0$) and also for all plane vortices with circular streamlines. Fields with a helical structure have a helicity proportional to $\sin\beta$, where β is the pitch angle of the helix. For plasma filaments described in MHD theory, the magnetic field helicity density can be significant; it is defined for the vector potential **A**, the electric field intensity **E**, and the velocity field **u**:

$$\begin{aligned}
\mathcal{H}_A &= \mathbf{A}\cdot(\nabla\times\mathbf{A}) \;= \mathbf{A}\cdot\mathbf{B}\,,\\
\mathcal{H}_E &= \mathbf{E}\cdot(\nabla\times\mathbf{E}) = -\,\mathbf{E}\cdot\frac{\partial\mathbf{B}}{\partial t}\,,\\
\mathcal{H}_u &= \mathbf{u}\cdot(\nabla\times\mathbf{u}) = \mathbf{u}\cdot\boldsymbol{\omega}\,.
\end{aligned} \tag{1.241}$$

The quantity $\boldsymbol{\omega}\equiv\nabla\times\mathbf{u}$ is called the vorticity. Fields satisfying the so-called Beltrami condition are considered, where the curl of the field is proportional to the field itself:

$$\nabla\times\mathbf{V} = \alpha\mathbf{V}\,, \qquad \text{or} \qquad \mathbf{V}\times(\nabla\times\mathbf{V}) = 0\,. \tag{1.242}$$

These *Betrami fields* are named after the Italian mathematician Eugenio Beltrami. The proportionality coefficient α may vary in time and space; however, it is treated here as a constant. A Beltrami field is 1) source-free, 2) helical, and 3) satisfies Helmholtz equation. The absence of a source (div **V** = 0) follows from applying the divergence operator to the condition. The helicity nature for a nonzero field is apparent from the definition:

$$\mathcal{H} \equiv \mathbf{V}\cdot(\nabla\times\mathbf{V}) = \alpha\mathbf{V}\cdot\mathbf{V} = \alpha V^2. \tag{1.243}$$

By applying the curl operator to condition (1.242), we find that Beltrami fields satisfy Helmholtz equation (this is a non-equivalent transformation; the reverse may not hold)

$$\nabla^2\,\mathbf{V} \;+\; \alpha^2\,\mathbf{V} \;=\; 0\,. \tag{1.244}$$

In this case, the vector **V** is an eigenvector of the Laplace operator in the corresponding geometry. A typical mathematical example of Beltrami fields are the ABC flow:

$$\mathbf{V} \;=\; (A\cos y + B\sin z,\;\; B\cos z + C\sin x\,,\;\; C\cos x + A\sin y)\,. \tag{1.245}$$

For ABC fields, curl **V** = **V** and $\nabla^2\,\mathbf{V} = -\mathbf{V}$. These flows are important in chaos theory.

In plasma physics, force-free configurations are often considered, in which the current density points in the direction of the magnetic field (**j** || **B**, so-called *Birkeland currents*). In this case, the Lorentz force density **j**×**B** is zero. This configuration possesses the lowest possible energy, and a dissipative plasma always gradually approaches this state. The magnetic field in a force-free configuration satisfies the Beltrami condition, as can be demonstrated using the Ampère law:

$$\mathbf{j} \parallel \mathbf{B} \quad \Rightarrow \quad \mathbf{j} \sim \mathbf{B} \quad \Rightarrow \quad \nabla \times \mathbf{B} \sim \mathbf{B} \quad \Rightarrow \quad \mathbf{B} \times (\nabla \times \mathbf{B}) = 0 \,. \tag{1.246}$$

The magnetic field in a force-free configuration is therefore always helical.

Conservation of Magnetic Helicity

Integral magnetic helicity is conserved under the following assumptions:

1. *Infinite plasma conductivity* (ideal plasma). Thus, only the frozen-in term dominates in the equation for the time evolution of the magnetic field

$$\frac{\partial \mathbf{B}}{\partial t} = (\nabla \times \mathbf{u}) \times \mathbf{B} \,. \tag{1.247}$$

   In the limit of infinite conductivity, the Ohm law (1.174) takes the form:

$$\mathbf{E} = -\mathbf{u} \times \mathbf{B} \,. \tag{1.248}$$

2. *Incompressibility of the plasma*. The magnetic field satisfies div **B** = 0. Due to freezing, the velocity field is required to satisfy the same equation, i.e.,

$$\operatorname{div} \mathbf{u} = 0 \,. \tag{1.249}$$

3. The *normal component of the magnetic field at the surface is zero*, implying closed magnetic field lines. At the surface of the system, the relation holds

$$\mathbf{B} \cdot \mathbf{n} = 0 \,, \tag{1.250}$$

   where **n** is the normal vector to the surface. For this assumption to hold, the entire magnetic tube must be considered as the system, or the system must be very extensive.

The integral helicity for the vector potential of the magnetic field is defined as

$$K = \int \mathbf{A} \cdot (\nabla \times \mathbf{A}) \, \mathrm{d}V = \int \mathbf{A} \cdot \mathbf{B} \, \mathrm{d}^3\mathbf{x} \,. \tag{1.251}$$

The total time derivative yields the expression

$$\frac{\mathrm{d}K}{\mathrm{d}t} = \int_V \left[\frac{\partial}{\partial t} (\mathbf{A} \cdot \mathbf{B}) + (\mathbf{u} \cdot \nabla)(\mathbf{A} \cdot \mathbf{B}) \right] \mathrm{d}^3\mathbf{x} \,,$$

The first term is differentiated as a product; and the second term is transformed into the form of a divergence (using the incompressibility condition div **u** = 0)

$$\frac{\mathrm{d}K}{\mathrm{d}t} = \int_V \left(\frac{\partial \mathbf{A}}{\partial t} \cdot \mathbf{B} + \mathbf{A} \cdot \frac{\partial \mathbf{B}}{\partial t} \right) \mathrm{d}^3\mathbf{x} \; + \; \int_V \operatorname{div} \left[\mathbf{u} (\mathbf{A} \cdot \mathbf{B}) \right] \mathrm{d}^3\mathbf{x} .$$

Using the Gauss theorem for the last term yields:

$$\frac{\mathrm{d}K}{\mathrm{d}t} = \int_V \left(\frac{\partial \mathbf{A}}{\partial t}\cdot \mathbf{B}\right)\mathrm{d}^3\mathbf{x} + \int_V \left(\mathbf{A}\cdot\frac{\partial \mathbf{B}}{\partial t}\right)\mathrm{d}^3\mathbf{x} + \int_{S=\partial V} (\mathbf{A}\cdot\mathbf{B})(\mathbf{u}\cdot\mathbf{n})\,\mathrm{d}S\,. \tag{1.252}$$

First, the middle term of the equation is simplified. For the time evolution of the magnetic field, the frozen-in term is substituted and simplified using the identity $\mathbf{A}\cdot(\boldsymbol{\nabla}\times\mathbf{B}) = \mathbf{B}\cdot(\boldsymbol{\nabla}\times\mathbf{A}) - \mathrm{div}\,(\mathbf{A}\times\mathbf{B})$, which can be found in *Selected Topics I*, Equation I.3.120:

$$\begin{aligned}
\int_V \mathbf{A}\cdot\frac{\partial \mathbf{B}}{\partial t}\mathrm{d}^3\mathbf{x} &= \int_V \mathbf{A}\cdot\mathrm{curl}(\mathbf{u}\times\mathbf{B})\,\mathrm{d}^3\mathbf{x} = \\
&= -\int_V \mathrm{div}\big[\mathbf{A}\times(\mathbf{u}\times\mathbf{B})\big]\,\mathrm{d}^3\mathbf{x} + \int_V (\mathbf{u}\times\mathbf{B})\cdot\mathrm{curl}\,\mathbf{A}\,\mathrm{d}^3\mathbf{x} = \\
&= -\int_V \mathrm{div}\big[(\mathbf{A}\cdot\mathbf{B})\mathbf{u} - (\mathbf{A}\cdot\mathbf{u})\mathbf{B}\big]\,\mathrm{d}^3\mathbf{x} + \int_V (\mathbf{u}\times\mathbf{B})\cdot\mathbf{B}\,\mathrm{d}^3\mathbf{x} = \\
&= -\int_V \mathrm{div}\big[(\mathbf{A}\cdot\mathbf{B})\mathbf{u} - (\mathbf{A}\cdot\mathbf{u})\mathbf{B}\big]\,\mathrm{d}^3\mathbf{x} = \\
&= -\int_S \big[(\mathbf{A}\cdot\mathbf{B})(\mathbf{u}\cdot\mathbf{n}) - (\mathbf{A}\cdot\mathbf{u})(\mathbf{B}\cdot\mathbf{n})\big]\,\mathrm{d}S = \\
&= -\int_S (\mathbf{A}\cdot\mathbf{B})(\mathbf{u}\cdot\mathbf{n})\,\mathrm{d}S\,.
\end{aligned}$$

The second term in the penultimate line vanishes because the normal component $\mathbf{B}\cdot\mathbf{n}$ is zero at the boundary by assumption (3). The remaining non-zero term cancels out with the last term in the equation, leaving:

$$\frac{\mathrm{d}K}{\mathrm{d}t} = \int_V \frac{\partial \mathbf{A}}{\partial t}\cdot\mathbf{B}\,\mathrm{d}^3\mathbf{x}\,. \tag{1.253}$$

The time derivative of the vector potential follows from the electric field equation:

$$\mathbf{E} = -\boldsymbol{\nabla}\phi - \frac{\partial \mathbf{A}}{\partial t} \tag{1.254}$$

and then substitution it into the equation: (1.253) yields:

$$\begin{aligned}
\frac{\mathrm{d}K}{\mathrm{d}t} &= -\int_V (\mathbf{E}\cdot\mathbf{B} + \nabla\phi\cdot\mathbf{B})\,\mathrm{d}^3\mathbf{x} = \\
&= -\int_V \big[(-\mathbf{u}\times\mathbf{B})\cdot\mathbf{B} + \mathrm{div}(\phi\mathbf{B})\big]\,\mathrm{d}^3\mathbf{x} = \\
&= -\int_S \phi(\mathbf{B}\cdot\mathbf{n})\,\mathrm{d}S = 0\,.
\end{aligned} \tag{1.255}$$

Under the assumptions mentioned above, the integral helicity is therefore conserved.

State with Minimum Magnetic Energy

Consider a magnetic tube filled with a perfectly conducting plasma, where the surface normal component of the magnetic field is zero. Diffusion is negligible, so the magnetic helicity K is conserved. The magnetic energy extremum is sought under the constraint of helicity conservation. Using the method of Lagrange multipliers, the necessary condition for extremality is:

$$\delta(W_\mathrm{M} + \lambda K) = 0 \qquad \Rightarrow$$

$$\delta \int \left(\frac{B^2}{2\mu_0} + \lambda \mathbf{A}\cdot\mathbf{B} \right) \mathrm{d}^3\mathbf{x} = 0 \qquad \Rightarrow$$

$$\int \left(\frac{1}{\mu_0}\mathbf{B}\cdot\delta\mathbf{B} + \lambda\,\delta\mathbf{A}\cdot\mathbf{B} + \lambda\,\mathbf{A}\cdot\delta\mathbf{B} \right) \mathrm{d}^3\mathbf{x} = 0\,.$$

The variation of the field $\delta\mathbf{B}$ is related to the variation of the magnetic potential $\delta\mathbf{A}$. Since $\mathbf{B} = \nabla\times\mathbf{A}$, the relation $\delta\mathbf{B} = \nabla\times\delta\mathrm{A}$ holds (derivatives and variations commute):

$$\int \left(\frac{1}{\mu_0}\mathbf{B}\cdot(\nabla\times\delta\mathbf{A}) + \lambda\,\delta\mathbf{A}\cdot\mathbf{B} + \lambda\,\mathbf{A}\cdot(\nabla\times\delta\mathbf{A}) \right) \mathrm{d}^3\mathbf{x} = 0\,.$$

The terms involving curl ($\nabla\times$) are converted to divergence using the identity (*Selected Topics I*, Eq. I3.120) $\mathbf{A}\cdot(\nabla\times\mathbf{B}) = \mathbf{B}\cdot(\nabla\times\mathbf{A}) - \mathrm{div}(\mathbf{A}\times\mathbf{B})$:

$$\int \left(-\frac{1}{\mu_0}\mathrm{div}\left(\mathbf{B}\times\delta\mathbf{A}\right) + \frac{1}{\mu_0}(\nabla\times\mathbf{B})\cdot\delta\mathbf{A} + \lambda\,\delta\mathbf{A}\cdot\mathbf{B} - \lambda\,\mathrm{div}\left(\mathbf{A}\times\delta\mathbf{A}\right) + \lambda(\nabla\times\mathbf{A})\cdot\delta\mathbf{A} \right) \mathrm{d}^3\mathbf{x} = 0.$$

Using the Gauss theorem, divergence integrals are converted into surface integrals over the magnetic tube by substituting $\nabla\times\mathbf{A} = \mathbf{B}$:

$$-\int_{\partial V} \left[\left(\frac{1}{\mu_0}\mathbf{B} + \lambda\,\mathbf{A} \right) \times \delta\mathbf{A} \right] \cdot \mathrm{d}\mathbf{S} \;+\; \int_V \left[\left(\frac{1}{\mu_0}\nabla\times\mathbf{B} + 2\lambda\mathbf{B} \right) \cdot \delta\mathbf{A} \right] \mathrm{d}^3\mathbf{x} = 0\,.$$

The variation of the vector potential must be zero at the boundary of the region, and therefore the first integral vanishes:

$$\int_V \left[\left(\frac{1}{\mu_0}\,\nabla\times\mathbf{B} + 2\lambda\mathbf{B} \right) \cdot \delta\mathbf{A} \right] \mathrm{d}^3\mathbf{x} = 0\,.$$

Since this result holds for any region and the variations of the vector potential components δA_k are independent, the integrand itself must be zero ("almost everywhere"):

$$\frac{1}{\mu_0}\,\nabla\times\mathbf{B} + 2\lambda\mathbf{B} = 0\,.$$

From this, the necessary condition for the extremality of the magnetic energy follows:

► $$\nabla\times\mathbf{B} = \alpha\mathbf{B}\,. \qquad (1.256)$$

In the state of minimum energy, under the condition of magnetic helicity conservation, the magnetic field is therefore a Beltrami field. The current density points in the direc-

tion of the field; this represents a force-free configuration in which currents flow along the magnetic field lines (so-called Birkeland currents). The state of minimum magnetic energy is necessarily helical. The magnetic field satisfies the Helmholtz equation, which is obtained by applying a curl operation to the equation (1.256):

► $$\left(\nabla^2 + \alpha^2\right)\mathbf{B} = 0\,. \tag{1.257}$$

However, not all solutions to equation (1.257) solve the original equation (1.256) since differentiation increased its order. The Helmholtz equation (1.257) is therefore no longer a necessary condition for energy extremality. If plasma has finite conductivity, energy dissipation and magnetic reconnection occur. The plasma strives for a force-free state with minimum magnetic energy, but helicity changes during these processes.

Dissipation of Magnetic Helicity

The details in this subsection may be skipped without loss of continuity. If the system has closed magnetic field lines (zero normal component of the magnetic field at the surface), the only ways to alter the field's helicity are through dissipative processes and field line reconnection. Performing the step-by-step derivation given above with the diffusion term included yields the simple relation:

$$\frac{\mathrm{d}K}{\mathrm{d}t} = -\frac{1}{\sigma}\int_V \mathbf{j}\cdot\mathbf{B}\,\mathrm{d}^3\mathbf{x}\,. \tag{1.258}$$

The energy of the magnetic field is given by the relation

$$W_\mathrm{M} = \frac{1}{2\mu}\int_V B^2\,\mathrm{d}^3\mathbf{x}\,. \tag{1.259}$$

The time derivative of the energy is given by Joule dissipation

$$\frac{\mathrm{d}W_\mathrm{M}}{\mathrm{d}t} = -\frac{1}{\sigma}\int_V j^2\,\mathrm{d}^3\mathbf{x}\,. \tag{1.260}$$

For further calculation, the Schwarz inequality (I.3.165) in the L^2 space is utilized:

$$\left|\langle \mathbf{j}|\mathbf{B}\rangle\right| \le \|\mathbf{j}\|\cdot\|\mathbf{B}\| \quad \Rightarrow \quad \left|\int \mathbf{j}\cdot\mathbf{B}\,\mathrm{d}^3\mathbf{x}\right| \le \sqrt{\int j^2\,\mathrm{d}^3\mathbf{x}}\,\sqrt{\int B^2\,\mathrm{d}^3\mathbf{x}}\,.$$

This immediately yields the estimate

$$\left|\frac{\mathrm{d}K}{\mathrm{d}t}\right| \le \left(\frac{2\mu}{\sigma}W_\mathrm{M}\left|\frac{\mathrm{d}W_\mathrm{M}}{\mathrm{d}t}\right|\right)^{1/2}. \tag{1.261}$$

The relation is further refined using two additional dimensional estimates. The ratio of magnetic energy to helicity is inversely proportional to the dimensions of the system:

$$\frac{W_\mathrm{M}}{|K|} \sim \frac{(B^2/2\mu)\Delta V}{|AB|\Delta V} \sim \frac{B^2/2\mu}{BL\cdot B} = \frac{1}{2\mu_0 L} \quad \Rightarrow \quad W_\mathrm{M} \sim \frac{|K|}{2\mu L}\,. \tag{1.262}$$

The second estimate is the characteristic magnetic field diffusion time (resistive time):

$$\partial \mathbf{B}/\partial t = \frac{1}{\sigma\mu}\nabla^2\mathbf{B} \quad \Rightarrow \quad B/\tau_\mathrm{R} \simeq \frac{1}{\sigma\mu}B/L^2 \quad \Rightarrow \quad \tau_\mathrm{R} \sim L^2\sigma\mu\,. \tag{1.263}$$

The estimate (1.261) can now be rewritten in the standard form:

$$\left|\frac{\Delta K}{\Delta t}\right| \lesssim \left(\frac{2\mu}{\sigma}\frac{|K|}{2\mu L}\frac{|K|}{2\mu L\,\Delta t}\right)^{1/2} = \left(\frac{K^2}{2\sigma\mu L^2\Delta t}\right)^{1/2} = \left(\frac{K^2}{2\tau_\mathrm{R}\Delta t}\right)^{1/2}$$

and for the relative change in helicity, the order-of-magnitude estimate is

► $$\left|\frac{\Delta K}{K}\right| < \left(\frac{\Delta t}{\tau_\mathrm{R}}\right)^{1/2}. \tag{1.264}$$

For rapid processes ($\Delta t \ll \tau_\mathrm{R}$), the change in helicity ΔK is negligible. For example, solar coronal eruptions with a reconnection time $\Delta t \sim 1{,}000$ s, linear dimensions $L \sim 5{,}000$ km, and a magnetic diffusion coefficient $\eta_\mathrm{M} \sim 10^{-6}$ km^{2}s^{-1} yield a characteristic resistive time $\tau_\mathrm{R} \sim 10^{13}$ s and a relative change in helicity $\Delta K/K < 10^{-5}$. The opposite situation occurs in tokamak plasma. The resistive time is on the order of seconds, and the residence time is in the tens of seconds. The change in helicity is significant here.

Fluid Dynamo

A very important aspect of magnetohydrodynamics is the generation of magnetic fields within the interiors of the Sun, stars, and planets. Current fluid dynamo theory does not explain the initial origin of these fields, but it successfully describes their maintenance, amplification, and periodic switching between dipolar and azimuthal components.

Cowling Anti-Dynamo Theorem

In 1934, the English astronomer Thomas George Cowling demonstrated that a stationary, axially symmetric magnetic field cannot be generated by an axially symmetric plasma flow. Consider a simple axially symmetric field as illustrated in the figure.

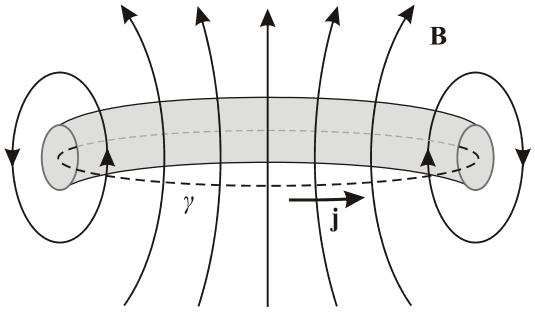


Fig. 1.35: Schematic representation of the anti-dynamo theorem.

The electric current generating the field flows within a current tube along a neutral line, where the magnetic field curl is nonzero while the field itself vanishes. The neutral line is shown by a dashed line in the figure. The current density along this neutral line is integrated using the Ohm law (1.174):

$$\oint_{\gamma} \mathbf{j} \cdot \mathrm{d}\mathbf{l} = \oint_{\gamma} \sigma \left(\mathbf{E} + \mathbf{u} \times \mathbf{B} \right) \cdot \mathrm{d}\mathbf{l} \, .$$

Since the magnetic field vanishes along the neutral line, the second term of the integral is identical to zero. Converting the first term to a surface integral via the Stokes theorem and simplifying using the Maxwell equations, stationarity implies that this term vanishes as well:

$$\oint_{\gamma} \mathbf{j} \cdot \mathrm{d}\mathbf{l} = \sigma \int_{S} (\nabla \times \mathbf{E}) \cdot \mathrm{d}\mathbf{S} = \sigma \int_{S} \left(-\frac{\partial \mathbf{B}}{\partial t} \right) \cdot \mathrm{d}\mathbf{S} = 0.$$

This contradicts the assumption that a stationary, axially symmetric field is generated by a nonzero current along the neutral line. Consequently, field generation must be more complex, requiring a continuous transfer between the dipole and azimuthal components.

Parker Fluid Dynamo Model

The fluid dynamo theory was developed by Eugene Parker, with key contributions from Yakov Zeldovich and Henry Moffatt. Differential rotation stretches initially dipolar field lines azimuthally in regions where rotation is faster (e.g., near the solar equator), thereby increasing their length. This mechanism is called the *Omega effect* (named after the symbol Ω for angular frequency and the characteristic shape of the field lines), which transforms the dipole component into an azimuthal one. On the Sun, this occurs near the tachocline – the radiative-convective transition region located ~220,000 km below the surface – where a magnetic field line takes about 8 months to loop the Sun. On Earth, a similar phenomenon takes place within the viscous conductive medium at the core-mantle boundary.

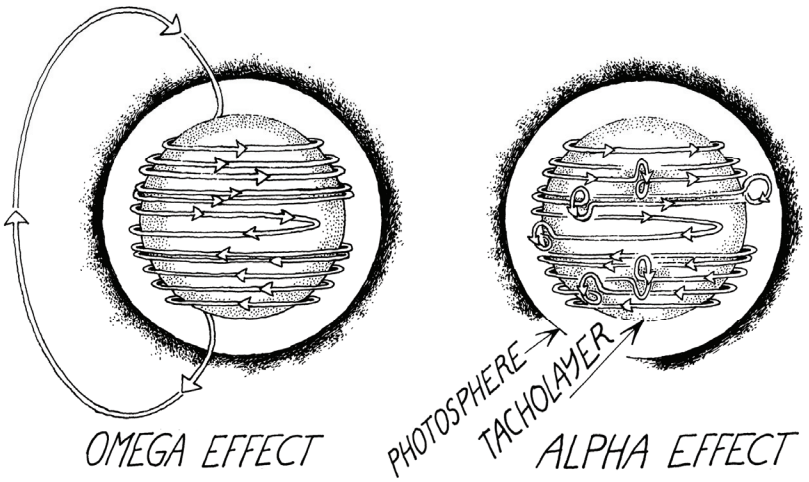


Fig. 1.36: Spatial mechanism of the solar dynamo.

The second significant phenomenon is the *alpha effect*. In this process, the magnetic tube is deflected by the Coriolis force, causing it to deform and twist back into a dipole component. This phenomenon is named after the shape of the deflected field line, which resembles the Greek letter α. These combined processes enable the mutual transforma-

tion of both field components and the long-term maintenance of the magnetic field by a fluid dynamo. One component is always gradually amplified at the expense of the other, and then vice versa, causing the magnetic dipole to reverse regularly. For the Sun, the full magnetic cycle (the time required for the magnetic north pole to return to its original position) lasts 22 years. During the dipole reversal period, the field exhibits significantly higher multipole moments (quadrupole and octupole), resembling a highly distorted sphere where multiple regions of emerging and receding magnetic field lines alternate across the surface.

Deriving the omega and alpha effects requires both differential rotation and macroturbulent fluctuations in the magnetic and velocity fields. Both fields are decomposed into a component averaged over *short-term fluctuations* and a fluctuating component:

$$\mathbf{u} = \langle \mathbf{u} \rangle + \delta\mathbf{u}\,; \qquad \mathbf{B} = \langle \mathbf{B} \rangle + \delta\mathbf{B}\,. \tag{1.265}$$

The mean values of the fluctuation components are clearly zero:

$$\langle \delta\mathbf{u} \rangle = 0\,; \qquad \langle \delta\mathbf{B} \rangle = 0\,. \tag{1.266}$$

Substituting decomposition (1.265) into the field equation ((1.177) yields:

$$\frac{\partial\left[\langle \mathbf{B} \rangle + \delta\mathbf{B}\right]}{\partial t} = \frac{1}{\sigma\mu}\nabla^2\left[\langle \mathbf{B} \rangle + \delta\mathbf{B}\right] + \operatorname{curl}\left[\left(\langle \mathbf{u} \rangle + \delta\mathbf{u}\right)\times\left(\langle \mathbf{B} \rangle + \delta\mathbf{B}\right)\right]. \tag{1.267}$$

By averaging this equation, the terms linear in the fluctuations disappear, and we thus obtain the equation for the mean value of the magnetic field:

► $$\frac{\partial\langle \mathbf{B} \rangle}{\partial t} = \frac{1}{\sigma\mu}\nabla^2\langle \mathbf{B} \rangle + \operatorname{curl}\left[\langle \mathbf{u} \rangle\times\langle \mathbf{B} \rangle\right] + \operatorname{curl}\left\langle \delta\mathbf{u}\times\delta\mathbf{B}\right\rangle. \tag{1.268}$$

If we now subtract the equation for the mean values (1.268) from (1.267), we obtain the equation for the fluctuations of the magnetic field

► $$\frac{\partial}{\partial t}\left(\delta\mathbf{B}\right) = \frac{1}{\sigma\mu}\nabla^2\left(\delta\mathbf{B}\right) + \operatorname{curl}\left[\langle \mathbf{u} \rangle\times\delta\mathbf{B} + \delta\mathbf{u}\times\langle \mathbf{B} \rangle + \delta\mathbf{u}\times\delta\mathbf{B} - \langle \delta\mathbf{u}\times\delta\mathbf{B} \rangle\right]. \tag{1.269}$$

We have thus obtained equations for both the time evolution of the mean field value and the time evolution of the fluctuation component. The first term on the right-hand side of equation (1.268) describes standard field diffusion; the second term is responsible for the *Ω effect*; and the third term is responsible for the *α effect*, which originates from fluctuations in the velocity and magnetic fields.

Omega Effect

The second term of equation (1.268) is essential for the *Ω* effect:

► $$\frac{\partial\langle \mathbf{B} \rangle}{\partial t} = \operatorname{curl}\left[\langle \mathbf{u} \rangle\times\langle \mathbf{B} \rangle\right]. \tag{1.270}$$

The mean magnetic field is frozen into the mean velocity field, meaning it follows the macroscopic plasma motion. If a body rotates at a constant angular velocity, the dipole field remains unchanged. However, the Sun undergoes differential rotation; the equatorial angular velocity is approximately one-third greater than at the poles, generating a strong azimuthal magnetic field component. Notably, solar differential rotation is also non-zero in the radial direction near the tachocline.

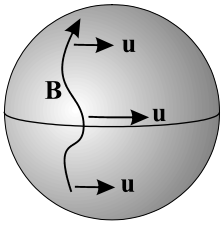


Fig. 1.37: Schematic of the omega effect driven by differential rotation.

Alpha Effect

The third term of equation (1.268) governs the α effect:

$$\frac{\partial \langle \mathbf{B} \rangle}{\partial t} = \operatorname{curl} \boldsymbol{\varepsilon}; \qquad \boldsymbol{\varepsilon} \equiv \left\langle \delta \mathbf{u} \times \delta \mathbf{B} \right\rangle. \tag{1.271}$$

The α effect transforms the azimuthal magnetic field component back into a dipole component, driven entirely by velocity and magnetic field fluctuations. Statistically, the expression $\boldsymbol{\varepsilon} \equiv \langle \delta \mathbf{u} \times \delta \mathbf{B} \rangle$ represents the correlation function between these fluctuating components. A vanishing value would imply a total lack of correlation, which does not hold for a turbulent conductive fluid. This correlation function is highly complex and typically requires numerical resolution of the magnetic field fluctuation equation (1.269). This equation demonstrates that the field fluctuation is directly proportional to its mean value; thus, for a slowly varying field, the correlation function takes the form:

$$\varepsilon_k = \alpha_{kl} \langle B_l \rangle + \beta_{klm} \partial_l \langle B_m \rangle + \cdots \tag{1.272}$$

The coefficients α and β depend on the statistical properties of the turbulent fluctuations. For isotropic turbulence, the correlation function simplifies to

$$\varepsilon_k = \alpha \langle B_k \rangle + \beta \varepsilon_{klm} \partial_l \langle B_m \rangle + \cdots \tag{1.273}$$

Substituting this into the equation (1.271) yields the relation

$$\frac{\partial \langle \mathbf{B} \rangle}{\partial t} = \alpha \operatorname{curl} \langle \mathbf{B} \rangle - \beta \Delta \langle \mathbf{B} \rangle + \cdots \tag{1.274}$$

The first term on the right-hand side describes the α effect – a positive feedback mechanism where the temporal variation of the mean field is proportional to the field itself, allowing a macroscopic order to emerge from turbulent fluctuations. The effect is named after the coefficient α. The second term ($\beta < 0$) represents turbulent diffusion. Since the mean field $\langle \mathbf{B} \rangle$ is an axial vector, α must be a pseudoscalar quantity that changes sign under a coordinate system inversion. A straightforward measure of this mirror symmetry loss is the kinetic helicity density. If the kinetic helicity is non-zero – for instance, due to the action of the Coriolis force – the magnetic field automatically becomes helical, developing a growing perpendicular component. In helical fields, a portion of the field represents a Beltrami field, where $\operatorname{curl} \langle \mathbf{B} \rangle \sim \langle \mathbf{B} \rangle$, and thus $\partial \langle \mathbf{B} \rangle / \partial t \sim \langle \mathbf{B} \rangle$. This feedback amplifies any statistical transverse component until saturation occurs. Consequently, three conditions are essential for the α effect:

1) The plasma possesses a finite, non-zero resistivity, as only then is magnetic helicity not strictly conserved, allowing the fields to become helical.
2) The velocity fluctuations are helical, ensuring the pseudoscalar nature of the coefficient α.
3) Positive feedback must occur, meaning small perturbations must grow, and linear perturbation analysis must indicate a plasma instability. For stellar plasma, this condition is satisfied.

In the Sun, the most critical region for the α effect is the tachocline at the bottom of the convective zone, where downflows reverse into upflows, resulting in large and predominantly helical fluctuations in the velocity field.

◖ **Example 1.2:** Consider a circularly polarized wave generated in the plasma propagating along the z-axis (locally, this can also represent the azimuthal direction):

$$\delta\mathbf{u} = \left(u_0 \cos(kz - \omega t),\, u_0 \sin(kz - \omega t),\, 0\right).$$

The result of such a perturbation is a nonzero vorticity field:

$$\delta\boldsymbol{\omega} = \operatorname{curl} \delta\mathbf{u} = -k\,\delta\mathbf{u}\,.$$

The considered velocity field fluctuation is a Beltrami field and has a helicity density

$$\mathcal{H} = \delta\mathbf{u} \cdot \delta\boldsymbol{\omega} = -ku_0^2\,.$$

Such a localized fluid flow immediately leads to the deformation of the magnetic field into a helical structure. ◗

The curl of the mean magnetic field is proportional to the mean current density; therefore, the newly emerging field develops a component in the direction of the flowing current. As a result of these fluctuations, the magnetic field acquires a component parallel to the current density, making the newly emerging and amplifying part of the field necessarily helical (a Beltrami field). This process creates a field component perpendicular to the original background field. If the velocity fluctuations are periodic, as in the case of a circularly polarized wave, the direction of the induced current also varies periodically, causing the magnetic field to form a twisted loop **Chyba! Nenalezen zdroj odkazů.**:

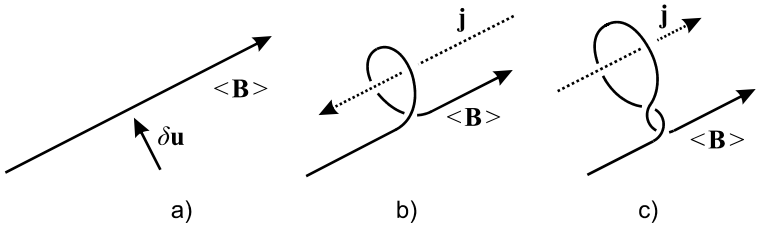


Fig. 1.38: Twisting of a magnetic flux loop driven by helical fluctuations.

Finally, the α effect alone is sufficient to flip both the toroidal component into the poloidal configuration and vice versa. A dynamo model based solely on the α effect is referred to as an $\alpha\alpha$ model. A much more effective mechanism, however, is the previously described Parker or $\alpha\Omega$ model.

◖ **Example 1.3:** An estimation of the correlation function for a plasma with a high magnetic Reynolds number. Such a situation occurs both on the Sun and in fusion plasmas. The details in this example may be skipped without loss of continuity.

Solution: In equation (1.269) for magnetic field fluctuations, the third term dominates on the right-hand side, since magnetic fluctuations are primarily caused by fluctuations in the velocity field. The first term is negligible given the assumption of a high magnetic Reynolds number, and terms involving the second powers of the fluctuations are of a higher order. Therefore, in our approximation, the field fluctuation is given by:

$$\frac{\partial}{\partial t}(\,\delta\mathbf{B}) \;\approx\; \mathrm{curl}\big[\,\delta\mathbf{u}\times\langle\mathbf{B}\rangle\big] \;\;\Rightarrow$$

$$\delta B_k \;\approx\; \int_0^t \varepsilon_{klm}\varepsilon_{mno}\partial_l \delta u_n(t')\langle B_o\rangle(t')\,\mathrm{d}t'\,,$$

where the fluctuation has been integrated over time and the vector triple product has been expanded. Obvious spatial dependencies are omitted from the notation. Expanding the vector triple product yields:

$$\delta B_k \;\approx\; \int_0^t \partial_n \delta u_k(t')\langle B_n\rangle(t')\,\mathrm{d}t' - \int_0^t \partial_n \delta u_n(t')\langle B_k\rangle(t')\,\mathrm{d}t'\,.$$

In the next step, the derivatives of the product are performed, assuming that the plasma behaves as an incompressible fluid (the divergences of both fields are zero):

$$\delta B_k \;\approx\; \int_0^t \delta u_{k,n}(t')\,\langle B_n\rangle(t')\,\mathrm{d}t' - \int_0^t \delta u_n(t')\big\langle B_{k,n}\big\rangle(t')\,\mathrm{d}t'\,.$$

Partial derivatives are written in shorthand as a subscript after a comma. The correlation function $\boldsymbol{\varepsilon} \equiv \langle\, \delta\mathbf{u}\times\delta\mathbf{B}\,\rangle$, which is responsible for the α effect, can now be calculated:

$$\varepsilon_i \equiv \varepsilon_{ijk}\left\langle \delta u_j \delta B_k \right\rangle =$$

$$= \left\langle \int_0^t \varepsilon_{ijk}\,\delta u_j(t)\,\delta u_{k,n}(t')\langle B_n\rangle(t')\,\mathrm{d}t' \right\rangle - \left\langle \int_0^t \varepsilon_{ijk}\,\delta u_j(t)\,\delta u_n(t')\big\langle B_{k,n}\big\rangle(t')\,\mathrm{d}t' \right\rangle.$$

The result expressed as follows:

$$\varepsilon_i = \left\langle \int_0^t \alpha_{in}(t,t')\,\langle B_n\rangle(t')\,\mathrm{d}t' \right\rangle - \left\langle \int_0^t \eta_{ikn}(t,t')\,\big\langle B_{k,n}\big\rangle(t')\,\mathrm{d}t' \right\rangle;$$

$$\alpha_{in}(t,t') \equiv \varepsilon_{ijk}\,\delta u_j(t)\,\delta u_{k,n}(t')\,, \qquad (1.275)$$

$$\eta_{ikn}(t,t') \equiv \varepsilon_{ijk}\,\delta u_j(t)\,\delta u_n(t')\,.$$

The correlation coefficients can be assumed to be a function of time separation, i.e.,

$$\alpha_{in}(t,t') \equiv \alpha_{in}(t-t')\,, \qquad (1.276)$$

$$\eta_{ikn}(t,t') \equiv \eta_{ikn}(t-t').$$

They rapidly converge to zero in the past. The slowly varying mean value of the field and its derivative can then be factored out of the integral (1.275):

$$\varepsilon_i(t) = \tilde{\alpha}_{in}(t)\langle B_n \rangle(t) - \tilde{\eta}_{ikn}(t)\langle B_{k,n} \rangle(t)\,;$$

$$\tilde{\alpha}_{in}(t) \equiv \left\langle \int_0^t \alpha_{in}(t-t')\ \mathrm{d}t' \right\rangle, \tag{1.277}$$

$$\tilde{\eta}_{ikn}(t) \equiv \left\langle \int_0^t \eta_{ikn}(t-t')\,\mathrm{d}t' \right\rangle.$$

In this approximation, the magnetic field fluctuation is therefore proportional to the mean value of the field itself and its derivatives. The proportionality coefficients are given by integrals over the fluctuations of the velocity field. If, for simplicity, the plasma is assumed to be isotropic (though not always true), the following relations hold:

$$\begin{aligned} \tilde{\alpha}_{in} &\sim \delta_{in}\,, \\ \tilde{\eta}_{ikn} &\sim \varepsilon_{ikn}\,. \end{aligned} \tag{1.278}$$

Under these simplifying assumptions, the correlation function $\boldsymbol{\varepsilon} \equiv \langle\, \delta\mathbf{u}\times\delta\mathbf{B} \,\rangle$ is given by

$$\boldsymbol{\varepsilon} = \alpha\langle \mathbf{B} \rangle - \eta\mathbf{J} \tag{1.279}$$

and indeed has a component proportional to the mean value of the field.

◗

In general, field component determination requires computationally intensive numerical simulations of the alpha-omega governing equations. The figure shows results of such Earth's dynamo simulations from a supercomputing center in San Diego.

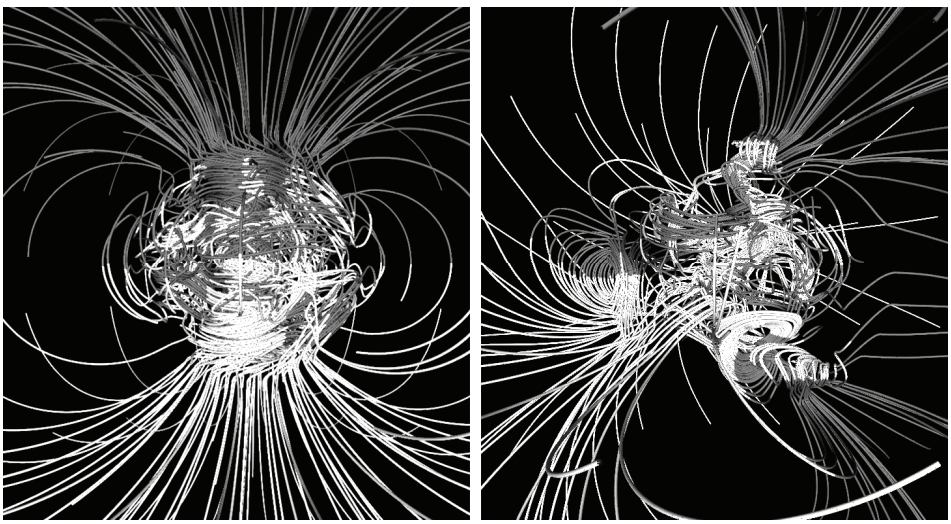


Fig. 1.39: Computer simulation of a fluid dynamo inside the Earth. The shades distinguish between incoming and outgoing magnetic field lines. On the left is a predominantly dipole field; on the right is the state during a pole reversal, when the Earth has several north and south poles. San Diego Supercomputer Center, 1999. Gary Glatzmaier, Paul Roberts.

Reconnection of Magnetic Field Lines

In nature, magnetic fields from different sources commonly interact, forming complex network structures. For example, a compass needle features both closed field lines and open lines that emanate from its poles. These lines connect directly to the Earth magnetic field lines, causing the compass needle to align toward the magnetic north.

During this interaction, magnetic field lines frequently break and reconnect – a process known as *magnetic reconnection*. Through this mechanism, a magnetic field transitions, often rapidly, to a lower-energy state by altering the topology of its field lines. The field lines rearrange into a different, energetically more favorable configuration, and the released magnetic energy heats the surrounding plasma. Magnetic reconnection typically occurs in regions where magnetic field lines point in opposite directions. This scenario takes place, for instance, within the magnetic loops of the solar corona, at the dayside boundary of the Earth magnetosphere, or within the Earth magnetotail.

No satisfactory analytical model describes reconnection across all scales; most balance inflow and outflow, leaving details to numerical simulations. Ideal MHD, assuming infinite conductivity, cannot describe reconnection. In ideal environments, the induction equation contains only the convective term, perfectly freezing the plasma to the magnetic field. For an incompressible fluid div $\mathbf{u} = 0$, corresponding to div $\mathbf{B} = 0$, plasma flow across field lines is impossible, dissipation is absent, magnetic flux and helicity are conserved, and particles remain trapped on their original field lines. Any topological change is strictly forbidden.

To describe the reconnection of magnetic field lines within fluid models, it is therefore necessary to employ *resistive magnetohydrodynamics*, which accounts for a finite plasma resistivity. The energy accumulated in the magnetic field can only be released via topological transitions if the plasma possesses a finite resistivity.

In resistive magnetohydrodynamics, the resistive time constant (1.263) – derived by dimensional analysis from the diffusion equation – plays a crucial role. This quantity represents the characteristic time constant of magnetic diffusion driven by the finite plasma resistivity.

Most macroscopic motions in a magnetized plasma are characterized by the Alfvén speed (1.237). The time required for a perturbation to propagate through the plasma at this speed is termed the Alfvén time. Both characteristic time scales are given by:

$$\tau_{\mathrm{R}} \sim L^2 \sigma \mu \,; \qquad \tau_{\mathrm{A}} \sim \frac{L}{v_{\mathrm{A}}} = \frac{L\sqrt{\mu\rho}}{B_0} \,. \tag{1.280}$$

Experiments indicate that the typical reconnection time scale lies between these two values and is approximately equal to their geometric mean:

$$\tau_{\mathrm{REC}} = \sqrt{\tau_{\mathrm{R}} \tau_{\mathrm{A}}} \,. \tag{1.281}$$

An important plasma characteristic is the *Lundquist number* $\#_{\mathrm{Lu}}$ (sometimes denoted by S), defined as the ratio of the resistive time to the Alfvén time:

$$\#_{\mathrm{Lu}} \equiv S \equiv \frac{\tau_{\mathrm{R}}}{\tau_{\mathrm{A}}} = \frac{L^2 \sigma \mu}{L / v_A} = L \sigma \mu v_{\mathrm{A}} \,. \tag{1.282}$$

The Lundquist number equals the magnetic Reynolds number if the flow velocity is replaced by the Alfvén velocity. For various plasmas, the following values hold [16]:

Plasma	L (m)	τ_R (s)	τ_A (s)	$\#_{Lu}$
Arc	10^{-1}	10^{-3}	10^{-3}	1
Tokamak	1	1	10^{-8}	10^{8}
Earth's core	10^{6}	10^{12}	10^{5}	10^{7}
Sunspot	10^{7}	10^{14}	10^{5}	10^{9}
Solar corona	10^{9}	10^{18}	10^{6}	10^{12}

Except for low-temperature arc plasmas, the Lundquist number is very high; for fusion and astrophysical plasmas, the convective term dominates the induction equation. Ideal MHD thus applies to most of the plasma volume. Reconnection regions, where diffusion dominates, are limited to narrow zones of weak or zero field. Within these diffusion regions, resistive MHD equations must be used and matched at boundaries to the external ideal MHD. Typically, the energy continuity equation is included, as energy transfer is highly significant.

Spontaneous 2D Reconnection in Magnetic Layer

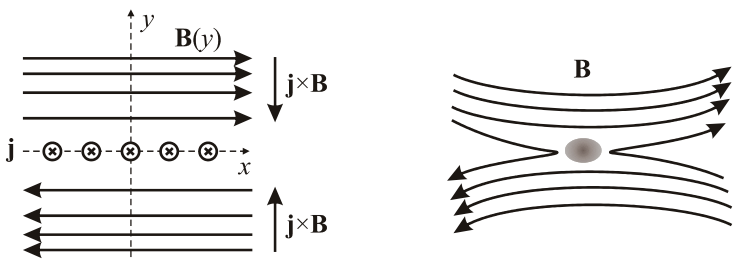


Fig. 1.40: Principle of magnetic field line reconnection.

The simplest possible configuration is illustrated in the figure. In the perpendicular direction (along the y-axis), the magnetic field gradually weakens to zero at $y = 0$, where the field reverses its direction and begins to grow again. In this region of zero magnetic field, a strong electric current must flow, as the magnetic field curl is non-zero. In the (xz) plane, a so-called neutral layer forms, with the current density directed along the z-axis. The Lorentz force $\mathbf{j}\times\mathbf{B}$ acts on the plasma, compressing it toward the neutral layer. In a plasma with zero resistivity, a static equilibrium is established between the magnitude of the Lorentz force and the plasma pressure gradient, and all macroscopic motion ceases.

However, if the plasma possesses a finite resistivity, the magnetic field lines are no longer frozen into the fluid, allowing the plasma to drift across the field lines. The velocity of this motion is given by the first term of the general drift equation(1.110):

$$\mathbf{u}_\mathrm{d} = \frac{\mathbf{E}\times\mathbf{B}}{B^2} \approx \frac{\mathbf{j}\times\mathbf{B}}{\sigma B^2} = \frac{\mathrm{curl}\,\mathbf{B}\times\mathbf{B}}{\sigma\mu B^2}\,. \tag{1.283}$$

The relative motion of the plasma and the magnetic field lines within a medium with a finite resistivity causes them to break and reconnect to alternative field lines. The released magnetic energy subsequently heats the plasma via the Joule effect. Depending on the geometry of the field lines, the specific point at which the reconnection takes place is termed an X-point. Frequently, a multitude of such points develop within the neutral layer, and so-called magnetic islands (plasmoids) form between them, at the centers of which O-points are located:

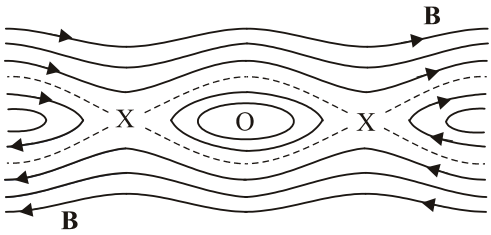


Fig. 1.41: X-points and O-points formed during field line reconnection.

The dashed line indicates the *separatrix*, a curve separating distinct magnetic field topologies. In the upper region, the magnetic field lines point in one direction, whereas in the lower region, they point in the opposite direction. Magnetic islands have formed in the vicinity of the neutral layer.

To evaluate the reconnection rate, a dimensionless quantity termed the *reconnection index* (or Mach–Alfvén number) is utilized. The reconnection index is defined as the ratio of the velocity of the plasma entering the reconnection region to the Alfvén velocity at which the plasma is spontaneously expelled from this region. For spontaneous 2D reconnection, the system yields:

$$\#_\mathrm{sp} = \frac{u_\mathrm{in}}{u_\mathrm{out}} \approx \frac{u_\mathrm{d}}{v_\mathrm{A}} \approx \frac{1/L\sigma\mu}{v_\mathrm{A}} = \frac{1}{L\sigma\mu\, v_\mathrm{A}} = \frac{1}{\#_\mathrm{Lu}}\,,$$

so it holds that:

► $$\#_\mathrm{sp} \approx \frac{1}{\#_\mathrm{Lu}}\,. \tag{1.284}$$

For spontaneous 2D reconnection, the reconnection index corresponds to the inverse of the Lundquist number. For both fusion and astrophysical plasmas, this index is extremely small ($u_\mathrm{in} << u_\mathrm{out}$), meaning that the reconnection process proceeds very slowly. It will be demonstrated in Section 1.3.3 that a neutral zero-field layer forms spontaneously within a sufficiently wide plasma filament. On opposite sides of this layer, the magnetic field possesses opposite polarities, triggering spontaneous 2D reconnection.

Driven 2D Reconnection (Sweet–Parker Model)

Field line reconnection does not always occur spontaneously. In the previous scenario, a neutral layer (or current sheet) formed within the plasma, and fluid motion was driven solely by relaxation processes.

Near the neutral layer, a significant resistivity increase frequently occurs due to poorly understood mechanisms. This area is termed the *diffusion region*, where plasma transport is driven by magnetic diffusion. Along the field lines, plasma flows freely out of this region at the Alfvén velocity, pushed by the magnetic pressure gradient. Typical examples include solar corona processes and subsequent flares, which represent macroscopic manifestations of the released magnetic energy.

A simple model of driven reconnection was proposed independently by the English astronomer Peter Alan Sweet in 1958 and by the American astrophysicist Eugene Parker in 1957. The model assumes that plasma regions with oppositely oriented magnetic field lines are forced by magnetic diffusion into a macroscopic diffusion region toward the neutral layer at an inflow speed u_{in}. In this narrow region, magnetic field line reconnection takes place. At the lateral boundaries, plasma is expelled out of the diffusion region at an outflow speed u_{out}, often forming high-velocity plasma jets. The Sweet–Parker model assumes that the dimensions of the region satisfy $\Delta \gg \delta$, meaning the diffusion region is highly elongated but extremely thin. The electric current flows within the x-z plane along the z-axis.

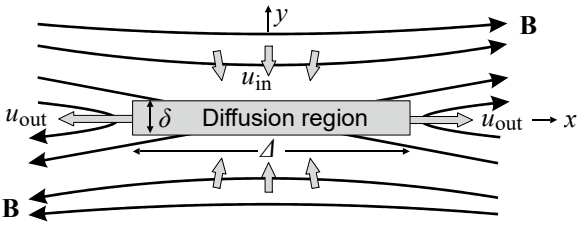


Fig. 1.42: Schematic diagram of the diffusion region.

The Sweet–Parker model is based on three fundamental assumptions:

1) The inflowing plasma follows the diffusing magnetic field lines, meaning the plasma velocity is governed by the resistive time scale τ_{R}, see (1.263):

$$u_{\text{in}} \approx \frac{\delta}{\tau_{\text{R}}} = \frac{\delta}{\delta^2 \sigma\mu} = \frac{1}{\delta\sigma\mu}. \tag{1.285}$$

2) The outflowing plasma moves freely under the influence of the magnetic pressure gradient, thereby attaining the Alfvén velocity:

$$\frac{B^2}{2\mu_0} \approx \frac{1}{2}\rho u_{\text{out}}^2 \qquad \Rightarrow \qquad u_{\text{out}} \approx v_{\text{A}} = \frac{B}{\sqrt{\mu\rho}}. \tag{1.286}$$

3) The relation between the inflow and outflow velocities is governed by mass conservation (the continuity equation expressed in the form $uS = \text{const}$)

$$u_{\text{in}}\Delta = u_{\text{out}}\delta. \tag{1.287}$$

Finally, the driven reconnection index, which equals the Mach–Alfvén number, can be determined. Starting from the continuity equation (1.287)) and relation (1.285) for u_{in}:

$$\#_{\text{dr}}^2 = \frac{u_{\text{in}}}{u_{\text{out}}} \cdot \frac{u_{\text{in}}}{u_{\text{out}}} \approx \frac{\delta}{\Delta} \cdot \frac{1/\delta\sigma\mu}{v_{\text{A}}} = \frac{1}{\Delta\sigma\mu v_{\text{A}}} \approx \frac{1}{\#_{\text{Lu}}}.$$

Taking the square root yields:

$$\#_{\mathrm{dr}} \approx 1/\sqrt{\#_{\mathrm{Lu}}}\ . \tag{1.288}$$

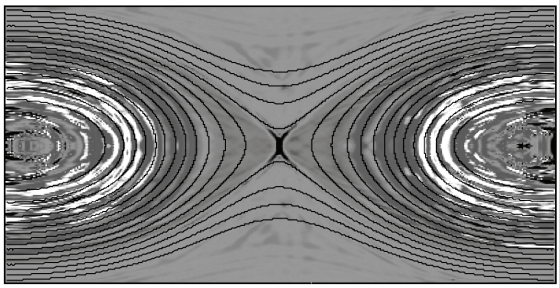


Fig. 1.43: MHD simulation of magnetic reconnection incorporating a diffusion region. The grayscale indicates current density. Simulation by Joachim Birn.

Fast 2D Reconnection (Petschek Model)

The driven reconnection index exceeds the spontaneous one, meaning driven reconnection proceeds at a faster rate. However, certain transient phenomena, such as coronal mass ejections, occur more rapidly than the Sweet–Parker model predicts. Reconnection is considered rapid if its index is ≥ 0.1. A model derived by Harry Petschek in 1964 is frequently utilized; here, reconnection is localized within a tiny region ($\Delta \approx \delta$) due to a tearing instability driven by MHD waves. A shock wave forms near the diffusion region, significantly accelerating the process. Inflow and outflow velocities differ minimally in this mechanism, and the reconnection index is given by:

$$\#_{\mathrm{P}} \approx \frac{1}{\ln(\#_{\mathrm{Lu}})}\,. \tag{1.289}$$

The Petschek model is highly effective for fast reconnection. Its primary limitation is that it does not address the physical formation of the localized enhanced resistivity region, making it internally inconsistent. It fails completely for plasma with a homogeneous resistivity profile. Furthermore, the resistivity governed by the Spitzer relation represents merely an approximation valid for small electric field values; during rapid reconnection, strong electric fields and anomalous resistivity profiles develop. The model occasionally fails even in astrophysical plasmas where the diffusion region is not spatially small. Despite these shortcomings, it represents the first model based on a tearing instability that accurately captures the fundamental physical mechanism.

Fast 2D Reconnection with the Hall Effect

For diffusion regions smaller than the ion Larmor radius, the Hall effect (the generation of electric and magnetic fields perpendicular to the flowing current) must be incorporated into the framework. The generalized Ohm law takes the form:

$$\mathbf{j} = \sigma\left(\mathbf{E} + \mathbf{u}\times\mathbf{B}\right) - \frac{\sigma}{Qn}\left(\mathbf{j}\times\mathbf{B} - \nabla p_{\mathrm{e}}\right) - \frac{\sigma}{\varepsilon_0 \omega_{\mathrm{p}}^2}\frac{\partial \mathbf{j}}{\partial t}\,. \tag{1.290}$$

The middle term involving $\mathbf{j}\times\mathbf{B}$ corresponds to the Hall effect, which significantly influences the field topology at spatial scales smaller than the characteristic periodicity of ion motion given by the Larmor radius, or the ion inertial scale:

$$R_{\mathrm{L}} = \frac{M v_{\perp}}{QB};, \tag{1.291}$$

$$R_{\mathrm{i}} = c/\omega_{\mathrm{pi}}\,. \tag{1.292}$$

At these micro-scales, electrons decouple from ions, enabling the formation of a Hall current. Under a finite resistivity, this configuration triggers rapid Petschek-type reconnection, as demonstrated by Michael Shay in 1999. If the Hall effect is considered, a collisional plasma is no longer required for reconnection to occur. This analogue of the Petschek model can be derived purely kinematically and without collisions, making it internally consistent. The resulting MHD waves belong to the group of whistler waves, and their frequency is proportional to the square of the wave vector:

$$\omega \sim k^2\,. \tag{1.293}$$

Small-scale waves reach high phase velocities, which they transfer to the plasma:

$$u_{\mathrm{out}} \sim \frac{\mathrm{d}\omega}{\mathrm{d}k} \sim k \sim \frac{1}{\delta}\,. \tag{1.294}$$

The Hall-type reconnection index is independent of the Lundquist number and is approximately equal to 0.1:

► $$\#_{\mathrm{H}} \approx 0{,}1\,. \tag{1.295}$$

A prominent example of Hall-type reconnection occurs within the Earth magnetic tail. The thickness of the current sheet is normally ~5,000 km. During geomagnetic storms, it thins drastically to ~200 km, which corresponds to the local ion Larmor radius. At that moment, rapid Hall-type reconnection occurs violently.

Turbulent 2D Reconnection (GS95 Model)

Reconnection processes can be further accelerated or influenced by the presence of waves and turbulence within the plasma. For example, in 1995, the turbulent GS95 model (named after Peter Goldreich and Seshadri Sridhar) was developed, wherein the reconnection index corresponds exactly to:

► $$\#_{\mathrm{GS}} \approx \#_{\mathrm{Lu}}^{1/4}\,. \tag{1.296}$$

Reconnection within this framework proceeds exceptionally rapidly. The diffusion region is fractal, with structures repeating down to the ion Larmor radius. Within this zone, numerous magnetic islands form a state referred to as magnetic foam. Turbulent reconnection accelerates cosmic-ray particles via the Fermi mechanism, and magnetic mirrors develop in stronger field regions. The resulting dynamic islands can also transfer energy to charged particles. Furthermore, turbulent reconnection influences star formation by effectively weakening the primordial field. If the field lines were strictly frozen, the gravitational contraction of a protostellar nebula would generate an unrealistically strong stellar magnetic field. The GS95 model was extended in 1999 by Alexander Lazarian and Ethan Vishniac into a *stochastic reconnection model* based on random field fluctuations in fully ionized, non-viscous plasma, where a growing α effect generates novel configurations.

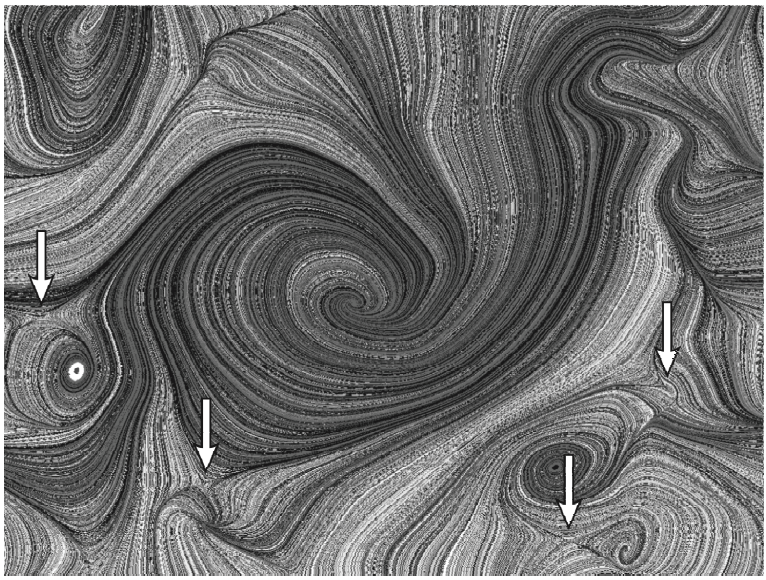


Fig. 1.44: Regions of magnetic field line reconnection obtained from the author's PIC simulations.

Three-Dimensional Reconnection and other Open Questions

If the magnetic field possesses a significant component perpendicular to the neutral layer, the process is classified as 3D reconnection. This scenario can resemble the structure illustrated in Figure 1.45; unlike in the idealized diagram, however, the fan of field lines in a realistic configuration may be further twisted into a helical spiral within the (*xy*) plane. The physical mechanisms governing 3D reconnection are currently the subject of intensive ongoing research, though many aspects remain unresolved.

Two-dimensional models describing reconnection are predominantly stationary; however, in many physical scenarios, reconnection exhibits an eruptive, transient character that these models cannot capture. Various other kinetic phenomena, such as electron-ion decoupling, anomalous resistivity, or the direct acceleration of charged particles, can also exert a significant influence on the topology changes of magnetic field lines. Furthermore, magnetic field line reconnection can occur in collisionless plasmas. The description of such collisionless processes is not based on fluid magnetohydrodynamics (which is inherently collision-dominated) but on statistical and kinetic plasma models. A complete, universally applicable description of reconnection is not currently available; it is highly probable that reconnection is driven by a variety of distinct mechanisms, most of which are investigated primarily via numerical simulations.

For macroscopic diffusion regions, the Sweet–Parker model operates successfully and was generalized to asymmetric configurations in 2007 (Paul Cassak, Michael Shay). For spatial scales smaller than the ion Larmor radius, the Hall effect must be incorporated, which entails catastrophic onset behavior and rapid Petschek-type reconnection with a reconnection index of ~0.1. A number of fundamental questions remain open: Is the rapid reconnection index universally equal to 0.1? What is the underlying physical reason? Can a strictly stationary reconnection state exist, or is it invariably an eruptive

phenomenon? How do macroscopic astrophysical phenomena (such as solar flares, magnetic storms, and coronal mass ejections) emerge from microscopic reconnection events? What is the exact role of turbulence in modulating the reconnection rate? How does three-dimensional reconnection progress in complex fields?

Finally, the foundational understanding of magnetic reconnection dates back to 1946, when the Australian astronomer Ronald Gordon Giovanelli proposed that X-shaped magnetic field null points could serve as the primary source of plasma heating and particle acceleration. The term *magnetic reconnection* was formally introduced by James Dungey, who discovered in 1953 that a change in the topology of magnetic field lines is possible exclusively in a plasma with a finite resistivity. In 1961, Dungey proposed that magnetic reconnection represents the key mechanism responsible for the transport of solar wind energy into the Earth magnetosphere. Previously, it was widely assumed that magnetic reconnection was also responsible for heating the solar corona. Today, it is well established that while micro-reconnection events do occur throughout the corona, the primary mechanism of coronal heating is the dissipation of magneto-acoustic waves.

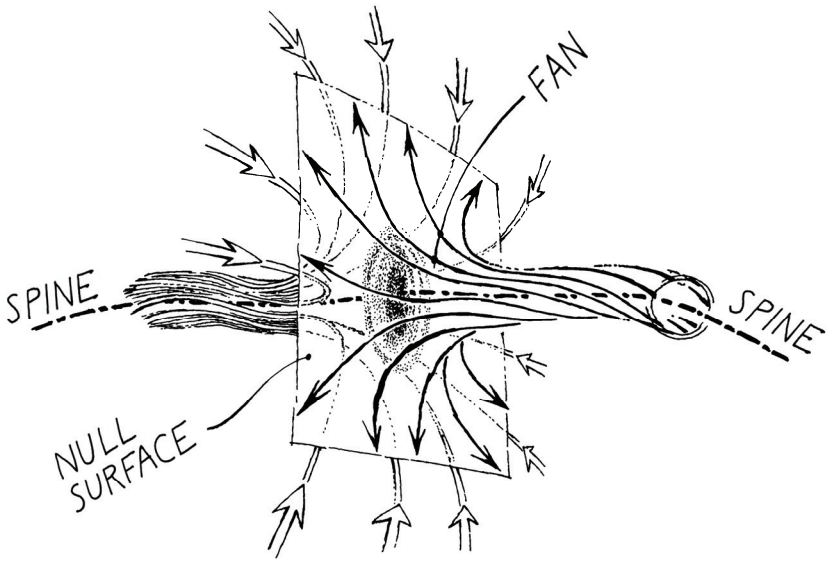


Fig. 1.45: Three-dimensional reconnection configuration of magnetic field lines.

1.3.3 Some Equilibrium Configurations in Plasma

Equilibrium in Plasma

In a steady state, where the plasma is in static equilibrium, the right-hand side of the equation of motion (1.213) vanishes:

► $$-\nabla p + \mathbf{j}\times\mathbf{B} = 0\,. \tag{1.297}$$

Viscous processes exert no influence in static equilibrium. Under these conditions, the fluid pressure gradient exactly balances the Lorentz force density. Taking the scalar product of the equilibrium equation (1.297) with either the current density or the magnetic field yields:

$$\begin{aligned} \mathbf{j}\cdot\nabla p &= 0\,, \\ \mathbf{B}\cdot\nabla p &= 0\,. \end{aligned} \tag{1.298}$$

Since the pressure gradient is orthogonal to surfaces of constant pressure, electric currents in equilibrium flow exclusively along isobaric surfaces. The same topology applies to the magnetic field lines. Consequently, current tubes are geometrically identical to magnetic flux tubes, even though the vectors **j** and **B** are generally not collinear.

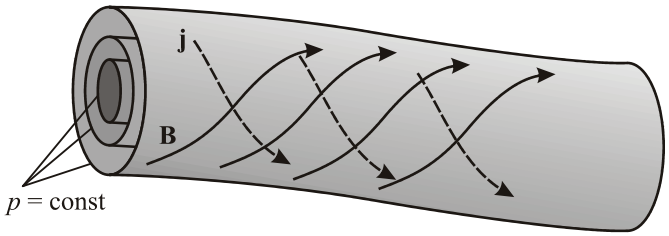


Fig. 1.46: Magnetic field and current density configurations in an equilibrium plasma.

Magnetic Surface

Assume there exists a scalar function $\psi(\mathbf{x})$ such that the surface of the magnetic flux tube is given by the equation

$$\psi(\mathbf{x}) = \text{const}\,. \tag{1.299}$$

The gradient of this function is normal to the magnetic tube surface, satisfying:

$$\mathbf{B}\cdot\nabla\psi = 0\,. \tag{1.300}$$

In cylindrical coordinates (r, φ, z), the magnetic field can be expressed via the vector potential through the relations:

$$B_r = \frac{1}{r}\frac{\partial A_z}{\partial\varphi} - \frac{\partial A_\varphi}{\partial z}\,; \qquad B_\varphi = \frac{\partial A_r}{\partial z} - \frac{\partial A_z}{\partial r}\,; \qquad B_z = \frac{1}{r}\frac{\partial}{\partial r}(rA_\varphi) - \frac{1}{r}\frac{\partial A_r}{\partial\varphi}\,. \tag{1.301}$$

The condition (1.300) can be satisfied in cylindrical coordinates for various geometric symmetries by utilizing the following formulations:

Translation symmetry ($\partial/\partial z = 0$):

$$\psi(r,\varphi) = A_z(r,\varphi)\,. \tag{1.302}$$

Axisymmetry ($\partial/\partial\varphi = 0$):

$$\psi(r,z) = rA_\varphi(r,z)\,. \tag{1.303}$$

Helical symmetry with pitch α:

$$\psi(r,\varphi-\alpha z) = A_z(r,\varphi-\alpha z)+\alpha r A_\varphi(r,\varphi-\alpha z)\,. \tag{1.304}$$

The function defining the surface of the magnetic flux tube is determined by appropriate combinations of the vector potential components under the specified spatial symmetries.

Equilibrium in Axisymmetry

Assuming axisymmetry, where all variables are independent of the toroidal angle φ (see Fig. 1.47), the magnetic surface shape function is determined from relation (1.303):

$$\psi(r,z) = rA_\varphi(r,z)\,.$$

The radial and axial components of the magnetic field follow from (1.301):

$$\begin{aligned} B_r &= -\frac{1}{r}\frac{\partial\psi}{\partial z}\,,\\ B_z &= +\frac{1}{r}\frac{\partial\psi}{\partial r}\,. \end{aligned} \tag{1.305}$$

The toroidal component is derived from the Ampère law:

$$B_\varphi = \frac{\mu_0 I(\psi)}{2\pi r}\,, \tag{1.306}$$

where $I(\psi)$ represents the poloidal electric current flowing through a circular area bounded by the magnetic surface (see Figure 1.47):

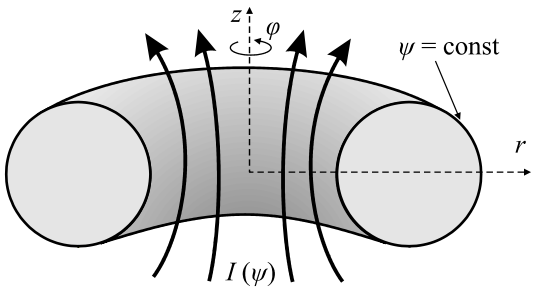


Fig. 1.47: Axisymmetric equilibrium configuration in a plasma.

The radial equilibrium condition (1.297) for this specific symmetry is derived by substituting the current density from the corresponding Maxwell equation:

$$-\frac{\partial p(\psi)}{\partial r}+j_\varphi B_z-j_z B_\varphi \;=\; 0\,;$$

$$-\frac{\partial p(\psi)}{\partial r}+\frac{1}{\mu_0}\left[\nabla\times\mathbf{B}\right]_\varphi B_z-\frac{1}{\mu_0}\left[\nabla\times\mathbf{B}\right]_z B_\varphi \;=\; 0\,;$$

$$-\frac{\partial p(\psi)}{\partial r}+\frac{1}{\mu_0}\left[\frac{\partial B_r}{\partial z}-\frac{\partial B_z}{\partial r}\right]B_z-\frac{1}{\mu_0}\left[\frac{1}{r}\frac{\partial}{\partial r}(rB_\varphi)\right]B_\varphi \;=\; 0\,.$$

Substituting the magnetic field components from relations (1.305) and (1.306) allows the spatial derivatives of pressure and current to be expressed as derivatives of a composite function: $\partial f(\psi)/\partial r = (\partial f/\partial\psi)\,(\partial\psi/\partial r)$. Following straightforward algebraic manipulations, the governing equation for ψ is established:

► $$\frac{\partial^2\psi}{\partial z^2}+r\frac{\partial}{\partial r}\frac{1}{r}\frac{\partial\psi}{\partial r}+\frac{\mu_0^2}{8\pi^2}\frac{\partial I^2}{\partial\psi}+\mu_0 r^2\frac{\partial p}{\partial\psi}=0\,. \qquad (1.307)$$

This is the *Grad–Shafranov equation* for axisymmetric plasma equilibrium, first derived in 1958 by Harold Grad and Hanan Rubin at New York University and, independently, in 1959 by Vitaly Dmitrievich Shafranov in the Soviet Union. The Shafranov work was not published in the West until 1966.

Current Filament (Pinch)

Current filaments, which form pinches, are among the most common structures observed in plasmas. In the simplest configuration, the electric current flows axially, generating an azimuthal magnetic field that exerts a compressing Lorentz force on the filament. In static equilibrium, the plasma pressure gradient expanding the fluid is exactly balanced by this compressive Lorentz force. Such a structure is termed a *z*-pinch, where the letter *z* denotes that the current flows along the cylinder *z*-axis.

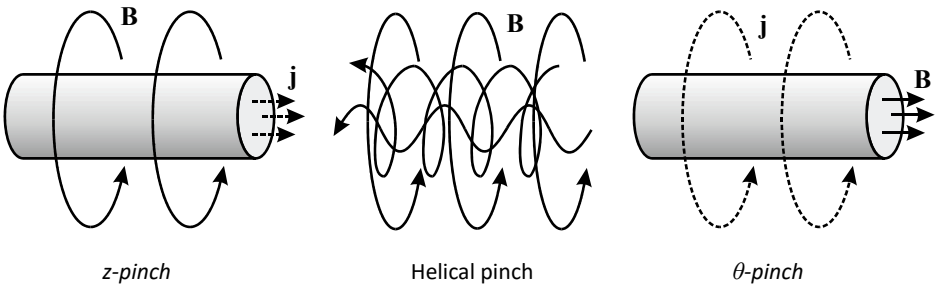


Fig. 1.48: Various types of current filaments in a plasma.

Section 1.5.2 demonstrates that this equilibrium is unstable, causing the pinch to collapse rapidly. However, twisting the magnetic field lines into a rope configuration achieves relative stability. In this regime, both current density and magnetic field have axial and azimuthal components: the axial current generates the azimuthal field, while the azimuthal current generates the axial field, forming a *helical pinch*. A well-known alternative is the *θ-pinch*, where current flows azimuthally along the surface, producing an axial magnetic field. Another setup is the *toroidal pinch* within *tokamaks* – essen-

tially a linear pinch twisted into a toroid, where it is standard practice to utilize the terms *toroidal* and *poloidal* instead of axial and azimuthal fields.

Bennett Equilibrium

The equilibrium of a *z*-pinch is analyzed here assuming a homogeneously distributed electric current and negligible radiation losses. The equilibrium conditions for a *z*-pinch under these assumptions were first derived by Willard Harrison Bennett in 1934. First, the azimuthal magnetic field $B(r)$ within a pinch of radius R is determined from the Ampère law expressed in cylindrical coordinates:

$$\nabla \times \mathbf{B} = \mu_0 \mathbf{j} \quad \Rightarrow$$

$$\frac{1}{r}\frac{\mathrm{d}}{\mathrm{d}r}(rB) = \mu_0 j \quad \Rightarrow$$

$$B(r) = \frac{\mu_0 j}{2} r + \frac{C}{r}.$$

The first term describes the magnetic field inside the pinch, whereas the second term diverges at the center, requiring the integration constant to be set to $C = 0$. Outside the pinch, the current density vanishes, causing the first term to disappear as well. Matching both solutions at the pinch boundary and substituting $j = I/\pi R^2$ yields:

$$B(r) = \begin{cases} \dfrac{\mu_0 I}{2\pi R^2} r, & r \le R; \\ \dfrac{\mu_0 I}{2\pi r}, & r \ge R. \end{cases} \tag{1.308}$$

The equilibrium equation (1.297) is then utilized to calculate the pressure profile:

$$\frac{\mathrm{d}p}{\mathrm{d}r} = -jB \quad \Rightarrow$$

$$\frac{\mathrm{d}p}{\mathrm{d}r} = -\frac{I}{\pi R^2}\frac{\mu_0 I}{2\pi R^2} r \quad \Rightarrow$$

$$p(r) = -\frac{\mu_0 I^2}{4\pi^2 R^4} r^2 + p_0 .$$

The integration is performed inside the pinch using the internal magnetic field solution. The physical significance of the constant p_0 is straightforward, representing the central pressure. The pressure must decrease toward the surface, where it vanishes, satisfying the boundary condition $p(R) = 0$. From this condition, p_0 and the general solution are determined:

► $$p(r) = p_0\left(1 - \frac{r^2}{R^2}\right); \qquad p_0 = \frac{\mu_0 I^2}{4\pi^2 R^2}. \tag{1.309}$$

This is the well-known Bennett solution featuring a parabolic pressure profile. The central pressure is directly proportional to the square of the total current. Substituting the electron and ion pressures from the ideal gas equation of state yields:

$$p_0 = n_\mathrm{e} k_\mathrm{B} T_\mathrm{e} + n_\mathrm{i} k_\mathrm{B} T_\mathrm{i} \approx n_\mathrm{e} k_\mathrm{B}\left(T_\mathrm{e} + T_\mathrm{i}/Z\right). \tag{1.310}$$

Subsequently substituting the particle number densities $n_\alpha = N_\alpha/V = N_\alpha/\pi R^2 l$ yields the relation between the temperature of the central region and the total flowing current:

► $$\mathcal{N}_\mathrm{e} k_\mathrm{B} \left(T_\mathrm{e} + T_\mathrm{i}/Z\right) = \frac{\mu_0}{4\pi} I^2 \; ; \qquad \mathcal{N}_\mathrm{e} \equiv \frac{N_\mathrm{e}}{l} = n_\mathrm{e} \pi R^2 \; . \tag{1.311}$$

The quantity $\mathcal{N}_\mathrm{e}$ is the number of electrons per unit length along the axis. The achieved temperature is therefore proportional to the square of the total current.

Force-Free Helical Pinch Configuration and Reverse Pinch

Assuming the helical pinch eventually reaches a minimum magnetic energy state, the field satisfies the Beltrami condition $\boldsymbol{\nabla}\times\mathbf{B} = \alpha\mathbf{B}$. In cylindrical geometry, the radial magnetic field component is zero, and both the azimuthal and axial components depend exclusively on r. Beltrami condition in cylindrical coordinates yields:

$$\boldsymbol{\nabla}\times\mathbf{B} = \alpha\mathbf{B} \; ; \qquad \Rightarrow \qquad \begin{aligned} 0 &= \alpha B_r \; , \\ -\frac{\mathrm{d}B_z}{\mathrm{d}r} &= \alpha B_\varphi \; , \\ \frac{1}{r}\frac{\mathrm{d}}{\mathrm{d}r}\left(rB_\varphi\right) &= \alpha B_z \; . \end{aligned} \tag{1.312}$$

Substituting the field component B_φ from the second equation into the third yields:

$$\frac{\mathrm{d}^2 B_z}{\mathrm{d}r^2} + \frac{1}{r}\frac{\mathrm{d}B_z}{\mathrm{d}r} + \alpha^2 B_z = 0 \; . \tag{1.313}$$

This represents the Bessel equation, which possesses the solution

► $$\begin{aligned} B_z(r) &= B_0 J_0(\alpha r) \; , \\ B_\varphi(r) &= B_0 J_1(\alpha r) \; . \end{aligned} \tag{1.314}$$

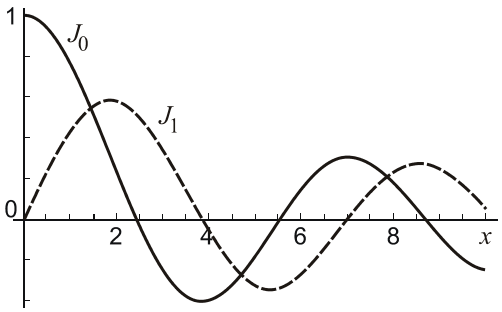


Fig. 1.49: Profiles of the Bessel functions J_0 and J_1.

The functions J_0 and J_1 are Bessel functions of the first kind; in cylindrical coordinates, they replace the Cartesian cosine and sine. Just as the derivative of the cosine is minus the sine, the derivative of J_0 equals minus J_1. The function J_0 changes sign at an argu-

ment of ~2.4. If the pinch radius is sufficiently large, the direction of B_z necessarily reverses for $r > 2.4/\alpha$, forming a *reverse pinch*. At the radius:

$$a = \frac{2,4}{\alpha} \tag{1.315}$$

a neutral layer forms, on opposite sides of which the field points in opposite directions. This geometry is highly conducive to magnetic field line reconnection and the development of the tearing instability.



Fig. 1.50: Lightning channel representing the most common natural plasma filament.
Source: Ing. Jaromír Jindra, Czech Astronomical Society.

Brief History of Pinch Research

1790	The Dutch scientist Martin van Marun discharged 100 Leyden jars through a wire, causing it to explode. This represents the first documented, though unexplained, pinch phenomenon.
1905	The Australian scientists James Arthur Pollock and Samuel Barraclough observed a crushed hollow lightning rod (photo on the right) near Sydney after a strike, correctly attributing the deformation to magnetic field pressure.
1934	Willard Harrison Bennett derived the pressure profile for a stationary *z*-pinch assuming a constant current density.
1946	George Thompson and Moses Blackman of Imperial College London patented a fusion device based on a toroidal pinch.
1946	George Thompson and Peter Thonemann conducted extensive experiments with the toroidal pinch.
1954	Martin David Kruskal and Martin Schwarzschild developed the initial theory of pinch instabilities, specifically addressing tearing and kink modes.
1956	Rendel Sebastian Pease and Stanislav Iosivovich Braginsky discovered a solution involving electromagnetic collapse, where radiative energy losses cause the pinch to contract uncontrollably toward the axis.
1957	The first large toroidal device, ZETA, featuring a diameter of 3 meters and a current of 900,000 A, was constructed in Harwell, England.
1958	The first fusion neutrons were detected in the SCYLLA toroidal pinch device at Los Alamos.



Plasma filament instabilities are discussed in detail in Section 1.5.2.

Current Sheet

A current sheet (or plasma wall) represents a two-dimensional analog of a current filament. An electric current flowing through a surface generates a magnetic field on both sides, which subsequently exerts a magnetic pressure on the sheet.

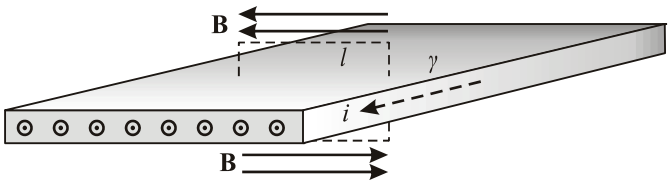


Fig. 1.52: General configuration of a plasma wall.

Applying the Ampère law in its integral form to the contour illustrated in the figure yields a straightforward relation:

$$\oint_{\gamma} \mathbf{B}\cdot \mathrm{d}\mathbf{l} = \mu_0 I \qquad \Rightarrow \qquad 2Bl = \mu_0 I \quad \Rightarrow$$

$$B = \frac{1}{2}\mu_0 i\,, \tag{1.316}$$

where i is the electric current per unit of transverse length. Current sheets are extremely thin relative to their width, differing by many orders of magnitude. The largest within the Solar System is the heliospheric current sheet – a rippled zero-field region around the Sun known as the *Parker surface*. Its near-Earth thickness is approximately 1,000 km, with opposite magnetic polarities on either side.

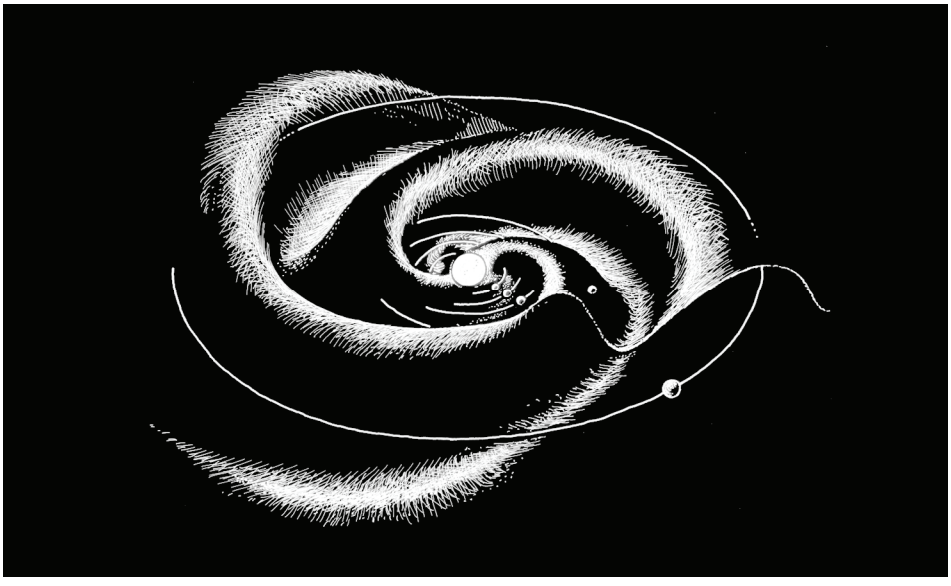


Fig. 1.53: Parker surface geometry near the Sun.

Planets pass alternately above and below the Parker surface, causing periodic reversals in the observed polarity of the solar magnetic field. Another prominent current sheet forms within the Earth magnetotail. Near these current sheets – where the magnetic field is oppositely oriented on either side – magnetic field line reconnection frequently occurs, promoting the development of the tearing instability.

Electrical Double Layer

A double layer (DL) represents a localized electric potential jump within a plasma. DLs occur frequently wherever electrons and ions exhibit counter-streaming motion. This relative macroscopic transport can trigger a two-stream instability, leading to a spatial potential jump $\Delta\phi$. The phenomenon is analogous to open-channel water flow, where hydraulic jumps or height discontinuities spontaneously form on the surface. Similarly, electrostatic potential steps develop spontaneously in a plasma with an electric potential gradient. Such double layers can also arise from random fluctuations in ion number density or from the parallel transport of charged particles along magnetic field lines.

Alternatively, an electric double layer can form at the interface between two plasma regions possessing different temperatures or electron number densities. Due to the local temperature or density gradient, electrons begin to diffuse preferentially into the adjacent region, generating a localized negative charge. This separation induces an electric field along with an associated potential step. No net electric current flows continuously through such equilibrium double layers.

The physical basis for the formation of an electric double layer is invariably the relative motion of electrons with respect to the background plasma, which locally disrupts quasi-neutrality and generates both an electric field and a spatial potential step.

The double-layer parameter, defined as the ratio of potential energy difference to the electron thermal energy, is utilized to evaluate the significance of the structure:

► $$\#_{\mathrm{DL}} \equiv \frac{e\,\Delta\phi}{k_{\mathrm{B}} T_{\mathrm{e}}}. \tag{1.317}$$

Double layers forming at the interface between regions with different temperatures typically possess a parameter value of approximately unity. In contrast, those generated by large potential gradients are highly pronounced, with $\#_{\mathrm{DL}} > 1$. For these strong double layers, particles are divided into four distinct groups (Figure 1.54):

1) ions accelerated by the potential drop,
2) electrons accelerated by the potential rise,
3) ions trapped on the low-potential side,
4) electrons trapped on the high-potential side.

The number density profiles n of these four particle types are shown in Fig. 1.54*b*; where negative particle number densities are plotted as dotted lines, and positive ones as solid lines. The corresponding total charge density ρ_Q is shown in Fig. 1.54*d*. This results in a net positive charge layer on the high-potential side and a net negative charge layer on the low-potential side, a configuration that gives the double layer its name. Before and after the potential step, the space charge vanishes, and the positive and negative charges exactly neutralize each other. The internal electric field E of the double layer (Fig. 1.54*c*), is localized strictly between the two charged layers and corresponds to the negative spatial derivative of the potential. Double layers can exist as long-term

stable structures where the potential step establishes the four particle populations, whose collective electric field in turn self-consistently sustains the potential step.

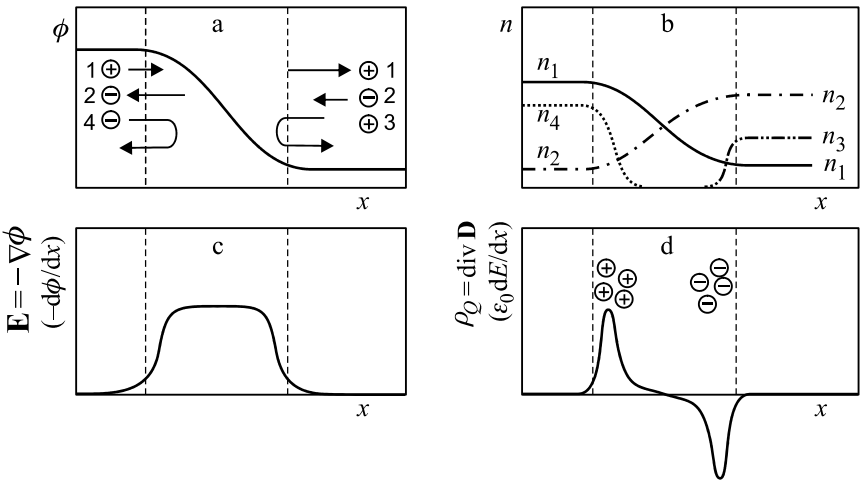


Fig. 1.54: Schematic structure of an electric double layer.

Double layers accelerate charged particles, acting as natural accelerators within both laboratory and space plasmas. Due to the macroscopic separation of positive and negative charges, these structures also function as natural capacitors. he electrostatic energy stored within these regions is transformed directly into the kinetic energy of the accelerated particles. The power dissipated across the double layer corresponds to the product of the potential drop and the net electric current traversing the structure:

$$P = \Delta\phi\, I\,. \tag{1.318}$$

Relativistic electrons can be generated within the double layer if the energy associated with the potential difference exceeds the rest energy of an electron; that is, if the relativistic double-layer parameter, defined by the relation:

► $$\#_{\mathrm{DLR}} \equiv \frac{e\Delta\phi}{m_{\mathrm{e}}c^2} \tag{1.319}$$

exceeds unity, $\#_{\mathrm{DLR}} > 1$.

Double layers typically form thin, warped sheets of varying spatial geometries. The characteristic thickness of a double layer is governed by the localized disruption of plasma quasi-neutrality, which cannot exceed a scale of several Debye lengths.

Even the thickest double layers exhibit a thickness of merely approximately ten Debye lengths. This spatial scale corresponds to millimeters in laboratory plasmas, centimeters in the planetary ionosphere, tens of meters within the interplanetary medium, and tens of kilometers within the intergalactic medium.

Double layers drift through the background plasma, rapidly thicken and break up, or gradually dissipate via standard diffusion processes. Conventional double layers orient perpendicularly to the magnetic field lines along which particles undergo transport, resulting in a parallel electric field. However, oblique double layers are also observed.

Within double layers, electrons and ions can accelerate to high velocities, converting the circuit magnetic energy into particle kinetic energy. Double layers develop wherever strong electric currents traverse a plasma. They exist within planetary magnetospheres; for instance, at distances of several Earth radii, energetic ions are generated in double layers along magnetic field lines. The potential drop in this region ranges between 10^2–10^4 V. Double layers likely develop within current-carrying solar filaments, where the potential drop is estimated up to 10^9–10^{11} V, accelerating protons to kinetic energies of several tens of gigaelectronvolts. If double layers form within plasma filaments near active galactic nuclei, the potential drop can reach 10^{17} V, with the released power on the order of 10^{37} W.

Ion thrusters represent a compelling practical application. In 2003, Christine Charles and Rod Boswell at the Australian National University developed an ion engine where a stable double layer forms at the interface between the high-density source plasma and the low-density plasma within the magnetic expansion nozzle. This double layer accelerates ions to high kinetic energies, significantly increasing the net thrust and boosting the overall efficiency of interplanetary spaceflight.

Double Layer Formed by Electron Density Variation

Assume that, driven by turbulent fluctuations, the electron density undergoes a spatial variation. A simple one-dimensional stationary solution is sought, neglecting magnetic fields and electron pressure gradients. The continuity equation then yields:

$$\frac{\partial}{\partial x}\left(n_\mathrm{e} u_\mathrm{e}\right) = 0 .$$

Since x represents the unique independent variable, this relation simplifies to:

$$n_\mathrm{e} u_\mathrm{e} = \text{const} \qquad \Rightarrow \qquad n_\mathrm{e} u_\mathrm{e} = -\frac{j_\mathrm{e}}{e} \qquad \Rightarrow$$

$$u_\mathrm{e}(x) = -\frac{j_\mathrm{e}}{e n_\mathrm{e}(x)} . \tag{1.320}$$

The electron current density remains constant, and the electron velocity within the perturbed density region adjusts dynamically to satisfy the continuity equation. For a steady state, the electron equation of motion reduces to:

$$n_\mathrm{e} m_\mathrm{e} u_\mathrm{e} \frac{\partial}{\partial x} u_\mathrm{e} = -n_\mathrm{e} e E .$$

From this equation of motion, the electric field arising from the spatial variation in electron velocity can be determined:

$$E = -\frac{\partial}{\partial x}\frac{m_\mathrm{e} u_\mathrm{e}^2}{2e} .$$

Substituting the velocity expression from (1.320) yields the following relation for the resulting electric field:

$$E(x) = -\frac{\partial}{\partial x}\frac{m_\mathrm{e} j_\mathrm{e}^2}{2e^3 n_\mathrm{e}^2(x)} . \tag{1.321}$$

An electron density variation thus generates a localized electric field. This field vanishes in uniform regions and remains non-zero only where a density gradient exists. The relation between the electric field and electrostatic potential yields:

$$\phi(x) = \frac{m_\mathrm{e} j_\mathrm{e}^2}{2e^3 n_\mathrm{e}^2(x)} . \tag{1.322}$$

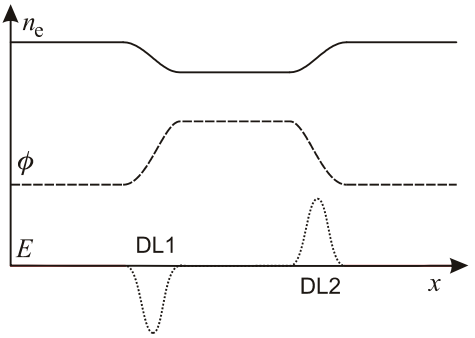


Fig. 1.55: Double layer pair formed by an electron number density well.

Where the electron density varies, the electric potential shifts accordingly, forming an electric double layer structure. A localized decrease in density thus leads directly to the generation of a double layer. This specific solution was derived by the Swedish physicists Hannes Alfvén and Per Carlqvist in 1968.

Solution for Potential Inside Two-Stream Maintained Double Layer

The electrostatic potential inside the double layer decreases from ϕ_DL to zero. A comprehensive calculation requires all four particle populations: the accelerated electron and ion streams, alongside trapped thermal electrons and ions. In this derivation, only streaming populations are considered, neglecting thermal kinetic effects. An electron stream traveling at constant velocity enters from the low-potential side, while an ion stream enters from the high-potential side. Both undergo acceleration across the double layer. The governing equations comprise the energy conservation law, the continuity equation, and the Poisson equation for the potential.

$$\begin{aligned} \frac{1}{2} m_\mathrm{e} u_\mathrm{e}^2 - e\phi &= \mathrm{const} = \frac{1}{2} m_\mathrm{e} u_\mathrm{e0}^2 ; \\ \frac{1}{2} m_\mathrm{i} u_\mathrm{i}^2 + Ze\phi &= \mathrm{const} = \frac{1}{2} m_\mathrm{i} u_\mathrm{i0}^2 + Ze\phi_\mathrm{DL} . \end{aligned} \tag{1.323}$$

$$\begin{aligned} n_\mathrm{e} u_\mathrm{e} &= \mathrm{const} = -\frac{j_\mathrm{e}}{e} ; \\ n_\mathrm{i} u_\mathrm{i} &= \mathrm{const} = \frac{j_\mathrm{i}}{Ze} ; \end{aligned} \tag{1.324}$$

$$\frac{\mathrm{d}^2\phi}{\mathrm{d}x^2} = \frac{e n_\mathrm{e}}{\varepsilon_0} - \frac{Z e n_\mathrm{i}}{\varepsilon_0} . \tag{1.325}$$

The energy conservation constant is evaluated at the boundary where the particles enter the double layer. Substituting particle densities from the continuity equation (1.324) and velocities from the energy conservation relation (1.323) into the Poisson equation (1.325) yields the final differential equation for the potential:

$$\frac{\mathrm{d}^2\phi}{\mathrm{d}x^2} = -\frac{j_\mathrm{e}/\varepsilon_0}{\sqrt{u_{\mathrm{e}0}^2 + \dfrac{2e}{m_\mathrm{e}}\phi}} - \frac{j_\mathrm{i}/\varepsilon_0}{\sqrt{u_{\mathrm{i}0}^2 + \dfrac{2Ze}{m_\mathrm{i}}(\phi_\mathrm{DL} - \phi)}}\,. \tag{1.326}$$

This ordinary second-order differential equation for $\phi(x)$ can be solved analytically via elliptic integrals, though it is usually solved numerically. The integration constants are determined uniquely by the boundary conditions: at both edges of the double layer, the electric field vanishes (implying a zero potential gradient), whereas the potential itself equals zero at one boundary and ϕ_DL at the other. This yields the Child–Langmuir law relating the total current density j, the layer thickness d, and the potential drop ϕ_DL:

$$jd^2 = A\phi_\mathrm{DL}^{3/2}\,; \qquad A \approx 0{,}20724\left(1+\sqrt{\frac{m_\mathrm{e}}{m_\mathrm{i}}}\right)\sqrt{\frac{2e}{m_\mathrm{e}}}\,; \qquad j = j_\mathrm{e} + j_\mathrm{i}\,. \tag{1.327}$$

In the general case, the population of trapped thermal particles must also be accounted for, with their density following the Boltzmann distribution assuming a non-zero temperature. Consequently, two additional terms are introduced to the right-hand side of the Poisson equation:

$$n_\alpha = n_{0\alpha}\exp\left[-Q_\alpha\phi/k_\mathrm{B}T_\alpha\right]; \qquad \alpha = \mathrm{e},\,\mathrm{i}\,.$$

Brief History of Double-Layer Research

1929	Irving Langmuir detects double layers within laboratory plasmas.
1958	Hannes Alfvén proposes that the electrons responsible for the aurora are accelerated toward Earth by double layers in the magnetosphere.
1967	Hannes Alfvén and Per Carlqvist propose a theory of solar flares wherein double layers play a key role.
1987	The Swedish Viking satellite in a polar orbit detects prominent double layers in the Earth magnetosphere using electric field sensors mounted on 40-meter booms.
1992	Noah Hershkowitz discovers multiple double layers featuring a stepped potential profile in laboratory plasmas.
2003	Christine Charles and Rod Boswell develop a spacecraft ion thruster utilizing a double layer to accelerate ions, with ESA conducting laboratory verification in 2005.

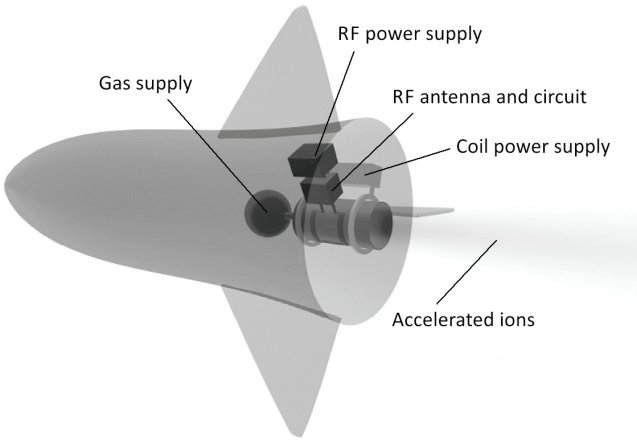


Fig. 1.56: ESA ion engine.

The European Space Agency ion propulsion system is designed for interplanetary flights. The plasma, generated by radio-frequency heating, is confined by magnetic field coils. A stable double layer forms at the chamber outlet, accelerating the ions to high kinetic energies. This mechanism generates the necessary thrust for this novel thruster.

Shock Waves

Regions often form in plasma where certain parameters – such as velocity, density, temperature, or magnetic field – change abruptly. Such regions are called shock waves; some of which can travel through the plasma. A typical example is the shock wave generated by the interaction of the solar wind with Earth magnetosphere. On the sunward side, a bow shock forms, similar to the shock wave created ahead of a ship moving across the sea. Shock waves also develop where the flow transitions from supersonic to subsonic and are characteristic features of both laboratory and astrophysical plasmas. Particles can be significantly accelerated across shock waves. The double layer discussed in the previous section is a special case of a shock wave.

In classical hydrodynamics, shock waves were studied by the Scottish engineer William John Macquorn Rankine and the French engineer Pierre Henri Hugoniot. The conditions that individual quantities must satisfy across a shock wave are called the *Rankine–Hugoniot conditions*. Suppose that for some extensive quantity A, the continuity equation takes the form:

$$\frac{\partial \rho_A}{\partial t} + \operatorname{div} \mathbf{j}_A = 0 \,, \tag{1.328}$$

Using a procedure similar to that for Maxwell equations (*Selected Topics*, *Volume II*, Section II.2.1.7), the condition holding in the rest frame of the shock wave is found:

$$\begin{gathered} (\mathbf{j}\cdot\mathbf{n})_1 = (\mathbf{j}\cdot\mathbf{n})_2 \quad \Rightarrow \quad (\mathbf{j}\cdot\mathbf{n})_2 - (\mathbf{j}\cdot\mathbf{n})_1 = 0 \quad \Rightarrow \\ [\mathbf{j}\cdot\mathbf{n}]_1^2 = 0 \,. \end{gathered} \tag{1.329}$$

The square brackets denote the jump in a quantity across the boundary, analogous to a definite integral. Subscripts indicate states on either side of the shock, and **n** is the normal vector. Mass and momentum conservation immediately yield:

► $$\left[\rho\,\mathbf{u}\cdot\mathbf{n}\right]_1^2 = 0\,, \tag{1.330}$$

► $$\left[\rho\mathbf{u}\left(\mathbf{u}\cdot\mathbf{n}\right)+\left(p+\frac{B^2}{2\mu_0}\right)\mathbf{n}-\frac{(\mathbf{B}\cdot\mathbf{n})\mathbf{B}}{\mu_0}\right]_1^2 = 0\,, \tag{1.331}$$

For energy, the situation is more complex; the energy flux is given by:

$$\mathbf{j}_\mathrm{E} = e\mathbf{u}+\frac{1}{2}\rho u^2\mathbf{u}+p\mathbf{u}+\mathbf{E}\times\mathbf{H}\,. \tag{1.332}$$

The individual terms represent, in order: the internal energy flux, the kinetic energy flux (directed bulk motion), the work done by pressure, and the Poynting vector expressing the electromagnetic energy flux. The corresponding jump condition across the shock wave takes the form:

$$\left[\left(e+\frac{\rho u^2}{2}+p\right)(\mathbf{u}\cdot\mathbf{n})+(\mathbf{E}\times\mathbf{H})\cdot\mathbf{n}\right]_1^2 = 0\,. \tag{1.333}$$

For a polytropic plasma, the internal energy is expressed via pressure:

$$p = nk_\mathrm{B}T\,, \tag{1.334}$$

$$e = \frac{f}{2}nk_\mathrm{B}T = \frac{f}{2}p\,. \tag{1.335}$$

Denoting the number of degrees of freedom of a particle by f, the adiabatic exponent is

$$\gamma = \frac{f+2}{f}\,, \tag{1.336}$$

from which f is calculated and substituted into the energy equation, yielding:

$$e = \frac{p}{\gamma-1}\,. \tag{1.337}$$

For discontinuous solutions, ideal magnetohydrodynamics is utilized (diffusion terms determine a finite shock wave thickness), substituting for **E**:

$$\mathbf{E} = -\mathbf{u}\times\mathbf{B}\,. \tag{1.338}$$

Consequently, the relation is directly obtained:

► $$\left[\left(\frac{\rho u^2}{2}+\frac{\gamma p}{\gamma-1}+\frac{B^2}{\mu_0}\right)(\mathbf{u}\cdot\mathbf{n})-\frac{(\mathbf{B}\cdot\mathbf{n})(\mathbf{B}\cdot\mathbf{u})}{\mu_0}\right]_1^2 = 0\,. \tag{1.339}$$

These conditions must be combined with the continuity of the normal magnetic field component (div **B** = 0) and the tangential electric field component (curl **E** = $-\partial\mathbf{B}/\partial t$). Recall that in ideal MHD, **E** = $-\mathbf{u}\times\mathbf{B}$:

► $$\left[\mathbf{B}\cdot\mathbf{n}\right]_1^2 = 0\,, \tag{1.340}$$

► $$\left[\mathbf{n}\times(\mathbf{u}\times\mathbf{B})\right]_1^2 = 0\,. \tag{1.341}$$

Relations (1.330) to (1.341) are known as the Rankine–Hugoniot conditions.

◖ **Example 1.4:** Traveling shock wave. Assume a shock wave formed by a parallel magnetic field jump moving through a plasma at rest at velocity V:

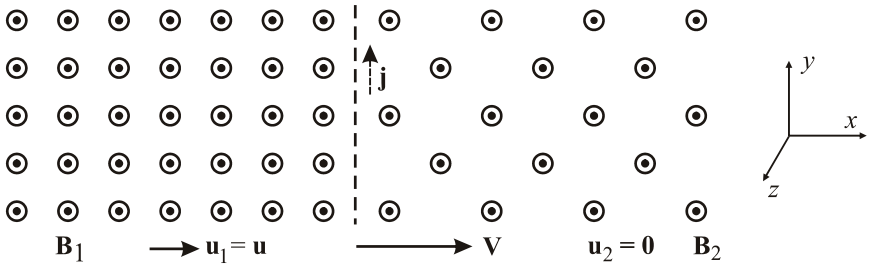


Fig. 1.57: Moving shock wave.

In front of the wavefront, the plasma velocity is zero; behind the wave, the plasma moves at a velocity **u**. Determine this velocity **u** from the magnetic field values on both sides of the shock wave.

Solution: In the rest frame of the shock wave, the magnetic field remains unchanged for non-relativistic velocities according to transformation (II.3.83) (see *Selected Topics*, *Volume II*). In this frame, the jump condition then implies that:

$$B_1(u-V) = B_2(-V)\,. \tag{1.342}$$

This directly yields the speed u of the medium behind the shock wave:

$$u = \left(1-\frac{B_2}{B_1}\right)V\,. \tag{1.343}$$

◗

1.4 Linear Waves in Plasma

1.4.1 Basic Concepts

Superposition of Plane Waves

Linear wave analysis was previously introduced in the *Electromagnetic waves* section of *Selected Topics*, *Volume II*. Here, the essential facts are briefly summarized. If the governing partial differential equations are linear, solutions can be directly constructed as a superposition of Fourier modes:

$$\psi(t,\mathbf{x}) = \int \psi_{\omega,\mathbf{k}}\, \mathrm{d}^3\mathbf{k}\,; \tag{1.344}$$

$$\psi_{\omega,\mathbf{k}} = a\,\mathrm{e}^{\mathrm{i}\varphi} = a(\omega,\mathbf{k})\,\mathrm{e}^{\mathrm{i}(\mathbf{k}\cdot\mathbf{x}-\omega t)}. \tag{1.345}$$

The complex wave function ψ is a symbolic representation of any wave where only the real part holds physical significance; $\psi_{\omega,\mathbf{k}}$ is the corresponding Fourier mode, a is its amplitude, and φ represents its phase. The superposition (1.344) represents a standard Fourier transform, physically describing the construction of the resulting solution from individual plane waves. The four-component set (ω, $\mathbf{k}$) is termed the wave four-vector, consisting of the angular frequency ω and the wave vector $\mathbf{k}$:

► $$\omega = -\frac{\partial\varphi}{\partial t}, \tag{1.346}$$

► $$\mathbf{k} = \frac{\partial\varphi}{\partial\mathbf{x}} = \nabla\varphi\,. \tag{1.347}$$

The minus sign in front of the angular frequency ensures both that the wave vector points in the direction of the wavefront propagation velocity (a surface of constant phase) and that the four-vector transforms correctly under the Lorentz transformation. Further details are available within the *Electromagnetic waves* section of *Selected Topics*, *Volume II*. For a plane wave, the following fundamental relations hold:

$$|\omega| = \frac{2\pi}{T}, \tag{1.348}$$

$$k = \frac{2\pi}{\lambda}, \tag{1.349}$$

where T represents the wave period and λ is its wavelength. The integration of modes is performed exclusively over **k**-space, since the components of the wave four-vector are interdependent. This functional dependence can be expressed via the dispersion relation

$$\phi(\omega,\mathbf{k}) = 0 \tag{1.350}$$

In many scenarios, the dispersion relation can be used to determine either $\omega = \omega(\mathbf{k})$ or $\mathbf{k} = \mathbf{k}(\omega)$. Individual modes then propagate at a characteristic phase velocity:

► $$v_\mathrm{f} = \frac{\omega}{k}; \qquad \mathbf{v}_\mathrm{f} = \frac{\omega}{k}\frac{\mathbf{k}}{k} = \frac{\omega}{k^2}\mathbf{k}. \tag{1.351}$$

There are no relativistic restrictions on the phase velocity; it can – and in specific media must – exceed the speed of light in vacuum. As a whole, a wave superposition, such as a wave packet, propagates at the group velocity:

► $$\mathbf{v}_\mathrm{g} = \frac{\partial\omega}{\partial\mathbf{k}} = \left(\frac{\partial\omega}{\partial k_x}, \frac{\partial\omega}{\partial k_y}, \frac{\partial\omega}{\partial k_z}\right). \tag{1.352}$$

In spherical coordinates (k, θ, φ), the corresponding relation takes the form of a gradient operator evaluated in **k**-space:

$$\mathbf{v}_\mathrm{g} = \left(\frac{\partial\omega}{\partial k}, \frac{1}{k}\frac{\partial\omega}{\partial\theta}, \frac{1}{k\sin\theta}\frac{\partial\omega}{\partial\varphi}\right). \tag{1.353}$$

Because a superposition of plane waves can carry information, the group velocity is strictly subluminal.

For a linear system of equations, the superposition principle holds, and individual modes (1.345) can be substituted directly into the governing equations. Spatial and temporal differential operations reduce to straightforward algebraic transformations:

Expression	Example
$\frac{\partial}{\partial t} \to -\mathrm{i}\omega$	$\frac{\partial f}{\partial t} = -\mathrm{i}\omega f$
$\frac{\partial}{\partial x_l} \to +\mathrm{i}k_l$	$\frac{\partial f}{\partial x_l} = +\mathrm{i}k_l f$
$\boldsymbol{\nabla} \to +\mathrm{i}\mathbf{k}$	$\boldsymbol{\nabla} f = +\mathrm{i}\mathbf{k} f$
$\mathrm{div} \to \mathrm{i}\mathbf{k}\cdot$	$\mathrm{div}\,\mathbf{V} = \mathrm{i}\mathbf{k}\cdot\mathbf{V}$
$\mathrm{curl} \to \mathrm{i}\mathbf{k}\times$	$\mathrm{curl}\,\mathbf{V} = \mathrm{i}\mathbf{k}\times\mathbf{V}$
$\boldsymbol{\nabla}^2 \to -k^2$	$\boldsymbol{\nabla}^2 f = -k^2 f$

This conversion transforms the partial differential equations into an algebraic system, equivalent to performing a Fourier transform. If possible, the system order is reduced at either the differential or algebraic level. Since the resulting system contains no right-hand sides, a non-zero solution requires a vanishing determinant of the matrix. This condition yields the dispersion relation between ω and **k**, determining both phase and group velocities. This procedure was explored within *Selected Topics*, *Volume II* for electromagnetic waves in vacuum, anisotropic, and conductive media. Finally, a return to the original equations determines the spatial orientations of individual vectors, such as the electric, magnetic, or fluid velocity fields.

◖ Example 1.5: Klein–Gordon Equation

The Klein–Gordon equation is the relativistic equation for a free particle with zero spin:

$$\left(\nabla^2 - \frac{1}{c^2}\frac{\partial^2}{\partial t^2} - \mu^2\right)\psi = 0\,; \qquad \mu^2 \equiv \frac{m^2c^2}{\hbar^2}\,. \tag{1.354}$$

This is a wave equation containing a constant term that reduces to the non-relativistic Schrödinger equation in the appropriate limit. Further details are available in *Selected Topics*, *Volume II*, Section I.2.7.3 (Klein–Gordon Equation). The equation is strictly linear, and its solution is interpreted as a superposition of plane waves. Performing a Fourier transform on the Klein–Gordon equation according to the established rules yields the dispersion relation:

$$\omega^2 = c^2k^2 + c^2\mu^2\,. \tag{1.355}$$

The phase and group velocities are determined using the standard analytical procedure:

$$v_\mathrm{f} = \frac{\omega}{k} = c\sqrt{1+\frac{\mu^2}{k^2}} = c\sqrt{1+\frac{\mu^2\lambda^2}{4\pi^2}}\,, \tag{1.356}$$

$$v_\mathrm{g} = \frac{\partial\omega}{\partial k} = \frac{c}{\sqrt{1+\dfrac{\mu^2}{k^2}}} = \frac{c}{\sqrt{1+\dfrac{\mu^2\lambda^2}{4\pi^2}}}\,. \tag{1.357}$$

Clearly, the group velocity remains subluminal, whereas the phase velocity is superluminal and carries no physical information. The two velocities satisfy the simple relation: $v_\mathrm{f}\,v_\mathrm{g} = c^2$. Both velocities depend on the wavelength, indicating physical dispersion. Only for a massless particle ($\mu = 0$) are both velocities equal to the speed of light in vacuum. A particle with zero rest mass and its associated wave packet cannot propagate at any other velocity. Plasma waves analyzed in Section 1.4.3 will exhibit similar behavior.

◗

Nonlinear System of Equations

Nonlinear models pose a significant challenge because they generally lack universal solution methods. Linearization helps overcome this, although it discards many intrinsic nonlinear properties. A linear approximation is justified exclusively for small-amplitude waves, interpreted as small perturbations of a known, preferably stationary, solution. However, linearization often represents the unique approach to analyzing the system. Using methods from theoretical mechanics, solution stability can be investigated based on the behavior of these small perturbations. Linearization involves two consecutive steps. First, a stationary solution is established. In a homogeneous, unbounded medium, this is typically a constant spatial profile; in bounded media (such as a cylindrical filament), its structure is more complex. Second, the wave is treated as a small perturbation. This implies that relative perturbations behave as a small dimensionless parameter, allowing powers higher than the first order to be neglected. Practically, the perturbed solution is substituted into the original equations, and all higher-order terms are

dropped. This yields a linear system for the perturbations, solvable via standard procedures. Before addressing magnetohydrodynamics, these steps are illustrated using ordinary sound waves in gases.

1.4.2 Sound Waves in Gases

For a nonlinear system of equations, a procedure based on linearization can be employed, which is analogous to the stability analysis of systems of ordinary differential equations [1]. Here, the behavior of small perturbations is examined, which may be damped (stability), grow exponentially (instability), or exhibit a wave-like character. The fundamental steps for solving a nonlinear system using the linearization method (also termed the perturbation method or the method of small perturbations) are summarized as follows:

1. Determining a preferably stationary solution.
2. Linearization utilizing small perturbations.
3. Elimination of variables (if necessary).
4. Fourier transform.
5. Algebraic elimination of remaining variables.
6. Deriving the dispersion relation (system determinant vanishes).
7. Investigating solution stability.
8. Calculating phase and group velocities.
9. Determining relative directions between vectors.

For linear systems, the procedure begins directly with step 3. For nonlinear systems, the entire sequence must be followed, as demonstrated below using sound waves propagating in a homogeneous, isotropic gas.

Static Medium

The following system of equations is considered as the starting point:

$$\frac{\partial \rho}{\partial t} + \operatorname{div} \rho \mathbf{u} \;=\; 0\,,$$

$$\rho \frac{\partial \mathbf{u}}{\partial t} + \rho \left(\mathbf{u} \cdot \nabla \right) \mathbf{u} \;=\; -\nabla\, p\,, \tag{1.358}$$

$$p = p(\rho) = K\, \rho^{\gamma}\,.$$

The first relation is the continuity equation for the density ρ, the second is the equation of motion for the velocity field $\mathbf{u}$, and the system is closed by a polytropic equation of state (where the pressure p depends on density via a power law, a behavior highly typical for both gases and plasmas). The system contains five unknowns (ρ, $\mathbf{u}$, p) and is inherently nonlinear due to the products of the unknown functions. The complete analytical procedure (steps 1 through 9) is performed as follows:

1. **Steady-State Solution**: For example, a stationary gas in a closed domain yields:

$$\rho = \rho_0 , \qquad \mathbf{u}_0 = 0 , \qquad p = p_0 .$$

2. **Linearization:** A small perturbation to the steady-state solution is assumed:

$$\rho = \rho_0 + \delta\rho , \qquad \mathbf{u} = \delta\mathbf{u} , \qquad p = p_0 + \delta p .$$

Substituting this perturbation into the system (1.358) yields:

$$\frac{\partial}{\partial t}(\rho_0 + \delta\rho) + \operatorname{div}\Big[(\rho_0 + \delta\rho)(\delta\mathbf{u})\Big] = 0 ,$$

$$(\rho_0 + \delta\rho)\frac{\partial(\delta\mathbf{u})}{\partial t} + \rho\big(\delta\mathbf{u}\cdot\boldsymbol{\nabla}\big)(\delta\mathbf{u}) = -\boldsymbol{\nabla}(p_0 + \delta p) ,$$

$$\delta p = \alpha(\rho_0)\delta\rho ; \qquad \alpha \equiv \frac{\partial p}{\partial \rho} .$$

Only first-order terms are retained, neglecting higher-order perturbations. Since the derivatives of constants vanish, the linearized system reduces to:

$$\begin{gathered} \frac{\partial}{\partial t}(\delta\rho) + \operatorname{div}\Big[\rho_0(\delta\mathbf{u})\Big] = 0 , \\ \rho_0 \frac{\partial(\delta\mathbf{u})}{\partial t} = -\boldsymbol{\nabla}(\delta p) , \\ \delta p = \alpha(\rho_0)\delta\rho . \end{gathered} \tag{1.359}$$

3. **Elimination of Variables:** The system (1.359) is linear with respect to $\delta\rho$, $\delta\mathbf{u}$, and δp. In principle, the pressure perturbation δp can be eliminated immediately by substitution from the last equation. However, this step can also be performed later.

4. **Fourier Transform:** The system is converted into an algebraic form using the Fourier transform. Since the system is already linear, this step is equivalent to assuming a plane-wave solution, yielding:

$$\begin{gathered} -\mathrm{i}\,\omega\delta\rho + \mathrm{i}\,\rho_0(\mathbf{k}\cdot\delta\mathbf{u}) = 0 , \\ -\mathrm{i}\,\omega\rho_0\,\delta\mathbf{u} = -\mathrm{i}\,\mathbf{k}\,\delta p , \\ \delta p = \alpha\,\delta\rho . \end{gathered} \tag{1.360}$$

5. **Elimination of Variables:** The resulting system contains five unknowns, which would require calculating the determinant of a 5×5 matrix. Using the last equation, the pressure perturbation is eliminated:

$$\begin{gathered} -\omega\delta\rho + \rho_0(\mathbf{k}\cdot\delta\mathbf{u}) = 0 , \\ \mathbf{k}\,\alpha\,\delta\rho - \omega\rho_0\,\delta\mathbf{u} = 0 . \end{gathered}$$

This leaves four equations (one scalar and one vector) for four unknowns $\delta\rho$ and $\delta\mathbf{u}$, reducing the problem to a 4×4 determinant. From the second (vector) equation, the velocity perturbation can be expressed and substituted into the first equation:

$$(-\omega^2 + \alpha k^2)\delta\rho = 0 .$$

This yields a single equation for the unknown $\delta\rho$, though completely eliminating variables is not always possible.

6. **Dispersion Relation:** The condition for a non-zero solution requires the expression in parentheses before $\delta\rho$ to vanish (it represents the determinant of a 1×1 matrix):

$$-\omega^2 + \alpha(\rho_0)k^2 = 0\,. \tag{1.361}$$

The dispersion relation is solved for ω. Substituting the definition of α yields:

$$\omega = \sqrt{\frac{\partial p}{\partial \rho}}\,k\,. \tag{1.362}$$

7. **Stability of the Solution:** The dispersion relation is purely real; a real wave vector **k** corresponds to a real angular frequency ω, meaning the solutions are strictly wave-like. The system exhibits neither damping nor instability.
8. **Phase and Group Velocities:** Since the resulting dispersion relation is linear, the phase and group velocities are identical, and sound propagates at the velocity:

$$c_\mathrm{s} = \frac{\omega}{k} = \sqrt{\frac{\partial p}{\partial \rho}}\,. \tag{1.363}$$

Specifically for polytropic processes, $p = K\rho^\gamma$ (m_0 is the mass of a single atom):

$$c_\mathrm{s} = \sqrt{\gamma\frac{p}{\rho}} = \sqrt{\gamma\frac{k_\mathrm{B}T}{m_0}}\,. \tag{1.364}$$

9. **Vector Relationships:** The second equation (1.360) demonstrates that the velocity perturbation aligns with the direction of wave propagation (along the wave vector **k**), confirming that this is a *longitudinal wave*.

Using the speed of sound, the dispersion relation for sound waves can be written as:

► $$\omega = c_\mathrm{s}\,k\,; \qquad c_\mathrm{s} \equiv \sqrt{\gamma\frac{p}{\rho}}\,. \tag{1.365}$$

Moving Medium

A non-zero velocity is now assumed in the steady-state solution (corresponding to sound propagation in a moving medium), seeking a solution of the form:

$$\begin{aligned} \rho &= \rho_0 + \delta\rho\,, \\ \mathbf{u} &= \mathbf{u}_0 + \delta\mathbf{u}\,, \\ p &= p_0 + \delta p\,. \end{aligned} \tag{1.366}$$

How does this affect the system? The calculation proceeds identically, but the convective term in the equation of motion now also contributes to the linearized equations. A straightforward calculation yields the dispersion relation:

$$\left(\omega - \mathbf{k}\cdot\mathbf{u}_0\right)^2 - \alpha(\rho_0)k^2 = 0\,; \qquad \alpha \equiv \frac{\partial p}{\partial \rho} \tag{1.367}$$

and from it the observed angular frequency

$$\omega = c_s k + \mathbf{k}\cdot\mathbf{u}_0 = c_s k + k u_0 \cos\varphi = c_s k\left(1 + \frac{u_0}{c_s}\cos\varphi\right). \tag{1.368}$$

The angle between the wave vector $\mathbf{k}$ and the medium velocity $\mathbf{u}_0$ is denoted as φ. Defining the sound frequency in a stationary medium as $\omega_0 = c_s k$ yields the relation:

► $$\omega = \omega_0\left(1 + \frac{u_0}{c_s}\cos\varphi\right), \tag{1.369}$$

which represents the Doppler formula for the frequency shift due to the motion of the wave source. For moving fluids, the dispersion relation therefore features the combination:

$$\Omega = \omega - \mathbf{k}\cdot\mathbf{u}_0. \tag{1.370}$$

Jeans Criterion

Waves are now described in a cloud of gas and dust governed by a gravitational field (a nebula). Specifically, the conditions under which a sound wave becomes unstable are investigated, causing a portion of the nebula to collapse and form a globule – a dense region serving as the precursor to a future star.

The following table compares the quantities describing electrostatic and gravitational fields. The correct coefficient for the Laplace–Poisson equation for gravitational potential can be obtained by comparing the potential energy relations in the first row.

Quantity	Electrostatic field	Gravitational field
Potential of a point source	$\phi_E = \frac{Q}{4\pi\varepsilon_0 r}$	$\phi_G = -G\frac{M}{r}$
Potential energy	$V_E = q\,\phi_E$	$V_G = m\,\phi_G$
Equation for the potential	$\nabla^2\phi_E = -\frac{\rho_Q}{\varepsilon_0}$	$\nabla^2\phi_G = 4\pi G\rho_M$
Force from energy	$\mathbf{F} = -\nabla V_E$	$\mathbf{F} = -\nabla V_G$
Force from potential	$\mathbf{F} = -q\nabla\phi_E$	$\mathbf{F} = -m\nabla\phi_G$
Force density	$\mathbf{f} = -\rho_Q\nabla\phi_E$	$\mathbf{f} = -\rho_M\nabla\phi_G$

As a starting point, the system (1.358) supplemented by the gravitational force density and the equation for the gravitational potential is considered:

$$\begin{aligned} \partial\rho/\partial t + \operatorname{div}\rho\mathbf{u} &= 0\,, \\ \rho\,\partial\mathbf{u}/\partial t + \rho(\mathbf{u}\cdot\nabla)\mathbf{u} &= -\nabla p - \rho\nabla\phi\,, \\ \nabla^2\phi &= 4\pi G\rho\,, \\ p &= p(\rho)\,. \end{aligned} \tag{1.371}$$

Since this is a purely gravitational problem without electric fields, there is no risk of confusing densities or potentials, so the subscript G is omitted. This yields a total of six equations for six unknowns ρ, $\mathbf{u}$, ϕ, and p. The solution is sought in the perturbed form:

$$\rho = \rho_0 + \delta\rho\,, \qquad \mathbf{u} = \delta\mathbf{u}\,, \qquad \phi = \phi_0 + \delta\phi\,, \qquad p = p_0 + \delta p\,.$$

The zero-order quantities must satisfy the equation $\Delta\phi_0 = 4\pi G\rho_0$, which implies that $\nabla\phi_0 \neq 0$. However, this contradicts the steady-state solution of the equation of motion for $p_0 = \text{const}$. This inconsistency arises from replacing a finite nebula with an infinite space filled with matter of constant density, pressure, and temperature. In the large-scale nebula approximation, boundary effects can be neglected while still enforcing $\nabla\phi_0 \neq 0$ in the perturbation analysis. This "inconsistency" was already present in Jeans original solution. Using a similar procedure, the dispersion relation for sound waves influenced by a gravitational field is obtained:

$$\omega^2 = c_\mathrm{s}^2\, k^2 - 4\pi G\rho_0\,; \qquad c_\mathrm{s}^2 \equiv \frac{\partial p}{\partial \rho}\,. \tag{1.372}$$

Unlike the original relation (1.365), an additional term appears on the right-hand side. The solution for the angular frequency ω is straightforward:

$$\omega = \pm\sqrt{c_\mathrm{s}^2\, k^2 - 4\pi G\rho_0}\ . \tag{1.373}$$

At first glance, the angular frequency need not be a real quantity. For

$$c_\mathrm{s}^2\, k^2 < 4\pi G\rho_0 \tag{1.374}$$

the angular frequency is purely imaginary, $\omega = \pm\mathrm{i}\,b$, and the terms

$$\mathrm{e}^{\mathrm{i}\omega t} = \mathrm{e}^{\mp bt}$$

appear in a plane wave. Certain perturbations can grow exponentially, causing instability. In such environments, stars form from originally small perturbations that grow to macroscopic sizes. Condition (1.374) is examined below in more detail:

$$c_\mathrm{s}^2 \frac{4\pi^2}{\lambda^2} < 4\pi G\rho_0 \quad \Rightarrow$$

$$\lambda > \sqrt{\frac{\pi}{G\rho_0}}\, c_\mathrm{s} = \sqrt{\frac{\pi}{G\rho_0}}\sqrt{\gamma\frac{k_\mathrm{B}T}{m_0}}\,.$$

Here, m_0 represents the mass of a single atom or molecule. Perturbations with wavelengths exceeding a certain threshold are gravitationally unstable. For stars to form, the nebula must be larger than this critical size. This statement is known as the Jeans criterion, derived in 1902:

► $$L > \sqrt{\frac{\pi\gamma k_\mathrm{B}T}{G\rho_0 m_0}}\,. \tag{1.375}$$

The dispersion relation (1.373) straightforwardly yields the phase and group velocities of perturbations. In an ionized medium with magnetic fields, star formation can occur even without satisfying the Jeans criterion.

If the Jeans criterion is satisfied and a spherical object forms within the nebula, its equilibrium conditions must then be determined. The gravitational force acting on a given layer inside the protostar is given by:

$$F_{\text{grav}} \sim \frac{1}{R^2}\,.$$

The pressure force on this layer is proportional to the pressure $p \sim \rho^{\gamma}$ and surface $S \sim R^2$:

$$F_{\text{pressure}} \sim \rho^{\gamma} R^2 \sim R^{-3\gamma} R^2 \sim \frac{1}{R^{3\gamma-2}}\,.$$

Both forces decrease as the star expands, establishing equilibrium when they balance. Their rates of decrease are identical for the coefficient:

$$\gamma = \frac{4}{3}.$$

Two cases are considered. First, for $\gamma > 4/3$, the pressure curve is steeper than the gravitational curve. If the star experiences a fluctuation that increases its size, the gravitational force prevails, causing it to contract. Conversely, if the star decreases in size, the pressure force prevails and forces it to expand back to its original size. The star is stable, and size fluctuations do not threaten its existence.

For $\gamma < 4/3$, the situation is reversed. If the star fluctuates toward a larger size, the pressure force prevails and forces the star to expand continuously. The star becomes unstable and will, at the very least, eject its outer envelope. If the star shrinks, gravity prevails and forces it to collapse.

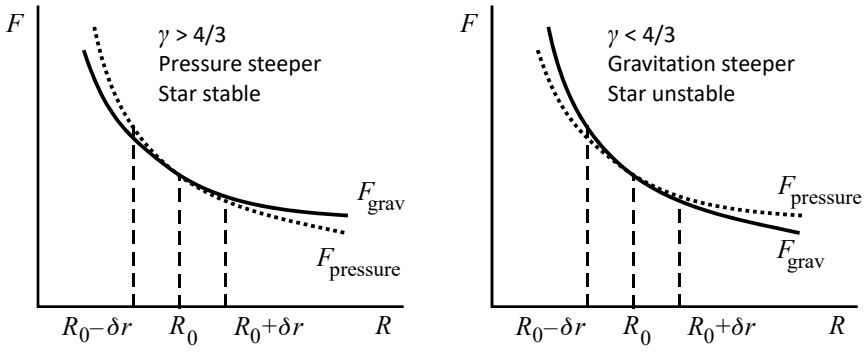


Fig. 1.58: Equilibrium of a polytropic star.

Note: The material of white dwarfs has a polytropic index close to 4/3, which varies slightly with the star's mass. At approximately 1.4 solar masses, the polytropic index is exactly 4/3; for higher masses, the white dwarf becomes unstable. This threshold is known as the Chandrasekhar limit.

1.4.3 Plasma Oscillations and Waves

A plasma medium can transmit numerous wave types in response to various external stimuli. In this section, the simplest plasma oscillations and waves occurring in the absence of a magnetic field are examined. The restoring force is driven solely by the electric field, enabling periodic motion. An initial perturbation causes the electron and ion fluids to oscillate at two characteristic frequencies while generating a global electric field. Because the electron fluid oscillates at significantly higher frequencies than the ion fluid, a single-fluid model is inadequate; instead, a two-fluid model must be employed. Viscous terms are neglected. For this wave type, the Maxwell equation curl $\mathbf{E} = 0$ applies (an electric field wave is possible even with a zero magnetic field), implying that $\mathbf{k} \times \delta\mathbf{E} = 0$. Consequently, $\delta\mathbf{E} \parallel \mathbf{k}$ holds, and the wave is longitudinal.

Derivation of the Dispersion Relation

The following is taken as the starting system of equations:

$$\begin{gathered}
\frac{\partial n_\mathrm{e}}{\partial t} + \operatorname{div}(n_\mathrm{e}\mathbf{u}_\mathrm{e}) = 0\,, \\
\frac{\partial n_\mathrm{i}}{\partial t} + \operatorname{div}(n_\mathrm{i}\mathbf{u}_\mathrm{i}) = 0\,, \\
m_\mathrm{e} n_\mathrm{e} \frac{\partial \mathbf{u}_\mathrm{e}}{\partial t} + m_\mathrm{e} n_\mathrm{e} (\mathbf{u}_\mathrm{e} \cdot \boldsymbol{\nabla}) \mathbf{u}_\mathrm{e} \;=\; -\boldsymbol{\nabla} p_\mathrm{e} - e n_\mathrm{e} \mathbf{E}\,, \\
m_\mathrm{i} n_\mathrm{i} \frac{\partial \mathbf{u}_\mathrm{i}}{\partial t} + m_\mathrm{i} n_\mathrm{i} (\mathbf{u}_\mathrm{i} \cdot \boldsymbol{\nabla}) \mathbf{u}_\mathrm{i} \;=\; -\boldsymbol{\nabla} p_\mathrm{i} + Z e n_\mathrm{i} \mathbf{E}\,, \\
\frac{\partial \mathbf{E}}{\partial t} = -\frac{1}{\varepsilon_0} (Z e n_\mathrm{i} \mathbf{u}_\mathrm{i} - e n_\mathrm{e} \mathbf{u}_\mathrm{e})\,, \\
p_\mathrm{e} = n_\mathrm{e} k_\mathrm{B} T_\mathrm{e} = C_\mathrm{e} n_\mathrm{e}^{\gamma_\mathrm{e}}\;; \\
p_\mathrm{i} = n_\mathrm{i} k_\mathrm{B} T_\mathrm{i} = C_\mathrm{i} n_\mathrm{i}^{\gamma_\mathrm{i}}\,.
\end{gathered} \tag{1.376}$$

These comprise the continuity equations for electrons and ions, the equations of motion including pressure and electric field terms, the equation for the electric field, and the polytropic equations of state. The electric field equation is derived from Maxwell equation $\boldsymbol{\nabla} \times \mathbf{H} = \mathbf{j} + \partial\mathbf{D}/\partial t$, where the magnetic field is zero and the current density is given by relation (1.170). A Z-times ionized plasma is assumed. These equations are linearized by perturbing the steady-state solution:

$$\begin{gathered}
n_\mathrm{e} = n_{\mathrm{e}0} + \delta n_\mathrm{e}\;; \quad n_\mathrm{i} = n_{\mathrm{i}0} + \delta n_\mathrm{i}\;; \quad \mathbf{u}_\mathrm{e} = \delta\mathbf{u}_\mathrm{e}\;; \quad \mathbf{u}_\mathrm{i} = \delta\mathbf{u}_\mathrm{i}\;; \\
\mathbf{E} = \delta\mathbf{E}\;; \quad p_\mathrm{e} = p_{\mathrm{e}0} + \delta p_\mathrm{e}\;; \quad p_\mathrm{i} = p_{\mathrm{i}0} + \delta p_\mathrm{i}\,.
\end{gathered} \tag{1.377}$$

Substituting into the original equations and dropping higher-order terms yields:

$$\frac{\partial \delta n_\mathrm{e}}{\partial t} + \mathrm{div}(n_{\mathrm{e}0}\,\delta \mathbf{u}_\mathrm{e}) = 0\,,$$

$$\frac{\partial \delta n_\mathrm{i}}{\partial t} + \mathrm{div}(n_{\mathrm{i}0}\,\delta \mathbf{u}_\mathrm{i}) = 0\,,$$

$$m_\mathrm{e} n_{\mathrm{e}0} \frac{\partial \delta \mathbf{u}_\mathrm{e}}{\partial t} = -\boldsymbol{\nabla}\,\delta p_\mathrm{e} - e n_{\mathrm{e}0}\,\delta \mathbf{E}\,,$$

$$m_\mathrm{i} n_{\mathrm{i}0} \frac{\partial \delta \mathbf{u}_\mathrm{i}}{\partial t} = -\boldsymbol{\nabla}\,\delta p_\mathrm{i} + Z e n_{\mathrm{i}0}\,\delta \mathbf{E}\,,$$

$$\frac{\partial \delta \mathbf{E}}{\partial t} = -\frac{e}{\varepsilon_0}\,(Z n_{\mathrm{i}0}\,\delta \mathbf{u}_\mathrm{i} - n_{\mathrm{e}0}\,\delta \mathbf{u}_\mathrm{e})\,,$$

$$\delta p_\mathrm{e} = m_\mathrm{e} c_\mathrm{e}^2\,\delta n_\mathrm{e}\,; \quad c_\mathrm{e}^2 \equiv \frac{\gamma_\mathrm{e} k_\mathrm{B} T_\mathrm{e}}{m_\mathrm{e}}\,,$$

$$\delta p_\mathrm{i} = m_\mathrm{i} c_\mathrm{i}^2\,\delta n_\mathrm{i}\,; \quad c_\mathrm{i}^2 \equiv \frac{\gamma_\mathrm{i} k_\mathrm{B} T_\mathrm{i}}{m_\mathrm{i}}\,.$$

The next step is straightforward. The number of equations is reduced by substituting the last two into the remaining ones, followed by a Fourier transform:

$$-\omega \delta n_\mathrm{e} + n_{\mathrm{e}0}\,(\mathbf{k}\cdot\delta \mathbf{u}_\mathrm{e}) = 0\,,$$

$$-\omega \delta n_\mathrm{i} + n_{\mathrm{i}0}\,(\mathbf{k}\cdot\delta \mathbf{u}_\mathrm{i}) = 0\,,$$

$$\mathrm{i}\,\omega m_\mathrm{e} n_{\mathrm{e}0}\,\delta \mathbf{u}_\mathrm{e} = \mathrm{i}\,\mathbf{k}\,m_\mathrm{e} c_\mathrm{e}^2\,\delta n_\mathrm{e} + e n_{\mathrm{e}0}\,\delta \mathbf{E}\,,$$

$$\mathrm{i}\,\omega m_\mathrm{i} n_{\mathrm{i}0}\,\delta \mathbf{u}_\mathrm{i} = \mathrm{i}\,\mathbf{k}\,m_\mathrm{i} c_\mathrm{i}^2\,\delta n_\mathrm{i} - Z e n_{\mathrm{i}0}\,\delta \mathbf{E}\,,$$

$$\mathrm{i}\,\omega \delta \mathbf{E} = \frac{e}{\varepsilon_0}\,(Z n_{\mathrm{i}0}\,\delta \mathbf{u}_\mathrm{i} - n_{\mathrm{e}0}\,\delta \mathbf{u}_\mathrm{e})\,.$$

This system contains 11 algebraic equations for the unknowns δn_e, δn_i, $\delta \mathbf{u}_\mathrm{e}$, $\delta \mathbf{u}_\mathrm{i}$, $\delta \mathbf{E}$. To reduce the system, $\delta \mathbf{u}_\mathrm{e}$ and $\delta \mathbf{u}_\mathrm{i}$ are expressed from the third and fourth equations and substituted into the rest. Next, $\delta \mathbf{E}$ is expressed from the last equation and substituted into the remaining two, yielding:

$$\left[(\omega^2 - \omega_\mathrm{pe}^2 - \omega_\mathrm{pi}^2)(\omega^2 - c_\mathrm{e}^2 k^2) - \omega_\mathrm{pe}^2 c_\mathrm{e}^2 k^2\right]\delta n_\mathrm{e} + \left[Z\omega_\mathrm{pe}^2 c_\mathrm{i}^2 k^2\right]\delta n_\mathrm{i} = 0\,,$$

$$\left[\frac{1}{Z}\omega_\mathrm{pi}^2 c_\mathrm{e}^2 k^2\right]\delta n_\mathrm{e} + \left[(\omega^2 - \omega_\mathrm{pe}^2 - \omega_\mathrm{pi}^2)(\omega^2 - c_\mathrm{i}^2 k^2) - \omega_\mathrm{pi}^2 c_\mathrm{i}^2 k^2\right]\delta n_\mathrm{i} = 0\,,$$

These combinations are denoted as the sound speed (for electrons, this is a formal designation; the ear cannot hear electron-carried sound) and the plasma frequency:

$$c_\mathrm{e}^2 \equiv \frac{\gamma_\mathrm{e} k_\mathrm{B} T_\mathrm{e}}{m_\mathrm{e}}\,; \qquad c_\mathrm{i}^2 \equiv \frac{\gamma_\mathrm{i} k_\mathrm{B} T_\mathrm{i}}{m_\mathrm{i}}\,, \tag{1.378}$$

$$\omega_{\mathrm{pe}}^2 \equiv \frac{n_{\mathrm{e}0}\, e^2}{m_{\mathrm{e}}\varepsilon_0}; \qquad \omega_{\mathrm{pi}}^2 \equiv \frac{n_{\mathrm{i}0} Z^2 e^2}{m_{\mathrm{i}}\varepsilon_0}, \tag{1.379}$$

For the resulting system to have a nonzero solution, its determinant must vanish:

$$\begin{pmatrix} \left[(\omega^2 - \omega_{\mathrm{pe}}^2 - \omega_{\mathrm{pi}}^2)(\omega^2 - c_{\mathrm{e}}^2 k^2) - \omega_{\mathrm{pe}}^2 c_{\mathrm{e}}^2 k^2\right] \times \\ \times\left[(\omega^2 - \omega_{\mathrm{pe}}^2 - \omega_{\mathrm{pi}}^2)(\omega^2 - c_{\mathrm{i}}^2 k^2) - \omega_{\mathrm{pi}}^2 c_{\mathrm{i}}^2 k^2\right] \end{pmatrix} - \omega_{\mathrm{pe}}^2 \omega_{\mathrm{pi}}^2 c_{\mathrm{e}}^2 c_{\mathrm{i}}^2 k^4 \;=\; 0\,.$$

Rearranging the terms (via Mathematica or MATLAB) yields the dispersion relation:

$$\begin{pmatrix} \left[\,(\omega^2 - \omega_{\mathrm{pe}}^2)(\omega^2 - \omega_{\mathrm{pi}}^2) - \omega_{\mathrm{pe}}^2 \omega_{\mathrm{pi}}^2\,\right] \times \\ \times\left[\,(\omega^2 - \omega_{\mathrm{pe}}^2 - c_{\mathrm{e}}^2 k^2)(\omega^2 - \omega_{\mathrm{pi}}^2 - c_{\mathrm{i}}^2 k^2) - \omega_{\mathrm{pe}}^2 \omega_{\mathrm{pi}}^2\,\right] \end{pmatrix} = 0\,.$$

This relation has two main branches: the first is independent of the wave vector (plasma oscillations, discussed below), while the second depends on it (plasma waves, see page 128, and ion waves, see page 129):

► $$\left[(\omega^2 - \omega_{\mathrm{pe}}^2)(\omega^2 - \omega_{\mathrm{pi}}^2) - \omega_{\mathrm{pe}}^2 \omega_{\mathrm{pi}}^2\right] = 0\,, \tag{1.380}$$

► $$\left[(\omega^2 - \omega_{\mathrm{pe}}^2 - c_{\mathrm{e}}^2 k^2)(\omega^2 - \omega_{\mathrm{pi}}^2 - c_{\mathrm{i}}^2 k^2) - \omega_{\mathrm{pe}}^2 \omega_{\mathrm{pi}}^2\right] = 0\,. \tag{1.381}$$

Plasma Oscillations

Expanding equation (1.380) yields a non-zero solution:

$$\omega^2 = \omega_{\mathrm{pe}}^2 + \omega_{\mathrm{pi}}^2\,.$$

The square of the electron plasma frequency is three orders of magnitude higher than that of the ions. The second term on the right-hand side represents a negligible ion mass correction and is usually ignored. Using quasi-neutrality ($n_{\mathrm{i}0} = n_{\mathrm{e}0}/Z$) yields:

$$\omega^2 = \omega_{\mathrm{pe}}^2 + \omega_{\mathrm{pi}}^2 = \omega_{\mathrm{pe}}^2\left(1 + \frac{\omega_{\mathrm{pi}}^2}{\omega_{\mathrm{pe}}^2}\right) = \omega_{\mathrm{pe}}^2\left(1 + \frac{n_{\mathrm{i}0} Z^2 e^2}{m_{\mathrm{i}}\varepsilon_0}\frac{m_{\mathrm{e}}\varepsilon_0}{n_{\mathrm{e}0} e^2}\right) = \omega_{\mathrm{pe}}^2\left(1 + \frac{Z m_{\mathrm{e}}}{m_{\mathrm{i}}}\right) \;\Rightarrow$$

► $$\omega^2 = \omega_{\mathrm{pe}}^2\left(1 + \frac{Z m_{\mathrm{e}}}{m_{\mathrm{i}}}\right)\,. \tag{1.382}$$

If the ions possessed infinite mass, the oscillations would occur exactly at the electron plasma frequency, leaving the ions completely stationary. The physics can be understood as an electron fluid oscillating against a fixed ion background. The second term in parentheses provides a small correction for the finite ion mass. This frequency represents one of the most critical plasma characteristics; a plasma frequently responds to external stimuli with oscillations or waves at this frequency, which typically lies within the radio frequency range.

Plasma Waves

The second branch (1.381) of the dispersion relation is now considered. The inequality $m_e << m_i$ is applied through the limit $m_i \to \infty$. In doing so, the high-frequency component of the waves is analyzed, where the ions cannot respond quickly enough and effectively behave as if they possessed infinite mass. This limiting process yields:

$$\omega_{pi}^2 \to 0\,; \qquad c_i^2 \to 0\,.$$

The dispersion relation (1.381) reduces directly to the relation:

$$\omega^2 - \omega_{pe}^2 - c_e^2 k^2 = 0\,,$$

which yields the dispersion relation for *plasma waves*:

► $$\omega^2 = \omega_{pe}^2 + c_e^2 k^2\,; \quad \text{resp.} \qquad \omega = \sqrt{\omega_{pe}^2 + c_e^2 k^2}\,. \tag{1.383}$$

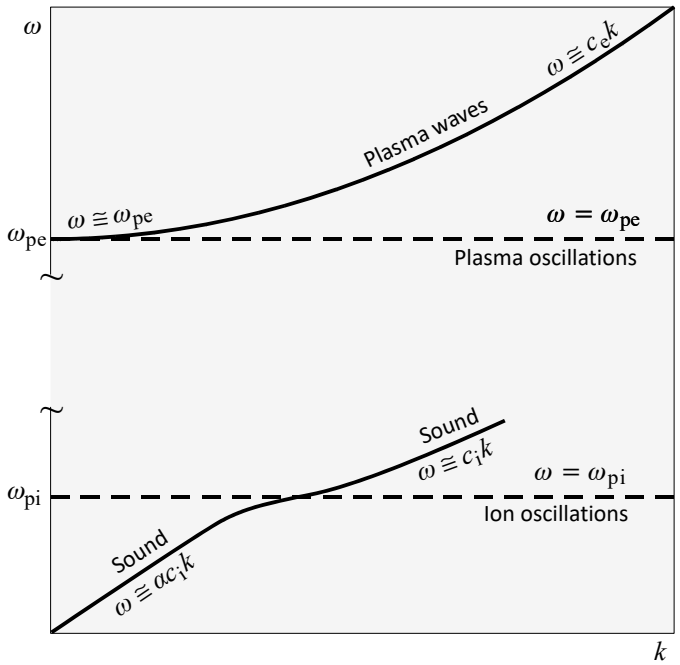


Fig. 1.59: Dispersion relation for plasma oscillations and waves.

Long-Wave Limit (small *k*)

The second term in the dispersion relation is negligible, corresponding to oscillations at the electron plasma frequency:

$$\omega = \omega_{pe}\,.$$

Short-Wave Limit (large *k*)

The first term in the dispersion relation is negligible, and the relation becomes linear:

$$\omega = c_e k\,.$$

The slope of the dispersion curve represents the electron "speed of sound" (approximately the electron thermal velocity). Real sound is carried by heavy particles (ions and neutrals) and exhibits a much lower frequency.

Note 1: Plasma waves are the most typical high-frequency waves in plasma, usually falling within the radio frequency range. The dispersion relation (1.383) admits solutions exclusively for

$$\omega > \omega_{\mathrm{pe}} . \tag{1.384}$$

At lower frequencies, the wave does not propagate. This behavior is evident directly from both the dispersion relation and the accompanying figure; for frequencies below the plasma frequency, the relation yields a complex solution, meaning the wave is evanescent.

Note 2: The distinction between small and large k depends on which of the two terms in expression (1.383) dominates. Since $\omega_{\mathrm{p}}^2/c^2k^2 = \lambda^2/4\pi^2\gamma\lambda_{\mathrm{D}}^2$, the small-$k$ limit corresponds to the long-wavelength region ($\lambda >> \lambda_{\mathrm{D}}$), while the large-$k$ limit to the short-wavelength region ($\lambda << \lambda_{\mathrm{D}}$), where λ_{D} is the Debye length.

Note 3: The second term in the dispersion relation (1.383) arises from the thermal motion of electrons. Without thermal motion, waves would not propagate, and only localized oscillations would occur.

Note 4: The dispersion relation (1.383) straightforwardly yields both the phase and group velocities:

$$v_{\mathrm{f}} = \frac{\omega}{k} = c_{\mathrm{e}} \sqrt{1 + \frac{\omega_{\mathrm{pe}}^2 \lambda^2}{4\pi^2 c_{\mathrm{e}}^2}} ; \qquad v_{\mathrm{g}} = \frac{\partial \omega}{\partial k} = c_{\mathrm{e}} \Big/ \sqrt{1 + \frac{\omega_{\mathrm{pe}}^2 \lambda^2}{4\pi^2 c_{\mathrm{e}}^2}} . \tag{1.385}$$

Consequently, the phase and group velocities satisfy the following relations:

$$v_{\mathrm{f}} > c_{\mathrm{e}} ; \qquad v_{\mathrm{g}} < c_{\mathrm{e}} ; \qquad v_{\mathrm{f}} v_{\mathrm{g}} = c_{\mathrm{e}}^2 . \tag{1.386}$$

Note 5: In the presence of a magnetic field, the high-frequency branch transitions into a more complex set of electromagnetic plasma waves. Conversely, the low-frequency branch described in the next section transitions into a complex of magnetoacoustic waves.

Ion Waves

The inequality $m_{\mathrm{e}} << m_{\mathrm{i}}$ is now applied through the limit $m_{\mathrm{e}} \to 0$. Electrons with zero mass effectively become a background negative charge cloud. Ions retain a finite, albeit large, mass and oscillate at very low frequencies against the electron background. This limiting process implies:

$$\omega_{\mathrm{pe}}^2 \to \infty ; \qquad c_{\mathrm{e}}^2 \to \infty .$$

Retaining the dominant terms in the dispersion relation (1.381) yields:

$$(-\omega_{\mathrm{pe}}^2 - c_{\mathrm{e}}^2 k^2)(\omega^2 - \omega_{\mathrm{pi}}^2 - c_i^2 k^2) - \omega_{\mathrm{pe}}^2 \omega_{\mathrm{pi}}^2 = 0 .$$

This relation is solved straightforwardly for ω:

$$\omega^2 = \omega_{\mathrm{pi}}^2 + c_{\mathrm{i}}^2 k^2 - \frac{\omega_{\mathrm{pi}}^2\, \omega_{\mathrm{pe}}^2}{\omega_{\mathrm{pe}}^2 + c_{\mathrm{e}}^2 k^2}$$

and after a simple rearrangement, it follows that:

► $$\omega^2 = \omega_{\mathrm{pi}}^2 \left[1 - \frac{1}{1 + c_{\mathrm{e}}^2 k^2 / \omega_{\mathrm{pe}}^2} \right] + c_{\mathrm{i}}^2 k^2 \ . \qquad (1.387)$$

The relation can also optionally be rewritten using the Debye length (discussed in Section 1.6.4, p. 231). A simple relation holds between the sound speed (1.378), the plasma frequency (1.379), and the Debye length:

$$c_\alpha^2 / \omega_{\mathrm{p}\alpha}^2 = \gamma_\alpha \lambda_\alpha^2 \ .$$

Using this expression, the dispersion relation for ion waves is sometimes expressed as:

► $$\omega^2 = \omega_{\mathrm{pi}}^2 \left[1 \ - \ \frac{1}{1 + \gamma_{\mathrm{e}} \lambda_{\mathrm{D}\,\mathrm{e}}^2 k^2} + \ \gamma_{\mathrm{i}} \lambda_{\mathrm{D}\,\mathrm{i}}^2 k^2 \right] . \qquad (1.388)$$

Long-Wave Limit (small k)

In the long-wave limit, the dispersion relation (1.387) can be approximated as:

$$\omega^2 = \omega_{\mathrm{pi}}^2 \left[1 - \frac{1}{1 + c_{\mathrm{e}}^2 k^2 / \omega_{\mathrm{pe}}^2} \right] + c_{\mathrm{i}}^2 k^2 \approx$$

$$\approx \ \omega_{\mathrm{pi}}^2 \left[1 - \left(1 - c_{\mathrm{e}}^2 k^2 / \omega_{\mathrm{pe}}^2 \right) \right] + c_{\mathrm{i}}^2 k^2 \ \Rightarrow$$

$$\omega^2 = c_{\mathrm{i}}^2 k^2 \left[1 + \frac{\omega_{\mathrm{pi}}^2}{\omega_{\mathrm{pe}}^2} \frac{c_{\mathrm{e}}^2}{c_{\mathrm{i}}^2} \right] .$$

Using the definitions of the sound speed (1.378), the plasma frequency (1.379), and quasi-neutrality $n_{\mathrm{i}0} = n_{\mathrm{e}0}/Z$ yields:

$$\omega^2 \ = \ c_{\mathrm{i}}^2 k^2 \left(1 + Z \frac{\gamma_{\mathrm{e}} T_{\mathrm{e}}}{\gamma_{\mathrm{i}} T_{\mathrm{i}}} \right); \quad \text{or}$$

$$\omega \ = \ c_{\mathrm{i}} k \sqrt{1 + Z \frac{\gamma_{\mathrm{e}} T_{\mathrm{e}}}{\gamma_{\mathrm{i}} T_{\mathrm{i}}}} \, .$$

These solutions represent sound waves propagating at the velocity:

$$c_{\mathrm{s}} = c_{\mathrm{i}} \sqrt{1 + Z \frac{\gamma_{\mathrm{e}} T_{\mathrm{e}}}{\gamma_{\mathrm{i}} T_{\mathrm{i}}}} \, .$$

Short-Wave Limit (large *k*)

In the short-wave limit, only a single term remains in the dispersion relation (1.387)

$$\omega^2 \approx c_\mathrm{i}^2 k^2 \; ; \quad \text{resp.} \qquad \omega = c_\mathrm{i} k \; .$$

These again correspond to sound waves propagating at the velocity:

$$c_\mathrm{s} = c_\mathrm{i} \; .$$

Low-frequency solutions are sound waves exhibiting weak dispersion.

Other Factors

Motion of the Medium

Plasma oscillations and waves are influenced by numerous other factors. If the medium in which the wave propagates moves at a velocity $\mathbf{u}_0$, the dispersion relation (1.381) becomes:

$$\left[(\omega - \mathbf{k} \cdot \mathbf{u}_0)^2 - \omega_\mathrm{pe}^2 - c_\mathrm{e}^2 k^2 \right] \cdot \left[(\omega - \mathbf{k} \cdot \mathbf{u}_0)^2 - \omega_\mathrm{pi}^2 - c_\mathrm{i}^2 k^2 \right] - \omega_\mathrm{pe}^2 \omega_\mathrm{pi}^2 = 0 \; .$$

This relation naturally incorporates the Doppler frequency shift.

Collisions

Collisions introduce a friction term on the right-hand side of the equation of motion, which is proportional to velocity and the collision frequency ν. Since electron plasma oscillations are strictly longitudinal, collision effects can be estimated in one dimension while neglecting other terms, such as pressure:

$$\frac{\partial n_\mathrm{e}}{\partial t} + \frac{\partial}{\partial x}(n_\mathrm{e} u_\mathrm{e}) = 0 \; ,$$

$$m_\mathrm{e} n_\mathrm{e} \frac{\partial u_\mathrm{e}}{\partial t} = -e\, n_\mathrm{e} E - n_\mathrm{e} m_\mathrm{e} \nu u_\mathrm{e} \; ,$$

$$\frac{\partial E}{\partial t} = \frac{1}{\varepsilon_0} e n_\mathrm{e} u_\mathrm{e} \; .$$

Applying perturbations and the Fourier transform yields the dispersion relation. In the absence of the collision term, it takes the form:

$$\omega^2 = \omega_\mathrm{pe}^2 \; ; \qquad \omega_\mathrm{pe}^2 \equiv \frac{n_0 e^2}{m_\mathrm{e} \varepsilon_0} \; .$$

This approach provides an efficient method for deriving the plasma frequency. With the collision term included, forcing the determinant to zero yields:

$$\omega^2 + \mathrm{i}\,\omega\nu - \omega_\mathrm{pe}^2 = 0 \qquad \Rightarrow \qquad \omega = -\mathrm{i}\frac{\nu}{2} \pm \sqrt{\omega_\mathrm{pe}^2 - \left(\frac{\nu}{2}\right)^2} \; .$$

Collisions cause the damping of plasma oscillations with a damping coefficient $\delta = \nu/2$.

Magnetic Field

A magnetic field deeply alters wave behavior. The high-frequency branch transitions into the *complex of anisotropic electromagnetic waves* (Sec. 1.4.5), while the low-frequency branch becomes a *complex of anisotropic magnetoacoustic waves* (Sec. 1.4.4).

1.4.4 Magnetoacoustic Waves

In this section, low-frequency waves driven by ion motion in the presence of a magnetic field are examined. The magnetic field introduces a completely new property – anisotropy. Other factors influencing wave behavior include the electric charge of the ions and the conductivity of the medium.

Derivation of the Dispersion Relation

As our starting point, classical single-fluid magnetohydrodynamics is considered:

$$\begin{aligned} \frac{\partial \rho}{\partial t} + \operatorname{div}(\rho \mathbf{u}) &= 0, \\ \rho \frac{\partial \mathbf{u}}{\partial t} + \rho (\mathbf{u}\cdot\nabla)\mathbf{u} &= -\nabla p + \frac{\nabla\times\mathbf{B}}{\mu_0}\times\mathbf{B}, \\ \frac{\partial \mathbf{B}}{\partial t} &= \frac{1}{\sigma\mu_0}\nabla^2\mathbf{B} + \nabla\times(\mathbf{u}\times\mathbf{B}), \\ p &= p(\rho). \end{aligned} \tag{1.389}$$

The diffusion term in the magnetic field equation is responsible for the damping of magnetoacoustic waves. For a highly conductive plasma ($\sigma \to \infty$), this term can be neglected, rendering the waves undamped. Retaining this term in the governing system would yield complex solutions for both the frequency and the wave vector, causing the plane wave to damp exponentially. The entire governing system is algebraically closed by the equation of state.

The analytical procedure continues analogously to the previous cases by perturbing the steady-state solution:

$$\rho = \rho_0 + \delta\rho; \qquad \mathbf{u} = \delta\mathbf{u}; \qquad \mathbf{B} = \mathbf{B}_0 + \delta\mathbf{B}; \qquad p = p_0 + \delta p. \tag{1.390}$$

Substituting the perturbed solution (1.390) into the system (1.389), neglecting higher-order terms, and assuming a plane-wave solution yields the linearized algebraic system:

$$\begin{aligned} -\omega\delta\rho + \rho_0 \mathbf{k}\cdot\delta\mathbf{u} &= 0, \\ \mathbf{k}\,\delta p - \rho_0\omega\delta\mathbf{u} + \frac{1}{\mu_0}(\mathbf{B}_0\cdot\delta\mathbf{B})\mathbf{k} - \frac{1}{\mu_0}(\mathbf{B}_0\cdot\mathbf{k})\delta\mathbf{B} &= 0, \\ \mathbf{k}\times(\mathbf{B}_0\times\delta\mathbf{u}) - \omega\delta\mathbf{B} &= 0, \\ \delta p - c_s^2\delta\rho &= 0; \qquad c_s^2 \equiv \frac{\partial p}{\partial \rho}. \end{aligned} \tag{1.391}$$

This is a homogeneous system of eight equations (two scalar and two vector). By successively eliminating variables, the system can be reduced to a single equation for velocity (the second equation). First, δp is substituted from the last equation, then $\delta\rho$ from the first equation, and finally $\delta\mathbf{B}$ from the third equation (simplifying the vector triple product). This yields a coupled system of equations for the velocity field perturbations:

$$\mathbf{M}\cdot\delta\mathbf{u}=\mathbf{0}\,. \tag{1.392}$$

The components of the symmetric matrix $\mathbf{M}$ are given by:

$$M_{kl}=\left[\omega^2-(\mathbf{k}\cdot\mathbf{v}_\mathrm{A})^2\right]\delta_{kl}+(\mathbf{k}\cdot\mathbf{v}_\mathrm{A})(k_k v_l^{(\mathrm{A})}+k_l v_k^{(\mathrm{A})})\;-\;\left(v_\mathrm{A}^2+c_\mathrm{s}^2\right)k_k k_l\,.$$

This matrix can also be expressed in the invariant form:

$$\mathbf{M}=\left[\omega^2-(\mathbf{k}\cdot\mathbf{v}_\mathrm{A})^2\right]\vec{\mathbf{1}}\;+\;(\mathbf{k}\cdot\mathbf{v}_\mathrm{A})\left[\mathbf{k}\otimes\mathbf{v}_\mathrm{A}+\mathbf{v}_\mathrm{A}\otimes\mathbf{k}\right]\;-\;\left(v_\mathrm{A}^2+c_\mathrm{s}^2\right)\;\mathbf{k}\otimes\mathbf{k}\,.$$

The quantity $\mathbf{v}_\mathrm{A}$ is termed the Alfvén velocity and is defined as:

$$\mathbf{v}_\mathrm{A}\equiv\frac{\mathbf{B}_0}{\sqrt{\mu_0\,\rho_0}}\,. \tag{1.393}$$

To derive the dispersion relation, a convenient coordinate system can be chosen. The z-axis is aligned with the direction of the magnetic field $\mathbf{B}_0$ (and thus the Alfvén velocity). The coordinate system is then rotated around this axis so that the wave vector $\mathbf{k}$ lies within the (x, z) plane. In this coordinate system, $\mathbf{B}_0=(0,0,B_0)$, $\mathbf{v}_\mathrm{A}=(0,0,v_\mathrm{A})$, and the wave vector is $\mathbf{k}=(k\sin\alpha,\,0,\,k\cos\alpha)$. The angle between the vectors $\mathbf{B}_0$ and $\mathbf{k}$ is α.

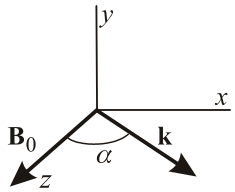


Fig. 1.60: Choice of the coordinate system.

For this choice, the matrix $\mathbf{M}$ takes a simple form:

$$\mathbf{M}=\begin{pmatrix}\omega^2-k^2v_\mathrm{A}^2-c_\mathrm{s}^2k^2\sin^2\alpha & 0 & -c_\mathrm{s}^2k^2\sin\alpha\cos\alpha\\ 0 & \omega^2-k^2v_\mathrm{A}^2\cos^2\alpha & 0\\ -c_\mathrm{s}^2k^2\sin\alpha\cos\alpha & 0 & \omega^2-c_\mathrm{s}^2k^2\cos^2\alpha\end{pmatrix}.$$

Since a non-zero solution to the system (1.392) is sought, the determinant of matrix $\mathbf{M}$ must vanish. This condition yields the dispersion relation for magnetoacoustic waves, expressed in a form independent of the chosen coordinate system:

$$\left[\omega^2-(\mathbf{k}\cdot\mathbf{v}_\mathrm{A})^2\right]\cdot\left[\omega^4-k^2\left(v_\mathrm{A}^2+c_\mathrm{s}^2\right)\omega^2+c_\mathrm{s}^2k^2\,(\mathbf{k}\cdot\mathbf{v}_\mathrm{A})^2\right]=0\,. \tag{1.394}$$

The Alfvén velocity vector points along the background magnetic field $\mathbf{B}_0$. It is immediately apparent that magnetoacoustic waves are far more complex than ordinary sound waves. When the expression in the first square bracket vanishes, the *Alfvén wave* (A) mode is established. When the expression in the second set of brackets vanishes, it yields an easily solvable bicubic equation for the angular frequency. Its solution provides two additional magnetoacoustic wave modes: the *slow wave* (S) and the *fast wave* (F). The dispersion relations for these individual modes are given by (where α is the angle between the wave vector and the magnetic field or the Alfvén velocity):

$$\begin{aligned}
\omega^2 &= v_\mathrm{A}^2 k^2 \cos^2\alpha\,, \\
\omega^2 &= \frac{1}{2}k^2\left(c_\mathrm{s}^2 + v_\mathrm{A}^2\right) - \frac{1}{2}k^2\sqrt{\left(c_\mathrm{s}^2 + v_\mathrm{A}^2\right)^2 - 4c_\mathrm{s}^2 v_\mathrm{A}^2\cos^2\alpha}\,, \\
\omega^2 &= \frac{1}{2}k^2\left(c_\mathrm{s}^2 + v_\mathrm{A}^2\right) + \frac{1}{2}k^2\sqrt{\left(c_\mathrm{s}^2 + v_\mathrm{A}^2\right)^2 - 4c_\mathrm{s}^2 v_\mathrm{A}^2\cos^2\alpha}\,.
\end{aligned} \qquad (1.395)$$

Notably, in some literature, all three magnetoacoustic wave modes introduced here are collectively referred to as Alfvén waves. In a classical sound wave, the energy density transfers between the thermal (pressure, p) and ordered (kinetic, $\rho v^2/2$) energy components. In a magnetoacoustic wave, the energy density of the magnetic field (magnetic pressure, $p_\mathrm{M} = B^2/2\mu_0$) acts as an additional equivalent component. Equating the kinetic energy density to the magnetic pressure yields the Alfvén velocity:

$$\frac{1}{2}\rho v^2 = \frac{1}{2}\frac{B^2}{\mu_0} \quad \Rightarrow \quad v = v_\mathrm{A} = \frac{B}{\sqrt{\mu_0\rho}}\,.$$

Wavefronts of Magnetoacoustic Waves

The dispersion relations (1.395) straightforwardly determine the phase velocities for the individual modes:

$$\begin{aligned}
v_\mathrm{Af}^2 &= v_\mathrm{A}^2\cos^2\alpha\,, \\
v_\mathrm{Sf}^2 &= \frac{1}{2}\left(c_\mathrm{s}^2 + v_\mathrm{A}^2\right) - \frac{1}{2}\sqrt{\left(c_\mathrm{s}^2 + v_\mathrm{A}^2\right)^2 - 4c_\mathrm{s}^2 v_\mathrm{A}^2\cos^2\alpha}\,, \\
v_\mathrm{Ff}^2 &= \frac{1}{2}\left(c_\mathrm{s}^2 + v_\mathrm{A}^2\right) + \frac{1}{2}\sqrt{\left(c_\mathrm{s}^2 + v_\mathrm{A}^2\right)^2 - 4c_\mathrm{s}^2 v_\mathrm{A}^2\cos^2\alpha}\,.
\end{aligned} \qquad (1.396)$$

These velocities are evaluated along the magnetic field $\mathbf{B}_0$ ($\alpha = 0$) and perpendicular to it ($\alpha = \pi/2$). The results are summarized in the following table:

Mode	A	S	F
$\alpha = 0$	v_A	$\min\{v_\mathrm{A}, c_\mathrm{s}\}$	$\max\{v_\mathrm{A}, c_\mathrm{s}\}$ (1.397)
$\alpha = \pi/2$	0	0	$\sqrt{v_\mathrm{A}^2 + c_\mathrm{s}^2}$ (1.398)

Along the background magnetic field, the phase velocity of the Alfvén wave equals the Alfvén velocity; the slow wave propagates at the lower of the two fundamental velocities (the sound speed and the Alfvén velocity), while the fast wave propagates at the

higher velocity. Perpendicular to the initial magnetic field, only the fast wave exhibits a non-zero propagation velocity; the slow and Alfvén waves have zero velocities.

This behavior is clearly illustrated in the polar diagram showing the phase velocity of all three modes as a function of the magnetic field. Such a diagram represents the shapes of the individual wavefronts. As the magnetic field decreases, the wavefronts of the Alfvén wave and the slow magnetoacoustic wave shrink, and the fast magnetoacoustic wavefront reduces to an ordinary sound wavefront. The magnetic field thus introduces a strong anisotropy into sound propagation. The behavior of wavefronts at various magnetic field intensities was visualized via Wolfram MATHEMATICA. The figures illustrate the wavefront shapes, or the polar diagram of the phase velocity, for various magnetic field strengths. In the presence of dust within the plasma, additional and more complex wavefronts structures emerge.

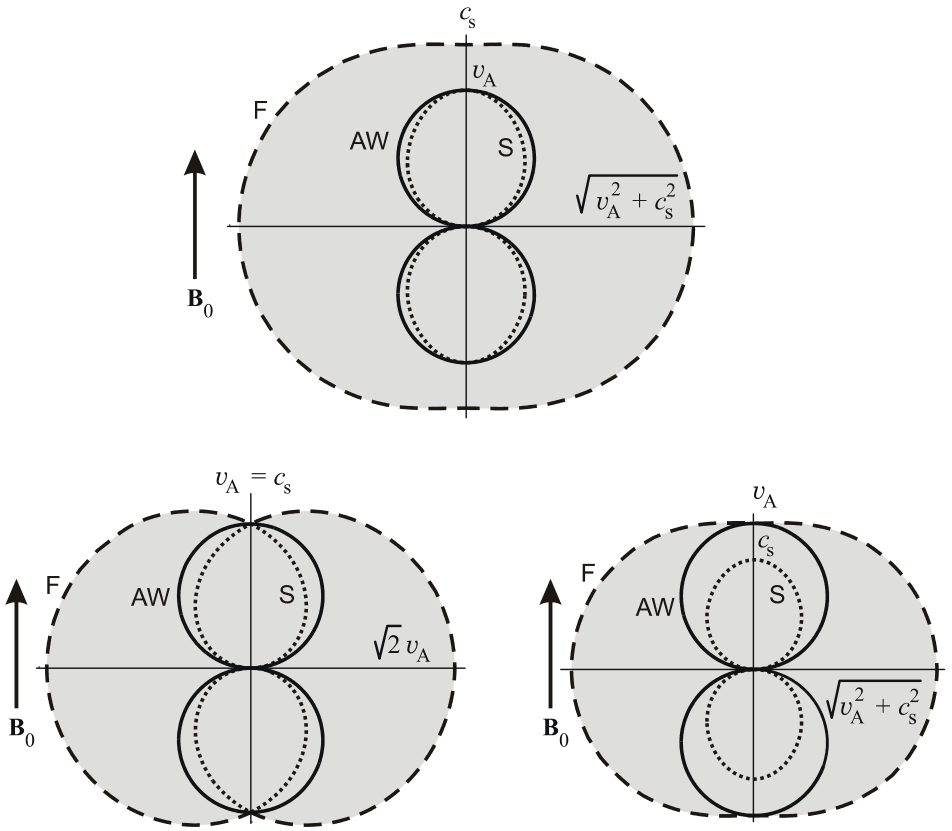


Fig. 1.61: The top panel illustrates the situation for a weak field ($v_A < c_s$), where the fast wave (F) represents a normal sound wave. In the lower-left panel, the effects of magnetic and thermal pressures are balanced ($v_A = c_s$). In the lower-right panel, the magnetic field dominates ($v_A > c_s$).

Directions of Vectors in Magnetoacoustic Waves

To examine the directions of individual perturbations for a specific mode, the corresponding dispersion relation is substituted into the original linearized system (1.391), keeping the coordinate system unchanged. This allows the determination of the direc-

tions of the individual vectors from (1.391). Magnetoacoustic waves represent a mixture of longitudinal and transverse waves. From the equation $\partial\mathbf{B}/\partial t = \text{curl}\,(\mathbf{u}\times\mathbf{B})$, it follows that $-\omega\delta\mathbf{B} = \mathbf{k}\times(\delta\mathbf{u}\times\mathbf{B}_0)$. The magnetic field perturbation is always perpendicular to the direction of wave propagation. Three critical scenarios are analyzed below.

Alfvén Wave

The Alfvén mode yields the simplest of the three dispersion relations. The system of equations (1.391) shows that the plasma oscillates perpendicular to both the magnetic field and the direction of propagation, classifying it as a transverse wave. The magnetic field perturbation is perpendicular to the initial magnetic field, causing the magnetic field lines to ripple. If the field is aligned with the z-axis, the dispersion relation takes the form $\omega = v_A k\cos\alpha = v_A k_z$, and the group velocity equals $\mathbf{v} = (0, 0, v_A)$. In an Alfvén wave, energy propagates exclusively along the magnetic field $\mathbf{B}_0$ at the Alfvén velocity.

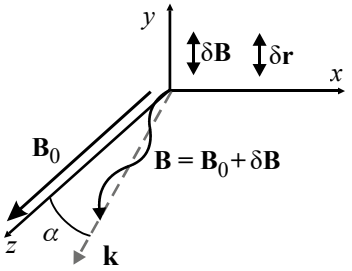


Fig. 1.62: relative vector directions within an Alfvén wave.

Compressional Wave

In a fast magnetoacoustic wave propagating perpendicular to the magnetic field ($\mathbf{k}\perp\mathbf{B}_0$), the perturbation is parallel to the initial field. This creates a wave of denser and sparser magnetic field lines, known as a compressional wave. The plasma oscillates along the direction of wave propagation $\mathbf{k}$ (perpendicular to field $\mathbf{B}_0$), making it a *longitudinal wave*. The wave behavior closely resembles "ordinary" sound; however, the role of the elastic medium is played by both the hydrostatic pressure p and the magnetic pressure $p_M = B^2/2\mu_0$. The wave velocity is determined by both effects, yielding $v_f = (c_s^2 + v_A^2)^{1/2}$. This mode is occasionally called the *compressional Alfvén longitudinal wave*.

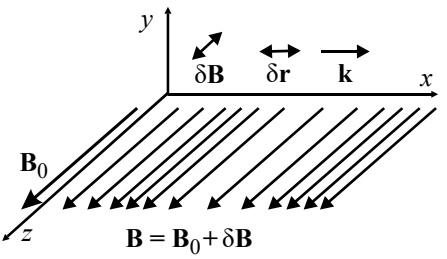


Fig. 1.63: Relative vector directions within an compressional wave.

Classical Sound Wave

Along $\mathbf{B}_0$, either a fast or slow wave propagates at the sound speed c_s (depending on the field strength). The plasma oscillates along the propagation direction and remains unaffected by the magnetic field, whose perturbation vanishes.

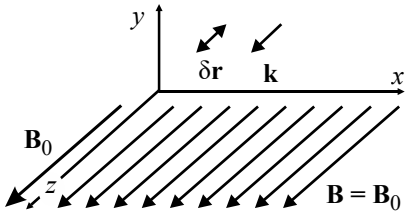


Fig. 1.64: Relative vector directions within a classical sound wave.

1.4.5 Electromagnetic Waves

Electromagnetic waves propagating through plasma interact primarily with electrons, as the heavier ions cannot respond quickly enough to high-frequency processes. For an electromagnetic wave, the following relations hold:

$$\begin{aligned} &\operatorname{div}\mathbf{B} = 0 \qquad \Rightarrow \qquad \delta\mathbf{B} \perp \mathbf{k}\,, \\ &\operatorname{curl}\mathbf{E} = -\frac{\partial \mathbf{B}}{\partial t} \qquad \Rightarrow \qquad \delta\mathbf{B} \perp \delta\mathbf{E}\,. \end{aligned} \tag{1.399}$$

A constant magnetic field $\mathbf{B}_0$ causes anisotropy in wave propagation. Perpendicular to the field, the plasma exhibits *ordinary* and *extraordinary* waves, similar to birefringent crystals. Along the field, however, these waves appear as a mixture of *left-* and *right-handed* modes. Plasma phenomena also include *whistlers* – low-frequency signals lasting several seconds that arise from lightning and propagate along Earth magnetic field lines. Understanding the material response to high-frequency waves and calculating *plasma permittivity* remain of major interest.

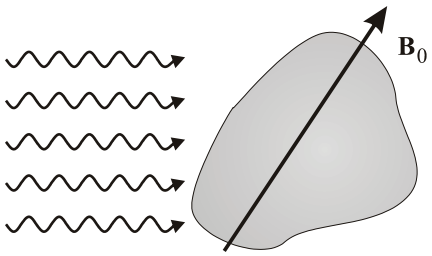


Fig. 1.65: Interaction of an electromagnetic wave with a plasma, where a wide variety of modes can be excited.

Dispersion Relations of the Electromagnetic Complex

As governing equations, the electron continuity equation, the electron equation of motion, and the Maxwell equations are selected. Due to the high frequency of these processes, Maxwell displacement current cannot be neglected. Throughout this analysis, the limit $m_\mathrm{i} \to \infty$ and $p \to 0$ is considered; that is, for electromagnetic wave propagation through plasma, ion motion and thermal processes are neglected, restricting the framework to a cold electron plasma:

$$\frac{\partial n_\mathrm{e}}{\partial t} + \mathrm{div}(n_\mathrm{e}\mathbf{u}_\mathrm{e}) = 0\,,$$

$$m_\mathrm{e} n_\mathrm{e} \frac{\partial \mathbf{u}_\mathrm{e}}{\partial t} + m_\mathrm{e} n_\mathrm{e} (\mathbf{u}_\mathrm{e} \cdot \nabla)\mathbf{u}_\mathrm{e} = -en_\mathrm{e}\mathbf{E} + \mathbf{j}\times\mathbf{B}\,, \tag{1.400}$$

$$\frac{\partial \mathbf{B}}{\partial t} = -\,\mathrm{curl}\,\mathbf{E}\,,$$

$$\frac{\partial \mathbf{E}}{\partial t} = \frac{1}{\varepsilon_0\mu_0}\,\mathrm{curl}\,\mathbf{B} - \frac{\mathbf{j}}{\varepsilon_0}\,; \qquad \mathbf{j} = -en_\mathrm{e}\mathbf{u}_\mathrm{e}\,.$$

Linearization is performed:

$$n_\mathrm{e} = n_0 + \delta n_\mathrm{e}\,, \qquad \mathbf{u}_\mathrm{e} = \delta\mathbf{u}_\mathrm{e}\,, \qquad \mathbf{B} = \mathbf{B}_0 + \delta\mathbf{B}\,, \qquad \mathbf{E} = \delta\mathbf{E} \tag{1.401}$$

and the Fourier transform (1.400) is applied using the standard procedure. Since number density perturbations vanish throughout, the continuity equation can be omitted. The current density from the last equation is substituted into the remaining equations:

$$\delta\mathbf{u}_\mathrm{e} = -\mathrm{i}\frac{e}{m_\mathrm{e}\omega}\delta\mathbf{E} - \mathrm{i}\frac{e}{m_\mathrm{e}\omega}\delta\mathbf{u}_\mathrm{e}\times\mathbf{B}_0\,,$$

$$\delta\mathbf{B} = \frac{1}{\omega}\,\mathbf{k}\times\delta\mathbf{E}\,, \tag{1.402}$$

$$\delta\mathbf{E} = -\frac{1}{\varepsilon_0\mu_0\omega}\,\mathbf{k}\times\delta\mathbf{B} + \mathrm{i}\frac{en_0}{\varepsilon_0\omega}\delta\mathbf{u}_\mathrm{e}\,.$$

The standard notation is introduced

$$c^2 \equiv \frac{1}{\varepsilon_0\mu_0}\,; \qquad \omega_\mathrm{p}^2 \equiv \frac{n_0 e^2}{m_\mathrm{e}\varepsilon_0}\,; \qquad \omega_\mathrm{c} \equiv \frac{eB_0}{m_\mathrm{e}} \tag{1.403}$$

for the speed of light, the plasma frequency, and the cyclotron frequency, and the unit vector along the magnetic field is defined as:

$$\mathbf{e}_B \equiv \frac{\mathbf{B}_0}{B_0}\,. \tag{1.404}$$

Variables are eliminated from system (1.402); from the second equation, $\delta\mathbf{B}$ is substituted into the remaining equations:

$$\delta\mathbf{u}_\mathrm{e} = -\mathrm{i}\frac{e}{m_\mathrm{e}\omega}\delta\mathbf{E} - \mathrm{i}\frac{\omega_\mathrm{c}}{\omega}\,\delta\mathbf{u}_\mathrm{e}\times\mathbf{e}_B,$$

$$\delta\mathbf{E} = -\frac{c^2}{\omega^2}\,\mathbf{k}\times(\mathbf{k}\times\delta\mathbf{E}) + \mathrm{i}\frac{en_0}{\varepsilon_0\omega}\delta\mathbf{u}_\mathrm{e}\,.$$

The velocity field perturbation is then expressed from the second equation and substituted it into the first (simplifying the vector triple products). This yields a separate equation for the electric field perturbation:

$$(\omega^2-\omega_\mathrm{p}^2-c^2k^2)\,\delta\mathbf{E}+\mathrm{i}\frac{\omega_\mathrm{c}}{\omega}(\omega^2-c^2k^2)(\delta\mathbf{E}\times\mathbf{e}_B)+$$

$$+c^2(\mathbf{k}\cdot\delta\mathbf{E})\mathbf{k}+\mathrm{i}\frac{\omega_\mathrm{c}}{\omega}c^2(\mathbf{k}\cdot\delta\mathbf{E})(\mathbf{k}\times\mathbf{e}_B)=0\,.$$

The same coordinate system as before is chosen: the z-axis points along the field $\mathbf{B}_0 = (0, 0, B_0)$, and the vector $\mathbf{k}$ lies in the (x, z) plane, such that $\mathbf{k} = (k \sin\alpha, 0, k \cos\alpha)$:

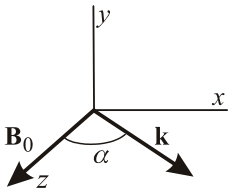


Fig. 1.66: Choice of the coordinate system.

In this coordinate system, the equation for the electric field perturbation takes the form:

$$\mathbf{M}_\mathbf{E}\cdot\delta\mathbf{E}=0\,; \tag{1.405}$$

$$\mathbf{M}_\mathrm{E}=\begin{pmatrix}\omega^2-\omega_\mathrm{p}^2-c^2k^2\cos^2\alpha, & \mathrm{i}\frac{\omega_\mathrm{c}}{\omega}(\omega^2-c^2k^2), & c^2k^2\cos\alpha\sin\alpha,\\ -\mathrm{i}\frac{\omega_\mathrm{c}}{\omega}(\omega^2-c^2k^2\cos^2\alpha), & \omega^2-\omega_\mathrm{p}^2-c^2k^2, & -\mathrm{i}\frac{\omega_\mathrm{c}}{\omega}c^2k^2\cos\alpha\sin\alpha,\\ c^2k^2\cos\alpha\sin\alpha, & 0, & \omega^2-\omega_\mathrm{p}^2-c^2k^2\sin^2\alpha.\end{pmatrix}.$$

For a non-trivial solution, the determinant of matrix $\mathbf{M}_\mathrm{E}$ must vanish, yielding:

$$-\left[c^4k^4\cos^2\alpha\sin^2\alpha\right]\cdot\left[\left(\omega^2-\omega_\mathrm{p}^2-c^2k^2\right)-\left(\frac{\omega_\mathrm{c}}{\omega}\right)^2\left(\omega^2-c^2k^2\right)\right]+$$

$$+\left[\omega^2-\omega_\mathrm{p}^2-c^2k^2\sin^2\alpha\right]\cdot\left[\begin{array}{l}\left(\omega^2-\omega_\mathrm{p}^2-c^2k^2\cos^2\alpha\right)\left(\omega^2-\omega_\mathrm{p}^2-c^2k^2\right)-\\ -\left(\frac{\omega_\mathrm{c}}{\omega}\right)^2\left(\omega^2-c^2k^2\right)\left(\omega^2-c^2k^2\cos^2\alpha\right)\end{array}\right]=0. \tag{1.406}$$

For electromagnetic waves, the refractive index, given by the relation

$$N=\frac{c}{v_\mathrm{f}}=\frac{c}{\omega/k}=\frac{ck}{\omega}\,. \tag{1.407}$$

is essential. It is therefore often advantageous to solve the dispersion relation for ck or ck/ω. The resulting refractive index becomes a function of the angular frequency:

$$N(\omega)\equiv\frac{ck(\omega)}{\omega}\,. \tag{1.408}$$

The refractive index also depends on the number density (via the plasma frequency) and the magnetic field (via the cyclotron frequency). Of particular interest are limiting situations where the refractive index becomes infinite (*resonance*) or zero (*cutoff*, representing the frequency below or above which a wave ceases to propagate):

$$\text{Resonance:} \qquad N \to \infty \;\; (v_\mathrm{f} \to 0)\,; \tag{1.409}$$

$$\text{Cut-off:} \qquad N \to 0 \;\; (v_\mathrm{f} \to \infty)\,. \tag{1.410}$$

Parallel Propagation: R and L Waves

Along the field ($\alpha = 0$), the dispersion relation reduces to a relatively simple expression:

$$\left[\omega^2 - \omega_\mathrm{p}^2\right] \cdot \left[\left(\omega^2 - \omega_\mathrm{p}^2 - c^2k^2\right)^2 - \left(\frac{\omega_\mathrm{c}}{\omega}\right)^2 \left(\omega^2 - c^2k^2\right)^2\right] = 0\,. \tag{1.411}$$

The solution for ω yields three fundamental modes. The first, obtained by setting the left parenthesis to zero, corresponds to electron plasma oscillations. No ion mass correction appears because the ions are considered infinitely massive. Setting the right parenthesis to zero yields the remaining two modes: the R and L waves.

R and L Waves

The dispersion relation is obtained from the condition:

$$\left(\omega^2 - \omega_\mathrm{p}^2 - c^2k^2\right)^2 - \left(\frac{\omega_\mathrm{c}}{\omega}\right)^2 \left(\omega^2 - c^2k^2\right)^2 = 0\,,$$

which allows to isolate the combination $\omega^2 - c^2k^2$. From this relation c^2k^2 is determined. Solving the dispersion relation for k in this way is straightforward procedure:

► $$c^2k^2 = \omega^2 - \frac{\omega_\mathrm{p}^2}{1 \mp \omega_\mathrm{c}/\omega}\,; \qquad \omega_\mathrm{c} = \left|\omega_\mathrm{ce}\right|. \tag{1.412}$$

The refractive index is then given by:

► $$N_\mathrm{R,L}^2 = 1 - \frac{(\omega_\mathrm{p}/\omega)^2}{1 \mp \omega_\mathrm{c}/\omega}\,. \tag{1.413}$$

Substituting c^2k^2 from the dispersion relation (1.412) into the linearized electric field equation (1.405) yields:

$$\delta E_y = \pm\,\mathrm{i}\,\delta E_x\,; \qquad \delta E_z = 0\,. \tag{1.414}$$

The imaginary unit denotes a mutual phase shift of $\pi/2$ between the components E_x and E_y (analogous to the superposition of two phase-shifted orthogonal oscillations). These represent right- and left-handed circularly polarized waves, known as the R wave (Right) and L wave (Left). The electric field perturbation is perpendicular to the background magnetic field ($\delta\mathbf{E} \perp \mathbf{B}_0$). For a wave $\delta E_x = A\,\exp(\mathrm{i}kz - \mathrm{i}\omega t)$, the real part of the time component equals $\mathrm{Re}(\delta E_x) \sim A\cos\omega t$, and according to the equation (1.414), $\mathrm{Re}(\delta E_y) \sim \pm A\sin\omega t$. The direction of rotation corresponds to the following figure:

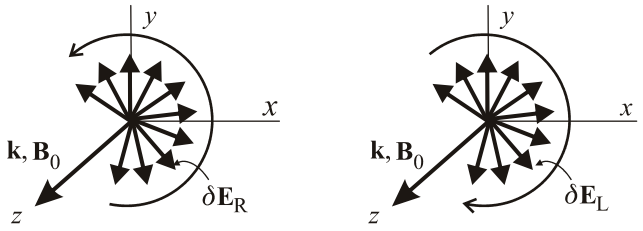


Fig. 1.67: Right-handed (R) and left-handed (L) circularly polarized wave topologies.

The handedness is determined by the rotation of the electric field vector when viewed along the magnetic field $\mathbf{B}_0$. Now the resonance and cutoff frequencies are determined:

Cyclotron Resonance. The condition $N \to \infty$ occurs only for the R wave at:

$$\omega = \omega_c \,. \tag{1.415}$$

The wave is absorbed at the Larmor frequency of the electrons. The L wave does not resonate with the electrons, as its electric field vector rotates opposite to the natural electron gyromotion around the magnetic field lines.

Cutoff Frequencies. The condition $N \to 0$ corresponds to wave reflection, defining the boundary of wave propagation. This occurs at the left and right cutoff frequencies:

$$\omega = \omega_{R,L} \equiv \pm\frac{1}{2}\omega_c + \frac{1}{2}\sqrt{\omega_c^2 + 4\omega_p^2} \,. \tag{1.416}$$

Only the positive root before the discriminant is retained to ensure a positive frequency. This choice accounts for all physically consistent combinations without losing solutions. Figure 1.68 illustrates the propagation regions for R and L waves.

Perpendicular Propagation: O and X Waves

For $\alpha = \pi/2$, the dispersion relation (1.406) reduces to:

$$\left[\omega^2 - \omega_p^2 - c^2k^2\right]\cdot\left[\left(\omega^2 - \omega_p^2\right)\left(\omega^2 - \omega_p^2 - c^2k^2\right) - \omega_c^2\left(\omega^2 - c^2k^2\right)\right] = 0 \,. \tag{1.417}$$

Ordinary Wave (O)

Setting the first parenthesis to zero yields the *ordinary wave* (O wave), whose dispersion relation resembles that of unmagnetized plasma waves:

► $$\omega^2 = \omega_p^2 + c^2k^2 \,. \tag{1.418}$$

The refractive index of the ordinary wave is given by:

► $$N_O^2 \equiv \frac{c^2k^2}{\omega^2} = 1 - \left(\frac{\omega_p}{\omega}\right)^2 = 1 - \frac{n_0e^2}{m_e\varepsilon_0\omega^2} \,. \tag{1.419}$$

Since the refractive index is frequency-dependent, different frequencies propagate at different velocities. Various plasma diagnostic methods are based on relation (1.419),

such as schlieren photography, which visualizes transverse gradients of the refractive index. In experimental physics, a simplified relation (valid for $\omega \gg \omega_p$) obtained from the first term of the Taylor expansion is frequently utilized:

$$N_O = \sqrt{1-\frac{n_0 e^2}{m_e \varepsilon_0 \omega^2}} \simeq 1-\frac{n_0 e^2}{2 m_e \varepsilon_0 \omega^2}. \tag{1.420}$$

Equations (1.418) or (1.419) represent the fundamental dispersion relation for electromagnetic wave propagation through plasma. The angular frequency and wave vector are real for $\omega > \omega_p$. For $\omega < \omega_p$, the wave vector becomes complex, meaning the wave is evanescent and ceases to propagate. Instead, it drives electron oscillations and undergoes reflection. The propagation regions for the O wave are illustrated in Figure 1.68.

Resonance. For the ordinary wave, no resonances occur ($N \to \infty$); the refractive index remains finite throughout the entire frequency spectrum.

Cutoff. The cutoff frequency ($N \to 0$) equals the electron plasma frequency, ω_p.

- The propagation of an ordinary wave is unaffected by the magnetic field; the wave propagates as if the field were absent.
- An ordinary wave features an electric field perturbation parallel to the background magnetic field ($\delta\mathbf{E} \parallel \mathbf{B}_0$).
- For frequencies exceeding the plasma frequency, the plasma is transparent to electromagnetic waves.

Extraordinary Wave (X)

Setting the second parenthesis in (1.417) to zero yields the dispersion relation for the extraordinary wave (X wave):

$$\left(\omega^2-\omega_p^2\right)\left(\omega^2-\omega_p^2-c^2k^2\right)-\omega_c^2\left(\omega^2-c^2k^2\right)=0. \tag{1.421}$$

Expressing the combination $\omega^2-c^2k^2$ allows us to determine c^2k^2 and, subsequently, the refractive index of the extraordinary wave:

► $$N_X^2 = 1-\left(\frac{\omega_p}{\omega}\right)^2 \frac{\omega^2-\omega_p^2}{\omega^2-\omega_p^2-\omega_c^2} \quad \text{or}$$

► $$N_X^2 = 1-\left(\frac{\omega_p}{\omega}\right)^2 \frac{1-(\omega_p/\omega)^2}{1-(\omega_p/\omega)^2-(\omega_c/\omega)^2}. \tag{1.422}$$

Standard limiting cases occur for:

$$N \to \infty \ (v_f \to 0) \qquad \Rightarrow$$

► $$\omega = \omega_h \equiv \sqrt{\omega_p^2 + \omega_c^2}\,. \tag{1.423}$$

$$N \to 0 \;\; (v_f \to \infty) \qquad \Rightarrow$$

► $$\omega = \omega_{L,R} \equiv \mp \frac{1}{2}\omega_c + \frac{1}{2}\sqrt{\omega_c^2 + 4\omega_p^2} \tag{1.424}$$

Deriving the cutoff frequencies (1.424) through direct calculation is algebraically tedious, as it involves nested square roots. It is more advantageous to prove, via direct substitution, that a highly useful identity holds between the refractive indices (formulas can be simplified during the proof by denoting $\omega_p/\omega=\mathscr{P}$, $\omega_c/\omega=\mathscr{C}$):

$$N_X^2 = \frac{2N_R^2 N_L^2}{N_R^2 + N_L^2}\,, \tag{1.425}$$

which implies $N_X =$ when $N_R = 0$ or $N_L = 0$, corresponding to the left and right cutoff frequencies.

Resonance (Upper Hybrid). Resonance occurs at the upper hybrid frequency ω_h, where the wave group velocity vanishes ($v_g = 0$) and the magnetic field perturbation disappears. Under these conditions, the oscillations become purely electrostatic electron oscillations at the upper hybrid frequency. This generalizes the plasma oscillations induced by an electromagnetic wave. In addition to the Coulomb force, the Lorentz force (associated with Larmor gyromotion around $\mathbf{B}_0$) acts as a restoring force; consequently, the frequency is higher than in pure, unmagnetized plasma oscillations. At a non-zero electron temperature (accounting for the pressure term), these oscillations begin to propagate as waves.

Cutoffs (Left and Right). The propagation boundaries of the X wave are determined by the right and left cutoff frequencies $\omega_{R,L}$. The extraordinary wave propagates within the intervals $\omega \in (\omega_L, \omega_h) \cup (\omega_R, \infty)$. The corresponding regions are illustrated in Fig. 1.68.

- The X wave is evanescent within the intervals $(0, \omega_L) \cup (\omega_h, \omega_R)$.
- The X wave is heavily influenced by the background magnetic field $\mathbf{B}_0$.
- In the X wave, the electric field perturbation is perpendicular to the background magnetic field: $\delta\mathbf{E} \perp \mathbf{B}_0$. The electrons oscillate along the electric field while simultaneously gyrating around the magnetic field lines.

In the case of an arbitrary wave propagation direction relative to the magnetic field $\mathbf{B}_0$, electromagnetic wave propagation is described by the general dispersion relation (1.406). At resonance frequencies, the electromagnetic wave is absorbed, leading to localized plasma heating. Such auxiliary heating by electromagnetic waves of suitable frequencies is utilized in various devices, including tokamaks. Because ion motion has not yet been incorporated into this framework, the ion cyclotron resonance for the L wave and the lower hybrid resonance for the X wave have not been derived here.

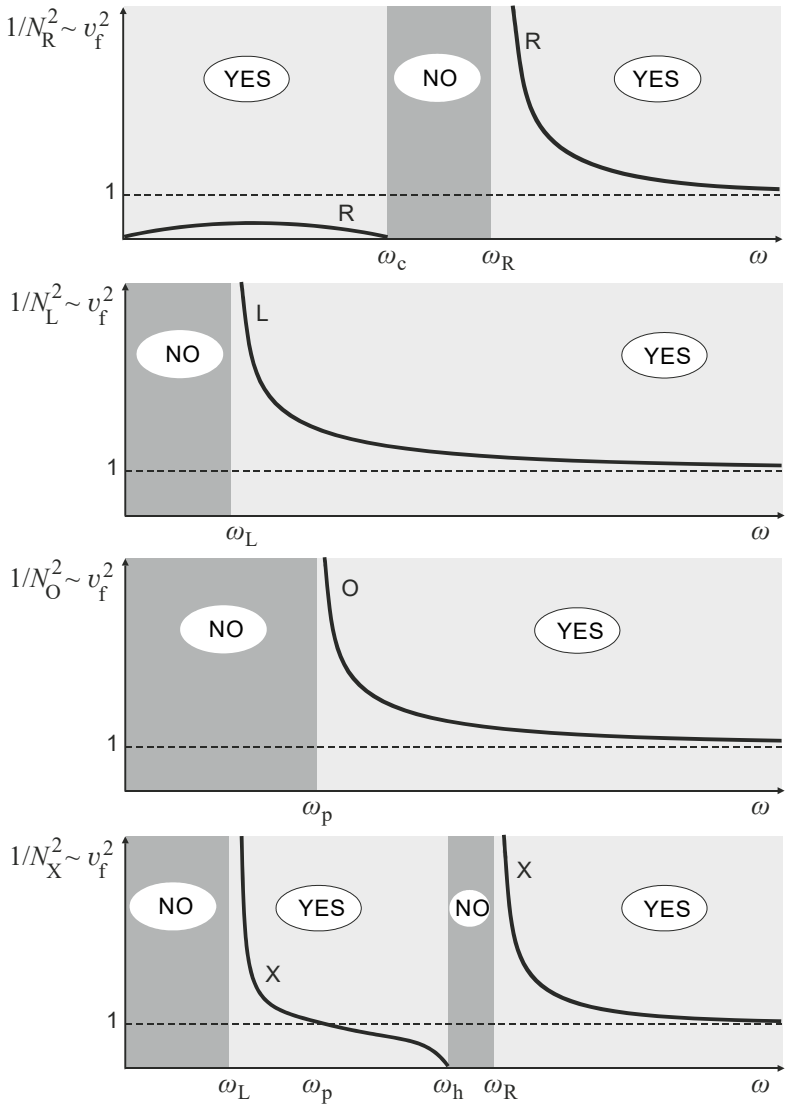


Fig. 1.68. Dispersion relations for L, R, O, and X waves. Propagation is limited to light gray bands.

Dispersion relations of electromagnetic waves for a cold electron plasma are illustrated in Figure 1.69. The curves are plotted for $\omega_c = 2.5\ \omega_p$. Neither ion nor thermal processes are considered in these plots; accounting for them would yield more complex dispersion relations. In the upper plot, resonances are easily identifiable where the corresponding branch of the dispersion relation approaches infinity (the refractive index diverges). The only electromagnetic wave mode capable of propagating at ultra-low frequencies is the R wave, commonly known as a *whistler*. The lower plot shows that the refractive index exceeds unity for the R wave in the region $\omega < \omega_c$ and for the X wave in the interval $\omega \in (\omega_p, \omega_h)$. The plots were generated in Wolfram Mathematica.

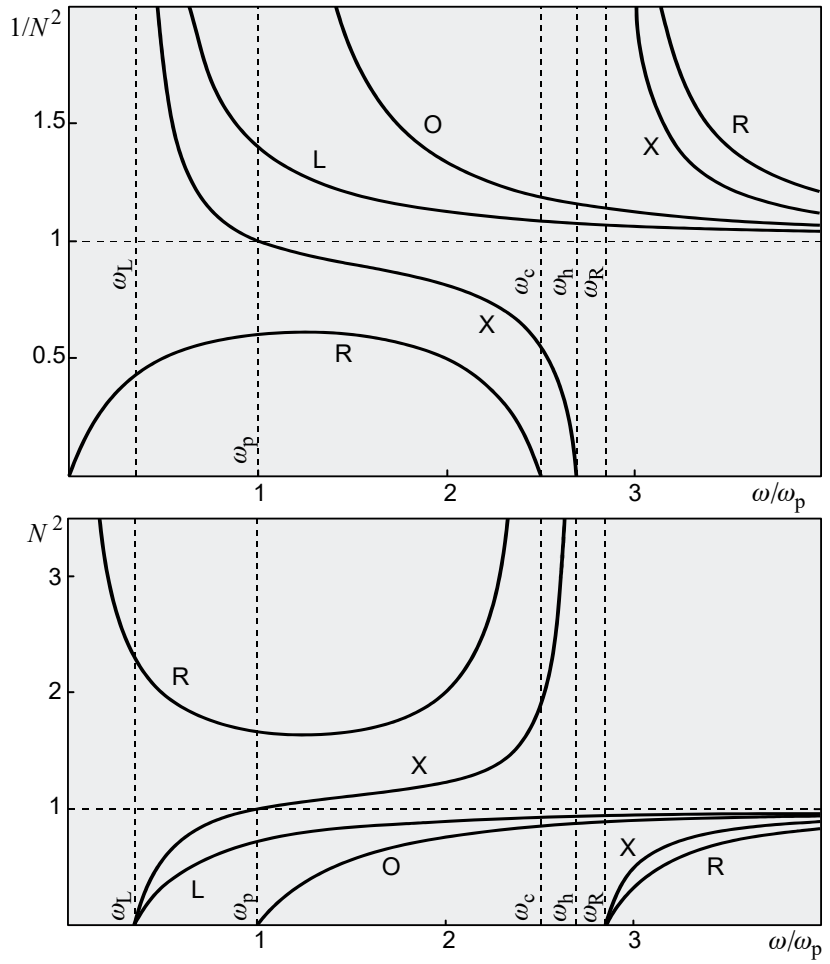


Fig. 1.69: Dispersion relations for electromagnetic waves and cold electron plasma.

Stix Coefficients and the CMA Diagram

The general dispersion relation $\phi(\omega, \mathbf{k}) = 0$ is solved either for the frequency ω or the wave vector $\mathbf{k}$. Frequently, it is also useful to determine the refractive index $N \equiv ck/\omega$ directly from it. This approach offers clear advantages: the refractive index is dimensionless, rendering the dispersion relation independent of units, while the resonance and cutoff frequencies correspond directly to the limits $N \to \infty$ and $N \to 0$. The following notation is frequently utilized for the squares of the refractive indices:

$$R \equiv N_{\mathrm{R}}^2 = 1 - \frac{\omega_{\mathrm{p}}^2/\omega^2}{1 - \omega_{\mathrm{c}}/\omega}; \qquad L \equiv N_{\mathrm{L}}^2 = 1 - \frac{\omega_{\mathrm{p}}^2/\omega^2}{1 + \omega_{\mathrm{c}}/\omega};$$

$$P \equiv N_{\mathrm{O}}^2 = 1 - \frac{\omega_{\mathrm{p}}^2}{\omega^2}; \qquad X \equiv N_{\mathrm{X}}^2 = \frac{2RL}{R+L}. \tag{1.426}$$

►

The last expression represents a rewritten form of relation (1.425). For a multi-fluid plasma, the sum is taken over all species components (where $\omega_{c\alpha} = \omega_{ce} = -eB/m$).

$$N_R^2 = 1 - \sum_\alpha \frac{\omega_{p\alpha}^2/\omega^2}{1 + \omega_{c\alpha}/\omega};$$

$$N_L^2 = 1 - \sum_\alpha \frac{\omega_{p\alpha}^2/\omega^2}{1 - \omega_{c\alpha}/\omega}; \tag{1.427}$$

$$N_O^2 = 1 - \sum_\alpha \frac{\omega_{p\alpha}^2}{\omega^2}.$$

Symmetric and antisymmetric combinations of N_R and N_L are introduced as follows:

$$\begin{aligned} S &\equiv \tfrac{1}{2}(R + L); \\ D &\equiv \tfrac{1}{2}(R - L). \end{aligned} \tag{1.428}$$

The quantity X can then be written as:

$$X = RL/S \ . \tag{1.429}$$

The coefficients S, D, P, and X are known as Stix coefficients, named after the American plasma physicist Thomas Howard Stix, who introduced them in 1962. In the previous section graphs, the vertical axis represents the reciprocal of the corresponding Stix coefficient, which is proportional to the square of the phase velocity. The general dispersion relation (1.406) can be solved for the refractive index:

► $$N^2 = 1 - \frac{\mathscr{P}^2}{1 - \frac{\frac{1}{2}\mathscr{C}^2 \sin^2\alpha}{1 - \mathscr{P}^2} \pm \frac{1}{1 - \mathscr{P}^2}\sqrt{\frac{1}{4}\mathscr{C}^4 \sin^4\alpha + \mathscr{C}^2\left[1 - \mathscr{P}^2\right]^2 \cos^2\alpha}}; \tag{1.430}$$

$$\mathscr{C} \equiv \frac{\omega_c}{\omega}; \qquad \mathscr{P} \equiv \frac{\omega_p}{\omega}.$$

The resulting expression is known as the Appleton–Hartree formula, named after the English physicist Edward Victor Appleton and the English mathematician and physicist Douglas Reyner Hartree. Independently, the German radio engineer Hans Karl Lassen derived this relation, though his research remained largely unknown in English-speaking countries. For a wave propagating parallel to an external magnetic field, the dispersion relation branches (via a ± sign in the denominator) into the R and L modes, whereas for perpendicular propagation, it splits into the O and X modes.

Considering a two-fluid plasma (electrons and ions) yields two additional resonance frequencies: the ion cyclotron resonance for the L wave (where the ion Larmor gyromotion shares the same sense of rotation as the electric field perturbation in the L wave) and the lower hybrid resonance for the X wave. The wavefront geometries are illustrated in the polar phase velocity diagram known as the CMA diagram, while all resonance and cutoff frequencies are summarized in the subsequent tables.

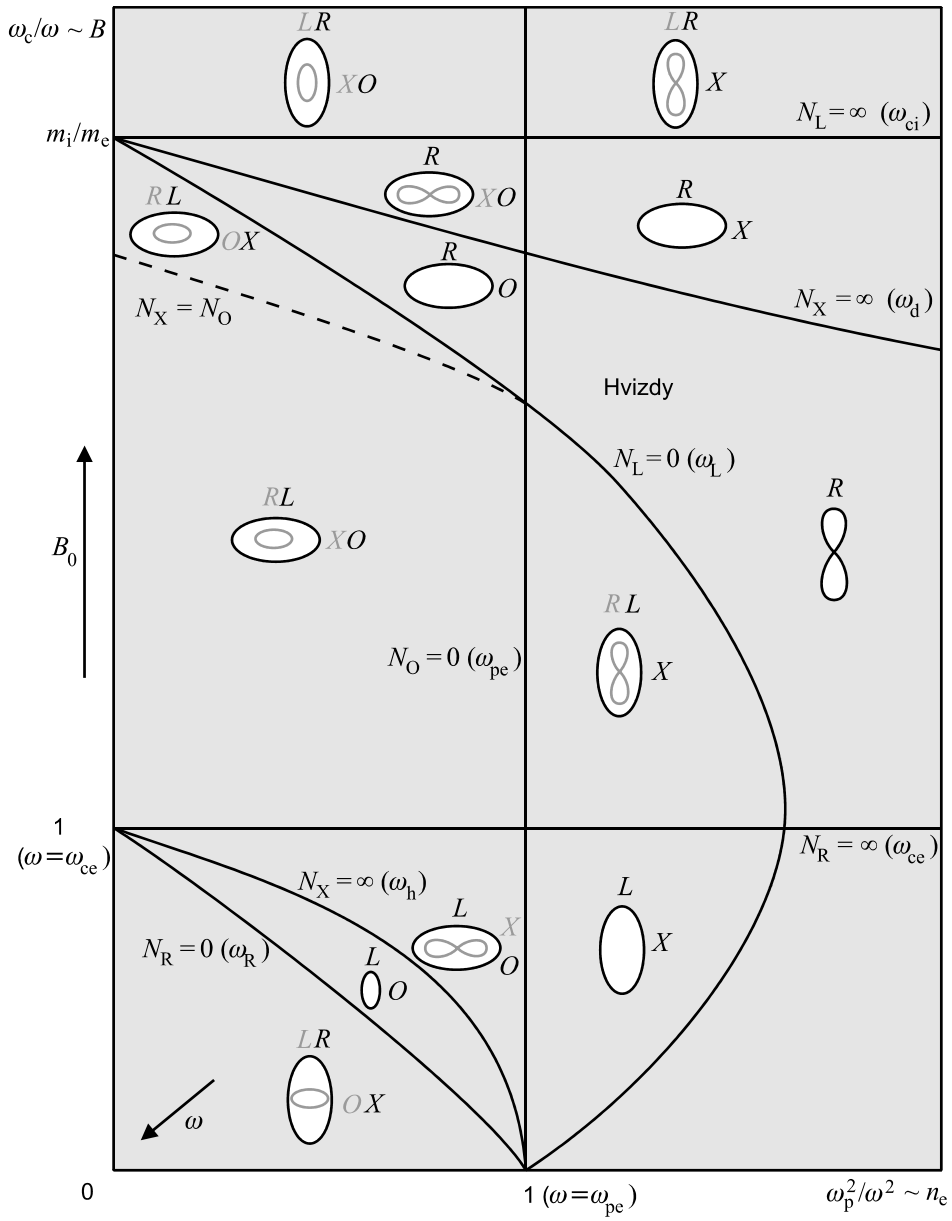


Fig. 1.70: CMA Diagram. The wavefront shapes (polar phase velocity diagrams) are mapped on the CMA diagram, named after the initials of its authors (Phillips Charles Clemmow, Terence Richard Mullaly, 1955; William Phelps Allis, 1959). The axes represent the background magnetic field and plasma density. The wavefronts change abruptly at boundaries where the refractive index of the various modes (*L*, *R*, *O*, *X*) vanishes or diverges. This diagram corresponds to a cold two-fluid electron-ion plasma. Note that in the right half ($\omega < \omega_{pe}$), the ordinary wave (O) is absent. The whistler region, where exclusively the R wave propagates, is bounded on the left by $\omega < \omega_{pe}$ and on the bottom by $\omega < \omega_{ce}$.

Resonance frequencies

$N_L \to \infty$	Cyclotron ion resonance	$\omega = \omega_{ci} = \dfrac{ZeB_0}{m_i}$
$N_R \to \infty$	Cyclotron electron resonance	$\omega = \lvert\omega_{ce}\rvert = \dfrac{eB_0}{m_e}$
$N_O \to \infty$	–	–
$N_X \to \infty$	Upper hybrid resonance	$\omega = \omega_h = \sqrt{\omega_{pe}^2 + \omega_{ce}^2}$
	Lower hybrid resonance	$\omega = \omega_d = \sqrt{\lvert\omega_{ci}\omega_{ce}\rvert}$

Cutoff frequencies

$N_L = 0$	L waves	$\omega = \omega_L = -\dfrac{1}{2}\lvert\omega_{ce}\rvert + \dfrac{1}{2}\sqrt{\omega_{ce}^2 + 4\omega_{pe}^2}$
$N_R = 0$	R waves	$\omega = \omega_R = +\dfrac{1}{2}\lvert\omega_{ce}\rvert + \dfrac{1}{2}\sqrt{\omega_{ce}^2 + 4\omega_{pe}^2}$
$N_O = 0$	O waves	$\omega = \omega_{pe} = \sqrt{\dfrac{n_e e^2}{m_e \varepsilon_0}}$
$N_X = 0$	L waves	$\omega = \omega_L = -\dfrac{1}{2}\lvert\omega_{ce}\rvert + \dfrac{1}{2}\sqrt{\omega_{ce}^2 + 4\omega_{pe}^2}$
	R waves	$\omega = \omega_R = +\dfrac{1}{2}\lvert\omega_{ce}\rvert + \dfrac{1}{2}\sqrt{\omega_{ce}^2 + 4\omega_{pe}^2}$

Summary of resonance and cutoff frequencies (assuming $\omega_{ce} \gg \omega_{ci}$, $\omega_{pe} \gg \omega_{pi}$).

Faraday Rotation

Consider a linearly polarized wave propagating through a cold plasma along the direction of the magnetic field. Such a wave can be constructed by superimposing right- and left-handed circularly polarized waves of equal amplitude. In the geometry adopted here (where the magnetic field aligns with the z-axis), the circularly polarized waves satisfy:

$$\begin{aligned} \mathbf{E}_R &= E_0\, e^{i(k_R z - \omega t)}(\mathbf{e}_x + i\,\mathbf{e}_y)\,; \\ \mathbf{E}_L &= E_0\, e^{i(k_L z - \omega t)}(\mathbf{e}_x - i\,\mathbf{e}_y)\,. \end{aligned} \tag{1.431}$$

The component E_y follows from relation (1.414), which can be verified by separating E_x and E_y. The propagation of a linearly polarized wave along the magnetic field is analyzed as a superposition of circularly polarized modes:

$$\mathbf{E} = \frac{1}{2}(\mathbf{E}_L + \mathbf{E}_R) = \frac{E_0}{2} e^{-i\omega t}\left[\left(e^{ik_L z} + e^{ik_R z}\right)\mathbf{e}_x - i\left(e^{ik_L z} - e^{ik_R z}\right)\mathbf{e}_y\right]. \tag{1.432}$$

If the wave vectors k_R and k_L were identical, the y-components would cancel, yielding a linearly polarized wave in the (x, z) plane. In a plasma, however, the wave vectors of the left- and right-handed waves differ slightly, leading to a continuous rotation of the polarization plane. This phenomenon is known as *Faraday rotation*, discovered by the prominent English physicist and chemist Michael Faraday in 1845.

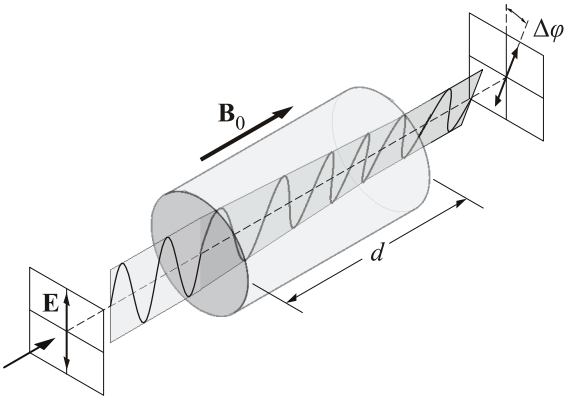


Fig. 1.71: Spatial mechanism of Faraday rotation.

For the wave vectors given by (1.412), the relation yields::

$$k_{R,L} = \frac{\omega}{c}\sqrt{1-\frac{\omega_p^2/\omega^2}{1\mp\omega_c/\omega}}\,.$$

In the high-frequency limit $\omega \gg \omega_c, \omega_p$, the expression can be approximated as:

$$k_{R,L} = \frac{\omega}{c}\left(1-\frac{1}{2}\frac{\omega_p^2/\omega^2}{(1\mp\omega_c/\omega)}+\cdots\right) \approx \frac{\omega}{c}\left(1-\frac{\omega_p^2}{2\omega^2}\mp\frac{\omega_p^2\omega_c}{2\omega^3}+\cdots\right)$$

or

$$\begin{aligned} k_{R,L} &= k \mp \Delta k\,; \\ k &\equiv \frac{k_L + k_R}{2} \approx \frac{\omega}{c}\left(1-\frac{\omega_p^2}{2\omega^2}\right); \\ \Delta k &\equiv \frac{k_L - k_R}{2} \approx \frac{1}{2}\frac{\omega_p^2}{\omega^2}\frac{\omega_c}{c}\,. \end{aligned} \tag{1.433}$$

Substituting (1.433) into (1.432) yields:

$$\mathbf{E} = \frac{1}{2}(\mathbf{E}_R + \mathbf{E}_L) = \frac{E_0}{2}e^{i(kz-\omega t)}\left[\left(e^{+i\Delta k z}+e^{-i\Delta k z}\right)\mathbf{e}_x - i\left(e^{+i\Delta k z}-e^{-i\Delta k z}\right)\mathbf{e}_y\right]$$

or

$$\mathbf{E} = E_0\, e^{i(kz-\omega t)}\left[\cos(\Delta k z)\,\mathbf{e}_x + \sin(\Delta k z)\,\mathbf{e}_y\right].$$

Consequently, the difference between the two wave vectors rotates the polarization plane by an angle per unit distance dz:

$$\frac{\mathrm{d}\varphi}{\mathrm{d}z} = \Delta k \, .$$

Integration over the total distance d yields:

$$\varphi = \varphi_0 + \frac{e^3}{2\varepsilon_0 c m_\mathrm{e}^2} \frac{1}{\omega^2} \int_0^d n_\mathrm{e}(z) B_0(z) \, \mathrm{d}z \, . \tag{1.434}$$

For a constant number density and magnetic field, the simple relation is established:

► $$\Delta\varphi = \frac{e^3}{2\varepsilon_0 c m_\mathrm{e}^2} \frac{1}{\omega^2} n_\mathrm{e} B_0 d \, . \tag{1.435}$$

In astronomy, pulsars (discovered in 1967) are typical sources of highly polarized radio emissions. Measuring the pulsar polarization angle for a known frequency and initial polarization plane yields the integrated product of the electron number density and the longitudinal galactic magnetic field along the line of sight to Earth.

A similar phenomenon occurs in transparent dielectrics (including liquids) within a strong magnetic field, where the following empirical relation holds:

► $$\Delta\varphi = \mathcal{V} B_0 d \, , \tag{1.436}$$

where $\mathcal{V}$ is the Verdet constant, whose value depends on the specific material properties. A positive value indicates counterclockwise rotation when viewed along the magnetic field direction, whereas a negative value indicates clockwise rotation. Terbium gallium garnet (TGG) crystals, widely used in magneto-optical components, such as optical isolators, exhibit a Verdet constant reaching $\mathcal{V} \sim -40$ rad T^{-1}m^{-1}.

Whistlers

Whistlers are generated as secondary effects of lightning in the lower atmosphere and also occur within magnetospheric plasma. These electromagnetic waves, with frequencies ranging from 300 Hz to 30 kHz, propagate energy approximately along Earth magnetic field lines. Whistlers were discovered by the German physicist Heinrich Barkhausen in 1919 and described in detail in 1953 by the British-French physicist and electrical engineer Lewelyn Robert Owen Storey. They represent a modification of R waves, featuring a non-zero angle between the Earth field and the propagation direction. The dispersion relation for whistlers resembles that of R waves and can be derived from the Appleton–Hartree formula (1.430) for small angles (sin $\alpha \approx 0$):

$$N^2 = 1 - \frac{(\omega_\mathrm{p}/\omega)^2}{1 - (\omega_\mathrm{c}/\omega)\cos\alpha} \, ; \qquad N \equiv \frac{ck}{\omega} \, . \tag{1.437}$$

Since $\omega \ll \omega_\mathrm{c}$ for most whistlers, neglecting the unity term in the denominator yields a simpler approximation:

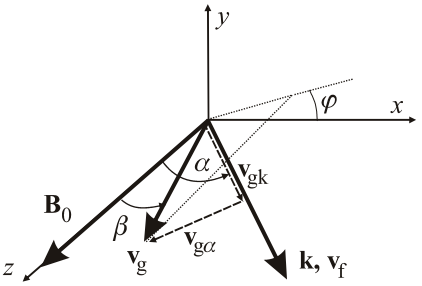
$$\omega^2 = c^2 k^2 - \frac{\omega_\mathrm{p}^2 \, \omega}{\omega_\mathrm{c} \cos\alpha} \, . \tag{1.438}$$

For ultra-low frequencies, the square of the frequency on the left-hand side can also be neglected, yielding an even simpler approximation for low-frequency whistlers:

$$\omega(k,\alpha) \cong \frac{c^2 k^2}{\omega_\mathrm{p}^2}\omega_\mathrm{c}\cos\alpha \ . \tag{1.439}$$

Phase and Group Velocity

Phase and group velocities are determined below (where α is the deviation of **k** from the magnetic field, and β is the deviation of the group velocity from the field):



The phase velocity is given by the relation:

$$\mathbf{v}_\mathrm{f} = v_\mathrm{f}\mathbf{e}_k \ ; \qquad v_\mathrm{f} \equiv \frac{\omega}{k} = \frac{c^2 k}{\omega_\mathrm{p}^2}\omega_\mathrm{c}\cos\alpha \, . \tag{1.440}$$

The group velocity components are derived from the gradient in **k**-space using spherical coordinates:

$$\mathbf{v}_\mathrm{g} = \frac{\partial\omega}{\partial k}\mathbf{e}_k + \frac{1}{k}\frac{\partial\omega}{\partial\alpha}\mathbf{e}_\alpha + \frac{1}{k\sin\alpha}\frac{\partial\omega}{\partial\varphi}\mathbf{e}_\varphi \, . \tag{1.441}$$

Differentiation yields the individual components:

$$\begin{aligned} v_{gk} &= 2\frac{c^2 k}{\omega_\mathrm{p}^2}\omega_\mathrm{c}\cos\alpha \, , \\ v_{g\alpha} &= -\frac{c^2 k}{\omega_\mathrm{p}^2}\omega_\mathrm{c}\sin\alpha \, , \\ v_{g\varphi} &= 0 \, . \end{aligned} \tag{1.442}$$

The geometric decomposition in the figure indicates that the α-component points opposite to the direction of the increasing angle α and is thus negative. This component is much smaller than the completely dominant component along the **k** direction. The final equation (1.442) confirms that $\mathbf{v}_\mathrm{g}$ lies strictly within the ($\mathbf{e}_z$, **k**) plane.

The energy propagation velocity is evaluated as a function of frequency by substituting the wave vector from the dispersion relation (1.439) into equations (1.442):

► $$v_\mathrm{gk} = \frac{2c}{\omega_\mathrm{p}}\sqrt{\omega_\mathrm{c}\cos\alpha}\ \omega^{1/2} \ ; \qquad v_{g\alpha} = -\frac{c}{\omega_\mathrm{p}}\sqrt{\frac{\omega_\mathrm{c}}{\cos\alpha}}\sin\alpha\ \omega^{1/2} . \tag{1.443}$$

Both velocity components are proportional to $\omega^{1/2}$. Given the small propagation angle, $v_{g\alpha} << v_{gk}$. The whistler propagates from the lightning strike location along Earth magnetic field lines. Higher frequencies travel faster, reaching the observer sooner. The whistler lasts several seconds as lower frequencies gradually arrive. Because of these low frequencies, electric field variations can be converted directly into audio signals. Whistlers propagate from pole to pole and can undergo multiple reflections. During storms, they likely accelerate electrons to relativistic speeds.

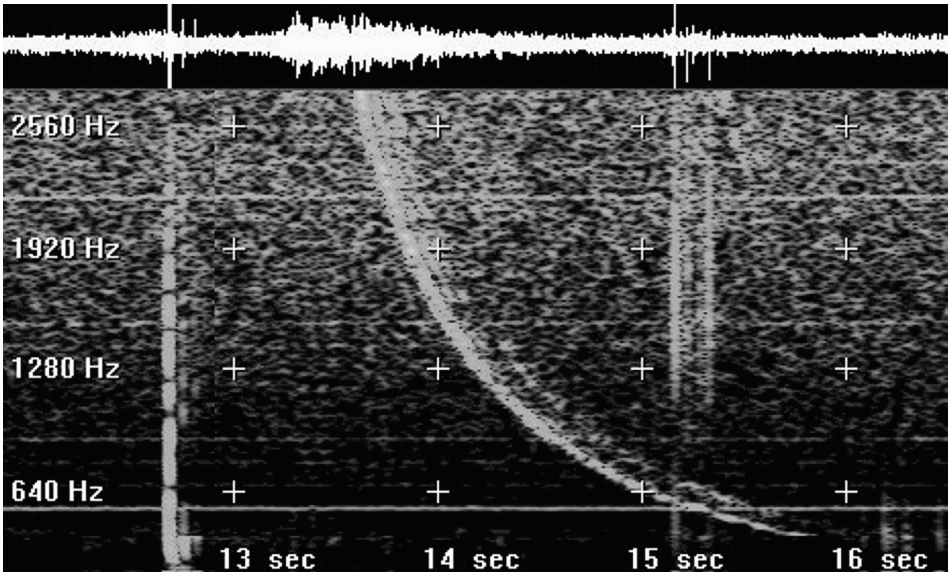


Fig. 1.73: Whistler spectrum exhibiting a gradually decreasing frequency. Source: NASA, 2001.

Maximum Deviation of Whistler Propagation from the Magnetic Field

The geometric relation from the figure satisfies:

$$\mathrm{tg}(\alpha-\beta)=-\frac{v_{g\alpha}}{v_{gk}} \quad \text{or}$$

$$\mathrm{tg}(\alpha-\beta)=\frac{1}{2}\mathrm{tg}\,\alpha\,.$$

Substituting (1.442) into the first relation yields the second. From this, the deviation angle β of the group velocity from the background magnetic field is determined:

$$2\frac{\sin(\alpha-\beta)}{\cos(\alpha-\beta)}=\frac{\sin\alpha}{\cos\alpha} \qquad \Rightarrow .$$

$$2\frac{\sin\alpha\cos\beta-\cos\alpha\sin\beta}{\cos\alpha\cos\beta+\sin\alpha\sin\beta}=\frac{\sin\alpha}{\cos\alpha} \qquad \Rightarrow$$

$$\beta = \operatorname{arctg}\left(\frac{\sin\alpha\cos\alpha}{1+\cos^2\alpha}\right) = \operatorname{arctg}\left(\frac{\sin 2\alpha}{3+\cos 2\alpha}\right).$$

To find the maximum value of β, the derivative with respect to α is set equal to zero, which yields $\cos 2\alpha = -1/3$, $\sin 2\alpha = (8/9)^{1/2}$

► $$\beta_{\max} = \operatorname{arctg}\left[2^{-3/2}\right] = 19°29'. \tag{1.444}$$

The maximum deviation of low-frequency whistler propagation from the direction of Earth magnetic field is 19°29′ (the Storey angle). At this maximum deviation, the direction of wave propagation corresponds to $\alpha = 54°44'$ ($2\alpha = 109°28'$).

Permittivity Tensor for Electromagnetic Waves in Plasma

At high frequencies and in the presence of a magnetic field, plasma behaves fundamentally differently from an isotropic conductive medium. Therefore, the permittivity tensor for a cold electron plasma with a background field $\mathbf{B}_0$ is determined by evaluating the electric displacement field in response to a high-frequency wave:

$$\delta\mathbf{D} = \varepsilon_0\delta\mathbf{E} + \delta\mathbf{P} = \varepsilon_0\delta\mathbf{E} - en_e\delta\mathbf{x}_e = \varepsilon_0\delta\mathbf{E} + \frac{en_e}{i\omega}\delta\mathbf{u}_e. \tag{1.445}$$

To relate the position coordinates to the velocity field, the corresponding plane Fourier component is integrated. The velocity field perturbation is derived from the electron equation of motion, using the linearized form after the Fourier transform (1.402):

$$\delta\mathbf{u}_e = -i\frac{e}{m_e\omega}\delta\mathbf{E} - i\frac{e}{m_e\omega}\delta\mathbf{u}_e\times\mathbf{B}_0.$$

Writing the equation in components yields the electron velocity field perturbation:

$$\delta u_k = -\frac{ie}{m_e\omega}\delta E_k - \frac{ie}{m_e\omega}\varepsilon_{klm}\delta u_l B_{0m} \quad \Rightarrow$$

$$\left(\delta_{kl} + i\frac{\omega_c}{\omega}\varepsilon_{klm}\beta_m\right)\delta u_l = -\frac{ie}{m_e\omega}\delta E_k .$$

The velocity equation takes a simple matrix form:

$$\mathbf{M}\cdot\delta\mathbf{u} = -\frac{ie}{m_e\omega}\delta\mathbf{E}; \tag{1.446}$$

$$\mathbf{M} \equiv \begin{pmatrix} 1 & i\omega_c/\omega & 0 \\ -i\omega_c/\omega & 1 & 0 \\ 0 & 0 & 1 \end{pmatrix}.$$

To determine the velocity field perturbation, it suffices to find the inverse of matrix **M**. According to (1.445), the perturbation of the electric displacement field then becomes:

$$\delta\mathbf{D} \;=\; \varepsilon_0\delta\mathbf{E} + \frac{en_\mathrm{e}}{i\omega}\delta\mathbf{u}_\mathrm{e} \;=\; \varepsilon_0\delta\mathbf{E} + \frac{en_\mathrm{e}}{i\omega}\left(-\frac{\mathrm{i}\,e}{m_\mathrm{e}\omega}\mathbf{M}^{-1}\delta\mathbf{E}\right) = \varepsilon_0\left(\mathbf{1} - \frac{\omega_\mathrm{p}^2}{\omega^2}\mathbf{M}^{-1}\right)\delta\mathbf{E}\,.$$

The resulting permittivity tensor is given by:

$$\ddot{\boldsymbol{\varepsilon}} = \varepsilon_0\left(\mathbf{1} - \frac{\omega_\mathrm{p}^2}{\omega^2}\mathbf{M}^{-1}\right). \tag{1.447}$$

The final step is to determine the inverse of matrix **M**. This is possible via any standard approach – such as cofactor expansion, Gaussian elimination, or spectral decomposition (the matrix is Hermitian with real eigenvalues 1, 1– ω_c/ω, 1+ ω_c/ω). This yields:

$$\mathbf{M}^{-1} = \frac{1}{1-(\omega_\mathrm{c}/\omega)^2}\begin{pmatrix} 1\,; & -\mathrm{i}(\omega_\mathrm{c}/\omega); & 0\,; \\ \mathrm{i}(\omega_\mathrm{c}/\omega); & 1\,; & 0\,; \\ 0\,; & 0\,; & 1-(\omega_\mathrm{c}/\omega)^2 \end{pmatrix}.$$

Substituting this expression into (1.447) results in the permittivity tensor:

► $$\ddot{\boldsymbol{\varepsilon}} = \varepsilon_0\begin{pmatrix} S & -\mathrm{i}\,D & 0 \\ \mathrm{i}\,D & S & 0 \\ 0 & 0 & P \end{pmatrix}. \tag{1.448}$$

The permittivity tensor is explicitly anisotropic, featuring non-zero off-diagonal elements, while the diagonal element corresponding to the magnetic field direction (*P*) differs from those in the other directions (*S*). Furthermore, the permittivity tensor is complex; multiplication by the imaginary unit introduces a phase shift between the electric displacement perturbation $\delta\mathbf{D}$, which contains the plasma response, and the initial electric field perturbation $\delta\mathbf{E}$.

Schlieren Photography

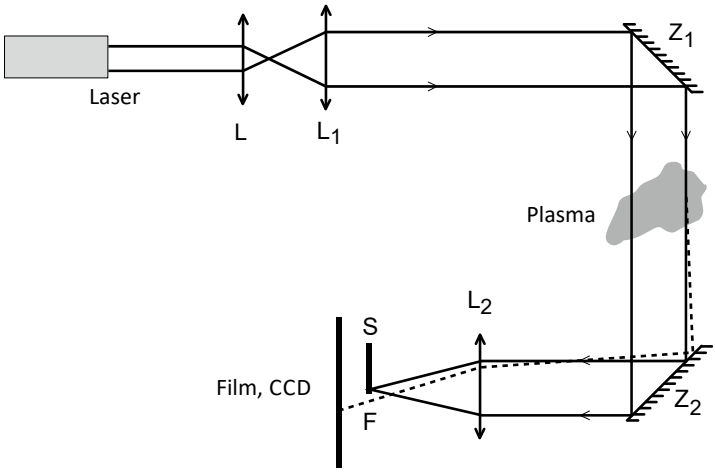


Fig. 1.74: Operational principle of schlieren photography.

Electromagnetic wave propagation through plasma is also utilized in various imaging techniques, among the most prominent being *schlieren photography*. A collimated beam, typically a laser, serves as the light source. The laser beam propagates through the plasma as an ordinary wave (O wave) with a refractive index given by (1.420). A transverse plasma density gradient causes spatial variations in the refractive index, deflecting the beam from its initial path. A knife-edge *S* positioned at the focal point *F* (Figure 1.74) blocks the undeflected light, allowing only the deflected rays to be imaged on a screen (film or CCD). The resulting photograph visualizes the transverse plasma density gradients. The term "schlieren" originates from the German word *Schlieren* (meaning streaks or smudges). This method applies to any optical inhomogeneities that alter the refractive index, including turbulence and shock waves in ordinary gases.

A schlieren photograph does not visualize the plasma itself, but rather regions featuring a non-zero refractive index (or density) gradient, thereby highlighting the boundaries of all plasma structures.

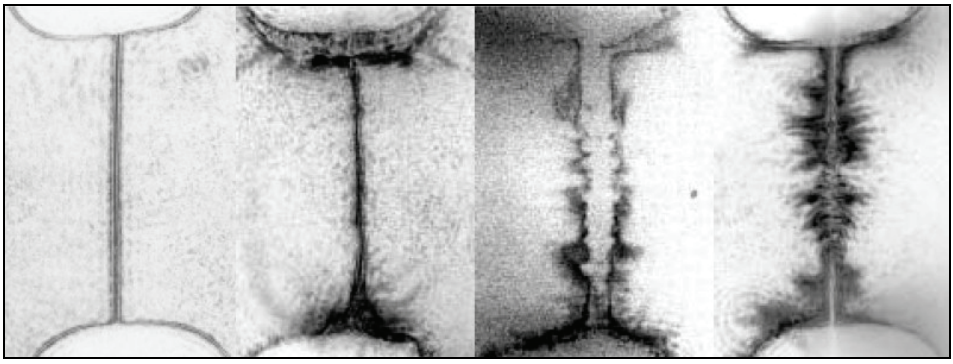


Fig. 1.75: Schlieren image of an exploding carbon filament (diameter 120 μm, length 7 mm) with an exposure time of 3 ns. Courtesy of Pavel Kubeš et al., FEE, CTU.

1.5 Instabilities in Plasma

1.5.1 Unbounded Cold Plasma

Basic Concepts

In most cases, the dispersion relation is obtained in the implicit form:

$$\phi(\omega, \mathbf{k}) = 0 \,. \tag{1.449}$$

Focus is placed on scenarios where the solution $\omega(\mathbf{k})$ or $\mathbf{k}(\omega)$ becomes complex. A complex frequency or wave vector implies that the oscillating exponential $\exp[\mathrm{i}(\mathbf{k}\cdot\mathbf{x}-\omega t)]$ transforms into a temporally or spatially growing or decaying exponential.

Solution in ω (Temporal Evolution)

Suppose the wave vector $\mathbf{k}$ is purely real and the dispersion relation has been solved for the angular frequency ω:

$$\omega = \omega(\mathbf{k}) \,; \qquad \text{resp.} \quad \omega = \omega_1(\mathbf{k}) + \mathrm{i}\,\omega_2(\mathbf{k}) \,. \tag{1.450}$$

Depending on the sign of ω_2, the temporal solution grows or is damped. For the growing case, the *instability growth rate* γ can be defined via the relation $\exp[\gamma t]$:

$$\gamma \equiv \omega_2 = \mathrm{Im}(\omega) \,. \tag{1.451}$$

Regarding temporal evolution, we distinguish between two main types of instability:

- **Convective instability**: At any fixed spatial point, the perturbation amplitude eventually decreases over time. The instability drifts to another location.
- **Absolute instability**: At any fixed spatial point, the perturbation amplitude continually increases over time.

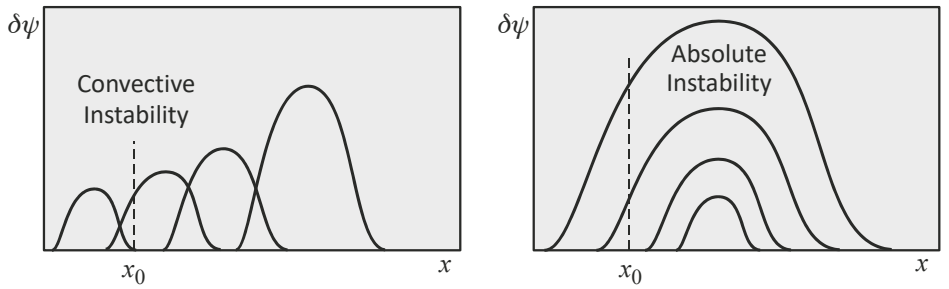


Fig. 1.76: Different regimes of instability growth: convective and absolute instabilities.

The distinction between absolute and convective instabilities may depend on the choice of the coordinate system. For example, a convective instability observed within a coordinate system moving along with the perturbation wave packet will appear to a stationary laboratory observer as an absolute instability.

Solution in k (Spatial Evolution)

Suppose the angular frequency ω is purely real and the dispersion relation has been solved for the wave vector:

$$\mathbf{k} = \mathbf{k}(\omega)\,; \qquad \text{resp.} \quad \mathbf{k} = \mathbf{k}_1(\omega) + \mathrm{i}\,\mathbf{k}_2(\omega)\,. \tag{1.452}$$

The spatial evolution of the perturbation can either decay exponentially away from the source (an *evanescent mode*) or grow (an *amplifying mode*).

Uncoupled Modes of the Dispersion Relation

Sometimes, the dispersion relation decomposes into individual uncoupled modes:

$$\left[\omega - \omega_1(\mathbf{k})\right] \cdot \left[\omega - \omega_2(\mathbf{k})\right] \cdots \left[\omega - \omega_N(\mathbf{k})\right] = 0\,. \tag{1.453}$$

Each bracket can be set to zero independently, contributing a single branch to the complete dispersion relation. For simplicity, the existence of only two branches in a single spatial dimension is assumed:

$$\left[\omega - \omega_1(k)\right] \cdot \left[\omega - \omega_2(k)\right] = 0\,, \tag{1.454}$$

which intersect at the point P = (ω_0, k_0):

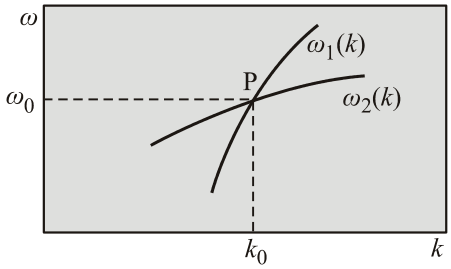


Fig. 1.77: Two uncoupled modes of the dispersion relation.

Near the intersection point, both modes are approximated linearly:

$$\begin{aligned} \omega_1(k) &\cong \omega_0 + \frac{\partial \omega_1}{\partial k}(k - k_0) = \omega_0 + v_1(k - k_0)\,; \\ \omega_2(k) &\cong \omega_0 + \frac{\partial \omega_2}{\partial k}(k - k_0) = \omega_0 + v_2(k - k_0)\,, \end{aligned} \tag{1.455}$$

where v_1 and v_2 represent the group velocities of the two branches.

Coupled Modes of the Dispersion Relation

When two waves with identical wavelengths and frequencies (generally driven by different mechanisms) coexist in a plasma, they naturally interact, transferring energy between the modes. The most straightforward way to couple these modes is to introduce a non-zero constant to the right-hand side of the dispersion relation (1.454):

$$\left[\omega - \omega_1(k)\right] \cdot \left[\omega - \omega_2(k)\right] = \varepsilon\,. \tag{1.456}$$

For a small ε relative to the left-hand side terms, this configuration represents weak coupling, where ε is defined as the *coupling constant*. A non-zero coupling constant fundamentally alters the intersection topology of the two branches, leading to an avoided crossing. Applying a linear approximation (1.455) in equation (1.456) yields:

$$\Big[\omega-\omega_0-v_1(k-k_0)\Big]\cdot\Big[\omega-\omega_0-v_2(k-k_0)\Big]=\varepsilon\,.$$

Due to the coupling constant, the individual modes can no longer be set to zero independently. In this linear approximation, the governing equation becomes quadratic for both ω and k. Solving for both variables via the substitution $\xi\equiv\omega-\omega_0$ – and utilizing the identity $(v_1+v_2)^2-4v_1v_2=(v_1-v_2)^2$ within the discriminant – yields the following analogous results for the angular frequency and wave vector:

$$\omega=\omega_0+\frac{1}{2}\left[(v_1+v_2)(k-k_0)\pm\sqrt{(v_1-v_2)^2(k-k_0)^2+4\varepsilon}\right];\qquad(1.457)$$

$$k=k_0+\frac{1}{2v_1v_2}\left[(v_1+v_2)(\omega-\omega_0)\pm\sqrt{(v_1-v_2)^2(\omega-\omega_0)^2+4\varepsilon v_1v_2}\right].\qquad(1.458)$$

Consequently, mode crossing no longer occurs. Depending on the signs of ε and v_1v_2, real solutions for either the angular frequency or the wave vector may vanish. This behavior leads to four distinct scenarios, illustrated in the figure.

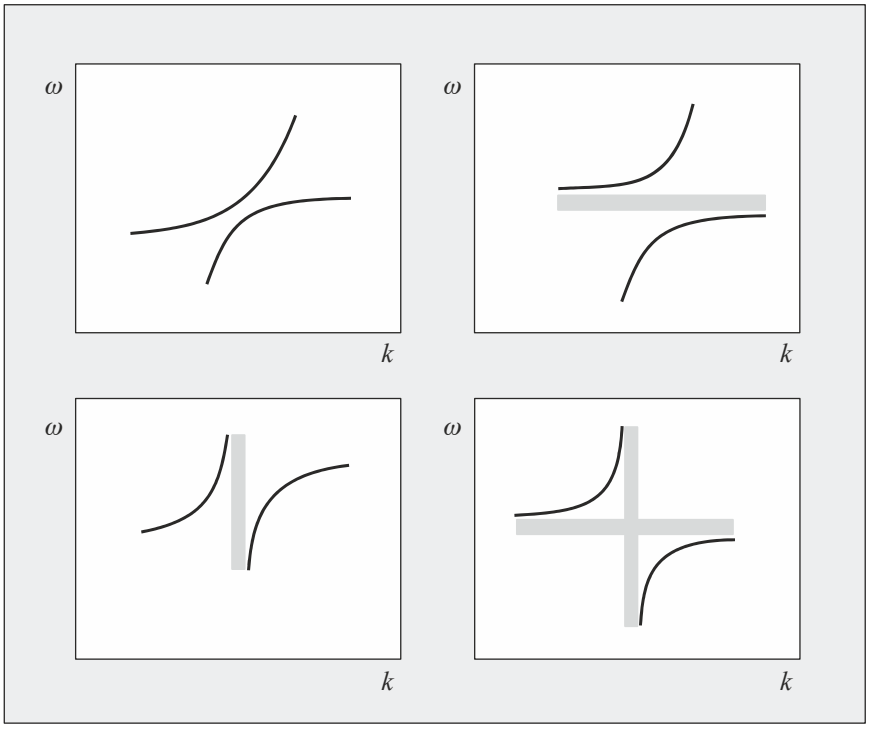


Fig. 1.78: Dispersion relations featuring weak mode coupling; gray bands indicate regions without real solutions.

Multistream Instability

Consider a plasma composed of multiple fluids α moving at distinct unperturbed velocities. In deriving the dispersion relation, the following assumptions are introduced:

1. *The plasma is unbounded*: There are no boundaries within the medium. Accounting for boundaries would require boundary conditions, a scenario addressed in the subsequent section.
2. *The plasma is cold*: The pressure gradient in the equation of motion is neglected. This simplifies the derivation and isolates the conditions for the onset of instability. As the instability develops, the plasma thermalizes, violating this assumption. Hot plasmas are more appropriately described using statistical methods (see Section 1.6).
3. *The instability is driven by an electric field*: The background magnetic field is neglected. From Faraday law curl $\mathbf{E} = -\partial\mathbf{B}/\partial t$, it follows that $\mathbf{k}\times\delta\mathbf{E} = 0$, meaning the perturbations are driven by a longitudinal electric field. In the absence of coupling between magnetic and electric field perturbations, Maxwell equations reduce to Gauss law: div $\mathbf{D} = \rho_Q$.

The following governing system is considered as the starting point:

$$\frac{\partial n_\alpha}{\partial t} + \operatorname{div} n_\alpha \mathbf{u}_\alpha = 0\,,$$

$$m_\alpha n_\alpha \frac{\partial \mathbf{u}_\alpha}{\partial t} + m_\alpha n_\alpha \left(\mathbf{u}_\alpha \cdot \nabla\right)\mathbf{u}_\alpha = Q_\alpha n_\alpha \mathbf{E}\,, \tag{1.459}$$

$$\operatorname{div}\mathbf{E} = \frac{1}{\varepsilon_0}\sum_\alpha n_\alpha Q_\alpha\,.$$

Perturbations of the following form are assumed:

$$n_\alpha = n_{0\alpha} + \delta n_\alpha\,; \qquad \mathbf{u}_\alpha = \mathbf{u}_{0\alpha} + \delta\mathbf{u}_\alpha; \qquad \mathbf{E} = \delta\mathbf{E}\,.$$

Linearizing the system and applying a Fourier transform yields:

$$\left(\omega - \mathbf{k}\cdot\mathbf{u}_{0\alpha}\right)\delta n_\alpha - n_{0\alpha}\left(\mathbf{k}\cdot\delta\mathbf{u}_\alpha\right) = 0\,,$$

$$\mathrm{i}\left(\omega - \mathbf{k}\cdot\mathbf{u}_{0\alpha}\right)\delta\mathbf{u}_\alpha = -\frac{Q_\alpha}{m_\alpha}\delta\mathbf{E}\,,$$

$$\mathrm{i}\mathbf{k}\cdot\delta\mathbf{E} = \frac{1}{\varepsilon_0}\sum_\alpha Q_\alpha \delta n_\alpha\,.$$

Expressing $\delta\mathbf{u}_\alpha$ from the second equation and substituting it into the continuity equation yields δn_α. Inserting this into Gauss law provides the general dispersion relation:

► $$\sum_\alpha \frac{\omega_{\mathrm{p}\alpha}^2}{\left(\omega - \mathbf{k}\cdot\mathbf{u}_{0\alpha}\right)^2} = 1\,; \qquad \omega_{\mathrm{p}\alpha}^2 \equiv \frac{n_{0\alpha}Q_\alpha^2}{m_\alpha\varepsilon_0}\,. \tag{1.460}$$

Consider a simple scenario involving two co-propagating beams (the *Buneman instability*; for counter-propagating beams, the system exhibits the classical *two-stream insta-*

bility). The electric field perturbation $\delta\mathbf{E}$ and the wave vector $\mathbf{k}$ are aligned. The dispersion relation takes the form:

$$f(\omega) = \frac{\omega_{\mathrm{p1}}^2}{(\omega - ku_1)^2} + \frac{\omega_{\mathrm{p2}}^2}{(\omega - ku_2)^2} = 1. \tag{1.461}$$

For simplicity, the subscript 0 for the unperturbed velocities is omitted. The function $f(\omega)$ on the left-hand side can be plotted as follows:

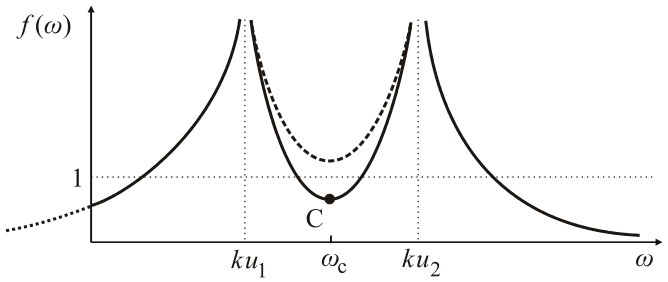


Fig. 1.79: Left-hand side of the dispersion relation for the Buneman instability.

The solutions correspond to points where the function $f(\omega)$ intersects the line $f(\omega) = 1$. The nature of these solutions depends on the position of point C, representing the local minimum of f. If $y_C < 1$, four real solutions exist. If $y_C > 1$ (dashed curve), only two real solutions remain. Since the dispersion relation is fourth-order in ω, the two missing roots must be complex, giving rise to an instability. The critical point is found from the condition:

$$\frac{\mathrm{d}f}{\mathrm{d}\omega} = 0 \qquad \Rightarrow \qquad \omega_{\mathrm{C}} = \frac{u_2\omega_{\mathrm{p1}}^{2/3} + u_1\omega_{\mathrm{p2}}^{2/3}}{\omega_{\mathrm{p1}}^{2/3} + \omega_{\mathrm{p2}}^{2/3}}k\,. \tag{1.462}$$

The *stability criterion* is derived from the relation $f(\omega_C) \leq 1$:

► $$k^2 \;\geq\; \frac{\left[\omega_{\mathrm{p1}}^{2/3} + \omega_{\mathrm{p2}}^{2/3}\right]^3}{(u_2 - u_1)^2}. \tag{1.463}$$

This relation was derived by Oscar Buneman in 1959. For sufficiently short wavelengths, a cold plasma remains stable, whereas instability always sets in for sufficiently long wavelengths. In a hot plasma, however, this does not necessarily hold, and the system is more appropriately analyzed using statistical physics (see Section 1.6). The beams will slow down through a collisionless mechanism; a strong electric field with a wavelength $\lambda > \lambda_C$ develops, leading to gradual thermalization of the plasma.

Two Symmetrical Beams

Consider two identical beams moving symmetrically toward each other. The dispersion relation takes a simple one-dimensional form:

► $$\frac{\omega_{\mathrm{p}}^2}{(\omega - ku_0)^2} + \frac{\omega_{\mathrm{p}}^2}{(\omega + ku_0)^2} = 1. \tag{1.464}$$

Expanding this yields a biquadratic equation for ω, which possesses the solution:

$$\omega^2 = \omega_\mathrm{p}^2 + k^2 u_0^2 \pm \omega_\mathrm{p} \sqrt{\omega_\mathrm{p}^2 + 4k^2 u_0^2} \,. \tag{1.465}$$

Evidently, evaluating the roots demonstrates that all solutions are purely real. The region of real solutions (and thus stability) can be determined either directly from relation (1.465) or from the *Buneman stability criterion* (1.463):

$$k^2 \geq 2\frac{\omega_\mathrm{p}^2}{u_0^2} \qquad \Rightarrow \qquad \bar{k} \equiv \frac{k u_0}{\omega_\mathrm{p}} \in \left(-\infty, -\sqrt{2}\right\rangle \cup \left\langle +\sqrt{2}, \infty\right) . \tag{1.466}$$

It is convenient to rewrite the dispersion relation (1.465) in the dimensionless form:

$$\begin{aligned} \bar{\omega}^2 &= 1 + \bar{k}^2 \pm \sqrt{1 + 4\bar{k}^2} \;; \\ \bar{\omega} &\equiv \frac{\omega}{\omega_\mathrm{p}} \;; \qquad \bar{k} \equiv \frac{k u_0}{\omega_\mathrm{p}} \,. \end{aligned} \tag{1.467}$$

Taking the square root provides four solutions, which are generally complex and of the form $\bar{\omega} = \bar{\omega}_1 + \mathrm{i}\bar{\omega}_2$. The real and imaginary branches are plotted below:

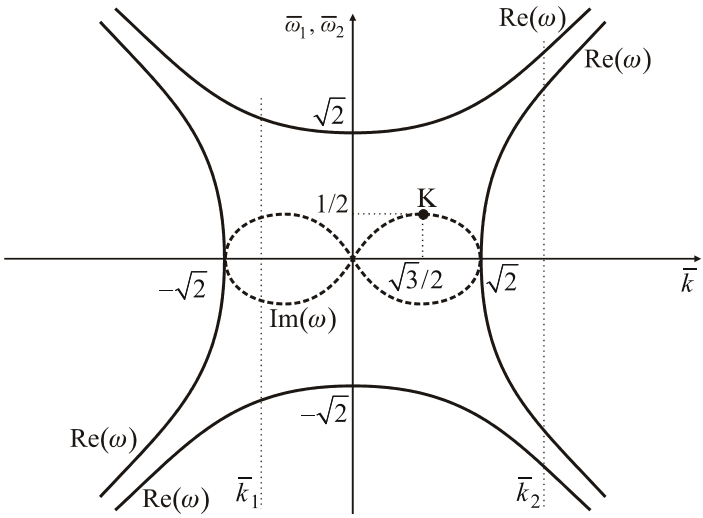


Fig. 1.80: Real and imaginary branches of the dispersion relation.

For large wave vectors ($\bar{k}_2$ in the figure), four real solutions for ω exist. For small (dimensionless) wave vectors within the interval ($-\sqrt{2}$, $\sqrt{2}$), only two real and two complex solutions remain ($\bar{k}_1$ in the figure). Point K corresponds to the maximum instability, where the imaginary part of the angular frequency – and thus the instability growth rate – reaches its highest value. Its horizontal coordinate is located at the local maximum of the dispersion relation (1.467). Setting the derivative of the right-hand side to zero yields $\bar{k} = \sqrt{3}/2$. At this point, the dispersion relation (1.467) has four solutions:

$$\bar{\omega} = \pm\frac{\sqrt{15}}{2}; \qquad \bar{\omega} = \pm\frac{\mathrm{i}}{2}.$$

Regarding the instability, focus is placed on the imaginary part of the solution; the co-ordinates of point K are (√3/2, 1/2), and the maximum growth rate is given by:

$$\gamma = \mathrm{Im}(\omega) = \mathrm{Im}(\bar{\omega})\,\omega_\mathrm{p} = \frac{\omega_\mathrm{p}}{2}. \tag{1.468}$$

A similar analysis applies to two distinct beams, although the dispersion relation is no longer symmetric. The two-stream instability leads to wave propagation and subsequent thermalization, converting directed kinetic energy into heat. However, the cold plasma approximation ceases to apply in this regime. This instability frequently benchmarks simulation algorithms for charged particle dynamics, as the analytical solution and the unstable region are straightforwardly verified.

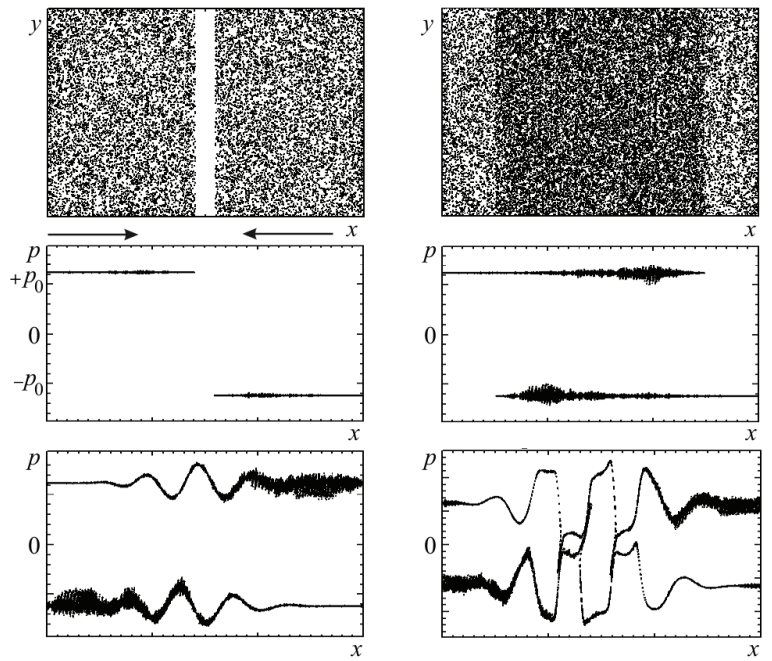


Fig. 1.81: Numerical simulation of a two-stream instability for two counter-streaming positron beams. Bottom four panels show the temporal evolution of the instability in phase space (x, p). Initially, the beam momentum was $\pm p_0$. Simulation by O. Hastings and E. Liang, Rice University.

Beam-Plasma Instability

Consider a beam interacting with a stationary plasma. The general dispersion relation (1.460) takes the form:

$$\frac{\omega_\mathrm{pb}^2}{(\omega - k u_\mathrm{b})^2} + \frac{\omega_\mathrm{p}^2}{\omega^2} = 1, \tag{1.469}$$

where ω_p represents the plasma frequency, ω_pb is the beam plasma frequency, and u_b denotes the unperturbed beam velocity. The stability criterion can be rewritten as:

$$k \geq \frac{\omega_\mathrm{p}}{u_\mathrm{b}}\left[1+\left(\frac{\omega_\mathrm{pb}}{\omega_\mathrm{p}}\right)^{2/3}\right]^{3/2} . \tag{1.470}$$

In the weak-beam limit ($\omega_\mathrm{pb} \ll \omega_\mathrm{p}$, which occurs, for example, when ions penetrate an electron plasma), the condition $k \geq \omega_\mathrm{p}/u_\mathrm{b}$ holds approximately. The dispersion relation can be recast into another elegant form:

$$\left[\omega^2-\omega_\mathrm{p}^2\right]\cdot\left[(\omega-ku_\mathrm{b})^2-\omega_\mathrm{pb}^2\right]=\omega_\mathrm{pb}^2\omega_\mathrm{p}^2 . \tag{1.471}$$

This formulation is analogous to (1.456), where four wave modes are coupled in a *four-wave interaction*. The weak-beam limit corresponds to the weak-coupling limit, characterized by a small coupling constant on the right-hand side.

Beam-plasma instabilities are highly common, occurring in the solar wind near planetary shock waves and when cosmic plasma jets propagate through the interstellar or intergalactic medium. The instability leads to beam thermalization, an effect that can be exploited to heat laboratory plasmas using charged particle beams.

Other Instabilities (Drift and Weibel)

Drift motions can also cause two fluid streams to move in opposite directions. In most drift-driven cases, electrons and ions move counter to each other, potentially triggering an instability, with the *stability criterion* (1.463) formulated as:

$$k \geq \frac{\omega_\mathrm{pe}}{|v_\mathrm{Di}-v_\mathrm{De}|}\left[1+\left(\frac{\omega_\mathrm{pi}}{\omega_\mathrm{pe}}\right)^{2/3}\right]^{3/2} . \tag{1.472}$$

Instabilities arising from the intermixing of two or more media with different velocities are generally referred to as multistream instabilities. This name is not entirely precise, as the media do not always form distinct streams. In the 1D case, where the velocities of all media, the electric field, and the wave vector are collinear, this reduces to the *Buneman instability*. In the presence of anisotropy in velocity space (2D and 3D cases), velocity differences give rise to the *Weibel instability* (Erich S. Weibel, 1959).

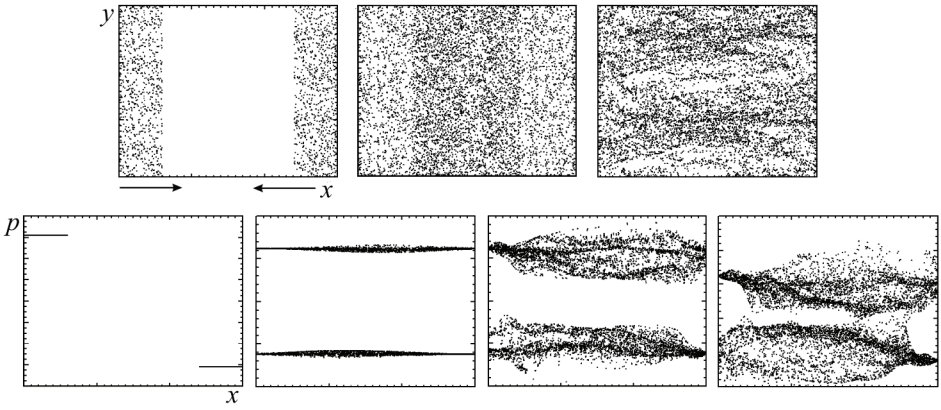


Fig. 1.82: Structural development of the Weibel instability. Top: (*x*, *y*) configuration space; bottom: (*x*, *p*) phase space. PIC simulation by O. P. Hastings, E. Liang, Rice University (2007).

1.5.2 Boundary and Interchange Instabilities

Governing Equations and the Displacement Vector

A bounded plasma is considered within the framework of ideal magnetohydrodynamics. Consequently, the diffusion term and the displacement current are neglected (restricting to low-frequency processes), and assuming that the process wavelength exceeds the mean free path of all particles (otherwise, continuum theory would be inapplicable).

The presence of a boundary significantly complicates the analysis, requiring solutions on both sides of the interface to be matched via appropriate boundary conditions. This task demands knowledge of the perturbed boundary behavior. Another complication arises because the equilibrium solution is generally no longer constant but depends on spatial variables, such as the distance from the boundary. Consequently, seeking a periodic perturbation in these variables is no longer possible. A planar interface is examined first, followed by a cylindrical interface (a plasma column).

Planar Interface

Assume an interface in the (x, z) plane, where the steady-state solution can vary with the distance y. The perturbation of the equilibrium solution thus takes the form:

$$\psi(t,\mathbf{x}) = \psi_0(y) + \delta\psi\,; \qquad \delta\psi = \psi_1(y)\,\mathrm{e}^{\mathrm{i}k_x x + \mathrm{i}k_z z - \mathrm{i}\omega t}\,. \tag{1.473}$$

The perturbation comprises two parts: a non-periodic component denoted by ψ_1, and a periodic component contained within the oscillating exponential. The periodic part leads to algebraic relations as before, whereas the non-periodic part yields differential equations. The subscript "1" on the non-periodic component indicates a first-order perturbation theory. Where applicable, variables are decomposed into partial waves, leading to the following rules for the corresponding Fourier transform:

► $$\partial_t \to -\mathrm{i}\omega\,; \qquad \partial_x \to \mathrm{i}k_x\,; \qquad \partial_y \to \mathrm{d}/\mathrm{d}y\,; \qquad \partial_z \to \mathrm{i}k_z\,. \tag{1.474}$$

The only modification is that for the non-periodic variable y, the derivative is retained. It reduces to an ordinary derivative because, after applying the Fourier transform, no other independent variable remains in the expressions.

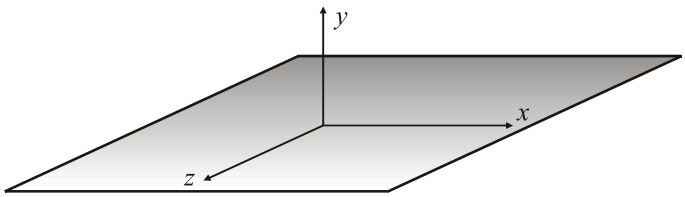


Fig. 1.83: Planar interface between two media.

Cylindrical Interface

A cylindrical plasma column or pinch is considered, where the equilibrium solution (e.g., the Bennett profile) varies with the radial distance r. The perturbation in cylindrical coordinates thus takes the form:

$$\psi(t,r,\varphi,z) = \psi_0(r) + \psi_1(r)\,\mathrm{e}^{\mathrm{i}k_\varphi \varphi + \mathrm{i}k_z z - \mathrm{i}\omega t}\,. \tag{1.475}$$

The perturbation $\delta\psi$ comprises a non-periodic component $\psi_1(r)$ and an oscillating exponential. The solution must satisfy periodicity in the azimuthal angle φ:

$$\psi(t,r,\varphi+2\pi,z)=\psi(t,r,\varphi,z)\,. \tag{1.476}$$

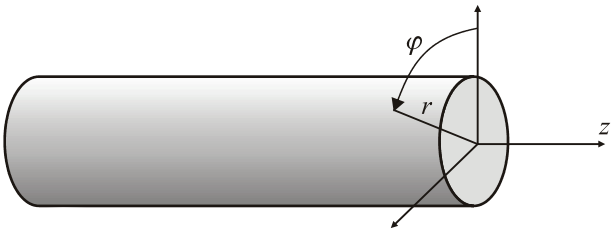


Fig. 1.84: Cylindrical interface between two media.

This periodicity requires that:

$$\mathrm{e}^{\mathrm{i}k_\varphi\varphi}=\mathrm{e}^{\mathrm{i}k_\varphi(\varphi+2\pi)} \quad\Rightarrow\quad \mathrm{e}^{2\pi\mathrm{i}k_\varphi}=1 \quad\Rightarrow\quad k_\varphi=m=0,\pm1,\pm2,\ldots$$

The integer m represents the azimuthal mode number, reducing (1.475) to:

$$\psi(t,r,\varphi,z)=\psi_0(r)+\psi_1(r)\,\mathrm{e}^{\mathrm{i}m\varphi+\mathrm{i}k_z z-\mathrm{i}\omega t}\;; \qquad m=0,\pm1,\pm2,\ldots \tag{1.477}$$

The corresponding rules for the partial-wave expansion are:

► $$\partial_t\to-\mathrm{i}\omega\,; \qquad \partial_r\to\mathrm{d}/\mathrm{d}\,r\,; \qquad \partial_\varphi\to\mathrm{i}m\,; \qquad \partial_z\to\mathrm{i}k_z\;. \tag{1.478}$$

The radial variable r is non-periodic, so both the variable and its derivatives are retained within the equations. The first three perturbation modes are illustrated below:

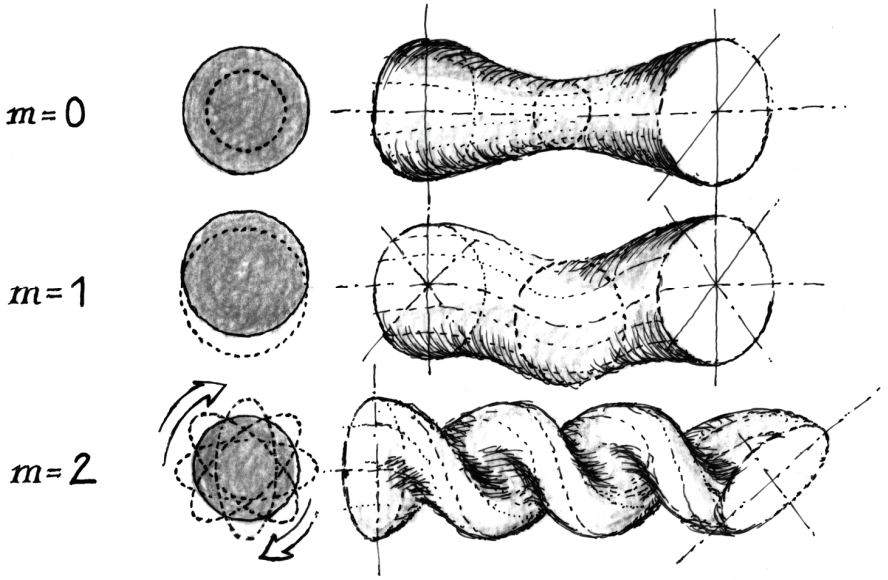


Fig. 1.85: First three modes of cylindrical perturbations.

Note 1: If the left and right boundaries of the plasma column are identified (a simple approximation of a toroidal geometry), the relation $\psi(t, r, \varphi, z) = \psi(t, r, \varphi, z+L)$ must hold, where L is the column length, yielding:

$$k_z = \frac{2\pi}{L} n\,; \quad \delta\psi = \psi_1(r) \exp\left[\mathrm{i}\, m\varphi + \mathrm{i} \frac{2\pi}{L} nz - \mathrm{i}\, \omega t \right]; \quad n = 0, 1, 2\ldots \tag{1.479}$$

Note 2: The general boundary condition leads to the perturbation:

$$\psi(t, \mathbf{q}_\mathrm{n}, \mathbf{q}_\mathrm{p},) = \psi_0(\mathbf{q}_\mathrm{n}) + \psi_1(\mathbf{q}_\mathrm{n})\, \mathrm{e}^{\mathrm{i}\mathbf{q}_\mathrm{p}\cdot\mathbf{k}_\mathrm{p} - \mathrm{i}\omega t}\,, \tag{1.480}$$

where $\mathbf{q}_\mathrm{n}$ represents non-periodic variables and $\mathbf{q}_\mathrm{p}$ represents periodic variables.

Displacement Vector

In boundary value problems, we typically focus on the displacement vector of a selected plasma region rather than the velocity field. This vector is defined by the relation:

► $$\delta\boldsymbol{\xi}(t, \mathbf{x}) = \int_{t_0}^{t} \delta\mathbf{u}(t', \mathbf{x})\, \mathrm{d}t'. \tag{1.481}$$

The inverse relation takes the form:

$$\delta\mathbf{u} = \frac{\partial\, \delta\boldsymbol{\xi}}{\partial t}\,. \tag{1.482}$$

Initially, the displacement vector vanishes. However, this property does not hold for its individual Fourier components, from which the total vector is constructed. These components again comprise both a periodic ($\mathbf{q}_\mathrm{p}$) and a non-periodic ($\mathbf{q}_\mathrm{n}$) part:

$$\begin{aligned} \delta\boldsymbol{\xi}_\omega \;&=\; \boldsymbol{\xi}_{1\omega}(\mathbf{q}_\mathrm{n})\, \mathrm{e}^{\mathrm{i}\mathbf{q}_\mathrm{p}\cdot\mathbf{k}_\mathrm{p} - \mathrm{i}\omega t}; \\ \delta\boldsymbol{\xi} &= \int \delta\boldsymbol{\xi}_\omega\, \mathrm{d}\omega. \end{aligned} \tag{1.483}$$

For partial waves, the subscript ω is typically omitted unless ambiguity arises. The displacement vector represents each plasma element's perturbation shift and uniquely defines the newly deformed boundary geometry.

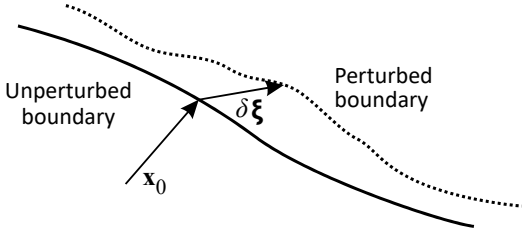


Fig. 1.86: Definition of the displacement vector.

Governing Equations for the Displacement Vector

The analysis begins with the standard system of ideal magnetohydrodynamics for a single-component plasma featuring a polytropic equation of state (1.222) and adding a gravitational acceleration term to the equation of motion:

$$\begin{gathered}\frac{\partial \rho}{\partial t}+\operatorname{div}(\rho \mathbf{u})=0, \\ \rho \frac{\partial \mathbf{u}}{\partial t}+\rho(\mathbf{u} \cdot \nabla) \mathbf{u} \;=\; -\nabla p \;+\rho \mathbf{g}+\frac{\operatorname{curl} \mathbf{B}}{\mu_0} \times \mathbf{B}, \\ \frac{\partial p}{\partial t}+(\mathbf{u} \cdot \nabla) p \;+\; \gamma p \operatorname{div} \mathbf{u} \;=\; 0, \\ \frac{\partial \mathbf{B}}{\partial t}=\operatorname{curl}(\mathbf{u} \times \mathbf{B}).\end{gathered} \tag{1.484}$$

Linearization yields:

$$\rho=\rho_0(\mathbf{q}_{\mathrm{n}})+\delta \rho ; \quad \mathbf{u}=\delta \mathbf{u} ; \quad p=p_0(\mathbf{q}_{\mathrm{n}})+\delta p ; \quad \mathbf{B}=\mathbf{B}_0(\mathbf{q}_{\mathrm{n}})+\delta \mathbf{B}. \tag{1.485}$$

Because the equilibrium solution depends on spatial variables, it can no longer be factored out of the spatial derivatives, nor can its gradients be assumed to vanish. The resulting linearized system, retaining only first-order terms, takes the form:

$$\begin{gathered}\frac{\partial \delta \rho}{\partial t}+\operatorname{div}(\rho_0 \delta \mathbf{u})=0, \\ \rho_0 \frac{\partial \delta \mathbf{u}}{\partial t}=\; -\nabla \delta p+\mathbf{g} \delta \rho+\frac{\operatorname{curl} \delta \mathbf{B}}{\mu_0} \times \mathbf{B}_0+\frac{\operatorname{curl} \mathbf{B}_0}{\mu_0} \times \delta \mathbf{B}, \\ \frac{\partial \delta p}{\partial t}+(\delta \mathbf{u} \cdot \nabla) p_0 \;+\; \gamma p_0 \operatorname{div} \delta \mathbf{u} \;=\; 0, \\ \frac{\partial \delta \mathbf{B}}{\partial t}=\operatorname{curl}(\delta \mathbf{u} \times \mathbf{B}_0).\end{gathered} \tag{1.486}$$

The substitution $\delta \mathbf{u}=\partial \delta \boldsymbol{\xi} / \partial t$ is then performed. In this linearized system, temporal dependence resides exclusively within the perturbation terms $\delta \psi$, whereas equilibrium quantities ψ_0 depend solely on spatial coordinates. Consequently, with the exception of the second equation, all relations can be integrated over time from 0 to t. The definite integrals yield no integration constants since the perturbations vanish at the lower limit:

$$\begin{gathered}\delta \rho+\operatorname{div}(\rho_0 \delta \boldsymbol{\xi})=0, \\ \rho_0 \frac{\partial^2 \delta \boldsymbol{\xi}}{\partial t^2}=-\nabla \delta p+\mathbf{g} \delta \rho+\frac{\operatorname{curl} \delta \mathbf{B}}{\mu_0} \times \mathbf{B}_0+\frac{\operatorname{curl} \mathbf{B}_0}{\mu_0} \times \delta \mathbf{B}, \\ \delta p+(\delta \boldsymbol{\xi} \cdot \nabla) p_0 \;+\; \gamma p_0 \operatorname{div} \delta \boldsymbol{\xi} \;=\; 0, \\ \delta \mathbf{B} \;=\operatorname{curl}(\delta \boldsymbol{\xi} \times \mathbf{B}_0).\end{gathered} \tag{1.487}$$

The second equation of motion serves as the equation for the displacement vector. Substituting δp and $\delta\mathbf{B}$ from the last two equations, and ρ from the first equation, yields:

$$\rho_0 \frac{\partial^2 \delta\boldsymbol{\xi}}{\partial t^2} = \boldsymbol{\nabla}(\delta\boldsymbol{\xi}\cdot\boldsymbol{\nabla})p_0 + \boldsymbol{\nabla}(\gamma p_0 \operatorname{div}\delta\boldsymbol{\xi}) - \mathbf{g}\operatorname{div}(\rho_0\,\delta\boldsymbol{\xi}) +$$

$$+ \frac{\operatorname{curl}\delta\mathbf{B}}{\mu_0}\times\mathbf{B}_0 + \frac{\operatorname{curl}\mathbf{B}_0}{\mu_0}\times\delta\mathbf{B}\,; \qquad \text{kde} \tag{1.488}$$

$$\delta\mathbf{B} \equiv \operatorname{curl}(\delta\boldsymbol{\xi}\times\mathbf{B}_0)\,.$$

The right-hand side is a linear differential operator acting on the displacement vector:

$$\rho_0 \frac{\partial^2 \delta\boldsymbol{\xi}}{\partial t^2} = \hat{\mathscr{L}}\,\delta\boldsymbol{\xi}\,. \tag{1.489}$$

Throughout this derivation, no Fourier decomposition into partial waves has been performed. Assuming a temporal evolution of the form $\exp[-i\omega t]$ yields:

$$\hat{\mathscr{L}}\,\delta\boldsymbol{\xi} = -\rho_0\omega^2\,\delta\boldsymbol{\xi}\,. \tag{1.490}$$

This represents an eigenvalue problem for the operator $\hat{\mathscr{L}}$, where the eigenvalue depends on the angular frequency. Whether the solution is continuous at the boundary depends on the operator's spectrum: a discrete spectrum corresponds to discrete-mode perturbations with frequencies ω_n, whereas a continuous spectrum allows for arbitrary frequencies ω. The general solution is then constructed via standard superposition:

$$\delta\boldsymbol{\xi} = \sum_n \mathbf{a}_n\,\mathrm{e}^{-\mathrm{i}\omega_n t} \qquad \text{or} \quad \delta\boldsymbol{\xi} = \int_{\omega} \mathbf{a}(\omega)\,\mathrm{e}^{-\mathrm{i}\omega t}\,\mathrm{d}\omega\,. \tag{1.491}$$

In ideal magnetohydrodynamics, the operator $\hat{\mathscr{L}}$ is Hermitian with respect to the scalar product:

$$\langle\,\mathbf{f}\,|\,\mathbf{g}\,\rangle \equiv \int \mathbf{f}^*(\mathbf{x})\cdot\mathbf{g}(\mathbf{x})\,\mathrm{d}^3\mathbf{x} = \int f_l^*(\mathbf{x})\,g_l(\mathbf{x})\,\mathrm{d}^3\mathbf{x}\,, \tag{1.492}$$

satisfying the identity:

$$\langle\,\mathbf{f}\,|\,\hat{\mathscr{L}}\,\mathbf{g}\,\rangle = \langle\,\hat{\mathscr{L}}\,\mathbf{f}\,|\,\mathbf{g}\,\rangle\,. \tag{1.493}$$

A complex vector space is assumed, as complex wave functions describe the waves. Consequently, the operator possesses real eigenvalues, restricting the solutions to either $\omega^2 > 0$ (stable) or $\omega^2 < 0$ (purely imaginary, unstable). In the purely imaginary case, the solution comprises both exponentially growing and decaying modes, with no oscillatory component. In non-ideal magnetohydrodynamics involving magnetic dissipation, the angular frequency can become fully complex, allowing the solution to include both exponential and oscillatory terms.

Evidently, equation (1.489) implies that the expression $\mathbf{f} \equiv \hat{\mathscr{L}}\,\delta\boldsymbol{\xi}$ represents the force density acting on the plasma. Expressing the potential energy as negative work yields:

$$\delta W = -\int \delta\boldsymbol{\xi}^*\cdot\hat{\mathscr{L}}\,\delta\boldsymbol{\xi}\;\mathrm{d}^3\mathbf{x} = -\int \delta\xi_l^*\hat{\mathscr{L}}\,\delta\xi_l\,\mathrm{d}^3\mathbf{x} = -\left\langle \delta\boldsymbol{\xi}\,\middle|\,\hat{\mathscr{L}}\,\delta\boldsymbol{\xi}\right\rangle. \tag{1.494}$$

If the potential energy δW decreases due to the perturbation, the plasma may or may not transition to a more energetically favorable configuration. Conversely, if the potential energy increases, such a motion will never occur spontaneously. A sufficient condition for *plasma stability* is therefore:

$$\langle \delta\boldsymbol{\xi} \,|\, \hat{\mathscr{I}}\, \delta\boldsymbol{\xi} \rangle < 0 \,. \tag{1.495}$$

Matching Fields at a Boundary

If a point on the unperturbed boundary is denoted by $\mathbf{x}_0$, the corresponding point on the deformed boundary is, in the first-order perturbation theory, given by:

$$\mathbf{x} = \mathbf{x}_0 + \delta\boldsymbol{\xi}(t, \mathbf{x}_0) \,. \tag{1.496}$$

After substituting the solution for the displacement vector into a specific scenario, the equation for the deformed boundary is obtained. From this, the normal vector can be derived via standard procedures (expressing the boundary in implicit form and evaluating its gradient). This normal vector comprises both zero- and first-order components:

$$\mathbf{n} = \mathbf{n}_0 + \delta\mathbf{n} \,. \tag{1.497}$$

Knowing the boundary equation and its normal vector allows us to match both vector and scalar fields at the interface.

Continuity of the Normal Component of a Vector Field

Suppose that the normal component of a vector field (such as the magnetic field **B**) is continuous across the interface, satisfying:

$$\mathbf{K} \cdot \mathbf{n} = \text{const} \,, \tag{1.498}$$

which, in first-order theory, yields the boundary condition:

$$\mathbf{K}_0 \cdot \delta\mathbf{n} + \delta\mathbf{K} \cdot \mathbf{n}_0 = \text{const} \,. \tag{1.499}$$

Substituting partial-wave perturbations and eliminating the periodic factors from both sides yields the final boundary condition:

► $$\mathbf{K}_0 \cdot \mathbf{n}_1 + \mathbf{K}_1 \cdot \mathbf{n}_0 = \text{const} \,. \tag{1.500}$$

Continuity of the Tangential Component of a Vector Field

Suppose the tangential component of a vector field (such as the electric field **E**) is continuous across the interface, satisfying:

$$\mathbf{K} \times \mathbf{n} = \text{const} \,. \tag{1.501}$$

Analogously to the previous case, we obtain the boundary condition is obtained:

► $$\mathbf{K}_0 \times \mathbf{n}_1 + \mathbf{K}_1 \times \mathbf{n}_0 = \text{const} \;. \tag{1.502}$$

Continuity of a Scalar Field

Consider a scalar field that remains continuous across the interface between two media (such as the total pressure):

$$\psi(t, \mathbf{x}) = \psi_0(\mathbf{x}) + \delta\psi(t, \mathbf{x}) \,. \tag{1.503}$$

At the deformed boundary, the field takes the value:

$$\psi(t,\mathbf{x}_0+\delta\boldsymbol{\xi}) = \psi_0(\mathbf{x}_0+\delta\boldsymbol{\xi}) + \delta\psi(t,\mathbf{x}_0+\delta\boldsymbol{\xi}) =$$

$$= \psi_0 + (\delta\boldsymbol{\xi}\cdot\boldsymbol{\nabla})\psi_0 + \delta\psi + (\delta\boldsymbol{\xi}\cdot\boldsymbol{\nabla})\delta\psi\,.$$

On the right-hand side, a first-order Taylor expansion is applied to both terms around $\mathbf{x}_0$. If the scalar field is continuous at zero order, enforcing continuity at first order yields:

$$(\delta\boldsymbol{\xi}\cdot\boldsymbol{\nabla})\psi_0 + \delta\psi = \text{const}\,.$$

Substituting partial waves and eliminating the periodic factors from both sides provides the final continuity condition for the scalar field:

► $$(\boldsymbol{\xi}_1\cdot\boldsymbol{\nabla})\psi_0 + \psi_1 = \text{const}\,. \tag{1.504}$$

Plasma Filament Instabilities

Consider the simplest possible plasma filament with cylindrical symmetry, where an electric current flows exclusively along the surface. (The next simplest scenario would be a Bennett pinch featuring a uniform current density across the cross-section and a parabolic pressure profile.) The only non-periodic variable is the radial distance; thus, every solution takes the form (1.477).

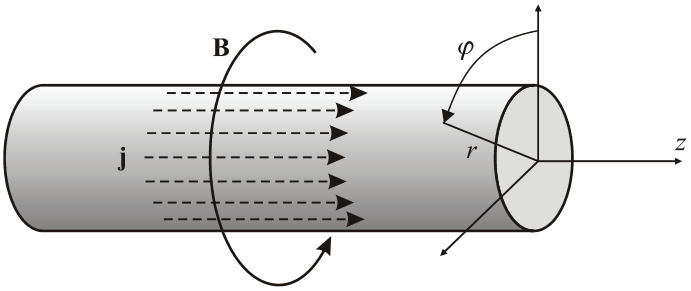


Fig. 1.87: Coordinate system selection for a cylindrical filament.

Internal Solution

In this simple scenario, Ampere law curl $\mathbf{H} = \mathbf{j}$ implies that the equilibrium magnetic field inside vanishes, and the MHD equilibrium condition $\mathbf{j}\times\mathbf{B} = -\boldsymbol{\nabla}p$ dictates that the pressure is uniform. Consequently, for the internal equilibrium solution, all quantities remain constant (a property that does not hold for a Bennett pinch):

$$\rho_0 = \text{const}\,; \qquad p_0 = \text{const}\,;$$
$$\mathbf{u}_0 = \mathbf{B}_0 = 0\,. \tag{1.505}$$

From the governing equation for the displacement vector (1.488), only the following terms remain:

$$-\rho_0\,\omega^2\delta\boldsymbol{\xi} = \gamma p_0 \boldsymbol{\nabla}\,\mathrm{div}\,\delta\boldsymbol{\xi}\,; \qquad \delta\boldsymbol{\xi} = \boldsymbol{\xi}_1(r)\,\mathrm{e}^{\mathrm{i}m\varphi + \mathrm{i}k_z z}\,. \tag{1.506}$$

In principle, this yields three coupled ordinary differential equations for ξ_{1r}, $\xi_{1\varphi}$, and ξ_{1z}.. However, this direct approach is unnecessarily complex. Instead, substituting the equilibrium solution into equations (1.487) yields:

$$\begin{aligned} \omega^2 \rho_0 \delta\boldsymbol{\xi} &= \boldsymbol{\nabla}\, \delta p\,, \\ \delta p + \gamma p_0\, \mathrm{div}\, \delta\boldsymbol{\xi} &= 0\,, \\ \delta\mathbf{B} &= 0\,. \end{aligned} \tag{1.507}$$

The final equation immediately demonstrates that the magnetic field perturbation inside the filament vanishes, which implies that its non-periodic component is also zero:

$$\mathbf{B}_1 = 0\,. \tag{1.508}$$

The first two relations (1.507) form a system of equations for the displacement vector $\delta\boldsymbol{\xi}$ and the pressure perturbation δp. Eliminating the pressure perturbation yields a single equation for the displacement vector (1.506). Conversely, substituting $\delta\boldsymbol{\xi}$ from the first equation into the second leads to a scalar equation for the pressure perturbation; once solved, the displacement vector can be straightforwardly evaluated from the first equation. This latter analytical approach is pursued here:

$$\left(\boldsymbol{\nabla}^2 + \frac{\omega^2}{c_\mathrm{s}^2}\right) \delta p = 0\,; \qquad c_\mathrm{s}^2 \equiv \frac{\gamma p_0}{\rho_0}\,. \tag{1.509}$$

The Laplace operator is expressed in cylindrical coordinates; for detailed derivations, see Volume I, Section 3.10.3 (*Operators in Curvilinear Coordinates*):

$$\frac{1}{r}\frac{\partial}{\partial r}\left(r\frac{\partial \delta p}{\partial r}\right) + \frac{1}{r^2}\frac{\partial^2 \delta p}{\partial \varphi^2} + \frac{\partial^2 \delta p}{\partial z^2} + \frac{\omega^2}{c_\mathrm{s}^2}\delta p = 0\,.$$

Applying the transform rules (1.478) or directly substituting $\delta p = p_1(r)\exp[\mathrm{i}m\varphi + \mathrm{i}kz]$ and eliminating the oscillating factor yields the equation:

$$r^2 \frac{\mathrm{d}^2 p_1}{\mathrm{d}r^2} + r\frac{\mathrm{d}p_1}{\mathrm{d}r} - \left[m^2 + \left(k^2 - \frac{\omega^2}{c_\mathrm{s}^2}\right) r^2\right] p_1 = 0\,. \tag{1.510}$$

The following notation is introduced:

$$q^2 \equiv k^2 - \frac{\omega^2}{c_\mathrm{s}^2}\,; \qquad x \equiv qr\,. \tag{1.511}$$

The quantity q can generally be complex. However, in the incompressible limit $\gamma \to \infty$ (corresponding to an isochoric process and an incompressible fluid), $q^2 > 0$ holds. With this notation, the relation takes the form of the modified Bessel equation:

$$x^2 \frac{\mathrm{d}^2 p_1}{\mathrm{d}x^2} + x\frac{\mathrm{d}p_1}{\mathrm{d}x} - \left[m^2 + x^2\right] p_1 = 0\,. \tag{1.512}$$

Details regarding this relation are provided in Volume I, Section 3.7.1 (*Bessel Functions*). The general solution takes the form:

$$p_1(r) = AI_m(qr) + BK_m(qr)\,. \tag{1.513}$$

Since the modified Bessel function of the second kind $K_m(qr)$ diverges as $r \to 0$, the constant B must vanish, reducing the solution to:

$$p_1(r) = AI_m(qr)\,. \tag{1.514}$$

Finally, the displacement vector is evaluated from the first equation of (1.507):

$$\delta\boldsymbol{\xi} = \frac{1}{\omega^2\rho_0}\nabla\delta p = \frac{1}{\omega^2\rho_0}\left(\frac{\partial}{\partial r}, \frac{1}{r}\frac{\partial}{\partial\varphi}, \frac{\partial}{\partial z}\right) AI_m(qr)\,\mathrm{e}^{\mathrm{i}m\varphi+\mathrm{i}kz-\mathrm{i}\omega t} =$$

$$= \left(\frac{Aq}{\omega^2\rho_0}I'_m, \frac{\mathrm{i}mA}{\omega^2\rho_0 r}I_m, \frac{\mathrm{i}kA}{\omega^2\rho_0}I_m\right)\mathrm{e}^{[\mathrm{i}m\varphi+\mathrm{i}kz-\mathrm{i}\omega t]}\,.$$

The non-periodic component of the displacement vector satisfies:

$$\boldsymbol{\xi}_1 = \left(\frac{Aq}{\omega^2\rho_0}I'_m, \frac{\mathrm{i}mA}{\omega^2\rho_0 r}I_m, \frac{\mathrm{i}kA}{\omega^2\rho_0}I_m\right). \tag{1.515}$$

Overall, the non-periodic components of the internal perturbations within the plasma filament are described by the following solutions in cylindrical coordinates (r, φ, z):

► (1.516)

$\mathbf{B}_0 = (0,0,0)$	$\mathbf{B}_1 = (0,0,0)$
$p_0 = \text{const}$	$p_1 = AI_m(qr)$
$\boldsymbol{\xi}_0 = (0,0,0)$	$\boldsymbol{\xi}_1 = \left(\frac{Aq}{\omega^2\rho_0}I'_m(qr), \frac{\mathrm{i}mA}{\omega^2\rho_0 r}I_m(qr), \frac{\mathrm{i}kA}{\omega^2\rho_0}I_m(qr)\right)$

External Solution

Outside the plasma filament, the equilibrium magnetic field decreases with radius as $1/r$ according to Ampere law, allowing the relation to be formulated as:

$$\mathbf{B}_0 = B_0(r_0)\frac{r_0}{r}\mathbf{e}_\varphi\,, \tag{1.517}$$

where r_0 represents the filament radius. Since no plasma exists externally, the perturbations p_1 and $\boldsymbol{\xi}_1$ vanish. The only non-zero contribution comes from the magnetic field perturbation. Because the external region is current-free, curl $\delta\mathbf{B} = 0$ holds, meaning the magnetic field perturbation is irrotational and can be expressed via a scalar potential:

$$\delta\mathbf{B} = \nabla\delta\phi\,. \tag{1.518}$$

The divergence of the magnetic field must vanish, satisfying $\mathrm{div}(\mathbf{B}_0+\delta\mathbf{B}) = 0$. Since $\mathrm{div}\,\mathbf{B}_0 = 0$ holds for the equilibrium solution, $\mathrm{div}\,\delta\mathbf{B} = 0$ must also satisfy this condition. Combining this with (1.518) yields Laplace equation for the perturbed potential:

$$\nabla^2\delta\phi = 0\,. \tag{1.519}$$

Expanding the Laplace operator in cylindrical coordinates provides the following equation for its non-periodic component:

$$r^2\frac{\mathrm{d}^2\phi_1}{\mathrm{d}r^2}+r\frac{\mathrm{d}\phi_1}{\mathrm{d}r}-\left[m^2+k^2r^2\right]\phi_1=0\,. \tag{1.520}$$

Introducing the internal variable:

$$x=kr\,, \tag{1.521}$$

the modified Bessel equation is obtained again

$$x^2\frac{\mathrm{d}^2\phi_1}{\mathrm{d}x^2}+r\frac{\mathrm{d}\phi_1}{\mathrm{d}x}-\left[m^2+x^2\right]\phi_1=0\,, \tag{1.522}$$

which has the general solution:

$$\phi_1(r)=CI_m(kr)+DK_m(kr)\,. \tag{1.523}$$

Outside the filament, as $r\to\infty$, the modified Bessel function of the first kind I_m (qr) diverges; consequently, the constant C must vanish, reducing the solution to:

$$\phi_1(r)=DK_m(kr)\,. \tag{1.524}$$

The magnetic field perturbation can then be evaluated directly from equation (1.518):

$$\delta\mathbf{B}=\nabla\delta\phi=\left(\frac{\partial}{\partial r},\frac{1}{r}\frac{\partial}{\partial\varphi},\frac{\partial}{\partial z}\right)\phi_1\,\mathrm{e}^{\mathrm{i}m\varphi+\mathrm{i}kz-\mathrm{i}\omega t}=\left(\frac{\partial}{\partial r},\frac{1}{r}\frac{\partial}{\partial\varphi},\frac{\partial}{\partial z}\right)DK_m(kr)\,\mathrm{e}^{\mathrm{i}m\varphi+\mathrm{i}kz-\mathrm{i}\omega t}\,.$$

Differentiating and eliminating the oscillating factor yields the final expression:

$$\mathbf{B}_1=\left(DkK_m',\frac{\mathrm{i}Dm}{r}K_m,\mathrm{i}kDK_m\right). \tag{1.525}$$

The results for the external region are summarized as follows:

► (1.526)

$\mathbf{B}_0=\left(0,B_0(r_0)\frac{r_0}{r},0\right)$	$\mathbf{B}_1=\left(DkK_m'(kr),\frac{\mathrm{i}Dm}{r}K_m(kr),\mathrm{i}kDK_m(kr)\right)$
$\boldsymbol{\xi}_0$: no plasma	$\boldsymbol{\xi}_1$: no plasma, doesn't make sense
$p_0=0$	$p_1=0$

Matching the Solution at the Interface

First, the normal vector to the boundary is determined, satisfying the relation:

$$r=r_0+\xi_{1r}(r_0)\,\mathrm{e}^{\mathrm{i}m\varphi+\mathrm{i}kz-\mathrm{i}\omega t}\,. \tag{1.527}$$

The boundary is expressed in the implicit form:

$$F(t,r,\varphi,z)=-r+r_0+\xi_{1r}(r_0)\,\mathrm{e}^{\mathrm{i}m\varphi+\mathrm{i}kz-\mathrm{i}\omega t}=0 \tag{1.528}$$

and the normal vector is defined via its gradient:

$$\mathbf{n}=\nabla F=\left(\frac{\partial F}{\partial r},\frac{1}{r}\frac{\partial F}{\partial\varphi},\frac{\partial F}{\partial z}\right)=\left(-1,\frac{\mathrm{i}m\xi_{1r}}{r}\mathrm{e}^{\mathrm{i}m\varphi+\mathrm{i}kz-\mathrm{i}\omega t},\mathrm{i}k\xi_{1r}\,\mathrm{e}^{\mathrm{i}m\varphi+\mathrm{i}kz-\mathrm{i}\omega t}\right). \tag{1.529}$$

The normal vector can be decomposed into an equilibrium and a perturbed part, $\mathbf{n} = \mathbf{n}_0 + \delta\mathbf{n}$, allowing us to isolate the non-periodic component of the perturbation:

$$\mathbf{n}_0 = (-1, 0, 0)\,, \tag{1.530}$$

$$\delta\mathbf{n} = \left(0, \frac{\mathrm{i}\, m\xi_{1r}}{r}, ik\xi_{1r}\right) \mathrm{e}^{\mathrm{i}\, m\varphi + \mathrm{i}\, kz - \mathrm{i}\omega t}\,, \tag{1.531}$$

$$\mathbf{n}_1 = \left(0, \frac{\mathrm{i}\, m\xi_{1r}}{r}, \mathrm{i}\, k\xi_{1r}\right). \tag{1.532}$$

This provides all the necessary components for a successful boundary matching: the internal solution (1.516), the external solution (1.526), and the normal vector components $\mathbf{n}_0$ and $\mathbf{n}_1$. First, $\mathbf{B}\cdot\mathbf{n}$ is matched according to relation (1.500):

$$\left[\mathbf{B}_0 \cdot \mathbf{n}_1 + \mathbf{B}_1 \cdot \mathbf{n}_0\right]_{\text{int}}^{\text{ext}} = 0\,. \tag{1.533}$$

Inside the filament, this expression vanishes, whereas outside the filament the relation yields $B_{0\varphi} n_{1\varphi} + B_{1r} n_{0r} = 0$. Since the boundary is shared, the displacement vector ξ_{1r} from the internal solution must be substituted. In all formulations, the limit as $r \to r_0$ is evaluated:

► $$A\left[\frac{\mathrm{i}\, mB_0(r_0)q}{\omega^2 \rho_0 r_0} I_m'(qr_0)\right] - D\left[kK_m'(kr_0)\right] = 0\,. \tag{1.534}$$

It remains to match the total pressure $\psi = p + B^2/2\mu_0$ according to relation (1.504):

$$\left[\xi_{1r}\, \frac{\mathrm{d}}{\mathrm{d}r} \frac{B_0^2}{2\mu_0} + p_1 + \frac{B_{0\varphi} B_{1\varphi}}{\mu_0}\right]_{\text{int}}^{\text{ext}} = 0\,.$$

Substituting the internal and external solutions into this boundary condition allows for the evaluation of the derivatives, taking the limit as $r \to r_0$:

► $$A\left[I_m(qr_0) + \frac{B_0^2 q}{\omega^2 \rho_0 \mu_0 r_0} I_m'(qr_0)\right] - D\left[\frac{\mathrm{i}\, mB_0}{\mu_0 r_0} K_m(kr_0)\right] = 0\,. \tag{1.535}$$

The relations (1.534) and (1.535) form a homogeneous system for the unknown integration constants A and D. A non-trivial solution exists only if the determinant of the system vanishes:

$$-\frac{\mathrm{i}\, mB_0(r_0)q}{\omega^2 \rho_0 r_0} I_m'(qr_0)\left[\frac{\mathrm{i}\, mB_0}{\mu_0 r_0} K_m(kr_0)\right] + kK_m'(kr_0)\left[I_m(qr_0) + \frac{B_0^2 q}{\omega^2 \rho_0 \mu_0 r_0} I_m'(qr_0)\right] = 0.$$

Multiplying the final two terms yields the explicit expression for ω^2:

► $$\omega^2 = -\frac{v_{\mathrm{A}}^2 q}{r_0} \frac{I_m'(qr_0)}{I_m(qr_0)}\left[1 + \frac{m^2}{kr_0} \frac{K_m(kr_0)}{K_m'(kr_0)}\right]; \qquad v_{\mathrm{A}}^2 \equiv \frac{B_0^2(r_0)}{\rho_0 \mu_0}\,. \tag{1.536}$$

The dispersion relation for this cylindrical scenario is thus established, which simultaneously provides the eigenvalues of the problem (1.490).

Analysis of the Solution

The derived dispersion relation confirms the previous assertion regarding the governing equation for the displacement vector: only the cases $\omega^2 > 0$ (stable solutions) and $\omega^2 < 0$ (purely imaginary, unstable solutions) can occur. The fundamental *stability criterion* is:

$$\frac{v_A^2}{r_0} q \frac{I'_m(qr_0)}{I_m(qr_0)} \left[1 + \frac{m^2}{kr_0} \frac{K_m(kr_0)}{K'_m(kr_0)} \right] < 0 .$$

Since the modified Bessel function of the first kind $I_m(qr)$ and its derivative $I'_m(qr)$ are strictly positive, and that $q^2 > 0$ holds in the near-incompressible limit ($\gamma \to \infty$), the final form of the *Kruskal–Shafranov stability criterion* is obtained:

► $$1 + \frac{m^2}{kr_0} \frac{K_m(kr_0)}{K'_m(kr_0)} < 0 . \tag{1.537}$$

Notably, the only quantity in the final equation that contains the material properties of the plasma is q. Defining $x \equiv kr_0$, the stability criterion can be rewritten as follows (where K_m is strictly positive and K'_m is negative):

$$F(x) \equiv xK'_m(x) + m^2 K_m(x) > 0 . \tag{1.538}$$

This formulation is well-suited for a graphical solution by plotting the left-hand side. The relation immediately demonstrates that for $m = 0$, no stable solution exists, rendering the filament inherently unstable against zero-mode perturbations. The same applies to the $m = 1$ mode.

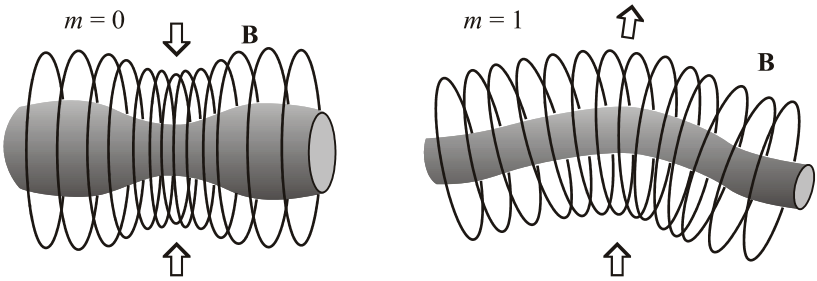
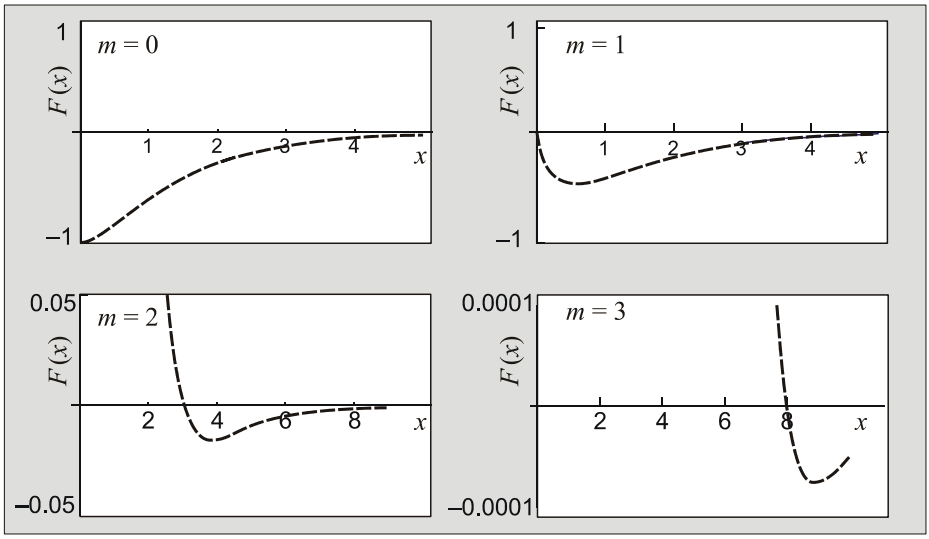


Fig. 1.88: Zero- and first-mode filament perturbations (sausage and kink).

The instability for $m = 0$ is known as the *sausage instability*, whereas the instability for $m = 1$ is termed the *kink instability*. In both scenarios, a stronger magnetic field (manifested by denser magnetic field lines) develops at the localized necking or deformation, where the enhanced magnetic pressure further drives the initial deformation.

The curves in Figure 1.89 plot left-hand side of the inequality (1.538). The first two modes are universally unstable. All higher modes ($m \geq 2$) are *stable* for $x < x_0$, with the critical values $x < x_0$ summarized in the table below.



Mode m	0	1	2	3	4	5
$x_0 = kr_0$	–	–	3,04	8,02	15,01	24,01

Fig. 1.89: Critical values x_0 for filament stability; the table lists the arguments, where the respective curves cross zero.

For x_0, the following approximate formula holds:

$$x_0 \approx m^2 - 1\,. \tag{1.539}$$

From mode $m = 2$, the system is stable for $kr_0 < x_0$, which corresponds to wavelengths:

► $$\lambda > \frac{2\pi r_0}{m^2 - 1}; \qquad m = 2, 3, \ldots\,. \tag{1.540}$$

Solution for a Non-Zero Axial Field

If an axial magnetic field B_{0z} is initially present, the first two modes become stabilized within certain parameter regimes. Thus, an axial field exerts a stabilizing effect on the current-carrying plasma filament.

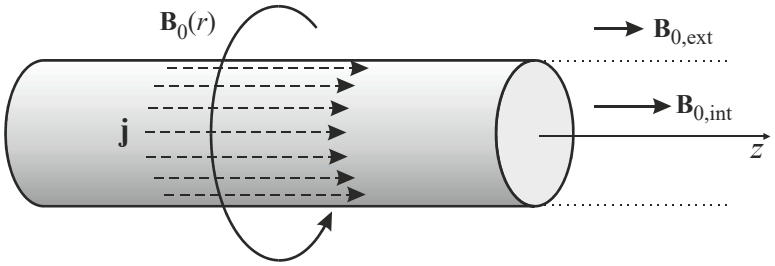


Fig. 1.90: Generalized configuration case of a plasma filament featuring an axial magnetic field.

Following a similar procedure, the general dispersion relation can be derived. The result requires a graphical solution, where stable regimes emerge for the first two modes:

$$\omega^2 = k^2 v_{\mathrm{A,int}}^2 - \left(k\, v_{\mathrm{A,ext}} + m \frac{v_{\mathrm{A}}}{r_0} \right)^2 \frac{q}{k} \frac{I_m'(qr_0)}{I_m(qr_0)} \frac{K_m(kr_0)}{K_m'(kr_0)} - \frac{v_{\mathrm{A}}^2 q}{r_0} \frac{I_m'(qr_0)}{I_m(qr_0)};$$

► $$v_{\mathrm{A}}^2 \equiv \frac{B_0^2(r_0)}{\rho_0 \mu_0}; \quad v_{\mathrm{A,int}}^2 \equiv \frac{B_{0,\mathrm{int}}^2}{\rho_0 \mu_0}; \quad v_{\mathrm{A,ext}}^2 \equiv \frac{B_{0,\mathrm{ext}}^2}{\rho_0 \mu_0}; \tag{1.541}$$

$$q^2 \equiv \frac{\left(k^2 - \omega^2/c_{\mathrm{s}}^2\right)\left(k^2 - \omega^2/v_{\mathrm{A,int}}^2\right)}{k^2 - \omega^2/c_{\mathrm{s}}^2 - \omega^2/v_{\mathrm{A,int}}^2}.$$

Rayleigh–Taylor Instability

The Rayleigh–Taylor instability (RT instability) arises at the interface between two fluids of different densities when a denser fluid rests above a less dense one in a gravitational field. For fluids in a constant gravitational field, this instability was first described by Lord Rayleigh in 1883. The English physicist and mathematician Geoffrey Ingram Taylor generalized this concept in 1950 to encompass any constant acceleration directed from the denser to the less dense fluid. In such scenarios, the denser fluid attempts to occupy a position below the less dense medium, causing initial perturbations at the interface to develop into characteristic finger-like plumes and, subsequently, mushroom-shaped structures. These processes are sometimes classified as interchange instabilities because different fluid regions exchange positions, minimizing the system's potential energy. Typical example involves two immiscible liquids poured into a glass such that the denser liquid rests above the less dense one. However, the RT instability also occurs during inversion at the interface between two air masses, or during the interaction of an expanding stellar wind stellar wind with the Crab Nebula – the remnant of a supernova explosion observed in 1054, or the buoyant rise of hot gases forming mushroom-shaped clouds in nuclear detonations.

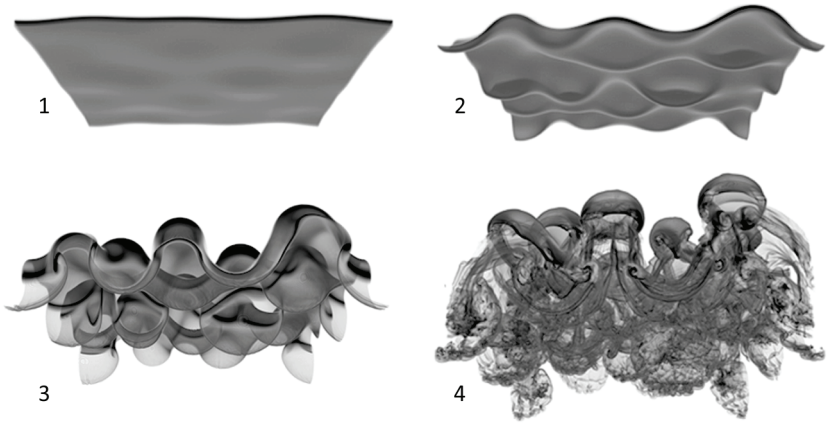


Fig. 1.91: Numerical simulation of the development of the Rayleigh–Taylor instability. Source: Pittsburgh Supercomputing Center.

In 1954, Martin Kruskal and Martin Schwarzschild demonstrated that a magnetic field can suppress this instability at the interface between two plasma media at short wavelengths.

A coordinate system is chosen where the interface between the two media lies in the plane $y = 0$. Assume that a homogeneous gravitational field acts along the y-axis and an external magnetic field $\mathbf{B}_0$, parallel to the interface, acts on the plasma. A small perturbation develops at the interface between the two media. We can align the z-axis with the magnetic field to ensure compatibility with previous derivations. Alternatively, aligning the z-axis with the perturbation propagation direction yields a simple periodic factor of $\exp(ikz)$. The subsequent derivation is independent of the z-axis choice; the essential requirement is that vectors $\mathbf{B}_0$ and $\mathbf{k}$ remain parallel to the interface. For clarity, the coordinate system illustrated below is adopted:

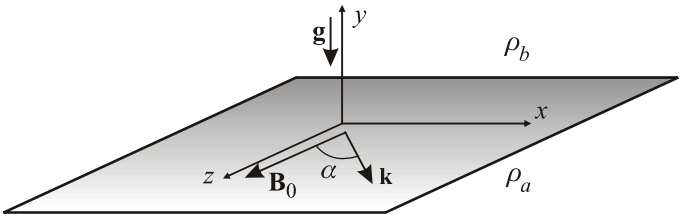


Fig. 1.92: Choice of coordinate system for the Rayleigh–Taylor instability analysis.

Evaluation of the Displacement Vector

With this choice of the coordinate system, the perturbations take the form:

$$\psi(t,\mathbf{x}) = \psi_0(y) + \delta\psi(t,\mathbf{x}); \qquad \delta\psi(t,\mathbf{x}) = \psi_1(y)\,\mathrm{e}^{\mathrm{i}[k_x x + k_z z - \omega t]}. \tag{1.542}$$

For simplicity, he subscript 1 for the displacement vector is omitted:

$$\delta\boldsymbol{\xi}(t,\mathbf{x}) = \boldsymbol{\xi}(y)\,\mathrm{e}^{\mathrm{i}[k_x x + k_z z - \omega t]}. \tag{1.543}$$

From the system geometry, the following relations hold for the individual quantities:

$$\begin{aligned} \mathbf{k} &= \mathbf{k}_{||} = (k_x, 0, k_z)\,, \\ \boldsymbol{\xi}(y) &= \xi_\perp \mathbf{e}_y + \boldsymbol{\xi}_{||} = (\xi_{||x}, \xi_\perp, \xi_{||z})\,, \\ \mathbf{B}_0 &= \mathbf{B}_0(y) = (B_{0x}, 0, B_{0z})\,, \\ \rho_0 &= \rho_0(y); \quad p_0 = p_0(y)\,. \end{aligned} \tag{1.544}$$

Symbols || and $\perp$ denote components parallel and perpendicular (along the y-axis) to the interface. Although $B_{0x} = 0$ here, this is not essential for subsequent derivations. For simplicity, an incompressible plasma is assumed, satisfying div $\delta\boldsymbol{\xi} = 0$. Upon expansion, this condition yields a straightforward relation:

$$\xi_\perp' + \mathrm{i}\,\mathbf{k}\cdot\boldsymbol{\xi}_{||} = 0 \quad \Rightarrow \quad \xi_\perp' + \mathrm{i}\,\mathbf{k}\cdot\boldsymbol{\xi} = 0 \quad \Rightarrow \quad \mathbf{k}\cdot\boldsymbol{\xi} = \mathrm{i}\,\xi_\perp'. \tag{1.545}$$

The prime in the notation denotes differentiation with respect to the sole non-periodic variable y. In the governing equation for the displacement vector (1.488), the magnetic field perturbation for the given geometry is determined first (div $\mathbf{B}_0 = 0$; div $\boldsymbol{\xi} = 0$):

$$\delta\mathbf{B} = \operatorname{curl}\left(\delta\boldsymbol{\xi}\times\mathbf{B}_0\right) = \left(\mathbf{B}_0\cdot\boldsymbol{\nabla}\right)\delta\boldsymbol{\xi} - \left(\delta\boldsymbol{\xi}\cdot\boldsymbol{\nabla}\right)\mathbf{B}_0 = \mathrm{i}\left(\mathbf{B}_0\cdot\mathbf{k}\right)\delta\boldsymbol{\xi} - \delta\xi_\perp\mathbf{B}_0' . \quad (1.546)$$

Substituting the perturbation into (1.488) yields for an incompressible plasma:

$$-\omega^2\rho_0\,\delta\boldsymbol{\xi} = \boldsymbol{\nabla}(\delta\boldsymbol{\xi}\cdot\boldsymbol{\nabla})p_0 - \mathbf{g}\operatorname{div}\left(\rho_0\delta\boldsymbol{\xi}\right) + \frac{\operatorname{curl}\delta\mathbf{B}}{\mu_0}\times\mathbf{B}_0 + \frac{\operatorname{curl}\mathbf{B}_0}{\mu_0}\times\delta\mathbf{B} . \quad (1.547)$$

Expanding all terms, evaluating the derivatives, eliminating the periodic factors, simplifying the vector triple products, and substituting for (**k**·**ξ**) from (1.545) provides:

$$-\omega^2\rho_0\xi_\perp = \left[\xi_\perp p_0' - \frac{\mathrm{i}}{\mu_0}\left(\mathbf{B}_0\cdot\boldsymbol{\xi}\right)\left(\mathbf{B}_0\cdot\mathbf{k}\right) + \frac{1}{\mu_0}\left(\mathbf{B}_0\cdot\mathbf{B}_0'\right)\xi_\perp\right]' - \frac{\xi_\perp}{\mu_0}\left(\mathbf{B}_0\cdot\mathbf{k}\right)^2 + g\rho_0'\xi_\perp ,$$

$$-\omega^2\rho_0\boldsymbol{\xi}_\parallel = \mathrm{i}\,\mathbf{k}\xi_\perp p_0' + \frac{1}{\mu_0}\mathbf{k}\left(\mathbf{B}_0\cdot\boldsymbol{\xi}\right)\left(\mathbf{B}_0\cdot\mathbf{k}\right) - \frac{1}{\mu_0}\boldsymbol{\xi}_\parallel\left(\mathbf{B}_0\cdot\mathbf{k}\right)^2 + \frac{\mathrm{i}}{\mu_0}\mathbf{k}\left(\mathbf{B}_0\cdot\mathbf{B}_0'\right)\xi_\perp .$$

These represent the three (1+2) equations for δ**ξ** components. Multiplying the second equation scalarly by **k**, substituting **k**·$\xi_\parallel$ = **k**·**ξ** from (1.545), the combination

$$\frac{\mathrm{i}}{\mu_0}\left(\mathbf{B}_0\cdot\boldsymbol{\xi}\right)\left(\mathbf{B}_0\cdot\mathbf{k}\right) = \xi_\perp p_0' + \frac{\omega^2}{k^2}\rho_0\xi_\perp' - \frac{1}{\mu_0 k^2}\left(\mathbf{B}_0\cdot\mathbf{k}\right)^2\xi_\perp' + \frac{\xi_\perp}{\mu_0}\left(\mathbf{B}_0\cdot\mathbf{B}_0'\right)$$

can be evaluated and then substituted into the first equation. It yields a single differential equation for the normal component of the displacement vector:

$$\left[\left(\omega^2\rho_0 - \frac{\left(\mathbf{k}\cdot\mathbf{B}_0\right)^2}{\mu_0}\right)\xi_\perp'\right]' - k^2\left(\omega^2\rho_0 - \frac{\left(\mathbf{k}\cdot\mathbf{B}_0\right)^2}{\mu_0}\right)\xi_\perp - gk^2\rho_0'\xi_\perp = 0 . \quad (1.548)$$

Denoting the expression in parentheses as $\mathcal{K}_0$, the governing equation for the normal component of the displacement vector reduces to the elegant form:

$$\left(\mathcal{K}_0\xi_\perp'\right)' - k^2\left(\mathcal{K}_0\xi_\perp\right) - gk^2\rho_0'\xi_\perp = 0 ;$$

► (1.549)

$$\mathcal{K}_0 \equiv \omega^2\rho_0 - \frac{1}{\mu_0}\left(\mathbf{k}\cdot\mathbf{B}_0\right)^2 .$$

Introducing the Alfvén velocity corresponding to the unperturbed magnetic field via the relation

$$\mathbf{v}_{0\mathrm{A}} \equiv \frac{\mathbf{B}_0}{\sqrt{\mu_0\rho_0}} , \quad (1.550)$$

the function $\mathcal{K}_0$ can be recast as:

$$\mathcal{K}_0 \equiv \rho_0\left[\omega^2 - \left(\mathbf{k}\cdot\mathbf{v}_{0\mathrm{A}}\right)^2\right] . \quad (1.551)$$

For an infinitesimally thin planar interface (transition layer), the equilibrium density $\rho_0(y)$ and magnetic field $\mathbf{B}_0(y)$ are uniform within both half-spaces but exhibit a step-

like discontinuity at the plane $y = 0$. Consequently, their derivatives ρ'_0 and $\mathbf{B}'_0$ generate Dirac delta distributions. For $y \neq 0$, however, $\rho'_0 = 0$ and the function $\mathcal{K}_0$ remains constant, reducing the governing equation in both half-spaces to:

$$\xi''_\perp - k^2 \xi_\perp = 0 \,. \tag{1.552}$$

The general solution is a linear combination of exponentials. In each half-space, only the mode decaying to zero at infinity is retained to ensure continuity:

$$\xi_\perp(y) = C\mathrm{e}^{-k|y|} = \begin{cases} C\mathrm{e}^{-ky} \,; & y > 0 \,, \\ C\mathrm{e}^{+ky} \,; & y < 0 \,. \end{cases} \tag{1.553}$$

Boundary Conditions and the Dispersion Relation

Evidently, the first derivative of the derived solution exhibits a jump discontinuity at the plane $y = 0$, meaning the second derivative behaves as a distribution. These jump conditions must be balanced within the governing equation (1.549), which allows for the matching of solutions across the interface. Substituting the solution into the governing equation (1.549) and integrating with respect to the variable y eliminates the derivative in the first term, thereby resolving the associated discontinuities. Since the second term contains no discontinuities, integration by parts is applied to the final term, converting the density step discontinuity into a derivative of the continuous normal component $\xi_\perp$:

$$\left[-\mathcal{K}_0 k \operatorname{sgn} y \, \mathrm{e}^{-k|y|} \right]_{-l}^{+l} - k^2 \int_{-l}^{+l} \mathcal{K}_0 \mathrm{e}^{-k|y|} \mathrm{d}y - \left[g k^2 \rho_0 \mathrm{e}^{-k|y|} \right]_{-l}^{+l} - \int_{-l}^{+l} g k^3 \rho_0 \operatorname{sgn} y \, \mathrm{e}^{-k|y|} \mathrm{d}y = 0 \,.$$

The limit as $l \to 0$ is evaluated, approaching the interface from both half-spaces. Because both integrands are bounded, the integrals vanish in the limit, yielding:

$$\left[-\mathcal{K}_0 k \operatorname{sgn} y \, \mathrm{e}^{-k|y|} - g k^2 \rho_0(y) \mathrm{e}^{-k|y|} \right]_{y \to 0^-}^{y \to 0^+} = 0 \,,$$

from which the dispersion relation immediately follows:

► $$\mathcal{K}_a + \mathcal{K}_b + g k (\rho_b - \rho_a) = 0 \,, \tag{1.554}$$

where the subscripts a and b denote the lower and upper half-spaces, respectively. Substituting the explicit form of $\mathcal{K}$ provides the final dispersion relation for the system:

► $$\omega^2 (\rho_a + \rho_b) - \frac{1}{\mu_0} \left[(\mathbf{k} \cdot \mathbf{B}_a)^2 + (\mathbf{k} \cdot \mathbf{B}_b)^2 \right] + g k (\rho_b - \rho_a) = 0 \,. \tag{1.555}$$

Analysis of the Solution (Zero Magnetic Field)

For a vanishing magnetic field, the relation reduces to:

► $$\omega^2 = -g k \frac{\rho_b - \rho_a}{\rho_a + \rho_b} \,. \tag{1.556}$$

Consequently, the configuration is always unstable if the denser fluid rests above the lighter one ($\omega^2 < 0$, $\rho_b > \rho_a$). The instability growth rate γ is given by:

$$\gamma = \sqrt{gk\frac{\rho_b - \rho_a}{\rho_a + \rho_b}}\,, \tag{1.557}$$

demonstrating that the instability develops fastest at short wavelengths and large density differences $\rho_b >> \rho_a$, with the denser fluid positioned above the less dense medium.

Analysis of the Solution (Non-Zero Magnetic Field)

In the presence of an equilibrium magnetic field, the dispersion relation satisfies:

► $$\omega^2 = -gk\frac{\rho_b - \rho_a}{\rho_a + \rho_b} + \frac{1}{\mu_0}\frac{(\mathbf{k}\cdot\mathbf{B}_a)^2 + (\mathbf{k}\cdot\mathbf{B}_b)^2}{\rho_a + \rho_b}\,, \tag{1.558}$$

yielding the stability criterion: ($\omega^2 \geq 0$)

$$-gk(\rho_b - \rho_a) + \frac{(\mathbf{k}\cdot\mathbf{B}_a)^2 + (\mathbf{k}\cdot\mathbf{B}_b)^2}{\mu_0} \geq 0\,. \tag{1.559}$$

This can be rewritten as:

► $$\lambda \leq \frac{2\pi\left(B_a^2\cos^2\alpha_a + B_b^2\cos^2\alpha_b\right)}{\mu_0 g(\rho_b - \rho_a)}\,, \tag{1.560}$$

where α denotes the angle between the magnetic field and the wave vector. For a perturbation propagating along the magnetic field, a stability region always exists for sufficiently short wavelengths, even when the denser fluid rests above the less dense one. For the stability cone, the following relation holds assuming equal angles $\alpha_a = \alpha_b = \alpha$):

► $$\begin{gathered}\alpha \in <0, \alpha_{\max})\,; \quad \alpha_{\max} = \arccos\sqrt{\frac{\lambda}{\lambda_{\max}}}\,; \\ \lambda \leq \lambda_{\max} \equiv \frac{2\pi\left(B_a^2 + B_b^2\right)}{\mu_0 g(\rho_b - \rho_a)}\,; \quad \rho_b > \rho_a\,.\end{gathered} \tag{1.561}$$

Kelvin–Helmholtz Instability

Another classic instability developing at the interface between two media is the Kelvin–Helmholtz (KH) instability. It arises when two media exhibit relative motion, such as wind blowing over a water surface, the solar wind streaming along the magnetopause, the shearing boundaries between planetary bands on gas giants, or interacting layers within Earth atmosphere. If the velocity shear is sufficiently large, the instability develops even under Rayleigh–Taylor stable configurations (i.e., with the lighter fluid resting above the denser one). The KH instability can also emerge within a single fluid subject to a strong velocity shear gradient. Stabilizing factors include gravitational fields, magnetic fields in plasmas, or a smooth transition layer where the velocity varies gradually rather than abruptly.

This instability was first described by Hermann von Helmholtz in 1868 and, independently, by Lord Kelvin in 1871. A complete solution for incompressible fluids was formulated by Subrahmanyan Chandrasekhar in 1961. In 1963, Amiya Sen generalized this solution to ideal magnetohydrodynamics, extending it to the compressible regime

a year later. This compressible formulation was subsequently generalized by Richard Gerwin and David John Southwood in 1968, with the latter focusing specifically on the magnetopause. In 1980, Attilio Ferrari derived a partial solution for relativistic velocities, a regime crucial for analyzing relativistic jets emanating from black holes.

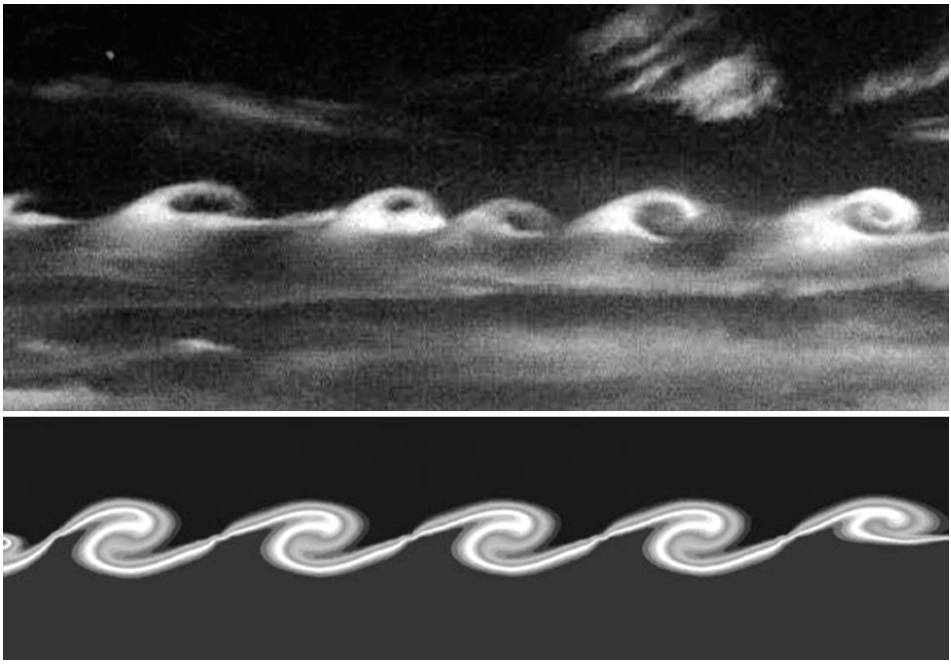


Fig. 1.93: Comparison of the KH instability in cloud formations with a numerical simulation. Photo: University of Notre Dame. Simulation: FLUENT software package.

Dispersion Relation

Consider conditions similar to the Rayleigh–Taylor instability, namely an incompressible plasma with an infinitesimally thin planar interface at $y = 0$. We assume that the equilibrium profiles depend solely on the y-coordinate, i.e., $\rho_0 = \rho_0(y)$, $\mathbf{B}_0 = \mathbf{B}_0(y)$, and $\mathbf{u}_0 = \mathbf{u}_0(y)$, where both $\mathbf{B}_0$ and $\mathbf{u}_0$ lie within the interface plane $y = 0$. A coordinate system analogous to the one used for the RT instability can be selected (though the resulting dispersion relation remains independent of this choice):

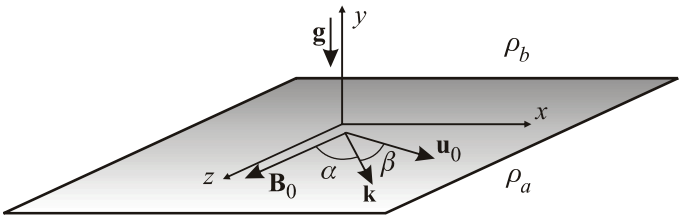


Fig. 1.94: Choice of coordinate system for the Kelvin–Helmholtz instability analysis.

The dispersion relation can be derived using the same procedure; compared to Equation (1.367), the formulation merely undergoes a Doppler shift modification:

$$\omega \to \omega - \mathbf{k}\cdot\mathbf{u}_0 . \tag{1.562}$$

The dispersion relation thus takes a form analogous to (1.554):

$$\begin{gathered} \mathcal{K}_a + \mathcal{K}_b + gk(\rho_b - \rho_a) = 0 ; \\ \mathcal{K}_0 \equiv \left[\omega - \mathbf{k}\cdot\mathbf{u}_0\right]^2 \rho_0 - \frac{1}{\mu_0}\left(\mathbf{k}\cdot\mathbf{B}_0\right)^2 . \end{gathered} \tag{1.563}$$

Substituting the explicit form of $\mathcal{K}$ yields the final dispersion relation:

► $$\left(\omega - \mathbf{k}\cdot\mathbf{u}_a\right)^2 \rho_a + \left(\omega - \mathbf{k}\cdot\mathbf{u}_b\right)^2 \rho_b - \frac{(\mathbf{k}\cdot\mathbf{B}_a)^2 + (\mathbf{k}\cdot\mathbf{B}_b)^2}{\mu_0} + gk(\rho_b - \rho_a) = 0. \tag{1.564}$$

Analysis of the Solution (Zero Gravity, Zero Magnetic Field)

Assuming the fluid in half-space *a* is at rest, velocity $\mathbf{u}_b$ represents the relative velocity $\Delta\mathbf{u}_0$ between the media. Measuring the angular frequency in this reference frame reduces the dispersion relation to:

$$\omega^2 \rho_a + \left(\omega - \mathbf{k}\cdot\Delta\mathbf{u}_0\right)^2 \rho_b = 0 ,$$

$$\omega^2 \rho_a + \omega^2 \rho_b - 2\omega(\mathbf{k}\cdot\Delta\mathbf{u}_0)\rho_b + \left(\mathbf{k}\cdot\Delta\mathbf{u}_0\right)^2 \rho_b = 0 ,$$

► $$\omega_{1,2} = (\mathbf{k}\cdot\Delta\mathbf{u}_0)\frac{r \pm \mathrm{i}\sqrt{r}}{(1+r)} ; \qquad r \equiv \frac{\rho_b}{\rho_a} . \tag{1.565}$$

Since the angular frequency possesses a non-zero imaginary part, the KH instability always develops, even for $r = 1$ – which corresponds to identical fluids in relative motion with a non-zero velocity. The instability growth rate (the positive imaginary part of the angular frequency) is given by:

$$\gamma = \frac{(\mathbf{k}\cdot\Delta\mathbf{u}_0)\sqrt{r}}{(1+r)} . \tag{1.566}$$

Analysis of the Solution (Effect of Gravity)

Assuming the fluid in half-space *a* is at rest, and the system is subject only to a homogeneous gravitational field, the solution for ω is evaluated as:

► $$\omega_{1,2} = \frac{(\mathbf{k}\cdot\Delta\mathbf{u}_0)r}{1+r} \pm \sqrt{\frac{gk(1-r)}{1+r} - \frac{(\mathbf{k}\cdot\Delta\mathbf{u}_0)^2 r}{(1+r)^2}} ; \qquad r \equiv \frac{\rho_b}{\rho_a} . \tag{1.567}$$

Evidently, gravity exerts a stabilizing effect, meaning the angular frequency is no longer inherently complex. The stability criterion requires the radicand to be non-negative:

$$gk(1-r^2) - (\mathbf{k}\cdot\Delta\mathbf{u}_0)^2 r \geq 0 .$$

Assuming a Rayleigh–Taylor stable configuration (i.e., the lighter fluid rests above the denser one, $r < 1$; otherwise, the RT instability would dominate), the stability criterion reduces to:

► $$\lambda \geq \lambda_{\max} \cos^2 \beta\,; \qquad \lambda_{\max} \equiv 2\pi \frac{\Delta u_0^2}{g} \frac{r}{1-r^2}\,; \qquad \beta = \sphericalangle(\mathbf{k}, \Delta \mathbf{u}_0)\,. \tag{1.568}$$

Perturbations with wavelengths $\lambda > \lambda_{\max}$ remain stable and do not grow. For example, considering wind blowing over water ($\beta = 0$, with compressibility neglected as a first approximation), waves propagate along the wind direction. Since the air density is orders of magnitude lower than that of water ($r << 1$), the stability criterion simplifies to:

$$\lambda \geq \lambda_{\max}\,; \qquad \lambda_{\max} \equiv 2\pi r \frac{\Delta u_0^2}{g}\,. \tag{1.569}$$

Notably, short-wavelength modes are stabilized by surface tension.

Analysis of the Solution (Effect of Gravity and the Magnetic Field)

For non-zero gravity and magnetic fields, the dispersion relation (1.564) yields:

$$\omega_{1,2} = \frac{(\mathbf{k}\cdot\Delta\mathbf{u}_0)r}{1+r} \pm \sqrt{\frac{gk(1-r)}{1+r} + \frac{\left[(\mathbf{k}\cdot\mathbf{v}_a)^2 + (\mathbf{k}\cdot\mathbf{v}_b)^2 r\right]}{1+r} - \frac{(\mathbf{k}\cdot\Delta\mathbf{u}_0)^2 r}{(1+r)^2}}\,,$$

► $$\mathbf{v}_a \equiv \frac{\mathbf{B}_a}{\sqrt{\mu_0 \rho_a}}\,; \qquad \mathbf{v}_\mathrm{b} \equiv \frac{\mathbf{B}_b}{\sqrt{\mu_0 \rho_b}}\,; \tag{1.570}$$

$$r \equiv \frac{\rho_b}{\rho_a}\,.$$

Simultaneous gravity and magnetic fields exert a stabilizing effect, contributing positively to the radicand. Assuming a Rayleigh–Taylor stable configuration $r < 1$), the stability criterion takes the form:

► $$k(\Delta u_0)^2 r \cos^2 \beta \leq g(1-r^2) + k\left(v_a^2 \cos^2\alpha_a + v_b^2 r \cos^2\alpha_b\right)(1+r)\,. \tag{1.571}$$

This relation yields the stability boundaries for specific parameter regimes.

Other Instabilities (Richtmyer–Meshkov and Diocotron)

Richtmyer–Meshkov Instability

The Richtmyer–Meshkov (RM) instability arises at the interface between two media subject to rapid acceleration, typically during the passage of a shock wave. This instability develops during supernova explosions, where the resulting mixing combines both the RM and RT instabilities. Another classic example is inertial confinement fusion, where a hot plasma envelope implodes onto a cold fuel pellet. The reflection of a shock wave at the interface can trigger the formation of vortical structures. The existence of this instability was theoretically predicted by Robert Davis Richtmyer at Los Alamos National Laboratory in 1953, and first observed experimentally by Evgeny Meshkov in 1970 in the Soviet Union.

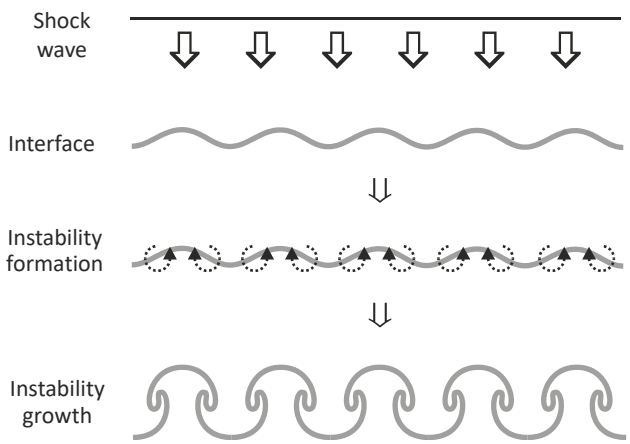


Fig. 1.95: Formation and development of the Richtmyer–Meshkov instability.

Diocotron Instability

The diocotron instability is the electrostatic analog of the KH instability, where plasma motion along the interface arises due to a violation of quasi-neutrality. The resulting electric field, combined with an external magnetic field, drives a charged particle drift that triggers the instability, forming characteristic vortices in the shear velocity region. The diocotron instability occurs on the surface of plasma filaments, during electron beam propagation through plasmas, within auroral curtains, or in the spiral arms of galaxies (e.g., NGC 3646). The name derives from the Greek word meaning "*to pursue.*" This instability was introduced by Hannes Alfvén in 1950 to explain vortex structures in the aurora.

The diocotron instability emerges whenever two layers of differently charged plasma slide past each other. It is most prevalent in plasma filaments where electric charge becomes radially separated. The resulting radial electric field, paired with an axial magnetic field B_z, induces an azimuthal drift at velocity v_φ. The entire filament undergoes differential rotation, meaning regions at varying radial distances possess different angular velocities. At the filament surface, two distinct velocity regions (the rotating filament and the surrounding medium) come into contact, triggering the instability.

Radial charge separation – the fundamental condition for the diocotron instability – can occur via multiple mechanisms. Most commonly, it stems from various drifts to which electrons and ions respond asymmetrically. Additionally, the column's own radiation can induce charge separation; radiative processes carry away thermal energy, creating a radial temperature gradient that causes both charge separation (analogous to the thermoelectric effect) and the separation of distinct chemical elements. Furthermore, other instability types can generate uncompensated space charge.

The diocotron instability is highly common in plasma filaments, having been documented in numerous laboratory experiments, space plasmas, and numerical simulations. Its development, driven by surface rotation, can serve as the dominant impetus for a filament's transition into a helical structure.

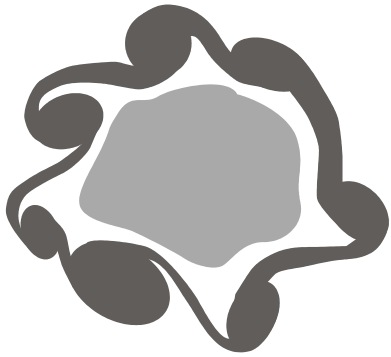


Fig. 1.96: Development of the diocotron instability at the plasma boundary.

Interchange Instabilities

The Rayleigh–Taylor instability occurs when a denser fluid rests above a lighter one. When the denser fluid moves beneath the lighter one, a rearrangement takes place, leading to a decrease in the system's potential energy. This same principle applies generally: if a plasma displacement reduces the internal energy of the system, the plasma is unstable. The *stability criterion* is therefore given by:

$$\delta W_{\text{int}} \geq 0\,; \qquad \delta W_{\text{int}} \equiv -\int \delta\boldsymbol{\xi}^{*} \cdot \hat{\mathscr{L}}\, \delta\boldsymbol{\xi}\, \mathrm{d}^{3}\mathbf{x}\,. \tag{1.572}$$

Equation (1.494) expresses this energy. Consider a plasma dominated by a strong magnetic field $\beta = p/p_{\text{M}} << 1$). The change in internal energy can be evaluated by assuming the plasma surrounding one magnetic field line is interchanged with the plasma surrounding an adjacent magnetic field line (exchanging the plasma within two neighboring magnetic flux tubes).

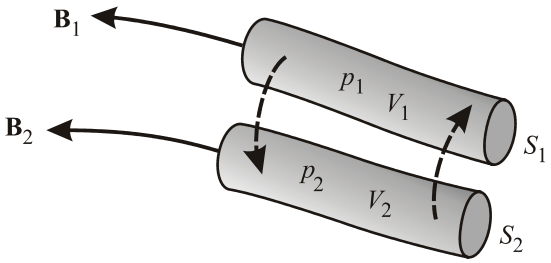


Fig. 1.97: Mechanism of the interchange instability.

For the internal energy, relation (1.337) dictates that:

$$W_{\text{int}} = \frac{pV}{\gamma - 1}\,, \tag{1.573}$$

where p is the plasma pressure inside the flux tube, V is its volume, and γ is the polytropic coefficient. The plasma pressure is assumed to satisfy a polytropic relation:

$$pV^{\gamma} = \text{const}\,. \tag{1.574}$$

If the plasma flows from tube 1 to tube 2, the change in internal energy equals:

$$\delta W_{1\to 2} = \frac{p_2' V_2 - p_1 V_1}{\gamma - 1} = \frac{p_1 (V_1/V_2)^{\gamma} V_2 - p_1 V_1}{\gamma - 1}\,.$$

Conversely, if the plasma flows from tube 2 to tube 1, the energy changes by:

$$\delta W_{2\to 1} = \frac{p_1' V_1 - p_2 V_2}{\gamma - 1} = \frac{p_2 (V_2/V_1)^{\gamma} V_1 - p_2 V_2}{\gamma - 1}\,.$$

The total energy variation for both flux tubes is given by:

$$\delta W = \delta W_{1\to 2} + \delta W_{2\to 1} = \frac{1}{\gamma - 1}\left[p_1 \left(\frac{V_1}{V_2}\right)^{\gamma} V_2 - p_1 V_1 + p_2 \left(\frac{V_2}{V_1}\right)^{\gamma} V_1 - p_2 V_2 \right].$$

Denoting equilibrium values as $p_1 = p$ and $V_1 = V$, and expressing the variations as $p_2 = p + \delta p$ and $V_2 = V + \delta V$, allows a perturbation expansion. Because the zero- and first-order terms vanish identically, the expansion must be retained up to second order:

$$\delta W = \frac{1}{\gamma - 1}\left[p \left(\frac{V}{V + \delta V}\right)^{\gamma} (V + \delta V) - pV + (p + \delta p)\left(\frac{V + \delta V}{V}\right)^{\gamma} V - (p + \delta p)(V + \delta V) \right],$$

$$\delta W = \frac{1}{\gamma - 1}\left[p \left(1 + \frac{\delta V}{V}\right)^{-\gamma} (V + \delta V) - pV + (p + \delta p)\left(1 + \frac{\delta V}{V}\right)^{\gamma} V - (p + \delta p)(V + \delta V) \right].$$

The binomial expansion is applied via the relation:

$$(1 + x)^n = 1 + nx + \frac{n(n-1)}{2} x^2 + \cdots$$

Multiplying these terms and retaining second-order contributions yields:

$$\delta W = \gamma \frac{p}{V} (\delta V)^2 + \delta p\, \delta V\,. \tag{1.575}$$

This relation assumes a dominant magnetic field. In the case of a weak magnetic field, variations in the magnetic flux and the corresponding magnetic energy of adjacent flux tubes must also be accounted for, altering the final formulation. The volume of a finite-length flux tube is given by:

$$V = \int S\, \mathrm{d}l\,.$$

Choosing a cross-sectional area perpendicular to the tube and applying the conservation of magnetic flux $\phi = BS$ yields:

$$V = \phi \int \frac{\mathrm{d}l}{B} = \phi U\,; \quad U \equiv \int \frac{\mathrm{d}l}{B}\,.$$

The quantity U represents the specific volume of the magnetic flux tube per unit of magnetic flux, evaluated as the line integral of the inverse magnetic field along the tube. The fundamental criterion for plasma stability against the interchange of adjacent flux tubes requires that the total energy variation remains non-negative:

$$\gamma \frac{p}{U}(\delta U)^2 + \delta p\, \delta U \geq 0\,; \qquad U \equiv \int \frac{\mathrm{d}l}{B}\,. \tag{1.576}$$

Sufficient Condition for Stability

Since the first term is strictly non-negative, the following relation serves as a sufficient stability criterion:

$$\delta p\, \delta U > 0\,; \qquad U \equiv \int \frac{\mathrm{d}l}{B}\,. \tag{1.577}$$

Both terms must share the same sign. For instance, as pressure increases, the quantity U must also increase, which implies a decreasing magnetic field. Consequently, stability is ensured if the magnetic field strength increases in the direction of decreasing plasma pressure.

◖ Example 1.6: Convex and Concave Mirrors

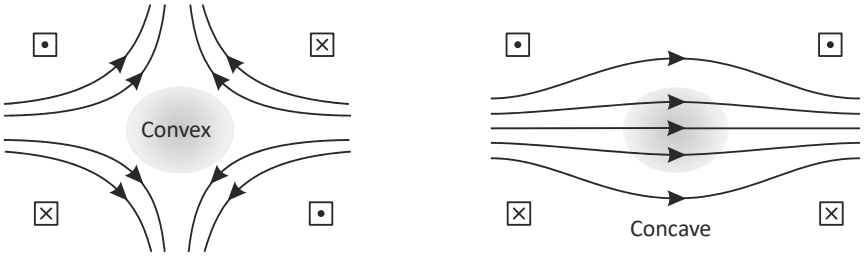


Fig. 1.98: Magnetic field line geometry for convex (cusp) and concave mirrors.

The left panel of Figure 1.98 illustrates an azimuthal, or convex (relative to the plasma), mirror, frequently termed a *cusp configuration*. Moving across the field lines – the direction governing plasma interchange between flux tubes – away from the plasma core results in a decreasing plasma pressure and an increasing magnetic field. This configuration satisfies the sufficient stability criterion, rendering the system stable against plasma penetration across the magnetic field lines.

With a classical (concave) mirror, the scenario is inverted. Moving across the field lines causes both plasma pressure and magnetic field to decrease. Such a configuration fails the sufficient criterion, meaning the system may exhibit instability.

◗

Necessary and Sufficient Condition for Stability

Evaluating the complete stability criterion (1.576) requires integrating the quantity $1/B$ along a magnetic field line to determine its spatial dependence. If individual field lines are parameterized by the radial coordinate r (e.g., the distance from the system axis), the pressure profile $p(r)$ and the specific volume function $U(r)$ must be specified. The system remains stable if and only if:

$$\gamma \frac{p}{U}\left(\frac{\mathrm{d}U}{\mathrm{d}r}\right)^2 + \frac{\mathrm{d}p}{\mathrm{d}r}\frac{\mathrm{d}U}{\mathrm{d}r} \geq 0\,; \qquad U \equiv \int \frac{\mathrm{d}l}{B}\,. \tag{1.578}$$

The *stability criterion* (1.576) can be recast into an alternative form:

$$\frac{\delta \ln p}{\delta \ln U} \geq -\gamma\,. \tag{1.579}$$

An equivalent stability criterion, expressed as a product, takes the form:

$$\delta U\, \delta\left[\ln\left(pV^{\gamma}\right)\right] \geq 0\,. \tag{1.580}$$

Since the onset or damping of these modes depends exclusively on the equilibrium pressure profile, instabilities of this class are classified as *pressure-gradient-driven*.

◖ Example 1.7: Infinite Conductor

Consider an infinite conductor carrying a constant current, surrounded by a plasma.

1) Determine the maximum rate at which the plasma pressure can decrease with distance from the conductor for the system to remain stable.
2) Find the dependence of the β parameter on the distance from the conductor at the boundary between stability and instability.

Solution: Assume that the pressure decreases with distance from the conductor as C/r^{α}. The magnetic field lines form concentric circles. Along a circle of radius r, the magnetic field is given by Ampere law, $B(r) = D/r$. Since this field is uniform along the entire circle, the two key quantities are:

$$p(r) = \frac{C}{r^{\alpha}}\,; \qquad U(r) = \int \frac{\mathrm{d}l}{B(l)} = \frac{2\pi r}{D/r} = Kr^2\,.$$

Substituting $p(r)$ and $U(r)$ into the stability criterion (1.578) yields:

$$\alpha \leq 2\gamma\,.$$

For $\alpha = 2\gamma$, the β parameter exhibits the following dependence:

$$\beta \equiv p/p_M \sim p/B^2 \sim 1/r^{\alpha+2} = 1/r^{2\gamma+2}\,.$$

Conclusion: The plasma surrounding the conductor remains stable against interchange perturbations between the flux tubes if the pressure decreases more slowly than $1/r^{2\gamma}$. If the pressure decreases more rapidly, the plasma is unstable. The critical value of the β parameter decreases with distance as $1/r^{2\gamma+2}$. ◗

◖ Example 1.8: Magnetic Dipole

Solve the previous problem for a conductor coiled into a loop of radius a, assuming a distance sufficiently far from the source $r \gg a$.

Solution: The derivation follows a procedure analogous to the previous example. At large distances from the source, the length of the magnetic field line is proportional to the distance, and the dipole magnetic field decreases as the cube of the distance:

$$B(r) \sim \frac{1}{r^3}; \qquad \Rightarrow \qquad U(r) \equiv \int \frac{\mathrm{d}l}{B} \sim r^4 .$$

Applying this criterion to a pressure profile C/r^{α} yields the stability condition:

$$\alpha \leq 4\gamma . \tag{1.581}$$

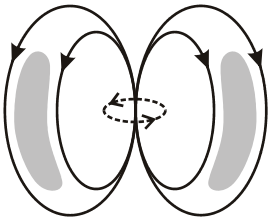


Fig. 1.99: Magnetic dipole configuration.

Conclusion: The plasma surrounding a magnetic dipole remains stable against interchange perturbations between the flux tubes if the pressure decreases more slowly than $1/r^{4\gamma}$. If the pressure decreases more rapidly, the plasma becomes unstable. The critical value of the β parameter decreases with distance as $1/r^{4\gamma+2}$. ◗

Note 1: The plasma within the Earth's Van Allen radiation belts is stable; consequently, the local plasma pressure decreases more slowly than $1/r^{4\gamma}$.

Note 2: A magnetic dipole configuration (analogous to the Van Allen belts) represents one of the concepts for plasma confinement in thermonuclear fusion. If the plasma pressure drops too sharply with distance from the center, the plasma escapes the confinement system via an interchange instability.

Note 3: For non-negligible values of the β parameter, variations in the magnetic energy must be explicitly incorporated into the derivation. In such scenarios, the stability criterion takes the form [3], [11]:

$$\gamma \frac{p}{U}(\delta U)^2 + \left(1 + \gamma \frac{pU}{I}\right) \delta p \, \delta U \geq 0 ; \quad U \equiv \int \frac{\mathrm{d}l}{B} ; \quad I \equiv \frac{1}{\mu_0} \int B \, \mathrm{d}l . \tag{1.582}$$

Note 4.: The presence of a sheared magnetic field (a field parallel to the interface whose magnitude depends on the distance) can stabilize pressure-gradient-driven instabilities, analogously to the stabilization of the RT instability.

Schwarzschild Convection Criterion

In 1958, the German physicist Martin Schwarzschild, son of the renowned Karl Schwarzschild, derived a criterion for the development of convective flow in stellar interiors. This criterion applies not only to stars but also to any fluid or plasma system. Suppose that, through some random perturbation, a localized region of plasma is displaced within a star. For clarity, consider a small plasma element moving from the stellar interior slightly upward along the z-axis (see Figure 1.100).

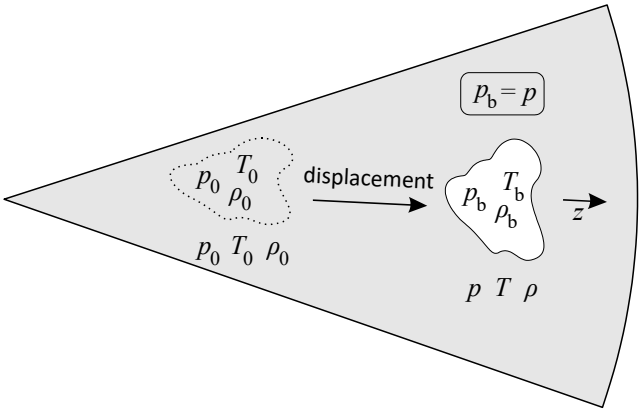


Fig. 1.100: Geometric schematic for the Schwarzschild convection criterion.

Initially, this hypothetical volume shares the ambient plasma parameters. After displacement, the internal parameters become T_b, ρ_b, and p_b, while the surrounding values are T, ρ, and p. Pressure equilibrium requires $p_b = p$. If the displaced element's density exceeds the surroundings ($\rho_b > \rho$), buoyancy forces return it downward, ensuring stability. Conversely, if $\rho_b < \rho$, the element continues rising, generating convective flow. This regime is convectively unstable, and the criterion for the onset of convection is therefore straightforward:

► $$\rho_b < \rho\,. \tag{1.583}$$

First, the left-hand side of this criterion is expanded. Assuming the element's displacement behaves as a rapid perturbation lasting for a short time, the bubble has insufficient time to exchange thermal energy with its surroundings, rendering the process adiabatic:

$$p_b = K\rho^{\gamma}\,; \qquad \gamma \equiv \frac{c_p}{c_V}. \tag{1.584}$$

A first-order Taylor expansion of this relation yields:

$$\begin{aligned} p_b = K\rho^{\gamma} &\approx p_0 + \frac{\partial p_b}{\partial \rho}(\rho_b - \rho_0) = \\ &= p_0 + K\gamma\rho_0^{\gamma-1}(\rho_b - \rho_0) = \\ &= p_0 + \frac{p_0}{\rho_0}\gamma(\rho_b - \rho_0)\,. \end{aligned} \tag{1.585}$$

The constant K is determined from equation (1.584). The bubble density for the left-hand side of the criterion can then be evaluated, incorporating the condition that the internal bubble pressure equals the ambient medium pressure ($p_b = p$):

$$\rho_b = \rho_0 + \frac{\rho_0}{\gamma p_0}(p - p_0). \tag{1.586}$$

The right-hand side of the criterion is expressed via the plasma equation of state:

$$p = A\rho T\,. \tag{1.587}$$

A first-order expansion allows the constant A to be evaluated from the final equation:

$$\begin{aligned} p &= p_0 + \frac{\partial p}{\partial \rho}(\rho - \rho_0) + \frac{\partial p}{\partial T}(T - T_0) = \\ &= p_0 + AT_0(\rho - \rho_0) + A\rho_0(T - T_0) = \\ &= p_0 + \frac{p_0}{\rho_0}(\rho - \rho_0) + \frac{p_0}{T_0}(T - T_0) \end{aligned} \tag{1.588}$$

The density for the first term of the criterion is then determined:

$$\rho = \rho_0 + \frac{\rho_0}{p_0}\left(p - p_0\right) - \frac{\rho_0}{T_0}(T - T_0) \tag{1.589}$$

Substituting (1.589) and (1.586) into (1.583) yields the convection criterion:

$$\frac{\rho_0}{\gamma p_0}\left(p - p_0\right) < \frac{\rho_0}{p_0}\left(p - p_0\right) - \frac{\rho_0}{T_0}(T - T_0)\,. \tag{1.590}$$

Further simplification straightforwardly leads to the relation:

$$\mathrm{d}T < \left(\frac{\gamma - 1}{\gamma}\right)\frac{T_0}{p_0}\mathrm{d}p\,. \tag{1.591}$$

In the geometry of Figure 1.100, both dT and dp are negative since pressure and temperature decrease with altitude. Omitting the subscript 0 to generalize the thought experiment, the formulation reduces to:

► $$\left|\mathrm{d}T\right| > \left(\frac{\gamma - 1}{\gamma}\right)\frac{T}{p}\left|\mathrm{d}p\right|\,. \tag{1.592}$$

Consequently, convective flow develops only if a sufficiently steep temperature gradient exists. Within the Sun, this criterion is satisfied exclusively at depths of 200,000 km or less below the surface. Energy from the solar interior is initially transported via radiation, with convection dominating only within this outermost 200,000-km layer. Conversely, in massive stars driven by the CNO cycle, the temperature gradient is maximized near the center, featuring a convective core surrounded by outer radiative layers. The Schwarzschild criterion can be expressed in alternative formulations, including:

► $$\frac{\left|\mathrm{d}T\right|}{T} > \left(\frac{\gamma - 1}{\gamma}\right)\frac{\left|\mathrm{d}p\right|}{p}\,, \tag{1.593}$$

► $$\frac{\mathrm{d}\ln T}{\mathrm{d}\ln p} < \frac{\gamma - 1}{\gamma}\,. \tag{1.594}$$

The Schwarzschild criterion holds generally: any strong temperature gradient within a plasma triggers a convective instability, generating macroscopically turbulent flows.

1.5.3 Resistive Instabilities

Governing Equations

A non-zero plasma resistivity primarily enables magnetic reconnection and the associated tearing instability, which develops at the interface between two regions with oppositely directed magnetic field lines. Near the boundaries of such regions, the diffusion term in the magnetic field equation (1.177) cannot be neglected. Furthermore, phenomena associated with a spatial resistivity gradient across the interface are highly significant. Consequently, the magnetic field equation is derived once more, explicitly incorporating a non-zero resistivity gradient. Throughout this chapter, perturbations are assumed to take the form:

$$\psi(t,\mathbf{q}_\mathrm{n},\mathbf{q}_\mathrm{p},) = \psi_0(\mathbf{q}_\mathrm{n}) + \psi_1(\mathbf{q}_\mathrm{n})\,\mathrm{e}^{\mathrm{i}\,\mathbf{q}_\mathrm{p}\cdot\mathbf{k}_\mathrm{p} - \mathrm{i}\,\omega t}\,, \tag{1.595}$$

where $\mathbf{q}_\mathrm{n}$ represents non-periodic variables (perpendicular to the interface) and $\mathbf{q}_\mathrm{p}$ represents periodic variables. The divergence-free property of the magnetic field, universally satisfied by Maxwell equations) and the incompressibility of the plasma are assumed. The latter condition is generally valid when magnetic convection dominates over diffusion, a regime applicable to the vast majority of both laboratory and space plasmas:

$$\mathrm{div}\,\mathbf{B} \;=\; 0\,, \tag{1.596}$$

$$\mathrm{div}\,\boldsymbol{\xi} \;=\; 0\,. \tag{1.597}$$

Equation for the Magnetic Field

The analysis begins with the Faraday law (magnetic field temporal evolution):

$$\mathrm{curl}\,\mathbf{E} = -\frac{\partial \mathbf{B}}{\partial t} \tag{1.598}$$

and Ohm law in differential form:

$$\mathbf{j} = \sigma(\mathbf{E} + \mathbf{u}\times\mathbf{B})\,; \qquad \sigma = \sigma(\mathbf{x})\,. \tag{1.599}$$

Substituting the electric field (1.599) into equation (1.598) and performing straightforward algebraic manipulations yields:

► $$\frac{\partial \mathbf{B}}{\partial t} \;=\; \frac{\eta}{\mu_0}\nabla^2\mathbf{B} + \mathrm{curl}\,(\mathbf{u}\times\mathbf{B}) - \frac{1}{\mu_0}(\nabla\eta)\times\mathrm{curl}\,\mathbf{B}\,, \tag{1.600}$$

where the resistivity is defined via the relation:

$$\eta(\mathbf{x}) = \frac{1}{\sigma(\mathbf{x})}\,. \tag{1.601}$$

The first term describes the diffusion of the magnetic field, the second represents magnetic freezing, and the third term acts as an effective force field that significantly influences the reconnection of magnetic field lines. The linearized induction equation for $\mathbf{u}_0 = 0$, where the equilibrium field $\mathbf{B}_0$ satisfies Laplace equation $\nabla^2\mathbf{B}_0 = 0$ (representing the stationary form of the field formulation), takes the form:

► $$\frac{\partial \delta \mathbf{B}}{\partial t} = \frac{\eta_0}{\mu_0}\nabla^2 \delta \mathbf{B} + \operatorname{curl}(\delta \mathbf{u} \times \mathbf{B}_0) - \frac{1}{\mu_0}(\nabla \eta_0) \times \operatorname{curl} \delta \mathbf{B} - \frac{1}{\mu_0}(\nabla \delta \eta) \times \operatorname{curl} \mathbf{B}_0 \,. \quad (1.602)$$

Equation for Resistivity

The origin of the plasma resistivity gradient can vary. Assuming the equilibrium profile of the resistivity is given, its variations driven by a wave or an instability must be determined. Without relying on a detailed micro-physical mechanism for plasma conductivity, it can be stated that plasma motions transport regions with a specific resistivity from one location to another; consequently, the material derivative $\mathrm{d}\eta/\mathrm{d}t = 0$ holds. Upon expansion, the transport equation for resistivity takes the form:

► $$\frac{\partial \eta}{\partial t} + (\mathbf{u} \cdot \nabla)\, \eta = 0 \,. \quad (1.603)$$

The linearized form of the resistivity formulation reduces to:

$$\frac{\partial \delta \eta}{\partial t} + (\delta \mathbf{u} \cdot \nabla)\, \eta_0 = 0 \,.$$

Both terms can be integrated directly with respect to time:

$$\delta \eta + (\delta \boldsymbol{\xi} \cdot \nabla)\, \eta_0 = 0 \,.$$

Eliminating the periodic variables yields the final formulation:

► $$\eta_1 + (\boldsymbol{\xi}_1 \cdot \nabla)\, \eta_0 = 0 \,. \quad (1.604)$$

Describing macroscopic displacements rather than specific micro-mechanisms, the perturbation η_1 can be evaluated directly from the displacement vector, rendering the resistivity equation straightforward in the linear approximation.

Significance of the Gradient η_0

The Ohm law (1.599) can be expressed in terms of resistivity as:

$$\eta \mathbf{j} = \mathbf{E} + \mathbf{u} \times \mathbf{B} \,.$$

In the linear approximation, this relation yields:

$$\delta \eta\, \mathbf{j}_0 + \eta_0\, \delta \mathbf{j} = \delta \mathbf{E} + \delta \mathbf{u} \times \mathbf{B}_0 \,.$$

Since these represent purely algebraic relations, the periodic factors can be eliminated from both sides of the equation:

$$\eta_1\, \mathbf{j}_0 + \eta_0\, \mathbf{j}_1 = \mathbf{E}_1 + \mathbf{u}_1 \times \mathbf{B}_0 \,.$$

Substituting the resistivity perturbation η_1 from relation (1.604) allows the current density perturbation $\mathbf{j}_1$ to be evaluated:

$$\mathbf{j}_1 = \frac{(\boldsymbol{\xi}_1 \cdot \nabla)\, \eta_0}{\eta_0}\, \mathbf{j}_0 + \frac{\mathbf{E}_1 + \mathbf{u}_1 \times \mathbf{B}_0}{\eta_0} \,.$$

This perturbed current is directly coupled with the Lorentz force density:

$$\mathbf{f}_1 \equiv \mathbf{j}_1 \times \mathbf{B}_0 = \frac{(\boldsymbol{\xi}_1 \cdot \nabla)\,\eta_0}{\eta_0}\left(\mathbf{j}_0 \times \mathbf{B}_0\right) + \frac{\mathbf{E}_1 \times \mathbf{B}_0 + (\mathbf{u}_1 \times \mathbf{B}_0) \times \mathbf{B}_0}{\eta_0}.$$

While the second term represents the standard variation in force density caused by perturbations, the first term is entirely new. This force arises due to the gradient of the equilibrium resistivity distribution, expressed as:

► $$\mathbf{f}_{\nabla\eta_0}^{(1)} \equiv \frac{(\boldsymbol{\xi}_1 \cdot \nabla)\,\eta_0}{\eta_0}\left(\mathbf{j}_0 \times \mathbf{B}_0\right). \tag{1.605}$$

With opposite magnetic fields across the interface, the equilibrium current $\mathbf{j}_0$ flows along it, directing this new force perpendicularly. This force significantly influences the instability onset (analogously to gravity in the Rayleigh–Taylor instability), promoting instability on one side while dampening it on the other.

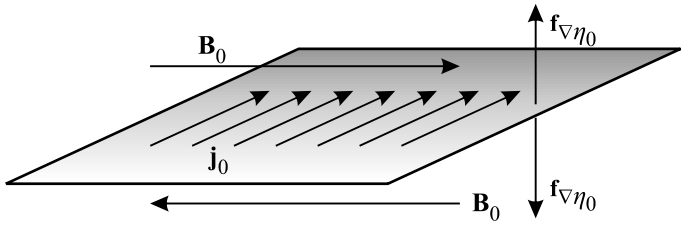


Fig. 1.101: Neutral layer configuration in resistive magnetohydrodynamics.

Equations for the Displacement Vector

The analysis incorporates the equation of motion in the form:

$$\rho\frac{\partial \mathbf{u}}{\partial t} + \rho(\mathbf{u}\cdot\nabla)\mathbf{u} = -\nabla p + \rho\mathbf{g} + \frac{1}{\mu_0}(\nabla\times\mathbf{B})\times\mathbf{B}. \tag{1.606}$$

Linearization yields:

► $$\rho_0\frac{\partial^2\delta\boldsymbol{\xi}}{\partial t^2} + = = -\nabla\delta p + \delta\rho\,\mathbf{g} + \frac{1}{\mu_0}(\nabla\times\mathbf{B}_0)\times\delta\mathbf{B} + \frac{1}{\mu_0}(\nabla\times\delta\mathbf{B})\times\mathbf{B}_0. \tag{1.607}$$

Additional Equations

Equations (1.602), (1.604), and (1.607) must be supplemented by the incompressibility condition or another appropriate closure of the system. Under the incompressibility assumption, both pressure and density advect with the moving plasma in a manner analogous to the resistivity. Consequently, by analogy with relation (1.604), these perturbations satisfy:

► $$\rho_1 + (\boldsymbol{\xi}_1 \cdot \nabla)\,\rho_0 = 0, \tag{1.608}$$

► $$p_1 + (\boldsymbol{\xi}_1 \cdot \nabla)\,p_0 = 0. \tag{1.609}$$

The fundamental relations reduce to the equations for the magnetic field and displacement vector; the remaining algebraic formulations are straightforward to solve.

Tearing Instability

Problem Geometry

Consider two regions with oppositely oriented magnetic fields separated by a planar interface. The coordinate system is chosen analogously to the one used for the Rayleigh–Taylor instability, where the interface lies in the $y = 0$ plane and the magnetic field vector points along the z-axis. Quantities are decomposed into components parallel to the interface (within the $y = 0$ plane) and perpendicular to it ($\perp$):

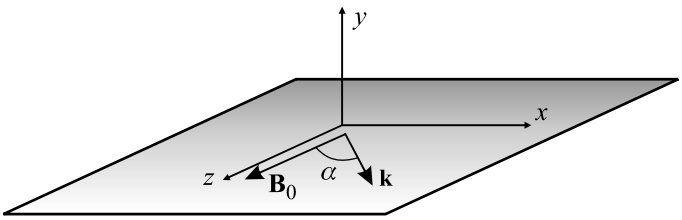


Fig. 1.102: Geometric configuration of the tearing instability.

The perturbation of any quantity takes the form:

$$\psi(t,\mathbf{x}) = \psi_0(y) + \delta\psi = \psi_0(y) + \psi_1(y)\,\mathrm{e}^{\mathrm{i}[k_x x + k_z y - \omega t]}\,. \tag{1.610}$$

The non-periodic variable is perpendicular to the interface, while the periodic variables span the x and z coordinates. Divergence-free condition of the magnetic field (1.596) and plasma incompressibility (1.597) yield:

$$\operatorname{div}\delta\mathbf{B} = 0 \qquad \Rightarrow$$

$$\frac{\partial\,\delta B_x}{\partial x} + \frac{\partial\,\delta B_y}{\partial y} + \frac{\partial\,\delta B_z}{\partial z} = 0 \qquad \Rightarrow$$

$$\blacktriangleright \qquad \frac{\mathrm{d}B_{1\perp}}{\mathrm{d}\,y} + \mathrm{i}\,\mathbf{k}\cdot\mathbf{B}_{1\parallel} = 0\,. \tag{1.611}$$

An identical formulation applies to the displacement vector (div $\boldsymbol{\xi} = 0$):

$$\blacktriangleright \qquad \frac{\mathrm{d}\xi_{1\perp}}{\mathrm{d}\,y} + \mathrm{i}\,\mathbf{k}\cdot\boldsymbol{\xi}_{1\parallel} = 0\,. \tag{1.612}$$

Analogously to the RT instability, the system requires determining the normal components of the displacement vector and the magnetic field perturbation; horizontal projections are subsequently eliminated via (1.611) and (1.612).

Given the equilibrium profiles $\mathbf{B}_0(y)$ and $\eta_0(y)$, and assuming symmetry (1.610), the entire problem reduces to a system of ordinary differential equations. These equations can either be solved numerically or analyzed via dimensional scaling involving the width of the transition region between the two field directions, εL, where the characteristic scale of the transition layer is governed by the parameter ε.

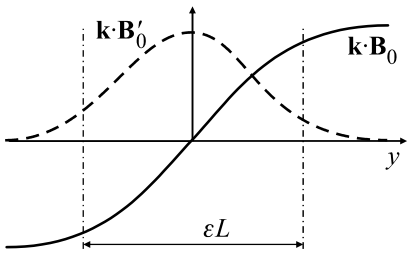


Fig. 1.103: Structure of the transition region.

The horizontal axis represents the distance from the interface. The quantity $\mathbf{k}\cdot\mathbf{B}_0$ corresponds to the projection of the magnetic field in the direction of wave propagation (up to a normalization constant). This quantity is positive in one half-space and negative in the other. The plane separating the half-spaces with oppositely directed fields is defined by the relation:

$$\mathbf{k}\cdot\mathbf{B}_0 = 0 \tag{1.613}$$

and is termed the resonance surface. The graph illustrates the derivative of this quantity as a dashed line, reaching its maximum at the resonance surface. Within the dimensional analysis of the problem, the derivative of $\mathbf{k}\cdot\mathbf{B}_0$ can be scaled as:

$$\mathbf{k}\cdot\mathbf{B}_0' \approx \frac{\mathbf{k}\cdot\mathbf{B}_0}{\varepsilon L}\,.$$

Conversely, the quantity $\mathbf{k}\cdot\mathbf{B}_0$, which vanishes at the resonance surface, is expressed as:

$$\mathbf{k}\cdot\mathbf{B}_0 \approx \varepsilon L\,\mathbf{k}\cdot\mathbf{B}_0'\,.$$

From the dimensional analysis of the governing equations within this geometry, the instability growth rate γ, defined by equation (1.451), can be estimated. The numerical solution of these equations yields a characteristic magnetic field topology around the resonance surface, featuring magnetic islands (O-points) and intersections of separatrices where magnetic reconnection occurs (X-points).

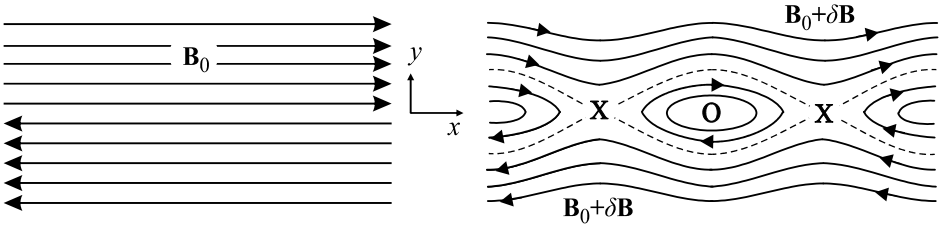


Fig. 1.104: Magnetic reconnection mechanism and the formation of X- and O-points.

The electric current continues to flow within the interface plane, but its distribution becomes highly inhomogeneous. The current density concentrates at the locations of the magnetic islands, leading to the filamentation (tearing) of the current sheet.

Driven Resistive Instabilities

A driven instability is characterized by behavior influenced directly by an external force. In the RT instability, this role is played by the gravitational field: in one direction, gravity exerts a stabilizing effect (denser fluid at the bottom), whereas in the opposite direction, a gravity-driven instability develops (denser fluid on top). The gravitational field can similarly drive resistive island modes, traditionally referred to as *g-modes*.

Crucially, an analogous driving force arises from a spatial plasma resistivity gradient directed perpendicular to the interface, which triggers the *rippling mode*. Such a gradient manifests as an effective force acting perpendicular to the interface. However, unlike gravitational acceleration, this resistive force possesses opposite directions within the two half-spaces (pointing either toward or away from the resonance surface). Consequently, this driving force stabilizes the perturbation on one side of the interface while promoting its growth on the other. The instability inherently develops within the half-space of lower resistivity, where higher perturbed current densities can be sustained.

Tokamak Instabilities

Denoting the toroidal angle as φ and the poloidal angle as θ within a tokamak geometry, the equilibrium and perturbed quantities are parameterized as:

$$\psi = \psi(\rho)\mathrm{e}^{\mathrm{i}[m\theta+n\varphi-\omega t]}\,; \qquad m,n = 0,\pm 1,\pm 2,\ldots \tag{1.614}$$

The solenoidality condition div $\mathbf{B} = 0$ for the magnetic field yields:

$$\frac{\mathrm{d}B_\rho}{\mathrm{d}\rho} + \frac{m}{\rho}B_\theta + \frac{n}{r}B_\varphi = 0\,. \tag{1.615}$$

The periodic component of this formulation directly defines the resonance surface:

$$\mathbf{k}\cdot\mathbf{B} = \frac{m}{\rho}B_\theta + \frac{n}{r}B_\varphi = 0\,. \tag{1.616}$$

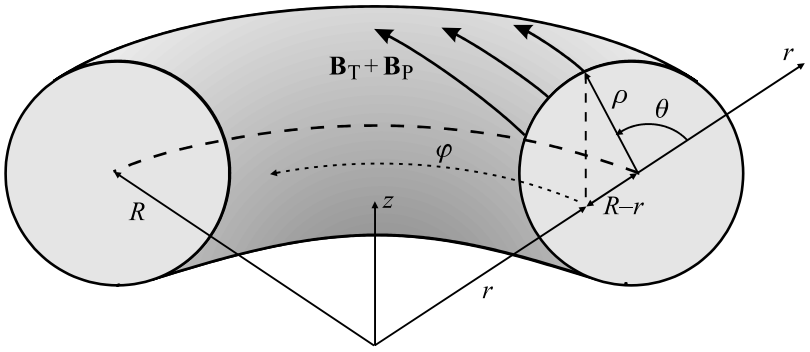


Fig. 1.105: Magnetic configuration and coordinate definitions within a tokamak.

This relation can be recast into the form:

$$\frac{\rho}{r}\frac{B_\varphi}{B_\theta} = \frac{m}{n}.$$

The sign remains arbitrary, as both the poloidal mode number m and the toroidal mode number n can take positive or negative integers. The safety factor (or rotation number) q, representing the average number of toroidal field line revolutions per single poloidal revolution, is defined as:

$$q(\rho) \equiv \frac{\mathrm{d}\varphi}{\mathrm{d}\theta} = \frac{\rho}{r}\frac{r\,\mathrm{d}\varphi}{\rho\,\mathrm{d}\theta} = \frac{\rho}{r}\frac{B_\varphi}{B_\theta} \approx \frac{\rho}{R}\frac{B_\mathrm{T}}{B_\mathrm{P}}.$$

In tokamaks satisfying the large-aspect-ratio approximation ($a << R$), the resonance surfaces adhere to the formulation:

► $$q(\rho) \simeq \frac{\rho}{R}\frac{B_\mathrm{T}}{B_\mathrm{P}} = \frac{m}{n}\ . \tag{1.617}$$

On these resonant "mn" rational surfaces, magnetic island (tearing) instabilities develop, manifesting as m localized islands along the flux surface. Their periodic formation and relaxation are heavily correlated with the characteristic sawtooth oscillations observed in the inductive electric field diagnostics.

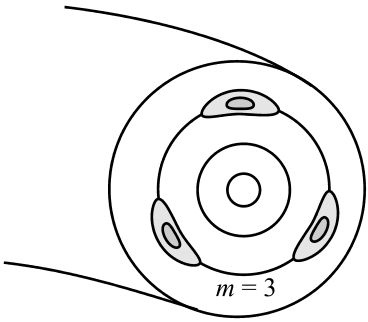


Fig. 1.106: Formation and topology of magnetic islands within a tokamak for the m = 3 mode.

1.6 Statistical Description of Plasma

When modeling a typical plasma, calculating the individual trajectories of all particles is computationally and technically impossible. Even the highly rarefied plasma of interstellar space contains millions of particles per cubic meter, whereas tokamak plasmas reach 10^{18} particles/m^3, and the solar core features up to 10^{31} particles/m^3. For such enormous multi-particle systems, it is advantageous to adopt a statistical description that relies on the distribution functions of individual particle species and their collective average behavior. This approach forms the core of the statistical description of plasmas analyzed throughout this chapter.

1.6.1 Boltzmann Equation

Assume several particle species (electrons, ions, neutral particles) denoted by the Greek subscript α. Throughout this chapter, Einstein summation convention applies exclusively to Latin indices ($i, j, k,\ldots$), whereas Greek indices are exempt from summation. The distribution function for species α is denoted by:

$$f_\alpha = f_\alpha(t, \mathbf{x}, \mathbf{v}_\alpha)\,.$$

In thermodynamic equilibrium, this distribution function is time-independent and coincides with the canonical or grand-canonical distribution ρ [2]. It is normalized to the total particle number:

► $$\begin{aligned} \int f_\alpha(t, \mathbf{x}, \mathbf{v}_\alpha)\,\mathrm{d}^3\mathbf{v}_\alpha &= n_\alpha(t, \mathbf{x})\,, \\ \int f_\alpha(t, \mathbf{x}, \mathbf{v}_\alpha)\,\mathrm{d}^3\mathbf{x}\,\mathrm{d}^3\mathbf{v}_\alpha &= N_\alpha(t)\,. \end{aligned} \tag{1.618}$$

Integrating over the velocity space defines the particle number density:

$$n_\alpha = \lim_{\Delta V \to 0} \frac{\Delta N_\alpha}{\Delta V}\,, \tag{1.619}$$

establishing the continuum limit. Further integration over space yields the total particle number N_α. Evaluating the average of a general dynamical variable A requires dividing by the normalization factor:

► $$\begin{aligned} \mathscr{A}(t, \mathbf{x}) &= \langle A \rangle_{\mathbf{v}} = \frac{\int A\, f_\alpha(t, \mathbf{x}, \mathbf{v}_\alpha)\,\mathrm{d}^3\mathbf{v}_\alpha}{\int f_\alpha(t, \mathbf{x}, \mathbf{v}_\alpha)\,\mathrm{d}^3\mathbf{v}_\alpha}\,; \\ \mathscr{A}(t) &= \langle A \rangle_{\mathbf{x},\mathbf{v}} = \frac{\int A\, f_\alpha(t, \mathbf{x}, \mathbf{v}_\alpha)\,\mathrm{d}^3\mathbf{x}\,\mathrm{d}^3\mathbf{v}_\alpha}{\int f_\alpha(t, \mathbf{x}, \mathbf{v}_\alpha)\,\mathrm{d}^3\mathbf{x}\,\mathrm{d}^3\mathbf{v}_\alpha}\,. \end{aligned} \tag{1.620}$$

Quantity $\mathscr{A}(t, \mathbf{x})$ represents the macroscopic density of the variable A. Due to the chosen normalization:

► $$\int A\, f_\alpha(t,\mathbf{x},\mathbf{v}_\alpha)\,\mathrm{d}^3\mathbf{v}_\alpha \;=\; n_\alpha(t,\mathbf{x})\,\mathscr{A}(t,\mathbf{x}) \;. \tag{1.621}$$

This expression is highly useful and applied here in its explicit form.

Various Forms of the Boltzmann Equation

The distribution function of a particle species α varies over time due to self-collisions and collisions with other particle species:

$$\frac{\mathrm{d}}{\mathrm{d}t} f_\alpha(t,\mathbf{x},\mathbf{v}_\alpha) = \sum_\beta S_{\alpha\beta} \;. \tag{1.622}$$

The right-hand side terms represent the Boltzmann collision integrals, evaluated in the next chapter. Expanding the total time derivative on the left yields:

$$\frac{\partial f_\alpha}{\partial t} + \frac{\partial f_\alpha}{\partial x_k}\frac{\mathrm{d}x_k}{\mathrm{d}t} + \frac{\partial f_\alpha}{\partial v_{\alpha k}}\frac{\mathrm{d}v_{\alpha k}}{\mathrm{d}t} = \sum_\beta S_{\alpha\beta} \;.$$

The Einstein summation convention applies exclusively to Latin indices, exempting Greek species indices. Time derivatives of positions correspond to velocities, and those of velocities represent accelerations, expressed via Newton second law:

$$\frac{\partial f_\alpha}{\partial t} + v_{\alpha k}\frac{\partial f_\alpha}{\partial x_k} + \frac{F_{\alpha k}}{m_\alpha}\frac{\partial f_\alpha}{\partial v_{\alpha k}} = \sum_\beta S_{\alpha\beta} \;.$$

Grouping the summed terms on the left using differential operators yields:

► $$\frac{\partial f_\alpha}{\partial t} \;+\; (\mathbf{v}_\alpha \cdot \boldsymbol{\nabla}_\mathbf{x})\, f_\alpha \;+\; \frac{1}{m_\alpha}(\mathbf{F}_\alpha \cdot \boldsymbol{\nabla}_\mathbf{v})\, f_\alpha \;=\; \sum_\beta S_{\alpha\beta} \;. \tag{1.623}$$

This formulation is the Boltzmann equation, the foundation for non-equilibrium statistical mechanics. The right-hand side contains the Boltzmann collision integral (see p. 208) over a region of phase space. Depending on its explicit form, the equation is referred to by distinct names:

Boltzmann Equation

Collisions are treated in a fully generalized framework and are evaluated using the standard collision integral (see p. 208). The Boltzmann equation is named after Ludwig Boltzmann, the Austrian physicist who founded statistical mechanics.

Fokker–Planck Equation and Landau Equation

The collision term accounts exclusively for pairwise Coulomb interactions, characterized by well-established effective cross-sections. The equation is named after Adriaan Daniël Fokker, a Dutch physicist and musician, and Max Planck, a German physicist and a pioneer of quantum theory. A closely related variant of the Fokker–Planck formulation is the *Landau equation*.

For the lower limit of pairwise Coulomb interactions, the impact parameter corresponding to a 90-degree deflection is chosen (as collisions at shorter impact parameters are statistically negligible). The maximum cutoff limit is defined by the Debye length,

which represents the natural screening distance for point charges. This equation is named after Lev Davidovich Landau, the Soviet theoretical physicist and recipient of the 1962 Nobel Prize in Physics.

BGK Equation

Assuming the system remains close to local thermodynamic equilibrium f_{LE}, the collision term reduces to a simplified relaxation-time formulation driven by collisions:

$$S_\alpha \simeq (\Delta f_\alpha/\Delta t)_{\mathrm{col}} = -(f_\alpha - f_{\mathrm{LE}})/\tau_{\mathrm{c}} = -\nu_{\mathrm{c}}(f_\alpha - f_{\mathrm{LE}}),$$

where τ_{c} is the mean time between collisions and ν_{c} is the collision frequency. The formulation is named after its authors: the Indian mathematician Prabhu Lal Bhatnagar, the American theoretical physicist Eugene Paul Gross, and the American mathematician and astrophysicist Max Krook.

Vlasov Equation

Collisions either cancel out or are neglected (rendering the right-hand side zero), and the macroscopically averaged Lorentz force acts as the sole governing force. It remains the most widely applied formulation in collisionless plasma physics. The equation is named after Anatoly Alexandrovich Vlasov, the Soviet theoretical physicist who established this foundational kinetic approach.

◖ **Example 1.9:** Show that the stationary solution of the collisionless (Vlasov) equation yields the canonical distribution. Solve the formulation in one dimension for a single, collisionless particle species subject to a conservative potential force field $F = -\,\mathrm{d}V/\mathrm{d}x$.

Solution: Under these specific conditions, the Boltzmann equation reduces to:

$$v\frac{\partial f}{\partial x} - \frac{1}{m}\frac{\mathrm{d}V}{\mathrm{d}x}\frac{\partial f}{\partial v} = 0\,.$$

The equation is solved via separation of variables by substituting $f(x,v) = A(x)\,B(v)$.

$$v\frac{\mathrm{d}A}{\mathrm{d}x}B - \frac{1}{m}\frac{\mathrm{d}V}{\mathrm{d}x}A\frac{\mathrm{d}B}{\mathrm{d}v} = 0 \quad \Rightarrow \quad \frac{\mathrm{d}A}{A\,\mathrm{d}V} = \frac{1}{m}\frac{\mathrm{d}B}{B\,v\,\mathrm{d}v}\,.$$

The left-hand side depends solely on position, while the right-hand side depends strictly on velocity. For two functions of independent variables to remain identically equal, both sides must equal a separation constant:

$$\frac{1}{A}\frac{\mathrm{d}A}{\mathrm{d}V} = C \quad \Rightarrow \quad \frac{\mathrm{d}A}{A} = C\,\mathrm{d}V \quad \Rightarrow \quad A(x) = K_x \exp[C\,V(x)]\,;$$

$$\frac{1}{mB\,v}\frac{\mathrm{d}B}{\mathrm{d}v} = C \quad \Rightarrow \quad \frac{\mathrm{d}B}{B} = C\,mv\,\mathrm{d}v \quad \Rightarrow \quad B(v) = K_v \exp[Cmv^2/2]\,.$$

The general solution is evaluated as:

$$f(x,v) = A(x)\cdot B(v) = K\exp\left[C\left(mv^2/2 + V(x)\right)\right].$$

This solution exhibits the mathematical structure of the canonical distribution. The coefficient C is determined through thermodynamic calibration, compatible with standard textbooks such as [2]:

$$C = -1/k_{\mathrm{B}}T\,. \tag{1.624}$$

Note (Saha Equation): From the equilibrium distribution and quasi-neutrality, an equation governing the relative proportions of ions of different charge states within a plasma follows immediately. This formulation was first derived by the Indian astrophysicist Meghnad Saha in 1920 and, independently, by the American physicist and chemist Irving Langmuir in 1923. Today, it is written in the form:

$$\frac{n_{i+1}n_{\mathrm{e}}}{n_i} = C\frac{g_{i+1}g_{\mathrm{e}}}{g_i}\exp\left[-\frac{\varepsilon_{i+1}-\varepsilon_i}{k_{\mathrm{B}}T}\right];$$
$$C = \frac{\left(2\pi m_{\mathrm{e}}k_{\mathrm{B}}T\right)^{3/2}}{\left(2\pi\hbar\right)^3}, \tag{1.625}$$

where g_i represents the statistical weight for ions of charge state i, g_{e} is the statistical weight of electrons (typically set to 2), and ε_i is the energy required to produce an ion of charge state i (by removing i electrons from the atomic shell, where $i = 0$ corresponds to neutral particles. The factor $(2\pi\hbar)^3$ represents the volume of a single quantum state of an electron in phase space; for further details, see [2]. The Saha equation is frequently utilized to determine the electron number density during single ionization, where $n_{\mathrm{i}} = n_{\mathrm{e}}$:

$$\frac{n_{\mathrm{e}}^2}{n_{\mathrm{n}}} = C\frac{2g_1}{g_0}\exp\left[-\frac{I}{k_{\mathrm{B}}T}\right], \tag{1.626}$$

where I denotes the ionization energy.

Boltzmann Equation in Random Velocities

The following three velocities must be distinguished:

$$\begin{aligned} &\mathbf{v}_\alpha && \text{phase variable,}\\ &\mathbf{u}_\alpha(t,\mathbf{x}) \equiv \left\langle \mathbf{v}_\alpha \right\rangle && \text{velocity field (mean or average velocity),}\\ &\mathbf{w}_\alpha \equiv \mathbf{v}_\alpha - \mathbf{u}_\alpha && \text{random (thermal) velocity.} \end{aligned} \tag{1.627}$$

Previously, the analysis utilized a phase space $(t, \mathbf{x}, \mathbf{v}_\alpha)$. The phase velocity contains a macroscopic flow component and a thermal component ($\mathbf{v}_\alpha = \mathbf{u}_\alpha + \mathbf{w}_\alpha$). Isolating the thermal motion by executing a transformation is often advantageous:

$$(t, \mathbf{x}, \mathbf{v}_\alpha) \quad \rightarrow \quad (t, \mathbf{x}, \mathbf{w}_\alpha)\,.$$

In the Boltzmann equation, derivatives are replaced according to the scheme:

$$\frac{\partial}{\partial t} \;\rightarrow\; \frac{\partial}{\partial t}+\frac{\partial w_k}{\partial t}\frac{\partial}{\partial w_k} \;=\; \frac{\partial}{\partial t}-\frac{\partial u_k}{\partial t}\frac{\partial}{\partial w_k},$$

$$\frac{\partial}{\partial x_j} \;\rightarrow\; \frac{\partial}{\partial x_j}+\frac{\partial w_k}{\partial x_j}\frac{\partial}{\partial w_k} \;=\; \frac{\partial}{\partial x_j}-\frac{\partial u_k}{\partial x_j}\frac{\partial}{\partial w_k},$$

$$\frac{\partial}{\partial v_j} \;\rightarrow\; \frac{\partial}{\partial w_j},$$

$$v_j \;\rightarrow\; w_j+u_j(t,\mathbf{x}).$$

This transformation yields:

$$\frac{\mathrm{d}f_\alpha}{\mathrm{d}t}+\left(\mathbf{w}_\alpha\cdot\boldsymbol{\nabla}_\mathbf{x}\right)f_\alpha+\left(\frac{\mathbf{F}_\alpha}{m_\alpha}-\frac{\mathrm{d}\mathbf{u}_\alpha}{\mathrm{d}t}\right)\cdot\frac{\partial f_\alpha}{\partial\mathbf{w}_\alpha}-$$

$$-\left[\left(\mathbf{w}_\alpha\cdot\boldsymbol{\nabla}_\mathbf{x}\right)\mathbf{u}_\alpha\right]\cdot\frac{\partial f_\alpha}{\partial\mathbf{w}_\alpha}=\sum_\beta S_{\alpha\beta}, \tag{1.628}$$

$$\text{where}\quad \frac{\mathrm{d}}{\mathrm{d}t}\equiv\frac{\partial}{\partial t}+\mathbf{u}_\alpha\cdot\boldsymbol{\nabla}_\mathbf{x}.$$

Relativistic Boltzmann Equation

This subsection may be omitted on a first reading. A general relativistic collision term is unavailable, but often unnecessary, since effective cross-sections decrease rapidly at high velocities. However, a relativistic description is essential in high-energy regimes. Conversely, the left-hand side of the equation can be easily recast into a Lorentz-covariant form. The derivation is evaluated here for a single particle species; consequently, Greek indices within this subsection denote exclusively the components of four-vectors. Instead of velocity as an independent variable, the formulation must employ momentum, or more specifically, the four-momentum:

$$f=f(x^\alpha,P^\alpha)=f(t,\mathbf{x},E,\mathbf{p}); \tag{1.629}$$

The components of the four-momentum are constrained by the invariant mass relation (where the magnitude of the four-momentum satisfies $-m_0^2c^2$), yielding:

$$E^2=\mathbf{p}^2c^2+m_0^2c^4, \tag{1.630}$$

which establishes $E = E(\mathbf{p})$. Normalization applies to momentum space instead of velocity space, requiring that:

$$\int f(x^\alpha,P^\alpha)\,\mathrm{d}^3p=n(t,\mathbf{x}). \tag{1.631}$$

This notation appears non-relativistic. However, accounting $E = E(\mathbf{p})$, the formulation can be expressed in a relativistic invariant form via the Dirac delta distribution:

► $$\int f(t,\mathbf{x},E,\mathbf{p})\,\delta\big(E-E(\mathbf{p})\big)\,\mathrm{d}^4P=n(t,\mathbf{x}). \tag{1.632}$$

Generalizing relation (1.622) within a relativistic framework requires replacing coordinate time with the proper time τ, which is an invariant under Lorentz transformations:

$$\frac{\mathrm{d}f}{\mathrm{d}\tau} = S\,; \tag{1.633}$$

Expanding the derivative on the left-hand side yields:

$$\frac{\partial f}{\partial x^\alpha}\frac{\mathrm{d}x^\alpha}{\mathrm{d}\tau} + \frac{\partial f}{\partial P^\alpha}\frac{\mathrm{d}P^\alpha}{\mathrm{d}\tau} = S\,. \tag{1.634}$$

The first term incorporates temporal and spatial derivatives, generalizing the first two terms on the left of the standard Boltzmann equation. Evaluating these time derivatives allows the formulation to be expressed as:

$$U^\alpha \frac{\partial f}{\partial x^\alpha} + F^\alpha \frac{\partial f}{\partial P^\alpha} = S\,. \tag{1.635}$$

The Lorentz four-force is expressed via relation I.1.267 (see the *Selected Topics I*)

$$U^\alpha \frac{\partial f}{\partial x^\alpha} + QF^{\alpha\beta}U_\beta \frac{\partial f}{\partial P^\alpha} = S\,. \tag{1.636}$$

As a final step, the four-velocities must be converted into four-momenta:

► $$P^\alpha \frac{\partial f}{\partial x^\alpha} + QF^{\alpha\beta}P_\beta \frac{\partial f}{\partial P^\alpha} = m_0 S\,. \tag{1.637}$$

This is the desired relativistically covariant Boltzmann equation. In the first term, the four-momentum can be moved inside the derivative with respect to the distribution function. In the second term, an analogous operation is valid because:

$$\frac{\partial}{\partial P^\alpha}\left(F^{\alpha\beta}P_\beta f\right) = F^{\alpha\beta}\delta_{\alpha\beta} f + F^{\alpha\beta}P_\beta \frac{\partial f}{\partial P^\alpha} = F^{\alpha\beta}P_\beta \frac{\partial f}{\partial P^\alpha}. \tag{1.638}$$

Upon differentiation, the first term vanishes due to the contraction of a symmetric and an antisymmetric tensor. However, this property does not hold for a generalized velocity-dependent force field. Consequently, the formulation reduces to:

► $$\frac{\partial}{\partial x^\alpha}\left(P^\alpha f\right) + \frac{\partial}{\partial P^\alpha}\left(QF^{\alpha\beta}P_\beta f\right) = m_0 S\,. \tag{1.639}$$

This form provides an elegant expression of the Boltzmann equation for a plasma subject to an electromagnetic field and the Lorentz four-force.

General Relativistic Variant

This subsection may be omitted on a first reading. An interesting extension is to recast the Boltzmann equation in general relativity, where particle trajectories are governed by the curvature of spacetime. The covariant derivative of a four-vector is defined as:

$$\frac{\mathrm{D}A^\alpha}{\mathrm{D}x^\nu} \equiv A^\alpha{}_{;\nu} = A^\alpha{}_{,\nu} + \Gamma^\alpha_{\mu\nu}A^\mu\,, \tag{1.640}$$

where the first term represents an ordinary partial derivative and the second term accounts for the variation of the four-vector A^α induced by spacetime curvature. The coefficients Γ are termed the Christoffel symbols, evaluated via the formula:

$$\Gamma^{\alpha}_{\mu\nu} = \frac{1}{2} g^{\alpha\beta} \left(g_{\beta\mu,\nu} + g_{\beta\nu,\mu} - g_{\mu\nu,\beta} \right). \tag{1.641}$$

The geodesic equation, describing the straightest path in curved spacetime, is:

$$\mathrm{d}^2 x^{\alpha} + \Gamma^{\alpha}_{\mu\nu} \mathrm{d}x^{\mu} \mathrm{d}x^{\nu} = 0 . \tag{1.642}$$

The four-force in equation (1.635) can be formulated via the geodesic equation:

$$F^{\alpha} = \frac{\mathrm{d}P^{\alpha}}{\mathrm{d}\tau} = m_0 \frac{\mathrm{d}U^{\alpha}}{\mathrm{d}\tau} = m_0 \frac{\mathrm{d}^2 x^{\alpha}}{\mathrm{d}\tau^2} = -m_0 \Gamma^{\alpha}_{\mu\nu} \frac{\mathrm{d}x^{\mu}}{\mathrm{d}\tau} \frac{\mathrm{d}x^{\nu}}{\mathrm{d}\tau} = -m_0 \Gamma^{\alpha}_{\mu\nu} U^{\mu} U^{\nu} . \tag{1.643}$$

In terms of four-momenta, the general relativistic Boltzmann equation (1.635) is:

► $$P^{\alpha} \frac{\partial f}{\partial x^{\alpha}} - \Gamma^{\alpha}_{\mu\nu} P^{\mu} P^{\nu} \frac{\partial f}{\partial P^{\alpha}} = m_0 S . \tag{1.644}$$

Boltzmann Collision Term

This chapter addresses the right-hand side of the non-relativistic Boltzmann equation, specifically collisions. Consider an elastic collision between two particles α and β.

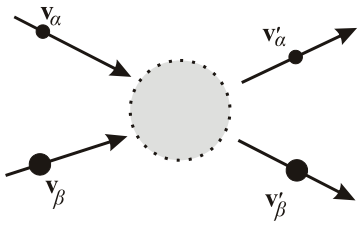


Fig. 1.107: Schematic of a two-particle elastic collision.

Initially, the formulation transforms the particle velocities $\mathbf{v}_{\alpha}$ and $\mathbf{v}_{\beta}$ into the relative velocity $\mathbf{g}$ (alternatively denoted as $\mathbf{v}_{\alpha\beta}$ and the center-of-mass velocity $\mathbf{v}_{\mathrm{cm}}$ (alternatively denoted as $\mathbf{v}_{(\alpha\beta)}$). The forward transformation takes the form:

$$\begin{aligned} \mathbf{g} &\equiv \mathbf{v}_{\alpha\beta} = \mathbf{v}_{\alpha} - \mathbf{v}_{\beta} ; \\ \mathbf{v}_{\mathrm{cm}} &\equiv \mathbf{v}_{(\alpha\beta)} = \frac{m_{\alpha}\mathbf{v}_{\alpha} + m_{\beta}\mathbf{v}_{\beta}}{m_{\alpha} + m_{\beta}} . \end{aligned} \tag{1.645}$$

The determinant of this transformation matrix equals unity; hence, the inverse matrix is evaluated via the standard cofactor method:

$$\begin{aligned} \mathbf{v}_{\alpha} &= \mathbf{v}_{\mathrm{cm}} + \frac{m_{\beta}}{m_{\alpha} + m_{\beta}} \mathbf{g} ; \\ \mathbf{v}_{\beta} &= \mathbf{v}_{\mathrm{cm}} - \frac{m_{\alpha}}{m_{\alpha} + m_{\beta}} \mathbf{g} . \end{aligned} \tag{1.646}$$

Energy and momentum conservation laws are formulated in these new variables:

$$\mathbf{p} = m_\alpha \mathbf{v}_\alpha + m_\beta \mathbf{v}_\beta = (m_\alpha + m_\beta)\,\mathbf{v}_\mathrm{T} = \text{const},$$
$$E = \frac{1}{2} m_\alpha \mathbf{v}_\alpha^2 + \frac{1}{2} m_\beta \mathbf{v}_\beta^2 = \frac{1}{2}(m_\alpha + m_\beta)\,\mathbf{v}_\mathrm{T}^2 + \frac{1}{2}\frac{m_\alpha m_\beta}{m_\alpha + m_\beta}\mathbf{g}^2 = \text{const}. \tag{1.647}$$

Momentum conservation dictates a constant center-of-mass velocity. Combined with energy conservation, this requires an invariant relative velocity magnitude. Consequently, during an elastic collision, both quantities are conserved:

- The center-of-mass velocity remains unchanged during the collision.
- The magnitude of the relative velocity remains unchanged during the collision.

► $$\begin{aligned} \mathbf{v}_\mathrm{cm} &= \text{const}\,, \\ |\,\mathbf{g}\,| &= \text{const}\,. \end{aligned} \tag{1.648}$$

The only quantity that varies during an elastic collision is the orientation of the relative velocity vector. Therefore, two new quantities characterizing the collision are used:

$$g_{\alpha\beta} \equiv |\,\mathbf{g}\,| = |\,\mathbf{v}_{\alpha\beta}\,|\,;$$
$$\mathbf{k}_{\alpha\beta} \equiv \frac{\mathbf{g}}{|\,\mathbf{g}\,|} = \frac{\mathbf{v}_{\alpha\beta}}{|\,\mathbf{v}_{\alpha\beta}\,|}\,. \tag{1.649}$$

The relative velocity magnitude remains constant, satisfying $g_{\alpha\beta} = g'_{\alpha\beta}$. The second quantity describes the orientation of the relative velocity vector, representing two degrees of freedom of the collision (two independent components of the unit vector $\mathbf{k}$, where the third is defined by the unit magnitude condition). In literature, the relative velocity vector is frequently denoted by the symbol $\mathbf{g}$, i.e., $\mathbf{v}_{\alpha\beta} = \mathbf{g}_{\alpha\beta}$.

Collision Cross Section

The collision cross section for species α striking target particles β is conventionally the proportionality coefficient within the formulation for the collision frequency:

$$\nu_\alpha \sim n_\beta \bar{v}_{\alpha\beta}\,; \qquad \nu_\alpha = \sum_\beta \nu_{\alpha\beta} = \sum_\beta \sigma_{\alpha\beta} n_\beta \bar{v}_{\alpha\beta}\,. \tag{1.650}$$

The effective cross section represents the geometric area of a target particle β presented to an incident particle α. The collision frequency is proportional to this cross section, the mean relative velocity, and the number density of the target particles. For elastic two-particle collisions, the cross section is introduced analogously as a conditional probability (under the constraint of a constant magnitude $g_{\alpha\beta}$, denoted by:

$$\sigma(\mathbf{k}_{\alpha\beta} \,|\, \mathbf{k}'_{\alpha\beta}\,;\, g_{\alpha\beta})$$

and normalized such that:

$$\frac{\mathrm{d}w}{\mathrm{d}t} = g_{\alpha\beta}\,\sigma(\mathbf{k}_{\alpha\beta} \,|\, \mathbf{k}'_{\alpha\beta}\,;\, g_{\alpha\beta})\,\mathrm{d}^2\mathbf{k}'_{\alpha\beta} \tag{1.651}$$

represents the time derivative of the conditional probability that the unit vector directing the relative velocity lies within the interval ($\mathbf{k}'_{\alpha\beta}$, $\mathbf{k}'_{\alpha\beta} + \mathrm{d}\,\mathbf{k}'_{\alpha\beta}$) after the collision. The cross section remains invariant under:

- time reversal: $\sigma(\mathbf{k}_{\alpha\beta} \,|\, \mathbf{k}'_{\alpha\beta} \,;\, g_{\alpha\beta}) \;=\; \sigma(-\mathbf{k}'_{\alpha\beta} \,|\, -\mathbf{k}_{\alpha\beta} \,;\, g_{\alpha\beta})\,,$
- spatial inversion: $\sigma(\mathbf{k}_{\alpha\beta} \,|\, \mathbf{k}'_{\alpha\beta} \,;\, g_{\alpha\beta}) \;=\; \sigma(-\mathbf{k}_{\alpha\beta} \,|\, -\mathbf{k}'_{\alpha\beta} \,;\, g_{\alpha\beta})\,.$

An important symmetry relation follows directly from both properties:

► $$\sigma(\mathbf{k}_{\alpha\beta} \,|\, \mathbf{k}'_{\alpha\beta} \,;\, g_{\alpha\beta}) \;=\; \sigma(\mathbf{k}'_{\alpha\beta} \,|\, \mathbf{k}_{\alpha\beta} \,;\, g_{\alpha\beta})\,. \tag{1.652}$$

Boltzmann Collision Integral

The collision term of the Boltzmann equation can be formulated as:

$$\begin{aligned} S_{\alpha\beta} = \int\Big[f_\alpha(t,\mathbf{x},\mathbf{v}'_\alpha) f_\beta(t,\mathbf{x},\mathbf{v}'_\beta) - f_\alpha(t,\mathbf{x},\mathbf{v}_\alpha) f_\beta(t,\mathbf{x},\mathbf{v}_\beta)\Big]\cdot \\ \cdot\, g_{\alpha\beta}\, \sigma(\mathbf{k}_{\alpha\beta} \,|\, \mathbf{k}'_{\alpha\beta} \,;\, g_{\alpha\beta})\, \mathrm{d}^2\mathbf{k}'_{\alpha\beta}\, \mathrm{d}^3\mathbf{v}_\beta\,. \end{aligned} \tag{1.653}$$

The physical interpretation is straightforward: the collision probability for two particles is proportional to the product of both distribution functions of both species (representing particle occupancy at a given point in phase space) multiplied by the differential collision cross section. The first term (gain term) describes particles scattered into the given phase space volume, while the second (loss term) describes particles scattered out. Integration is evaluated over the free kinematic parameters of the collision. Due to symmetry property (1.652), both cross sections can be formulated uniformly and factored out of the brackets. The collision term (1.653) inherently assumes that the colliding particle pair remains *uncorrelated* prior to the interaction. This foundational assumption is known as the *molecular chaos assumption*.

Collision Invariant

Let ψ_α be a summational invariant (mass, momentum, or energy) satisfying:

$$\psi_\alpha + \psi_\beta = \psi'_\alpha + \psi'_\beta\,. \tag{1.654}$$

Consequently, a fundamental relation holds for the collision operator:

► $$\sum_{\alpha,\beta} \int \psi_\alpha S_{\alpha\beta}\, \mathrm{d}^3\mathbf{v}_\alpha \;=\; 0\,. \tag{1.655}$$

Note: This proof may be omitted on a first reading.

Proof:

$$\begin{aligned} S &= \sum_{\alpha,\beta} \int \psi_\alpha S_{\alpha\beta} \mathrm{d}^3\mathbf{v}_\alpha = \\ &= \sum_{\alpha\beta} \int \psi_\alpha \Big[f'_\alpha f'_\beta - f_\alpha f_\beta \Big] \cdot g_{\alpha\beta}\, \sigma(\mathbf{k}_{\alpha\beta} \,|\, \mathbf{k}'_{\alpha\beta} \,;\, g_{\alpha\beta})\, \mathrm{d}^2\mathbf{k}'_{\alpha\beta}\, \mathrm{d}^3\mathbf{v}_\alpha \mathrm{d}^3\mathbf{v}_\beta\,. \end{aligned}$$

Next, a transformation to center-of-mass and relative velocities is executed:

$$\mathrm{d}^3\mathbf{v}_\alpha\, \mathrm{d}^3\mathbf{v}_\beta = \mathrm{d}^3\mathbf{v}_{(\alpha\beta)}\, \mathrm{d}^3\mathbf{v}_{\alpha\beta} = \mathrm{d}^3\mathbf{v}_{(\alpha\beta)}\, g_{\alpha\beta}^2\, \mathrm{d}g_{\alpha\beta}\, \mathrm{d}^2\mathbf{k}_{\alpha\beta}\,,$$

where the differential element $\mathrm{d}^2\mathbf{k}_{\alpha\beta}$ accounts for all angular dependencies. This transformation yields:

$$S = \sum_{\alpha\beta} \int \psi_\alpha \left[f'_\alpha f'_\beta - f_\alpha f_\beta \right] g^3_{\alpha\beta}\, \sigma(\mathbf{k}_{\alpha\beta} \,|\, \mathbf{k}'_{\alpha\beta}\,;\, g_{\alpha\beta})\, \mathrm{d}^2\mathbf{k}'_{\alpha\beta}\, \mathrm{d}^2\mathbf{k}_{\alpha\beta}\, \mathrm{d}g_{\alpha\beta}\, \mathrm{d}^3\mathbf{v}_{(\alpha\beta)} \,.$$

Interchanging the primed and unprimed quantities and applying the relations:

$$g'_{\alpha\beta} = g_{\alpha\beta}\,; \qquad \mathbf{v}'_{(\alpha\beta)} = \mathbf{v}_{(\alpha\beta)}\,; \qquad \sigma(\mathbf{k} \,|\, \mathbf{k}'; g_{\alpha\beta}) = \sigma(\mathbf{k}' \,|\, \mathbf{k}\,; g_{\alpha\beta})$$

yields:

$$S = \sum_{\alpha\beta} \int \psi'_\alpha \left[f_\alpha f_\beta - f'_\alpha f'_\beta \right] g^3_{\alpha\beta}\, \sigma(\mathbf{k}_{\alpha\beta} \,|\, \mathbf{k}'_{\alpha\beta}\,;\, g_{\alpha\beta})\, \mathrm{d}^2\mathbf{k}'_{\alpha\beta}\, \mathrm{d}^2\mathbf{k}_{\alpha\beta}\, \mathrm{d}g_{\alpha\beta}\, \mathrm{d}^3\mathbf{v}_{(\alpha\beta)} \,.$$

The next step involves symmetrization, expressing the formulation as the arithmetic mean of the two preceding results:

$$S = \frac{1}{2} \sum_{\alpha\beta} \int (\psi_\alpha - \psi'_\alpha) \left[f'_\alpha f'_\beta - f_\alpha f_\beta \right] g^3_{\alpha\beta}\, \sigma(\mathbf{k}_{\alpha\beta} \,|\, \mathbf{k}'_{\alpha\beta}\,;\, g_{\alpha\beta})\, \mathrm{d}^2\mathbf{k}'_{\alpha\beta}\, \mathrm{d}^2\mathbf{k}_{\alpha\beta} \mathrm{d}g_{\alpha\beta}\, \mathrm{d}^3\mathbf{v}_{(\alpha\beta)} \,.$$

Subsequently, interchanging the species indices α and β followed by a secondary symmetrization yields:

$$S = \frac{1}{4} \sum_{\alpha\beta} \int (\psi_\alpha + \psi_\beta - \psi'_\alpha - \psi'_\beta) \left[f'_\alpha f'_\beta - f_\alpha f_\beta \right] g^3_{\alpha\beta}\, \sigma(\cdots)\, \mathrm{d}^2\mathbf{k}'_{\alpha\beta}\, \mathrm{d}^2\mathbf{k}_{\alpha\beta}\, \mathrm{d}g_{\alpha\beta}\, \mathrm{d}^3\mathbf{v}_{(\alpha\beta)} \,.$$

For summational invariants, the first parenthetical term vanishes identically, leading to the final result $S = 0$.

■

Transport Equation

Often, probabilistic information regarding the entire phase space is unnecessary; instead, knowing the evolution of macroscopic variables in time and position is sufficient. This state is evaluated by averaging over the velocity distribution, where the normalization corresponds to the particle number according to relation (1.620):

$$\mathbf{u}_\alpha(t, \mathbf{x}) = \frac{\int \mathbf{v}_\alpha f_\alpha(t, \mathbf{x}, \mathbf{v}_\alpha)\, \mathrm{d}^3\mathbf{v}_\alpha}{\int f_\alpha(t, \mathbf{x}, \mathbf{v}_\alpha)\, \mathrm{d}^3\mathbf{v}_\alpha} \,.$$

The reduction of velocity space variables via this averaging process transitions the description from kinetic statistics to continuum equations. Multiplying the Boltzmann equation (1.623) by an arbitrary velocity-dependent function $\phi_\alpha(\mathbf{v}_\alpha)$ (which may or may not be a summational invariant) and subsequently integrating the formulation over the velocity variables yields:

$$\int \phi_\alpha \frac{\partial f_\alpha}{\partial t} \mathrm{d}^3\mathbf{v}_\alpha \;+\; \int \phi_\alpha\, (\mathbf{v}_\alpha \cdot \nabla_{\mathbf{x}})\, f_\alpha\, \mathrm{d}^3\mathbf{v}_\alpha \;+\; \int \frac{\phi_\alpha}{m_\alpha} (\mathbf{F}_\alpha \cdot \nabla_{\mathbf{v}})\, f_\alpha\, \mathrm{d}^3\mathbf{v}_\alpha \;=$$

$$= \int \phi_\alpha \sum_\beta S_{\alpha\beta}\, \mathrm{d}^3\mathbf{v}_\alpha \,.$$

The three terms on the left-hand side are simplified successively:

First term:

$$\int \phi_\alpha(\mathbf{v}_\alpha)\frac{\partial f_\alpha}{\partial t}\mathrm{d}^3\mathbf{v}_\alpha = \frac{\partial}{\partial t}\int \phi_\alpha\, f_\alpha\, \mathrm{d}^3\mathbf{v}_\alpha = \frac{\partial}{\partial t} n_\alpha(t,\mathbf{x})\langle\phi_\alpha\rangle_{\mathbf{v}} = \frac{\partial}{\partial t}\langle n_\alpha\,\phi_\alpha\rangle_{\mathbf{v}} \,.$$

Second term:

$$\int \phi_\alpha(\mathbf{v}_\alpha) v_{\alpha k}\frac{\partial f_\alpha}{\partial x_k}\mathrm{d}^3\mathbf{v}_\alpha = \frac{\partial}{\partial x_k}\int \phi_\alpha(\mathbf{v}_\alpha) v_{\alpha k} f_\alpha\, \mathrm{d}^3\mathbf{v}_\alpha = \frac{\partial}{\partial x_k} n_\alpha(t,\mathbf{x})\langle\phi_\alpha v_{\alpha k}\rangle_{\mathbf{v}} =$$

$$= \frac{\partial}{\partial x_k}\langle n_\alpha \phi_\alpha v_{\alpha k}\rangle_{\mathbf{v}} \,.$$

Third term:

$$\int \frac{\phi_\alpha(\mathbf{v}_\alpha)}{m_\alpha} F_{\alpha k}(t,\mathbf{x},\mathbf{v}_\alpha)\frac{\partial f_\alpha}{\partial v_{\alpha k}}\mathrm{d}^3\mathbf{v}_\alpha \overset{\text{(p.p.)}}{=}$$

$$= \left[\frac{\phi_\alpha F_{\alpha k} f_\alpha}{m_\alpha}\nu_k\right]_{\partial\Omega} - \frac{1}{m_\alpha}\int \frac{\partial}{\partial v_{\alpha k}}[\phi_\alpha\, F_{\alpha k}]\, f_\alpha\, \mathrm{d}^3\mathbf{v}_\alpha =$$

$$= -\frac{1}{m_\alpha}\left\langle n_\alpha \frac{\partial}{\partial \mathbf{v}_\alpha}(\phi_\alpha \mathbf{F}_\alpha)\right\rangle_{\mathbf{v}} \,.$$

Simplifying the third term requires assuming that the force field can depend on velocity (e.g., the magnetic component of the Lorentz force). Executing integration by parts, the first resulting term vanishes because the distribution function is assumed to vanish at the boundaries of the velocity space; the symbol ν_k denotes the components of the normal vector. Averaging the Boltzmann equation over the velocity space yields:

► $$\frac{\partial}{\partial t}\langle n_\alpha\,\phi_\alpha\rangle_{\mathbf{v}} + \frac{\partial}{\partial x_i}\langle n_\alpha\,\phi_\alpha\, v_{i\alpha}\rangle_{\mathbf{v}} - \frac{1}{m_\alpha}\left\langle n_\alpha \frac{\partial}{\partial \mathbf{v}_\alpha}(\phi_\alpha \mathbf{F}_\alpha)\right\rangle_{\mathbf{v}} = \int \phi_\alpha \sum_\beta S_{\alpha\beta}\,\mathrm{d}^3\mathbf{v}_\alpha \,. \quad (1.656)$$

This general transport equation forms the foundation of *continuum theory*. Prior to further analysis, it can be written for the electromagnetic interaction:

$$\mathbf{F}_\alpha = Q_\alpha \mathbf{E} + Q_\alpha\, \mathbf{v}_\alpha \times \mathbf{B} \,.$$

Evaluating the velocity derivative in the third term requires either component-wise decomposition or utilizing the cross-product definition expressed via the Levi-Civita tensor. This straightforward procedure yields:

► $$\frac{\partial}{\partial t}\langle n_\alpha\,\phi_\alpha\rangle_{\mathbf{v}} + \nabla_{\mathbf{x}}\cdot\langle n_\alpha\,\phi_\alpha\,\mathbf{v}_\alpha\rangle_{\mathbf{v}} - \frac{Q_\alpha}{m_\alpha}\left\langle n_\alpha\,(\mathbf{E}+\mathbf{v}_\alpha\times\mathbf{B})\cdot\frac{\partial\phi_\alpha}{\partial\mathbf{v}_\alpha}\right\rangle_{\mathbf{v}} = \int \phi_\alpha \sum_\beta S_{\alpha\beta}\,\mathrm{d}^3\mathbf{v}_\alpha \,. \quad (1.657)$$

Note 1: Statistical physics utilizes the variables $(t, \mathbf{x}, \mathbf{v}_\alpha)$. Averaging over the velocity space reduces the statistical information regarding the velocity component of the phase space, making the averaged variables functions of $(t, \mathbf{x})$ alone. However, the mean fluid velocity $\mathbf{u}_\alpha(t, \mathbf{x})$ naturally reappears within the continuum formulations.

Note 2: The transport equation possesses the mathematical structure of a continuity equation. The first term represents the temporal derivative of the additive quantity density, followed by its flux divergence. The third term corresponds to field-driven sources, while the right-hand side contains collision sources. It describes how physical quantities are transported.

Note 3: The transport equation incorporates a test function ϕ_α. Substituting successive powers of velocity yields the Boltzmann equation moments, which is why the transport formulation is alternative referred to as the *moment equation*.

Note 4: If the function ϕ_α represents a summational invariant, summing over all species renders the right-hand side of equation (1.657) zero, meaning the collision terms cancel out. This result follows directly from relation (1.655):

$$\sum_\alpha \frac{\partial}{\partial t}\left\langle n_\alpha \phi_\alpha \right\rangle_{\mathbf{v}} + \nabla_{\mathbf{x}} \cdot \left\langle n_\alpha \phi_\alpha \, \mathbf{v}_\alpha \right\rangle_{\mathbf{v}} - \frac{Q_\alpha n_\alpha}{m_\alpha} \left\langle (\mathbf{E} + \mathbf{v}_\alpha \times \mathbf{B}) \frac{\partial \phi_\alpha}{\partial \mathbf{v}_\alpha} \right\rangle_{\mathbf{v}} = 0 .$$

This specific approximation constitutes the widely utilized *single-fluid model*.

Note 5: For the zeroth-order moment, setting $\phi_\alpha = m_\alpha$ within the single-fluid approximation yields the macroscopic continuity equation:

$$\frac{\partial}{\partial t}\rho + \frac{\partial}{\partial x_k} j_k = 0 ; \qquad \rho \equiv \sum_\alpha \rho_\alpha , \qquad \mathbf{j} \equiv \sum_\alpha m_\alpha n_\alpha \mathbf{u}_\alpha .$$

The continuity equation governs the temporal evolution of mass density (the zeroth moment of the Boltzmann equation). However, the second term introduces a new variable – the mass flux **j** containing the mean flow velocity. Evaluating the temporal evolution of this mass flux (momentum density) requires a new relation, the equation of motion, obtained as the first moment by setting $\phi_\alpha = m_\alpha v_{i\alpha}$:

$$\frac{\partial}{\partial t} j_k + \frac{\partial}{\partial x_l} P_{kl} = 0 .$$

The equation of motion introduces another new variable – the pressure tensor, which incorporates dynamic pressure (momentum flux), the standard thermal pressure (the scalar component driven by random motion), the viscosity (the anisotropic tensor component), and the Maxwell stress tensor. The subsequent moment yields the evolution equation for this pressure tensor, corresponding to the energy transport equation involving quadratic velocity terms:

$$\frac{\partial}{\partial t} P_{kl} + \frac{\partial}{\partial x_n} Q_{kln} = 0 .$$

The second term of this formulation introduces yet another variable describing the heat flux. This procedure can be extended indefinitely, generating an infinite hierarchy of fluid moment equations. In practical applications, the system is closed after a finite number of moments via an algebraic closure relation, such as the Fourier law for heat conduction.

Note 6: Plasma physics frequently employs the multi-fluid model, treating the plasma as a mixture of electron, neutral, and distinct ion fluids. In this framework, inter-species collision terms do not vanish and must be explicitly incorporated.

Note 7: Complete system information requires solving the kinetic Boltzmann equation coupled with the corresponding field equations. Conversely, a macroscopic description can rely exclusively on fluid moment equations.

The following section provides the derivation of the first three moments of the Boltzmann equation, reformulated in terms of the mean fluid velocity $\mathbf{u}_\alpha \equiv \langle\, \mathbf{v}_\alpha \,\rangle$ and the random (thermal) velocity $\mathbf{w}_\alpha \equiv \mathbf{v}_\alpha - \mathbf{u}_\alpha$. Within the transport formulation (1.657), the test function ϕ_α is successively replaced by m_α (or Q_α), $m_\alpha v_{\alpha k}$, and $m_\alpha v_\alpha^2/2$. The phase velocity is then decomposed into macroscopic and thermal components: $v_{\alpha k} = u_{\alpha k} + w_{\alpha k}$. By definition, the expectation value of the thermal component vanishes: $\langle\, \mathbf{w}_\alpha \,\rangle = 0$.

1.6.2 Transition from Kinetics to Continuum

Zeroth-Order Moment and Charge Conservation for Particles

Substituting the scalars m_α, Q_α, and 1 for the function ϕ_α yields the mass, charge, and particle number conservation laws. For this zeroth moment, collision integrals vanish identically for each species because ϕ_α is velocity-independent; thus, relation (1.655) holds without summing over α. Elastic Coulomb collisions conserve mass, charge, and particle number, yielding the continuity equations:

$$\frac{\partial \rho_{\mathrm{m},\alpha}}{\partial t} + \frac{\partial j_k^{(\mathrm{m},\alpha)}}{\partial x_k} = 0\,,$$

$$\frac{\partial \rho_{\mathrm{Q},\alpha}}{\partial t} + \frac{\partial j_k^{(\mathrm{Q},\alpha)}}{\partial x_k} = 0\,, \qquad \alpha = \mathrm{e,\ i,\ ii,\ n,\ldots} \tag{1.658}$$

$$\frac{\partial n_\alpha}{\partial t} + \frac{\partial n_\alpha u_{\alpha k}}{\partial x_k} = 0\,.$$

Throughout this chapter, the Einstein summation convention applies exclusively to Latin indices ($i, j, k,\ldots$), whereas Greek species indices are exempt. Superscript indices are enclosed in parentheses to distinguish them from exponents. Variables subject to substitution are set in italics. Where appropriate, the component notation can be recast into a coordinate-independent, invariant formulation:

$$\begin{aligned}
&\frac{\partial \rho_{\mathrm{m},\alpha}}{\partial t} + \boldsymbol{\nabla} \cdot \mathbf{j}_{\mathrm{m},\alpha} = 0 \,, \\
&\frac{\partial \rho_{\mathrm{Q},\alpha}}{\partial t} + \boldsymbol{\nabla} \cdot \mathbf{j}_{\mathrm{Q},\alpha} = 0 \,, \qquad \alpha = \mathrm{e,\ i,\ ii,\ n,\ldots} \\
&\frac{\partial n_\alpha}{\partial t} + \boldsymbol{\nabla} \cdot \left(n_\alpha \mathbf{u}_\alpha \right) = 0 \,.
\end{aligned} \tag{1.659}$$

The temporal derivatives govern the mass density, charge density, and particle number density of species α, respectively. The spatial derivatives incorporate the mass flux, charge flux, and particle number flux. These macroscopic variables depend solely on time and spatial coordinates, defined via the invariant formulations:

$$\begin{aligned}
\rho_{\mathrm{m},\alpha} &= m_\alpha n_\alpha = \int m_\alpha f_\alpha \, \mathrm{d}^3 \mathbf{v}_\alpha \,, \\
\rho_{\mathrm{Q},\alpha} &= Q_\alpha n_\alpha = \int Q_\alpha f_\alpha \, \mathrm{d}^3 \mathbf{v}_\alpha \,, \\
\mathbf{j}_{\mathrm{m},\alpha} &= m_\alpha n_\alpha \mathbf{u}_\alpha = \int m_\alpha \mathbf{v}_\alpha f_\alpha \, \mathrm{d}^3 \mathbf{v}_\alpha \,, \\
\mathbf{j}_{\mathrm{Q},\alpha} &= Q_\alpha n_\alpha \mathbf{u}_\alpha = \int Q_\alpha \mathbf{v}_\alpha f_\alpha \, \mathrm{d}^3 \mathbf{v}_\alpha \,.
\end{aligned} \tag{1.660}$$

Summing the moment equations over all particle species α yields:

$$\begin{aligned}
&\frac{\partial \rho_{\mathrm{m}}}{\partial t} + \boldsymbol{\nabla} \cdot \mathbf{j}_{\mathrm{m}} = 0 \,, \\
&\frac{\partial \rho_{\mathrm{Q}}}{\partial t} + \boldsymbol{\nabla} \cdot \mathbf{j}_{\mathrm{Q}} = 0 \,, \\
&\frac{\partial n}{\partial t} + \boldsymbol{\nabla} \cdot \left(n \mathbf{u} \right) = 0 \,,
\end{aligned} \tag{1.661}$$

where the collective parameters are defined as:

$$\begin{aligned}
\rho_{\mathrm{m}} &\equiv \sum_\alpha \rho_{\mathrm{m},\alpha} = \sum_\alpha m_\alpha n_\alpha \,, & \mathbf{j}_{\mathrm{m}} &\equiv \sum_\alpha \mathbf{j}_{\mathrm{m},\alpha} = \sum_\alpha m_\alpha n_\alpha \mathbf{u}_\alpha \,, \\
\rho_{\mathrm{Q}} &\equiv \sum_\alpha \rho_{\mathrm{Q},\alpha} = \sum_\alpha Q_\alpha n_\alpha \,, & \mathbf{j}_{\mathrm{Q}} &\equiv \sum_\alpha \mathbf{j}_{\mathrm{Q},\alpha} = \sum_\alpha Q_\alpha n_\alpha \mathbf{u}_\alpha \,, \\
n &\equiv \sum_\alpha n_\alpha \,, & \mathbf{u} &\equiv \frac{\sum_\alpha m_\alpha n_\alpha \mathbf{u}_\alpha}{\sum_\alpha m_\alpha n_\alpha} \,.
\end{aligned} \tag{1.662}$$

Zeroth-Order Moment and Charge Conservation for Fields

Evaluating the electromagnetic fields for the Boltzmann or moment formulations requires the system of Maxwell equations:

$$\operatorname{div} \mathbf{D} = \rho_{\mathrm{Q}} \,, \tag{1.663}$$

$$\operatorname{div} \mathbf{B} = 0 \,, \tag{1.664}$$

$$\nabla\times\mathbf{E} = -\frac{\partial\mathbf{B}}{\partial t}, \tag{1.665}$$

$$\nabla\times\mathbf{H} = \mathbf{j}_{\mathrm{Q}} + \frac{\partial\mathbf{D}}{\partial t}. \tag{1.666}$$

The corresponding macroscopic source terms are defined by the relations:

$$\begin{aligned}\rho_{\mathrm{Q}} &= \sum_{\alpha} Q_{\alpha} n_{\alpha} = \sum_{\alpha} \int Q_{\alpha} f_{\alpha}\, \mathrm{d}^3\mathbf{v}_{\alpha}\,,\\ \mathbf{j}_{\mathrm{Q}} &= \sum_{\alpha} Q_{\alpha} n_{\alpha}\mathbf{u}_{\alpha} = \sum_{\alpha} \int Q_{\alpha}\mathbf{v}_{\alpha} f_{\alpha}\, \mathrm{d}^3\mathbf{v}_{\alpha}\,.\end{aligned} \tag{1.667}$$

These source terms within the Maxwell equations are fully consistent with the zeroth-order moment of the Boltzmann equation. Differentiating equation (1.663) over time and adding the divergence of (1.666) yields the charge conservation law:

► $$\frac{\partial\rho_{\mathrm{Q}}}{\partial t} + \nabla\cdot\mathbf{j}_{\mathrm{Q}} = 0\,,$$

related with the formulation derived via the zeroth-order Boltzmann moment (1.661). For the derivation of higher-order moments, a linear constitutive relationship is assumed between the electric vectors **E** and **D**, as well as between the magnetic vectors **B** and **H**.

First-Order Moment and Momentum Conservation for Particles

To derive the momentum equation, the test function within the transport relation is replaced by the k-th component of momentum, $\phi_{\alpha} = m_{\alpha}v_{\alpha k}$, which represents a summational invariant. Following substitution, the moment equations take the form:

$$\frac{\partial}{\partial t}\left(n_{\alpha}m_{\alpha}u_{\alpha k}\right) + \frac{\partial}{\partial x_l}\left(n_{\alpha}m_{\alpha}\left\langle v_{\alpha k}v_{\alpha l}\right\rangle_{\mathbf{v}}\right) = n_{\alpha}Q_{\alpha}\left(\mathbf{E}+\mathbf{u}_{\alpha}\times\mathbf{B}\right)_k + \int m_{\alpha}v_{\alpha k}\sum_{\beta} S_{\alpha\beta}\,\mathrm{d}^3\mathbf{v}_{\alpha}\,.$$

The first term is the temporal variation of the momentum density for species α, and the second is the spatial derivative of the second-order momentum flux tensor, where each momentum component can advect in three directions. Within this term, the phase velocity is decomposed ($v_{\alpha k} = u_{\alpha k} + w_{\alpha k}$). Upon expansion, terms proportional to the first power of random velocity vanish, leaving two non-zero terms: the dynamic pressure tensor D_{kl} driven by macroscopic flow, and the thermal pressure tensor P_{kl} driven by random motion. This entire left-hand side has the structure of a continuity equation, expressing momentum conservation for the k-th component. The first right-hand side term describes momentum variation driven by electromagnetic fields, which transfer momentum to the particles, whereas the second term represents collision-driven momentum transfer. The resulting formulation takes the form:

$$\frac{\partial}{\partial t}\gamma_{\alpha k} + \frac{\partial}{\partial x_l}T_{kl}^{(\alpha)} = f_{\alpha k} + \Gamma_{\alpha k}\,, \tag{1.668}$$

where the individual macroscopic quantities are defined as:

$$\gamma_{\alpha k} \equiv n_\alpha m_\alpha u_{\alpha k} = m_\alpha \int v_{\alpha k} f_\alpha \, \mathrm{d}^3\mathbf{v}_\alpha \, ;$$

$$T_{kl}^{(\alpha)} \equiv n_\alpha m_\alpha u_{\alpha k} u_{\alpha l} + n_\alpha m_\alpha \langle \, w_{\alpha k} \, w_{\alpha l} \, \rangle_{\mathbf{v}} = D_{kl}^{(\alpha)} + P_{kl}^{(\alpha)} \, ; \tag{1.669}$$

$$D_{kl}^{(\alpha)} \equiv n_\alpha m_\alpha u_{\alpha k} u_{\alpha l} \, ;$$

$$P_{kl}^{(\alpha)} \equiv n_\alpha m_\alpha \langle \, w_{\alpha k} w_{\alpha l} \, \rangle_{\mathbf{v}} = m_\alpha \int (v_{\alpha k} - u_{\alpha k})(v_{\alpha l} - u_{\alpha l}) f_\alpha \, \mathrm{d}^3\mathbf{v}_\alpha \, ;$$

$$f_{\alpha k} \equiv n_\alpha Q_\alpha \left(\mathbf{E} + \mathbf{u}_\alpha \times \mathbf{B} \right)_k = \left(\rho_{\mathrm{Q},\alpha} \mathbf{E} + \mathbf{j}_{\mathrm{Q},\alpha} \times \mathbf{B} \right)_k \, ;$$

$$\Gamma_{\alpha k} \equiv m_\alpha \int v_{\alpha k} \sum_\beta S_{\alpha\beta} \, \mathrm{d}^3\mathbf{v}_\alpha \, .$$

These variables, parameterized for particle species α, represent the momentum density, momentum flux tensor, dynamic pressure tensor, thermal pressure tensor, Lorentz force density, and the collision-driven momentum variation rate. The momentum conservation law for species α can be expressed in an invariant formulation:

$$\frac{\partial}{\partial t} \boldsymbol{\gamma}_\alpha + \boldsymbol{\nabla} \cdot \ddot{\mathbf{T}}_\alpha = \mathbf{f}_\alpha + \boldsymbol{\Gamma}_\alpha \, , \tag{1.670}$$

where the variables in the terms are defined as:

$$\boldsymbol{\gamma}_\alpha \equiv n_\alpha m_\alpha \mathbf{u}_\alpha = m_\alpha \int \mathbf{v}_\alpha f_\alpha \, \mathrm{d}^3\mathbf{v}_\alpha \, ;$$

$$\ddot{\mathbf{T}}_\alpha \equiv n_\alpha m_\alpha \mathbf{u}_\alpha \otimes \mathbf{u}_\alpha + n_\alpha m_\alpha \left\langle \mathbf{w}_\alpha \otimes \mathbf{w}_\alpha \right\rangle_{\mathbf{v}} = \ddot{\mathbf{D}}_\alpha + \ddot{\mathbf{P}}_\alpha \, ;$$

$$\ddot{\mathbf{D}}_\alpha \equiv n_\alpha m_\alpha \mathbf{u}_\alpha \otimes \mathbf{u}_\alpha \, ;$$

$$\ddot{\mathbf{P}}_\alpha \equiv n_\alpha m_\alpha \left\langle \mathbf{w}_\alpha \otimes \mathbf{w}_\alpha \right\rangle_{\mathbf{v}} = m_\alpha \int (\mathbf{v}_\alpha - \mathbf{u}_\alpha) \otimes (\mathbf{v}_\alpha - \mathbf{u}_\alpha) f_\alpha \, \mathrm{d}^3\mathbf{v}_\alpha \, ; \tag{1.671}$$

$$\mathbf{f}_\alpha \equiv \rho_{\mathrm{Q},\alpha} \mathbf{E} + \mathbf{j}_{\mathrm{Q},\alpha} \times \mathbf{B} \, ;$$

$$\boldsymbol{\Gamma}_\alpha \equiv \int m_\alpha \mathbf{v}_\alpha \sum_\beta S_{\alpha\beta} \, \mathrm{d}^3\mathbf{v}_\alpha \, .$$

Conventionally, the thermal pressure tensor is formally decomposed into a scalar isotropic pressure and a traceless anisotropic tensor. This traceless component corresponds to viscosity, where the viscous stress tensor is assigned a negative sign because it opposes the macroscopic momentum flux:

$$\begin{aligned} P_{kl}^{(\alpha)} &\equiv p_\alpha \delta_{kl} - V_{kl}^{(\alpha)} = \frac{1}{3} n_\alpha m_\alpha \left\langle w_\alpha^2 \right\rangle_{\mathbf{v}} \delta_{kl} - n_\alpha m_\alpha \left\langle \frac{1}{3} w_\alpha^2 \delta_{kl} - w_{\alpha k} w_{\alpha l} \right\rangle_{\mathbf{v}} \, ; \\ \ddot{\mathbf{P}}_\alpha &\equiv p_\alpha \ddot{\mathbf{I}} - \ddot{\mathbf{V}}_\alpha = \frac{1}{3} n_\alpha m_\alpha \left\langle w_\alpha^2 \right\rangle_{\mathbf{v}} \ddot{\mathbf{I}} - n_\alpha m_\alpha \left\langle \frac{1}{3} w_\alpha^2 \ddot{\mathbf{I}} - \mathbf{w}_\alpha \otimes \mathbf{w}_\alpha \right\rangle_{\mathbf{v}} \, . \end{aligned} \tag{1.672}$$

To model the plasma as a single collective fluid, the moment formulations (1.670) are summed over all species α. Because the test function ϕ_α is a summational invariant,

inter-species collision terms cancel out identically, yielding a simplified single-fluid momentum conservation law in invariant form:

► $$\frac{\partial}{\partial t}\boldsymbol{\gamma}_{\mathrm{P}} + \boldsymbol{\nabla}\cdot\ddot{\mathbf{T}}_{\mathrm{P}} = \mathbf{f}\,; \tag{1.673}$$

where the collective single-fluid parameters are defined as:

$$\begin{gathered}\boldsymbol{\gamma}_{\mathrm{P}} \equiv \sum_{\alpha} n_\alpha m_\alpha \mathbf{u}_\alpha\,, \\ \ddot{\mathbf{T}}_{\mathrm{P}} \equiv \ddot{\mathbf{D}} + \ddot{\mathbf{P}} = \sum_{\alpha}\left(n_\alpha m_\alpha\, \mathbf{u}_\alpha \otimes \mathbf{u}_\alpha\right) + \sum_{\alpha}\left(n_\alpha m_\alpha \left\langle \mathbf{w}_\alpha \otimes \mathbf{w}_\alpha \right\rangle_{\mathrm{v}}\right), \\ \mathbf{f} \equiv \rho_{\mathrm{Q}}\mathbf{E} + \mathbf{j}_{\mathrm{Q}}\times\mathbf{B}\,.\end{gathered} \tag{1.674}$$

The subscript *P* denotes the particle contribution. An analogous conservation law can be derived for electromagnetic fields, where the Lorentz force density corresponds to the momentum transfer rate from fields to particles. Vector arrows are somewhere retained to prevent ambiguity between vectors and second-order tensors.

First-Order Moment and Momentum Conservation for Fields

Although the momentum conservation law for the electromagnetic field is derived in the Selected Topics II (*Electromagnetic Field*), its fundamental steps are outlined here. The field can be treated as a collection of photons with zero rest mass, satisfying:

$$\mathcal{E}^2 = p^2c^2 + m_0^2c^4 \qquad \Rightarrow$$

$$\mathcal{E} = pc.$$

In terms of volumetric densities, this relation takes the form:

$$\rho_{\mathcal{E}} = \gamma_{\mathrm{EM}}\, c\,.$$

Multiplying by the propagation velocity yields the energy flux density on the left:

$$\rho_{\mathcal{E}}\mathbf{c} = \gamma_{\mathrm{EM}} c\mathbf{c}$$

The energy flux on the left corresponds to the Poynting vector, while the propagation direction is absorbed into the momentum density vector on the right:

$$\mathbf{E}\times\mathbf{H} = \boldsymbol{\gamma}_{\mathrm{EM}} c^2\,.$$

Expressing the speed of light via the permittivity and permeability ($c^2 = 1/\varepsilon\mu$) yields the final formulation for the field momentum density:

$$\boldsymbol{\gamma}_{\mathrm{EM}} = \mathbf{D}\times\mathbf{B}\,. \tag{1.675}$$

The objective is to establish the momentum conservation law for the electromagnetic field by evaluating the temporal derivative of relation (1.675). This evaluation incorporates the Maxwell equations (1.663) through (1.666):

$$\frac{\partial\boldsymbol{\gamma}_{\mathrm{EM}}}{\partial t} = \frac{\partial}{\partial t}\left(\mathbf{D}\times\mathbf{B}\right) = \frac{\partial\mathbf{D}}{\partial t}\times\mathbf{B} + \mathbf{D}\times\frac{\partial\mathbf{B}}{\partial t} = \left(\boldsymbol{\nabla}\times\mathbf{H} - \mathbf{j}_{\mathrm{Q}}\right)\times\mathbf{B} + \mathbf{D}\times\left(-\boldsymbol{\nabla}\times\mathbf{E}\right) = \cdots$$

Standard algebraic manipulations follow, where terms involving spatial derivatives are recast into a divergence form. This vector remapping can be performed by expanding the cross products via the Levi-Civita tensor. Utilizing the Maxwell relations, these elementary operations yield:

► $$\frac{\partial}{\partial t}\boldsymbol{\gamma}_{\mathrm{EM}} + \boldsymbol{\nabla}\cdot\ddot{\mathbf{T}}_{\mathrm{EM}} = -\mathbf{f}\,, \tag{1.676}$$

where the individual invariant terms are defined as:

$$\begin{aligned}
&\boldsymbol{\gamma}_{\mathrm{EM}} \equiv \mathbf{D}\times\mathbf{B}\,,\\
&\ddot{\mathbf{T}}_{\mathrm{EM}} \equiv \ddot{\mathbf{T}}_{\mathrm{E}} + \ddot{\mathbf{T}}_{\mathrm{M}}\,,\\
&\ddot{\mathbf{T}}_{\mathrm{E}} \equiv \frac{\mathbf{E}\cdot\mathbf{D}}{2}\,\ddot{\mathbf{1}} - \mathbf{E}\otimes\mathbf{D}\,; \qquad T^{(\mathrm{E})}_{kl} \equiv \frac{\mathbf{E}\cdot\mathbf{D}}{2}\delta_{kl} - E_k D_l\,,\\
&\ddot{\mathbf{T}}_{\mathrm{M}} \equiv \frac{\mathbf{H}\cdot\mathbf{B}}{2}\,\ddot{\mathbf{1}} - \mathbf{H}\otimes\mathbf{B}\,; \qquad T^{(\mathrm{M})}_{kl} \equiv \frac{\mathbf{H}\cdot\mathbf{B}}{2}\delta_{kl} - H_k B_l\,,\\
&\mathbf{f} \equiv \rho_{\mathrm{Q}}\mathbf{E} + \mathbf{j}_{\mathrm{Q}}\times\mathbf{B}\,.
\end{aligned} \tag{1.677}$$

The field momentum flux tensor $\mathbf{T}_{\mathrm{EM}}$ is known as the *Maxwell stress tensor*. Evidently, the momentum of the isolated field is not conserved due to transfer between fields and particles. A strict conservation law is established only for the combined system. Summing equations (1.673) and (1.676) yields:

► $$\frac{\partial}{\partial t}\left(\rho_{\mathrm{m}}\,\mathbf{u} + \mathbf{D}\times\mathbf{B}\right) + \boldsymbol{\nabla}\cdot\left[\sum_{\alpha}\ddot{\mathbf{T}}_{\alpha} + \ddot{\mathbf{T}}_{\mathrm{E}} + \ddot{\mathbf{T}}_{\mathrm{M}}\right] = 0\,. \tag{1.678}$$

This formulated equation represents the total momentum conservation law for the coupled particle-field system. The first term under the temporal derivative corresponds to the *matter momentum density* $\rho_{\mathrm{m}}\mathbf{u}$, which simultaneously represents the mass flux from the continuity equation. The second term, $\mathbf{D}\times\mathbf{B}$, constitutes the *electromagnetic field momentum density*. The spatial derivatives incorporate the momentum flux tensors of the particles, the electric field, and the magnetic field.

In summary, the partial momentum formulations verify that neither the isolated particle system nor the isolated field system conserves momentum independently:

$$\frac{\partial}{\partial t}\left(\mathbf{D}\times\mathbf{B}\right) + \boldsymbol{\nabla}\cdot\left(\ddot{\mathbf{T}}_{\mathrm{E}} + \ddot{\mathbf{T}}_{\mathrm{M}}\right) = -\rho_{\mathrm{Q}}\mathbf{E} - \rho_{\mathrm{Q}}\,\mathbf{u}\times\mathbf{B},$$

$$\frac{\partial}{\partial t}\left(\rho_{\mathrm{m}}\,\mathbf{u}\right) + \boldsymbol{\nabla}\cdot\left(\sum_{\alpha}\ddot{\mathbf{T}}_{\alpha}\right) = \rho_{\mathrm{Q}}\mathbf{E} + \rho_{\mathrm{Q}}\,\mathbf{u}\times\mathbf{B}.$$

For the particles, the temporal variation of the momentum density equals the Lorentz force density on the right-hand side. For the electromagnetic field, the relation contains the identical coupling term with the opposite sign. Summing these equations thus yields a vanishing right-hand side. Without summing over α, uncompensated inter-species collision terms remain:

$$\frac{\partial}{\partial t}\left(\rho_{\mathrm{m},\alpha}\,\mathbf{u}_\alpha\right) + \vec{\nabla}\cdot\vec{\mathbf{T}}_\alpha = \rho_{\mathrm{Q},\alpha}\mathbf{E} + \rho_{\mathrm{Q},\alpha}\,\mathbf{u}_\alpha\times\mathbf{B} + \sum_\beta\int m_\alpha \mathbf{v}_\alpha S_{\alpha\beta}\,\mathrm{d}^3\mathbf{v}_\alpha\,.$$

Note: If a momentum conservation law is expressed in the form $\partial\boldsymbol{\gamma}/\partial t + \nabla\cdot\vec{\mathbf{T}}$, the corresponding angular momentum conservation law can be simply written as $\partial\mathscr{L}_{kl}/\partial t + \partial\mathscr{N}_{kln}/\partial x_n = 0$, where the angular momentum density is $\mathscr{L}_{kl} = x_k\gamma_l - x_l\gamma_k$ and the angular momentum flux is $\mathscr{N}_{kln} = x_k T_{ln} - x_l T_{kn}$. Comprehensive details are provided in the Selected Topics II (*Electromagnetic Field*).

Second-Order Moment and Energy Conservation for Particles

Let the test function ϕ_α represent the kinetic energy of a particle of species α:

$$\phi_\alpha = m_\alpha v_\alpha^2/2 = m_\alpha v_{\alpha k} v_{\alpha k}/2\,.$$

The derivation is identical to the first moment. Following substitution, the phase velocity is decomposed into macroscopic and thermal components ($v_{\alpha k} = u_{\alpha k} + w_{\alpha k}$) and expanded. Expectation values for terms proportional to the first power of the random velocity vanish identically, yielding the energy conservation law in the form:

$$\frac{\partial}{\partial t}\left(\frac{\rho_{\mathrm{m},\alpha}u_\alpha^2}{2} + e_\alpha\right) + \nabla\cdot\left(\frac{\rho_{\mathrm{m},\alpha}u_\alpha^2}{2}\mathbf{u}_\alpha + e_\alpha\mathbf{u}_\alpha + \vec{\mathbf{P}}_\alpha\cdot\vec{\mathbf{u}}_\alpha + \mathbf{q}_\alpha\right) = \mathbf{j}_{\mathrm{Q},\alpha}\cdot\mathbf{E} + \mathscr{S}_\alpha\,, \quad (1.679)$$

where the constituent variables are defined as:

$$e_\alpha \equiv \rho_{\mathrm{m},\alpha}\left\langle\frac{w_\alpha^2}{2}\right\rangle; \quad \mathbf{q}_\alpha \equiv \rho_\alpha\left\langle\frac{w_\alpha^2}{2}\mathbf{w}_\alpha\right\rangle; \quad \mathscr{S}_\alpha \equiv \sum_\beta\int\frac{m_\alpha v_\alpha^2}{2}S_{\alpha\beta}\,d^3v_\alpha\,;$$

The symbol e_α represents the internal energy associated with random thermal motion, $\mathbf{q}_\alpha$ denotes the heat flux, and $\mathscr{S}_\alpha$ is the collision integral. The temporal derivative incorporates the kinetic energy density and the internal energy density of species α. The spatial derivative governs the individual *energy fluxes*: the kinetic energy flux, internal energy flux, pressure-driven energy flux, and heat flux. The right-hand side of equation (1.679) contains terms driving non-conservation of energy: the Joule heating density (Joule power density) and a term corresponding to inter-species collisional energy transfer.

Within the single-fluid approximation, summing all formulations (1.679) over all species α causes the collision terms to cancel out identically since ϕ_α is a summational invariant. This yields a simplified single-fluid energy conservation law:

► $$\frac{\partial}{\partial t}\left(\frac{\rho_{\mathrm{m}}u^2}{2} + e\right) + \nabla\cdot\left(\frac{\rho_{\mathrm{m}}u^2}{2}\mathbf{u} + e\mathbf{u} + \vec{\mathbf{P}}\cdot\vec{\mathbf{u}} + \mathbf{q}\right) = \mathbf{j}_{\mathrm{Q}}\cdot\mathbf{E}\,; \quad e = \sum_\alpha e_\alpha\,; \quad \mathbf{q} = \sum_\alpha \mathbf{q}_\alpha\,. \quad (1.680)$$

The remaining macroscopic parameters correspond to definitions from preceding moments. The fluid energy is not conserved alone, as the plasma is heated by electromagnetic fields. A closed conservation law requires the combined particle-field system.

Second-Order Moment and Energy Conservation for Fields

Although the energy conservation law for the electromagnetic field is derived in the second volume of Selected Topics (*Electromagnetic Field* section), the derivation is outlined here within this statistical framework. From classical electrodynamics, the electric field energy density is expressed as $\mathbf{E}\cdot\mathbf{D}/2$ (analogous to the energy density of a capacitor), and the magnetic field energy density is $\mathbf{H}\cdot\mathbf{B}/2$ (analogous to an inductor). Evaluating the temporal variation of the total field energy density via the Maxwell equations (1.663) through (1.666) yields the conservation form under the assumption of linear constitutive relations:

$$\frac{\partial}{\partial t}\left(\frac{\mathbf{E}\cdot\mathbf{D}}{2}+\frac{\mathbf{H}\cdot\mathbf{B}}{2}\right) = \mathbf{E}\cdot\frac{\partial\mathbf{D}}{\partial t}+\mathbf{H}\cdot\frac{\partial\mathbf{B}}{\partial t} = \mathbf{E}\cdot\left(\operatorname{curl}\mathbf{H}-\mathbf{j}_{\mathrm{Q}}\right) + \mathbf{H}\cdot\left(-\operatorname{curl}\mathbf{E}\right) =$$
$$= \mathbf{E}\cdot\operatorname{curl}\mathbf{H}-\mathbf{H}\cdot\operatorname{curl}\mathbf{E}-\mathbf{j}_{\mathrm{Q}}\cdot\mathbf{E} = -\operatorname{div}\left(\mathbf{E}\times\mathbf{H}\right)-\mathbf{j}_{\mathrm{Q}}\cdot\mathbf{E}.$$

The resulting field energy conservation law takes the form:

► $$\frac{\partial}{\partial t}\left(\frac{\mathbf{E}\cdot\mathbf{D}}{2}+\frac{\mathbf{H}\cdot\mathbf{B}}{2}\right) + \nabla\cdot\left(\mathbf{E}\times\mathbf{H}\right) = -\mathbf{j}_{\mathrm{Q}}\cdot\mathbf{E}. \tag{1.681}$$

The temporal derivative incorporates the electric and magnetic energy densities. The spatial derivative governs the electromagnetic energy flux $\mathbf{E}\times\mathbf{H}$, defined as the Poynting vector. The right-hand side term represents the Joule power density transferred from the fields to plasma heating. The total energy conservation law is recovered by summing the particle contribution (1.680) and the field contribution (1.681):

► $$\frac{\partial}{\partial t}\left(\frac{\rho u^2}{2}+e+\frac{\mathbf{E}\cdot\mathbf{D}}{2}+\frac{\mathbf{H}\cdot\mathbf{B}}{2}\right) + \nabla\cdot\left(\frac{\rho u^2}{2}\mathbf{u}+e\mathbf{u}+\ddot{\mathbf{P}}\cdot\vec{\mathbf{u}}+\mathbf{q}+\mathbf{E}\times\mathbf{H}\right) = 0. \tag{1.682}$$

The temporal derivative encompasses the collective *energy densities* (kinetic, internal, electric, and magnetic), while the spatial derivative governs the total energy fluxes (kinetic, internal, pressure, thermal, and electromagnetic). Energy conservation holds strictly for the coupled multi-species particle-field system. The individual, isolated conservation formulations retain non-zero source terms governed by the Joule power density.

Analyzing the energy equations for each particle species separately without summation retains the inter-species collision integrals. Assuming a polytropic plasma behavior for particles possessing f degrees of freedom yields:

$$p = Kn^{\gamma}; \qquad \gamma \equiv \frac{f+2}{f}. \tag{1.683}$$

The pressure satisfies the equation of state in the form:

$$p = nk_{\mathrm{B}}T \tag{1.684}$$

Consequently, the internal energy density reduces to:

$$e = \frac{f}{2}nk_{\mathrm{B}}T = \frac{p}{\gamma-1}. \tag{1.685}$$

Deriving higher-order Boltzmann moments remains feasible, though their structure grows increasingly complex and physical interpretation more difficult. If a generalized power of velocity is substituted for ϕ_α without representing a summational invariant, inter-species collision integrals do not cancel out upon summation.

Each subsequent moment introduces a higher-order tensor variable, requiring an additional transport relation and generating an infinite hierarchy of moment equations. In practical continuum modeling, this hierarchy is terminated after a finite number of moments by introducing an empirical relation, such as the Fourier law for heat conduction at the second-order moment level.

1.6.3 Simple Transport Phenomena

The statistical framework addresses three categories of phenomena:

1. *Transport phenomena*: Evaluating the transport of mass, momentum, energy, and other macroscopic variables driven by particle collision processes.
2. *Relaxation phenomena*: Analyzing the collision-driven relaxation of a perturbed system back to equilibrium and its relaxation times.
3. *Microinstabilities and Landau damping*: A class of kinetic phenomena governed by the velocity component of the distribution function that cannot be captured via magnetohydrodynamics (continuum theory). If the characteristic frequencies of these processes significantly exceed the collision frequency, the collisionless Vlasov framework is employed.

Initially, the formulation utilizes the relatively simple yet highly effective BGK approximation, named after Prabhu Lal Bhatnagar, Eugene Paul Gross, and Max Krook. This approach assumes that the collision operator is directly proportional to the deviation from the local equilibrium configuration and that the interactions drive the distribution back toward equilibrium:

$$S_\alpha \simeq (\Delta f_\alpha/\Delta t)_{\text{col}} = -(f_\alpha - f_{\text{LE}})/\tau = -\nu(f_\alpha - f_{\text{LE}})\,.$$

Unless multi-species interactions are analyzed simultaneously, the species subscript α is omitted. The BGK kinetic equation is formulated as:

$$\frac{\partial f}{\partial t} + (\mathbf{v}\cdot\boldsymbol{\nabla}_{\mathbf{x}})f + \left(\frac{\mathbf{F}}{m}\cdot\boldsymbol{\nabla}_{\mathbf{v}}\right)f = -\nu\left(f - f_{\text{LE}}\right); \tag{1.686}$$

$$f_{\text{LE}} \equiv n(\mathbf{x})\left(\frac{m}{2\pi k_{\text{B}}T(\mathbf{x})}\right)^{3/2}\exp\left[-\frac{m\left(\mathbf{v}-\mathbf{u}(\mathbf{x})\right)^2}{2k_{\text{B}}T(\mathbf{x})}\right]. \tag{1.687}$$

The function f_{LE} represents the local thermodynamic equilibrium canonical (Gibbs) velocity distribution, termed the Maxwellian distribution, which can vary spatially. The solution for the distribution function is sought via a perturbation series expansion:

$$f = f_0 + \varepsilon f_1 + \varepsilon^2 f_2 + \cdots \tag{1.688}$$

In subsequent derivations, f_0 constitutes the established unperturbed solution, the expansion is restricted to first-order perturbations, and the limit $\varepsilon \to 1$ is executed. This framework assumes small deviations from the Maxwellian distribution.

Charge Transport and Ohm Law

Assume a homogeneous equilibrium plasma characterized by:

$$f_0 = f_{\mathrm{LE}} \equiv n\left(\frac{m}{2\pi k_{\mathrm{B}}T}\right)^{3/2} \exp\left[-\frac{m\,\mathbf{v}^2}{2k_{\mathrm{B}}T}\right]. \tag{1.689}$$

The objective is to evaluate a stationary ($\partial/\partial t = 0$) and homogeneous ($\boldsymbol{\nabla} = 0$) first-order perturbation f_1 induced by a weak external electric field $\varepsilon\mathbf{E} = -\varepsilon\boldsymbol{\nabla}\phi$ (treated as a first-order perturbation associated with a small potential gradient $\varepsilon\boldsymbol{\nabla}\phi$). Within first-order perturbation theory, relation (1.686) reduces to:

$$\frac{Q\mathbf{E}}{m}\cdot\frac{\partial f_0}{\partial \mathbf{v}} = -\nu f_1 .$$

Substituting for f_0, the distribution function perturbation is evaluated as:

$$f_1 = \frac{Q(\mathbf{E}\cdot\mathbf{v})}{\nu k_{\mathrm{B}}T}\, n\left(\frac{m}{2\pi k_{\mathrm{B}}T}\right)^{3/2} \exp\left[-\frac{m\,\mathbf{v}^2}{2k_{\mathrm{B}}T}\right]. \tag{1.690}$$

The Maxwellian distribution of a charged particle ensemble becomes characteristically deformed up to first order, satisfying $f = f_0 + f_1$. Fig. 1.108 illustrates the distribution function for the velocity component aligned with the external electric field.

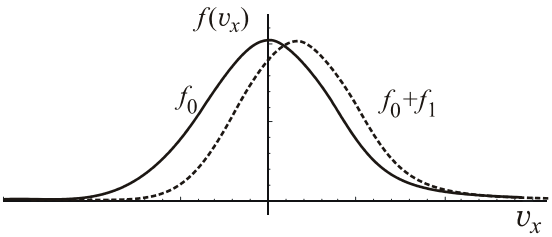


Fig. 1.108: Perturbation of the Maxwellian velocity distribution.

The *charge flux*, or the electrical current density in the plasma, is defined as:

$$\mathbf{j}_Q = Qn\mathbf{u} = \int Q\mathbf{v}f\,\mathrm{d}^3\mathbf{v} = \int Q\mathbf{v}(f_0 + f_1)\,\mathrm{d}^3\mathbf{v} = \int Q\mathbf{v}f_1\,\mathrm{d}^3\mathbf{v} .$$

The integral involving $\mathbf{v}f_0$ vanishes identically because it represents an odd function over velocity space. Substituting the formulation for f_1, integration yields:

$$j_{Qk} = n\frac{Q^2E_l}{\nu k_{\mathrm{B}}T}\left(\frac{m}{2\pi k_{\mathrm{B}}T}\right)^{3/2} \int_{-\infty}^{\infty}\int_{-\infty}^{\infty}\int_{-\infty}^{\infty} v_k v_l \,\exp\left[-\frac{m(v_1^2+v_2^2+v_3^2)}{2k_{\mathrm{B}}T}\right]\mathrm{d}v_1\mathrm{d}v_2\mathrm{d}v_3 .$$

All off-diagonal velocity integrals (with $v_k v_l$) vanish identically as odd functions. The diagonal components are symmetric, allowing the evaluation of the first component:

$$j_{Qk} = n\frac{Q^2 E_l}{\nu k_B T}\left(\frac{m}{2\pi k_B T}\right)^{3/2} \delta_{kl} \int_{-\infty}^{\infty}\int_{-\infty}^{\infty}\int_{-\infty}^{\infty} v_1^2 \exp\left[-\frac{m(v_1^2+v_2^2+v_3^2)}{2k_B T}\right] \mathrm{d}v_1 \mathrm{d}v_2 \mathrm{d}v_3 .$$

Two of these velocity integrations reduce to standard Gaussian integrals, while the remaining component is evaluated via the relations established in the *Selected Topics I*:

► $$\mathbf{j}_Q = \sigma \mathbf{E} = -\sigma \nabla \phi ; \qquad \sigma \equiv \frac{Q^2 n}{m\nu} . \tag{1.691}$$

The driving force behind the charge flux is the electric field (the negative gradient of the scalar potential). The proportionality coefficient σ is termed the *differential conductivity*. Relation (1.691) represents Ohm law, named after the German physicist Georg Simon Ohm. An identical relation can be recovered from the elementary Drude model of conductivity, proposed in 1900 by Paul Drude. Consider a charged particle subject to an electric field force and an effective collisional friction force that is proportional to the momentum loss rate. The proportionality coefficient is defined by the collision frequency $\nu = 1/\tau$, where τ represents the mean free time between collisions:

$$m\frac{\mathrm{d}\mathbf{u}}{\mathrm{d}t} = Q\mathbf{E} - \frac{m\mathbf{u}}{\tau} = Q\mathbf{E} - \nu m\mathbf{u} .$$

In a stationary state, the particle achieves a drift velocity $\mathbf{u} = Q\mathbf{E}/m\nu$, yielding:

$$\mathbf{j}_Q = Qn\mathbf{u} = \frac{Q^2 n}{m\nu}\mathbf{E} ,$$

coinciding with the kinetic result (1.691). In anisotropic media, the electrical conductivity generalizes to a second-order tensor, and Ohm law takes the form:

$$j_{Q,k} = \sigma_{kl} E_l = -\sigma_{kl}\frac{\partial \phi}{\partial x_l} . \tag{1.692}$$

Particle Transport and Fick Law

Assume an initially homogeneous equilibrium plasma. The driving force behind particle transport is a small spatial gradient in the particle number density. The local equilibrium Maxwellian distribution reflects these density spatial variations via:

$$f_{\mathrm{LE}} \equiv n(\mathbf{x})\left(\frac{m}{2\pi k_B T}\right)^{3/2} \exp\left[-\frac{m\mathbf{v}^2}{2k_B T}\right] .$$

In the absence of external force fields, the local particle number density near any given spatial coordinate satisfies:

$$n(\mathbf{x}) = n(\mathbf{x}_0) + \varepsilon \left.\frac{\partial n}{\partial x_l}\right|_{\mathbf{x}_0} \left(x_l - x_{0l}\right) \qquad \Rightarrow \qquad \nabla n \sim \varepsilon .$$

Consequently, the spatial derivative (∇) is treated as a first-order operator within perturbation theory (where ∇f_{LE} is of first order, ∇f_1 of second order, and ∇f_2 of third order). This classification arises because spatial dependence is absent in a standard Max-

wellian distribution. Within first-order perturbation theory, substituting $f = f_{\mathrm{LE}} + f_1 + \cdots$ into the BGK equation yields:

$$(\mathbf{v}\cdot\boldsymbol{\nabla}) f_{\mathrm{LE}} = -\nu f_1 \,.$$

The first-order perturbation f_1 is evaluated directly in the form:

$$f_1 = -\frac{(\mathbf{v}\cdot\boldsymbol{\nabla} n)}{\nu}\left(\frac{m}{2\pi k_{\mathrm{B}} T}\right)^{3/2} \exp\left[-\frac{m\,\mathbf{v}^2}{2k_{\mathrm{B}} T}\right]. \tag{1.693}$$

The particle flux is obtained through averaging process:

$$\mathbf{j}_N = n\mathbf{u} = \int \mathbf{v}(f_{\mathrm{LE}} + f_1)\,\mathrm{d}^3\mathbf{v} = \int \mathbf{v} f_1\,\mathrm{d}^3\mathbf{v} \,.$$

The integration is evaluated identically to the charge transport case. The individual components of the integral remain non-zero exclusively for the diagonal terms $v_k v_l$, which are integrated via the relation I.3.574 (*Selected Chapters I*):

► $$\mathbf{j}_N = -D\boldsymbol{\nabla} n \,; \qquad D \equiv \frac{k_{\mathrm{B}} T}{m\nu} \,. \tag{1.694}$$

The driving force of the particle flux is the negative gradient of the number density. The proportionality coefficient D is termed the diffusion coefficient. Relation (1.694) represents Fick law of diffusion, named after the German physiologist Adolf Eugen Fick.

Note 1: Substituting the particle flux formulation into the macroscopic continuity equation yields the diffusion equation:

$$\left.\begin{aligned} &\partial n/\partial t + \mathrm{div}\,\mathbf{j}_{\mathrm{N}} = 0\,, \\ &\mathbf{j}_N = -D\boldsymbol{\nabla} n \end{aligned}\right\} \quad \Rightarrow \quad \frac{\partial n}{\partial t} = D\boldsymbol{\nabla}^2 n \,. \tag{1.695}$$

Mathematically, this relation constitutes a parabolic partial differential equation, serving as a physical prototype for transport processes describing the dissipation of a given quantity into its surroundings. Analogous formulations govern heat conduction [1] or, as shown later, magnetic field diffusion.

Note 2: Dimensional analysis reveals that the diffusion coefficient corresponds to the product of the mean free path squared and the collision frequency:

$$D \sim \lambda^2 \nu \tag{1.696}$$

Ambipolar Diffusion

Because electrons possess a significantly lower mass than ions, they respond faster to forces and tend to leave the plasma core rapidly. This directional charge separation induces an electrostatic field that couples the two species. The field decelerates the electrons and accelerates the ions, ensuring that both species preserve macroscopically a zero net charge density. This coupled, synchronized transport of electrons and ions is termed *ambipolar diffusion*.

A crucial parameter in ambipolar diffusion is particle mobility. The mobility constitutes the proportionality coefficient between the mean drift velocity and the driving electric field:

$$\mathbf{u}_\alpha = \mu_\alpha \mathbf{E} \tag{1.697}$$

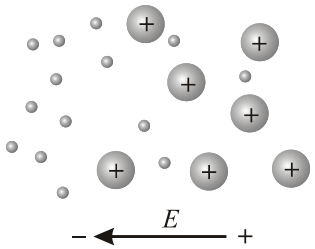


Fig. 1.109: Schematic representation of ambipolar diffusion mechanisms.

Analyzing a multi-fluid system with coexisting electron and ion components requires retaining the species subscript α. Utilizing the mobility, both the charge flux (current density) and the field-driven particle flux are formulated as:

$$\mathbf{j}_{Q,\alpha} = Q_\alpha n_\alpha \mathbf{u}_\alpha = Q_\alpha n_\alpha \mu_\alpha \mathbf{E}\,, \tag{1.698}$$

$$\mathbf{j}_{N,\alpha} = n_\alpha \mathbf{u}_\alpha = n_\alpha \mu_\alpha \mathbf{E}\,. \tag{1.699}$$

The explicit formulation for mobility is evaluated directly from the current density relation (1.691):

$$\mu_\alpha = \frac{Q_\alpha}{m_\alpha \nu_\alpha}\,. \tag{1.700}$$

Electron mobility is negative, reflecting motion opposite to the electric field vector. In an unmagnetized plasma, the collective transport of electrons and ions is driven simultaneously by the internal electric field and the particle density gradient:

$$\begin{aligned} \mathbf{j}_{N,\mathrm{e}} &= n_\mathrm{e}\mu_\mathrm{e}\mathbf{E} - D_\mathrm{e}\boldsymbol{\nabla} n_\mathrm{e}\,, \\ \mathbf{j}_{N,\mathrm{i}} &= n_\mathrm{i}\mu_\mathrm{i}\mathbf{E} - D_\mathrm{i}\boldsymbol{\nabla} n_\mathrm{i}\,. \end{aligned} \tag{1.701}$$

For a plasma with Z-times ionized species, the twin constraints of quasi-neutrality and equal fluid drift velocities are expressed as:

$$\begin{aligned} &Q_\mathrm{e} = -e\,, && Q_\mathrm{i} = Ze\,; \\ &n_\mathrm{e} \equiv n = Zn_\mathrm{i}\,, && n_\mathrm{i} = n/Z\,; \\ &\mathbf{j}_{N,\mathrm{e}} \equiv \mathbf{J}\,, && \mathbf{j}_{N,\mathrm{i}} \equiv \mathbf{J}/Z\,. \end{aligned}$$

Substituting the respective number densities and particle fluxes into (1.701) yields:

$$\begin{aligned} \mathbf{J} &= n\mu_\mathrm{e}\mathbf{E} - D_\mathrm{e}\boldsymbol{\nabla} n\,, \\ \mathbf{J}/Z &= n\mu_\mathrm{i}\mathbf{E}/Z - D_\mathrm{i}\boldsymbol{\nabla} n/Z\,. \end{aligned}$$

Eliminating the internal electric field from these coupled equations yields the result:

► $$\mathbf{J} = -D_\mathrm{a}\nabla n\,; \qquad D_\mathrm{a} \equiv \frac{\mu_\mathrm{e} D_\mathrm{i} - \mu_\mathrm{i} D_\mathrm{e}}{\mu_\mathrm{e} - \mu_\mathrm{i}}\,. \tag{1.702}$$

Since $|\mu_\mathrm{e}| \gg |\mu_\mathrm{i}|$ holds universally, the relation (1.702) simplifies to:

$$D_\mathrm{a} \approx D_\mathrm{i} - \frac{\mu_\mathrm{i}}{\mu_\mathrm{e}} D_\mathrm{e}\,. \tag{1.703}$$

Using the mobility definition (1.700), the diffusion coefficient (1.694) becomes:

$$D_\alpha \equiv \frac{k_\mathrm{B} T_\alpha}{m_\alpha \nu_\alpha} = \mu_a \frac{k_\mathrm{B} T_\alpha}{Q_\alpha}\,. \tag{1.704}$$

This formulation represents the Einstein relation, shifting the collision frequency dependency within the diffusion coefficient into the species mobility. Assuming identical temperatures for electron and ion plasma components, the Einstein relation (1.704) yields $D_\mathrm{e} = -(Z\mu_\mathrm{e}/\mu_\mathrm{i})D_\mathrm{i}$, reducing the ambipolar diffusion coefficient (1.703) to:

$$D_\mathrm{a} \approx (1+Z)\, D_\mathrm{i}\,. \tag{1.705}$$

Consequently, the effective ambipolar diffusion rate is governed by the massive ions.

Diffusion in a Magnetic Field

Assume a small density gradient and a homogeneous magnetic field $\mathbf{B} = (0,0,B_0)$. Allowing a number density gradient both parallel to the field (z-axis) and perpendicular to it (x-axis) enables the investigation of transport mechanisms along and across the magnetic fieldlines, such that $n = n(x, z)$. The magnetic field introduces spatial anisotropy into the plasma system; consequently, the random velocity components and temperatures can vary between the parallel and perpendicular directions. The local equilibrium distribution is thus formulated in an anisotropic form:

$$f_\mathrm{LE} \equiv n(x,z)\left(\frac{m}{2\pi k_\mathrm{B} T_\perp}\right)\left(\frac{m}{2\pi k_\mathrm{B} T_\parallel}\right)^{1/2} \exp\left[-\frac{m(v_x^2 + v_y^2)}{2k_\mathrm{B} T_\perp} - \frac{m v_z^2}{2k_\mathrm{B} T_\parallel}\right]. \tag{1.706}$$

Within first-order perturbation theory, the BGK equation retains the terms (where spatial derivatives continue to act as first-order operations):

$$\left(\mathbf{v}\cdot\frac{\partial f_\mathrm{LE}}{\partial \mathbf{x}}\right) + \left(\frac{Q\,\mathbf{v}\times\mathbf{B}_0}{m}\cdot\frac{\partial f_1}{\partial \mathbf{v}}\right) = -\nu f_1\,;$$

The local equilibrium distribution incorporates the spatial perturbation, thus appearing as the primary perturbation term within the spatial derivatives. Conversely, it contains no velocity perturbation; hence, the first-order perturbation f_1 only appears linearly within the velocity derivative term. The particle flux is evaluated by multiplying the governing relation by velocity and subsequently averaging over the velocity space:

$$\int \mathbf{v}\left(\mathbf{v}\cdot\frac{\partial f_\mathrm{LE}}{\partial \mathbf{x}}\right)\mathrm{d}^3\mathbf{v} + \int \mathbf{v}\left(\frac{Q\,\mathbf{v}\times\mathbf{B}_0}{m}\cdot\frac{\partial f_1}{\partial \mathbf{v}}\right)\mathrm{d}^3\mathbf{v} = -\nu\int \mathbf{v} f_1\,\mathrm{d}^3\mathbf{v}\,;$$

The integral on the right-hand side represents the particle flux explicitly. The first integral on the left is evaluated directly, while the second integral is expanded into components and integrated by parts, yielding:

$$\frac{k_B T_\perp}{m}\frac{\partial n}{\partial x} - \frac{QB_0}{m} j_{N,y} = -\nu j_{N,x} ,$$

$$\frac{QB_0}{m} j_{N,x} = -\nu j_{N,y} ,$$

$$\frac{k_B T_\parallel}{m}\frac{\partial n}{\partial z} = -\nu j_{N,z} .$$

The parameter QB_0/m denotes the gyration (cyclotron or Larmor) frequency at which the charged particle orbits the magnetic fieldlines. The two respective particle fluxes are evaluated from the first two components as:

$$j_{N\perp} = j_{N,x} = -D_\perp \frac{\partial n}{\partial x}, \qquad j_{N\parallel} = j_{N,z} = -D_\parallel \frac{\partial n}{\partial z}, \qquad j_{N,y} = -\frac{\omega_c}{\nu} j_{N\perp};$$

$$D_\perp \equiv \frac{k_B T_\perp}{m\nu}\left[\frac{1}{1+(\omega_c/\nu)^2}\right]; \qquad D_\parallel \equiv \frac{k_B T_\parallel}{m\nu}; \qquad \omega_c \equiv \frac{QB_0}{m}. \tag{1.707}$$

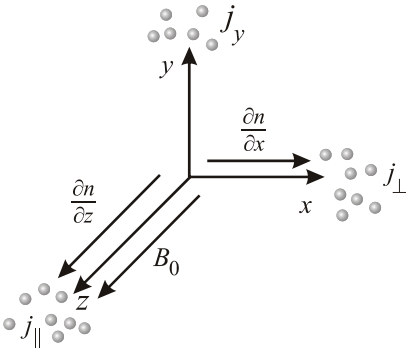


Fig. 1.110: Schematic representation of particle diffusion mechanisms in a magnetized plasma.

Along the magnetic fieldlines, diffusion is identical to the unmagnetized case and remains completely unaffected. Conversely, cross-field transport is constrained, with the perpendicular diffusion coefficient modified by the denominator factor. This anisotropy explains two distinct solar wind regimes: slow and fast. Near the solar equator, particles escape across fieldlines at 300 to 500 km/s, whereas in polar regions, they advect parallel to the fieldlines at 700 to 900 km/s.

In the weak-field limit, the perpendicular diffusion coefficient reduces to the standard unmagnetized coefficient. Conversely, in the strong-field limit, unity in the denominator is negligible, and the cross-field diffusion coefficient reduces to:

$$D_\perp \approx \frac{k_B T_\perp m\nu}{Q^2 B_0^2} = R_L^2 \nu \approx \frac{1}{B_0^2}; \qquad \omega_c \gg \nu . \tag{1.708}$$

Within a strong magnetic field, the particle is tightly bound to its Larmor orbit, and the role of the mean free path λ in relation (1.696) is assumed by the Larmor radius $R_\mathrm{L} = mv_\mathrm{T}/QB_0$ of the gyration motion for the thermal velocity $v_\mathrm{T} = (k_\mathrm{B}T_\perp/m)^{1/2}$. This substitution is physically intuitive because the mean free path represents the distance over which a particle deflects by 90° from its original path, which matches the Larmor radius in an extremely strong magnetic field.

Gyromagnetic Transport and Non-Classical Diffusion

An additional mechanism constitutes particle transport perpendicular to both the density gradient and the magnetic field, corresponding to the non-zero flux component $j_{N,y}$ within (1.707). This mode operates analogously to particle drifts, yielding:

► $$j_{N,y} = \frac{\omega_\mathrm{c} k_\mathrm{B} T_\perp}{m\nu^2}\left[\frac{1}{1+(\omega_\mathrm{c}/\nu)^2}\right]\frac{\partial n}{\partial x}. \tag{1.709}$$

For strong magnetic fields, unity within the denominator is negligible, and substituting the cyclotron frequency from (1.707) yields:

$$j_{N,y} = \frac{k_\mathrm{B}T_\perp}{QB_0}\frac{\partial n}{\partial x} \approx \frac{1}{B_0}. \tag{1.710}$$

Several specific characteristics are noteworthy:

1. The particle flux is perpendicular to the magnetic field and the number density gradient, aligning with the drift vector driven by the effective force $-\nabla n$.
2. Unlike relation (1.708), this net flux scales inversely with the first power of the magnetic field magnitude ($1/B_0$); consequently, this transport mode dominates in strong magnetic field regimes.
3. The final relation (1.710) is independent of the collision frequency; thus, this flux is not a consequence of collisions and is not classical diffusion.

This non-zero flux arises from spatial asymmetries. For a zero density gradient, individual gyration trajectories cancel out identically. Conversely, under a non-zero gradient, particle trajectories along the positive and negative y-axis do not balance, producing a net macroscopic flux independent of collisions. This phenomenon is termed *gyromagnetic transport*, exhibiting a $1/B_0$ proportionality underlying Bohm diffusion.

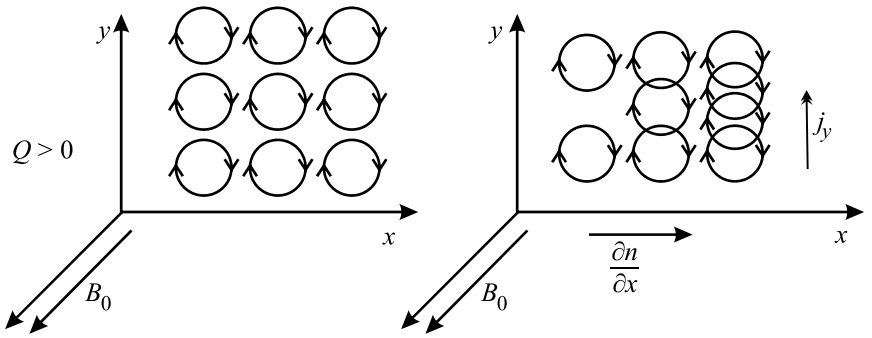


Fig. 1.111: Kinematic mechanism of gyromagnetic particle transport.

Neoclassical and Anomalous Diffusion

In inhomogeneous magnetic fields, such as tokamak configurations, additional drifts occur, predominantly the grad B drift driven by magnitude variations and the curvature drift. The resulting guiding center displacement typically exceeds the Larmor radius, significantly increasing the effective mean free path. Trapped particle dynamics, including banana orbits, must also be incorporated.

The first approach involves a direct kinetic calculation. An alternative method estimates the effective mean free path in the presence of drifts, subsequently utilizing relation (1.696). Both frameworks yield the *neoclassical diffusion* formulation accounting for field gradients and curvature, which enhances cross-field transport by several orders of magnitude.

However, experimentally measured diffusion rates in toroidal confinement are typically 10 to 100 times higher than neoclassical predictions. This phenomenon is termed *anomalous diffusion*, where turbulent plasma processes dominate the macroscopic transport. Anomalous transport is investigated via high-performance numerical simulations, and the precise underlying mechanisms remain a subject of active research.

Heat Transport and Fourier Law

Assume an initially homogeneous equilibrium plasma. The driving force behind the thermal energy transport is a small spatial temperature gradient. The local equilibrium Maxwellian distribution tracks these spatial variation dynamics via:

$$f_{\mathrm{LE}} \equiv n(\mathbf{x})\left(\frac{m}{2\pi k_{\mathrm{B}} T(\mathbf{x})}\right)^{3/2} \exp\left[-\frac{m\,\mathbf{v}^2}{2k_{\mathrm{B}} T(\mathbf{x})}\right].$$

The formulation incorporates the spatial dependence of the particle number density, as it remains coupled to the temperature profile. Assuming heat conduction at a constant isotropic pressure $p = nk_{\mathrm{B}}T$, evaluation of the spatial derivative yield

$$T\,\nabla n + n\,\nabla T = 0\,. \tag{1.711}$$

An analogous coupling between these variables manifests in a polytropic plasma $p = Kn^{\gamma}$). Similarly to particle transport, the local equilibrium distribution constitutes the zeroth-order solution, where the spatial gradient acts as a first-order operator within perturbation theory. Substituting $f = f_{\mathrm{LE}} + f_1 + \cdots$ into the BGK equation (1.686) yields:

$$v_l \frac{\partial}{\partial x_l}\left[n(\mathbf{x})\left(\frac{m}{2\pi k_{\mathrm{B}} T(\mathbf{x})}\right)^{3/2} \exp\left[-\frac{m\,\mathbf{v}^2}{2k_{\mathrm{B}} T(\mathbf{x})}\right]\right] = -\nu f_1\,.$$

Evaluating the product derivative while utilizing relation (1.711) yields:

$$f_1 = -n\frac{(\mathbf{v}\cdot\boldsymbol{\nabla} T)}{\nu}\frac{1}{T}\left[\frac{m\mathbf{v}^2}{2k_{\mathrm{B}}T} - \frac{5}{2}\right]\left(\frac{m}{2\pi k_{\mathrm{B}}T}\right)^{3/2} \exp\left[-\frac{m\,\mathbf{v}^2}{2k_{\mathrm{B}}T}\right]. \tag{1.712}$$

The remaining objective is to evaluate the heat flux vector:

$$\mathbf{q} \equiv mn\frac{1}{2}\left\langle w^2\,\mathbf{w}\right\rangle = \frac{1}{2}\int m(\mathbf{v}-\mathbf{u})^2(\mathbf{v}-\mathbf{u}) f_1\,\mathrm{d}^3\mathbf{v} \;=\; \frac{1}{2}\int m v^2\mathbf{v}\, f_1\,\mathrm{d}^3\mathbf{v}\,.$$

Substituting f_1 from (1.712), velocity integration is executed identically to preceding modes. The integration is tedious due to the sixth power of velocity. This evaluation is efficiently performed via symbolic software (e.g., Mathematica, MATLAB) or the relations tabulated in the first volume of *Selected Topics I*, p. 369::

► $$\mathbf{q} = -\kappa \nabla T\,; \qquad \kappa \equiv \frac{5nk_\mathrm{B}^2 T}{2m\nu}\,. \tag{1.713}$$

The driving force of the heat flux is the negative temperature gradient, and the proportionality coefficient κ is termed the *thermal conductivity*. Relation (1.713) represents the *Fourier law*, named after the French mathematician and physicist Jean-Baptiste Joseph Fourier. Standard introductory textbooks frequently mention a simplified one-dimensional variant of the Fourier law for a homogeneous rod with cross-section ΔS and length l, describing the heat transfer across a time interval Δt:

$$\frac{\Delta Q}{\Delta S \cdot \Delta t} = \kappa \frac{T_2 - T_1}{l} \qquad \Rightarrow \qquad \Delta Q = \kappa \frac{\Delta S}{l} \cdot \left(T_2 - T_1\right) \Delta t\,.$$

Entropy Production and Onsager Relations

Previous chapters covered phenomena restoring thermodynamic equilibrium. Small gradients in electric potential, number density, or temperature induce macroscopic fluxes:

► $$\begin{aligned} \mathbf{j}_Q &= -\sigma \nabla \phi\,, \\ \mathbf{j}_N &= -D \nabla n\,, \\ \mathbf{q} &= -\kappa \nabla T\,, \end{aligned}$$

which decay and vanish at equilibrium, where the system recovers a Maxwellian distribution. The negative gradients of macroscopic variables constitute the driving forces of transport processes, termed thermodynamic forces X_k. Generally, a single thermodynamic force can drive multiple macroscopic fluxes, and conversely, a given flux mode is frequently driven by several forces simultaneously. Density and temperature gradients can induce particle, charge, and heat fluxes alike. For instance, a temperature-gradient-driven charge flux constitutes a *thermoelectric effect*, whereas a similar particle flux defines *thermodiffusion*. Close to equilibrium, linear combinations provide a robust approximation, allowing each flux to be expressed as a linear combination of all thermodynamic forces:

$$J_i = c_{ik} X_k\,. \tag{1.714}$$

The relaxation toward thermodynamic equilibrium is an irreversible process, inherently driving entropy production. This foundational mechanism was extensively investigated by the Norwegian-American chemist and theoretical physicist Lars Onsager. For example, evaluating the entropy production $\mathrm{d}S = \mathrm{d}Q/T$ driven by a charge flux (current density) utilizes the Joule heating power density $\mathbf{j}\cdot\mathbf{E}$ transferred to the charged particles. This coupling term appeared with opposing signs on the right-hand sides of the energy conservation equations for particles and fields. In this elementary configuration, the entropy production rate reduces to:

$$\frac{\mathrm{d}S}{\mathrm{d}t} = \frac{1}{T}\frac{\mathrm{d}Q}{\mathrm{d}t} \qquad \Rightarrow \qquad \frac{\mathrm{d}s}{\mathrm{d}t} = \frac{1}{T}\mathbf{j}\cdot\mathbf{E} \qquad \Rightarrow \qquad \frac{\mathrm{d}S}{\mathrm{d}t} = \int \frac{\mathbf{j}\cdot\mathbf{E}}{T}\mathrm{d}V = \int \frac{\mathbf{j}\cdot\left(-\nabla\phi\right)}{T}\mathrm{d}V,$$

where s is entropy density. Generally, the entropy production rate within a process is proportional to the volume integral of the flux and its thermodynamic force. For multiple processes, the rate proportional to the summation of these terms:

$$\frac{\mathrm{d}S}{\mathrm{d}t} \sim \int J_k X_k \,\mathrm{d}V \;>\; 0\,. \tag{1.715}$$

Combining relations (1.714) and (1.715) yields the total entropy production rate:

► $$\frac{\mathrm{d}S}{\mathrm{d}t} = \int L_{ik} X_i X_k \,\mathrm{d}V \;>\; 0\,. \tag{1.716}$$

Evidently, entropy production is a positive-definite quadratic form of thermodynamic forces, where the coefficients L_{ik} are termed *kinetic coefficients*. Based on microscopic reversibility under time reversal, Onsager demonstrated the *reciprocal relations*:

► $$L_{ik} = L_{ki}\,. \tag{1.717}$$

These reciprocal relations establish fundamental couplings between kinetic coefficients that cannot be derived within thermodynamics (it is necessary to use the microscopic reversibility). The relations are also referred to as the *fourth law of thermodynamics*, treated as an independent axiomatic principle. For the discovery of these reciprocal relations, Lars Onsager was awarded the 1968 Nobel Prize in Chemistry. Applying the Sylvester criterion to the positive-definite quadratic form (1.716) yields:

$$L_{11} > 0\,; \qquad \begin{vmatrix} L_{11} & L_{12} \\ L_{21} & L_{22} \end{vmatrix} > 0\,; \quad \cdots \tag{1.718}$$

The Onsager reciprocal relations directly imply the symmetry of the electrical conductivity tensor since:

$$\frac{\mathrm{d}S}{\mathrm{d}t} = \int \frac{j_k E_k}{T}\,\mathrm{d}V = \int \frac{\sigma_{kl} E_k E_l}{T}\,\mathrm{d}V = \int L_{kl} E_k E_l \,\mathrm{d}V = \int L_{kl} X_k X_l \,\mathrm{d}V\,.$$

Analogously, the thermal conductivity tensor must be symmetric in anisotropic media. In summary, the generalized diffusion equation is obtained directly from the macroscopic continuity equation:

$$\frac{\partial \rho_k}{\partial t} + \boldsymbol{\nabla} \cdot \mathbf{j}_k = 0.$$

Under the assumption that:

$$\mathbf{j}_k = c_{kl} \mathbf{X}_l = -c_{kl} \boldsymbol{\nabla} \psi_l\,; \qquad \rho_k = a_{kl} \psi_l\,.$$

yields the generalized diffusion equation in the form:

$$a_{kl} \frac{\partial \psi_l}{\partial t} = \boldsymbol{\nabla} \cdot c_{kl} \boldsymbol{\nabla} \psi_l\,. \tag{1.719}$$



1.6.4 Coulomb Interaction

Debye Shielding

Consider a multi-species plasma configuration. Evaluating the electrostatic potential profile around a selected point source (either a test particle or a localized perturbation) reveals that the potential field is significantly altered by surrounding charged particles. Near thermodynamic equilibrium, particles of opposite polarity collectively migrate toward the source, shielding its charge. This shielding produces an exponential decay of the electrostatic field characterized by the Debye length λ_D, the distance at which the potential drops to 1/e of its vacuum Coulomb value. This parameter is named after the Dutch-American physicist and chemist Peter Debye. Combining the Maxwell relation $\boldsymbol{\nabla}\cdot\mathbf{D} = \rho_Q$ with the electrostatic potential definition $\mathbf{E} = -\boldsymbol{\nabla}\phi$ yields the Poisson equation for the electrical potential:

$$\boldsymbol{\nabla}^2\phi = -\frac{\rho_Q}{\varepsilon_0}. \tag{1.720}$$

The charge density on the right-hand side can be evaluated from the equilibrium Maxwellian velocity distribution. Assuming a near-equilibrium plasma state allows a first-order Taylor expansion of the exponential Boltzmann factor:

$$\frac{\rho_Q}{\varepsilon_0} = \frac{1}{\varepsilon_0}\sum_\alpha Q_\alpha n_\alpha(\mathbf{x}) = \frac{1}{\varepsilon_0}\sum_\alpha Q_\alpha n_{\alpha 0}\exp\left[-\frac{Q_\alpha\phi(\mathbf{x})}{k_B T_\alpha}\right] \approx$$

$$\approx \frac{1}{\varepsilon_0}\left(\sum_\alpha Q_\alpha n_{\alpha 0}\right) - \left(\sum_\alpha \frac{Q_\alpha^2 n_{\alpha 0}}{\varepsilon_0 k_B T_\alpha}\right)\phi(\mathbf{x}) \pm \cdots$$

The first term vanishes identically due to plasma quasi-neutrality, an intrinsic property within the definition of a plasma. The second term remains proportional to the local electrostatic potential; hence, the Poisson equation (1.720) reduces to:

$$\boldsymbol{\nabla}^2\phi = \alpha\phi; \qquad \alpha \equiv \sum_\alpha \frac{Q_\alpha^2 n_{\alpha 0}}{\varepsilon_0 k_B T_\alpha}.$$

Formulating the solution in spherical coordinates centered on the point source yields:

$$\frac{1}{r}\frac{\mathrm{d}^2}{\mathrm{d}r^2}[r\phi(r)] = \alpha\phi \quad \Rightarrow \quad \frac{\mathrm{d}^2\psi}{\mathrm{d}r^2} = \alpha\psi; \quad \psi(r) \equiv r\phi(r) \quad \Rightarrow$$

$$\psi(r) = C_1\,\mathrm{e}^{\sqrt{\alpha}\,r} + C_2\,\mathrm{e}^{-\sqrt{\alpha}\,r} \quad \Rightarrow \quad \phi(r) = \frac{C_1}{r}\mathrm{e}^{\sqrt{\alpha}\,r} + \frac{C_2}{r}\mathrm{e}^{-\sqrt{\alpha}\,r}.$$

Since the electrostatic potential of a localized source must remain finite at infinity, the integration constant C_1 vanishes identically ($C_1 = 0$). The remaining constant C_2 is evaluated by imposing the boundary condition that the potential reduces to the classical vacuum Coulomb formulation for a source charge Q_0 in the limit of small distances:

$$\phi(r) = \frac{Q_0}{4\pi\varepsilon_0 r}\,\mathrm{e}^{-\frac{r}{\lambda_\mathrm{D}}}\,; \qquad \lambda_\mathrm{D} \equiv \sqrt{\frac{\varepsilon_0 k_\mathrm{B}}{\sum_\alpha Q_\alpha^2 n_{\alpha 0}/T_\alpha}}\,. \tag{1.721}$$

For the specific case of a Z-times ionized plasma containing electrons and a single ion species at identical temperatures ($Q_\mathrm{e} = -e$, $Q_\mathrm{i} = Ze$, $n_{\mathrm{i}0} = n_{\mathrm{e}0}/Z$, $T_\mathrm{e} = T_\mathrm{i} = T$), the Debye length simplifies to the widely utilized formulation:

$$\lambda_\mathrm{D} = \sqrt{\frac{\varepsilon_0 k_\mathrm{B} T}{(1+Z) n_{\mathrm{e}0} e^2}}\,. \tag{1.722}$$

A critical plasma parameter is the plasma parameter N_D, representing the total number of electrons enclosed within a Debye sphere. This sphere defines the volume inside which a particle interacts with individual neighbors as discrete point charges; beyond this screening boundary, the collective plasma behaves as a continuous medium:

$$N_\mathrm{D} = \frac{4}{3}\pi\lambda_\mathrm{D}^3\, n_{\mathrm{e}0}\,. \tag{1.723}$$

If $N_\mathrm{D} >> 1$, the net average particle force vanishes, characterizing an ideal plasma governed by the ideal gas equation of state. Such plasma states require either high temperatures (and consequently high conductivity) or low particle number densities.

Coulomb Scattering and Rutherford Formula

Consider a charged particle beam incident on a stationary target. Selecting one particle from the beam and one from the target enables the analysis of the interaction within the center-of-mass frame as motion in a central field, provided the kinetic energy is defined as $T = \mu\mathbf{g}^2/2$. Here, $\mu \equiv m_\alpha m_\beta/(m_\alpha+m_\beta)$ represents the reduced mass, and $\mathbf{g}$ denotes the relative velocity according to decomposition (1.647), where the center-of-mass velocity in this frame vanishes identically. Because the Coulomb interaction is not instantaneous, the magnitude of the relative velocity varies during the collision; however, it approaches an identical asymptotic value g_0 in the limits $t \to \pm\infty$ before and after the interaction.

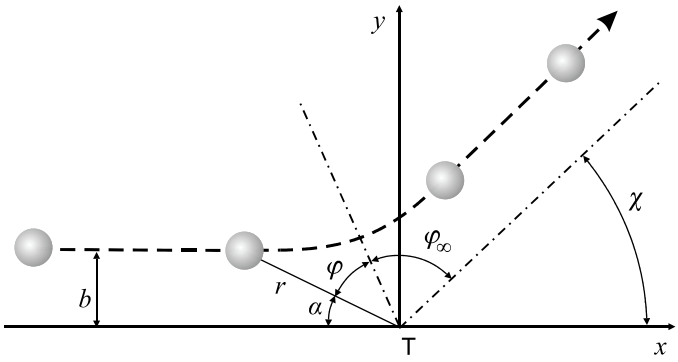


Fig. 1.112: Kinematic scheme of Coulomb scattering in the center-of-mass frame. The letter T denotes the center of mass, and the polar angle is measured from the periapsis.

The objective is to evaluate the asymptotic state following scattering, establishing a relation between the scattering angle χ, the impact parameter b, and the initial relative velocity g_0. The final step involves computing the differential collision cross section for the Coulomb interaction. The trajectory constitutes a planar problem, allowing the Lagrangian of the incident particle to be formulated as:

$$L = \frac{1}{2}\mu\dot{r}^2 + \frac{1}{2}\mu r^2\dot{\varphi}^2 - \frac{Q_\alpha Q_\beta}{4\pi\varepsilon_0 r}.$$

Since the Lagrangian is independent of the polar angle φ, the angular momentum p_φ is conserved. Furthermore, because it does not depend explicitly on time, the total energy is conserved. Instead of solving the equations of motion, these conservation laws are utilized directly (α represents the angle between relative velocity and radius vector):

$$p_\varphi \equiv \frac{\partial L}{\partial\dot{\varphi}} = \mu r^2\dot{\varphi} = \text{const} = \mu r g_\varphi = \mu r g\sin\alpha = \mu g r\sin\alpha = \mu g_0 b\,,$$

$$E = \frac{1}{2}\mu\dot{r}^2 + \frac{1}{2}\mu r^2\dot{\varphi}^2 + \frac{Q_\alpha Q_\beta}{4\pi\varepsilon_0 r} = \frac{1}{2}\mu(g_r^2 + g_\varphi^2) + \frac{Q_\alpha Q_\beta}{4\pi\varepsilon_0 r} == \text{const} = \frac{1}{2}\mu g_0^2\,.$$

The integration constants are evaluated for $t \to -\infty$ ($r \to \infty$), where b is the impact parameter. The first relation yields the angular temporal variation, and the second governs the radial derivative, substituting the angular derivative from the first expression:

$$\frac{\mathrm{d}\varphi}{\mathrm{d}t} = \frac{b g_0}{r^2}, \qquad \frac{\mathrm{d}r}{\mathrm{d}t} = \sqrt{g_0^2 - \frac{Q_\alpha Q_\beta}{2\pi\varepsilon_0\mu r} - \frac{b^2 g_0^2}{r^2}}\,.$$

Since evaluating the asymptotic state for $t \to \infty$ is sufficient, computing the full temporal trajectory is unnecessary. Dividing the two equations eliminates time parameterization, and separating variables yields:

$$\int \frac{\dfrac{b}{r^2}}{\sqrt{1 - \dfrac{Q_\alpha Q_\beta}{2\pi\varepsilon_0\mu b g_0^2}\dfrac{b}{r} - \dfrac{b^2}{r^2}}}\,\mathrm{d}r = \int \mathrm{d}\varphi\,,$$

Introducing the substitution:

$$\xi = \frac{b}{r} + \xi_0\,; \qquad \xi_0 \equiv \frac{Q_\alpha Q_\beta}{4\pi\varepsilon_0\mu b\, g_0^2}$$

and executing elementary algebraic manipulations yields:

$$-\int \frac{1}{\sqrt{a^2 - \xi^2}}\,\mathrm{d}\xi = \varphi - \varphi_0\,; \qquad a^2 \equiv 1 + \xi_0^2\,.$$

Integration is straightforward, leading to:

$$\arccos\left(\frac{\xi}{a}\right) = \varphi - \varphi_0 \quad \Rightarrow \quad \xi = a\cos(\varphi - \varphi_0) \quad \Rightarrow \quad \frac{b}{r} + \xi_0 = \sqrt{1 + \xi_0^2}\,\cos(\varphi - \varphi_0)\,.$$

Measuring the angle from the periapsis (the shortest distance) matches standard laboratory frame conventions. Consequently, the radial distance r must exhibit an extremum at $\varphi = 0$. Differentiating this relation determines $\mathrm{d}r/\mathrm{d}\varphi$, and enforcing the necessary extremum condition $\mathrm{d}r/\mathrm{d}\varphi = 0$ at $\varphi = 0$ implies that the integration constant φ_0 vanishes identically ($\varphi_0 = 0$). Long after the scattering event ($r \to \infty$), the relation reduces to:

$$\xi_0 = \sqrt{1+\xi_0^2}\cos\varphi_\infty \quad \Rightarrow \quad \cos\varphi_\infty = \frac{1}{\sqrt{1+(1/\xi_0)^2}}.$$

Comparing this expression with the trigonometric identity between cosine and tangent functions established in the *Selected Topics I* (relation I.3.558) reveals that:

$$\operatorname{tg}\varphi_\infty = \frac{1}{\xi_0}.$$

The asymptotic angle φ_∞ relates to the scattering angle χ via the geometric condition (see Fig. 1.112) $\chi + 2\varphi_\infty = \pi$, which yields:

$$\operatorname{tg}\left(\frac{\pi}{2}-\frac{\chi}{2}\right) = \frac{1}{\xi_0} \qquad \Rightarrow \qquad \operatorname{cotg}\frac{\chi}{2} = \frac{4\pi\varepsilon_0\mu\, b\, g_0^2}{Q_\alpha Q_\beta} \qquad \Rightarrow$$

$$\blacktriangleright \qquad b(\chi) = b_0 \operatorname{cotg}\frac{\chi}{2}; \qquad \chi(b) = 2\operatorname{arccotg}\frac{b}{b_0}, \tag{1.724}$$

where the characteristic parameters are defined as:

$$b_0 \equiv \frac{Q_\alpha Q_\beta}{4\pi\varepsilon_0\mu\, g_0^2}; \qquad g \equiv \left|\mathbf{v}_\alpha - \mathbf{v}_\beta\right|; \qquad \mu \equiv \frac{m_\alpha m_\beta}{m_\alpha + m_\beta}.$$

The physical meaning of the parameter b_0 is straightforward, representing the *critical impact parameter* at which the scattering angle equals 90°. This parameter establishes the lower bound for collisional interactions incorporated into the Landau kinetic framework. The remaining objective is to evaluate the differential cross section for the Coulomb interaction. Consider a segment of the incident beam forming an annular ring with an impact parameter within the interval $(b, b + \mathrm{d}b)$, which subsequently scatters into the angular interval $(\chi, \chi + \mathrm{d}\chi)$. The differential cross section is formulated as:

$$\blacktriangleright \qquad \mathrm{d}\sigma = 2\pi b\mathrm{d}b = 2\pi b\left|\frac{\mathrm{d}b}{\mathrm{d}\chi}\right|\mathrm{d}\chi = \pi b_0^2 \frac{\cos\dfrac{\chi}{2}}{\sin^3\dfrac{\chi}{2}}\mathrm{d}\chi. \tag{1.725}$$

The absolute value is required because the scattering angle decreases with increasing impact parameter, rendering the derivative negative. The cross section can alternative be expressed via the differential solid angle element (see Fig. 1.113):

$$\mathrm{d}\Omega \equiv \frac{\mathrm{d}S}{R^2} = \frac{2\pi R\sin\chi\, R\mathrm{d}\chi}{R^2} = 2\pi\sin\chi\,\mathrm{d}\chi \quad \Rightarrow$$

$$\mathrm{d}\chi = \frac{\mathrm{d}\Omega}{2\pi\sin\chi} = \frac{\mathrm{d}\Omega}{4\pi\sin\dfrac{\chi}{2}\cos\dfrac{\chi}{2}}.$$

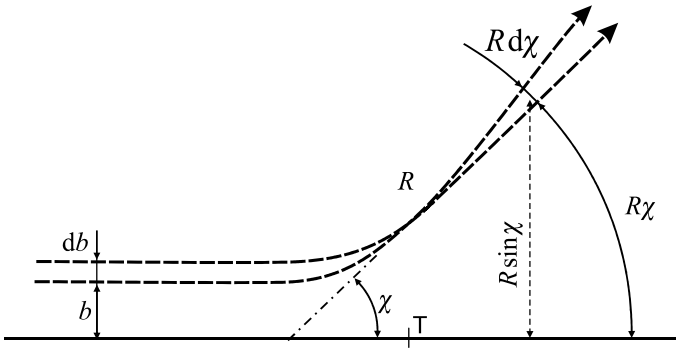


Fig. 1.113: Geometric configuration for the derivation of the differential collision cross section.

Consequently, the resulting differential cross section formulation yields:

$$\mathrm{d}\sigma = \frac{b_0^2}{4\sin^4\dfrac{\chi}{2}}\,\mathrm{d}\Omega\,;$$

$$b_0 \equiv \frac{Q_\alpha Q_\beta}{4\pi\varepsilon_0 \mu\, g_0^2}\,; \quad g \equiv \left|\mathbf{v}_\alpha - \mathbf{v}_\beta\right|\,; \quad \mu \equiv \frac{m_\alpha m_\beta}{m_\alpha + m_\beta}\,. \tag{1.726}$$

This relation constitutes the celebrated Rutherford formula, originally derived by the New Zealand physicist Ernest Rutherford during alpha particle scattering experiments on thin gold foils that led to the discovery of the atomic nucleus. Notably, the final formulation is independent of the charge signs of the interacting particles, making it identical for both attractive and repulsive Coulomb potentials. In historical literature, the Rutherford formula was alternative expressed utilizing the cosecant function:

$$\mathrm{d}\sigma = \frac{1}{4} b_0^2 \,\mathrm{cosec}^4\frac{\chi}{2}\,\mathrm{d}\Omega\,.$$

Fokker–Planck Equation

The objective is to evaluate the collision operator for the Coulomb interaction within the limit of weak, highly repetitive small-angle collisions. Unless strictly necessary, the species subscript α is omitted. The derivation incorporates the following assumptions:

1. Each particle undergoes a large number of collisions within a small but finite time interval Δt, during which its velocity vector changes slowly; hence, the net velocity change $\Delta\mathbf{v} = \mathbf{v}' - \mathbf{v}$ remains small.
2. Collisions are purely elastic, conserving total kinetic energy.
3. The electrostatic field surrounding a test particle constitutes a superposition of fields from particles within its Debye sphere. These neighbors are treated as point charges. Interactions beyond the Debye boundary are neglected.
4. Large-angle scattering events are neglected due to their low probability in a plasma, as large deviations would violate the small-perturbation condition.

Within the Landau framework, only collisions with a scattering angle under 90° (impact parameter $b > b_0$) are considered.

5. Collisions constitute a Markov process; the interaction hierarchy retains no memory of historical states or events. Consequently, the transition probability $\mathscr{P}(\mathbf{v}, \Delta\mathbf{v})\, \mathrm{d}^3(\Delta\mathbf{v})$ for a particle to alter its velocity from $\mathbf{v}$ to $\mathbf{v}+\Delta\mathbf{v}$ across Δt is time-independent. This approximation significantly simplifies the formulation.

Based on these assumptions, the Boltzmann equation collision operator governing the variation of the distribution function is formulated as:

$$S = \left(\frac{\partial f}{\partial t}\right)_{\mathrm{col}} = \frac{f(t,\mathbf{x},\mathbf{v}) - f(t-\Delta t,\mathbf{x},\mathbf{v})}{\Delta t}. \tag{1.727}$$

Standardly for Markov chains, the transition probabilities satisfy:

$$w_k = \sum_l w_l P_{lk} \ ,$$

where w_k denotes the probability of configuration k, and P_{lk} represents the transition probability from state l to state k. Analogously, the resulting distribution function at time t is expressed as a superposition of all possible transitions from time $t–\Delta t$:

$$f(t,\mathbf{x},\mathbf{v}) = \int f(t-\Delta t,\mathbf{x},\mathbf{v}-\Delta\mathbf{v})\mathscr{P}(\mathbf{v}-\Delta\mathbf{v},\Delta\mathbf{v})\,\mathrm{d}^3(\Delta\mathbf{v}). \tag{1.728}$$

The transition function $\mathscr{P}(\mathbf{v}, \Delta\mathbf{v})$ from state $\mathbf{v}$ to $\mathbf{v}+\Delta\mathbf{v}$ for the Coulomb potential is evaluated in the subsequent section. Its primary property is the normalization constraint ensuring that a transition always occurs:

$$\int \mathscr{P}(\mathbf{v},\Delta\mathbf{v})\,\mathrm{d}^3(\Delta\mathbf{v}) = 1. \tag{1.729}$$

The integrand within (1.728) is expanded to second order via a Taylor series expansion in the velocity argument $\mathbf{v}$ (justified by the first assumption ensuring small velocity variations over Δt):

$$f(t,\mathbf{x},\mathbf{v}) = \int\left[f(t-\Delta t,\mathbf{x},\mathbf{v})\mathscr{P}(\mathbf{v},\Delta\mathbf{v}) - \Delta v_l \frac{\partial(f\mathscr{P})}{\partial v_l} + \frac{1}{2}\Delta v_l \Delta v_k \frac{\partial^2(f\mathscr{P})}{\partial v_l \partial v_k} \pm \cdots \right]\mathrm{d}^3(\Delta\mathbf{v}).$$

Integrating the first term is trivial; factoring f out and applying the normalization constraint (1.729) allows the remaining parameters to be factored out:

$$f(t,\mathbf{x},\mathbf{v}) \cong f(t-\Delta t,\mathbf{x},\mathbf{v}) - \frac{\partial}{\partial v_l} f\int \Delta v_l\, \mathscr{P}\, \mathrm{d}^3(\Delta\mathbf{v}) + \frac{1}{2}\frac{\partial^2}{\partial v_l \partial v_k} f\int \Delta v_l \Delta v_k \mathscr{P}\, \mathrm{d}^3(\Delta\mathbf{v}).$$

Shifting the first term to the left-hand side, the two integrals on the right-hand side represent the expectation values of the velocity variations:

$$f(t,\mathbf{x},\mathbf{v}) - f(t-\Delta t,\mathbf{x},\mathbf{v}) = -\frac{\partial}{\partial v_l}\left(f\left\langle \Delta v_l \right\rangle\right) + \frac{1}{2}\frac{\partial^2}{\partial v_l \partial v_k}\left(f\left\langle \Delta v_l \Delta v_k \right\rangle\right).$$

Strictly, the distribution function on the right-hand side should be expanded via a temporal Taylor series as $f(t-\Delta t, \mathbf{x}, \mathbf{v}) - \Delta t\, \partial f(t, \mathbf{x}, \mathbf{v})/\partial t \pm \cdots$. However, since Δt is small,

restricting the linear approximation to the leading term $f(t, \mathbf{x}, \mathbf{v})$, is sufficient. In Markov processes, both expectation values scale linearly with Δt because both the mean deviation and the mean square deviation of random walk processes scale linearly over time. Retaining both terms on the right-hand side while evaluating f at time t preserves all terms linear in Δt. Algebraic simplification yields the collision operator in the Fokker–Planck approximation:

$$\frac{f(t,\mathbf{x},\mathbf{v})-f(t-\Delta t,\mathbf{x},\mathbf{v})}{\Delta t}=-\frac{1}{\Delta t}\frac{\partial}{\partial v_l}\left(f\left\langle\Delta v_l\right\rangle\right)+\frac{1}{2\Delta t}\frac{\partial^2}{\partial v_l\partial v_k}\left(f\left\langle\Delta v_l\Delta v_k\right\rangle\right).$$

The resulting Fokker–Planck equation takes the form:

$$\frac{\partial f}{\partial t}+\left(\mathbf{v}\cdot\boldsymbol{\nabla}_{\mathbf{x}}\right)f+\left(\frac{\mathbf{F}}{m}\cdot\boldsymbol{\nabla}_{\mathbf{v}}\right)f=-\frac{1}{\Delta t}\frac{\partial f\left\langle\Delta v_l\right\rangle}{\partial v_l}+\frac{1}{2\Delta t}\frac{\partial^2 f\left\langle\Delta v_l\Delta v_k\right\rangle}{\partial v_l\partial v_k};$$

► $$\left\langle\Delta v_l\right\rangle\equiv\int\Delta v_l\,\mathscr{P}\,\mathrm{d}^3(\Delta\mathbf{v}), \qquad (1.730)$$

$$\left\langle\Delta v_l\Delta v_k\right\rangle\equiv\int\Delta v_l\Delta v_k\,\mathscr{P}\,\mathrm{d}^3(\Delta\mathbf{v}).$$

Alternatively, it is frequently expressed in an invariant formulation:

$$\frac{\partial f}{\partial t}+\left(\mathbf{v}\cdot\boldsymbol{\nabla}_{\mathbf{x}}\right)f+\left(\frac{\mathbf{F}}{m}\cdot\boldsymbol{\nabla}_{\mathbf{v}}\right)f=-\frac{1}{\Delta t}\boldsymbol{\nabla}_{\mathbf{v}}\cdot\left(f\left\langle\Delta\mathbf{v}\right\rangle\right)+\frac{1}{2\Delta t}\left(\boldsymbol{\nabla}_{\mathbf{v}}\otimes\boldsymbol{\nabla}_{\mathbf{v}}\right):\left(f\left\langle\Delta\mathbf{v}\otimes\Delta\mathbf{v}\right\rangle\right);$$

► $$\left\langle\Delta\mathbf{v}\right\rangle\equiv\int\Delta\mathbf{v}\,\mathscr{P}\,\mathrm{d}^3(\Delta\mathbf{v}), \qquad (1.731)$$

$$\left\langle\Delta\mathbf{v}\otimes\Delta\mathbf{v}\right\rangle\equiv\int\Delta\mathbf{v}\otimes\Delta\mathbf{v}\,\mathscr{P}\,\mathrm{d}^3(\Delta\mathbf{v}).$$

The double-dot notation represents the double scalar product according to definition (1.730). The tensor product symbol is sometimes omitted. The Fokker–Planck collision operator incorporates two distinct components: the term containing $\langle\,\Delta\mathbf{v}\,\rangle$ is defined as the *dynamical friction term*, describing the collision-driven deceleration of the incident beam, while the term containing $\langle\,\Delta\mathbf{v}\otimes\Delta\mathbf{v}\,\rangle$constitutes the *diffusion term*, governing the velocity-space scattering of the particle ensemble.

Evaluating both coefficients for the Coulomb interaction in the subsequent chapter shows that they can be expressed via the Rosenbluth potentials. Since only small-angle collisions dominate, evaluating the impact parameter within the boundary interval $(b_{\min}, b_{\max})$, where $b_{\min} = b_0$ (corresponding to a 90° scattering angle) and $b_{\max} = \lambda_D$, renders the Fokker–Planck formulation fully equivalent to the Landau kinetic equation.

Rosenbluth Potentials

Evaluating the explicit values for $\langle\,\Delta\mathbf{v}\,\rangle$ and $\langle\,\Delta\mathbf{v}\otimes\Delta\mathbf{v}\,\rangle$ requires a formal distinction between the incident particle and the target particle. Following the established notation, the incident particle is indexed as α and the target particle as β. The pre-collision velocities are denoted as $\mathbf{v}_\alpha$, $\mathbf{v}_\beta$, and the post-collision velocities as $\mathbf{v}'_\alpha$, $\mathbf{v}'_\beta$. The relative velocity vector is defined as $\mathbf{g}\equiv\mathbf{v}_{\alpha\beta}=\mathbf{v}_\alpha-\mathbf{v}_\beta$. Relation (1.648) establishes that the magnitude of the relative velocity remains invariant during an elastic collision; hence, g

characterizes the interaction, whereas the relative velocity unit vector $\mathbf{k} \equiv \mathbf{g}/g$ rotates. Relation (1.724) governs the functional dependence between the impact parameter b and the scattering angle χ for the Coulomb potential:

$$b(\chi) = b_0 \operatorname{cotg}\frac{\chi}{2}; \qquad \chi(b) = 2\operatorname{arccotg}\frac{b}{b_0},$$
$$b_0 \equiv \frac{Q_\alpha Q_\beta}{4\pi\varepsilon_0 \mu g^2}; \quad g \equiv \left|\mathbf{v}_\alpha - \mathbf{v}_\beta\right|; \quad \mu \equiv \frac{m_\alpha m_\beta}{m_\alpha + m_\beta}. \tag{1.732}$$

These relations verify that the critical impact parameter b_0 corresponds to a 90° scattering angle, defining the lower bound of the impact parameter interval under evaluation. Evaluating the friction and diffusion terms within the Fokker–Planck equation requires expressing the incident particle velocity via the center-of-mass and relative velocities according to (1.646):

$$\mathbf{v}_\alpha = \mathbf{v}_{(\alpha\beta)} + \frac{m_\beta}{m_\alpha + m_\beta}\mathbf{v}_{\alpha\beta} = \mathbf{v}_\mathrm{T} + \frac{m_\beta}{m_\alpha + m_\beta}\mathbf{g}.$$

Evaluating the post- and pre-collision velocity difference and denoting the relative velocity $\mathbf{g}$ yields:

$$\Delta\mathbf{v}_\alpha = \frac{m_\beta}{m_\alpha + m_\beta}\Delta\mathbf{g}.$$

Since the center-of-mass velocity remains invariant during the collision, it vanishes within the difference relation. The corresponding variations are given by:

$$\left\langle \Delta\mathbf{v}_\alpha \right\rangle \equiv \frac{m_\beta}{m_\alpha + m_\beta}\int \Delta\mathbf{g}\,\mathscr{P}\,\mathrm{d}^3(\Delta\mathbf{v}),$$

$$\left\langle \Delta\mathbf{v}_\alpha \otimes \Delta\mathbf{v}_\alpha \right\rangle \equiv \left(\frac{m_\beta}{m_\alpha + m_\beta}\right)^2 \int \Delta\mathbf{g}\otimes\Delta\mathbf{g}\,\mathscr{P}\,\mathrm{d}^3(\Delta\mathbf{v}).$$

The transition probability element is formulated analogously to (1.653), scaling proportionally with the magnitude of the relative velocity (governing the collision frequency), the target particle velocity distribution function, the time interval, and the differential collision cross section for the Coulomb interaction:

$$\mathscr{P}\,\mathrm{d}^3(\Delta\mathbf{v}) = g\, f_\beta \Delta t\, \mathrm{d}\sigma\, \mathrm{d}^3\mathbf{v}_\beta,$$

$$\left\langle \Delta\mathbf{v}_\alpha \right\rangle \equiv \frac{m_\beta}{m_\alpha + m_\beta}\Delta t \int \Delta\mathbf{g}\, g\, \mathrm{d}\sigma\, f_\beta\, \mathrm{d}^3\mathbf{v}_\beta,$$

$$\left\langle \Delta\mathbf{v}_\alpha \otimes \Delta\mathbf{v}_\alpha \right\rangle \equiv \left(\frac{m_\beta}{m_\alpha + m_\beta}\right)^2 \Delta t \int \Delta\mathbf{g}\otimes\Delta\mathbf{g}\, g\, \mathrm{d}\sigma\, f_\beta\, \mathrm{d}^3\mathbf{v}_\beta.$$

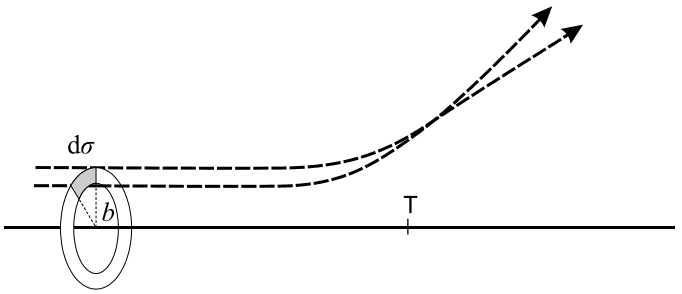


Fig. 1.114: Geometric configuration for the cross-section integration.

Fig. 1.114 shows that $\mathrm{d}\sigma = b\,\mathrm{d}b\,\mathrm{d}\varphi$. Thus, cross-section integration covers all impact parameters and the azimuthal angle, covering the entire annular area of the incident particle beam. Because integration over the cross section operates exclusively on the relative velocity terms g, the auxiliary tensor coefficients are evaluated first:

$$\gamma_k \equiv \int \Delta g_k \, g \, \mathrm{d}\sigma = \int \Delta g_k \, g \, b \, \mathrm{d}b \, \mathrm{d}\varphi \,; \tag{1.733}$$

$$\xi_{kl} \equiv \int \Delta g_k \Delta g_l \, g \, \mathrm{d}\sigma = \int \Delta g_k \Delta g_l \, g \, b \, \mathrm{d}b \, \mathrm{d}\varphi \,. \tag{1.734}$$

These coefficients determine the dynamical friction and diffusion terms:

$$\begin{aligned} \left\langle \Delta \mathbf{v}_\alpha \right\rangle &\equiv \frac{m_\beta}{m_\alpha + m_\beta} \Delta t \int \boldsymbol{\gamma} f_\beta(\mathbf{v}_\beta) \, \mathrm{d}^3 \mathbf{v}_\beta \,. \\ \left\langle \Delta \mathbf{v}_\alpha \otimes \Delta \mathbf{v}_\alpha \right\rangle &\equiv \left(\frac{m_\beta}{m_\alpha + m_\beta} \right)^2 \Delta t \int \ddot{\boldsymbol{\xi}} f_\beta(\mathbf{v}_\beta) \, \mathrm{d}^3 \mathbf{v}_\beta \,. \end{aligned} \tag{1.735}$$

Evaluating the coefficients γ_k and ξ_{kl}. constitutes the key to determining the Fokker–Planck collision operator. Structural symmetry dictates that these coefficients are formulated exclusively as functions of the relative velocity vector $\mathbf{g}$:

$$\begin{aligned} \gamma_k &= A \, g_k \,; \\ \xi_{kl} &= B \, \delta_{kl} + C \, g_k g_l \,. \end{aligned} \tag{1.736}$$

Consequently, the objective reduces to evaluating the scalar constants A, B, and C. These parameters depend solely on the relative velocity magnitude g, which remains invariant during elastic interactions. Without loss of generality, the constants A, B, and C can be evaluated in an arbitrary coordinate system. The derivation utilizes a frame where the pre-collision relative velocity $\mathbf{g} = \mathbf{v}_{\alpha\beta}$ aligns with the $\mathbf{e}_3$ basis axis. Since $\mathbf{g}$ and $\mathbf{g}'$ possess an identical magnitude g and differ only by rotation, the components of the velocity variation vector $\Delta\mathbf{g}$ governing integrals(1.733) and (1.734) are given by:

$$\Delta g_1 = g \sin\chi \cos\varphi \,;$$

$$\Delta g_2 = g \sin\chi \sin\varphi \;\; ;$$

$$\Delta g_3 = -g(1 - \cos\chi) \,.$$

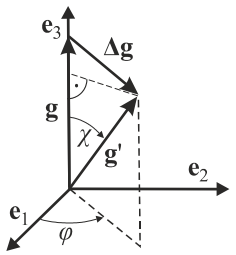


Fig. 1.115: Coordinate frame alignment with the pre-collision relative velocity vector.

Executing integrations (1.733) and (1.734) over the impact parameter b requires expressing the scattering angle χ dependencies via the relation $b = b_0 \operatorname{cotg}(\chi/2)$, transforming $\sin\chi$ and $\cos\chi$ functions into $\operatorname{cotg}\chi/2$ formulations. This mapping utilizes the trigonometric identities established in the first volume of *Selected Topics*:

$$\sin\chi = \frac{2\operatorname{cotg}(\chi/2)}{1+\operatorname{cotg}^2(\chi/2)} = \frac{2bb_0}{b^2+b_0^2},$$

$$\cos\chi = \frac{\operatorname{cotg}^2(\chi/2)-1}{\operatorname{cotg}^2(\chi/2)+1} = \frac{b^2-b_0^2}{b^2+b_0^2}.$$

The resulting expressions for the components of the vector $\Delta\mathbf{g}$ yield:

$$\Delta g_1 = g\frac{2bb_0}{b^2+b_0^2}\cos\varphi;$$

$$\Delta g_2 = g\frac{2bb_0}{b^2+b_0^2}\sin\varphi; \qquad (1.737)$$

$$\Delta g_3 = -g\frac{2b_0^2}{b^2+b_0^2}.$$

In accordance with (1.736), integral (1.733) within this coordinate frame possesses a single non-zero component along the $\mathbf{e}_3$ axis, evaluating the constant as $A = \gamma_3/g$. Furthermore, relation (1.736) implies $\xi_{11} = B$ and $\xi_{22} = B$; hence, B is determined via ξ_{11}, ξ_{22}, or the average $(\xi_{11} + \xi_{22})/2$. Under the assumption that $\lambda_D >> b_0$, integration is executed from zero since large-angle collisions with $b < b_0$ are highly improbable and their cumulative contribution is negligible:

$$A = \gamma_3/g \equiv \frac{1}{g}\int \Delta g_3\, g\, b\,\mathrm{d}b\,\mathrm{d}\varphi = \int\left(-\frac{2b_0^2}{b^2+b_0^2}\right) g\, b\,\mathrm{d}b\,\mathrm{d}\varphi = -2\pi b_0^2 g\int_0^{\lambda_D}\frac{2b}{b^2+b_0^2}\mathrm{d}b =$$

$$= -2\pi b_0^2 g\left[b^2+b_0^2\right]_0^{\lambda_D} = -2\pi b_0^2 g\ln\frac{\lambda_D^2+b_0^2}{b_0^2} \approx -4\pi b_0^2 g\ln\frac{\lambda_D}{b_0}.$$

An analogous procedure evaluates the constant B, utilizing a algebraic substitution for $b^2 + b_0^2$ within the integration:

$$B = \frac{\xi_{11} + \xi_{22}}{2} \equiv \int \left(\Delta g_1 \Delta g_1 + \Delta g_2 \Delta g_2 \right) g\, b\, \mathrm{d}b\, \mathrm{d}\varphi = \frac{1}{2} \int g^2 \left(\frac{2bb_0}{b^2 + b_0^2} \right)^2 g\, b\, \mathrm{d}b\, \mathrm{d}\varphi =$$

$$= \pi g^3 b_0^2 \int_0^{\lambda_\mathrm{D}} \frac{4b^3}{\left(b^2 + b_0^2 \right)^2} \mathrm{d}b = 2\pi g^3 b_0^2 \left[\frac{b_0^2}{b^2 + b_0^2} + \ln\left(b^2 + b_0^2 \right) \right]_0^{\lambda_\mathrm{D}} \approx 4\pi g^3 b_0^2 \ln \frac{\lambda_\mathrm{D}}{b_0}.$$

The remaining objective is to determine the final constant C. Within the selected coordinate frame, decomposition (1.736) implies $\xi^{33} = B + Cg^2$:

$$B + Cg^2 = \xi_{33} = \int \Delta g_3 \Delta g_3\, g\, b\, \mathrm{d}b\, \mathrm{d}\varphi = \int \left(-g \frac{2b_0^2}{b^2 + b_0^2} \right)^2 g\, b\, \mathrm{d}b\, \mathrm{d}\varphi =$$

$$= \pi g^3 4b_0^4 \int_0^{\lambda_\mathrm{D}} \frac{2b}{\left(b^2 + b_0^2 \right)^2} \mathrm{d}b = \pi g^3 4b_0^4 \left[-\frac{1}{b^2 + b_0^2} \right]_0^{\lambda_\mathrm{D}} \approx 0.$$

This final integral lacks the dominant logarithmic singularity, rendering it a factor of $\ln(\lambda_\mathrm{D}/b_0)$ smaller than A and B. Consequently, within this approximation, the relation simplifies to $C = -B/g^2$. The generalized formulation of the complete integration yields:

$$A \approx -4\pi b_0^2 g \ln\left(\frac{\lambda_\mathrm{D}}{b_0} \right); \quad B \approx 4\pi b_0^2 g^3 \ln\left(\frac{\lambda_\mathrm{D}}{b_0} \right); \quad C \approx -4\pi b_0^2 g \ln\left(\frac{\lambda_\mathrm{D}}{b_0} \right). \tag{1.738}$$

The collisional contribution within the interval from 0 to b_0 is negligible, justifying the integration lower bound executed from zero. Conversely, truncation at the upper bound via the Debye length remains critical, as the integral diverges without this shielding boundary. Substituting the constants A, B, and C into decomposition (1.736) and combining the result with the friction and diffusion expressions (1.735) yields the finalized formulations. Simplifying via the definition of the critical impact parameter b_0 leads to:

$$\begin{aligned} \gamma_k &\approx C_{\alpha\beta} \ln \Lambda_{\alpha\beta} \left(-\frac{g_k}{g^3} \right); \\ \xi_{kl} &\approx C_{\alpha\beta} \ln \Lambda_{\alpha\beta} \left(\frac{g^2 \delta_{kl} - g_k g_l}{g^3} \right), \end{aligned} \tag{1.739}$$

where the parameters are defined as:

$$C_{\alpha\beta} \equiv \frac{\left(Q_\alpha Q_\beta \right)^2}{4\pi\varepsilon_0^2 \mu^2}; \qquad \ln \Lambda_{\alpha\beta} \equiv \ln\left(\frac{\lambda_\mathrm{D}}{b_0} \right); \qquad \mu \equiv \frac{m_\alpha m_\beta}{m_\alpha + m_\beta}. \tag{1.740}$$

The slowly varying function $\ln \Lambda$ is the Coulomb logarithm, treated as a constant with respect to velocity derivatives and integrations. (For equilibrium plasma, $g^2 = k_\mathrm{B}T/m$, rendering its argument equal to the number of particles in a Debye sphere up to a factor

of three.) The components g_{kl} and the magnitude $g = (g_k g_k)^{1/2}$ act as integrands, expanding via the identities:

$$\frac{\partial g}{\partial g_k} = \frac{g_k}{g}\,; \qquad \frac{\partial}{\partial g_k}\left(\frac{1}{g}\right) = -\frac{g_k}{g^3}\,; \qquad \frac{\partial^2 g}{\partial g_k \partial g_l} = \frac{g^2\delta_{kl} - g_k g_l}{g^3}\,. \tag{1.741}$$

Since $g_k = v_{\alpha k} - v_{\beta k}$, the identity $\partial/\partial g_k = \partial/\partial v_{\alpha k}$ holds universally, allowing the friction and diffusion terms to be recast in the form:

$$\begin{gathered}\left\langle \Delta v_{\alpha k} \right\rangle \approx \Delta t \frac{m_\beta}{m_\alpha + m_\beta} C_{\alpha\beta} \ln \Lambda_{\alpha\beta} \frac{\partial}{\partial v_{\alpha k}} \int \frac{f_\beta(\mathbf{v}_\beta)}{g} \mathrm{d}^3\mathbf{v}_\beta\,. \\ \left\langle \Delta v_{\alpha k} \Delta v_{\alpha l} \right\rangle \approx \Delta t \left(\frac{m_\beta}{m_\alpha + m_\beta}\right)^2 C_{\alpha\beta} \ln \Lambda_{\alpha\beta} \frac{\partial^2}{\partial v_{\alpha k} \partial v_{\alpha l}} \int g\, f_\beta(\mathbf{v}_\beta)\, \mathrm{d}^3\mathbf{v}_\beta\,.\end{gathered} \tag{1.742}$$

The Rosenbluth potentials H and G are defined via the governing formulations:

► $$\begin{aligned} H_{\alpha\beta}(\mathbf{v}_\alpha) &\equiv \int \frac{f_\beta}{g} \mathrm{d}^3\mathbf{v}_\beta\,; \\ G_{\alpha\beta}(\mathbf{v}_\alpha) &\equiv \int g\, f_\beta\, \mathrm{d}^3\mathbf{v}_\beta \end{aligned}\,. \tag{1.743}$$

These potentials are named after the prominent American plasma physicist Marshall Nicholas Rosenbluth and quantify the statistical influence of the scattering target species β on the incident test species α. Utilizing relations (1.742) and (1.743), the collision operator on the right-hand side of the Fokker–Planck equation (1.730) reduces to:

$$\begin{gathered} S_{\alpha\beta} = -K_{\alpha\beta} \ln \Lambda_{\alpha\beta} \frac{\partial}{\partial v_{\alpha l}} \left(f_\alpha \frac{\partial H_{\alpha\beta}}{\partial v_{\alpha l}} \right) + D_{\alpha\beta} \ln \Lambda_{\alpha\beta} \frac{\partial^2}{\partial v_{\alpha l} \partial v_{\alpha k}} \left(f_\alpha \frac{\partial^2 G_{\alpha\beta}}{\partial v_{\alpha k} \partial v_{\alpha l}} \right); \\ S_{\alpha\beta} = -K_{\alpha\beta} \ln \Lambda_{\alpha\beta} \boldsymbol{\nabla}_{\mathbf{v}} \cdot \left(f_\alpha \boldsymbol{\nabla}_{\mathbf{v}} H_{\alpha\beta} \right) + D_{\alpha\beta} \ln \Lambda_{\alpha\beta} \left(\boldsymbol{\nabla}_{\mathbf{v}} \boldsymbol{\nabla}_{\mathbf{v}} \right) : \left(f_\alpha\, \boldsymbol{\nabla}_{\mathbf{v}} \boldsymbol{\nabla}_{\mathbf{v}} G_{\alpha\beta} \right); \\ K_{\alpha\beta} \equiv C_{\alpha\beta} \frac{m_\beta}{m_\alpha + m_\beta} = \frac{1}{4\pi} \left(\frac{Q_\alpha Q_\beta}{\varepsilon_0 m_\alpha} \right)^2 \frac{m_\alpha + m_\beta}{m_\beta}; \\ D_{\alpha\beta} \equiv \frac{1}{2} C_{\alpha\beta} \left(\frac{m_\beta}{m_\alpha + m_\beta} \right)^2 = \frac{1}{8\pi} \left(\frac{Q_\alpha Q_\beta}{\varepsilon_0 m_\alpha} \right)^2 . \end{gathered} \tag{1.744}$$

The first expression provides the component notation, whereas the second constitutes the invariant formulation. For clarity, dyadic product symbols are omitted; the tensor contraction hierarchy is uniquely specified by the component indices. The velocity gradients operate exclusively on the incident particle coordinates, as target coordinates are already integrated within the Rosenbluth potentials.

Rosenbluth potentials are widely utilized in plasma transport theory. Evaluating the target distribution function yields differential equations analogous to the classical electrostatic Poisson equation. Consequently, these potentials can be expanded into spherical harmonics to efficiently solve spherically symmetric kinetic configurations. Comparing the electrostatic potential of a dual-charge system with H yields:

$$\phi_{\alpha\beta}(\mathbf{r}_\alpha) = \frac{1}{4\pi\varepsilon_0}\int \frac{\rho_\beta}{\left|\mathbf{r}_\alpha - \mathbf{r}_\beta\right|}\mathrm{d}^3\mathbf{r}_\beta \,;$$

$$H_{\alpha\beta}(\mathbf{v}_\alpha) \equiv \int \frac{f_\beta}{\left|\mathbf{v}_\alpha - \mathbf{v}_\beta\right|}\mathrm{d}^3\mathbf{v}_\beta \,.$$

The electrostatic potential satisfies the classical Poisson equation:

$$\nabla^2\phi_{\alpha\beta} = -\frac{\rho_\beta}{\varepsilon_0}.$$

By mathematical analogy, the relation for the first potential evaluates to:

$$\nabla^2{}_{\mathbf{v}} H_{\alpha\beta} = -4\pi f_\beta \,. \tag{1.745}$$

Furthermore, direct differentiation of the definition yields $\nabla^2_{\mathbf{v}} G_{\alpha\beta} = 2H_{\alpha\beta}$. Consequently, the second potential satisfies the higher-order differential equation:

$$\nabla^2{}_{\mathbf{v}}\nabla^2{}_{\mathbf{v}} G_{\alpha\beta} = -8\pi f_\beta \,. \tag{1.746}$$

Given the velocity distribution function of the target species, the last two coupled relations determine the specific Rosenbluth potentials governing the incident beam interaction. In summary, the complete Fokker–Planck equation for an incident test particle species α interacting with a background target species β via Rosenbluth potentials is expressed as:

$$\frac{\partial f_\alpha}{\partial t} + \left(\mathbf{v}_\alpha \cdot \nabla_{\mathbf{x}}\right) f_\alpha + \left(\frac{\mathbf{F}_\alpha}{m_\alpha}\cdot\nabla_{\mathbf{v}}\right) f_\alpha = \sum_\beta S_{\alpha\beta} \,;$$

$$\blacktriangleright \qquad S_{\alpha\beta} \equiv K_{\alpha\beta}\ln\Lambda_{\alpha\beta}\left[\begin{array}{c} -\nabla_{\mathbf{v}}\cdot\left(f_\alpha \nabla_{\mathbf{v}} H_{\alpha\beta}\right) + \\ + \dfrac{1}{2}\dfrac{m_\beta}{m_\alpha + m_\beta}\left(\nabla_{\mathbf{v}}\nabla_{\mathbf{v}}\right) : \left(f_\alpha\, \nabla_{\mathbf{v}}\nabla_{\mathbf{v}}\nabla_{\mathbf{v}} G_{\alpha\beta}\right) \end{array}\right]; \tag{1.747}$$

$$H_{\alpha\beta}(\mathbf{v}_\alpha) \equiv \int \frac{1}{g} f_\beta \,\mathrm{d}^3\mathbf{v}_\beta \,,$$

$$G_{\alpha\beta}(\mathbf{v}_\alpha) \equiv \int g\, f_\beta \,\mathrm{d}^3\mathbf{v}_\beta \,.$$

The subsequent section introduces the error function and the Chandrasekhar function, both critical for evaluating the Rosenbluth potentials for a Maxwellian background target. The corresponding integration requires a series expansion in Legendre polynomials. The underlying mathematical framework is tabulated within the *Selected Topics I* (Special Functions, section I.3.7.2). If the explicit derivation details are omitted, the finalized formulations for the Rosenbluth potentials can be directly accepted.

Error Function and Chandrasekhar Function

Evaluating the Rosenbluth potentials utilizes the error function ϕ and the related Chandrasekhar function ψ:

► $$\phi(x) \equiv \frac{2}{\sqrt{\pi}} \int_0^x \mathrm{e}^{-\xi^2}\, \mathrm{d}\xi\,; \tag{1.748}$$

► $$\psi(x) \equiv \frac{2}{\sqrt{\pi}\, x^2} \int_0^x \xi^2\, \mathrm{e}^{-\xi^2}\, \mathrm{d}\xi\,. \tag{1.749}$$

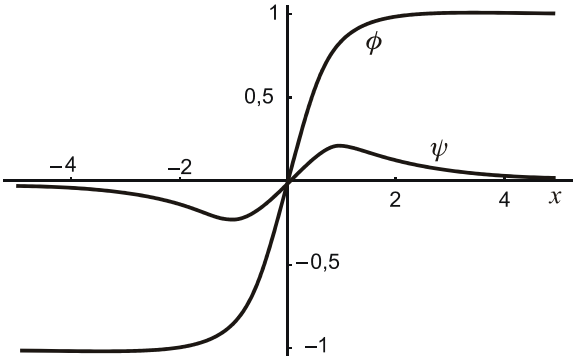


Fig. 1.116: Functional behavior of the error function and the Chandrasekhar function.

The asymptotic limits of both functions for small and large arguments are evaluated as:

$$\begin{aligned} x \ll 1\!:\quad & \psi(x) \equiv \frac{2}{\sqrt{\pi}\, x^2} \int_0^x \xi^2 (1 \pm \cdots)\, \mathrm{d}\xi \approx \frac{2}{3\sqrt{\pi}}\, x, \quad \phi(x) = \frac{2}{\sqrt{\pi}} \int_0^x (1 \pm \cdots)\, \mathrm{d}\xi \approx \frac{2}{\sqrt{\pi}}\, x, \\ x \gg 1\!:\quad & \psi(x) \approx \frac{2}{\sqrt{\pi}\, x^2} \int_0^\infty \xi^2\, \mathrm{e}^{-\xi^2}\, \mathrm{d}\xi = \frac{1}{2x^2}, \qquad \phi(x) \approx \frac{2}{\sqrt{\pi}} \int_0^\infty \mathrm{e}^{-\xi^2}\, \mathrm{d}\xi = 1\,. \end{aligned} \tag{1.750}$$

Fig. 1.116 illustrates the functional behavior. The Chandrasekhar function is named after the Indian-American astrophysicist Subrahmanyan Chandrasekhar. The functions ϕ and ψ are coupled via the relation:

► $$\psi(x) = \frac{\phi - x\phi'}{2x^2}\,. \tag{1.751}$$

The mathematical proof is straightforward. Substituting the Chandrasekhar function definition into the left-hand side and the error function definition into the right-hand side, while omitting the common denominator x^2, yields:

$$\frac{2}{\sqrt{\pi}} \int_0^x \xi^2\, \mathrm{e}^{-\xi^2}\, \mathrm{d}\xi \overset{?}{=} \frac{1}{\sqrt{\pi}} \int_0^x \mathrm{e}^{-\xi^2}\, \mathrm{d}\xi - x \frac{1}{\sqrt{\pi}}\, \mathrm{e}^{-x^2}\,.$$

Canceling coefficients and differentiating both sides with respect to x yields:

$$2x^2\,\mathrm{e}^{-x^2} \overset{?}{=} \mathrm{e}^{-x^2} - \left(\mathrm{e}^{-x^2} - 2x^2\,\mathrm{e}^{-x^2}\right).$$

Since both derivatives are equal, the original functions can differ only by an integration constant, which evaluates to zero. Consequently, the formulation of the Chandrasekhar function via the error function in (1.751) is verified. Utilizing the identity:

$$\phi' = \frac{2}{\sqrt{\pi}}\mathrm{e}^{-x^2}, \tag{1.752}$$

relation (1.751) between the Chandrasekhar and error functions can be inverted to yield:

► $$\phi = 2x^2\psi + \frac{2x}{\sqrt{\pi}}\mathrm{e}^{-x^2}. \tag{1.753}$$

Rosenbluth Potentials for a Maxwellian Target

Assume a Maxwellian velocity distribution for the background target species β:

$$f_\beta = n_\beta\left(\frac{m_\beta}{2\pi k_\mathrm{B}T_\beta}\right)^{3/2}\mathrm{e}^{-\frac{m v_\beta^2}{2k_\mathrm{B}T_\beta}}. \tag{1.754}$$

Evaluation of the Potential H

Due to the isotropic nature of the target distribution function f_β, the resulting potential depends exclusively on the velocity magnitude v_α. The denominator of the integrand is expanded into a series of Legendre polynomials via the relations established in *Selected Topics I* (Eq. I.3.456):

$$H(v_\alpha) \equiv \int \frac{f_\beta}{\left|\mathbf{v}_\alpha - \mathbf{v}_\beta\right|}\mathrm{d}^3\mathbf{v}_\beta =$$

$$= \sum_{l=0}^{\infty}\iiint f_\beta(v_\beta)\frac{\min^l(v_\alpha, v_\beta)}{\max^{l+1}(v_\alpha, v_\beta)}P_l(\cos\theta)\,v_\beta^2\sin\theta\,\mathrm{d}\varphi\,\mathrm{d}\theta\,\mathrm{d}v_\beta.$$

Integration over the azimuthal angle φ evaluates trivially to 2π. Integration over the polar angle θ between vectors $\mathbf{v}_\alpha$ and $\mathbf{v}_\beta$ is executed via the substitution $x = \cos\theta$:

$$H(v_\alpha) = 2\pi\sum_{l=0}^{\infty}\left[\int_0^\infty \frac{v_\beta^2\min^l(v_\alpha, v_\beta)}{\max^{l+1}(v_\alpha, v_\beta)}\left(\int_{-1}^{1}P_l(x)\,\mathrm{d}x\right)f_\beta(v_\beta)\,\mathrm{d}v_\beta\right].$$

The integration of Legendre polynomials simplifies via their symmetry property:

$$\int_{-1}^{1}P_l(x)\,\mathrm{d}x = 2\delta_{0l} \tag{1.755}$$

The Legendre polynomial integral is non-zero exclusively for $l = 0$, yielding a value of 2. Consequently, the infinite series collapses, leaving only the zeroth-order term:

$$H(v_\alpha) = 4\pi \int_0^\infty \frac{v_\beta^2 f_\beta(v_\beta)}{\max(v_\alpha, v_\beta)}\, \mathrm{d}v_\beta \qquad \Rightarrow$$

$$\blacktriangleright \qquad H(v_\alpha) = 4\pi \left[\frac{1}{v_\alpha} \int_0^{v_\alpha} v_\beta^2 f_\beta(v_\beta)\, \mathrm{d}v_\beta \; + \; \int_{v_\alpha}^\infty v_\beta f_\beta(v_\beta)\, \mathrm{d}v_\beta \right]. \tag{1.756}$$

The singularity within the original integrand divides the integration domain into two regions. This generalized formulation accommodates arbitrary isotropic target distribution functions f_β, such as Maxwellian or Fermi–Dirac distributions. Substituting the Maxwellian distribution (1.754) yields:

$$H(v_\alpha) = n_\beta \sqrt{\frac{m_\beta}{2k_\mathrm{B}T_\beta}}\, \frac{4}{\sqrt{\pi}}\, \frac{1}{x} \int_0^x \xi^2 \mathrm{e}^{-\xi^2}\, \mathrm{d}\xi \; + \; n_\beta \sqrt{\frac{m_\beta}{2k_\mathrm{B}T_\beta}}\, \frac{2}{\sqrt{\pi}}\, \mathrm{e}^{-x^2} \; ;$$

$$x \equiv \frac{v_\alpha}{\sqrt{2k_\mathrm{B}T_\beta/m_\beta}}.$$

This result can be recast via the Chandrasekhar function definition (1.749) as:

$$H(v_\alpha) = n_\beta \sqrt{\frac{m_\beta}{2k_\mathrm{B}T_\beta}} \left[2x\, \psi(x) \; + \; \frac{2}{\sqrt{\pi}}\, \mathrm{e}^{-x^2} \right].$$

Utilizing relation (1.753) directly yields the final expression for the potential H

$$\blacktriangleright \qquad H(v_\alpha) = \left(\frac{2k_\mathrm{B}T_\beta}{m_\beta} \right)^{-1/2} n_\beta\, \frac{\phi(x)}{x}\,; \qquad x \equiv \frac{v_\alpha}{\sqrt{2k_\mathrm{B}T_\beta/m_\beta}}. \tag{1.757}$$

Evaluation of the Potential G

The evaluation procedure is analogous, utilizing the structural identity:

$$\left|\mathbf{v}_\alpha - \mathbf{v}_\beta\right| = \frac{\left|\mathbf{v}_\alpha - \mathbf{v}_\beta\right|^2}{\left|\mathbf{v}_\alpha - \mathbf{v}_\beta\right|} = \frac{v_\alpha^2 - 2v_\alpha v_\beta \cos\theta + v_\beta^2}{\left|\mathbf{v}_\alpha - \mathbf{v}_\beta\right|}.$$

The denominator is expanded into a series of Legendre polynomials, proceeding identically to the evaluation of potential H:

$$G(v_\alpha) \equiv \int \left|\mathbf{v}_\alpha - \mathbf{v}_\beta\right| f_\beta\, \mathrm{d}^3\mathbf{v}_\beta = \int \frac{v_\alpha^2 - 2v_\alpha v_\beta \cos\theta + v_\beta^2}{\left|\mathbf{v}_\alpha - \mathbf{v}_\beta\right|} f_\beta\, \mathrm{d}^3\mathbf{v}_\beta =$$

$$= \sum_{l=0}^\infty \iiint f_\beta(v_\beta) \left(v_\alpha^2 - 2v_\alpha v_\beta \cos\theta + v_\beta^2 \right) \frac{\min^l(v_\alpha, v_\beta)}{\max^{l+1}(v_\alpha, v_\beta)} P_l(\cos\theta)\, v_\beta^2 \sin\theta\, \mathrm{d}\varphi\, \mathrm{d}\theta\, \mathrm{d}v_\beta =$$

$$= 2\pi \sum_{l=0}^{\infty} \left[\int_0^{\infty} \frac{\min^l(v_\alpha, v_\beta)}{\max^{l+1}(v_\alpha, v_\beta)} v_\beta^2 f_\beta(v_\beta) \left(\int_{-1}^{1} \left(v_\alpha^2 - 2v_\alpha v_\beta x + v_\beta^2 \right) P_l(x)\, \mathrm{d}x \right) \mathrm{d}v_\beta \right].$$

In accordance with (1.755), each integration over a Legendre polynomial retains a single non-zero term. An analogous procedure to potential H yields:

$$G(v_\alpha) = \frac{4\pi v_\alpha}{3} \left[\int_0^{v_\alpha} \left(3v_\beta^2 + \frac{v_\beta^4}{v_\alpha^2} \right) f_\beta(v_\beta)\, \mathrm{d}v_\beta + \int_{v_\alpha}^{\infty} \left(\frac{3v_\beta^3}{v_\alpha} + v_\alpha v_\beta \right) f_\beta(v_\beta)\, \mathrm{d}v_\beta \right]. \quad (1.758)$$

This expression remains valid for an arbitrary isotropic distribution f_β.. For a Maxwellian target, the evaluation proceeds analogously to potential H. The final result is expressed via the error function and its derivative:

► $$G(v_\alpha) = \left(\frac{2k_\mathrm{B}T_\beta}{m_\beta} \right)^{+1/2} n_\beta \left[x\phi(x) + \frac{\phi(x)}{2x} + \frac{1}{\sqrt{\pi}} \mathrm{e}^{-x^2} \right]; \quad x \equiv \frac{v_\alpha}{\sqrt{2k_\mathrm{B}T_\beta / m_\beta}}. \quad (1.759)$$

The first derivative of this potential with respect to velocity magnitude simplifies to:

$$\frac{\partial G(v_\alpha)}{\partial v_\alpha} = n_\beta \left[\phi(x) - \psi(x) \right]. \quad (1.760)$$

Decelerated and Runaway Test Particles

Consider a monochromatic beam α with uniform velocity and constant density injecting into a homogeneous, isotropic, Maxwellian background plasma, undergoing deceleration to a velocity $\mathbf{v}(t)$. No external force fields operate within the plasma. The beam distribution function is governed by a Dirac delta distribution, whereas the background target satisfies a Maxwellian framework:

$$f_\alpha = n_\alpha\, \delta\left(\mathbf{v}_\alpha - \mathbf{v}(t) \right);$$

$$f_\beta = n_\beta \left(\frac{m_\beta}{2\pi k_\mathrm{B} T_\beta} \right)^{3/2} \mathrm{e}^{-\frac{m v_\beta^2}{2k_\mathrm{B}T_\beta}}. \quad (1.761)$$

Consider the Fokker–Planck equation (1.747). The monochromatic beam behaves as a single test particle, exhibiting no velocity-space diffusion. Consequently, the analysis reduces to evaluating the first Rosenbluth potential H (friction term). Multiplying the Fokker–Planck equation by $\mathbf{v}_\alpha$ and integrating over velocity space evaluates its first moment. Because the distribution function f is spatially uniform ($\nabla f_\alpha = 0$), the second term on the left-hand side vanishes. In the absence of external fields, the third term also vanishes. The right-hand side incorporates exclusively the first Rosenbluth potential, as the second vanishes due to spatial isotropy:

$$\int \mathbf{v}_\alpha \frac{\partial f_\alpha}{\partial t} \mathrm{d}^3\mathbf{v}_\alpha = -K_{\alpha\beta} \ln \Lambda_{\alpha\beta} \int \mathbf{v}_\alpha \, \boldsymbol{\nabla}_\mathbf{v} \cdot \left(f_\alpha \boldsymbol{\nabla}_\mathbf{v} H \right) \mathrm{d}^3\mathbf{v}_\alpha \tag{1.762}$$

Substituting the Dirac delta distribution $n_\alpha \delta(\mathbf{v}_\alpha - \mathbf{v}(t))$ for the incident particle distribution function, averaging over the incident velocity coordinates is executed. Evaluating the left-hand side of relation (1.762) yields:

$$\mathbf{LHS} = \int \mathbf{v}_\alpha \frac{\partial f_\alpha}{\partial t} \mathrm{d}^3\mathbf{v}_\alpha = n_\alpha \int \mathbf{v}_\alpha \frac{\partial \delta\left(\mathbf{v}_\alpha - \mathbf{v}(t)\right)}{\partial t} \mathrm{d}^3\mathbf{v}_\alpha =$$

$$= n_\alpha \frac{\partial}{\partial t} \int \mathbf{v}_\alpha \delta\left(\mathbf{v}_\alpha - \mathbf{v}(t)\right) \mathrm{d}^3\mathbf{v}_\alpha = n_\alpha \frac{\partial \mathbf{v}}{\partial t}.$$

The remaining task is to evaluate the right-hand side of the Fokker–Planck relation:

$$\mathbf{RHS} = -K_{\alpha\beta} \ln \Lambda_{\alpha\beta} \int \mathbf{v}_\alpha \frac{\partial}{\partial \mathbf{v}_\alpha} \cdot \left(n_\alpha \delta\left(\mathbf{v}_\alpha - \mathbf{v}(t)\right) \frac{\partial H(\mathbf{v}_\alpha)}{\partial \mathbf{v}_\alpha} \right) \mathrm{d}^3\mathbf{v}_\alpha \overset{(1)}{=}$$

$$= n_\alpha K_{\alpha\beta} \ln \Lambda_{\alpha\beta} \int \left(\delta\left(\mathbf{v}_\alpha - \mathbf{v}(t)\right) \frac{\partial H(\mathbf{v}_\alpha)}{\partial \mathbf{v}_\alpha} \right) \mathrm{d}^3\mathbf{v}_\alpha =$$

$$= n_\alpha K_{\alpha\beta} \ln \Lambda_{\alpha\beta} \frac{\partial H(\mathbf{v})}{\partial \mathbf{v}}.$$

Label (1) denotes integration by parts. Retaining the second Rosenbluth potential would require a double integration by parts, yielding zero due to spatial isotropy. The first moment of the Fokker Planck equation for a test particle yields:

$$\frac{\partial \mathbf{v}}{\partial t} = K_{\alpha\beta} \ln \Lambda_{\alpha\beta} \frac{\partial H(\mathbf{v})}{\partial \mathbf{v}}; \qquad H(\mathbf{v}) \equiv n_\beta \frac{1}{v} \phi\left(\frac{v}{v_{0\beta}} \right). \tag{1.763}$$

Evidently, potential H governs the particle velocity variation, justifying its terminology as dynamical friction. Differentiating the right-hand side yields:

$$\frac{\partial}{\partial \mathbf{v}} \left(\frac{1}{v} \phi\left(v/v_{0\beta}\right) \right) = \frac{\partial}{\partial v} \left(\frac{1}{v} \phi\left(v/v_{0\beta}\right) \right) \frac{\partial v}{\partial \mathbf{v}} = \frac{\phi' \dfrac{v}{v_{0\beta}} - \phi}{v^2} \frac{\mathbf{v}}{v} = -2 v_{0\beta}^{-2} \psi\left(v/v_{0\beta}\right) \frac{\mathbf{v}}{v},$$

where the relation (1.751) for the Chandrasekhar function was utilized. The averaged Fokker–Planck equation (1.763) simplifies to the compact form:

$$\frac{\partial \mathbf{v}}{\partial t} = -K_{\alpha\beta} \ln \Lambda_{\alpha\beta} 2 n_\beta v_{0\beta}^{-2} \frac{\psi\left(v/v_{0\beta}\right)}{v} \mathbf{v}. \tag{1.764}$$

The result is intentionally structured as $\partial \mathbf{v}/\partial t = -\nu_{\alpha\beta} \mathbf{v}$, which explicitly isolates the collision frequency of a test particle traversing a Maxwellian background distribution:

$$\nu_{\alpha\beta} \equiv 2 K_{\alpha\beta} \ln \Lambda_{\alpha\beta} n_\beta v_{0\beta}^{-2} \frac{\psi\left(v/v_{0\beta}\right)}{v}. \tag{1.765}$$

Note 1: This method evaluates collision frequencies governing specific physical processes, whose inverse defines the relaxation time. Injecting a test particle and averaging the Fokker–Planck equation over a specific velocity moment yields the macroscopic evolution (momentum transport for the first moment, energy for the second). Restructuring to $\partial A/\partial t = -\nu A$ isolates the frequency ν, whose reciprocal value represents the relaxation time.

Note 2: Relaxation times and their corresponding frequencies scale differently depending on the specific transport process, as momentum equilibration and thermal energy equilibration with the surroundings occur at disparate rates.

Note 3: Generally, the second Rosenbluth potential also contributes, reflecting the velocity-space diffusion of the incident beam. The diffusion tensor is expressed as $D_{kl} = A\partial^2 G/\partial v_k \partial v_l$.

Note 4: In this framework, the collision frequency depends on the particle velocity via the functional scaling $\psi(v/v_0)/v$. For low velocities (e.g., standard Ohmic current conduction), the asymptotic expansion yields $\psi(x) \approx 2x/3\pi^{1/2}$, rendering the collision frequency velocity-independent. Conversely, for highly relativistic velocities, the scaling reduces to $\psi(x) \approx 1/2x^2$, causing the collision frequency to decay precipitously as $1/v^3$.

Note 5: Generally, collision frequencies must be evaluated numerically, particularly in the presence of fields or within non-Maxwellian plasma systems.

If a weak external electric field accelerates the particle, the macroscopic equation of motion is formulated as:

$$\frac{\mathrm{d}v}{\mathrm{d}t} = \frac{QE}{m} - \nu(v)v \qquad \Rightarrow \qquad \frac{\mathrm{d}v}{\mathrm{d}t} = \frac{QE}{m} - C\psi(v/v_0)\,. \tag{1.766}$$

Particle acceleration or deceleration depends on which term dominates.

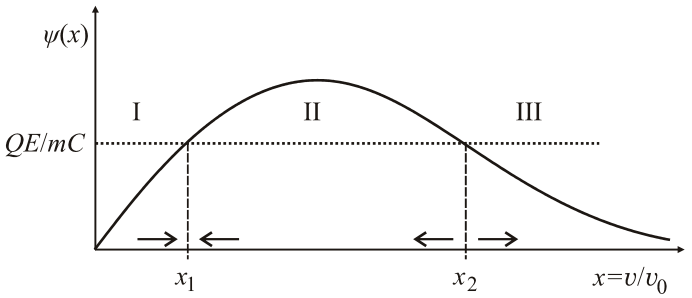


Fig. 1.117: Friction and acceleration regimes governing runaway particles.

In Region I, low-velocity particles accelerate via the electric field, as its force exceeds Chandrasekhar friction. Conversely, in Region II, friction dominates and decelerates particles. The equilibrium x_1 represents a stable node where field acceleration balances friction, resulting in constant drift velocity and standard Ohmic conduction.

In contrast, for velocities exceeding the crossover intersection x_2 (Region III), the particle undergoes *runaway acceleration*. The frictional interaction with the background plasma decays to a negligible level, allowing the electric field to continuously accelerate

the particle to progressively higher velocities. These entities are termed runaway particles, analyzed thoroughly in Section 1.7.2.

The equilibrium x_2 constitutes an unstable threshold. To trigger runaway acceleration, the initial velocity within a given field must exceed x_2. For instance, secondary electrons from atmospheric cosmic ray interactions can possess initial velocities exceeding this threshold within thundercloud electric fields. Such electrons achieve relativistic velocities, driving terrestrial gamma-ray flashes during thunderstorms and penetrating into the Van Allen radiation belts, where they act as *killer electrons* hazardous to spacecraft electronics and crews.

Relaxation Times and Collision Frequencies

Evaluating relaxation times or collision frequencies follows the preceding section methodology, primary requiring numerical computation. Analytical solutions always constitute approximations, typically valid for low velocities or small energy transfers, where the Chandrasekhar function can be expanded for a small argument. This analysis evaluates the velocity moments of the Fokker–Planck equation for specific transport phenomena. Generally, four distinct types of collision frequencies are computed:

1) test particle deceleration within the background plasma,
2) test particle diffusion perpendicular to the magnetic field,
3) test particle diffusion parallel to the magnetic field,
4) test particle energy loss.

The evaluated values are tabulated in the limits of low or high velocities, as found in the annually updated *NRL Plasma Formulary* [26]. For illustrative purposes, consider the collision frequency governing the deceleration of species α by the background species β. The evaluation of the first category computes the perpendicular velocity component transport because the time interval between collisions is defined by a 90° deflection of the particle velocity vector. This procedure yields the formulation:

$$\nu_{\alpha\beta} = n_\beta \frac{Q_\alpha^2 Q_\beta^2 \ln \Lambda_{\alpha\beta}}{2\pi\varepsilon_0^2 m_\alpha^2 v_{0\alpha}^3} \left[\phi(v_{0\alpha}/v_{0\beta}) - \psi(v_{0\alpha}/v_{0\beta}) \right] . \tag{1.767}$$

Evidently, $\nu_{ei} \sim Z\nu_{ee} >> \nu_{ii} >> \nu_{ie}$, driven primarily by the disparate masses and thermal velocities of electrons and ions. Within this formulation, $v_{0\alpha}$ represents the most probable velocity of the incident species at a given temperature, and $v_{0\beta}$ denotes the most probable velocity of the background target species. The basic collision frequencies satisfy the ratios:

$$\begin{array}{ccccccc} \nu_{ei} & : & \nu_{ee} & : & \nu_{ii} & : & \nu_{ie} \\ Z & : & 1 & : & \sqrt{m_e/m_i} & : & m_e/m_i \end{array} \tag{1.768}$$

◖ **Example 1.10:** Evaluate the electron conductivity in the limit of low velocities.

Solution: Substituting (1.767) into the conductivity formula (1.691) yields:

$$\sigma_{ee} \approx \frac{2m_e\pi\varepsilon_0^2}{e^2 \ln \Lambda \left[\phi(1) - \psi(1)\right]} \left(\frac{k_B T_e}{m_e} \right)^{3/2} ; \qquad \phi(1) - \psi(1) \approx 0,6 \qquad \Rightarrow$$

$$\sigma_{\mathrm{ee}} \approx \frac{10\pi}{3} \frac{m_{\mathrm{e}} \varepsilon_0^2}{e^2 \ln \Lambda} \left(\frac{k_{\mathrm{B}} T_{\mathrm{e}}}{m_{\mathrm{e}}} \right)^{3/2} \propto T_{\mathrm{e}}^{3/2} \,. \tag{1.769}$$

Plasma electron conductivity is independent of number density. Although a higher density increases charge carriers, potentially enhancing conductivity, it simultaneously scales the collision frequency, suppressing transport. These competing factors balance identically; thus, electrical conductivity depends exclusively on temperature. Formulation (1.769) represents the Spitzer formula, named after Lyman Spitzer. Under specific conditions, plasma can exhibit lower effective conductivity – termed *anomalous resistivity* – driven by drifts, turbulence, or wave-particle interactions.

1.6.5 Microinstabilities

Governing Relations

Transitioning from a statistical description to a fluid continuum (such as magnetohydrodynamics) removes the detailed kinetic information regarding the velocity-space distribution function within phase space. This transition filters out an entire class of microinstabilities driven by velocity-space particle distributions. This section focuses on linear instabilities within a collisionless plasma framework using a statistical approach. This configuration constitutes the opposite physical extreme compared to the collision-dominated continuum model; here, collisional interactions are neglected entirely, focusing exclusively on instabilities driven by wave-particle interactions. The governing kinetic framework utilizes the Vlasov equation for the species distribution function f_α:

$$\frac{\partial f_\alpha}{\partial t} + (\mathbf{v}_\alpha \cdot \boldsymbol{\nabla}_{\mathbf{x}}) f_\alpha + \frac{Q_\alpha}{m_\alpha} \left[(\mathbf{E} + \mathbf{v}_\alpha \times \mathbf{B}) \cdot \boldsymbol{\nabla}_{\mathbf{v}} \right] f_\alpha = 0 \,, \tag{1.770}$$

complemented by the Maxwell equations for the electromagnetic fields:

$$\boldsymbol{\nabla} \cdot \mathbf{D} = \rho_{\mathrm{Q}} \,, \tag{1.771}$$

$$\boldsymbol{\nabla} \cdot \mathbf{B} = 0 \,, \tag{1.772}$$

$$\boldsymbol{\nabla} \times \mathbf{E} = -\frac{\partial \mathbf{B}}{\partial t} \,, \tag{1.773}$$

$$\boldsymbol{\nabla} \times \mathbf{H} = \mathbf{j}_{\mathrm{Q}} + \frac{\partial \mathbf{D}}{\partial t} \,. \tag{1.774}$$

Particle kinetics and electromagnetic fields are coupled via the source terms:

$$\begin{aligned} \rho_{\mathrm{Q}} &= \sum_\alpha Q_\alpha n_\alpha = \sum_\alpha \int Q_\alpha f_\alpha \, \mathrm{d}^3 \mathbf{v}_\alpha \,, \\ \mathbf{j}_{\mathrm{Q}} &= \sum_\alpha Q_\alpha n_\alpha \mathbf{u}_\alpha = \sum_\alpha \int Q_\alpha \mathbf{v}_\alpha f_\alpha \, \mathrm{d}^3 \mathbf{v}_\alpha \,. \end{aligned} \tag{1.775}$$

This coupled system undergoes a linear perturbation analysis analogous to fluid continuum theory. The respective phenomena are classified into the following categories:

- *High-frequency unmagnetized processes*: a generalization of electrostatic plasma waves incorporating electron Landau damping.
- *Low-frequency unmagnetized processes*: a generalization of ion-acoustic waves incorporating ion Landau damping.
- *High-frequency magnetized processes*: mutual resonant interactions between particles and the electromagnetic wave complex.
- *Low-frequency magnetized processes*: mutual resonant interactions between particles and the magnetoacoustic wave complex.

Electron Landau Damping

Section 1.4.3 addressed electrostatic plasma waves associated with electron oscillations at the plasma frequency. These waves are driven exclusively by the self-consistent electric field, requiring no ambient background magnetic field. According to the dispersion relation derived from the fluid model, waves with frequencies exceeding the plasma frequency propagate without attenuation.

In reality, even linear kinetic theory predicts wave attenuation driven by the statistical behavior of resonant particles. This collisionless attenuation mechanism constitutes *Landau damping* (Lev Davidovich Landau, 1946). It cannot be derived via fluid models, where averaging the Boltzmann equation over velocity moments discards essential kinetic information. Consequently, the derivation requires the kinetic Boltzmann equation for the electron distribution function. Because this damping mechanism manifests without collisions, the collisionless Vlasov equation is utilized.

Consider a collisionless plasma to investigate electron interactions with longitudinal plasma waves near the electron plasma frequency in an infinite medium. Assuming the interaction is mediated solely by the electrostatic field ($\nabla \times \mathbf{E} = 0$) implies a longitudinal wave configuration with $\delta\mathbf{E} \parallel \mathbf{k}$. Aligning the coordinate frame such that the x-axis coincides with the wave propagation direction yields:

$$\mathbf{k} = (k, 0, 0); \qquad \delta\mathbf{E} = (\delta E, 0, 0). \tag{1.776}$$

A general harmonic perturbation takes the form:

$$\psi = \psi_0 + \delta\psi = \psi_0 + \psi_1 \, \mathrm{e}^{\mathrm{i}[kx - \omega t]}. \tag{1.777}$$

Tracking exclusively electron dynamics and neglecting ion motion near the plasma frequency reduces the governing equations ($Q_\mathrm{e} = -e$, $m = m_\mathrm{e}$) to:

$$\begin{gathered} \frac{\partial f}{\partial t} + \mathbf{v} \cdot \frac{\partial f}{\partial \mathbf{x}} - \frac{e}{m_\mathrm{e}} \mathbf{E} \cdot \frac{\partial f}{\partial \mathbf{v}} = 0, \\ \operatorname{div} \mathbf{E} = -\frac{en}{\varepsilon_0}, \\ n(t, \mathbf{x}) = \int f(t, \mathbf{x}, \mathbf{v}) \, \mathrm{d}^3\mathbf{v}, \end{gathered} \tag{1.778}$$

where $f = f(t, \mathbf{x}, \mathbf{v})$ is the electron distribution function. Crucially, the velocity coordinate $\mathbf{v}$ here acts as an independent phase-space variable rather than an averaged macroscopic fluid velocity. The electrostatic Poisson equation suffices because $\mathbf{B}_0 = 0$ and $\delta\mathbf{E} \parallel \mathbf{k}$ reduce the system to a one-dimensional problem. (In the presence of an ambient

magnetic field, the Maxwell–Faraday equation $\nabla \times \mathbf{E} = -\partial \mathbf{B}/\partial t$ must be incorporated). Linearizing the governing equations (1.778) via small-amplitude perturbations yields:

$$\begin{aligned} f &= f_0 + \delta f\,; \\ \mathbf{E} &= \delta \mathbf{E}\,; \\ n &= n_0 + \delta n\,. \end{aligned} \tag{1.779}$$

The unperturbed solution is assumed to be a stationary, homogeneous state (independent of t, x), governed by a Boltzmann velocity distribution f_0:

$$f_0(\mathbf{v}) \equiv n_0 \left(\frac{m_\mathrm{e}}{2\pi k_\mathrm{B} T} \right)^{3/2} \exp\left[-\frac{m_\mathrm{e} \mathbf{v}^2}{2 k_\mathrm{B} T} \right], \tag{1.780}$$

which factors into independent one-dimensional distribution functions:

$$f_0(\mathbf{v}) \equiv n_0 f_{0x}(v_x) f_{0y}(v_y) f_{0z}(v_z)\,, \tag{1.781}$$

where:

$$f_{0l}(v_l) \equiv \left(\frac{m_\mathrm{e}}{2\pi k_\mathrm{B} T} \right)^{1/2} \exp\left[-\frac{m_\mathrm{e} v_l^2}{2 k_\mathrm{B} T} \right]. \tag{1.782}$$

First-order linearization of the governing equations (1.778) yields:

$$\begin{aligned} \frac{\partial\, \delta f}{\partial t} + \mathbf{v} \cdot \frac{\partial\, \delta f}{\partial \mathbf{x}} - \frac{e}{m_\mathrm{e}} \delta \mathbf{E} \cdot \frac{\partial f_0}{\partial \mathbf{v}} &= 0\,, \\ \mathrm{div}\, \delta \mathbf{E} &= -\frac{e\, \delta n}{\varepsilon_0}\,, \\ \delta n(t, \mathbf{x}) &= \int \delta f(t, \mathbf{x}, \mathbf{v})\, \mathrm{d}^3 \mathbf{v}\,. \end{aligned} \tag{1.783}$$

Assuming planar perturbations $\delta\psi = \psi_1 \exp[\mathrm{i}(kx - \omega t)]$ moving along the x-axis yields:

$$\begin{aligned} -\mathrm{i}\omega\, \delta f + \mathrm{i} v_x k\, \delta f - \frac{e}{m_\mathrm{e}} \delta E_x \cdot \frac{\partial f_0}{\partial v_x} &= 0\,, \\ \mathrm{i} k\, \delta E_x &= -\frac{e\, \delta n}{\varepsilon_0}\,, \\ \delta n(t, x) &= \int \delta f\, \mathrm{d}^3 \mathbf{v}\,. \end{aligned} \tag{1.784}$$

Substituting δn from the second equation and δf from the first equation into the linearized Poisson relation, integration over the velocity coordinates v_y and v_z yields the kinetic dispersion relation:

► $$k^2 = \omega_\mathrm{p}^2 \int_{-\infty}^{+\infty} \frac{\mathrm{d} f_{0x}/\mathrm{d} v_x}{v_x - \omega/k}\, \mathrm{d} v_x\,; \qquad \omega_\mathrm{p}^2 \equiv \frac{n_0 e^2}{m_\mathrm{e} \varepsilon_0}\,. \tag{1.785}$$

The parameters relate exclusively to the electrons. The challenge is the first-order pole in the velocity space at $v_x = \omega/k$, corresponding to the wave phase velocity. Such integrals are evaluated via the residue theorem (see Section I.3.2.7 in the *Selected Topics I*, which also defines the Cauchy principal value, V.P.). The integration contour cannot be closed via an infinite semicircle in either the upper or lower complex half-plane because the integrand diverges at infinity along the imaginary axis due to the factor $\exp[-\alpha v^2]$). Consequently, the integration path follows the contour illustrated in Fig. 1.118:

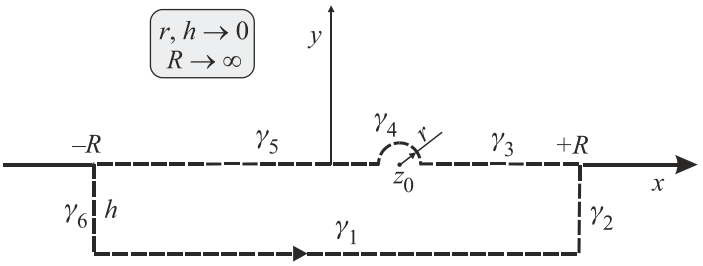


Fig. 1.118: Integration contour in the complex velocity plane for evaluating the Landau residue.

For a holomorphic function $g(z)$ in the numerator, the Cauchy theorem yields:

$$\oint_{\gamma} \frac{g(z)}{z-z_0}\,\mathrm{d}z \;=\; 2\pi\mathrm{i}\,\mathrm{Rez}\left(\frac{g(z)}{z-z_0}; z_0\right) \;=\; 2\pi\mathrm{i}g(z_0) = 2\pi\mathrm{i}g(x_0)\,.$$

The left-hand contour integral expands into a sum over individual segments:

$$\int_{\gamma_1} \frac{g(z)}{z-z_0}\,\mathrm{d}z \;+\; \int_{\gamma_2+\gamma_6} \frac{g(z)}{z-z_0}\,\mathrm{d}z \;+\; \int_{\gamma_3+\gamma_5} \frac{g(z)}{z-z_0}\,\mathrm{d}z \;+\; \int_{\gamma_4} \frac{g(z)}{z-z_0}\,\mathrm{d}z = 2\pi\mathrm{i}g(x_0)\,.$$

In the limit $h \to 0$, the line integrals over γ_2 and γ_6 vanish identically. Executing the limits $R \to \infty$ and $r \to 0$, the individual segments yield:

$$\int_{-\infty}^{+\infty} \frac{g(x)}{x-x_0}\,\mathrm{d}x \;+0+\; \lim_{\substack{R\to\infty\\ r\to 0}} \left(\int_{R}^{x_0+r} \frac{g(x)}{x-x_0}\,\mathrm{d}x \;+\; \int_{x_0-r}^{-R} \frac{g(x)}{x-x_0}\,\mathrm{d}x \right) + \int_{\gamma_4} \frac{g(z)}{z-z_0}\,\mathrm{d}z \;= 2\pi\mathrm{i}g(x_0)\,,$$

$$\int_{-\infty}^{+\infty} \frac{g(x)}{x-x_0}\,\mathrm{d}x \;-\; \lim_{\substack{R\to\infty\\ r\to 0}} \left(\int_{-R}^{x_0-r} \frac{g(x)}{x-x_0}\,\mathrm{d}x \;+\; \int_{x_0+r}^{R} \frac{g(x)}{x-x_0}\,\mathrm{d}x \right) + \int_{\gamma_4} \frac{g(z)}{z-z_0}\,\mathrm{d}z = 2\pi\mathrm{i}g(x_0)\,,$$

$$\int_{-\infty}^{+\infty} \frac{g(x)}{x-x_0}\,\mathrm{d}x \;-\; \mathrm{V.P.}\int_{-\infty}^{+\infty} \frac{g(x)}{x-x_0}\,\mathrm{d}x \;+\; \lim_{r\to 0} \int_{0}^{\pi} \frac{g(z_0 + r\,\mathrm{e}^{\mathrm{i}\varphi})}{r\,\mathrm{e}^{\mathrm{i}\varphi}}\,\mathrm{i}r\,\mathrm{e}^{\mathrm{i}\varphi}\,\mathrm{d}\varphi = 2\pi\mathrm{i}g(x_0)\,,$$

$$\int_{-\infty}^{+\infty} \frac{g(x)}{x-x_0}\,\mathrm{d}x \;-\; \mathrm{V.P.}\int_{-\infty}^{+\infty} \frac{g(x)}{x-x_0}\,\mathrm{d}x \;+\; \mathrm{i}\int_{0}^{\pi} g(x_0)\,\mathrm{d}\varphi \;= 2\pi\mathrm{i}g(x_0)\,,$$

$$\int_{-\infty}^{+\infty} \frac{g(x)}{x-x_0}\,\mathrm{d}x = \text{V.P.}\int_{-\infty}^{+\infty} \frac{g(x)}{x-x_0}\,\mathrm{d}x + \pi \mathrm{i} g(x_0) = I_1 + I_2 \,. \tag{1.786}$$

The first term represents the Cauchy principal value (see I.3.2.7 in the *Selected Topics I*), evaluated analytically as if the variable were strictly real and the pole did not exist, integrating across infinite boundaries. The integral I_1 lacks a closed-form analytical solution. For high-frequencies, a Taylor series expansion in powers of kv_x/ω yields:

$$I_1 \equiv \text{V.P.}\int_{-\infty}^{+\infty} \frac{\mathrm{d}f_{0x}/\mathrm{d}v_x}{v_x - \omega/k}\,\mathrm{d}v_x = -\frac{k}{\omega}\,\text{V.P.}\int_{-\infty}^{+\infty} \frac{\mathrm{d}f_{0x}/\mathrm{d}v_x}{1-\dfrac{kv_x}{\omega}}\,\mathrm{d}v_x =$$

$$= -\frac{k}{\omega}\int_{-\infty}^{+\infty}\left[1+\left(\frac{kv_x}{\omega}\right)+\left(\frac{kv_x}{\omega}\right)^2+\left(\frac{kv_x}{\omega}\right)^3+\cdots\right]\frac{\mathrm{d}f_{0x}}{\mathrm{d}v_x}\,\mathrm{d}v_x \,.$$

Integrating by parts, where the unperturbed distribution f_{0x} vanishes at the infinite integration boundaries, yields:

$$I_1 = \frac{k}{\omega}\int_{-\infty}^{+\infty}\left[\frac{k}{\omega}+2\frac{k^2}{\omega^2}v_x+3\frac{k^3}{\omega^3}v_x^2+\cdots\right] f_{0x}\,\mathrm{d}v_x =$$

$$= \frac{k}{\omega}\left[\frac{k}{\omega}+2\frac{k^2}{\omega^2}\langle v_x\rangle+3\frac{k^3}{\omega^3}\langle v_x^2\rangle+\cdots\right] = \frac{k^2}{\omega^2}++3\frac{k^4}{\omega^4}\frac{k_\mathrm{B}T_\mathrm{e}}{m_\mathrm{e}} \,.$$

Integrals of this Boltzmann form are standard within statistical physics [2]. The remaining task is to evaluate the second component, which constitutes π i times the residue of the integrand at the singularity. The mathematical procedure for residue evaluation is tabulated in the *Selected Topics I*, Section I.3.2.6:

$$I_2 = \mathrm{i}\pi\cdot\mathrm{Res}\left(\frac{\mathrm{d}f_{0x}/\mathrm{d}v_x}{v_x-\omega/k}\right) = \mathrm{i}\pi\left.\frac{\mathrm{d}f_{0x}}{\mathrm{d}v_x}\right|_{\frac{\omega}{k}} =$$

$$= -\mathrm{i}\pi\frac{m}{k_\mathrm{B}T_\mathrm{e}}\frac{\omega}{k}f_{0x}(\omega/k) \,.$$

The final expression executes the derivative of the Boltzmann distribution. Substituting both evaluated integral components into the dispersion relation (1.785) yields:

$$k^2 = \omega_\mathrm{p}^2\left[I_1+I_2\right] = \omega_\mathrm{p}^2\left[\frac{k^2}{\omega^2}+3\frac{k^4}{\omega^4}\frac{k_\mathrm{B}T_\mathrm{e}}{m_\mathrm{e}}+\cdots-\mathrm{i}\pi\frac{m}{k_\mathrm{B}T_\mathrm{e}}\frac{\omega}{k}f_{0x}(\omega/k)\right].$$

Algebraic simplification (multiplying the relation by ω^2/k^2) yields the kinetic dispersion relation in the form:

$$\omega^2 = \omega_\mathrm{p}^2+\frac{\omega_\mathrm{p}^2}{\omega^2}v_\mathrm{t}^2k^2+\cdots-\mathrm{i}\frac{3\pi\omega_\mathrm{p}^2}{v_\mathrm{t}^2}\frac{\omega^3}{k^3}f_{0x}(\omega/k) \,, \tag{1.787}$$

where the squared plasma frequency and thermal velocity are defined as:

$$\omega_{\mathrm{p}}^2 \equiv \frac{n_0 e^2}{m_{\mathrm{e}} \varepsilon_0}; \qquad v_{\mathrm{t}}^2 \equiv \frac{3 k_{\mathrm{B}} T_{\mathrm{e}}}{m_{\mathrm{e}}}.$$

Both parameters relate strictly to the electrons. The first term represents the classical cold plasma oscillations. The second term arises from thermal kinetic processes; if it remains small compared to the first term, approximating $\omega \sim \omega_{\mathrm{p}}$ recovers the standard warm plasma wave dispersion. The final term is completely new, representing the collisionless Landau damping mechanism, which is typically small compared to the first two terms. This smallness allows a binomial expansion of expression (1.787):

$$\omega^2 = a - \mathrm{i}\, b; \qquad b \ll a; \qquad \Rightarrow$$

$$\omega^2 = A \exp[\mathrm{i}\varphi]; \qquad A = \sqrt{a^2 + b^2} \sim a; \qquad \mathrm{tg}\,\varphi = \mathrm{arctg}(-b/a) \approx -\frac{b}{a} \qquad \Rightarrow$$

$$\omega^2 \approx a \exp\left[-\mathrm{i}\frac{b}{a}\right] \qquad \Rightarrow$$

$$\omega \approx \sqrt{a}\cos\left(-\frac{b}{2a}\right) + \mathrm{i}\sqrt{a}\sin\left(\frac{-b}{2a}\right) \approx \sqrt{a} - \mathrm{i}\frac{b}{2\sqrt{a}}.$$

The resulting complex frequency yields (the imaginary part from (1.787) is negative):

$$\blacktriangleright \qquad \omega \approx \omega_0 - \mathrm{i}\frac{3\pi\omega_{\mathrm{p}}^2}{2 v_{\mathrm{t}}^2 \omega_0}\frac{\omega^3}{k^3} f_{0x}(\omega/k); \qquad \omega_0 \equiv \sqrt{\omega_{\mathrm{p}}^2 + \frac{\omega_{\mathrm{p}}^2}{\omega^2} v_{\mathrm{t}}^2 k^2 + \cdots}. \qquad (1.788)$$

Physical Interpretation of Landau Damping

Equation (1.788) demonstrates that the imaginary part of the frequency is negative, confirming wave attenuation. The derivation of this collisionless attenuation via contour integration initially represented a surprising theoretical result, subsequently verified by experiments. Plasma waves undergo damping without particle collisions. This mechanism is analogous to a surfer on a wave crest; electrons track the longitudinal electrostatic plasma wave. Particles with velocities far from the phase velocity experience phase-mixing and exchange no net energy. Conversely, resonant electrons with velocities close to the phase velocity (corresponding to the pole in the complex integration) undergo strong energy exchange. If the initial electron velocity is slightly below the phase velocity, particles accelerate by trapping energy from the electric field. If their velocity exceeds the phase velocity, particles decelerate, transferring kinetic energy back into the wave field.

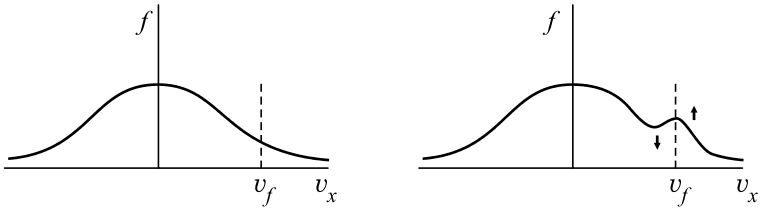


Fig. 1.119. Physical mechanism of Landau damping in velocity space.

According to the Boltzmann distribution, the thermal population contains more slow electrons than fast ones. Consequently, net wave attenuation dominates via energy absorption from the field. This represents the physical basis of Landau damping. The unperturbed distribution function deforms, generating a resonant perturbation that appears as a secondary peak (δf). The resulting velocity distribution exhibits two local maxima, potentially triggering a secondary two-stream (Buneman) instability. At extremely low phase velocities, Landau damping driven by resonant ions also becomes accessible.

Laser Wake Field Accelerators (LWFA)

Conventional particle accelerators utilize circular trajectories within betatrons or synchrotrons, exemplified by the Tevatron facility with a 6.3-km circumference. Alternative configurations employ linear radio-frequency structures with oscillating electric fields. However, the accelerating fields in these conventional cavities are limited to approximately 100 MV/m due to material breakdown. In 1979, Toshiki Tajima and John Myrick Dawson proposed a novel accelerator paradigm utilizing a plasma wave to accelerate electrons, analogous to a surfer riding a wake. This concept transition to practical implementation required over a quarter of a century. Modern table-top setups now routinely achieve high-gradient electron acceleration.

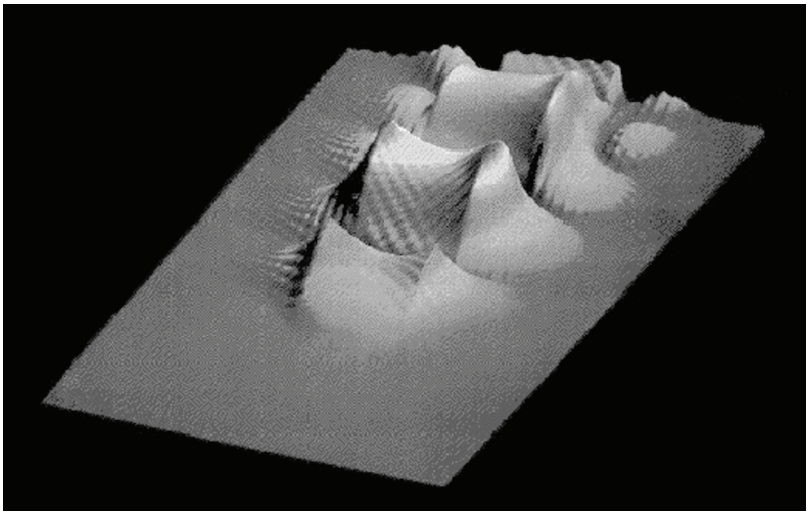


Fig. 1.120: Electrostatic wakefield generated behind an intense laser pulse propagating through a plasma medium. The gray scale indicates the longitudinal field intensity.

An intense laser pulse propagating through a gaseous medium ionizes the gas into a plasma and drags the lighter electrons along. This effect generates a localized electron density perturbation and a longitudinal electrostatic wakefield directly behind the pulse.

Under optimal momentum and energy conditions, a co-propagating electron can be trapped and accelerated by the electrostatic wave. Only a fraction of the background electrons undergo trapping, forming discrete accelerated bunches. This process constitutes the fundamental principle of a Laser Wake Field Accelerator (LWFA). Practical devices typically employ short (≤ 1 ps), high-intensity ($\geq 10^{18}$ W/cm^2) laser pulses. The generated wakefield routinely reaches gradients of 100 GV/m, exceeding conventional

RF cavity limits by three orders of magnitude. Electron bunches containing 10^9 particles (several hundred picocoulombs) accelerate up to energies of 60 MeV. However, this represents a minute fraction of the total plasma inventory, and controlling the ambient plasma and wakefield parameters remains challenging. Consequently, early single-pulse configurations served primarily as proof-of-principle laboratory studies.

The architecture advanced significantly after 2004 with the introduction of multi-pulse LWFA configurations. In addition to the primary drive pulse generating the wakefield, two auxiliary pulses interfere to establish a trailing optical standing wave. The longitudinal electric field component provides electron pre-acceleration, while the transverse component focuses the electron bunch. These auxiliary pulses permit active control over the plasma parameters within the wake. Acceleration in this configuration follows a two-stage process. Electrons are initially pre-accelerated in a slowly moving ($\Delta\omega/2k_0$) standing wave generated by the auxiliary pulses, before injection into the relativistic ($\sim c$) wakefield of the main drive pulse. Modern systems achieve accelerating wakefields up to 270 GV/m, yielding monoenergetic electron beams with energies up to 250 MeV within a 2-mm propagation length.

LWFA technologies revolutionize charged particle acceleration by significantly reducing the required physical footprint, enabling table-top configurations. Pre-acceleration via auxiliary pulses provides the parameter control necessary for practical applications. Ongoing development continues at the University of Colorado, UCB, UCLA, LLNL, and other research institutions

Maximum Longitudinal Field δE

The maximum attainable field magnitude can be estimated from the governing equation $\mathrm{div}\,\mathbf{E} = -e\delta n/\varepsilon_0$:

$$\mathrm{i}\,k\,\delta E = -e\,\delta n/\varepsilon_0 \qquad \Rightarrow$$

$$(\delta E)_{\max} < \left| \mathrm{i}\frac{e\delta n}{k\varepsilon_0} \right| < \frac{en_0}{k\varepsilon_0} = \frac{m_\mathrm{e}\omega_\mathrm{p}^2}{ke} = \frac{\omega_\mathrm{p}}{k}\frac{m_\mathrm{e}\omega_\mathrm{p}}{e} < \frac{cm_\mathrm{e}\omega_\mathrm{p}}{e}.$$

Consequently, the maximum accelerating gradient scales according to the relation:

► $$(\delta E)_{\max} < \frac{cm_\mathrm{e}\omega_\mathrm{p}}{e}. \tag{1.789}$$

Ion Landau Damping

Analogous to electron trapping within electrostatic plasma waves, ions can become trapped by ion waves. These structures represent the plasma equivalent of acoustic waves, frequently termed ion-acoustic waves. Due to the large mass disparity between electrons and ions, their respective Boltzmann velocity distributions differ substantially, as illustrated in Fig. 1.121.

For ion-acoustic waves, the primary restoring force is governed by the macroscopic thermal pressure of the hot electron species combined with ion inertia, rather than the self-consistent electrostatic field alone. The corresponding ion-acoustic dispersion relation was derived in Section~1.4.3, yielding expression (1.387):

$$\omega^2 = \omega_{\mathrm{pi}}^2 \left[1 + c_{\mathrm{i}}^2 k^2 / \omega_{\mathrm{pi}}^2 - \frac{1}{1 + c_{\mathrm{e}}^2 k^2 / \omega_{\mathrm{pe}}^2} \right]. \tag{1.790}$$

In the long-wavelength limit ($k \to 0$), this relation reduces to the form:

$$\omega = c_{\mathrm{i}} k \sqrt{1 + Z \frac{\gamma_{\mathrm{e}} T_{\mathrm{e}}}{\gamma_{\mathrm{i}} T_{\mathrm{i}}}}.$$

Consequently, the phase velocity of long-wavelength ion-acoustic waves is defined as:

$$v_{\mathrm{f}} = c_{\mathrm{i}} \sqrt{1 + Z \frac{\gamma_{\mathrm{e}} T_{\mathrm{e}}}{\gamma_{\mathrm{i}} T_{\mathrm{i}}}}. \tag{1.791}$$

Equation (1.791) demonstrates that under thermal equilibrium ($T_{\mathrm{e}} \approx T_{\mathrm{i}}$), the wave phase velocity corresponds to the region v_{f1} in Fig. 1.121. This velocity coincides with the steepest gradient of the ion Boltzmann distribution, allowing a significant population of ions to resonate with the ion-acoustic wave. Energy is absorbed from the wave by ions traveling slightly slower than the phase velocity, whereas resonant ions traveling faster transfer kinetic energy back into the wave field. Because the population of slower ions is substantially larger, the ion-acoustic wave undergoes strong attenuation via ion Landau damping phenomenon.

Conversely, when $T_{\mathrm{e}} >> T_{\mathrm{i}}$, the wave phase velocity shifts to the region v_{f2} in Fig. 1.121. In this domain, the probability density gradient is minimal and the absolute number of resonant ions is negligible. Under these conditions, ion Landau damping becomes negligible, allowing the ion-acoustic wave to propagate nearly unattenuated. An elevated electron temperature relative to the ion temperature ($T_{\mathrm{e}} >> T_{\mathrm{i}}$) thus ensures the propagation of long-wavelength ion-acoustic modes.

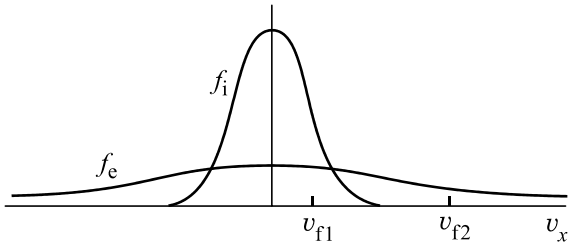


Fig. 1.121: Boltzmann velocity distributions for electrons and ions, indicating resonant phase velocity domains.

In the short-wavelength limit, relation (1.790) reduces to $\omega \approx c_{\mathrm{i}} k$, yielding the short-wavelength ion wave phase velocity:

$$v_{\mathrm{f}} \approx c_{\mathrm{i}}. \tag{1.792}$$

For short waves, the phase velocity of the ion-acoustic wave lies in the v_{f1} region in Figure 1.121, and the Landau damping on ions is always substantial.

Bernstein Modes

The presence of an ambient magnetic field introduces substantial complexity to wave-particle interactions. This problem was first solved analytically by Ira B. Bernstein in 1958. Consider ion-acoustic waves propagating in the presence of an external magnetic field. Comprehensive analysis indicates that wave propagation depends strongly on both the propagation angle and the wave frequency. The modes undergo attenuation via ion cyclotron resonance as well as ion Landau damping.

Perpendicular to the magnetic field ($\mathbf{k} \perp \mathbf{B}_0$), attenuation decreases significantly, permitting wave propagation provided the frequency does not coincide with harmonics (integer multiples) of the ion cyclotron frequency. These waves are designated as *Bernstein modes*; the real part of their frequency lies bounded between two consecutive harmonics of the ion cyclotron frequency:

$$m\,\omega_{\mathrm{ci}} < \left|\mathrm{Re}(\omega)\right| < (m+1)\omega_{\mathrm{ci}}\,; \qquad m = 1, 2, 3, \ldots \tag{1.793}$$

The imaginary frequency component, responsible for attenuation, increases sharply as the propagation deviates from perpendicularity ($\mathbf{k}\cdot\mathbf{B} \neq 0$). Furthermore, damping scales directly with the mode number m, meaning only the lowest-order Bernstein modes propagate nearly unattenuated. The electric field perturbation of Bernstein modes aligns approximately parallel to the wave vector $\mathbf{k}$.

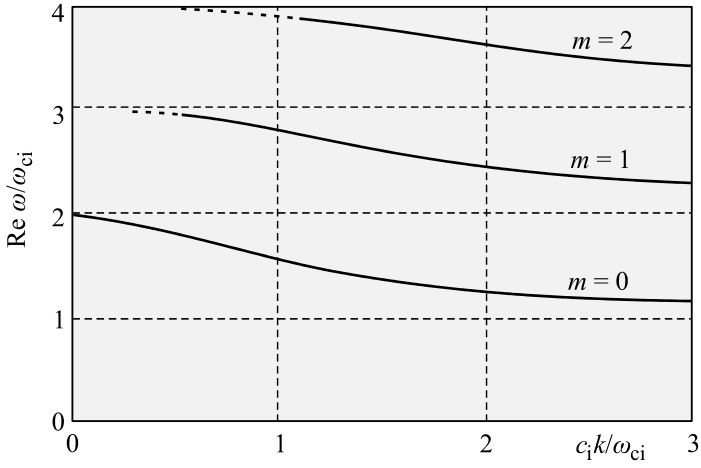


Fig. 1.122: Dispersion curves for the first three ion Bernstein modes. The horizontal axis represents the dimensionless wave vector, and the vertical axis indicates the real part of the dimensionless frequency.

An analogous family of Bernstein modes exists for the electron species. These electron plasma wave modes likewise propagate perpendicular to the ambient magnetic field, where damping is minimized, with frequencies bounded between consecutive harmonics of the electron cyclotron frequency.

1.7 Topics in Nonlinear Phenomena

The following section addresses several compelling nonlinear phenomena: the dynamics of a radiating particle whose momentum is modified by its own electromagnetic emission, the problem of runaway electrons capable of damaging experimental plasma devices, soliton solutions manifesting as isolated waves propagating through space, and specific aspects of turbulent plasma behavior.

1.7.1 Equation of Motion of a Radiating Particle

An accelerating charged particle emits electromagnetic radiation. The resulting loss of momentum and energy due to this self-emission modifies the trajectory of the particle. Formulating a completely consistent and satisfactory description of this radiation reaction remains an open problem in classical electrodynamics.

Potentials Generated in the Vicinity of a Particle

Consider the retarded and advanced four-potentials generated by a charged particle:

$$A^{\alpha}_{\mathrm{ret}}(t,\mathbf{r}) = A^{\alpha}_{-}(t,\mathbf{r}) = \frac{\mu_0}{4\pi}\int \frac{J^{\alpha}(t-\Delta t,\mathbf{r}')}{|\mathbf{r}-\mathbf{r}'|}\,\mathrm{d}^3\mathbf{r}' \tag{1.794}$$

$$A^{\alpha}_{\mathrm{adv}}(t,\mathbf{r}) = A^{\alpha}_{+}(t,\mathbf{r}) = \frac{\mu_0}{4\pi}\int \frac{J^{\alpha}(t+\Delta t,\mathbf{r}')}{|\mathbf{r}-\mathbf{r}'|}\,\mathrm{d}^3\mathbf{r}' \tag{1.795}$$

Formally, both potentials are expressed compactly as:

$$A^{\alpha}_{\mp}(t,\mathbf{r}) = \frac{\mu_0}{4\pi}\int \frac{J^{\alpha}(t\mp\Delta t,\mathbf{r}')}{|\mathbf{r}-\mathbf{r}'|}\,\mathrm{d}^3\mathbf{r}'\,. \tag{1.796}$$

In the immediate vicinity of the particle, the time interval between emission and observation is small. Consequently, a Taylor series expansion of the four-current is executed in powers of Δt:

$$A^{\alpha}_{\mp}(t,\mathbf{r}) = \frac{\mu_0}{4\pi}\int \left(\sum_{k=0}^{\infty}\frac{(\mp\Delta t)^k}{k!}\frac{\partial^k J^{\alpha}(t,\mathbf{r}')}{\partial t^k}\right)\frac{\mathrm{d}^3\mathbf{r}'}{|\mathbf{r}-\mathbf{r}'|}\,. \tag{1.797}$$

Substituting the retarded time from the relation

$$\Delta t = \frac{|\mathbf{r}-\mathbf{r}'|}{c} \tag{1.798}$$

yields the four-potential (assuming interchangeable summation and integration). Hereafter, only the retarded potential is tracked due to causality:

$$A^{\alpha}(t,\mathbf{r}) = \frac{\mu_0}{4\pi}\sum_{k=0}^{\infty}\left[\frac{(-1)^k}{c^k k!}\frac{\partial^k}{\partial t^k}\int |\,\mathbf{r}-\mathbf{r}'\,|^{k-1}\,J^{\alpha}(t,\mathbf{r}')\,\mathrm{d}^3\mathbf{r}'\right], \tag{1.799}$$

The resulting expansion is separated into even and odd terms:

$$\begin{aligned} A^{\alpha}(t,\mathbf{r}) = {} & \frac{\mu_0}{4\pi}\sum_{k=0,2,4}^{\infty}\left[\frac{1}{c^k k!}\frac{\partial^k}{\partial t^k}\int |\,\mathbf{r}-\mathbf{r}'\,|^{k-1}\,J^{\alpha}(t,\mathbf{r}')\,\mathrm{d}^3\mathbf{r}'\right] \mp \\ & - \frac{\mu_0}{4\pi}\sum_{k=1,3,5}^{\infty}\left[\frac{1}{c^k k!}\frac{\partial^k}{\partial t^k}\int |\,\mathbf{r}-\mathbf{r}'\,|^{k-1}\,J^{\alpha}(t,\mathbf{r}')\,\mathrm{d}^3\mathbf{r}'\right], \end{aligned} \tag{1.800}$$

The even components diverge on the particle worldline (for $k = 0$), corresponding to Coulomb-like fields. Although these fields diverge, the resulting force configuration for all even terms is symmetric relative to the particle, yielding a zero net force. Conversely, the odd component yields a non-vanishing net force, representing the radiation reaction to its own self-field.

This reaction force is evaluated within a co-moving, locally inertial Lorentz coordinate frame associated with an initial phase of the particle motion. In this localized frame, a non-relativistic approximation is valid, and tracking only the first non-vanishing term suffices. The final solution is subsequently transformed back into a general inertial frame to restore manifest covariance. For the scalar potential, the $k = 1$ term vanishes identically because the corresponding integral yields the total charge, whose time derivative is zero. Thus, the first non-vanishing contribution occurs at $k = 3$:

$$\frac{\phi}{c} = -\frac{\mu_0}{4\pi}\frac{1}{c^3 3!}\frac{\partial^3}{\partial t^3}\int |\,\mathbf{r}-\mathbf{r}'\,|^2\,\rho_Q(t,\mathbf{r}')\,c\,\mathrm{d}^3\mathbf{r}' \tag{1.801}$$

For the vector potential, the first non-vanishing term occurs at $k = 1$:

$$\mathbf{A} = -\frac{\mu_0}{4\pi}\frac{1}{c}\frac{\partial}{\partial t}\int \mathbf{j}_Q(t,\mathbf{r}')\,\mathrm{d}^3\mathbf{r}' \tag{1.802}$$

For a point particle characterized by the worldline $x_0^{\alpha}(\tau)$, the current density reduces to:

$$\rho_Q(t,\mathbf{r}) = Q\,\delta(\mathbf{r}'-\mathbf{r}_0), \tag{1.803}$$

$$\mathbf{j}_Q(t,\mathbf{r}) = Q\,\mathbf{v}\,\delta(\mathbf{r}'-\mathbf{r}_0). \tag{1.804}$$

Following integration, the corresponding potentials in the immediate vicinity of the particle yield:

► $$\phi = -\frac{\mu_0 Q}{24\pi c}\frac{\partial^3}{\partial t^3}\big(\mathbf{r}-\mathbf{r}_0(t)\big)^2, \tag{1.805}$$

► $$\mathbf{A} = -\frac{\mu_0 Q}{4\pi c}\frac{\mathrm{d}}{\mathrm{d}t}\mathbf{v}(t). \tag{1.806}$$

Abraham–Lorentz Equation of Motion

The corresponding self-fields are:

$$\mathbf{B} = \operatorname{curl} \mathbf{A} = 0\,, \tag{1.807}$$

$$\begin{aligned}
\mathbf{E} &= -\nabla\phi - \frac{\partial \mathbf{A}}{\partial t} = \\
&= \frac{\mu_0 Q}{24\pi c}\frac{\partial^3}{\partial t^3}\nabla\left(\mathbf{r} - \mathbf{r}_0(t)\right)^2 + \frac{\partial}{\partial t}\frac{\mu_0 Q}{4\pi c}\frac{\mathrm{d}}{\mathrm{d}t}\mathbf{v}(t) = \\
&= \frac{\mu_0 Q}{24\pi c}\frac{\partial^3}{\partial t^3} 2\left(\mathbf{r} - \mathbf{r}_0\right) + \frac{\mu_0 Q}{4\pi c}\frac{\mathrm{d}\mathbf{a}}{\mathrm{d}t} = \\
&= -\frac{\mu_0 Q}{12\pi c}\frac{\mathrm{d}\mathbf{a}}{\mathrm{d}t} + \frac{\mu_0 Q}{4\pi c}\frac{\mathrm{d}\mathbf{a}}{\mathrm{d}t} = \frac{\mu_0 Q}{6\pi c}\frac{\mathrm{d}\mathbf{a}}{\mathrm{d}t}.
\end{aligned} \tag{1.808}$$

To determine the force on the particle itself, an detector located at position $\mathbf{r}$ approaches the particle at $\mathbf{r}_0$. Consequently, the radiation reaction force takes the form:

$$\mathbf{F}_{\mathrm{rad}} = Q\,\mathbf{E} = \frac{\mu_0 Q^2}{6\pi c}\dot{\mathbf{a}} \tag{1.809}$$

This mechanism constitutes the Abraham–Lorentz force, named after the German physicist Max Abraham, who derived its formulation in 1905 [48]. The corresponding governing equation is designated as the Abraham–Lorentz (AL) equation of Motion:

► $$m_0\mathbf{a} = \mathbf{F}_{\mathrm{ext}} + \frac{\mu_0 Q^2}{6\pi c}\dot{\mathbf{a}} \tag{1.810}$$

Within the co-moving local Lorentz frame of the particle, the distinction between rest mass and relativistic mass vanishes, allowing the equation of motion to reduce to:

$$m_0\,\ddot{\mathbf{r}} = \mathbf{F}_{\mathrm{ext}} + m_0\,\tau_0\dddot{\mathbf{r}}\,;$$

► $$\tau_0 \equiv \frac{\mu_0 Q^2}{6\pi c m_0}. \tag{1.811}$$

The constant τ_0 has the dimension of time, and its physical interpretation is analyzed below. For an electron, its value is approximately 10^{-24} s. Three fundamental pathologies of this equation are immediately apparent:

I. The third-order time derivative requires an ambiguous initial condition
Classical mechanics uniquely defines the state of a system via its position and velocity (momentum). The initial position and velocity determine the integration constants arising during the solution of the equation of motion. However, the presence of a third-order time derivative introduces additional integration constants whose physical significance is ambiguous and, from the standpoint of classical mechanics, redundant.

II. In the absence of an external force, non-physical runaway solutions exist
One such solution is readily obtained by setting the external force to zero and integrating equation (1.811) three consecutive times, assuming the first and second integration constants vanish:

$$\begin{aligned} \dddot{\mathbf{r}} &= \tau_0 \ddot{\mathbf{r}}, \\ \ddot{\mathbf{r}} &= \tau_0 \dot{\mathbf{r}}, \\ \dot{\mathbf{r}} &= \tau_0 \mathbf{r}, \\ \mathbf{r} &= \mathbf{r}_0 \, \mathrm{e}^{t/\tau_0}. \end{aligned} \tag{1.812}$$

This result represents a *runaway solution*. Such behavior is non-physical, as a particle cannot experience exponential acceleration without any external force acting upon it. The Abraham–Lorentz equation thus yields solutions that do not correspond to physical reality. The general solution for a free particle (with zero external force) is expressed as:

$$\mathbf{r}(t) = \mathbf{c}_0 \, \mathrm{e}^{t/\tau_0} + \mathbf{c}_1 t + \mathbf{c}_2. \tag{1.813}$$

Choosing $\mathbf{c}_0 = 0$ eliminates the non-physical runaway solution, thereby reducing the number of integration constants to a physically acceptable count.

III. Abraham–Lorentz equation yields solutions violating causality

For an external force acting after t_0, the solution at $t < t_0$ depends on its future values, which is physically unacceptable. Such non-causal solutions exist for any external force that depends solely on time, as exemplified by this solution:

$$\mathbf{a} = \frac{1}{m_0 \tau_0} \int_t^\infty \mathbf{F}_{\mathrm{ext}}(t') \, \mathrm{e}^{-\frac{(t'-t)}{\tau_0}} \, \mathrm{d}t'. \tag{1.814}$$

Differentiating both sides of equation (1.814) with respect to time verifies that it satisfies the AL equation. For the derivative of the right-hand side, each occurrence of the variable t is differentiated independently via the Leibniz integral rule:

$$\frac{\mathrm{d}}{\mathrm{d}t} \int_C^t f(t,t') \, \mathrm{d}t' = f(t,t) + \int_C^t \frac{\partial f(t,t')}{\partial t} \mathrm{d}t' \tag{1.815}$$

yielding:

$$\frac{\mathrm{d}\mathbf{a}}{\mathrm{d}t} = -\frac{1}{m_0 \tau_0} \mathbf{F}_{\mathrm{ext}}(t) + \frac{1}{m_0 \tau_0^2} \int_t^\infty \mathbf{F}_{\mathrm{ext}}(t') \, \mathrm{e}^{-\frac{(t'-t)}{\tau_0}} \, \mathrm{d}t'. \tag{1.816}$$

The negative sign in the first term arises from interchanging integration limits to differentiate by the upper bound. Isolating the integral from (1.814) yields:

$$\frac{\mathrm{d}\mathbf{a}}{\mathrm{d}t} = -\frac{1}{m_0 \tau_0} \mathbf{F}_{\mathrm{ext}}(t) + \frac{1}{\tau_0} \mathbf{a} \quad \Rightarrow \tag{1.817}$$

$$m_0 \mathbf{a} = \mathbf{F}_{\mathrm{ext}}(t) + m_0 \tau_0 \frac{\mathrm{d}\mathbf{a}}{\mathrm{d}t}, \tag{1.818}$$

which recovers the AL equation, confirming that acceleration formulation (1.814) is a valid solution. However, the instantaneous acceleration is computed from the future values of the external force $\mathbf{F}_{\mathrm{ext}}(t)$, rendering the solution manifestly non-causal. The future force is integrated with an exponentially decaying weight, dictating the acceleration by the immediate future. The characteristic time constant τ_0 is designated as the *pre-acceleration* time. For an electron, this value is approximately 10^{-24} s.

The power associated with the generation of self-fields is expressed as:

$$P = \mathbf{F}_{\text{rad}} \cdot \mathbf{v} = m_0 \tau_0 \, \dot{\mathbf{a}} \cdot \mathbf{v} = m_0 \tau_0 \left[\frac{\mathrm{d}}{\mathrm{d}t} (\mathbf{a} \cdot \mathbf{v}) - \mathbf{a}^2 \right]. \tag{1.819}$$

This power vanishes at constant velocity, but the particle radiates during periodic motion; then, its time-averaged first component vanishes, yielding:

$$\langle P \rangle = -\frac{\mu_0 Q^2}{6\pi c} \langle a^2 \rangle . \tag{1.820}$$

Consequently, the particle loses energy via radiation as physically expected, confirming that the energy balance of the AL equation remains consistent. Substituting the acceleration of an oscillatory motion into this relation recovers the standard Larmor formula for dipole radiation (see *Selected Topics II*).

Lorentz–Dirac Equation of Motion

Outside the particle local co-moving Lorentz frame, covariant generalization of the equation of motion (1.811) to an arbitrary reference frame takes the form:

► $$m_0 \frac{\mathrm{d}U^\alpha}{\mathrm{d}\tau} = F^\alpha_{\text{ext}} + m_0 \tau_0 \left(\frac{\mathrm{d}a^\alpha}{\mathrm{d}\tau} - \frac{a^2}{c^2} U^\alpha \right); \qquad a^2 \equiv a^\beta a_\beta . \tag{1.821}$$

The second term in the parentheses ensures the correct normalization of the four-vectors. Multiplying the equation containing the external Lorentz force by U_α yields:

$$m_0 \frac{\mathrm{d}U^\alpha}{\mathrm{d}\tau} U_\alpha = Q F^{\alpha\beta} U_\beta U_\alpha + m_0 \tau_0 \left(\frac{\mathrm{d}a^\alpha}{\mathrm{d}\tau} U_\alpha - \frac{a^2}{c^2} U^\alpha U_\alpha \right)$$

The left-hand side vanishes because the four-acceleration is always orthogonal to the four-velocity (see *Selected Topics II*, expression II.3.99). The first term on the right-hand side also vanishes as a contraction of a symmetric and an antisymmetric tensor. The third term is modified via the product rule for differentiation, and the fourth term incorporates the four-velocity magnitude from the relation $U_\alpha U^\alpha = -c^2$:

$$0 = 0 + m_0 \tau_0 \left(\frac{\mathrm{d}}{\mathrm{d}\tau} \left(a^\alpha U_\alpha \right) - a^\alpha a_\alpha - \frac{a^2}{c^2} (-c^2) \right)$$

The first term in the parentheses vanishes due to the orthogonality of four-velocity and four-acceleration, causing the remaining terms to cancel identically:

$$0 = 0 + m_0 \tau_0 \left(0 - a^2 + a^2 \right)$$

Without the final compensating term, the Lorentz–Dirac equation (1.821) would lack manifest covariance. This relation was derived by the British physicist Paul A. M. Dirac) in 1938 utilizing four-momentum conservation of the combined particle-field system [49]. The present derivation follows the review article [51]. The compensating term can be transformed into its most common formulation by utilizing the identity $a_\beta U^\beta = 0$:

$$a^2 U^\alpha = a^\beta a_\beta U^\alpha = a^\beta \frac{\mathrm{d}U_\beta}{\mathrm{d}\tau} U^\alpha = \left(\frac{\mathrm{d}}{\mathrm{d}\tau}\left(a^\beta U_\beta\right) - \frac{\mathrm{d}a^\beta}{\mathrm{d}\tau} U_\beta \right) U^\alpha = -\frac{\mathrm{d}a^\beta}{\mathrm{d}\tau} U^\alpha U_\beta \,.$$

Consequently, the Lorentz–Dirac equation can be expressed in an alternative form, where the radiation reaction force is proportional to the proper-time derivative of acceleration, analogous to the AL equation:

► $$m_0 \frac{\mathrm{d}U^\alpha}{\mathrm{d}\tau} = F^\alpha_{\mathrm{ext}} \; + \; m_0 \tau_0 \left(g^\alpha{}_\beta + \frac{U^\alpha U_\beta}{c^2} \right) \frac{\mathrm{d}a^\beta}{\mathrm{d}\tau}. \tag{1.822}$$

Pauli Representation of Radiation Reaction

In the general Lorentz–Dirac equation (1.821), the radiation reaction force is given by:

$$F^\alpha_{\mathrm{rad}} = m_0 \tau_0 \left(\frac{\mathrm{d}a^\alpha}{\mathrm{d}\tau} - \frac{a^2}{c^2} U^\alpha \right). \tag{1.823}$$

The transformation from proper time τ to coordinate time t can be derived from the spacetime interval invariant:

$$\mathrm{d}s^2 = -c^2 \mathrm{d}\tau^2 = -c^2 \mathrm{d}t^2 + \mathrm{d}x^2 + \mathrm{d}y^2 + \mathrm{d}z^2 \qquad \Rightarrow \tag{1.824}$$

$$\mathrm{d}\tau = \mathrm{d}t \sqrt{1 - \mathbf{v}^2/c^2} \tag{1.825}$$

yields the operational derivative transformation:

$$\frac{\mathrm{d}f}{\mathrm{d}\tau} = \frac{\mathrm{d}f}{\mathrm{d}t} \frac{\mathrm{d}t}{\mathrm{d}\tau} = \gamma \frac{\mathrm{d}f}{\mathrm{d}t} = \gamma \dot{f} \,. \tag{1.826}$$

Dots designate derivatives with respect to coordinate time. Velocity is represented by the dimensionless velocity $\boldsymbol{\beta}$, whose value is independent of the choice of units:

$$\boldsymbol{\beta} \equiv \mathbf{v}/c \tag{1.827}$$

First, the time derivative of the Lorentz factor γ is evaluated:

$$\frac{\mathrm{d}\gamma}{\mathrm{d}t} = \frac{\mathrm{d}}{\mathrm{d}t}\left(\frac{1}{\sqrt{1 - \mathbf{v}^2/c^2}} \right) = \frac{\mathrm{d}}{\mathrm{d}t}\left(1 - \mathbf{v}^2/c^2\right)^{-1/2} = \frac{\mathbf{v}\cdot\dot{\mathbf{v}}}{c^2}\left(1 - \mathbf{v}^2/c^2\right)^{-3/2} = \gamma^3 \boldsymbol{\beta}\cdot\dot{\boldsymbol{\beta}} \,. \tag{1.828}$$

Evaluating the individual components required to construct the radiation reaction (1.823) yields:

$$x^\alpha = \begin{pmatrix} ct \\ \mathbf{x} \end{pmatrix}; \tag{1.829}$$

$$U^\alpha \equiv \frac{\mathrm{d}x^\alpha}{\mathrm{d}\tau} = \gamma \frac{\mathrm{d}x^\alpha}{\mathrm{d}t} = \gamma \begin{pmatrix} c \\ \mathbf{v} \end{pmatrix} = \gamma c \begin{pmatrix} 1 \\ \boldsymbol{\beta} \end{pmatrix}; \tag{1.830}$$

$$a^\alpha \equiv \frac{\mathrm{d}U^\alpha}{\mathrm{d}\tau} = \gamma \frac{\mathrm{d}U^\alpha}{\mathrm{d}t} = \gamma \frac{\mathrm{d}}{\mathrm{d}t}\begin{pmatrix} \gamma c \\ \gamma c \boldsymbol{\beta} \end{pmatrix} = \cdots = \\ = c\begin{pmatrix} \gamma^4 (\boldsymbol{\beta}\cdot\dot{\boldsymbol{\beta}}) \\ \gamma^4 (\boldsymbol{\beta}\cdot\dot{\boldsymbol{\beta}})\boldsymbol{\beta} + \gamma^2 \dot{\boldsymbol{\beta}} \end{pmatrix}. \tag{1.831}$$

The resulting expression possesses the correct dimension of acceleration, where the leading speed of light provides $[c]$ = m/s, and the coordinate time derivative introduces s^{-1}. The condition $a^\alpha U_\alpha = 0$ remains satisfied. Next, the scalar a^2 is evaluated:

$$a^2 = a^\alpha a_\alpha = -(a^0)^2 + \mathbf{a}\cdot\mathbf{a} = \cdots = \\ = c^2\left[\gamma^6 (\boldsymbol{\beta}\cdot\dot{\boldsymbol{\beta}})^2 + \gamma^4 \dot{\beta}^2\right], \tag{1.832}$$

The final component required for the radiation reaction is $\mathrm{d}a^\alpha/\mathrm{d}\tau$. Straightforward differentiation yields the concise expression:

$$\frac{\mathrm{d}a^\alpha}{\mathrm{d}\tau} = \gamma \frac{\mathrm{d}a^\alpha}{\mathrm{d}t} = \cdots = c\begin{pmatrix} 4\gamma^7 (\boldsymbol{\beta}\cdot\dot{\boldsymbol{\beta}})^2 + \gamma^5\left[\boldsymbol{\beta}\cdot\ddot{\boldsymbol{\beta}} + \dot{\beta}^2\right] \\ 4\gamma^7 (\boldsymbol{\beta}\cdot\dot{\boldsymbol{\beta}})^2\boldsymbol{\beta} + \gamma^5\left[(\boldsymbol{\beta}\cdot\ddot{\boldsymbol{\beta}})\boldsymbol{\beta} + 3(\boldsymbol{\beta}\cdot\dot{\boldsymbol{\beta}})\dot{\boldsymbol{\beta}} + \dot{\beta}^2\boldsymbol{\beta}\right] + \gamma^3\ddot{\boldsymbol{\beta}} \end{pmatrix} \tag{1.833}$$

Combining these expressions yields the radiation component of the right-hand side of the Lorentz–Dirac equation:

$$\frac{\mathrm{d}a^\alpha}{\mathrm{d}\tau} - \frac{a^2}{c^2}U^\alpha = c\begin{pmatrix} 3\gamma^7 (\boldsymbol{\beta}\cdot\dot{\boldsymbol{\beta}})^2 + \gamma^5 (\boldsymbol{\beta}\cdot\ddot{\boldsymbol{\beta}}) \\ 3\gamma^7 (\boldsymbol{\beta}\cdot\dot{\boldsymbol{\beta}})^2\boldsymbol{\beta} + \gamma^5\left[(\boldsymbol{\beta}\cdot\ddot{\boldsymbol{\beta}})\boldsymbol{\beta} + 3(\boldsymbol{\beta}\cdot\dot{\boldsymbol{\beta}})\dot{\boldsymbol{\beta}}\right] + \gamma^3\ddot{\boldsymbol{\beta}} \end{pmatrix} \tag{1.834}$$

The equation of motion (1.821) then takes the form:

$$\frac{\mathrm{d}p^\alpha}{\mathrm{d}\tau} = F^\alpha_{\mathrm{ext}} + m_0 c\,\tau_0 \begin{pmatrix} 3\gamma^7 (\boldsymbol{\beta}\cdot\dot{\boldsymbol{\beta}})^2 + \gamma^5 (\boldsymbol{\beta}\cdot\ddot{\boldsymbol{\beta}}) \\ 3\gamma^7 (\boldsymbol{\beta}\cdot\dot{\boldsymbol{\beta}})^2\boldsymbol{\beta} + \gamma^5\left[(\boldsymbol{\beta}\cdot\ddot{\boldsymbol{\beta}})\boldsymbol{\beta} + 3(\boldsymbol{\beta}\cdot\dot{\boldsymbol{\beta}})\dot{\boldsymbol{\beta}}\right] + \gamma^3\ddot{\boldsymbol{\beta}} \end{pmatrix}, \tag{1.835}$$

where p^α is the particle four-momentum. Transforming the left-hand side to coordinate time yields the radiation component:

► $$\frac{\mathrm{d}E_{\mathrm{rad}}}{\mathrm{d}t} = m_0 c^2 \tau_0 \left[3\gamma^6 (\boldsymbol{\beta}\cdot\dot{\boldsymbol{\beta}})^2 + \gamma^4 (\boldsymbol{\beta}\cdot\ddot{\boldsymbol{\beta}})\right]; \tag{1.836}$$

► $$\mathbf{F}_{\mathrm{rad}} \equiv \frac{\mathrm{d}\mathbf{p}_{\mathrm{rad}}}{\mathrm{d}t} = m_0 c\,\tau_0 \left[3\gamma^6 (\boldsymbol{\beta}\cdot\dot{\boldsymbol{\beta}})^2\boldsymbol{\beta} + \gamma^4 (\boldsymbol{\beta}\cdot\ddot{\boldsymbol{\beta}})\boldsymbol{\beta} + 3\gamma^4 (\boldsymbol{\beta}\cdot\dot{\boldsymbol{\beta}})\dot{\boldsymbol{\beta}} + \gamma^2\ddot{\boldsymbol{\beta}}\right]. \tag{1.837}$$

The final two expressions represent the loss of particle energy and momentum caused by self-emission. Expression (1.837) was derived in 1958 by Wolfgang Pauli [50] and is widely cited within the runaway electron research community. For ultrarelativistic particles ($\gamma \gg 1$), the terms inside the brackets are ordered by decreasing powers of the Lorentz factor γ.

Iterative Solution: Landau–Lifshitz Equation

An elegant resolution to these pathologies relies on the assumption that the radiation reaction term in equation (1.811) remains small, permitting an iterative estimation of the acceleration. The zeroth-order approximation is formulated as:

$$\mathbf{a}_0 = \frac{\mathbf{F}_{\text{ext}}}{m_0} \tag{1.838}$$

Substituting this first iteration back into the right-hand side of equation (1.811) yields:

$$m\,\mathbf{a}_1 \approx \mathbf{F}_{\text{ext}} + \tau_0 \dot{\mathbf{F}}_{\text{ext}}. \tag{1.839}$$

This formulation circumvents the ambiguities associated with third-order derivatives. However, the precise boundaries validity for higher-order iterations remain a subject of discussion. This iterative approach is fundamentally applicable to external forces depending explicitly on time (such as an electron interacting with a laser pulse field). The relativistic generalization of this iterative substitution (1.839) is straightforward:

$$m_0 \frac{\mathrm{d}U^\alpha}{\mathrm{d}\tau} = F^\alpha_{\text{ext}} \;+\; \tau_0 \left(g^\alpha{}_\beta + U_\beta U^\alpha \right) F^\beta_{\text{ext},\,\gamma} U^\gamma. \tag{1.840}$$

When the external force is specified as the Lorentz force, the resulting relation constitutes the *Landau–Lifshitz equation*:

► $$m_0 \frac{\mathrm{d}U^\alpha}{\mathrm{d}\tau} = QF^{\alpha\beta}U_\beta \;+\; \tau_0 \left(g^\alpha{}_\beta + U_\beta U^\alpha \right) QF^{\beta\alpha}{}_{,\gamma} U_\alpha U^\gamma. \tag{1.841}$$

Various equivalent representations of this equation exist. The primary criterion for its validity requires the radiation reaction force to be substantially smaller than the driving Lorentz force. Additionally, the transit time of an electromagnetic signal across the interaction region must be significantly shorter than the characteristic timescale of field variations. Generally, these constraints are formulated as [54]:

$$E \ll E_{\text{S}}/\alpha\,; \qquad \lambda \gg \alpha\,\lambda_{\text{C}}, \tag{1.842}$$

where E_{S} represents the Schwinger limit (the threshold field intensity for electron-positron pair production from vacuum), λ_{C} is the Compton wavelength (characterizing the photon wavelength shift during electron scattering), and α denotes the fine-structure constant (governing the electromagnetic interaction strength). These three fundamental physical quantities are defined as:

$$E_{\text{S}} \equiv \frac{m_{\text{e}}^2 c^3}{e\,\hbar} \approx 1.3\times10^{18}\ \text{V/m}, \tag{1.843}$$

$$\lambda_{\text{C}} \equiv \frac{2\pi\hbar}{m_{\text{e}} c} \approx 2.4\times10^{-12}\ \text{m}, \tag{1.844}$$

$$\alpha \equiv \frac{e^2}{4\pi\varepsilon_0\,\hbar c} \approx \frac{1}{137}. \tag{1.845}$$

Avenues for Resolving Pathologies

The solution to equation (1.811) can be reformulated to eliminate non-physical exponentially growing modes. This formulation is obtained from expression (1.816) via the substitution:

$$s = (t' - t)/\tau_0 \,, \tag{1.846}$$

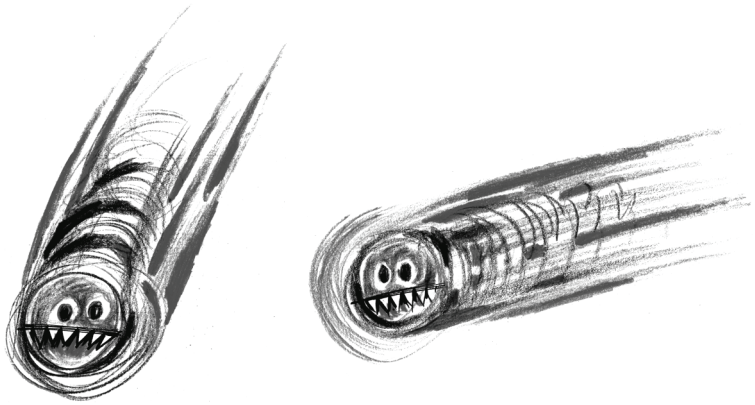
which yields the regularized solution:

$$\mathbf{a}(t) = \frac{1}{m}\int_0^\infty \mathbf{F}_{\text{ext}}(t + s\tau_0)\,\mathrm{e}^{-s}\,\mathrm{d}s \tag{1.847}$$

Nevertheless, the violation of causality persists. The general solution of equation (1.811) for a time-dependent force can be expressed in an alternative integral form:

$$\mathbf{a}(t) = \mathrm{e}^{t/\tau_0}\left[\mathbf{C} - \frac{1}{m_0\tau_0}\int_{-\infty}^{t} \mathbf{F}_{\text{ext}}(t')\,\mathrm{e}^{-t'/\tau_0}\,\mathrm{d}t'\right] \tag{1.848}$$

For a step-function constant force initiated at time t_0, the integration constant $\mathbf{C}$ can be selected to eliminate the non-physical exponential runaway behavior. However, the solution at times $t < t_0$ remains dependent on the force magnitude at $t > t_0$, which violates classical causality. These persistent ambiguities suggest that radiation reaction is inherently a quantum-mechanical process, and a fully consistent description within classical mechanics may be fundamentally unattainable.



1.7.2 Runaway Electrons

An electron moving through a plasma experiences a frictional drag force driven by Coulomb collisions (1.765) with background electrons and ions, as derived in Section 1.6.4. Initially, this collisional drag force increases proportionally with the electron velocity. However, at velocities significantly exceeding the ion thermal velocity, the frictional force peaks and subsequently scales as v^{-2}. Consequently, high-velocity collisions become highly inefficient. The maximum drag occurs near the ion thermal velocity; a detailed derivation of this profile is presented below.

Consider an external electric field accelerating an electron, while collisions act to decelerate it. Within the velocity interval (v_Ω, v_C) designated as the Ohmic regime in Fig. 1.124, these competing processes establish a steady-state velocity v_Ω. At lower velocities, the electric field dominates and accelerates the electron, whereas at higher velocities, collisional drag provides deceleration. The sole exception occurs when the applied electric field exceeds the maximum collisional drag force E_M. In such strong fields, acceleration unconditionally overcomes collisional drag, continuously driving the electron to higher velocities.

If the electron velocity exceeds the threshold value corresponding to the intersection point C between the electric field and the collisional drag curve, the particle enters the runaway regime. In this domain, collisions cannot compensate for the electric field acceleration, allowing the electron to attain substantial kinetic energy. Such high-energy electrons pose a severe damage risk to diagnostic and experimental equipment. As illustrated in Fig. 1.124, the *runaway regime* (conventionally abbreviated as REs) can be bounded by the synchrotron radiation emission of the electron. The radiation-induced momentum loss of a highly relativistic, accelerating electron exerts a braking effect analogous to collisional drag at low velocities.

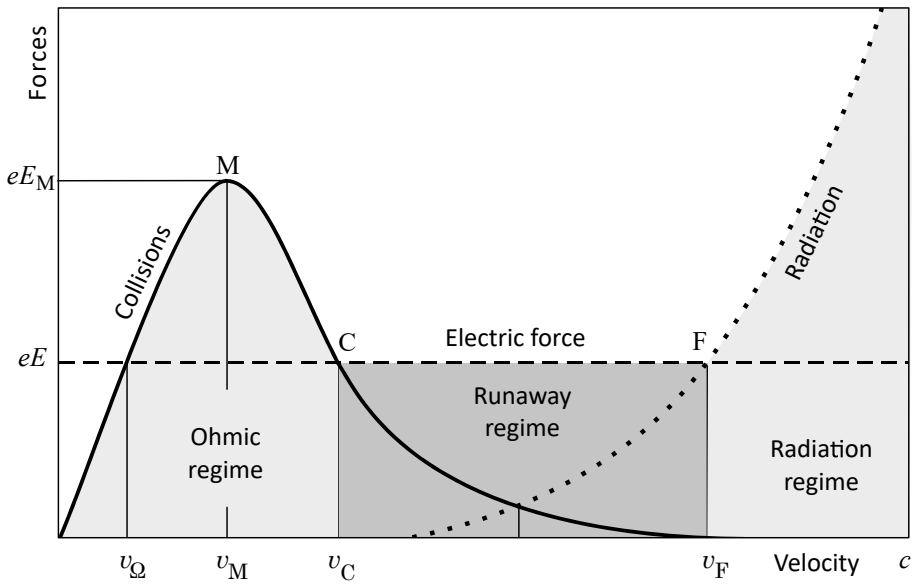


Fig. 1.124: Forces acting on a moving electron (excluding the magnetic Lorentz force).

Historical Background

The runaway electron regime manifests where electrostatic acceleration overcomes both collisional drag and radiative momentum loss. At a given velocity, the electric field must exceed a critical threshold to trigger continuous acceleration. The possibility of generating runaway electrons was first proposed in 1925 by Charles T. R. Wilson [73]. A more detailed theoretical framework was formulated by Ronald G. Giovanelli in 1949 [71]. In 1959, Harry Dreicer analytically evaluated the critical field threshold required for absolute runaway generation [69]. In 1992, Aleksandr V. Gurevich proposed an avalanche breakdown mechanism for lightning during atmospheric storms [70], initiated by relativistic seed electrons from cosmic ray showers. In 2003, Joseph R. Dwyer demonstrated that a single megaelectronvolt electron suffices to trigger such an avalanche [74]. Extensive research into runaway electrons accelerated primarily due to their frequent generation within large-scale tokamak vessels, where runaway electron beams present a severe threat to structural integrity.

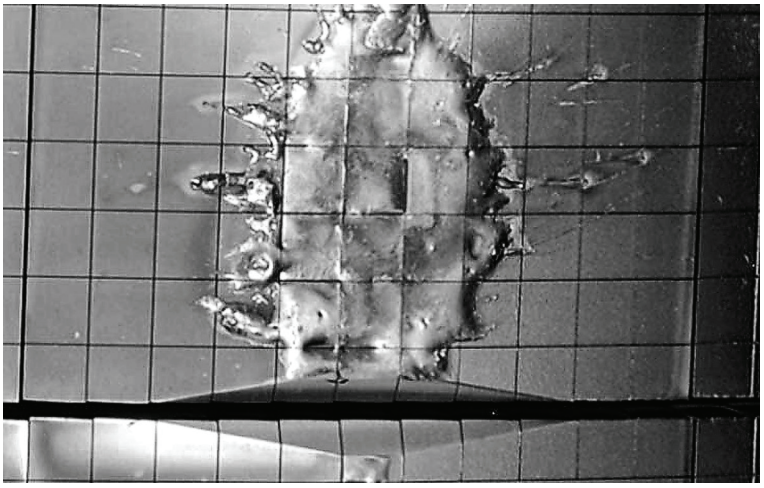


Fig. 1.125: Historical documentation of structural damage to the inner vacuum vessel wall of the JET tokamak caused by localized runaway electron impact. Eurofusion 2015.

Electrons can also gain energy through synergistic wave-particle interactions. For example, within the terrestrial magnetosphere, electrons execute helical motion around magnetic field lines. In the presence of right-hand circularly polarized electromagnetic waves (R-waves), where the electric field vector rotates in the same direction as the electron gyration, resonant energy transfer occurs provided the electron cyclotron frequency matches the wave frequency. This mechanism generates highly energetic “killer electrons” capable of damaging satellite instrumentation.

Runaway electrons manifest across diverse plasma environments, playing a key role in lightning dynamics, terrestrial gamma-ray flashes, and astrophysical jets from compact objects. Within magnetic confinement fusion plasma, such as in tokamaks aimed at thermonuclear fusion, runaway electrons represent a highly detrimental phenomenon. Incidents of localized first-wall damage caused by runaway electron impact are well documented. Consequently, understanding and mitigating their behavior has become a primary focus for research teams, particularly with the construction of the ITER toka-

mak. Runaway electrons are generated whenever the ambient electric field exceeds the Dreicer limit, or when the initial electron velocity exceeds a critical threshold. A fraction of electrons within the high-energy tail of a Maxwellian distribution naturally satisfy this super-thermal velocity condition. Although initially few, under favorable conditions an avalanche process can occur, where primary runaway electrons secondary-ionize the background plasma via close collisions, generating exponential populations.

In tokamaks, runaway electron beams typically form during plasma disruptions. During a disruption, the plasma temperature drops rapidly, causing a sharp decline in plasma conductivity and a subsequent collapse of the plasma current. This collapse induces a rapid decay of the poloidal magnetic field. According to Faraday law of induction, this rapid temporal variation of the magnetic flux generates a strong inductive toroidal electric field, triggering the runaway electron population.

Runaway electrons dissipate energy through multiple channels, including collisions with heavy ions, turbulence, kinetic instabilities, scattering by electric and magnetic fluctuations, electron-positron pair production, and synchrotron radiation.

Frictional Collisional Drag Force

An electron moving through a plasma undergoes Coulomb collisions with background electrons and ions, with the corresponding frequencies governed by relation:

$$\mathbf{F}_{\text{col}} = -m_{\text{e}}\mathbf{v}_{\text{e}}\left(\nu_{\text{ee}} + \nu_{\text{ei}}\right) \tag{1.849}$$

The collision frequencies are governed by relation (1.765). Substituting these frequencies yields the simplified expression:

$$\mathbf{F}_{\text{col}} = -\frac{n_{\text{e}}e^4 \ln\Lambda}{2\pi\varepsilon_0^2 m_{\text{e}}}\left[\frac{Z_{\text{eff}}}{v_{\text{Ti}}^2}\psi(v/v_{\text{Ti}}) + \frac{2}{v_{\text{Te}}^2}\psi(v/v_{\text{Te}})\right]\frac{\mathbf{v}}{v}, \tag{1.850}$$

where ψ denotes the Chandrasekhar function and Z_{eff} represents the effective ion charge state summed over all ion species:

$$Z_{\text{eff}} = \frac{1}{n_{\text{e}}}\sum_k Z_k^2 n_k\,. \tag{1.851}$$

The total collisional drag force formulation can be rewritten in the form:

$$\blacktriangleright \qquad \mathbf{F}_{\text{col}} = -2F_0\left[Z_{\text{eff}}\frac{m_i}{m_e}\psi(v/v_{\text{Ti}}) + 2\psi(v/v_{\text{Te}})\right]\frac{\mathbf{v}}{v}; \qquad F_0 \equiv \frac{n_{\text{e}}e^4\ln\Lambda}{4\pi\varepsilon_0^2 m_{\text{e}}v_{\text{Te}}^2}, \tag{1.852}$$

The first Chandrasekhar function peaks near the ion thermal velocity, and the second near the electron thermal velocity (the horizontal coordinate of the maximum evaluates numerically to $x \approx 0.967$). These maxima scale with the mass ratio $(m_i/m_e)^{1/2}$. Furthermore, the ion-induced peak is significantly higher because the leading coefficients scale as m_i/m_e; thus, the electron-ion (e-i) collision peak exceeds the electron-electron (e-e) contribution by three orders of magnitude (see Fig. 1.126.

The combined maximum practically coincides with the ion contribution, while the electron maximum manifests only as a minor modulation. Consequently, up to approximately 50 % of the electron thermal velocity, electron-ion collisions dominate entirely and electron-electron contributions are negligible. For higher velocities, both collisional terms must be incorporated.

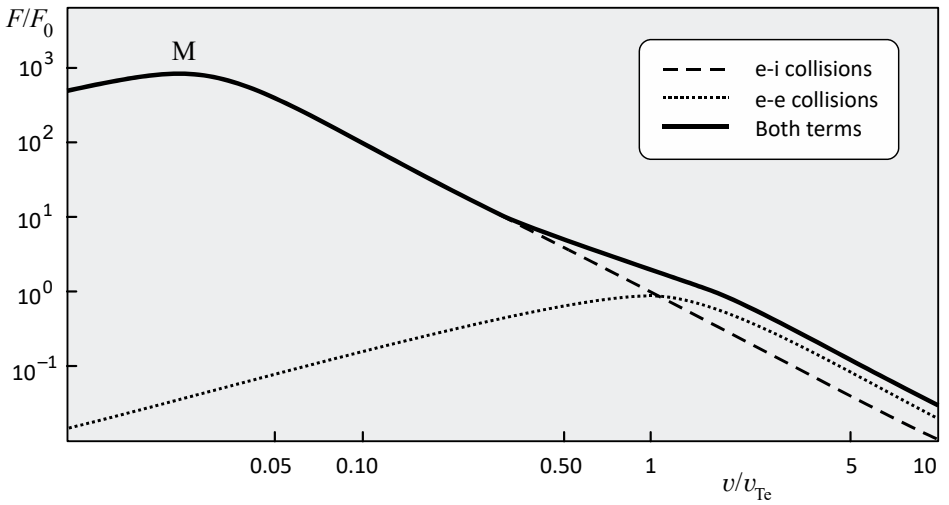


Fig. 1.126: Dependence of the collisional drag force on electron velocity in a logarithmic scale, illustrating the locations of both maxima. At low velocities, e-i collisions dominate entirely and e-e effects are negligible, whereas both components become non-negligible at higher velocities.

The limiting behavior of the Chandrasekhar function $\psi(x)$ is given by the relations:

$$\psi(x) = \frac{2}{3\sqrt{\pi}} x\,; \qquad x \ll 1\,, \tag{1.853}$$

$$\psi(x) = \frac{1}{2x^2}\,; \qquad x \gg 1\,. \tag{1.854}$$

Consequently, below the maximum, formula (1.852) can be approximated by a linear scaling. For velocities exceeding the electron thermal velocity, the asymptotic approximation (1.854) applies, reducing the collisional force to a simplified form:

► $$\mathbf{F}_{\text{col}} = -\frac{n_e e^4 \ln\Lambda}{4\pi\varepsilon_0^2 m_e v^2}\left(Z_{\text{eff}} + 2\right)\frac{\mathbf{v}}{v}\,; \qquad v_{\text{Te}} < v \ll c\,. \tag{1.855}$$

Formulation (1.852) is non-relativistic; however, this approximation introduces negligible error at high velocities since collisional drag becomes minor. Nevertheless, if required for extreme relativistic velocities, the relativistic formulation can be utilized [68]:

► $$\mathbf{F}_{\text{col}} = -\frac{n_e e^4 \ln\Lambda}{4\pi\varepsilon_0^2 m_e c^2}\left(\frac{\gamma}{\gamma^2 - 1} Z_{\text{eff}} + \frac{1}{\gamma - 1}\right)\frac{\mathbf{v}}{v}\,; \qquad v > v_{\text{Te}}\,. \tag{1.856}$$

Executing a Taylor expansion of the Lorentz factor γ in powers of velocity reduces (1.856) to the non-relativistic limit (1.855) in the lowest order. For scoping calculations, the Chandrasekhar function can be approximated via a simpler rational function:

$$\psi(x) \approx G(x) = \frac{2x}{3\pi^{1/2} + 4|x|^3}\,. \tag{1.857}$$

The model $G(x)$ exhibits identical behavior to $\psi(x)$ for small and large x. The maximum discrepancy occurs near the peak (< 10 %), which is acceptable for baseline estimates.

Radiation Reaction

An accelerating electron emits radiation driven by longitudinal acceleration and gyration within the magnetic field, causing a systemic loss of particle momentum and energy. This momentum loss acts as a braking force bounding the runaway regime (neglecting alternative channels, such as electron-positron pair production). The radiation reaction force is governed by the Pauli formulation (1.837):

$$\mathbf{F}_{\text{rad}} = \frac{e^2}{6\pi\varepsilon_0 c^2}\left[3\gamma^6\left(\boldsymbol{\beta}\cdot\dot{\boldsymbol{\beta}}\right)^2\boldsymbol{\beta} + \gamma^4\left(\boldsymbol{\beta}\cdot\ddot{\boldsymbol{\beta}}\right)\boldsymbol{\beta} + 3\gamma^4\left(\boldsymbol{\beta}\cdot\dot{\boldsymbol{\beta}}\right)\dot{\boldsymbol{\beta}} + \gamma^2\ddot{\boldsymbol{\beta}}\right], \tag{1.858}$$

where the dot denotes the coordinate time derivative d/dt. A fully four-vector evaluation additionally yields the corresponding energy loss rate:

$$\frac{\mathrm{d}E_{\text{rad}}}{\mathrm{d}t} = \frac{e^2}{6\pi\varepsilon_0 c}\left[3\gamma^6(\boldsymbol{\beta}\cdot\dot{\boldsymbol{\beta}})^2 + \gamma^4(\boldsymbol{\beta}\cdot\ddot{\boldsymbol{\beta}})\right]. \tag{1.859}$$

The parameter $\boldsymbol{\beta}$ denotes the dimensionless velocity $\mathbf{v}/c$, and γ represents the Lorentz factor. Two limiting configurations exist: (i) radiation associated with a change in velocity magnitude (e.g., bremsstrahlung), and (ii) radiation driven by a change in velocity direction (e.g., cyclotron or synchrotron emission).

Electron Radiation in Tokamaks

Electrons gyrating within a toroidal field B_{tor} emit synchrotron radiation; their orbital motion along the vessel induces betatron radiation, supplemented by bremsstrahlung from velocity modulations. Bremsstrahlung scales with the local ion density and impurity content, becoming significant during disruptions. Quantifying this power requires explicit knowledge of the specific discharge parameters. For radiation driven strictly by electron gyration within the toroidal field, relations (1.858) and (1.859) yield the scaling laws:

$$\left|\mathbf{F}_{\text{T, rad}}\right| = \frac{e^4}{6\pi\varepsilon_0 c^2}\frac{B_{\text{tor}}^2}{m_{\text{e}}^2}\frac{\beta_\perp}{1-\beta_\perp^2}; \tag{1.860}$$

$$\frac{\mathrm{d}E_{\text{T, rad}}}{\mathrm{d}t} = -\frac{e^4}{6\pi\varepsilon_0 c}\frac{B_{\text{tor}}^2}{m_{\text{e}}^2}\frac{\beta_\perp}{1-\beta_\perp^2}, \tag{1.861}$$

where $\beta_\perp$ is the dimensionless electron velocity component perpendicular to the local magnetic field line. Similarly, formulations (1.858) and (1.859) yield the betatron radiation power generated by electron transit along the toroidal circumference:

$$\left|\mathbf{F}_{\text{b, rad}}\right| = \frac{e^2}{6\pi\varepsilon_0 R_{\text{maj}}^2}\frac{\beta_\parallel^3}{1-\beta_\parallel^2}; \tag{1.862}$$

$$\frac{\mathrm{d}E_{\text{b, rad}}}{\mathrm{d}t} = -\frac{e^2 c}{6\pi\varepsilon_0 R_{\text{maj}}^2}\frac{\beta_\parallel^4}{1-\beta_\parallel^2}, \tag{1.863}$$

where $\beta_{||}$ is the parallel projection of the dimensionless velocity along the magnetic field line, and R_{maj} denotes the tokamak major radius. For example, in the COMPASS tokamak with a 10° pitch angle at thermal velocity, betatron emission is eight orders of magnitude lower than gyroradiation due to the vastly larger trajectory curvature radius. Consequently, betatron radiation is neglected in nearly all operational regimes.

Key Parameters of the Runaway Regime

The critical parameters governing the runaway regime (see Fig. 1.124) comprise: the maximum collisional drag force M and its associated threshold electric field E_M, the coordinates of point C defining the onset of the runaway regime, and the coordinates of point F representing the termination of the runaway regime driven by self-radiation.

Point M: Maximum Collisional Drag

Because e-e collisions are negligible near the peak of the total collisional drag force, only the e-i component is utilized to evaluate the coordinates of point M. The Chandrasekhar function exhibits an extremum at $x \approx 0{,}968$ with $\psi \approx 0{,}214$, yielding:

$$\begin{gathered} eE_M \approx \frac{n_e e^4 \ln\Lambda}{2\pi\varepsilon_0^2 m_e} \frac{Z_{eff}}{v_{Ti}^2} \psi(v_M/v_{Ti}); \\ v_M/v_{Ti} \approx 0{,}968; \\ \psi(v_M/v_{Ti}) \approx 0{,}214. \end{gathered} \tag{1.864}$$

This extremum directly defines the velocity and electric field corresponding to the coordinates of point M:

$$\begin{gathered} v_M \approx 0{,}968\, v_{Ti} \approx 0{,}968 \sqrt{\frac{m_e}{m_i}}\, v_{Te}, \\ E_M \approx 0{,}107 \frac{n_e e^3 \ln\Lambda}{\pi\varepsilon_0^2 m_e} \frac{Z_{eff}}{v_{Ti}^2} \approx 0{,}107 \frac{m_i}{m_e^2} \frac{n_e e^3 \ln\Lambda}{\pi\varepsilon_0^2} \frac{Z_{eff}}{v_{Te}^2}. \end{gathered} \tag{1.865}$$

The conversion of the ion thermal velocity to the electron thermal velocity applies strictly to a thermalized plasma. For a given electron thermal velocity, the maximum of the collision frequency along the horizontal axis occurs at a value approximately forty times lower – scaled by the mass ratio $(m_i/m_e)^{1/2}$ – than the electron thermal velocity. Thus, the horizontal coordinate of the extremum M corresponds approximately to the ion thermal velocity. The vertical coordinate defines the critical field E_M, above which an electron unconditionally enters the runaway regime regardless of its initial velocity.

Point C: Runaway Onset, Critical Velocity, and the Dreicer Field

Evaluating the coordinates of point C – representing the threshold velocity and the corresponding electric field required for the onset of the runaway regime – depends on the electron velocity domain and is classified into three distinct regions. The ion component peaks at 0.968 of the ion thermal velocity, whereas the electron component peaks at 0.968 of the electron thermal velocity. The horizontal coordinates (velocities) differ by the factor $(m_i/m_e)^{1/2}$, while the vertical coordinates (collisional drag force) scale as

m_i/m_e. Consequently, for a hydrogen plasma, the ion peak is approximately 1800 times higher than the electron peak.

In the velocity domain between these two extrema (i.e., below the electron thermal velocity), the electron contribution is minor and can be neglected. The ion component occupies the descending region and is approximated by expression (1.854). Between the two maxima (i.e., for velocities exceeding the electron thermal velocity), the electron contribution can no longer be neglected, and both components of the collisional drag force are approximated via relation (1.854)). Near the electron thermal velocity, the ion component remains also scalable via expression (1.854), whereas the electron component is replaced by the maximum of the Chandrasekhar function:

$$E_C = \frac{n_e e^3 \ln\Lambda}{4\pi\varepsilon_0^2 m_e v^2} \times \begin{cases} Z_{\text{eff}}; & v_M < v \ll v_{Te}, \\ Z_{\text{eff}} + 0.856; & v \approx v_{Te}, \\ Z_{\text{eff}} + 2; & v_{Te} \ll v \ll c. \end{cases} \tag{1.866}$$

The first expression corresponds to the formulation introduced in the original 1959 paper by Harry Dreicer [69]. The second relation defines the modern Dreicer field E_D, representing the electric field threshold at which bulk thermal electrons are continuously driven into the runaway regime. The electron contribution, which cannot be neglected near the thermal velocity, shifts the required electric field to higher values compared to the original Dreicer formulation. All three branches of expression (1.866) can be unified into a single formula:

► $$E_C = E_0 \left(Z_{\text{eff}} + \alpha \right); \qquad E_0 = \frac{n_e e^3 \ln\Lambda}{4\pi\varepsilon_0^2 m_e v^2}; \qquad \alpha = \begin{cases} 0; & v_M < v \ll v_{Te}, \\ 0.856; & v \approx v_{Te}, \\ 2; & v_{Te} \ll v \ll c. \end{cases} \tag{1.867}$$

Equations (1.866) and (1.867) permit the calculation of the threshold electric field required for a given electron velocity to enter the runaway regime.

Point F: Termination of the Runaway Regime

As an electron accelerates within the runaway regime, its kinetic energy increases, causing a sharp decline in the effective collision cross-section and the associated collisional drag force. At the upper bound of the runaway regime, the radiative deceleration force balances the accelerating electrostatic force, rendering collisional effects negligible:

$$eE_C = \frac{e^4}{6\pi\varepsilon_0 c^2} \frac{B_{\text{tor}}^2}{m_e^2} \frac{\beta_\perp}{1-\beta_\perp^2}. \tag{1.868}$$

Determining the threshold field E_C required for runaway onset via expression (1.866) for a given initial velocity allows the termination velocity to be evaluated from relation (1.868) based on the specific problem geometry. This optimization problem reduces to a quadratic equation.

1.7.3 Solitons

From the Union Canal to Solitons

In certain configurations, nonlinear equations provide highly interesting solutions: solitary waves that do not undergo dispersion and propagate through a medium without altering their shape. Such a wave constitutes a soliton. Mathematically, solitons are as fundamental in nonlinear theories as the harmonic oscillator is in linear theories. Experimentally, a soliton was first observed in a narrow water channel (the Union Canal in Hermiston, near Edinburgh) by the Scottish scientist John Scott Russell in 1834.

The origins of soliton physics are permanently linked with Russell's name. Russell was an outstanding physicist, shipbuilder, steam-car constructor, and innovator. He graduated from the University of St Andrews and possessed such profound knowledge that he became a professor at the University of Edinburgh at the age of 24. Two years later, in 1834, he introduced a steam-car transport service between Glasgow and Paisley. His initial success was opposed by competing operators, who orchestrated a traffic accident resulting in four passenger fatalities – likely the first automobile accident in history. Consequently, Russell accepted an offer from the Union Canal Company to test and design boats. This narrow canal, constructed between 1818 and 1822, connected Edinburgh and Glasgow. It primarily served for transporting coal and passengers in barges towed by horses along the bank. The canal is 50 kilometers long, mostly follows a contour line, and overcomes terrain irregularities via aqueducts or tunnels, the longest measuring 631 meters. In August 1834, Russell made an extraordinary discovery, which he described as follows:

"*I was observing the motion of a boat which was rapidly drawn along a narrow channel by a pair of horses, when the boat suddenly stopped – not so the mass of water in the channel which it had put in motion; it accumulated round the prow of the vessel in a state of violent agitation, then suddenly leaving it behind, rolled forward with great velocity, adopting the form of a large solitary elevation, a rounded, smooth and well-defined heap of water, which continued its course along the channel apparently without change of form or diminution of speed. I followed it on horseback, and overtook it still rolling on at a rate of some eight or nine miles an hour, preserving its original figure some thirty feet long and a foot to a foot and a half in height. Its height gradually diminished, and after a chase of one or two miles I lost it in the windings of the canal. Such, in the month of August 1834, was my first chance interview with that singular and beautiful phenomenon which I have called the Wave of Translation.*"

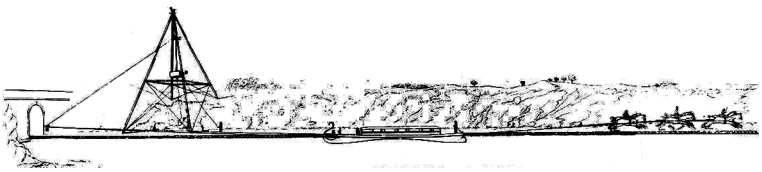


Fig. 1.127: Historical drawing by John Scott Russell of a horse-drawn barge on the Union Canal.

Russell was fully aware of the exceptional nature of the phenomenon. The *Great Wave of Translation* he discovered contradicted the hydrodynamics described by Newton and Bernoulli. Russell constructed a pond at his Edinburgh New Town home and spent three

years conducting various experiments there and on the Union Canal. He discovered that the wave possessed highly unusual and unexpected properties:

- The propagation velocity depends on the wave amplitude, and its width on the water depth. This wave is exceptionally stable, retaining its shape over several miles.
- Unlike normal waves, waves of translation never merge. A faster wave passes through a slower one and overtakes it.

If the wave is too large relative to the canal depth, it splits into a large and a small wave. Russell's research initially met a lack of interest. Scholars were unprepared for such a discovery, refusing to believe in phenomena contradicting Newton and Bernoulli. Its true significance was fully appreciated in the 1960s, when physicists began systematically investigating nonlinear phenomena. Today, light pulses travel thousands of kilometers through optical fibers without any loss of shape.

In 1895, the Dutch mathematicians Diederik Korteweg and Gustav de Vries derived the governing equation for wave propagation in shallow water. The equation is nonlinear, and wave dispersion can be precisely compensated by nonlinear effects. Sixty years after Russell's observations, the problem was solved. Waves can indeed propagate along a water channel without changing their shape and size, and their existence can be theoretically explained through nonlinear phenomena. The equation describing this wave is known today as the KdV (Korteweg–de Vries) equation. Currently, a wide range of other equations from various fields of science are known to provide soliton solutions.

What is the mathematical principle behind solitons? In linear equations, solutions are built from plane wave fronts. However, a wave packet undergoes *dispersion* because different wavelengths propagate at different velocities, causing it to spread out. In nonlinear theories, certain terms induce *modulational instability*, making the group velocity amplitude-dependent. Smaller amplitudes are suppressed, leading to packet collapse. In specific configurations, dispersion balances modulational instability, yielding a *soliton* of constant shape and size. As solutions to nonlinear equations, solitons manifest across numerous fields, ranging from hydrodynamics to nonlinear electrodynamics, plasma physics, biophysics, elementary particle physics, solid-state physics, and even economic market models.

Three Illustrative Examples

To analyze the interplay between dispersion and nonlinearity, consider the following three foundational equations:

1. Standard Wave Equation with no dispersion:

$$\left(\Delta - \frac{1}{c^2}\frac{\partial^2}{\partial t^2}\right)\phi = 0 \quad \Rightarrow \quad \omega = ck \quad \Rightarrow \quad v_f = v_g = c. \tag{1.869}$$

   The angular frequency scales linearly with the wave vector, rendering the phase and group velocities equal and constant. Consequently, all wavelengths propagate at identical velocities, and the wave packet undergoes no dispersion.

2. Klein–Gordon Equation with linear mass term and dispersion:

$$\left(\Delta - \frac{1}{c^2}\frac{\partial^2}{\partial t^2} - \mu^2\right)\phi = 0 \quad \Rightarrow \quad \omega = c\sqrt{k^2 + \mu^2} \quad \Rightarrow \quad \begin{matrix} v_f = c\sqrt{1 + (\mu/k)^2}\,, \\ v_g = c/\sqrt{1 + (\mu/k)^2}\,. \end{matrix} \tag{1.870}$$

Both phase and group velocities depend on the wave vector and thus on the wavelength ($\lambda = 2\pi/k$). This dispersion causes the wave packet to gradually broaden. For a packet of linear dimension L, the spatial spreading scales as:

$$\Delta L = \frac{\partial L}{\partial t}\Delta t \approx \Delta v_g \Delta t = \frac{\partial v_g}{\partial k}\Delta k \Delta t \approx \frac{\partial v_g}{\partial k}\frac{2\pi}{L}\Delta t \,. \tag{1.871}$$

3. Wave Equation with nonlinear term:

$$\left(\Delta - \frac{1}{c^2}\frac{\partial^2}{\partial t^2}\right)\phi + \gamma\phi^3 = 0\,. \tag{1.872}$$

Due to the nonlinearity, plane waves are no longer valid solutions, nor can solutions be constructed via standard linear superposition. Numerical simulations indicate that this equation undergoes *modulational instability*, where localized regions of the wave packet collapse depending on their amplitude.

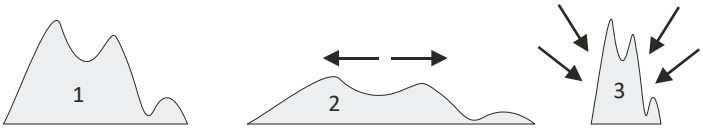


Fig. 1.128: Evolution and profile profiles of the wave packet solutions for Examples 1, 2, and 3.

Nonlinear effects can balance dispersion, yielding soliton solutions that propagate as solitary waves propagating without altering their shape:

$$\left(\Delta - \frac{1}{c^2}\frac{\partial^2}{\partial t^2}\right)\phi - \kappa^2\phi + \gamma\phi^3 = 0\,, \tag{1.873}$$

The added terms represent force densities corresponding to the "Mexican-hat" potential configuration $\mathscr{V}(\phi) = a\phi^2 - b\phi^4$. This potential is widely utilized in quantum field theory, the description of second-order phase transitions, and bifurcation analysis.

Solitons vs. Solitary Waves

For a continuous medium, the Lagrangian L, energy E, and momentum P are replaced by the Lagrangian density $\mathscr{L}$, energy density $\mathscr{E}$, and momentum density $\mathscr{P}$, respectively. These quantities depend on the spacetime events $(t, \mathbf{x})$ rather than time alone. The primary quantity of interest is the energy density:

► $$\mathscr{E}(t,\mathbf{x}) \equiv \pm\left(\frac{\partial \mathscr{L}}{\partial \phi_{k,t}}\phi_{k,t} - \mathscr{L}\right). \tag{1.874}$$

If energy conservation is enforced strictly via invariance under time translation, the global sign remains arbitrary. However, ensuring that forces directed toward the energy minimum recover the classical limit for compact bodies requires the kinetic term (squared field derivatives) to be non-negative. This choice depends on the metric tensor signature; for the convention utilized here, a negative sign must be chosen for the energy density expression. For the three preceding examples, formulated in one spatial

dimension for simplicity, the Lagrangian density, energy density, and governing Euler–Lagrange field equations are expressed as:

Standard Wave Equation

$$\mathscr{L} = \frac{1}{2}\left(\partial_\alpha \phi\right)\left(\partial^\alpha \phi\right) = -\frac{1}{2c^2}\left(\frac{\partial \phi}{\partial t}\right)^2 + \frac{1}{2}\left(\frac{\partial \phi}{\partial x}\right)^2, \tag{1.875}$$

$$\mathscr{E} = -\left(\frac{\partial \mathscr{L}}{\partial \phi_{k,t}}\phi_{k,t} - \mathscr{L}\right) = \frac{1}{2c^2}\left(\frac{\partial \phi}{\partial t}\right)^2 + \frac{1}{2}\left(\frac{\partial \phi}{\partial x}\right)^2, \tag{1.876}$$

$$\left(\frac{\partial^2}{\partial x^2} - \frac{1}{c^2}\frac{\partial^2}{\partial t^2}\right)\phi = 0\,. \tag{1.877}$$

Klein–Gordon Equation

$$\mathscr{L} = \frac{1}{2}\left(\partial_\alpha \phi\right)\left(\partial^\alpha \phi\right) + \frac{1}{2}\mu^2\phi^2\,, \tag{1.878}$$

$$\mathscr{E} = -\left(\frac{\partial \mathscr{L}}{\partial \phi_{k,t}}\phi_{k,t} - \mathscr{L}\right) = \frac{1}{2c^2}\left(\frac{\partial \phi}{\partial t}\right)^2 + \frac{1}{2}\left(\frac{\partial \phi}{\partial x}\right)^2 + \frac{1}{2}\mu^2\phi^2\,, \tag{1.879}$$

$$\left(\frac{\partial^2}{\partial x^2} - \frac{1}{c^2}\frac{\partial^2}{\partial t^2} - \mu^2\right)\phi = 0\,. \tag{1.880}$$

Nonlinear Klein–Gordon Equation

$$\mathscr{L} = \frac{1}{2}\left(\partial_\alpha \phi\right)\left(\partial^\alpha \phi\right) + \frac{1}{2}\mu^2\phi^2 - \frac{1}{4}\delta\phi^4\,, \tag{1.881}$$

$$\mathscr{E} = -\left(\frac{\partial \mathscr{L}}{\partial \phi_{k,t}}\phi_{k,t} - \mathscr{L}\right) = \frac{1}{2c^2}\left(\frac{\partial \phi}{\partial t}\right)^2 + \frac{1}{2}\left(\frac{\partial \phi}{\partial x}\right)^2 + \frac{1}{2}\mu^2\phi^2 - \frac{1}{4}\delta\phi^4\,, \tag{1.882}$$

$$\left(\frac{\partial^2}{\partial x^2} - \frac{1}{c^2}\frac{\partial^2}{\partial t^2} - \mu^2\right)\phi + \delta\phi^3 = 0\,. \tag{1.883}$$

The nonlinear Klein–Gordon equation with a ϕ^3 term yields a moving kink (step-like) solution. This is not a true soliton because the field is non-localized (it does not vanish far from the wave). However, its energy density remains strictly localized, concentrating within the step and propagating as a compact packet. This category of solutions is designated as a *solitary wave*. Conversely, a true *soliton* is strictly localized in space, translates at a constant velocity without shape deformation, and retains its asymptotic identity after colliding with other solitary waves, experiencing at most a spatial phase shift. A true soliton inherently features a fully localized energy density distribution.

Definition: A soliton is defined as a strictly localized solution of a partial differential equation that propagates at a constant velocity without changing its shape. If a system of N solitons possesses an initial energy density before a collision formulated as:

$$\mathscr{E}(t,x) = \sum_{k=1}^{N} \mathscr{E}_0(x - x_{0k} - v\,t)\,, \tag{1.884}$$

then neither the soliton number nor their profiles alter post-interaction. The collision induces at most a spatial phase shift; thus, the final state satisfies:

$$\mathscr{E}_{\text{fin}}(t,x) = \sum_{k=1}^{N} \mathscr{E}_0(x - x_{0k} - v\,t + \delta_k)\,. \tag{1.885}$$

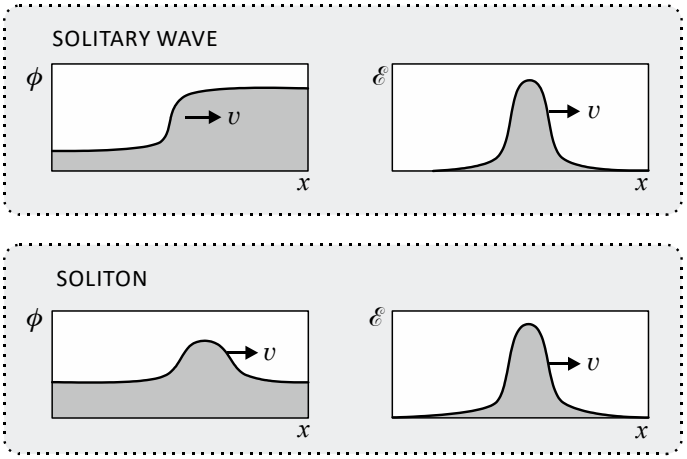


Fig. 1.129: Profiles of a soliton compared to a solitary wave configuration.

The property that a soliton retains its structural shape during propagation implies that within a co-moving coordinate frame, the solution becomes stationary (time-independent). Restricting the analysis to a single spatial dimension reduces the governing partial differential equation to an ordinary differential equation devoid of time derivatives, which may be analytically solvable. Once a solution is established within the co-moving reference frame, it is subsequently transformed back into the laboratory coordinate system where the soliton translates.

Sine-Gordon Solitary Wave

Typical soliton solutions arise directly from physical phenomena. Mathematical reduction of the underlying partial differential equations frequently yields one of four foundational formulations: the sine-Gordon, Korteweg–de Vries (KdV), nonlinear Schrödinger (NLS), or Burgers equation. The analysis below focuses initially on the first case.

The potential energy density within the Lagrangian and Hamiltonian frameworks for the nonlinear Klein–Gordon equation (1.881)–(1.883) is given by:

$$\mathscr{V} = \frac{1}{2}\mu^2\phi^2 - \frac{1}{4}\delta\phi^4\,. \tag{1.886}$$

The linear quadratic term governs dispersion, whereas the second introduces a nonlinearity driving the modulational instability that counteracts this broadening. Close

inspection reveals that for specific parameter values, these expressions correspond to the first two non-constant terms in the Taylor expansion of the cosine function (the zero-order constant term is physically irrelevant and vanishes). Utilizing the standard metric signature, the Lagrangian density is formulated as:

$$\mathscr{L} = -\mathscr{T} + \mathscr{V}. \tag{1.887}$$

Consequently, a periodic potential can be introduced:

$$\mathscr{V} = -\mu^2 \cos\phi\,, \tag{1.888}$$

which models physical phenomena near periodic lattice structures and reduces to the nonlinear Klein–Gordon potential (1.886) for small field amplitudes ϕ. The corresponding Lagrangian density, energy density, and Euler–Lagrange field equation evaluate to:

$$\mathscr{L} = \frac{1}{2}(\partial_\alpha\phi)\left(\partial^\alpha\phi\right) - \mu^2\cos\phi\,, \tag{1.889}$$

$$\mathscr{E} = -\frac{1}{2}(\partial_\alpha\phi)\left(\partial^\alpha\phi\right) - \mu^2\cos\phi\,, \tag{1.890}$$

$$\Box\phi - \mu^2\sin\phi = 0. \tag{1.891}$$

In the field equation, the negative sign before the second term combines contributions from the Lagrangian density, the cosine derivative, and the Euler–Lagrange structure, yielding a net negative sign. The presence of the sine function designates this relation as the *sine-Gordon equation*. In a single spatial dimension, these relations reduce to:

$$\mathscr{L} = -\frac{1}{2c^2}\left(\frac{\partial\phi}{\partial t}\right)^2 + \frac{1}{2}\left(\frac{\partial\phi}{\partial x}\right)^2 - \mu^2\cos\phi\,, \tag{1.892}$$

$$\mathscr{E} = +\frac{1}{2c^2}\left(\frac{\partial\phi}{\partial t}\right)^2 + \frac{1}{2}\left(\frac{\partial\phi}{\partial x}\right)^2 - \mu^2\cos\phi\,, \tag{1.893}$$

► $$\frac{\partial^2\phi}{\partial x^2} - \frac{1}{c^2}\frac{\partial^2\phi}{\partial t^2} = \mu^2\sin\phi. \tag{1.894}$$

A mechanical analogy is provided by a particle moving within a periodic cosine potential, driven by a force scaling as the sine of its position. Expanding the right-hand side to first order ($\sin\phi \sim \phi$) recovers the standard linear Klein–Gordon equation, which dictates the designation of the coefficient as μ^2. A third-order expansion ($\sin\phi \sim \phi - \phi^3/3!$) yields the nonlinear Klein–Gordon equation with a ϕ^3 term, corresponding to the Mexican-hat potential. An analytical solitary wave solution to the full sine-Gordon equation is evaluated below, demonstrating that a regularized solitary wave solution exists. The solution is evaluated initially within a co-moving frame tracking the wave. Because the profile remains invariant at constant velocity, the solution becomes stationary, reducing the system to a single ordinary differential equation:

► $$\frac{\mathrm{d}^2\phi}{\mathrm{d}x^2} = \mu^2\sin\phi. \tag{1.895}$$

It can be verified that a valid solution is expressed as:

► $$\phi_{\pm}(x) = 4\,\mathrm{atg}\left[\mathrm{e}^{\pm\mu x}\right]. \tag{1.896}$$

Verifying that this formulation satisfies the sine-Gordon equation constitutes a straightforward analytical exercise. This can be achieved either by direct second-order differentiation or by differentiating the implicit relation $\mathrm{tg}(\phi/4) = \exp(\pm\mu x)$ to isolate the first derivative before evaluating the second. Wherever the exponential term $\exp(\pm\mu x)$ appears, it is substituted via $\mathrm{tg}(\phi/4)$. For clarity, the positive branch (+) is analyzed below, as the negative branch follows an analogous procedure:

$$\begin{aligned}
&\mathrm{tg}(\phi/4) = \exp(\mu x) && \left|\ \mathrm{d}/\mathrm{d}x,\right.\\
&\frac{1}{4}\frac{\mathrm{d}\phi}{\mathrm{d}x}\frac{1}{\cos^2(\phi/4)} = \mu\exp(\mu x) && \left|\ \exp(\mu x) = \mathrm{tg}(\phi/4),\right.\\
&\frac{\mathrm{d}\phi}{\mathrm{d}x} = 4\mu\cos^2(\phi/4)\ \mathrm{tg}(\phi/4) && \left|\ \mathrm{tg}(\phi/4) = \sin(\phi/4)/\cos(\phi/4),\right.\\
&\frac{\mathrm{d}\phi}{\mathrm{d}x} = 2\mu\sin(\phi/2) && \left|\ \mathrm{d}/\mathrm{d}x,\right.\\
&\frac{\mathrm{d}^2\phi}{\mathrm{d}x^2} = \mu\frac{\mathrm{d}\phi}{\mathrm{d}x}\cos(\phi/2) && \left|\ \frac{\mathrm{d}\phi}{\mathrm{d}x} = 2\mu\sin(\phi/2),\right.\\
&\frac{\mathrm{d}^2\phi}{\mathrm{d}x^2} = \mu^2\sin\phi\,. &&
\end{aligned}$$

This relation satisfies the original governing equation. To transform this solution from the co-moving reference frame to the laboratory frame, the relativistic covariance of the equation permits the application of the Lorentz transformation:

$$x_{\mathrm{sol}} = \frac{x_{\mathrm{lab}} - x_0 - vt}{\sqrt{1 - v^2/c^2}}\,. \tag{1.897}$$

Consequently, the propagating solitary wave within the laboratory frame takes the form:

► $$\phi_{\pm}(t,x) = 4\,\mathrm{atg}\left[\mathrm{e}^{\left[\pm\mu\gamma(x - x_0 - vt)\right]}\right]\ ; \qquad \gamma \equiv \frac{1}{\sqrt{1 - v^2/c^2}}\,. \tag{1.898}$$

Evaluating the corresponding energy density according to relation (1.893) yields:

► $$\mathscr{E}_{\pm}(t,x) = \frac{8\mu^2\gamma^2(1 + v^2/c^2)\,\mathrm{e}^{[\pm2\mu\gamma(x - x_0 - vt)]}}{\left\{1 + \exp[\pm2\mu\gamma(x - x_0 - vt)]\right\}^2} - \mu^2\cos\left\{4\,\mathrm{atg}\left[\mathrm{e}^{[\pm\mu\gamma(x - x_0 - vt)]}\right]\right\}. \tag{1.899}$$

This solution represents a moving kink (step-like profile). Structurally, this is not a true soliton because the field is non-localized; however, its energy density remains strictly localized within the step. The solitary wave amplitude is invariant and independent of velocity or other parameters. Conversely, the total energy scales explicitly with velocity (analogous to how the kinetic energy of a macroscopic wave depends on its speed). The profiles for $\phi_{\pm}$, $\mathscr{E}_{\pm}$ are illustrated in Fig. 1.130.

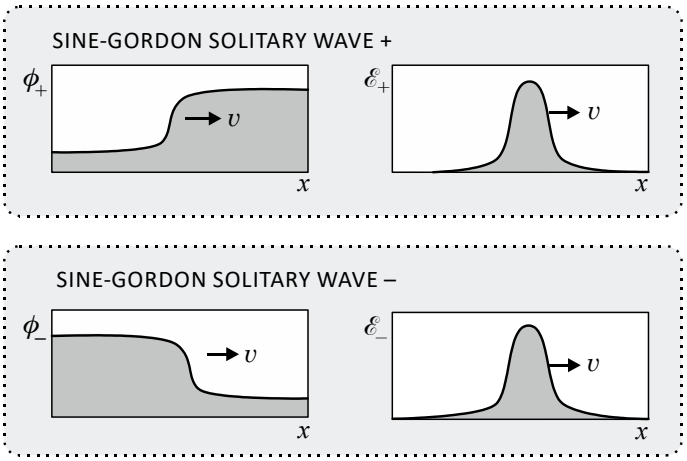


Fig. 1.130: Field profiles and corresponding energy density distributions for the sine-Gordon equation solutions.

Numerous physical phenomena are governed by the sine-Gordon equation. Key examples include mechanical domino chains, electrostatic double layers, crystal dislocations, the Josephson effect, and laser pulse propagation through two-level media.

Mechanical Domino Chains. A row of dominoes standing on their narrow edges represents a discrete mechanical chain. When perturbed, a cascade occurs where a localized wave of falling dominoes propagates through the sequence. If the field variables represent the height of the upper domino edge above the surface, $\phi = h(t, x)$, where x denotes the horizontal position, this controlled collapse corresponds to the ϕ_- solution. The sine-Gordon equation accurately models this behavior. The potential periodicity reflects the periodic spacing of the dominoes, and the propagating wavefront corresponds to the localized energy density $\mathscr{E}_-$, which acts as a quasiparticle (a translating energy packet). The amplitude of this solitary wave is fixed by the physical height of the dominoes and is independent of the propagation velocity.

Electrostatic Double Layers. Plasmas frequently exhibit propagating regions characterized by a sharp spatial transition of the electrostatic potential. Such localized structures feature a non-zero electric field that redistributes ambient plasma charges into a characteristic double layer, with positive charge accumulated on one side and negative charge on the opposite (see Subsection *Electrical Double Layer*, page 108). An electrostatic double layer represents a sine-Gordon solitary wave of the electric potential. The localized energy within the double layer, which must exceed the ambient thermal energy, can accelerate local particles to high kinetic energies. These structures manifest in both laboratory and space plasmas.

Crystal Dislocations. Consider a crystal lattice modeled by two atomic chains, where a fixed substrate chain exerts a periodic potential $V(x) = A[1-\cos(2\pi x/a)]$ on a secondary mobile chain, with a denoting the lattice constant. This configuration yields a sine-Gordon equation governing the atomic displacement from equilibrium. The solution (1.898) describes a dislocation propagating along the crystal. The solution transitions from zero displacement to a displacement exactly equal to one lattice constant a. The

dislocation energy is strictly localized within this transition region, representing a classical example of a sine-Gordon solitary wave.

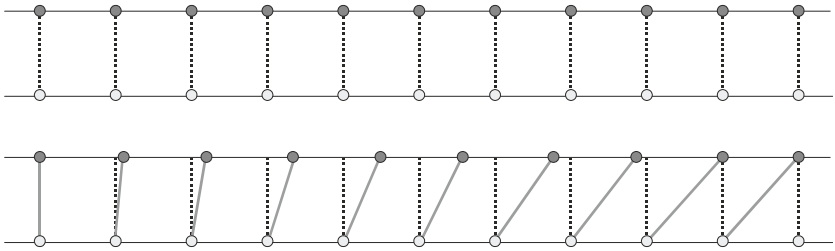


Fig. 1.131: Schematic of a crystal dislocation propagating through a periodic lattice potential.

Josephson Effect. When a current passes through a thin insulating barrier separating two superconductors, Cooper pairs tunnel through the insulator via the Josephson effect. The current density depends on the external magnetic field and temperature, a principle utilized in *Superconducting Quantum Interference Devices* (SQUIDs). The magnetic flux penetrates the Josephson junction in quantized units, which behave as quasiparticles known as *fluxons* or *magnons*. The transmission of the magnetic flux ϕ across the junction is governed by the sine-Gordon equation and exhibits a solitary wave character. The magnon acts as a quasiparticle describing a localized energy packet centered at the magnetic flux step.

Laser Pulse Propagation in Two-Level Media. Consider an optical medium composed of atoms with two distinct energy levels. When a resonant laser pulse matches the transition frequency between these levels, its intensity envelope is governed by the sine-Gordon equation, manifesting as a solitary wave. The ϕ_+ solution corresponds to stimulated emission under population inversion, describing pulse amplification. Conversely, the ϕ_- solution describes resonant absorption, corresponding to pulse attenuation.

KdV and NLS Solitons

Korteweg–de Vries Soliton. The most common categories of solitons comprise the KdV soliton satisfying the Korteweg–de Vries equation and the NLS soliton satisfying the nonlinear Schrödinger equation. The KdV equation constitutes the historically first discovered formulation yielding a soliton solution. Diederik Korteweg and Gustav de Vries derived this relation within a hydrodynamic description of shallow water waves. Its fundamental representation takes the form:

► $$\frac{\partial \phi}{c\,\partial t} + \alpha \phi \frac{\partial \phi}{\partial x} + \delta \frac{\partial^3 \phi}{\partial x^3} = 0\,, \tag{1.900}$$

where the constant c determines the phase velocity of perturbations within the given medium. The constant α governs the nonlinear term, structurally analogous to a material derivative of a velocity field and physically associated with convective fluid transport. The final constant δ scales the dispersive term, which is proportional to the third-order spatial derivative of the field. A soliton solution exists for arbitrary values of these parameters, as a wave velocity and amplitude can always be established such that dispersion is exactly counteracted by nonlinear compression. Multiplying by the constant c reduces the system to two independent coefficients:

►
$$\frac{\partial \phi}{\partial t} + A\phi\frac{\partial \phi}{\partial x} + D\frac{\partial^3 \phi}{\partial x^3} = 0\,; \tag{1.901}$$

$$A \equiv c\alpha; \qquad D \equiv c\delta. \tag{1.902}$$

Here, the dispersion is governed by the constant D, and nonlinear phenomena are scaled by the constant A. Although these parameters could be absorbed into the independent variables x and ϕ via appropriate substitutions, the KdV equation is retained in the general form (1.901) to preserve the manifest physical meaning of A and D. The target solution possesses two fundamental properties:

$$\lim_{x\to\pm\infty} \phi = 0\,, \tag{1.903}$$

$$\phi = \phi(\eta)\,; \qquad \eta \equiv x - x_0 \pm vt. \tag{1.904}$$

The first property (1.903) establishes the strict localization of the solution, meaning the field ϕ vanishes asymptotically far from the soliton core. The second property (1.904) describes the invariant propagation of the wavefront to the right (−) or left (+). Seeking a right-propagating solution (−) and substituting relation (1.904) into expression (1.901) yields the ordinary differential equation:

$$-v\frac{\mathrm{d}\phi}{\mathrm{d}\eta} + A\phi\frac{\mathrm{d}\phi}{\mathrm{d}\eta} + D\frac{\mathrm{d}^3\phi}{\mathrm{d}\eta^3} = 0\,. \tag{1.905}$$

Modifying the convective term via $\phi\phi' = (\phi^2/2)'$ and integrating the entire equation with respect to η yields a second-order ordinary differential equation:

$$-v\phi + \frac{A}{2}\phi^2 + D\frac{\mathrm{d}^2\phi}{\mathrm{d}\eta^2} = C_1\,. \tag{1.906}$$

The integration constant C_1 vanishes identically due to the localized boundary conditions (1.903). Multiplying the resulting equation by the first derivative ϕ' yields:

$$-v\phi\,\mathrm{d}\phi + \frac{A}{2}\phi^2\mathrm{d}\phi + D\frac{\mathrm{d}^2\phi}{\mathrm{d}\eta^2}\mathrm{d}\phi = 0\,, \tag{1.907}$$

where the final term is rewritten via (the prime denotes derivative according to η):

$$\frac{\mathrm{d}^2\phi}{\mathrm{d}\eta^2}\mathrm{d}\phi = \frac{\mathrm{d}^2\phi}{\mathrm{d}\eta^2}\frac{\mathrm{d}\phi}{\mathrm{d}\eta}\mathrm{d}\eta = \phi''\phi'\mathrm{d}\eta = \frac{1}{2}\frac{\mathrm{d}(\phi')^2}{\mathrm{d}\eta}\mathrm{d}\eta = \frac{1}{2}\,\mathrm{d}(\phi')^2\,. \tag{1.908}$$

Substituting this relation into equation (1.907) and performing integration yields:

$$-v\frac{\phi^2}{2} + \frac{A}{6}\phi^3 + \frac{D}{2}(\phi')^2 = C_2 \tag{1.909}$$

Imposing the localization requirement implies that the second integration constant also vanishes, reducing the KdV equation to a first-order ordinary differential equation:

$$\left(\frac{\mathrm{d}\phi}{\mathrm{d}\eta}\right)^2 = \frac{1}{D}\,\phi^2\left(v - \frac{A}{3}\phi\right), \tag{1.910}$$

which is readily separable. Following separation of variables, direct integration via appropriate substitution yields the solution:

$$\phi(\eta) = \frac{3v}{A}\cosh^{-2}\left[\sqrt{\frac{v}{4D}}\ \eta\right]. \tag{1.911}$$

Consequently, a soliton solution to the KdV equation exists for arbitrary parameters:

► $$\phi(t,x) = \frac{3v}{A}\cosh^{-2}\left[\sqrt{\frac{v}{4D}}\ (x - x_0 - vt)\right]. \tag{1.912}$$

The solution represents a localized crest propagating to the right at velocity v. The maximum amplitude is fundamentally coupled to its propagation velocity via:

► $$\phi_{\max} = \frac{3v}{A}. \tag{1.913}$$

Solitons of varying amplitudes propagate at different velocities, a hallmark characteristic of the KdV system. This relation can also be extracted directly from expression (1.910); at the peak amplitude, the first derivative on the left-hand side vanishes, immediately yielding the matching condition.

Note 1: The KdV equation is frequently expressed in a dimensionless form with coefficients absorbed into the variables, utilizing subscript notation for derivatives:

$$\phi_t + 6\phi\phi_x + \phi_{xxx} = 0. \tag{1.914}$$

The coefficient 6 is chosen conventionally to simplify the analytical solution. Within the present SI framework, setting $A = 6$ and $D = 1$ immediately recovers the normalized solution:

$$\phi(t,x) = \frac{v}{2}\cosh^{-2}\left[\frac{\sqrt{v}}{2}\ (x - x_0 - vt)\right]. \tag{1.915}$$

Note 2: The KdV equation serves as the simplest generalization of the wave equation of the type:

$$\frac{\partial\phi}{c\partial t} + \frac{\partial\phi}{\partial x} = 0. \tag{1.916}$$

This elementary wave equation yields the linear dispersion relation:

$$\omega = ck \tag{1.917}$$

Generalizing this dispersion relation by considering higher-order terms in the expansion yields:

$$\omega = c(k)k \approx (c_0 - c_1k^2)k = c_0k - c_1k^3 \tag{1.918}$$

The second term governs energy dissipation (implying a complex wave vector k) and must vanish for conservative solitons. The third term must be negative to ensure real k. Utilizing expression (1.918) as the baseline dispersion relation requires modifying the wave equation to the form:

$$\frac{\partial \phi}{c_0 \partial t} + \frac{\partial \phi}{\partial x} + c_1 \frac{\partial^3 \phi}{\partial x^3} = 0 \tag{1.919}$$

This modified wave equation can be formulated as a continuity equation:

$$\frac{\partial \phi}{\partial t} + \frac{\partial}{\partial x}\left[c_0 \phi + c_0 c_1 \frac{\partial^2 \phi}{\partial x^2} \right] = 0, \tag{1.920}$$

where the expression in the brackets denotes the flux of the quantity ϕ. Its primary generalization incorporating nonlinear phenomena is expressed as:

$$j = c_0 \phi + \alpha \phi^2 + c_0 c_1 \frac{\partial^2 \phi}{\partial x^2}, \tag{1.921}$$

yielding the partial differential equation:

$$\frac{\partial \phi}{\partial t} + c_0 \frac{\partial \phi}{\partial x} + 2\alpha \phi \frac{\partial \phi}{\partial x} + c_0 c_1 \frac{\partial^3 \phi}{\partial x^3} = 0 . \tag{1.922}$$

Shifting the independent spatial coordinate via $x \to x - c_0 t$ eliminates the second term, transforming the generalized wave equation into the standard KdV formulation (1.901):

$$\frac{\partial \phi}{\partial t} + A \phi \frac{\partial \phi}{\partial x} + D \frac{\partial^3 \phi}{\partial x^3} = 0 ; \qquad A = 2\alpha ; \quad D = c_0 c_1 . \tag{1.923}$$

Originally derived for shallow water waves, the KdV equation provided the first theoretical validation of the solitary wave observed by John Scott Russell in 1834. The resulting solution represents a robust solitary wave that retains its identity upon interaction with other waves, and whose velocity is uniquely determined by its height.

Nonlinear Schrödinger Soliton (NLS). A wide range of problems in quantum theory, plasma physics (Langmuir oscillations), and nonlinear optics are governed by the nonlinear Schrödinger equation. Its dimensionless representation is formulated as:

► $$\mathrm{i} \frac{\partial \phi}{\partial t} + \frac{\partial^2 \phi}{\partial x^2} + \sigma_\mathrm{D} \frac{\partial^2 \phi}{\partial y^2} + 2\sigma_\mathrm{N} \phi^2 \phi^* = 0. \tag{1.924}$$

The coefficient σ_D determines the NLS dispersion regime, yielding three categories:

- $\sigma_\mathrm{D} = +1$: elliptic NLS,
- $\sigma_\mathrm{D} = -1$: hyperbolic NLS,
- $\sigma_\mathrm{D} = 0$: (1+1)D NLS.

The final term represents the nonlinearity, which is cubic in this configuration but can be more complex. The coefficient σ_N dictates the type of modulational instability:

- $\sigma_\mathrm{N} = +1$: focusing,
- $\sigma_\mathrm{N} = -1$: defocusing.

The solution for the focusing (1+1)D NLS framework yields the Davydov soliton:

$$\phi(t,x) = \sqrt{\omega}\,\cosh^{-1}\left[\sqrt{\omega}\,(x - x_0 - vt)\right]\exp\left[\mathrm{i}\frac{vx}{2} - \mathrm{i}\left(\frac{v}{2}\right)^2 t + \mathrm{i}\,\omega t + \mathrm{i}\,\delta\right]. \quad (1.925)$$

A free parameter ω appears within the solution; the NLS soliton incorporates a plane wave modulated by a $\cosh^{-1}$ envelope. The amplitude is independent of velocity, scaling instead with the frequency of the wave packet trapped within the envelope. A comparison between both soliton classes reveals key distinctions:

- The KdV soliton is a single localized elevation (e.g., a surface water wave), whereas the NLS soliton manifests as a wave packet where a high-frequency carrier wave is modulated by a localized envelope.
- The propagation velocity of a KdV soliton depends on its amplitude, whereas the velocity of an NLS soliton is independent of its amplitude.
- For a KdV soliton, the product of the wave height and the square of its width remains constant; no such constraint applies to the NLS soliton.
- KdV solitons perfectly retain their shape post-collision, experiencing at most a phase shift. NLS solitons preserve their identity upon interaction, though their profile undergoes minor structural modifications.

The simplest analytical avenue to derive an equation yielding solitary solutions relies on modifying the 1D Navier–Stokes equation

$$\rho\frac{\partial u}{\partial t} + \rho u \cdot \nabla u = \eta\,\Delta u \quad (1.926)$$

into the simplified structure:

$$\frac{\partial u}{\partial t} + \frac{\partial}{\partial x}\left(\frac{u^2}{2}\right) = \frac{\eta}{\rho}\frac{\partial^2 u}{\partial x^2}. \quad (1.927)$$

This formulation represents the **Burgers equation**

$$\frac{\partial u}{\partial t} + A\frac{\partial}{\partial x}\left(u^2\right) - D\frac{\partial^2 u}{\partial x^2} = 0 \quad (1.928)$$

incorporating both nonlinear and dispersive terms. The Burgers equation similarly provides solitary wave solutions. The analytical procedure is fully analogous to the KdV framework: substituting t and x via the co-moving coordinate $\eta = x - vt$ reduces the partial differential equation to an integrable ordinary differential equation, subsequently solved via separation of variables.

Under specific boundary conditions, multiple solitons can organize into a coherent moving formation designated as a *soliton train*. Alternatively, a solitary wave can exhibit localized periodic internal oscillations while radiating no energy, periodically returning to its initial state. Although not constituting a true soliton due to this shape modulation, this related phenomenon is conventionally designated as a *breather*.

Solitons in Plasma Environments

Langmuir Solitons. Under specific assumptions, the fluid equations governing magnetohydrodynamics reduce to either the KdV or NLS equation. A key phenomenon constitutes the nonlinear modification of electron plasma (Langmuir) oscillations at the electron plasma frequency, which become highly localized. This process forms a density cavity filled with a high-frequency electric field, where the plasma density is depleted according to the relation:

$$\frac{\delta n}{n} \approx \frac{p_{\mathrm{E}}}{p_{\mathrm{T}}} \approx \frac{\varepsilon E^2/2}{2nk_{\mathrm{B}}T}. \tag{1.929}$$

Consequently, a Langmuir soliton is frequently referred to as a density well. The electric field envelope satisfies the relation:

$$E(x) \approx E_0 \cosh^{-1}(k_0 x)$$

and the corresponding energy density is governed by a KdV soliton profile:

$$\mathscr{E}(x) = \varepsilon E^2/2 \approx E_0^2 \cosh^{-2}(k_0 x)$$

This represents a simplified limiting configuration. Langmuir solitons exhibit significant complexity, manifesting as NLS solitons under certain regimes. A Langmuir soliton can oscillate, generating low-frequency ion-acoustic waves; conversely, at long wavelengths, it can absorb energy from ion-acoustic waves via parametric instability. At short wavelengths, it dissipates energy via Landau damping, establishing a stationary energy flux in *k*-space. A soliton exchanging energy with its environment is designated as a dissipative soliton. Langmuir solitons typically generate during the decay of intense electron plasma oscillations. These structures can be artificially generated in laboratories utilizing the *Double Plasma* device discussed below.

Davydov Solitons. This solution relates to Langmuir waves and is governed by the *Zakharov–Kuznetsov* system of partial differential equations:

$$\begin{aligned} \mathrm{i}\frac{\partial \phi}{\partial t} + \frac{\partial^2 \phi}{\partial x^2} &= \phi\psi\,; \\ \frac{\partial^2 \psi}{\partial x^2} - \frac{\partial^2 \psi}{\partial t^2} &= \frac{\partial^2 (\phi^2)}{\partial x^2}. \end{aligned} \tag{1.930}$$

►

Analogous mathematical structures arise in quantum chemistry and quantum field theory. In plasma physics, this system models electron-beam instabilities and Langmuir wave dynamics. The variable ϕ corresponds to the electric field potential, and ψ represents the ion density perturbation from equilibrium. The electric field satisfies a Schrödinger-type equation with a nonlinear source driven by the ion density perturbation. Conversely, the ion density satisfies a wave equation driven by a ponderomotive source term (proportional to the second derivative of the electric field square, representing the radiation pressure). This system yields a solitary wave solution known as the Davydov soliton:

$$\phi(t,x) = \sqrt{2(1-v^2)\omega}\,\cosh^{-1}\left[\sqrt{\omega}(x-vt)\right]\exp\left[\mathrm{i}\frac{vx}{2}-\mathrm{i}\left(\frac{v}{2}\right)^2 t+\mathrm{i}\,\omega t+\mathrm{i}\,\delta\right];$$
$$\psi(t,x) = -2\omega\cosh^{-2}\left[\sqrt{\omega}\,(x-vt)\right]. \tag{1.931}$$

The parameters comprise the soliton velocity v, a spatial phase shift δ, and a scaling parameter ω. Under specific constraints, the Zakharov–Kuznetsov equations reduce to either the NLS or KdV equation, where the Davydov soliton simplifies to a standard Langmuir soliton.

Trivelpiece–Gould Solitons. This soliton configuration is associated with electron plasma waves propagating within bounded geometry, manifesting as a plasma compression that scales according to the KdV equation. These solitons are most readily generated within a Q-machine, which consists of a cylindrical vacuum vessel terminated by planar hot metallic plates coated with an alkali metal (such as cesium or potassium). Thermionic emission from these heated plates generates electrons and ions. A strong axial magnetic field constrains the plasma, suppressing cross-field radial diffusion.

The resulting plasma features equal electron and ion temperatures ($T_\mathrm{e} \sim T_\mathrm{i}$), which presents a distinct experimental limitation; when the ion temperature matches the electron temperature, the phase velocity of the ion-acoustic wave becomes comparable to the ion thermal speed. Under this condition, resonant ions travel at the wave speed, absorbing wave energy via severe ion Landau damping. Conversely, when $T_\mathrm{e} >> T_\mathrm{i}$, ion Landau damping becomes negligible, which is ideal for soliton excitation. The soliton can be driven within the cylinder via an external voltage pulse.

Experimental validation indicates that the product of the wave height and the square of its width remains constant, and the propagation velocity depends strictly on the amplitude. A minor oscillatory wake is typically observed trailing the soliton. The bounded modes associated with this soliton were first documented in 1959 by Alvin W. Trivelpiece and Roy W. Gould at the California Institute of Technology.

Ion-Acoustic Solitons. This class of solitons evolves from acoustic modes propagating through a plasma. Unlike sound waves in neutral gases, these modes are carried by ions interacting via self-consistent electrostatic fields. Ion-acoustic solitons represent the most thoroughly investigated plasma solitons, generated easily within *Double Plasma* (DP) devices via a tailored voltage pulse. This setup permits the reliable generation of planar, cylindrical, or spherical solitons. Structurally, ion-acoustic solitons are governed by the KdV equation, and experimental observations align precisely with its analytical predictions in laboratory plasma environments.

The Double Plasma (DP) device constitutes the most significant experimental apparatus utilized in soliton research. A conventional configuration is illustrated in Fig. 1.132; the pioneering device of this type was constructed by Rudolf Limpaecher and Keneth R. MacKenzie in 1973. The system consists of a dual plasma chamber separated by a fine metallic mesh. This grid is electrically isolated, self-biasing to a negative potential of several tens of volts, which acts as an electrostatic barrier preventing electron transport between the two volumes. The voltages ϕ_HD and ϕ_HT govern the filament heating required for thermionic electron emission, while ϕ_AD and ϕ_AT accelerate these primary electrons to ionize the background working gas. To optimize plasma confinement, rows of permanent dipole magnets (arranged in an alternating polarity configura-

tion) line the chamber circumference, numbering between one and two thousand depending on the vessel dimensions. A carefully selected bias voltage ϕ_B controls ion transport between the chambers.

The baseline configuration provided approximately 1 m^3 of quiescent, collisionless plasma (where the mean free path exceeded the device dimensions), featuring an electron density of 10^7 to 10^{10} cm^{-3}, an electron temperature of 1 to 3 eV, and an ion temperature below 0.1 T_e. This low ion temperature suppresses ion Landau damping, ensuring that the generated ion-acoustic waves propagate without severe attenuation. The permanent magnets provided a surface field of 0.2 T, spaced 10 cm apart.

A soliton can be triggered via multiple methods, primarily by applying a voltage pulse ϕ_S that induces a localized ion density perturbation propagating from the driver chamber into the target (diagnostic) chamber. Alternative excitation techniques include direct grid modulation, biasing a metallic object immersed within the driver chamber (where a cylindrical object excites a cylindrical soliton), planar photoionization via focused light (yielding a planar soliton), or utilizing driven wire arrays. Such devices represent the standard framework for investigating ion-acoustic solitons, with modern variants incorporating spherical or cylindrical geometry.

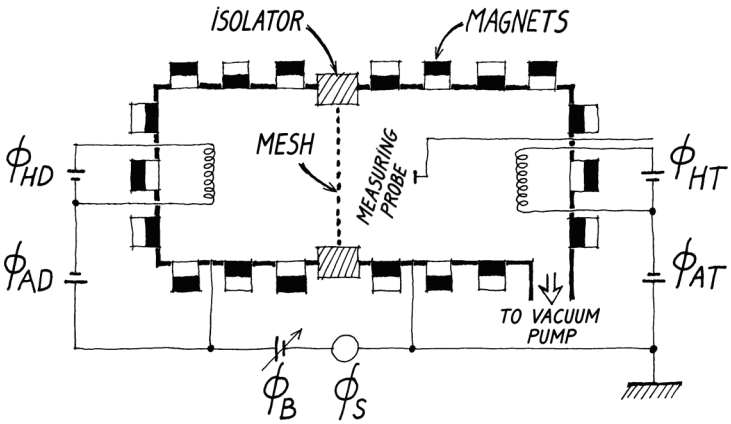


Fig. 1.132: Schematic diagram of a Double Plasma (DP) apparatus utilized for the excitation and diagnostics of ion-acoustic solitons.

1.7.4 Turbulence

The final section of plasma theory addresses turbulence. Turbulent dynamics represent some of the most ubiquitous motions in nature. These ubiquitous dynamics lack a closed analytical solution. Investigating turbulent processes relies on dimensional analysis, magnetohydrodynamics, statistical formulations, or numerical simulations. The following overview outlines baseline relations as an introductory summary; comprehensive developments are available in specialized textbooks.

Turbulent Structures

Turbulence predominantly manifests at high flow velocities, where excess kinetic energy triggers a transition from laminar to turbulent regimes. Nonlinear mechanisms store this energy within the rotational motion of vortices across a wide spectrum of spatial scales. Turbulent fields arise during flow separation around obstacles and govern atmospheric dynamics. In plasma environments, turbulent motions occur frequently, characterizing the solar wind, astrophysical systems, industrial reactors, and magnetic confinement fusion devices. In plasmas, turbulence typically evolves from the growth and saturation of various microinstabilities.

Although turbulence exhibits apparent chaos driven by millions of degrees of freedom, its defining attribute constitutes the *energy cascade*. Flow dynamics generate vortices across a vast range of spatial dimensions, where the largest eddies possess scales comparable to the macroscopic system boundaries. These structures stretch and fragment into smaller configurations. Consequently, kinetic energy is continuously transported via nonlinear coupling down to the *Kolmogorov scale*. At this minimum bound, the cascade ceases, and dissipative mechanisms driven by fluid viscosity convert the microscopic kinetic energy into chaotic thermal energy. Additionally, these dynamics drive macroscopic transport via turbulent diffusion. The turbulent velocity field can be decomposed via a standard Fourier expansion:

► $$\mathbf{u}(t,\mathbf{x}) = \int \mathcal{U}(\omega,\mathbf{k})\, \mathrm{e}^{\mathrm{i}[\mathbf{k}\mathbf{x}-\omega t]}\, \mathrm{d}^3\,\mathbf{k}\ , \tag{1.932}$$

where the four parameters ω, $\mathbf{k}$ characterizing the Fourier components are coupled via the linear or nonlinear dispersion relation. The magnitude of the wave vector $\mathbf{k}$ characterizes the spatial dimensions of the structures associated with a given mode:

► $$k = \frac{2\pi}{\lambda} \sim \frac{2\pi}{R} \tag{1.933}$$

The largest vortices possess a scale R_C comparable to the system geometry, whereas the minimum corresponds to the Kolmogorov scale R_K. In magnetized plasmas, the lower limit is the ion Larmor radius R_Li. Characterizing turbulence requires the energy spectrum, where kinetic energy per unit mass is compiled from Fourier modes:

► $$\langle\, \mathbf{u}\cdot\mathbf{u}/2\,\rangle = \int_0^\infty \mathcal{E}(k)\, \mathrm{d}k\ . \tag{1.934}$$

$\mathcal{E}(k)$ denotes the turbulent energy spectrum. As illustrated in Fig. 1.133 energy spectrum exhibits three distinct operational regimes classified by vortex scale:

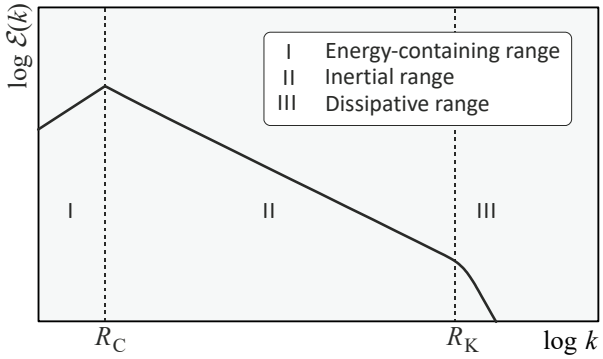


Fig. 1.133. Schematic representation of the three fundamental regimes in the energy spectrum.

The largest scales occupy Regime I, designated as the *energy-containing range*. Viscous effects are negligible here, and these large structures undergo minimal energy transfer to smaller configurations. These large eddies are neither homogeneous nor isotropic, rendering this range minor for local spectral energy transfer. Conversely, standard turbulence is characterized by Regime II, termed the *inertial range*, which hosts the turbulent energy cascade. Larger vortices transfer energy strictly to smaller scales. Fluid viscosity influences these dynamics but does not dominate. For conventional unmagnetized fluids, the vortex distribution is homogeneous and isotropic, yielding an energy spectrum proportional to $k^{-5/3}$ (the Kolmogorov spectrum). The existence of this subrange and the associated directional energy cascade distinguishes turbulence from other stochastic or chaotic phenomena. In plasma media, vortices are strongly modified by the background magnetic field, inducing severe anisotropy where the spectral scaling differs between the parallel and perpendicular wave vector components. The final domain constitutes the *dissipative range* (Regime III), where viscous mechanisms dominate, rapidly suppressing small-scale vortices and converting their kinetic energy into heat.

Kolmogorov Turbulence Model

The first successful phenomenological model of turbulence was formulated by the Soviet mathematician Andrey Nikolaevich Kolmogorov in 1941, conventionally designated as the K41 model. Kolmogorov postulated that all vortices within the inertial subrange are spatially and temporally microscopic relative to the macroscopic system scales ($r \ll L$, $\delta t \ll L/u$). These small-scale eddies possess no preferred orientation, exhibiting local homogeneity and isotropy. All directional memory from the large-scale forcing is lost during the cascade. Consequently, the resulting vortex statistics exhibit a universal character, depending strictly on the wave number k and the energy dissipation rate $\varepsilon \equiv \mathrm{d}(u^2/2)/\mathrm{d}t$ governed by viscous processes. The scaling laws can be derived via dimensional analysis. Evaluating the dimensions of the core quantities from relation (1.934) and the energy dissipation rate ε yields:

$$[u^2/2] = \mathrm{m}^2\mathrm{s}^{-2}; \qquad [k] = \mathrm{m}^{-1}; \qquad [\mathcal{E}] = \mathrm{m}^3\mathrm{s}^{-2}; \qquad [\varepsilon] = \mathrm{m}^2\mathrm{s}^{-3}. \tag{1.935}$$

Dimensional analysis dictates that the energy spectrum can only satisfy the unique functional scaling law:

► $$\mathcal{E} = K_0\, \varepsilon^{2/3}\, k^{-5/3}, \tag{1.936}$$

where K_0 represents a universal dimensionless constant. This scaling governs numerous unmagnetized fluids within the inertial range. In plasma applications, electrostatic potential fluctuations are highly significant, with their spectrum expressed as:

$$\langle (\delta\phi)^2 \rangle = \int_0^\infty S(k)\,\mathrm{d}k. \tag{1.937}$$

Dimensional analysis yields the scaling law:

$$S(k) \sim k^{-5}. \tag{1.938}$$

However, expression (1.938) remains valid strictly under the assumption that the electrostatic potential fluctuations are independent of the ion Larmor radius. Incorporating the Larmor radius would introduce an additional spatial parameter (with dimensions of meters) into the dimensional formulation, preventing a unique algebraic solution. Consequently, relation (1.938) must be interpreted with caution.

Similarly, the Kolmogorov microscale R_K can be evaluated via dimensional analysis. Combining the kinematic viscosity v and the energy dissipation rate $\mathscr{P}$ to form a unique parameter with the dimension of length yields the scaling law:

$$R_\mathrm{K} \approx v^{3/4} / \mathscr{P}^{1/4}. \tag{1.939}$$

This relation applies exclusively to processes where ion gyration dynamics do not dictate the baseline interactions. Consequently, its application is restricted to conventional fluid turbulence in the absence of external magnetic fields.

Turbulence in Magnetohydrodynamics

Consider the foundational framework of magnetohydrodynamics (MHD) incorporating viscous incompressible fluid. The governing equations are expressed as:

► $$\rho\frac{\partial \mathbf{u}}{\partial t} + \rho(\mathbf{u}\cdot\nabla)\mathbf{u} = \eta_\mathrm{L}\Delta\mathbf{u} - \nabla p_\mathrm{L} + \frac{1}{\mu}\operatorname{curl}\mathbf{B}\times\mathbf{B}, \tag{1.940}$$

► $$\frac{\partial \mathbf{B}}{\partial t} = \frac{1}{\sigma\mu}\Delta\mathbf{B} + \operatorname{curl}\mathbf{u}\times\mathbf{B}. \tag{1.941}$$

The first expression represents the plasma equation of motion, where the right-hand side sequentially incorporates the viscous force density, the pressure gradient force density, and the Lorentz force density. The second equation governs the temporal evolution of the magnetic field, where the first term describes magnetic diffusion and the second represents magnetic field freezing. These formulations are supplemented by the divergence constraints. For an incompressible fluid, these relations reduce to

$$\operatorname{div}\mathbf{B} = 0, \tag{1.942}$$

$$\operatorname{div}\mathbf{u} = 0. \tag{1.943}$$

Equation (1.943) dictates that the plasma is incompressible, rendering its mass density constant. Dividing equation (1.940) by the density and absorbing the magnetic permeability into the magnetic field yields

► $$\frac{\partial \mathbf{u}}{\partial t} + (\mathbf{u}\cdot\nabla)\,\mathbf{u} = \nu_{\mathrm{L}}\Delta\mathbf{u} - \nabla P_{\mathrm{L}} + \mathrm{curl}\,\mathbf{b}\times\mathbf{b}\,, \tag{1.944}$$

► $$\frac{\partial \mathbf{b}}{\partial t} = \nu_{\mathrm{M}}\Delta\mathbf{b} + \mathrm{curl}\,\mathbf{u}\times\mathbf{b}\,, \tag{1.945}$$

where the rescaled fields are defined as:

$$\mathbf{b} \equiv \frac{\mathbf{B}}{\sqrt{\mu\rho}}; \qquad P_{\mathrm{L}} \equiv \frac{p_{\mathrm{L}}}{\rho}; \qquad \nu_{\mathrm{M}} \equiv \frac{1}{\sigma\mu} \tag{1.946}$$

The rescaled magnetic field **b** possesses the dimensions of velocity, corresponding directly to the Alfvén velocity associated with the local field configuration. Consequently, the equations for the velocity and magnetic fields share identical dimensions. Comparing the individual terms yields the dimensionless characteristics of the flow:

$$\#_{\mathrm{Re}} \equiv \frac{|(\mathbf{u}\cdot\nabla)\,\mathbf{u}|}{|\nu_{\mathrm{L}}\Delta\mathbf{u}|} \approx \frac{Lu}{\nu_{\mathrm{L}}}; \tag{1.947}$$

$$\#_{\mathrm{ReM}} \equiv \frac{|\mathrm{curl}\,\mathbf{u}\times\mathbf{b}|}{|\nu_{\mathrm{M}}\Delta\mathbf{b}|} \approx \frac{Lu}{\nu_{\mathrm{M}}}; \tag{1.948}$$

$$\#_{\mathrm{Pr}} \equiv \frac{\#_{\mathrm{ReM}}}{\#_{\mathrm{Re}}} \approx \frac{\nu_{\mathrm{M}}}{\nu_{\mathrm{L}}}; \tag{1.949}$$

The Reynolds number $\#_{\mathrm{Re}}$ expresses the ratio of the convective term to the viscous term. High Reynolds numbers signify an excess of kinetic energy, triggering a transition to the turbulent regime. Thus, the magnitude of $\#_{\mathrm{Re}}$ dictates the spontaneous onset of turbulence, which can be further accelerated in plasmas by the growth of microinstabilities.

The magnetic Reynolds number $\#_{\mathrm{ReM}}$ represents the ratio of the convective freezing term to the magnetic diffusion term. In most laboratory and astrophysical plasmas, $\#_{\mathrm{ReM}}$ is exceptionally high, rendering magnetic freezing dominant over diffusion. The magnitude of $\#_{\mathrm{ReM}}$ does not explicitly govern the onset of fluid turbulence.

Finally, the magnetic Prandtl number $\#_{\mathrm{Pr}}$ expresses the ratio of magnetic diffusion to kinematic viscosity. In astrophysics, $\#_{\mathrm{Pr}}$ is 10^{29} in the intergalactic medium, ~ 1 in the solar wind and $\ll 1$ in the solar convective zone, quantifying the relative impact of Ohmic versus viscous dissipation.

Elsässer Variables

Equations (1.944) and (1.945) can be cast into a symmetric formulation by expanding the vector triple products on the right-hand sides. In the equation of motion, this decomposition separates the Lorentz force density into a magnetic pressure gradient and a magnetic tension contribution driven by field line curvature. In the induction equation, this transformation yields a total time derivative on the left-hand side. The resulting symmetric formulations are expressed as:

$$\frac{\partial \mathbf{u}}{\partial t} + (\mathbf{u}\cdot\nabla)\,\mathbf{u} = \nu_{\mathrm{L}}\Delta\mathbf{u} - \nabla\left(P_{\mathrm{L}} + P_{\mathrm{M}}\right) + (\mathbf{b}\cdot\nabla)\,\mathbf{b}\,, \tag{1.950}$$

$$\frac{\partial \mathbf{b}}{\partial t} + (\mathbf{u}\cdot\nabla)\,\mathbf{b} = \nu_{\mathrm{M}}\Delta\mathbf{b} + (\mathbf{b}\cdot\nabla)\,\mathbf{u}\,. \tag{1.951}$$

The magnetic pressure contribution within the equation of motion is expressed as:

$$P_{\mathrm{M}} \equiv \frac{p_{\mathrm{M}}}{\rho} = \frac{\mathbf{B}^2}{2\mu\rho} = \frac{\mathbf{b}^2}{2} \tag{1.952}$$

Equations (1.950) and (1.951) share identical dimensions. In a co-moving reference frame, the fields decompose into background and fluctuating components:

$$\mathbf{u} = \delta\mathbf{u}\,, \tag{1.953}$$

$$\mathbf{b} = \mathbf{b}_0 + \delta\mathbf{b}\,. \tag{1.954}$$

The velocity field retains only fluctuations, while the magnetic field comprises background and fluctuating fields. In 1950, Walter M. Elsässer introduced new variables:

$$\mathbf{z} = \delta\mathbf{u} - \delta\mathbf{b}\,, \tag{1.955}$$

$$\mathbf{w} = \delta\mathbf{u} + \delta\mathbf{b}\,. \tag{1.956}$$

These Elsässer variables are frequently designated via the symbols $\mathbf{z}_{\pm}$. Summing and subtracting the equations of motion and induction (1.950)–(1.951) yields:

► $$\frac{\partial \mathbf{z}}{\partial t} + (\mathbf{b}_0 \cdot \nabla)\mathbf{z} + (\mathbf{w} \cdot \nabla)\mathbf{z} = \Delta\left[\frac{\nu_{\mathrm{L}} - \nu_{\mathrm{M}}}{2}\mathbf{w} + \frac{\nu_{\mathrm{L}} + \nu_{\mathrm{M}}}{2}\mathbf{z}\right] - \nabla\left(P_{\mathrm{L}} + P_{\mathrm{M}}\right), \tag{1.957}$$

► $$\frac{\partial \mathbf{w}}{\partial t} - (\mathbf{b}_0 \cdot \nabla)\mathbf{w} + (\mathbf{z} \cdot \nabla)\mathbf{w} = \Delta\left[\frac{\nu_{\mathrm{L}} + \nu_{\mathrm{M}}}{2}\mathbf{w} + \frac{\nu_{\mathrm{L}} - \nu_{\mathrm{M}}}{2}\mathbf{z}\right] - \nabla\left(P_{\mathrm{L}} + P_{\mathrm{M}}\right). \tag{1.958}$$

The formulations for the Elsässer variables serve as the foundational starting point for analytical, scaling, and numerical investigations of MHD turbulence. Neglecting the background magnetic field, or assuming homogeneous and isotropic fluctuations where the characteristic timescale is driven exclusively by nonlinear interactions, i.e.,

$$\tau_{\mathrm{NL}} \simeq (kw)^{-1} \simeq (kz)^{-1}\,, \tag{1.959}$$

which recovers the standard Kolmogorov spectrum via dimensional analysis:

► $$\mathcal{E}_{\mathrm{K}} \sim \varepsilon^{2/3} k^{-5/3}\,. \tag{1.960}$$

Conversely, the primary focus concerns the influence of a strong background magnetic field, where the characteristic timescale is governed by the Alfvén transit time:

$$\tau_{\mathrm{A}} \simeq \frac{L}{v_{\mathrm{A}}} = \frac{L}{b_0}\,. \tag{1.961},$$

Maintaining the assumption of isotropic fluctuations (valid for weak background fields and small-scale eddies) yields the IK64 model, named after the Soviet astrophysicist Pyotr Savich Iroshnikov and the American theorist Robert Henry Kraichnan. Iroshnikov formulated this turbulence model in 1964, and Kraichnan derived it independently in 1965. The resulting spectral scaling relation is expressed as:

► $$\mathcal{E}_{\mathrm{IK}}(k) \sim \left(v_{\mathrm{A}}\varepsilon\right)^{1/2} k^{-3/2}\,. \tag{1.962}$$

Thus, the IK64 energy spectrum depends on the background magnetic field.



Fig. 1.134: Turbulent structures within Jupiter's northern hemisphere atmosphere, captured by the Juno spacecraft on May 23, 2018 (NASA/JPL).

Strong Anisotropic Turbulence

A strong background magnetic field introduces severe anisotropy into the plasma, rendering the assumption of homogeneous and isotropic turbulence invalid. Unlike the one-dimensional Kolmogorov description (1.934), the energy spectrum must be defined via a three-dimensional formulation:

$$\langle \mathbf{u} \cdot \mathbf{u} / 2 \rangle = \int_0^\infty \mathcal{E}(k_{\|}, k_{\perp}) \, \mathrm{d}^3 \mathbf{k} \, . \tag{1.963}$$

The dimensions of the energy spectrum differ from the one-dimensional representation. Anisotropic turbulence models are classified into weak and strong regimes. In *weak turbulence* (WT), both Elsässer fluctuations are significantly smaller than the background magnetic field, a constraint that breaks down in the strong turbulence regime. The weak MHD turbulence framework yields the energy spectrum scaling:

► $$\mathcal{E}_{\mathrm{WT}}(k) \sim k_{\|}^{1/2} k_{\perp}^{-2} \, . \tag{1.964}$$

However, weak turbulence conditions are rarely sustained in fully developed plasma systems; once turbulence develops, it typically transitions into a *strong regime*. The conditions for strong MHD turbulence were investigated by the American astrophysicist Peter Goldreich and the Indian physicist Seshadri Sridhar. Their 1995 results are designated as the GS95 model. The resulting energy spectrum exhibits highly interesting properties. Assuming the fluctuations remain isotropic at least within the plane perpendicular to the background magnetic field, the spectrum collapses into a one-dimensional form, recovering the Kolmogorov scaling:

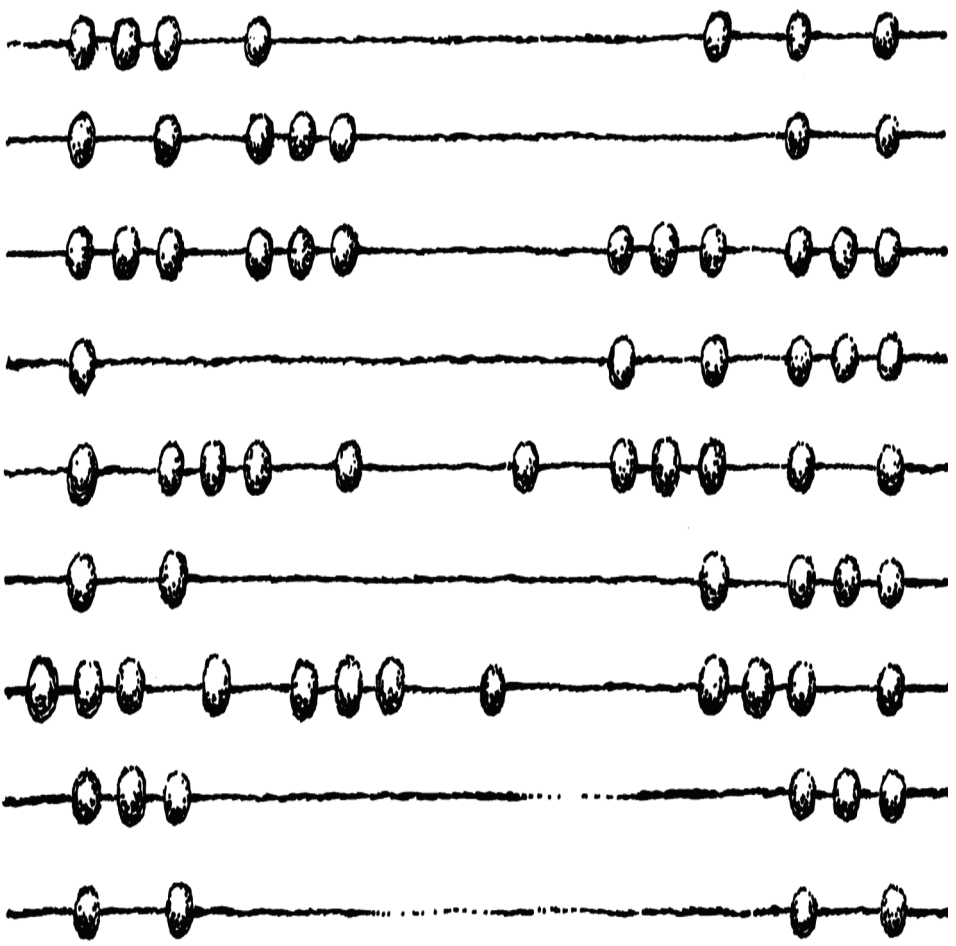
► $$\mathcal{E}_{\mathrm{GS}}(k) \sim \varepsilon^{2/3} k_{\perp}^{-5/3} \, . \tag{1.965}$$

For the parallel component, a critical balance is established between both wave vector components, satisfying the relation:

► $$k_{\|} \sim k_{\perp}^{2/3} \, . \tag{1.966}$$

The proportionality coefficients within the GS95 model depend explicitly on the Alfvén velocity and other local parameters, rendering direct experimental validation challenging. Numerical simulations indicate that in fully developed turbulence with a background magnetic field, the results for weak fields approach the GS95 scaling, whereas strong background fields align with the IK64 model. The physics of plasma turbulence remains an open discipline with numerous unresolved questions.

2. Numerical Simulations



2.1 Particle Motion Simulations

Analytical expressions for the trajectory of a charged particle in a homogeneous electric or magnetic field were derived in the previous chapters. In a more general case, obtaining an analytical expression for the trajectory is either highly difficult or entirely impossible. The systems of differential equations resulting from the equations of motion are nonlinear and rarely solvable analytically. Although solutions can be expanded into an infinite series with subsequent truncation to the first few terms, or simplification can be achieved via specific approximations – such as the adiabatic approximation for slowly varying fields – numerical simulations remain the primary recourse in most scenarios.

Physics was traditionally considered to consist of two inseparable components: experiment and theory. With the rapid advancement of computing technology in recent decades, all physical branches can now be described as comprising three interconnected and indispensable components: experiment, theory, and numerical simulations. Numerical simulations assist in verifying theories without costly experiments, obtaining information on the behavior of the investigated subject, and designing experiments to maximize results with minimal resources. Numerical simulations are also instrumental in processing large volumes of experimental data. Contemporary plasma physics can no longer be conceptualized without numerical simulations.

This textbook does not primarily focus on numerical methods in plasma physics. Nevertheless, the opportunity to simulate the discussed phenomena on a computer is provided for the inquisitive reader proficient in basic programming. This part of the textbook therefore serves as a sort of "cookbook" of selected algorithms that will make this possible. This selection comprises only one or a few algorithms out of many, presented without detailed explanation. Readers interested in numerical methods are referred to specialized publications dedicated to numerical simulations in plasma physics.

2.1.1 Newton-Euler Scheme (NE)

The simplest method for solving differential equations involves their conversion into difference equations, where derivatives are replaced by finite differences. This procedure is demonstrated using a simple problem of charged particle motion in a capacitor:

◖ **Example 2.1:** Find a difference scheme for the acceleration of a charged particle between capacitor plates. Consider the electric field to be homogeneous and the motion to be non-relativistic.

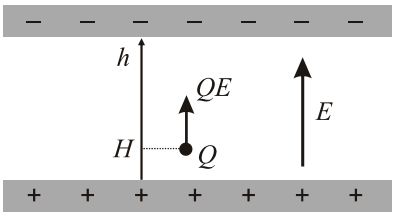


Fig. 2.1: Particle in Capacitor.

Solution: The equation of motion follows from the Newton second law:

$$m\ddot{h} = QE\,. \tag{2.1}$$

The resulting differential equation $\mathrm{d}^2h/\mathrm{d}t^2 = QE/m$ is exceptionally simple, and its analytical solution could be easily found. The formulation of the difference scheme is intentionally demonstrated on this simple equation. The same procedure can be applied to more complex equations that lack analytical solutions.

First, the second-order differential equation is converted into a system of two first-order equations, utilizing the definition of velocity as the first derivative of the position variable with respect to time:

$$\frac{\mathrm{d}h}{\mathrm{d}t} = v\,,$$
$$\frac{\mathrm{d}v}{\mathrm{d}t} = \frac{QE}{m}\,.$$

Solutions are sought only at discrete time intervals (difference equations) rather than for all continuous times. In practice, the actual solution is approximated by a piecewise linear curve. The focus is therefore restricted to specific values:

$$h_n = h(t_n)\,,$$
$$v_n = v(t_n)\,,$$
$$t_n = t_0 + n\,\Delta t\,; \qquad n = 1, 2, \ldots$$

The actual derivatives are replaced by finite differences:

$$\frac{h_{n+1} - h_n}{\Delta t} \cong v_n\,,$$
$$\frac{v_{n+1} - v_n}{\Delta t} \cong \frac{QE}{m}\,. \tag{2.2}$$

The values at time t_{n+1} are calculated using the values from time t_n:

$$h_{n+1} = h_n + v_n \Delta t\,,$$
$$v_{n+1} = v_n + \frac{QE}{m}\Delta t\,. \tag{2.3}$$

A difference scheme is thus obtained, through which individual sequential values are calculated:

$$h_0, v_0 \quad \Rightarrow \quad h_1, v_1 \quad \Rightarrow \quad h_2, v_2 \quad \Rightarrow \quad \cdots \quad .$$

For the numerical construction of the solution, knowledge of the initial height and initial velocity (the initial conditions) is sufficient:

$$h_0 = H, \quad v_0 = 0\,.$$

◗

Although the described procedure appears simple and straightforward, specific limitations exist. The computer-generated trajectory eventually deviates from the actual trajectory due to both rounding errors and the replacement of derivatives with differences.

Rounding errors can be partially eliminated by an appropriate choice of dimensionless variables. The error resulting from the use of differences instead of derivatives can be reduced by selecting a smaller time step. However, a compromise between the number of executed operations and the achieved accuracy must always be made. The time step does not need to remain constant throughout the entire calculation. In regions with large field gradients where the particle rapidly changes its position and velocity, a finer time step can be chosen compared to regions with minimal particle motion changes.

The derived scheme is designated as the Newton-Euler scheme and belongs to the class of *explicit schemes*. This classification arises because the right-hand side of equation (2.2) is expressed using the earlier time t_n after replacing the derivatives with differences. This choice enables an explicit expression (2.3) for the variables at the new time t_{n+1}. If the right-hand sides of (2.2) were expressed at the newer time t_{n+1}, an algebraic system of equations for h_{n+1} and v_{n+1} would be obtained. The new values h_{n+1} and v_{n+1} could then be determined from h_n and v_n only after solving this system. Such a scheme is called *implicit*. Although generally more stable and accurate than an explicit scheme, it requires solving a system of algebraic equations at each time step.

Order of the Scheme

Difference schemes are thus categorized as either explicit or implicit. Another important characteristic is the *order of the scheme*. When derivatives are replaced by differences, a certain error is introduced, which can be denoted as R (residual):

$$f'(t_n) = \frac{f(t_{n+1}) - f(t_n)}{\Delta t} + R(\Delta t)\,. \tag{2.4}$$

The objective of any numerical method is to minimize the residual R. If its dependence on the time step is linear, the method is classified as a first-order method. If the residual behaves as $(\Delta t)^n$, the method is termed an n-th order method. A higher order of the method corresponds to a more robust difference scheme that provides superior results. The derived Newton-Euler scheme is an explicit first-order scheme. For instance, if this scheme is used to describe harmonic oscillations, the amplitude of the oscillations grows numerically (non-physically). Consequently, the Newton-Euler scheme can only be utilized for short-term simulations.

Stability of the Scheme

Only *stable schemes* can be utilized for numerical simulations. Stable schemes are defined as those in which a numerical error introduced in one time step does not cause an error growth in subsequent time steps.

◖ **Example 2.2:** Design a Newton-Euler difference scheme for the motion of a charged particle in a homogeneous magnetic field

Solution: The corresponding difference scheme is easily obtained from the Hamilton equations (1.13) to (1.18):

$$x_{n+1} = x_n + \frac{p_x^{(n)}}{m}\Delta t\,,$$

$$y_{n+1} = y_n + \frac{p_y^{(n)} - QB\,x_n}{m}\Delta t\,,$$

$$z_{n+1} = z_n + \frac{p_z^{(n)}}{m}\Delta t\,,$$

$$p_x^{(n+1)} = p_x^{(n)} + \frac{QB\,(p_y^{(n)} - QB\,x_n)}{m}\Delta t\,,$$

$$p_y^{(n+1)} = p_y^{(n)}\,,$$

$$p_z^{(n+1)} = p_z^{(n)}\,.$$

Due to numerical errors, the Larmor radius of a particle moving in a homogeneous magnetic field slowly increases. Achieving better results requires a refined time step, increasing the operation count and subsequent rounding errors.

2.1.2 Leap-Frog Scheme (LF)

The deficiencies of the Newton-Euler scheme can be mitigated easily. If position and velocity are calculated at alternating times, the order of the scheme increases by one. The calculation of new velocities utilizes intermediate position values, and vice versa. In Example 2.1, the right-hand sides of the equations contain intermediate values instead of old or new values. The scheme remains explicit and as fast as the Newton-Euler scheme, but achieves second-order accuracy. In harmonic motion simulations, the Leap-Frog method preserves the genuine sinusoidal wave form.

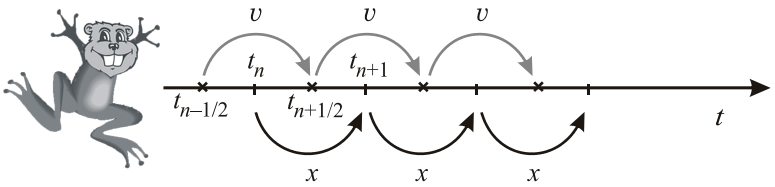


Fig. 2.2: Principle of leap-frog scheme.

The described procedure involves a single complication. Initially, the velocity at time $t_0 - \Delta t/2$ must be calculated; subsequently, new values are computed analogously to the Newton-Euler scheme. The calculation process for a one-dimensional case is outlined below. The differential equations are assumed to be:

$$\begin{aligned} \frac{\mathrm{d}x}{\mathrm{d}t} &= v\,, \\ \frac{\mathrm{d}v}{\mathrm{d}t} &= \frac{F(x,v)}{m}\,. \end{aligned} \tag{2.5}$$

First, the velocity value at time $t_0 - \Delta t/2$ is calculated in a standard manner. The Newton-Euler scheme is utilized to step backward by a negative time step $-\Delta t/2$:

$$v_{-1/2} = v_0 - \frac{F(x_0, v_0)}{m}\frac{\Delta t}{2}\,. \tag{2.6}$$

Subsequently, a repetitive computational cycle is initiated:

$$v_{n+1/2} = v_{n-1/2} + \frac{F(x_n, v_{n-1/2})}{m}\Delta t\,, \qquad x_{n+1} = x_n + v_{n+1/2}\Delta t\,. \tag{2.7}$$

The sequential values are determined as:

$$v_{-1/2}, x_0 \;\rightarrow\; v_{1/2}, x_1 \;\rightarrow\; v_{3/2}, x_2 \;\rightarrow\; v_{5/2}, x_3 \;\rightarrow\; \cdots$$

The Leap-Frog scheme is widely utilized in plasma physics. The explicit nature and high computational speed of the Newton-Euler scheme are retained, but the accuracy is improved to the second order.

2.1.3 Higher-Accuracy Schemes (RK, BB)

Runge-Kutta Scheme (RK)a

If higher demands are placed on simulation quality, numerical schemes with a higher order of accuracy must be utilized. The fourth-order Runge-Kutta method is among the most popular. The system of equations of motion is assumed to be converted into a system of first-order ordinary differential equations in the form:

$$\frac{\mathrm{d}\xi_k}{\mathrm{d}t} = f_k(t, \xi_1, \cdots, \xi_N)\,. \tag{2.8}$$

First, a set of four constants is determined at time t for each variable ξ_k:

$$\begin{aligned}
K_{1,k} &= f_k\left(t, \xi_1(t), \cdots, \xi_N(t)\right),\\
K_{2,k} &= f_k\left(t + \frac{1}{2}\Delta t, \xi_1(t) + \frac{1}{2}K_{1,1}\Delta t, \cdots, \xi_N(t) + \frac{1}{2}K_{1,N}\Delta t\right),\\
K_{3,k} &= f_k\left(t + \frac{1}{2}\Delta t, \xi_1(t) + \frac{1}{2}K_{2,1}\Delta t, \cdots, \xi_N(t) + \frac{1}{2}K_{2,N}\Delta t\right),\\
K_{4,k} &= f_k\left(t + \Delta t, \xi_1(t) + K_{3,1}\Delta t, \cdots, \xi_N(t) + K_{3,N}\Delta t\right).
\end{aligned} \tag{2.9}$$

The components of the quadruplet must be calculated in the specified order, as each subsequent constant utilizes the value of the preceding constant. These quadruplets are calculated for each of the N sought variables. The numerical solution at time $t + \Delta t$ is obtained from the relations:

$$\xi_k(t + \Delta t) \cong \xi_k(t) + \frac{1}{6}(K_{1,k} + 2K_{2,k} + 2K_{3,k} + K_{4,k}) \cdot \Delta t\,; \quad k = 1, \ldots, N\,. \tag{2.10}$$

The solution at time $t + \Delta t$ is thus known, and the procedure can be repeated. As an example, this scheme is applied to the Lorentz equation of motion:

$$\frac{\mathrm{d}\mathbf{x}}{\mathrm{d}t} = \mathbf{v}\,,$$
$$\frac{\mathrm{d}\mathbf{v}}{\mathrm{d}t} = \frac{Q}{m}(\mathbf{E} + \mathbf{v}\times\mathbf{B})\,. \tag{2.11}$$

First, auxiliary fields are calculated at the particle position:

$$\tilde{\mathbf{E}} \equiv \frac{Q}{m}\frac{\Delta t}{2}\mathbf{E}(\mathbf{x}_n)\,,$$
$$\tilde{\mathbf{B}} \equiv \frac{Q}{m}\frac{\Delta t}{2}\mathbf{B}(\mathbf{x}_n)\,. \tag{2.12}$$

Next, the vector constants **K** (for position) and **L** (for velocity) are determined:

$$\begin{aligned}
&\mathbf{K}_1 = \mathbf{v}_n\,, && \mathbf{L}_1 = \tilde{\mathbf{E}} + \mathbf{v}_n\times\tilde{\mathbf{B}}\,;\\
&\mathbf{K}_2 = \mathbf{v}_n + \mathbf{L}_1\,, && \mathbf{L}_2 = \tilde{\mathbf{E}} + \mathbf{K}_2\times\tilde{\mathbf{B}}\,;\\
&\mathbf{K}_3 = \mathbf{v}_n + \mathbf{L}_2\,, && \mathbf{L}_3 = \tilde{\mathbf{E}} + \mathbf{K}_3\times\tilde{\mathbf{B}}\,;\\
&\mathbf{K}_4 = \mathbf{v}_n + 2\mathbf{L}_3, && \mathbf{L}_4 = \tilde{\mathbf{E}} + \mathbf{K}_4\times\tilde{\mathbf{B}}\,.
\end{aligned} \tag{2.13}$$

The new values of positions and velocities are determined from the relations:

$$\mathbf{x}_{n+1} = \mathbf{x}_n + (\mathbf{K}_1 + 2\mathbf{K}_2 + 2\mathbf{K}_3 + \mathbf{K}_4)\Delta t/6\,,$$
$$\mathbf{v}_{n+1} = \mathbf{v}_n + (2\mathbf{L}_1 + 2\mathbf{L}_2 + 2\mathbf{L}_3 + 2\mathbf{L}_4)/6\,. \tag{2.14}$$

Boris-Buneman Scheme (BB)

The Boris-Buneman scheme is tailored for calculating charged particle trajectories in electric and magnetic fields. First, half of the acceleration in the electric field is calculated (2.16), followed by the particle rotation in the magnetic field (2.17), and the remaining part of the acceleration in the electric field is executed in the final step (2.18). The BB scheme is a highly efficient and fast fourth-order difference scheme:

$$\tilde{\mathbf{E}} \equiv \frac{Q}{m}\frac{\Delta t}{2}\mathbf{E},$$
$$\tilde{\mathbf{B}} \equiv \frac{Q}{m}\frac{\Delta t}{2}\mathbf{B}\,; \tag{2.15}$$

$$\tilde{\mathbf{v}} = \mathbf{v}_n + \tilde{\mathbf{E}}\,, \tag{2.16}$$

$$\tilde{\tilde{\mathbf{v}}} = \tilde{\mathbf{v}} + 2\frac{\left(\tilde{\mathbf{v}} + \tilde{\mathbf{v}}\times\tilde{\mathbf{B}}\right)\times\tilde{\mathbf{B}}}{1+\tilde{\mathbf{B}}^2}\,, \tag{2.17}$$

$$\mathbf{v}_{n+1} = \tilde{\tilde{\mathbf{v}}} + \tilde{\mathbf{E}}\,, \tag{2.18}$$

$$\mathbf{x}_{n+1} = \mathbf{x}_n + \mathbf{v}_{n+1}\Delta t\,. \tag{2.19}$$

2.1.4 Relativistic Schemes

At high velocities, the relativistic Lorentz equation of motion must be applied:

$$\frac{\mathrm{d}}{\mathrm{d}t}(\gamma\mathbf{v}) = \frac{Q}{m_0}\left[\mathbf{E} + \mathbf{v}\times\mathbf{B}\right]; \qquad \gamma \equiv \frac{1}{\sqrt{1 - v^2/c^2}}. \tag{2.20}$$

The primary issue is that velocity appears on both the left and right sides of this differential equation. If the substitution is applied:

$$\mathbf{u} \equiv \gamma\mathbf{v}, \tag{2.21}$$

the Lorentz equation of motion can be rewritten into the form:

$$\frac{\mathrm{d}\mathbf{u}}{\mathrm{d}t} = \frac{Q}{m_0}\left[\mathbf{E} + \frac{\mathbf{u}}{\gamma}\times\mathbf{B}\right]; \qquad \gamma = \sqrt{1 + \frac{\mathbf{u}^2}{c^2}}, \tag{2.22}$$

which serves as the initial relation for the formulation of relativistic numerical schemes:

Newton-Euler	**Leap-frog**
$\gamma_n = 1/\sqrt{1 - \mathbf{v}_n^2/c^2}$;	$\gamma_n = 1/\sqrt{1 - \mathbf{v}_n^2/c^2}$;
$\tilde{\mathbf{E}} = \frac{Q\Delta t}{m_0}\mathbf{E}$; $\quad \tilde{\mathbf{B}} = \frac{Q\Delta t}{m_0\gamma_n}\mathbf{B}$;	$\tilde{\mathbf{E}} \equiv \frac{Q\Delta t}{m_0}\mathbf{E}$, $\quad \tilde{\mathbf{B}} \equiv \frac{Q}{m_0}\frac{\Delta t}{2\gamma_n}\mathbf{B}$;
$\mathbf{u}_n = \gamma_n\mathbf{v}_n$;	$\mathbf{u}_{n-1/2} = \frac{\mathbf{v}_{n-1/2}}{\sqrt{1 - \mathbf{v}_{n-1/2}^2/c^2}}$;
$\mathbf{u}_{n+1} = \mathbf{u}_n + \tilde{\mathbf{E}} + \mathbf{u}_n\times\tilde{\mathbf{B}}$;	$\tilde{\mathbf{u}} = \tilde{\mathbf{u}}_{n-1/2} + \tilde{\mathbf{E}} + \tilde{\mathbf{u}}_{n-1/2}\times\tilde{\mathbf{B}}$;
$\mathbf{v}_{n+1} = \frac{\mathbf{u}_{n+1}}{\sqrt{1 + \mathbf{u}_{n+1}^2/c^2}}$;	$\mathbf{u}_{n+1/2} = \tilde{\mathbf{u}} + \frac{\left[\tilde{\mathbf{u}} + \tilde{\mathbf{u}}\times\tilde{\mathbf{B}}\right]\times\tilde{\mathbf{B}}}{1 + \tilde{\mathbf{B}}^2}$;
$\mathbf{x}_{n+1} = \mathbf{x}_n + \frac{\mathbf{v}_{n+1} + \mathbf{v}_n}{2}\Delta t$.	$\mathbf{v}_{n+1/2} = \frac{\mathbf{u}_{n+1/2}}{\sqrt{1 + \mathbf{u}_{n+1/2}^2/c^2}}$;
	$\mathbf{x}_{n+1} = \mathbf{x}_n + \frac{\mathbf{u}_{n+1/2}}{\gamma_{n+1/2}}\Delta t$.

Runge-Kutta	Boris-Buneman
$\gamma_n = 1/\sqrt{1-\mathbf{v}_n^2/c^2}$;	$\gamma_n = 1/\sqrt{1-\mathbf{v}_n^2/c^2}$;
$\tilde{\mathbf{E}} \equiv \frac{Q}{m}\frac{\Delta t}{2}\mathbf{E}, \quad \tilde{\mathbf{B}} \equiv \frac{Q}{m}\frac{\Delta t}{2}\mathbf{B}$,	$\tilde{\mathbf{E}} \equiv \frac{Q}{m_0}\frac{\Delta t}{2}\mathbf{E}$, $\quad \tilde{\mathbf{B}} \equiv \frac{Q}{m_0}\frac{\Delta t}{2\gamma_n}\mathbf{B}$;
$\mathbf{u}_n = \gamma_n \mathbf{v}_n$;	$\mathbf{u}_n = \gamma_n \mathbf{v}_n$;
$\mathbf{K}_1 = \frac{\mathbf{u}_n}{\gamma_n}$, $\quad \mathbf{L}_1 = \tilde{\mathbf{E}} + \mathbf{K}_1 \times \tilde{\mathbf{B}}$,	$\tilde{\mathbf{u}} = \mathbf{u}_n + \tilde{\mathbf{E}}$;
$\mathbf{K}_2 = \frac{\mathbf{u}_n + \mathbf{L}_1}{\gamma_{K_2}}$, $\quad \mathbf{L}_2 = \tilde{\mathbf{E}} + \mathbf{K}_2 \times \tilde{\mathbf{B}}$,	$\tilde{\tilde{\mathbf{u}}} = \tilde{\mathbf{u}} + 2\frac{(\tilde{\mathbf{u}} + \tilde{\mathbf{u}} \times \tilde{\mathbf{B}}) \times \tilde{\mathbf{B}}}{1+\tilde{\mathbf{B}}^2}$;
$\mathbf{K}_3 = \frac{\mathbf{u}_n + \mathbf{L}_2}{\gamma_{K_3}}$, $\quad \mathbf{L}_3 = \tilde{\mathbf{E}} + \mathbf{K}_3 \times \tilde{\mathbf{B}}$,	$\mathbf{u}_{n+1} = \tilde{\tilde{\mathbf{u}}} + \tilde{\mathbf{E}}$;
$\mathbf{K}_4 = \frac{\mathbf{u}_n + 2\mathbf{L}_3}{\gamma_{K_4}}$, $\quad \mathbf{L}_4 = \tilde{\mathbf{E}} + \mathbf{K}_4 \times \tilde{\mathbf{B}}$,	$\mathbf{v}_{n+1} = \frac{\mathbf{u}_{n+1}}{\sqrt{1+\mathbf{u}_{n+1}^2/c^2}}$;
$\mathbf{x}_{n+1} = \mathbf{x}_n + \frac{1}{6}\Delta t\left(\mathbf{K}_1 + 2\mathbf{K}_2 + 2\mathbf{K}_3 + \mathbf{K}_4\right)$,	$\mathbf{x}_{n+1} = \mathbf{x}_n + \mathbf{v}_{n+1}\Delta t$.
$\mathbf{u}_{n+1} = \mathbf{u}_n + \frac{1}{3}\left(\mathbf{L}_1 + \mathbf{L}_2 + \mathbf{L}_3 + \mathbf{L}_4\right)$,	
$\mathbf{v}_{n+1} = \frac{\mathbf{u}_{n+1}}{\sqrt{1+\mathbf{u}_{n+1}^2/c^2}}$.	

2.2 Difference Schemes in Magnetohydrodynamics

Magnetohydrodynamics is based on partial differential equations. Analytical solutions can be obtained only in exceptional cases; thus, reliance on numerical methods is necessary. Solutions can be determined via series expansions, variational methods, Green functions, characteristics, or finite element methods. Very frequently, partial differential equations are solved using difference schemes on a grid, analogously to ordinary differential equations in Chapter 2.1. Unlike ordinary differential equations, discretization in magnetohydrodynamics must be performed not only in time but also in space. At each time instant t_n, space is replaced by a discrete grid, and values are determined exclusively at the grid nodes. This textbook does not serve as a comprehensive manual of numerical methods, therefore it presents only the fundamentals of difference scheme formulation to enable simple computer simulations.

2.2.1 Partial Differential Equations

Classification of the Equations

Second-order partial differential equations are encountered most frequently in plasma physics. A general equation is assumed in the form:

$$F\left(\frac{\partial^2\psi}{\partial x_k \partial x_l}, \frac{\partial\psi}{\partial x_k}, \psi, x_k\right) = 0\,; \qquad k,l = 1,2,\ldots,N\,. \tag{2.23}$$

The unknown is a function of N variables, typically comprising one temporal and three spatial variables. An equation is classified as *quasilinear* if it is linear with respect to the second derivatives, taking the form:

$$\sum_{k,l} A_{kl}(\mathbf{x},\psi,\nabla\psi)\frac{\partial^2\psi}{\partial x_k \partial x_l} + B(\mathbf{x},\psi,\nabla\psi) = 0\,, \tag{2.24}$$

where the coefficients A_{kl} and B depend on x_k, ψ, and $\partial_k\psi$. An equation is classified as *linear* if it takes the form:

$$\sum_{k,l} A_{kl}(\mathbf{x})\frac{\partial^2\psi}{\partial x_k \partial x_l} + \sum_k B_k(\mathbf{x})\frac{\partial\psi}{\partial x_k} + C(\mathbf{x})\psi = f(\mathbf{x})\,. \tag{2.25}$$

The function $f(\mathbf{x})$ is designated as the right-hand side of the equation. If $f = 0$, the equation is referred to as *homogeneous*. An equation is termed *linear with constant coefficients* if the coefficients A_{kl}, B_k, and C are constant.

An equation can be converted into a simpler form via an appropriate transformation of variables. Linear equations are classified into three groups based on the coefficients of the second derivatives. An equation is defined as *elliptic* at a point $\mathbf{x}_0$ if a transformation exists that converts it at this point into the form:

$$\sum_k \frac{\partial^2 \psi}{\partial x_k^2} + \sum_k B_k(\mathbf{x}) \frac{\partial \psi}{\partial x_k} + C(\mathbf{x})\psi = f(\mathbf{x}) . \tag{2.26}$$

Examples of elliptic equations include the Laplace equation and the Poisson equation. An equation is defined as *hyperbolic* at a point $\mathbf{x}_0$ if a transformation exists that converts it at this point into the form:

$$\sum_{k=1}^{N-1} \frac{\partial^2 \psi}{\partial x_k^2} - \frac{\partial^2 \psi}{\partial x_N^2} + \sum_k B_k(\mathbf{x}) \frac{\partial \psi}{\partial x_k} + C(\mathbf{x})\psi = f(\mathbf{x}) . \tag{2.27}$$

One of the second derivatives thus possesses an opposite sign compared to the others. The wave equation serves as an example of such a hyperbolic equation. If minus and plus signs occur more than once among the second derivatives, the equation is termed *ultrahyperbolic*. An equation is defined as *parabolic* at a point $\mathbf{x}_0$ if a transformation exists that converts it at this point into:

$$\sum_{k=1}^{N-1} \frac{\partial^2 \psi}{\partial x_k^2} + \sum_k B_k(\mathbf{x}) \frac{\partial \psi}{\partial x_k} + C(\mathbf{x})\psi + D(\mathbf{x}) = 0 , \tag{2.28}$$

meaning that one second derivative (typically temporal) is absent. Examples include heat conduction, magnetic field diffusion, and time-dependent Schrödinger equations. If multiple second derivatives are absent, the equation is *parabolic in a broader sense*. Because equations are typically parabolic, hyperbolic, or elliptic over a domain in R^N, this classification does not exclusively constitute a single-point property.

◖ **Example 2.3:** Examples of typical equations are presented in the following table

Equation	Name	Type
$\nabla^2 \phi = 0$	Laplace equation	Elliptic
$\nabla^2 \phi = f(\mathbf{x})$	Poisson equation	Elliptic
$\nabla^2 \psi - \frac{1}{c^2}\frac{\partial^2 \psi}{\partial t^2} = 0$	Wave equation	Hyperbolic
$\frac{\partial T}{\partial t} = \kappa \nabla^2 T$	Heat conduction	Parabolic
$\frac{\partial^2 \psi}{\partial x^2} + \frac{\partial^2 \psi}{\partial y^2} - \frac{\partial^2 \psi}{\partial z^2} - \frac{\partial^2 \psi}{\partial w^2} = 0$		Ultrahyperbolic
$\frac{\partial^2 \psi}{\partial x^2} + \frac{\partial \psi}{\partial y} - \frac{\partial \psi}{\partial z} = 0$		Parabolic in a broader sense
$y\frac{\partial^2 \psi}{\partial t^2} + \frac{\partial \psi}{\partial t} - \frac{\partial^2 \psi}{\partial x^2} = 0$		$y = 0$ Parabolic, $y > 0$ Hyperbolic, $y < 0$ Elliptic

◗

Initial and Boundary Conditions

Analogously to ordinary differential equations, solving time-dependent partial differential equations requires an initial condition. However, initial conditions are insufficient for obtaining a solution. The problem is solved over a spatial domain Ω, and a solution requires defining the function behavior on the domain boundary. For instance, in determining circular membrane oscillations, the solution depends on whether the boundary of the membrane is free or fixed.

Evidently, the initial and boundary conditions imposed on the equation or systems of equations must be correctly formulated prior to solving partial differential equations:

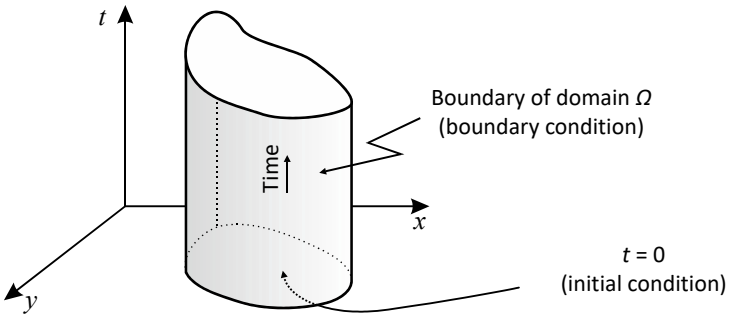


Fig. 2.3: Initial and boundary conditions of problem.

In most cases, a unique solution for a function $\psi(t, \mathbf{x})$ requires the specification of the initial condition:

$$\psi(0, \mathbf{x}) = g_0(\mathbf{x}), \tag{2.29}$$

and a boundary condition, with the most frequent types outlined below:

Dirichlet boundary condition – the value of the sought function is specified on the domain boundary:

$$\psi(t, \mathbf{x}_0) = G_0(t, \mathbf{x}_0) \text{ pro } \forall \mathbf{x}_0 \in \partial\Omega . \tag{2.30}$$

The symbol $\partial\Omega$ denotes the boundary of the domain Ω. The Dirichlet boundary condition is utilized, for example, in the heat conduction equation if the boundary of a rod or domain is maintained at a constant temperature, in the Laplace equation if the domain boundary has a specified potential, or in the wave equation if the boundary of an oscillating domain is fixed.

Neumann boundary condition – the normal derivative of the sought function is specified on the domain boundary, such as a free end of an oscillating membrane:

$$(\mathbf{n} \cdot \nabla)\psi(t, \mathbf{x}_0) = G_1(t, \mathbf{x}_0) \text{ pro } \forall \mathbf{x}_0 \in \partial\Omega . \tag{2.31}$$

Mixed boundary condition – a linear combination of the function and its derivatives is specified on the domain boundary:

$$\alpha\psi(t, \mathbf{x}_0) + \sum_k \beta_k \partial_k \psi(t, \mathbf{x}_0) = G_2(t, \mathbf{x}_0) \text{ pro } \forall \mathbf{x}_0 \in \partial\Omega . \tag{2.32}$$

Cauchy problem – for an N-th order equation, initial conditions are specified for the first $N-1$ derivatives, with no boundary conditions required.

2.2.2 Designing Differential Schemes

Temporal and spatial discretization is performed for the sought function, meaning that values are determined exclusively at times t_n and at nodes of the spatial grid x_j, y_k, z_l:

$$\psi^n_{j,k,l} = \psi(t_n, x_j, y_k, z_l); \qquad n = 0,1,2,\ldots; \qquad j,k,l = 0,\pm1,\pm2,\ldots$$
$$t_n = t_0 + n\Delta t, \qquad x_j = j\Delta x, \qquad y_k = k\Delta y, \qquad z_l = l\Delta z. \tag{2.33}$$

The superscript represents the discrete time, whereas the subscripts denote the discrete spatial dependence. The fundamental principle of difference scheme formulation is demonstrated first in one spatial dimension:

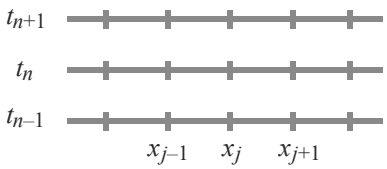


Fig. 2.4: Spatiotemporal discretization.

Spatial values at the new time layer t_{n+1} must be determined from known spatial values at the time layer t_n, and potentially t_{n-1}. Analogously to ordinary differential equations, schemes can be classified as either explicit or implicit:

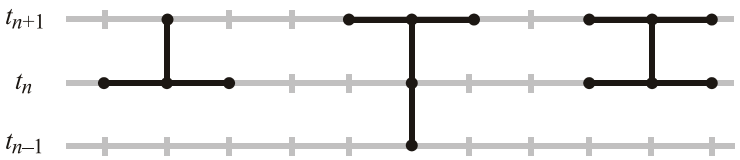


Fig. 2.5: Various difference schemes.

An explicit scheme is illustrated on the left in Figure 2.5, predicting the new time-level value from three known values at the current time level. An implicit scheme is shown in the center. A relationship among three values at the new level is obtained from values at two preceding time levels. For implicit schemes, solving a system of algebraic equations for the values at the new level is unavoidable. An implicit scheme where interconnected information about three values at the new level is obtained from three values at the current time level is depicted on the right. Explicit schemes are computationally simple, but their stability domain is generally significantly smaller than that of implicit schemes. Difference scheme formulation is introduced by defining spatial differences:

$$D^+\psi = \frac{\psi_{j+1} - \psi_j}{\Delta x}, \qquad D^-\psi = \frac{\psi_j - \psi_{j-1}}{\Delta x},$$
$$D^c\psi = \frac{\psi_{j+1} - \psi_{j-1}}{2\Delta x}, \qquad D^0\psi = \frac{\psi_{j+1/2} - \psi_{j-1/2}}{\Delta x}. \tag{2.34}$$

►

All four expressions can replace $\partial\psi/\partial x$ in a partial differential equation. These represent the forward difference, backward difference, centered difference, and two-point centered difference, respectively. In certain scenarios, a more complex three-point substitution for the spatial derivative can be utilized, such as:

$$D\psi = \frac{(\alpha+1)\psi_{j+1} - 2\alpha\psi_j + (\alpha-1)\psi_{j-1}}{2\Delta x}. \tag{2.35}$$

The expression yields D^- for $\alpha = -1$, D^c for $\alpha = 0$, and D^+ for $\alpha = +1$. Second derivatives can be replaced by various combinations of these differences, for instance

$$\frac{\partial^2\psi}{\partial x^2} \rightarrow D^+D^-\psi = D^+\frac{\psi_j - \psi_{j-1}}{\Delta x} =$$

$$= \frac{(\psi_{j+1} - \psi_j) - (\psi_j - \psi_{j-1})}{(\Delta x)^2} = \frac{\psi_{j+1} - 2\psi_j + \psi_{j-1}}{(\Delta x)^2}.$$

An identical result is obtained using two centered differences:

$$\frac{\partial^2\psi}{\partial x^2} \rightarrow D^+D^-\psi = D^cD^c\psi = \cdots = \frac{\psi_{j+1} - 2\psi_j + \psi_{j-1}}{(\Delta x)^2}. \tag{2.36}$$

Other substitutions for the second derivative are obtained by utilizing alternative combinations from (2.34); however, expression (2.36) is utilized most frequently. Temporal derivative differences are formulated analogously to ordinary differential equations:

$$\begin{aligned} \frac{\partial\psi}{\partial t} &\rightarrow \frac{f_j^{n+1} - f_j^n}{\Delta t}; \\ \frac{\partial\psi}{\partial t} &\rightarrow \frac{f_j^n - f_j^{n-1}}{\Delta t}. \end{aligned} \tag{2.37}$$

The first variant leads to an explicit scheme, whereas the second variant results in an implicit scheme. For the constructed scheme, the order of accuracy, conditions for convergence to the actual solution, and stability conditions must be verified to ensure that the obtained variables do not oscillate or diverge exponentially from the true solution. Frequently utilized schemes are outlined below.

Simple Explicit Scheme for the Diffusion Equation

A diffusion equation is assumed in the form:

$$\frac{\partial\psi}{\partial t} = \eta\frac{\partial^2\psi}{\partial x^2}. \tag{2.38}$$

Discretization leading to an explicit scheme is performed:

$$\frac{\psi_j^{n+1} - \psi_j^n}{\Delta t} = \eta\frac{\psi_{j-1}^n - 2\psi_j^n + \psi_{j+1}^n}{(\Delta x)^2}, \tag{2.39}$$

from which follows:

► $$\psi_j^{n+1} = \psi_j^n + \eta \frac{\psi_{j-1}^n - 2\psi_j^n + \psi_{j+1}^n}{(\Delta x)^2} \Delta t \,. \tag{2.40}$$

Values at the layer t_{n+1} are determined from the layer t_n if boundary conditions for calculating values at the boundary points are specified. This scheme corresponds to the graphical symbol on the left in Fig. 2.5. The scheme is highly efficient and convenient; however, stability requires the fulfillment of the condition (see Example 2.4, p. 319):

► $$\frac{\eta \Delta t}{(\Delta x)^2} \le \frac{1}{2} \,. \tag{2.41}$$

Du Fort-Frankel Scheme for the Diffusion Equation

Unconditional stability of the difference scheme for the diffusion (2.38) can be achieved via a simple modification. Discretization is chosen in a form analogous to (2.39):

$$\frac{\psi_j^{n+1} - \psi_j^{n-1}}{2\Delta t} = \eta \frac{\psi_{j-1}^n - (\psi_j^n + \psi_j^{n+1}) + \psi_{j+1}^n}{(\Delta x)^2} \,, \tag{2.42}$$

A central temporal difference is now on the left, and the middle term of the spatial derivative is replaced by the arithmetic mean of the current and new values. This scheme is implicit in the spatial value x_j since the new value appears on both the left and right sides. However, no numerical complication arises in this case, as the sought values at the new time level can be easily calculated from relation (2.42):

► $$\psi_j^{n+1} = \left(\frac{1-K}{1+K}\right)\psi_j^{n-1} + \left(\frac{K}{1+K}\right)\psi_{j-1}^n + \left(\frac{K}{1+K}\right)\psi_{j+1}^n \,; \qquad K \equiv \frac{2\eta \Delta t}{(\Delta x)^2} \,. \tag{2.43}$$

This approach is designated as the Du Fort-Frankel scheme and is unconditionally stable. It can also be utilized for a diffusion equation with an added convective term:

$$\frac{\partial \psi}{\partial t} + C \frac{\partial \psi}{\partial x} = \eta \frac{\partial^2 \psi}{\partial x^2} \,. \tag{2.44}$$

The formulation procedure remains identical; the first derivative with respect to x in the second term is replaced by the centered difference $D^{\mathrm{c}}\psi$, and the sought value at the new time level is subsequently calculated.

Lax-Wendroff Scheme

The flow behavior of specific variables is solved numerically. The corresponding equations are assumed to be written in conservative form:

$$\frac{\partial F}{\partial t} + \frac{\partial G}{\partial x} + \frac{\partial}{\partial x} A \frac{\partial H}{\partial x} = 0 \,. \tag{2.45}$$

Variables describing the flux represent ordered n–tuples:

$$F = \begin{pmatrix} F_1 \\ \vdots \\ F_N \end{pmatrix}; \quad G = \begin{pmatrix} G_1 \\ \vdots \\ G_N \end{pmatrix}; \quad H = \begin{pmatrix} H_1 \\ \vdots \\ H_N \end{pmatrix}. \tag{2.46}$$

Spatial discretization of the final term on the left side is solved first:

$$\frac{\partial}{\partial x}A\frac{\partial H}{\partial x} \rightarrow D^0 A D^0 H = D^0 A_j\left(\frac{H_{j+1/2}-H_{j-1/2})}{\Delta x}\right) =$$

$$= \frac{1}{(\Delta x)^2}\left[A_{j+1/2}\left(H_{j+1}-H_j\right)-A_{j-1/2}\left(H_j-H_{j-1}\right)\right].$$

Since $A = A(F)$, the values at half-arguments are given by the relations:

$$A_{j+1/2} \equiv A\left(\frac{F_{j+1}+F_j}{2}\right); \qquad A_{j-1/2} \equiv A\left(\frac{F_j+F_{j-1}}{2}\right).$$

A relatively robust explicit scheme for equations (2.45) is:

► $$\frac{F_j^{n+1}-F_j^n}{\Delta t}+\frac{G_{j+1}^n-G_{j-1}^n}{2\Delta x}+\frac{A_{j+1/2}^n\left(H_{j+1}^n-H_j^n\right)-A_{j-1/2}^n\left(H_j^n-H_{j-1}^n\right)}{(\Delta x)^2}=0. \qquad (2.47)$$

The values of F_j at the new time layer are easily determined from the expression. The Lax-Wendroff scheme can be generalized to two or three spatial dimensions.

Crank-Nicolson Scheme

The implicit scheme utilizing the arithmetic mean of the current and new time layers for spatial derivatives exhibits high stability; for the diffusion equation, this scheme is unconditionally stable:

► $$\frac{\partial \psi}{\partial x} \rightarrow \frac{1}{2}\frac{\psi_{j+1}^{n+1}-\psi_{j-1}^{n+1}}{2\Delta x}+\frac{1}{2}\frac{\psi_{j+1}^{n}-\psi_{j-1}^{n}}{2\Delta x},$$

$$\frac{\partial^2 \psi}{\partial x^2} \rightarrow \frac{1}{2}\frac{\psi_{j-1}^{n+1}-2\psi_j^{n+1}+\psi_{j+1}^{n+1}}{(\Delta x)^2}+\frac{1}{2}\frac{\psi_{j-1}^{n}-2\psi_j^{n}+\psi_{j+1}^{n}}{(\Delta x)^2}. \qquad (2.48)$$

This configuration corresponds to the diagram on the far right in Fig. 2.5.

Richtmyer-Morton Scheme

Another widely utilized implicit scheme incorporates a standard expression for spatial derivatives and expresses the temporal derivative using an optional parameter:

$$\frac{\partial \psi}{\partial x} \rightarrow \frac{\psi_{j+1}^{n+1}-\psi_{j-1}^{n+1}}{2\Delta x},$$

$$\frac{\partial^2 \psi}{\partial x^2} \rightarrow \frac{\psi_{j-1}^{n+1}-2\psi_j^{n+1}+\psi_{j+1}^{n+1}}{(\Delta x)^2}, \qquad (2.49)$$

$$\frac{\partial \psi}{\partial t} \rightarrow \frac{(\alpha+1)\psi^{n+1}-2\alpha\psi^n+(\alpha-1)\psi^{n-1}}{2\Delta t}.$$

For $\alpha = 2$, a frequently used asymmetric relation for the temporal derivative is obtained:

► $$\frac{\partial \psi}{\partial t} \rightarrow \frac{3\psi^{n+1} - 4\psi^{n} + \psi^{n-1}}{2\Delta t}. \tag{2.50}$$

Multiple Spatial Dimensions

Difference schemes in multiple spatial dimensions are formulated analogously. In certain scenarios, predicting the solution by performing difference operations exclusively in one specific spatial direction is advantageous. The resulting estimate is subsequently corrected via operations in another direction, with these directions alternating cyclically. This algorithm is designated as the Alternating Direction Implicit (ADI) method, and its detailed description can be found in specialized literature.

Tridiagonal Matrices

Equations of the following type are frequently encountered in implicit schemes:

$$-A_j\psi_{j+1}^{n+1} + B_j\psi_j^{n+1} - C_j\psi_{j-1}^{n+1} = D_j^n. \tag{2.51}$$

The new values at adjacent points are linked in triplets, analogously to the center diagram in Fig. 2.5. Determining these values requires solving a system of numerous equations with a sparse tridiagonal matrix:

$$\begin{pmatrix} B_1 & -A_1 & 0 & 0 & 0 \\ -C_2 & B_2 & -A_2 & 0 & 0 \\ 0 & -C_3 & B_3 & -A_3 & 0 \\ 0 & 0 & \ddots & \ddots & \ddots \end{pmatrix} \cdot \begin{pmatrix} \psi_1^{n+1} \\ \psi_2^{n+1} \\ \vdots \\ \psi_N^{n+1} \end{pmatrix} = \begin{pmatrix} D_1 \\ D_2 \\ \vdots \\ D_N \end{pmatrix}. \tag{2.52}$$

The boundary values ψ_1 and ψ_N are known at any time from the boundary conditions. The solution is sought in the form:

$$\psi_j^{n+1} = E_j\psi_{j-1}^{n+1} + F_j. \tag{2.53}$$

Substituting this expression into (2.51) yields the relations:

$$\begin{aligned} E_j &= \frac{C_j}{B_j - A_jE_{j+1}}, \\ F_j &= \frac{D_j + A_jF_{j+1}}{B_j - A_jE_{j+1}}. \end{aligned} \tag{2.54}$$

Expression (2.53) is applied to the final grid point $j = N$, where the value of the sought function is determined at all times by the right boundary condition:

$$\psi_N = E_N\psi_{N-1}^{n+1} + F_N.$$

Since the right boundary condition is predetermined and cannot depend on the sought solution, $E_N = 0$. The constant F_N must equal ψ_N, meaning:

$$E_N = 0, \qquad F_N = \psi_N. \tag{2.55}$$

At this stage, the values of both constants E and F at the right boundary are known. From equations (2.54), the following values are determined sequentially:

$$E_N, F_N \rightarrow E_{N-1}, F_{N-1} \rightarrow \cdots \rightarrow E_1, F_1 \,. \tag{2.56}$$

Once all constants E_j and F_j are known, the sought solution is determined sequentially from equation (2.53):

$$\psi_1 \rightarrow \psi_2^{n+1} \rightarrow \cdots \rightarrow \psi_{N-1}^{n+1} \,. \tag{2.57}$$

The grid is thus traversed from right to left, starting from the right boundary condition, to determine coefficients E and F. Subsequently, the grid is traversed from left to right starting from the left boundary condition to determine the sought solution.

2.2.3 Assessment of Scheme Stability

The von Neumann method for assessing the stability of a numerical scheme is described. For simplicity, the method is derived in one temporal and one spatial dimension, with generalization being straightforward. Numerical calculations are invariably performed on a finite grid. If the wave vector is denoted as $\boldsymbol{\kappa}$, a Fourier decomposition of the sought solution into partial waves can be executed:

$$\psi_{\boldsymbol{\kappa}}(\mathbf{x}) \equiv F(\boldsymbol{\kappa})\, \mathrm{e}^{\mathrm{i}\,\boldsymbol{\kappa}\cdot\mathbf{x}} \,. \tag{2.58}$$

In one dimension, the expression takes the form:

$$\psi_{\kappa}(x) \equiv F(\kappa)\, \mathrm{e}^{\mathrm{i}\,\kappa x} \,. \tag{2.59}$$

On a finite grid, both space and the wave vector are discrete, with the wave vector being multiples of the fundamental spatial frequency $\kappa_0 = \partial\varphi/\partial x = 2\pi/\Delta x$:

$$x_j = j\Delta x \,; \qquad \kappa_k = k\frac{2\pi}{\Delta x} \,; \qquad j,k = 1,2,\ldots \tag{2.60}$$

The subscript j indexes the spatial grid, and k the wave vector. The partial wave from which the solution is superposed is given by:

► $$\psi_k(x_j) \equiv F_k\, \mathrm{e}^{\mathrm{i}\,2\pi k\, j} \,;. \tag{2.61}$$

and the total composite solution is expressed as:

$$\psi(x_j) = \sum_k F_k\, \mathrm{e}^{\mathrm{i}\,2\pi k\, j} \,. \tag{2.62}$$

The selected difference scheme is stable if individual partial waves do not grow with time, meaning that the following condition is satisfied

► $$|g| \;\le\; 1 \,; \qquad g \equiv \frac{F_k^{n+1}}{F_k^n} \,. \tag{2.63}$$

This relation is designated as the *von Neumann stability criterion*. In practice, a less stringent condition for scheme stability suffices:

$$|g| \le 1 + \mathcal{O}(\Delta t). \tag{2.64}$$

To determine whether a designed scheme is stable, a single specific partial wave (2.61) is substituted into the scheme, the amplification factor g is determined, and the conditions under which its absolute value is less than or equal to unity are verified.

◖ **Example 2.4:** Investigate the stability of scheme (2.40) for the diffusion equation.

Solution: The analyzed difference scheme takes the form:

$$\psi_j^{n+1} = \psi_j^n + \eta \frac{\psi_{j-1}^n - 2\psi_j^n + \psi_{j+1}^n}{(\Delta x)^2} \Delta t .$$

Substituting the partial wave (2.61) into the scheme yields:

$$F_k^{n+1} e^{i2\pi k j} = F_k^n e^{i2\pi k j} + \eta \frac{F_k^n e^{i2\pi k(j-1)} - 2F_k^n e^{i2\pi k j} + F_k^n e^{i2\pi k(j+1)}}{(\Delta x)^2} \Delta t \quad \Rightarrow$$

$$F_k^{n+1} e^{i2\pi k j} = F_k^n \left[e^{i2\pi k j} + \frac{\eta \Delta t}{(\Delta x)^2} \left(e^{i2\pi k(j-1)} - 2 e^{i2\pi k j} + e^{i2\pi k(j+1)} \right) \right] \quad \Rightarrow$$

$$g_k \equiv \frac{F_k^{n+1}}{F_k^n} = \left[1 + \frac{\eta \Delta t}{(\Delta x)^2} \left(e^{-i2\pi k} - 2 + e^{+i2\pi k} \right) \right] \quad \Rightarrow$$

$$g_k = 1 + \frac{2\eta \Delta t}{(\Delta x)^2} \left[\cos(2\pi k) - 1 \right].$$

Since the cosine function ranges between −1 and +1, it follows that:

$$g_k \in \left\langle 1 - 4\eta \Delta t / (\Delta x)^2, 1 \right\rangle .$$

Condition (2.63) is satisfied in the right part of the interval; in the left part, the value must not drop below −1, meaning:

$$1 - 4\eta \Delta t / (\Delta x)^2 \ge -1 \quad \Rightarrow \quad \frac{\eta \Delta t}{(\Delta x)^2} \le \frac{1}{2},$$

which yields criterion (2.41).

◗

◖ **Example 2.5:** Investigate the stability of an explicit scheme utilizing centered differences for the wave equation.

Solution: A wave equation is assumed in the form:

$$\frac{\partial^2 \psi}{\partial x^2} - \frac{1}{c^2} \frac{\partial^2 \psi}{\partial t^2} = 0 .$$

The corresponding difference scheme is:

$$\frac{\psi_{j+1}^n - 2\psi_j^n + \psi_{j-1}^n}{(\Delta x)^2} - \frac{1}{c^2}\frac{\psi_j^{n+1} - 2\psi_j^n + \psi_j^{n-1}}{(\Delta t)^2} = 0\,.$$

The scheme exhibits second-order accuracy in both Δx and Δt and is explicit, as the value of ψ at the new time level appears only once. After substituting the partial wave, an equation for the factor g is obtained:

$$\begin{aligned} g - 2 + g^{-1} &= -4c^2\left(\frac{\Delta t}{\Delta x}\right)^2 \sin^2(\pi k) \quad \Rightarrow \\ \left(g^{1/2} - g^{-1/2}\right)^2 &= -4c^2\left(\frac{\Delta t}{\Delta x}\right)^2 \sin^2(\pi k) \quad \Rightarrow \\ g^{1/2} - g^{-1/2} &= \pm 2\,\mathrm{i}\,c\frac{\Delta t}{\Delta x}\sin(\pi k) \quad \Rightarrow \\ g \mp 2\,\mathrm{i}\,c\frac{\Delta t}{\Delta x}\sin(\pi k)g^{1/2} - 1 &= 0\,, \end{aligned}$$

which constitutes a quadratic equation for $g^{1/2}$. The solution is easily found as:

$$g^{1/2} = \pm\,\mathrm{i}\,c\frac{\Delta t}{\Delta x}\sin(\pi k) \pm \sqrt{1 - c^2\left(\frac{\Delta t}{\Delta x}\right)^2 \sin^2(\pi k)}\,.$$

Evidently, $|g|$ and $|g^{1/2}|$ are bounded by unity if the *Courant-Friedrichs-Lewy* (CFL) condition is satisfied:

▶
$$c\frac{\Delta t}{\Delta x} \le 1\,. \tag{2.65}$$

This constitutes a general condition for explicit schemes, expressing that the information propagation speed determined by the discretization must exceed all physical velocities tracked by the scheme, in this case $\Delta x/\Delta t \ge c$.

◗

2.3 Numerical Root-Finding for Polynomial Equations

Analyzing dispersion relation properties frequently requires finding the roots of a polynomial equation in the complex domain:

$$P(z) \equiv \sum_{k=0}^{N} c_k z^k = 0 . \tag{2.66}$$

The polynomial coefficients c_k are real. Numerous algorithms exist; in this brief overview, three distinct methods suitable for practical application are presented.

2.3.1 Weyl Algorithm

This efficient numerical algorithm is purely geometric and was formulated by the German mathematician Hermann Klaus Hugo Weyl. In the complex plane, a square large enough to contain all roots of equation (2.66) is initially constructed. Subsequently, the square is subdivided into four smaller quadrants, and sub-squares containing no roots in their vicinity are discarded. The remaining potential areas are further subdivided, continuously eliminating sections devoid of roots. After sufficient iterations, the roots are localized within the immediate vicinity of the remaining squares. The entire algorithm is structured into four sequential steps:

1. Input

The polynomial degree, coefficients, and the desired accuracy ε for solving equation (2.66) are specified.

2. Polynomial Rescaling

The roots z_k of the polynomial equation (2.66) are generally complex; the maximum absolute magnitude of all roots does not exceed the upper bound explicitly estimated by the American computer scientist Donald Erwin Knuth as:

► $$A_{\max} = 2 \cdot \max_k \left\{ \left| c_k / c_N \right| \right\} . \tag{2.67}$$

An alternative bound is expressed as:

► $$A_{\max} = 1 + \max_k \left\{ \left| c_k / c_N \right| \right\} . \tag{2.68}$$

The polynomial $P(A_{\max} z)$ possesses roots $z_k/A_{\max}$, therefore, it is rescaled to:

$$Q(\bar{z}) \equiv \sum_{k=0}^{N} \bar{c}_k \bar{z}^k ; \qquad \bar{z} \equiv \frac{z}{A_{\max}} , \qquad \bar{c}_k \equiv c_k A_{\max}^k . \tag{2.69}$$

The roots of the new polynomial satisfy:

$$Q(\bar{z}_k) = 0 \qquad \Rightarrow \qquad |\bar{z}_k| < 1\,, \tag{2.70}$$

meaning all roots lie within the unit circle in the complex plane. After locating these roots, transformation back to the original variables is required.

3. Generation and Testing of Square Systems

A system of potential squares is constructed. In the initial step, a single square centered at the origin with a side length $a = 2$ is defined. Its vertices possess coordinates (+1,+i), (+1,−i), (−1,−i), (−1,+i), and relation (2.70) guarantees that all sought roots lie within this boundary. In the subsequent step, each existing square is subdivided into four smaller quadrants, and a test is conducted to determine whether a root lies within the circumscribed circle (coefficients c_k are recalculated relative to the square center). Only squares satisfying the following test are retained:

► $$|\bar{c}_0| < \sum_{k=1}^{N} |\bar{c}_k| r^k\,, \tag{2.71}$$

where r is the radius of the circle circumscribed around the square with side length a:

$$r = \frac{a\sqrt{2}}{2}\,. \tag{2.72}$$

Root containment is guaranteed only for the initial square. For subsequent sub-squares, test (2.71) merely indicates a root within or near the boundary. The number of active squares initially increases exponentially but later decreases linearly.

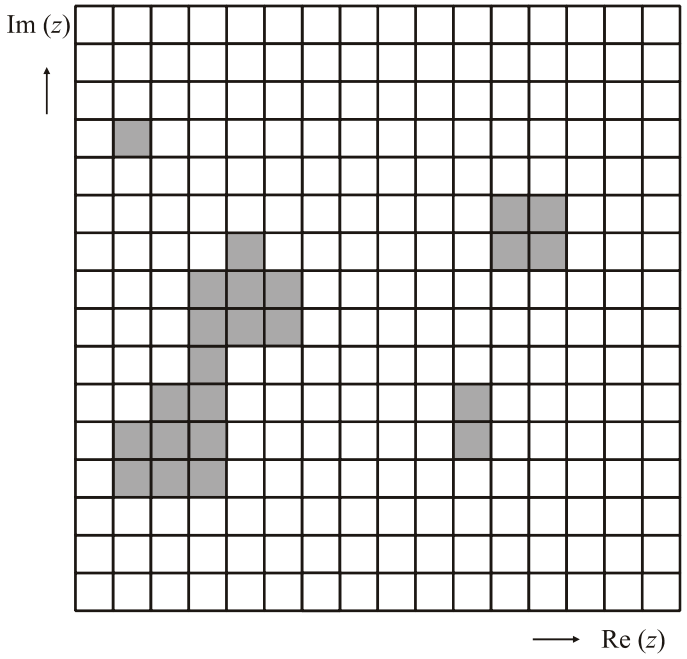


Fig. 2.6: Weyl algorithm after four steps. Potential squares are shaded gray, indicating the immediate vicinity of the polynomial roots. The region on the bottom-left will likely separate into two sub-regions upon further refinement.

4. Root Estimation

The system of squares is clustered into groups, where each group comprises a set of mutually touching squares. For each group, the center or centroid $\bar{z}_K$ is determined. This center constitutes an estimate of the root for the rescaled polynomial equation. The unscaled root value is obtained via:

$$z_k = A_{\max} \bar{z}_k \,. \tag{2.73}$$

Steps 3 and 4 are repeated iteratively until the specified accuracy is achieved. The computation can be terminated, for instance, when the dimension of the square or the largest group reaches a predefined value ε. The described algorithm does not determine root multiplicities; however, simple methods exist to estimate root multiplicity.

2.3.2 Newton Algorithm

The Newton algorithm is the simplest method for solving an equation $f(x) = 0$. Initializing from an arbitrary point x_0 on the x-axis as shown in Fig. 2.7, the subsequent point is obtained as the intersection of the x-axis with the tangent line to the function graph at $[x_0, f(x_0)]$. If the initial point is chosen appropriately, the sequence of constructed points converges to the intersection of the function graph with the x-axis, representing the solution to $f(x_0) = 0$:

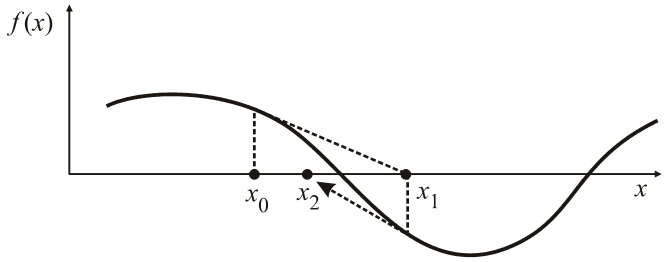


Fig. 2.7: Newton algorithm

The mathematical formulation of the algorithm is highly straightforward. The equation of the tangent line at x_n is expressed as:

$$y - f(x_n) = f'(x_n)(x - x_n) \tag{2.74}$$

The new point constitutes the intersection with the x-axis, which requires:

$$x = x_{n+1} \,; \quad y = 0 \,. \tag{2.75}$$

Substituting condition (2.75) into the tangent line equation (2.74) immediately yields the fundamental formulation of the Newton algorithm:

$$x_{n+1} = x_n - \frac{f(x_n)}{f'(x_n)} \,. \tag{2.76}$$

Analogously, complex and real roots of equation (2.66) can be determined:

$$z_{n+1} = z_n - \frac{P(z_n)}{P'(z_n)} \,. \tag{2.77}$$

Although the Newton algorithm is computationally fast, a major limitation involves the selection of the initial point. The method converges to different roots from different initial regions, and regions where the method fails to converge to any root also exist. While attempting random initial points to verify convergence is possible, this approach is inefficient for high-degree polynomials and does not guarantee locating all roots. If the Newton algorithm is utilized, determining a specific set of initial points to ensure convergence to all roots of the given polynomial equation is critical.

2.3.3 Generalized Newton Algorithm

John Hubbard, Dierk Schleicher, and Scott Sutherland [34] augmented the Newton method with an efficient grid-selection algorithm for initial points, ensuring convergence to all solutions of the polynomial equation (multiple grid points may converge to identical solutions, but no solution is omitted). The baseline algorithm comprises five steps:

1. Input

The polynomial degree, coefficients, and target accuracy ε are specified.

2. Polynomial Rescaling

Ensuring that all roots lie within the unit circle is necessary for method success. Therefore, identical rescaling to the Weyl algorithm is performed

► $$A_{\max} = 1 + \max_k \left\{ \left| c_k / c_N \right| \right\} \tag{2.78}$$

and operations are conducted with the polynomial

$$Q(\bar{z}) \equiv \sum_{k=0}^{N} \bar{c}_k \bar{z}^k \; ; \qquad \bar{z} \equiv \frac{z}{A_{\max}} , \qquad \bar{c}_k \equiv c_k A_{\max}^k , \tag{2.79}$$

whose roots lie within the unit circle in the complex plane.

3. Initial Grid Selection

The initial grid ensures that points converging to all roots of the polynomial via the Newton method are included. The derivation of this grid is provided in [34]. First, a grid of appropriate radii and angles for the initial points in the complex plane is determined:

$$r_l \equiv \left(1+\sqrt{2}\right)\left(\frac{N-1}{N}\right)^{\frac{2l-1}{4L}} \; ; \qquad l = 1,\ldots,L \; ; \qquad L \equiv \left\lceil 0,26632 \ln N \right\rceil , \tag{2.80}$$

$$\varphi_m \equiv \frac{2\pi m}{M} ; \qquad m = 0,\ldots,M-1 \; ; \qquad M \equiv \left\lceil 8,32547\, N \ln N \right\rceil . \tag{2.81}$$

The sought initial grid of points is subsequently given by:

$$\bar{z}_{lm} = r_l \exp(\mathrm{i}\,\varphi_m) \; ; \qquad l = 1,\ldots,L \; ; \qquad m = 0,\ldots,M-1 . \tag{2.82}$$

The initial grid contains LM points. The brackets $\lceil x \rceil$ denote the ceiling function, representing the smallest integer greater than or equal to x, commonly designated as CEILING or CEIL in programming languages.

4. Iteration

Iteration ensuring that the K-th term of the sequence solves the equation $Q(z) = 0$ with an accuracy of $|Q(\bar{z}_K)| < \varepsilon$ is performed via the standard Newton scheme for each grid point (2.82). This point is considered to be the initial value of the generated sequence, meaning $z_0 = z_{lm}$:

$$\bar{z}_{k+1} = \bar{z}_k - \frac{Q(\bar{z}_k)}{Q'(\bar{z}_k)}; \qquad k = 1 \ldots K; \qquad K \equiv \left\lceil \frac{\ln(1+\sqrt{2}) \; - \; \ln \varepsilon}{\ln N \; - \; \ln(N-1)} \right\rceil. \tag{2.83}$$

The method outlined above guarantees that the specified accuracy is achieved in fewer than K steps. Many roots are obtained duplicately from the initial grid, yet none of the roots are omitted. Iterations failing to converge are identified when the final term fails to satisfy the relation $|Q(\bar{z}_K)| < \varepsilon$.

5. Roots

The approximation of the sought root after back-scaling is given by:

$$z_k = A_{\max} \bar{z}_k \, . \tag{2.84}$$



2.4 PIC Simulations

The Particle-in-Cell (PIC) algorithm is widely utilized method in plasma physics. It constitutes a hybrid simulation approach where particles move freely in continuous space according to the equation of motion, whereas fields are evaluated exclusively at the nodes of a predefined grid. Rather than interacting with all other individual particles, each particle interacts with the mean field generated by the entire ensemble. If N denotes the particle count, this approach reduces the computational complexity from N^2 (for binary interactions) to $N \log N$. In numerous simulations, each simulation particle represents a macroparticle comprising an entire cluster of actual particles.

The PIC algorithm is suitable for describing plasma waves and instabilities, magnetic reconnection, plasma heating, laser-plasma interactions, and turbulence evolution. Simulation accuracy is conditioned on an appropriate choice of temporal and spatial steps. Generally, the time step of the particle integrator must be significantly shorter than the period corresponding to the electron plasma frequency, and the spatial grid step must be smaller than or at least comparable to the Debye length in the simulated plasma. The baseline cycle of the PIC method is structured into four core steps:

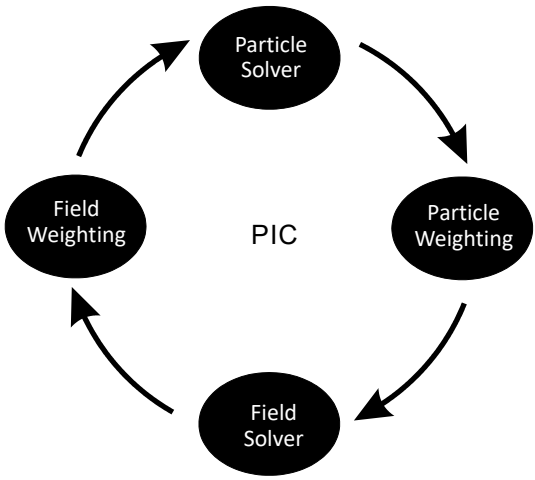


Fig. 2.8: Baseline cycle of PIC algorithm.

1. *Particle Weighting*. Charge and current densities at the grid nodes are determined from known particle positions and velocities. Particles are typically distributed among the nearest nodes according to a specific assignment rule ensuring that the largest fraction is allocated to the closest node. Following this step, the source terms of the Maxwell equations are defined at the grid nodes.
2. *Field Solver.* Electric and magnetic field values at the grid nodes are determined from the Maxwell equations, typically solved for potentials prior to evaluating the electromagnetic fields. Any available method for solving partial differential equations can be utilized (grids, finite elements, fast Fourier transform, etc.). Following this step, field values are known at the grid nodes.

3. *Field Weighting.* Since fields are evaluated at the grid nodes, field values must be determined at the continuous particle positions. The fields are interpolated to the position of a specific particle, reversing the particle weighting procedure. Following this step, the field value at the position of any selected particle is known.
4. *Particle Solver.* Individual particles are processed with known local fields, updating their positions and velocities in accordance with the equations of motion. Integration of the equations of motion is performed using standard numerical methods (e.g., Runge-Kutta, Leap-Frog; see Chapter 2.1).

Although this baseline cycle constitutes the core of the PIC method, implementation requires numerous auxiliary procedures. Initial conditions (generating the initial particle distribution in the plasma) and boundary conditions (defining plasma behavior at the domain boundaries) are critical. Visualization of particles and fields is indispensable, offering numerous methodologies: particle colors can represent charge, color shades can indicate temperature, particles can leave decaying tracks, or they can be rendered as moving points, spheres, or polyhedra. Fields are typically visualized via field lines, either in three dimensions or across various cross-sections. Plasma diagnostics are essential, calculating macroscopically verifiable plasma parameters (temperature, concentration, specific heats, susceptibility, permeability, permittivity, etc.) during runtime. Collisions between charged particles and neutrals can be incorporated using Monte Carlo methods. Since intra-cell interactions between charged particles are underrepresented in the standard PIC method, the computation can be augmented by a Monte Carlo module that accounts for random binary collisions within individual grid cells. Because a simulation particle usually represents an entire cluster, the method is alternative designated as the Cloud-in-Cell (CIC) method.

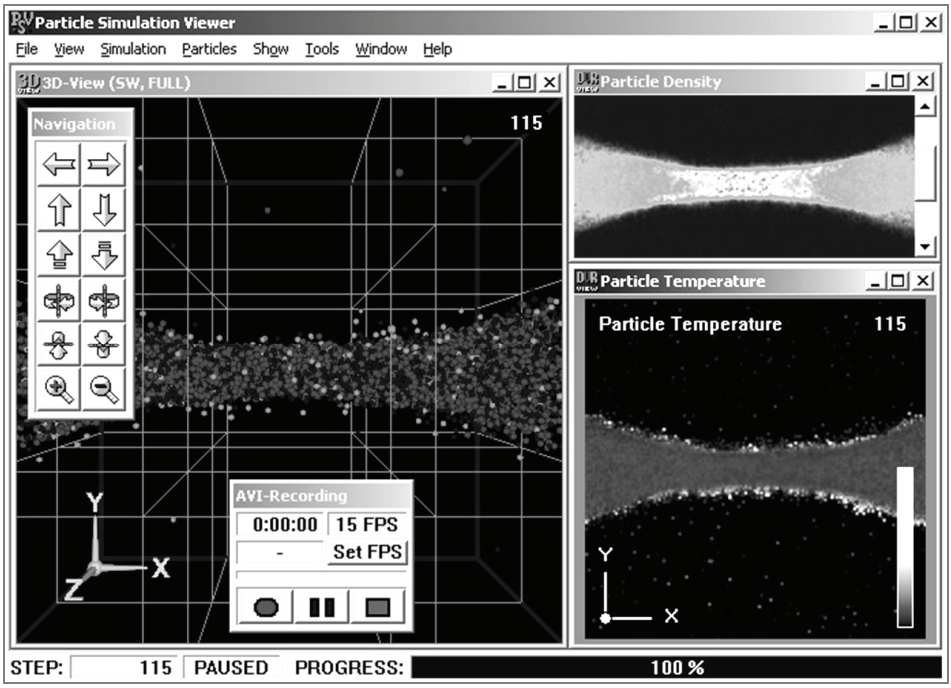


Fig. 2.9: Graphical user interface of PIC software package developed at author workplace.

2.4.1 Weighting

Weighting is performed twice within the PIC method. First, particles are weighted to the grid nodes, and subsequently, fields are interpolated from the grid nodes to the particles. Both weighting types must be of the identical order of accuracy. The particle weighting procedure is described below; reverse field weighting is analogous.

The simplest approach is *zero-order weighting*, assuming a particle belongs entirely to the nearest grid node. Although this scheme is computationally highly efficient, specific disadvantages exist. Consider a particle traversing the grid and observe the charge density at a specific node. The charge density remains zero until the particle approaches the observed node sufficiently, at which point it jumps to a maximum value, subsequently dropping to zero after particle departure. Such step changes can induce numerical instabilities.

Consequently, first-order (or higher-order) weighting is typically utilized, outlined here for a two-dimensional case. A particle is distributed to the nearest nodes (four nodes in a plane) proportionally to the opposite areas, ensuring that the closest node receives the largest fraction and the most distant node receives the smallest.

In a three-dimensional scenario, weighting is performed to the nearest eight neighbors proportionally to the opposite volumes. Higher-order weighting schemes exist, providing superior quality at significantly higher computational cost.

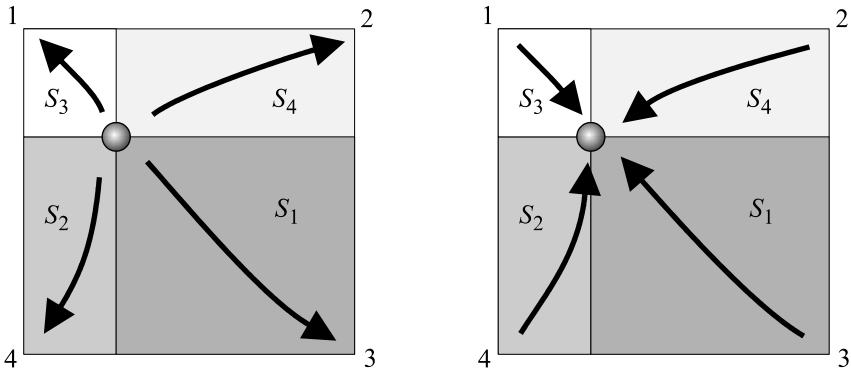


Fig. 2.10: First-order weighting illustrating particle weighting on left and field interpolation on right. Principle is identical.

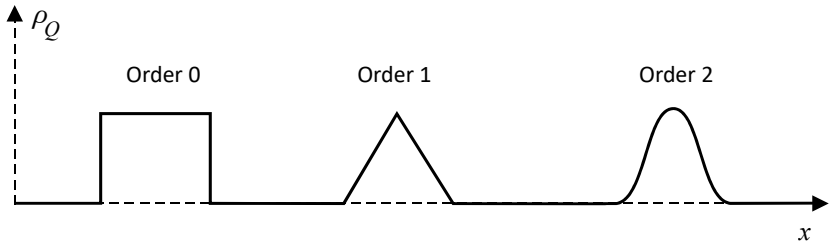


Fig. 2.11. Charge density profile at grid node induced by traversing particle across variable weighting schemes.

2.4.2 Field Solvers

A vast number of diverse methods exist for solving fields at grid nodes. If fields vary minimally over the selected time step, solving the Poisson equations for potentials suffices (ρ_Q denotes charge density, $\mathbf{j}_Q$ is current density):

$$\nabla^2\phi = -\frac{\rho_Q}{\varepsilon_0}; \qquad \nabla^2\mathbf{A} = -\mu_0\mathbf{j}_Q . \tag{2.85}$$

Following potential determination (via any numerical method), fields are evaluated from the relations:

$$\mathbf{E} = -\nabla\phi; \qquad \mathbf{B} = \nabla\times\mathbf{A} . \tag{2.86}$$

A solution method based on the Fourier transform is described briefly, suitable for a cuboidal domain ($L_x \times L_y \times L_z$) with periodic boundary conditions. The entire algorithm comprises five steps:

1. Discretization of Poisson equation.
2. Discrete Fourier transform (DFT) of equations.
3. Algebraic solution in **k**-space.
4. Inverse discrete Fourier transform (IDFT) to obtain potential.
5. Calculation of fields at grid nodes.

These steps are described for the electric field potential Poisson equation. Discretization can be performed, for instance, via centered differences (charge density is denoted as ρ):

$$\begin{aligned}
&\frac{\Delta_x^2\varphi}{(\Delta x)^2} + \frac{\Delta_y^2\varphi}{(\Delta y)^2} + \frac{\Delta_z^2\varphi}{(\Delta z)^2} = -\frac{\rho_{n_1,n_2,n_3}}{\varepsilon_0};\\
&\frac{\Delta_x^2\varphi}{(\Delta x)^2} \equiv \frac{\varphi_{n_1+1,n_2,n_3} - 2\varphi_{n_1,n_2,n_3} + \varphi_{n_1-1,n_2,n_3}}{(\Delta x)^2},\\
&\frac{\Delta_y^2\varphi}{(\Delta y)^2} \equiv \frac{\varphi_{n_1,n_2+1,n_3} - 2\varphi_{n_1,n_2,n_3} + \varphi_{n_1,n_2-1,n_3}}{(\Delta y)^2},\\
&\frac{\Delta_z^2\varphi}{(\Delta z)^2} \equiv \frac{\varphi_{n_1,n_2,n_3+1} - 2\varphi_{n_1,n_2,n_3} + \varphi_{n_1,n_2,n_3-1}}{(\Delta z)^2}.
\end{aligned} \tag{2.87}$$

The discrete Fourier transform (DFT) of a function F and the inverse discrete Fourier transform (IDFT) are given by the relations:

$$\tilde{F}(k_1,k_2,k_3) = \frac{1}{N_1N_2N_3}\sum_{n_1=0}^{N_1-1}\sum_{n_2=0}^{N_2-1}\sum_{n_3=0}^{N_3-1} F(n_1,n_2,n_3)\exp\left[2\pi\mathrm{i}\left(\frac{k_1n_1}{N_1}+\frac{k_2n_2}{N_2}+\frac{k_3n_3}{N_3}\right)\right];$$

$$F(n_1,n_2,n_3) = \sum_{k_1=0}^{N_1-1}\sum_{k_2=0}^{N_2-1}\sum_{k_3=0}^{N_3-1} \tilde{F}(k_1,k_2,k_3)\exp\left[-2\pi\mathrm{i}\left(\frac{k_1n_1}{N_1}+\frac{k_2n_2}{N_2}+\frac{k_3n_3}{N_3}\right)\right].$$

Applying the DFT transforms equation (2.87) into **k**-space:

$$\left[\frac{4N_1^2}{L_x^2}\sin^2\frac{\pi k_1}{N_1}+\frac{4N_2^2}{L_y^2}\sin^2\frac{\pi k_2}{N_2}+\frac{4N_3^2}{L_z^2}\sin^2\frac{\pi k_3}{N_3}\right]\tilde{\varphi}(k_1,k_2,k_3)=\frac{\tilde{\rho}(k_1,k_2,k_3)}{\varepsilon_0}. \quad (2.88)$$

The continuous Fourier transform for a continuous variable would yield $k^2\tilde{\varphi}=\tilde{\rho}/\varepsilon_0$. The squared sine functions appearing in the result are caused by grid effects. The algebraic solution of the equation is straightforward:

$$\tilde{\varphi}(k_1,k_2,k_3)=\frac{\tilde{\rho}(k_1,k_2,k_3)}{\varepsilon_0\left[\frac{4N_1^2}{L_x^2}\sin^2\frac{\pi k_1}{N_1}+\frac{4N_2^2}{L_y^2}\sin^2\frac{\pi k_2}{N_2}+\frac{4N_3^2}{L_z^2}\sin^2\frac{\pi k_3}{N_3}\right]}. \quad (2.89)$$

The sought potential is obtained via the inverse discrete Fourier transform:

$$\varphi=\mathrm{IDFT}(\tilde{\varphi}). \quad (2.90)$$

The electric field at the grid nodes is easily determined from the potential. Instead of the DFT/IDFT algorithm, a fast Fourier transform (FFT/IFFT) algorithm can be utilized, accelerating the process by requiring $N\log N$ operations instead of N^2; it is implemented in most numerical libraries.

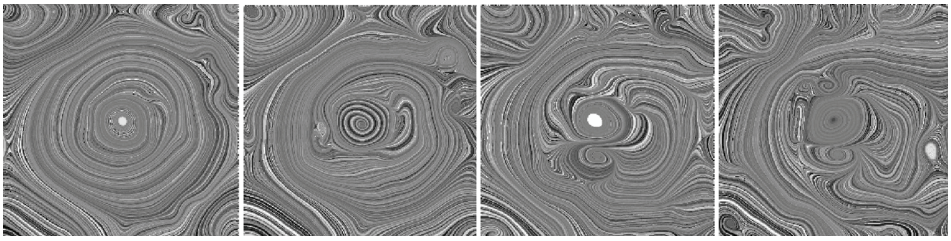


Fig. 2.12: Temporal evolution of magnetic field lines in transverse cross-section of plasma filament (400,000 electrons and ions). Result of PIC simulation by author, with field visualized via line integral convolution (LIC) method.

2.4.3 Particle Motion Solvers

The solution of charged particle motion in a known field was covered in detail in Chapter 2.1. For solving the ordinary differential equations, any of the described methods or other techniques documented in literature suitable for simulating charged particle trajectories in electric and magnetic fields can be selected.

2.5 Monte Carlo Simulations

The *Monte Carlo methods* represent a prominent group of numerical techniques in statistical physics, based on random number sequences. In physics, these methods were reportedly first utilized by Enrico Fermi in the 1930s to describe neutron properties. However, was not published and has not been preserved. The first documented application dates to the late 1940s at the Los Alamos National Laboratory. Pioneers included Nicholas Metropolis (who reportedly named the method), John von Neumann, Enrico Fermi, Stanislaw Ulam, Edward Teller, and Marshall Rosenbluth. Since then, Monte Carlo calculations have expanded across physics, mathematics, chemistry, economics, and alternative scientific disciplines.

Analogous techniques, termed *statistical sampling*, were utilized by mathematicians in the 18th century for multidimensional definite integrals, using specialized tables instead of computers. Today, nearly all programming languages implement random number generators for the interval <0, 1), though their quality may be insufficient for robust Monte Carlo calculations. The fundamental principles and specific applications are demonstrated in this chapter, beginning with two introductory examples.

◖ **Example 2.6:** The calculation of the Ludolf constant π serves as a highly illustrative demonstration of Monte Carlo methods. The procedure requires generating random points within the unit square<0, 1>×<0, 1>.

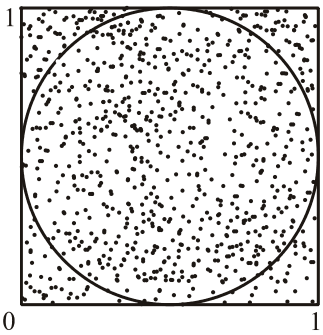


Fig. 2.13: Monte Carlo calculation of constant π.

A built-in generator of numbers γ_k within the interval <0, 1) is utilized to generate numerous points falling inside the square area:

$$x_k = \gamma_{2k-1}\,,$$
$$y_k = \gamma_{2k}\quad,\qquad k = 1, 2, \ldots$$

The total number of points generated within the unit square ($N_\square$) and the number of points falling inside the unit circle ($N_\circ$, satisfying the relation $x^2 + y^2 < 1$) are monitored according to Fig. 2.13. For a sufficiently large number of points, these counts are proportional to the geometric areas:

$$\frac{N_{\bigcirc}}{N_{\square}} \approx \frac{S_{\bigcirc}}{S_{\square}} = \frac{\pi R^2}{(2R)^2} = \frac{\pi}{4} \qquad \Rightarrow \qquad \pi \approx 4\frac{N_{\bigcirc}}{N_{\square}}.$$

By counting the generated points, the constant π can be determined with high precision given a substantial number of steps. ◗

◖ **Example 2.7:** An algorithm for calculating a definite integral is presented:

$$I = \int_a^b f(x)\,\mathrm{d}x\,.$$

A point is repeatedly generated from the domain of the sought integral (a, b):

$$x_k = a + \gamma_k (b-a)\,.$$

The mean value of the integrated function f over the integration interval (a, b) is:

$$\overline{f} = \frac{1}{n}\sum_{k=1}^{n} f(x_k)\,.$$

The integral is then approximately equal to the area of a rectangle with a height equal to the mean value of f:

$$\int_a^b f(x)\,\mathrm{d}x \doteq \overline{f}\cdot(b-a)\,.$$

This method is inefficient for evaluating one-dimensional integrals. The integral equals the area under the curve, and approximating this area using a larger number of trapezoids with subsequent summation is significantly faster. However, multidimensional integrals exist where Monte Carlo methods often constitute the unique option for estimating their value. ◗

2.5.1 Random Number Generators

The quality and speed of the random number generator are critical for Monte Carlo calculations. An ideal generator is derived from a genuinely random variable, such as electronic component noise or a quantum phenomenon. Such hardware generators are utilized exclusively for specialized calculations, with their primary disadvantage being the inability to replicate a previously executed calculation. Typically, software generators based on pseudorandom sequences generated by a specific mathematical algorithm are utilized. The period of these generators is finite, and the generated numbers repeat after a certain duration. The baseline requirements for a robust generator comprise:

1) a sufficiently long generator period,
2) high generation speed of pseudorandom numbers,
3) uniform distribution of generated numbers,
4) minimal correlation between individual groups of generated numbers.

The DIEHARD software suite developed at Florida State University can be utilized to test generator quality. The most frequently utilized generators in Monte Carlo calculations include:

Linear Multiplicative Congruential Generator (LCG)

The generator was proposed in 1949 by the American mathematician Derrick Henry Lehmer. The sequence of pseudorandom numbers is generated using the relation:

$$\gamma_k = (\lambda \cdot \gamma_{k-1} + C) \bmod P\,, \tag{2.91}$$

where the generation process is influenced by four parameters: λ, C, P, and γ_0. The maximum possible period is $P - 1$. The initial value of the sequence, γ_0, constitutes the seed, deterministically defining the subsequent sequence. Utilizing the identical seed enables the replication of a previously executed calculation. The IBM RANDU LCG generator was highly popular between the 1960s and 1980s, utilizing the parameters:

$$P = 2^{31}\,, \quad \lambda = 2^{16} + 3\,, \quad C = 0\,.$$

However, correlations of the type 2^n occur in sequences generated this way, entirely invalidating specific calculations. Points generated within a 3D cube are not distributed uniformly but are localized within fifteen planes, clearly discernible from certain viewing angles. Today, LCG generators are utilized exclusively as components of combined systems, such as coupling two interdependent LCG generators:

$$\begin{aligned} \xi_k &= (\lambda_1 \cdot \xi_{k-1} + C_1) \bmod P_1\,, \\ \eta_k &= (\lambda_2 \cdot \eta_{k-1} + C_2) \bmod P_2\,; \\ \gamma_k &= (\xi_k + \eta_k) \bmod \max(P_1, P_2)\,. \end{aligned} \tag{2.92}$$

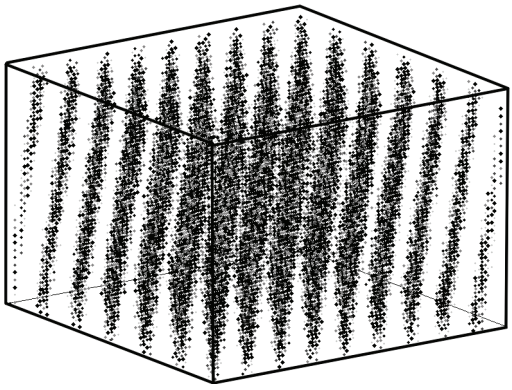


Fig. 2.14: Example of unsuitable random number generator IBM RANDU. Within a 3D cube, numbers are generated exclusively across fifteen planes.

Fibonacci Generators

These generators utilize preceding terms of the sequence to generate random numbers:

$$\gamma_k = f(\gamma_{k-p}, \gamma_{k-q}) \bmod P\,. \tag{2.93}$$

These generators typically exhibit excellent properties, although storing a specific number of generated values is necessary. The function f can represent simple multiplication, subtraction, or addition. A robust generator suitable for Monte Carlo calculations is the Lehmer-L'Ecuyer generator:

$$\begin{gathered}\gamma_k = (a_1\gamma_{k-1} + a_5\gamma_{k-5}) \bmod P; \\ a_1 = 107374182, \\ a_5 = 104480, \\ P = 2^{31} - 1\end{gathered} \tag{2.94}$$

or a highly efficient combined L'Ecuyer generator:

$$\begin{gathered}\gamma_k = (\xi_k - \eta_k) \bmod P_1; \\ \xi_k = (a_1\xi_{k-1} + a_2\xi_{k-2} + a_3\xi_{k-3}) \bmod P_1; \\ \eta_k = (b_1\eta_{k-1} + b_2\eta_{k-2} + b_3\eta_{k-3}) \bmod P_2; \\ a_1 = 0, \quad a_2 = 63308, \quad a_3 = -183326, \\ b_1 = 86098, \quad b_2 = 0, \quad b_3 = -539608, \\ P = 2^{31} - 1, \quad P_2 = 2145483479.\end{gathered} \tag{2.95}$$

Alternative specialized random number generators can be utilized in Monte Carlo simulations, but their description exceeds the scope of this textbook.

2.5.2 Implementation of Probability Distributions

Generators alternative to the uniform type are frequently required. For instance, constructing a generator that simulates events in accordance with a specific probability distribution may be necessary. Methods for realizing probability distributions are introduced in this section.

Rejection Method

Assume N events exist with probabilities w_1, w_2, $\cdots w_N$. A random variable ξ is introduced, where the first row denotes the event order and the second row represents the event probability:

$$\xi = \begin{pmatrix} 1 & 2 & 3 & \cdots & N \\ w_1 & w_2 & w_3 & \cdots & w_N \end{pmatrix} \tag{2.96}$$

The probability distribution can be visualized graphically (five events are selected in the illustration):

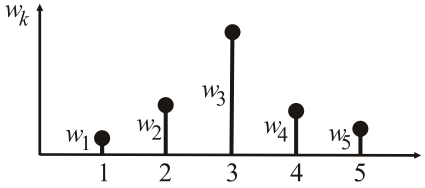


Fig. 2.15: Discrete probability distribution.

Steps are constructed where the height of each increment corresponds to the magnitude of the event probability. In mathematics, such steps are designated as a *distribution sequence* (or a *distribution function* in a continuous case). The final step must be at

a height of unity, representing the sum of all probabilities. The distribution sequence is defined by a simple relation:

$$D_k \equiv \sum_{j=1}^{k} w_j \,. \tag{2.97}$$

The sequence is illustrated in the subsequent figure, where the step height always corresponds to the given probability, and the total height of the staircase equals unity.

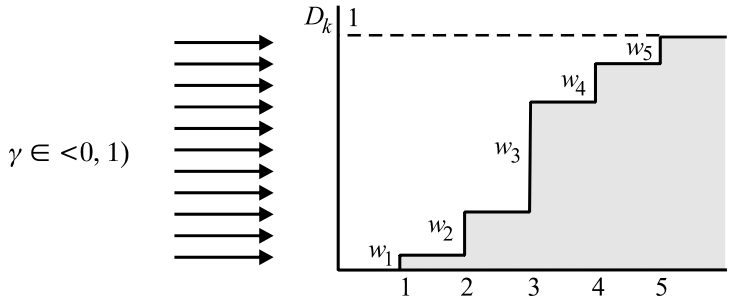


Fig. 2.16: Distribution sequence for discrete case.

The sequence is invariably monotonically increasing, with values ranging between 0 and 1. This property is exploited in the Monte Carlo realization of an event. A random number from the interval <0, 1) is generated repeatedly, conceptualized as a projectile striking the staircase from the left to determine which step is hit (see Figure 2.16). If it falls into step k, event k is declared to have occurred. Since the step height corresponds to the event probability, random events are generated precisely in accordance with the probability distribution. A similar procedure is applied in continuous scenarios. If the probability density is $f(x)$, a distribution function is defined by the relation:

$$D(x) = \int_{-\infty}^{x} f(x)\,\mathrm{d}x \,. \tag{2.98}$$

The function is monotonically increasing, with the limit at the right boundary defined by the sum of all probabilities: $\lim_{x\to\infty} D(x) = 1$.

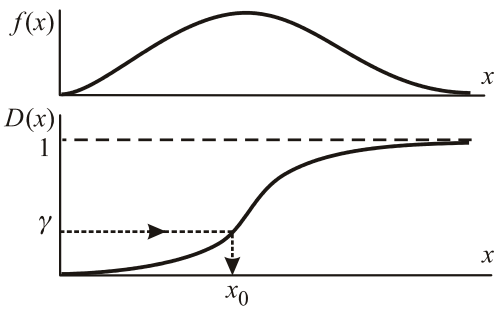


Fig. 2.17: Probability density and corresponding distribution function for continuous case.

Analogously to the discrete case, the rejection method allows the realization of a distribution using a uniform generator γ from the interval <0, 1). An event x_0 is declared to occur if $D(x_0) = \gamma$. For the realized event, the following relation holds:

$$x = D^{-1}(\gamma)\,. \tag{2.99}$$

The procedure for realizing a given continuous distribution is structured as follows:

1. The distribution function $D(x)$ is determined.
2. The inverse function to $D(x)$ is found.
3. A uniformly distributed random number $\gamma \in$ <0, 1) is generated.
4. The event $x = D^{-1}(\gamma)$ is declared to have occurred.

◖ **Example 2.8:** Realize a uniform distribution on the interval (a, b).

Solution: The probability density of a uniform distribution is a constant function $f(x)$. The constant value is determined from the normalization condition:

$$f(x) = K\,; \qquad \int_a^b f(x)\,\mathrm{d}x = 1 \qquad \Rightarrow$$

$$K\,(b-a) = 1 \qquad \Rightarrow \qquad .$$

$$f(x) = \frac{1}{b-a}$$

The distribution function is easily obtained:

$$D(x) = \int_a^x f(x)\,\mathrm{d}x = \frac{x-a}{b-a}$$

and set equal to a random number γ from the interval <0, 1), followed by inversion:

$$D(x) = \gamma \qquad \Rightarrow \qquad \frac{x-a}{b-a} = \gamma \qquad \Rightarrow \qquad x = a + \gamma(b-a)\,.$$

The result is natural: the random number γ between 0 and 1 is scaled to the required interval by the coefficient $(b-a)$ and shifted by the value a to the interval origin.

◗

◖ **Example 2.9:** Realize the distribution Kx^2 on the interval $(-1, +1)$.
Solution: First, the normalization constant K of the distribution is determined:

$$f(x) = Kx^2\,; \qquad \int_{-1}^{+1} f(x)\,\mathrm{d}x = 1 \qquad \Rightarrow \qquad K = \frac{3}{2} \qquad \Rightarrow \qquad f(x) = \frac{3}{2}x^2\,.$$

As the next step, the distribution function $D(x)$ is found:

$$D(x) \;=\; \int_{-1}^{x} f(x)\,\mathrm{d}x \;=\; \frac{x^3+1}{2}\,.$$

The distribution function is set equal to a random number γ from the interval <0, 1), and inversion is performed:

$$D(x) = \gamma \quad \Rightarrow \quad \frac{x^3 + 1}{2} = \gamma \quad \Rightarrow \quad x = \sqrt[3]{2\gamma - 1}\,.$$

The result is a non-uniform generator on the interval (−1, +1). In accordance with the parabolic probability density, values occur most frequently at the interval boundaries and least frequently in the center. The distribution function clearly indicates that hitting the position $x = 0$ with a "projectile arriving from the left" is nearly impossible:

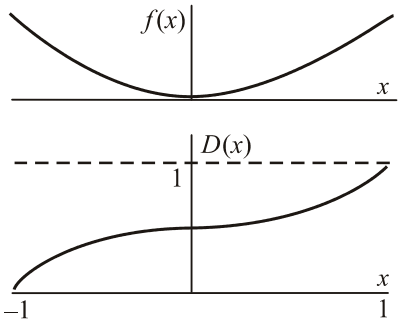


Fig. 2.18: Probability density and corresponding distribution function.

◗

◖ **Example 2.10:** Realize the distribution exp[−x] on the interval (0, ∞).

Solution: The normalized probability density is $f(x)$ = exp[−x], and integration yields the distribution function $D(x)$ = 1−exp[−x]. Setting $D(x) = \gamma$ yields 1−exp[−x] = γ, which upon inversion results in $x = -\ln(1-\gamma)$. Since γ and $1-\gamma$ share the identical uniform distribution on the interval (0, 1), selecting the following expression suffices:

$$x = -\ln \gamma\,.$$

◗

Note: Attention must be paid to the terminology: in physics, the *probability density* is alternative termed the *distribution function*. In mathematics, the distribution function is invariably defined as the integral of the probability density with an upper variable limit.

Von Neumann Method

Let a probability density $f(x)$ be defined on a finite interval (a, b). A bounding rectangle of minimal area enclosing the curve $f(x)$ is determined. The choice of height M is arbitrary provided $M > f(x)$ for all x; however, the method is most efficient for the minimal possible value of M. First, a random point within the rectangle is generated:

$$\begin{aligned} \eta_1 &= a + \gamma_1 (b - a)\,, \\ \eta_2 &= M \gamma_2\,. \end{aligned} \tag{2.100}$$

The probability of an event within the interval Δx is proportional to the area under the curve since $\Delta P = f \Delta x$. Therefore, augmenting the algorithm suffices:

$$\begin{aligned} \eta_2 < f(\eta_1) \quad &\Rightarrow \quad \text{Event } x = \eta_1 \text{ occured;} \\ \eta_2 \geq f(\eta_1) \quad &\Rightarrow \quad \text{New point } [\eta_1, \eta_2] \text{ is chosen.} \end{aligned} \tag{2.101}$$

The von Neumann method is universally applicable but lacks the efficiency of the rejection method (inverse function method). The latter approach is superior if the inverse to the distribution function can be analytically determined.

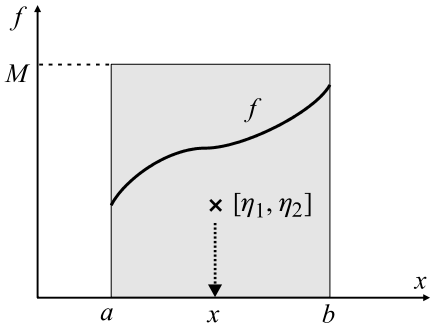


Fig. 2.19: Von Neumann method.

Superposition Method

Let the following three conditions be satisfied:

$$\begin{gathered} f(x) = \sum_{k=1}^{m} c_k \, f_k(x) \, ; \\ \int_{\Omega} f(x)\,\mathrm{d}x = \int_{\Omega} f_k(x)\,\mathrm{d}x = 1 \quad \text{pro } \forall k; \\ \sum_{k=1}^{m} c_k = 1 \, . \end{gathered} \tag{2.102}$$

The probability density is given by a sum (superposition) of several functions. Each partial probability density is normalized to unity, as is the total probability density. This requirement leads to the condition that the sum of the superposition coefficients equals unity. A sum of partial distribution functions for individual functions f_k is introduced:

$$D(x) = \sum_{k=1}^{m} c_k D_k(x) \, . \tag{2.103}$$

The following algorithm is utilized to realize the distribution:

1. A random variable is introduced:

$$\xi = \begin{pmatrix} 1 & 2 & \cdots & m \\ c_1 & c_2 & \cdots & c_m \end{pmatrix}$$

A uniformly distributed random number $\gamma_1 \in <0, 1)$ is generated. According to one of the preceding techniques (preferably the rejection method), an $k \in \{1, 2, \cdots, m\}$ is subsequently selected based on the probabilities of the coefficients $c_1, c_2, \cdots, c_m$.

2. A random number $\gamma_2 \in <0, 1)$ is generated, and the distribution $f_k(x)$ is realized via the inverse function or von Neumann method.

◖ **Example 2.11:** Realize the distribution $f(x) = \frac{5}{12}\left[1 + (x-1)^4\right]$ on the interval (0, 2).

Solution: Utilizing the rejection method for the entire probability density is theoretically possible but unnecessarily complex. The probability density is decomposed as follows (partial functions f_1 and f_2 are determined with coefficients such that they are normalized to unity, and subsequent coefficients c_1 and c_2 are found):

$$f_1(x) = \frac{1}{2}; \quad f_2(x) = \frac{5}{2}(x-1)^4 \qquad \Rightarrow \qquad f(x) = \frac{5}{6} f_1(x) + \frac{1}{6} f_2(x).$$

The distribution function is expressed as:

$$D(x) = \frac{5}{6} D_1(x) + \frac{1}{6} D_2(x); \qquad D_1(x) = \frac{x}{2}; \quad D_2(x) = \frac{1}{2}\left[1 + (x-1)^5\right].$$

First, the number γ_1 is generated, and a decision is made according to the relation:

$$\gamma_1 < \frac{5}{6} \qquad \Rightarrow \qquad \text{Event 1 occured;}$$

$$\gamma_1 \geq \frac{5}{6} \qquad \Rightarrow \qquad \text{Event 2 occured.}$$

Subsequently, the rejection method is applied. Generating γ_2 utilizes the relation:

For event 1: $\quad x = 2\gamma_2$;

For event 2: $\quad x = 1 + \sqrt[5]{2\gamma_2 - 1}$.

The entire method can be summarized as follows: a pair of random numbers within the interval (0, 1) is generated, utilizing the relation:

$$x = \begin{cases} 2\gamma_2, & \gamma_1 < \frac{5}{6}; \\ 1 + \sqrt[5]{2\gamma_2 - 1}, & \gamma_1 \geq \frac{5}{6}. \end{cases}$$

◗

Useful Implementations of Specific Distributions

Gaussian Distribution

$$f(x) = \frac{1}{\sqrt{2\pi}} \exp[-\frac{x^2}{2}]; \qquad x \in (-\infty, \infty). \tag{2.104}$$

A pair of random numbers γ_1, γ_2 is generated from the interval (0, 1). Two values of the Gaussian distribution are subsequently expressed as:

$$\begin{aligned} x_1 &= \sqrt{-2\ln\gamma_1}\,\cos(2\pi\gamma_2); \\ x_2 &= \sqrt{-2\ln\gamma_1}\,\sin(2\pi\gamma_2). \end{aligned} \tag{2.105}$$

Gamma Distribution

$$f(x)=\frac{a^n}{(n-1)!}x^{n-1}\exp[-ax]\,;\qquad x\in(0,\infty)\,;\quad ;a>0;\quad n=1,2,\ldots. \tag{2.106}$$

Numbers $\gamma_1, \gamma_2 \cdots \gamma_n$ are generated, determining the values:

$$x_n=-\frac{1}{a}\ln(\gamma_1\cdot\gamma_2\cdots\gamma_n)\,. \tag{2.107}$$

Points Inside Sphere of Radius *R*

Uniformly generated points within a sphere of radius R in spherical coordinates (r, φ, θ):

$$r=R\sqrt[3]{\gamma_1}\,;\qquad \varphi=2\pi\gamma_2\,;\qquad \cos\theta=2\gamma_3-1\,. \tag{2.108}$$

2.5.3 Metropolis Method

One of the most successful numerical algorithms, currently known as the *Metropolis method*, was published in 1953. The algorithm was formulated by a research group working on the development of the first nuclear reactors at the Los Alamos National Laboratory. The authors primarily comprised the Greek-American physicist Nicholas Metropolis, the American theorist Edward Teller, and the American plasma physicist Marshall Rosenbluth.

The Metropolis algorithm enables a straightforward approach to sampling the Boltzmann distribution. A system is assumed to be in thermodynamic equilibrium at a temperature T. The corresponding statistical ensemble undergoes the equilibrium Boltzmann distribution:

$$P_{\text{eq}}(H)=C\exp[-\beta H]\,. \tag{2.109}$$

In realizing the distribution, the primary limitation involves determining the normalization constant C. This determination requires evaluating the partition function by summing or integrating the exponential factors on the right-hand side over all degrees of freedom. Since the factor $\exp[-\beta H]$ can vary by many orders of magnitude, numerical integration is complicated.

The Metropolis method enables generating a representative sampling sequence of states S_n with energies $H_n = H(S_n)$. If a sufficient number of sequence terms is generated, the sequence simulates the Boltzmann distribution. Consequently, evaluating the mean values of dynamic variables via integration over the phase space is not required:

$$\langle A\rangle=\frac{\int A(S)\exp[-\beta H(S)]\,\mathrm{d}\Gamma}{\int\exp[-\beta H(S)]\,\mathrm{d}\Gamma}\,.$$

Instead, if the sequence contains a sufficiently large number of terms, determining the arithmetic mean of the sequence terms suffices:

$$\langle A\rangle\;=\;\lim_{N\to\infty}\frac{1}{N}\sum_{n=1}^{N}A(S_n)\,. \tag{2.110}$$

The Metropolis algorithm enables the formulation of such a representative sequence without calculating the partition function:

1) An initial state of the system is chosen randomly. The algorithm guarantees that the generated sequence simulates the properties of the Boltzmann distribution regardless of the initial term choice.

2) An alternative state of the system is chosen using a random number generator, which uniformly covers the possible generalized coordinates and momenta.

3) The new state is accepted with a probability:

$$P_{n\to n+1} = \begin{cases} \exp[-\beta\,\Delta H] & \text{pro } \Delta H > 0 \\ 1 & \text{pro } \Delta H \le 0 \end{cases}; \quad \Delta H \equiv H(S_{n+1}) - H(S_n)\,. \quad (2.111)$$

4) The procedure continues from step 2.

Note 1: Step 3 can be realized as follows: if $\Delta H \le 0$, the state S_{n+1} is considered the subsequent term of the representative sequence. If $\Delta H > 0$, a random number $\gamma \in (0, 1)$ is generated; for $\gamma \le \exp[-\beta\Delta H]$, S_{n+1} is accepted as the new sequence term, whereas for $\gamma > \exp[-\beta\Delta H]$, the original state is retained. Thus, a state with lower energy is invariably selected. The probability of choosing a higher energy configuration decreases exponentially with the energy difference.

Note 2: The generation of the representative sequence is performed at a constant temperature. Subsequent calculations can be initiated with incrementally modified temperatures to simulate the thermal dependence of variables. If the temperature is decreased sufficiently slowly, the ground state of the system can be located via the *simulated annealing* method. Although locating the ground state is critical, the Metropolis algorithm may occasionally isolate a local minimum rather than the absolute energy minimum.

Note 3: Monte Carlo methods typically fail near phase transitions, where relaxation times and the required number of sequence terms increase disproportionately.

Note 4: The Metropolis generation of a representative sequence belongs to the class of *Markov processes*, as the subsequent term depends exclusively on the preceding term rather than the historical generation of the sequence.

Note 5: This algorithm was generalized for arbitrary statistical distributions by the Canadian mathematician Keith Hastings in 1970. Let $P_{\text{eq}}(S)$ be a given probability distribution and $P_{n\to n+1}$ denote the proposed transition probability. A random number $\gamma \in (0, 1)$ is generated, and the new state is accepted if the following relation holds:

$$\gamma < \min\left\{\frac{P_{\text{eq}}(S_{n+1})P_{n\to n+1}}{P_{\text{eq}}(S_n)P_{n+1\to n}}, 1\right\}.$$

Due to the ratio formulation, normalization of the probabilities to unity is not required.

2.5.4 Monte Carlo Simulation of Binary Collisions

In multi-particle plasma, calculating actual collision trajectories is generally impossible, requiring Monte Carlo simulations. The procedure is structured as follows:

1) A decision is made whether a collision between two particles occurs (e.g., if they are within the Debye sphere) based on a predefined criterion.
2) A distribution sequence is constructed from the cross-sections σ_k of various possible processes (Coulomb collision, excitation, ionization, charge exchange, etc.), and the rejection method is applied to select the occurring process:

$$D_l = \frac{\sum_{k=1}^{l} \sigma_k}{\sigma_{\text{tot}}}; \quad \sigma_{\text{tot}} \equiv \sum_{k=1}^{N} \sigma_k \,. \tag{2.112}$$

3) A suitable post-collision state is generated from the pre-collision state using a Monte Carlo algorithm.

Although Monte Carlo estimates of final states are inaccurate for a single specific collision, statistically correct results are obtained for large ensembles. A widely utilized Monte Carlo algorithm for Coulomb collisions, proposed by Tomonori Takizuka and Hirotada Abe in 1977, is described below.

Coulomb Collisions

Two particles with masses m_α, m_β and laboratory velocities $\mathbf{v}^t{}_\alpha$, $\mathbf{v}^t{}_\beta$ are assumed to collide at time t. The relative velocity at time t is denoted as:

$$\mathbf{g}^t \equiv \mathbf{v}^t_\alpha - \mathbf{v}^t_\beta \tag{2.113}$$

Let $\mathbf{g}_z$ and $\mathbf{g}_{xy}$ represent the projections of the relative velocity onto the z-axis and the xy-plane, respectively. Furthermore, angles θ and φ are introduced:

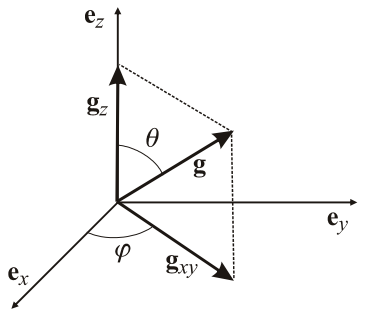


Fig. 2.20: Decomposition of relative velocity into projections $\mathbf{g}_{xy}$ and $\mathbf{g}_z$.

To describe the collision, a rotated coordinate system S' is chosen, rotated by angle φ about the z-axis and angle θ about the y-axis, aligning the relative velocity vector with the third axis:

$$\begin{pmatrix} \cos\theta & 0 & -\sin\theta \\ 0 & 1 & 0 \\ \sin\theta & 0 & \cos\theta \end{pmatrix} \cdot \begin{pmatrix} \cos\varphi & \sin\varphi & 0 \\ -\sin\varphi & \cos\varphi & 0 \\ 0 & 0 & 1 \end{pmatrix} \begin{pmatrix} g_x \\ g_y \\ g_z \end{pmatrix}_S^t = \begin{pmatrix} 0 \\ 0 \\ g \end{pmatrix}_{S'}^t . \tag{2.114}$$

The total transformation matrix takes the form:

$$\mathbb{R} = \begin{pmatrix} \cos\theta\cos\varphi & \cos\theta\sin\varphi & -\sin\theta \\ -\sin\varphi & \cos\varphi & 0 \\ \sin\theta\cos\varphi & \sin\theta\sin\varphi & \cos\theta \end{pmatrix}. \tag{2.115}$$

To return to the original system, the inverse matrix is required, obtained by transposing this unitary matrix:

$$\mathbb{R}^{-1} = \begin{pmatrix} \cos\theta\cos\varphi & -\sin\varphi & \sin\theta\cos\varphi \\ \cos\theta\sin\varphi & \cos\varphi & \sin\theta\sin\varphi \\ -\sin\theta & 0 & \cos\theta \end{pmatrix}. \tag{2.116}$$

During a Coulomb collision, the magnitude of the relative velocity remains constant, whereas only its direction changes. Therefore, the vector $(0, 0, g)^t$ is rotated by angles Θ and Φ.

Generation of Angles Θ and Φ

Due to symmetry, generating the angle Φ is straightforward by assuming a uniform distribution, where a random number $\gamma_1 \in (0, 1)$ is generated to define:

$$\Phi = 2\pi\gamma_1 . \tag{2.117}$$

The selection of the angle Θ depends on the cross-section of the specific collision type. Takizuka and Abe demonstrated that a correct statistical representation is achieved by:

$$\Theta = \operatorname{arctg}(2\delta) , \tag{2.118}$$

where $\delta \in (-\infty, \infty)$ is a normally distributed random variable with a mean of zero and a standard deviation σ given by:

$$\sigma = \sqrt{\frac{Q_\alpha^2 Q_\beta^2 \min\{n_\alpha, n_\beta\} \ln \Lambda_{\alpha\beta}}{8\pi\varepsilon_0^2 \mu^2 g^3} \Delta t} , \tag{2.119}$$

where μ is the reduced mass, $\ln \Lambda_{\alpha\beta}$ denotes the Coulomb logarithm, g is the relative velocity magnitude, and Δt represents the time step.

Return to Original Variables

The new relative velocity in the rotated system S' is evaluated from angles Θ and Φ. Laboratory velocity in system S is then found via the inverse matrix $\mathbb{R}^{-1}$:

$$\begin{pmatrix} g_x \\ g_y \\ g_z \end{pmatrix}_S^{t+\Delta t} = \mathbb{R}^{-1} \begin{pmatrix} g_x \\ g_y \\ g_z \end{pmatrix}_{S'}^{t+\Delta t} = \begin{pmatrix} \cos\theta\cos\varphi & -\sin\varphi & \sin\theta\cos\varphi \\ \cos\theta\sin\varphi & \cos\varphi & \sin\theta\sin\varphi \\ -\sin\theta & 0 & \cos\theta \end{pmatrix} \cdot \begin{pmatrix} g\sin\Theta\cos\Phi \\ g\sin\Theta\sin\Phi \\ g\cos\Theta \end{pmatrix}. \tag{2.120}$$

The difference between the post-collision and pre-collision relative velocities is defined by the relation:

$$\Delta\mathbf{g} = \mathbf{g}^{t+\Delta t} - \mathbf{g}^{t}. \tag{2.121}$$

Substitution from (2.120) yields:

$$\begin{aligned}
\Delta g_x &= \frac{g_x^t}{g_{xy}^t} g_z^t \sin\Theta\cos\Phi - \frac{g_y^t}{g_{xy}^t} g \sin\Theta\sin\Phi - g_x^t\left(1-\cos\Theta\right),\\
\Delta g_y &= \frac{g_y^t}{g_{xy}^t} g_z^t \sin\Theta\cos\Phi + \frac{g_x^t}{g_{xy}^t} g \sin\Theta\sin\Phi - g_y^t\left(1-\cos\Theta\right),\\
\Delta g_z &= -g_{xy}^t \sin\Theta\cos\Phi - g_z^t\left(1-\cos\Theta\right).
\end{aligned} \tag{2.122}$$

The variable g denotes the magnitude of $\mathbf{g}$, and g_{xy} represents the magnitude of the projection $\mathbf{g}_{xy}$:

$$g^t = \sqrt{\left(g_x^t\right)^2 + \left(g_y^t\right)^2 + \left(g_z^t\right)^2}, \qquad g_{xy}^t = \sqrt{\left(g_x^t\right)^2 + \left(g_y^t\right)^2}. \tag{2.123}$$

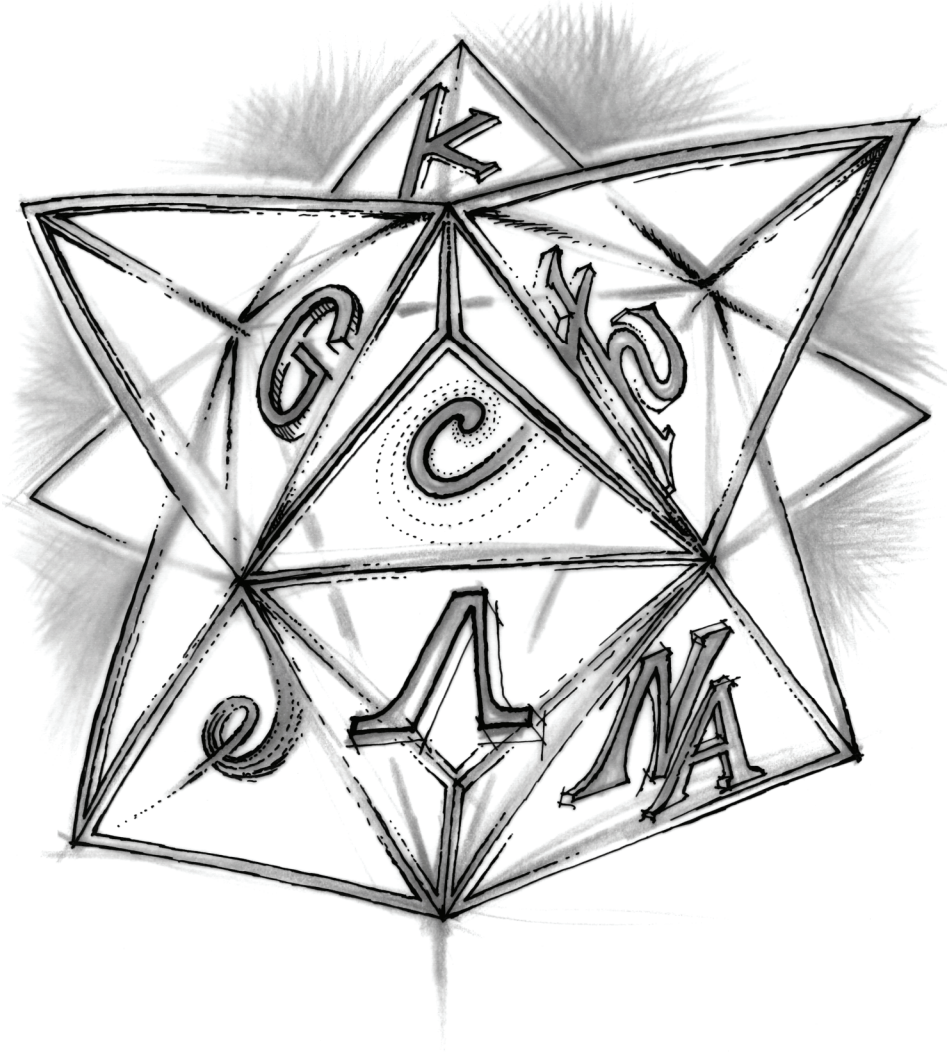
The velocities of the particles after the collision are ultimately determined using transformation (1.646):

$$\mathbf{v}_\alpha^{t+\Delta t} = \mathbf{v}_\alpha^t + \frac{m_\beta}{m_\alpha + m_\beta}\Delta\mathbf{g}, \qquad \mathbf{v}_\beta^{t+\Delta t} = \mathbf{v}_\beta^t - \frac{m_\alpha}{m_\alpha + m_\beta}\Delta\mathbf{g}. \tag{2.124}$$

The described algorithm is repeated iteratively for the observed particle system.



List of Symbols



$\#_{Al}$ Alfvén number
$\#_{Bt}$ Batchelor number
$\#_{dr}$ driven reconnection index
$\#_{DL}$ double layer parameter
$\#_{DL,rel}$ relativistic double layer parameter
$\#_{GS}$ GS95 model reconnection index
$\#_{Ha}$ Hartmann number
$\#_{Lu}$ Lundquist number
$\#_{M}$ Mach number
$\#_{MA}$ Mach-Alfvén number
$\#_{P}$ Petschek model reconnection index
$\#_{Re}$ Reynolds number
$\#_{Re,M}$ magnetic Reynolds number]
$\#_{rec}$ reconnection index
$\#_{sp}$ spontaneous reconnection index
$\#_{St}$ Stuart number
$\mathbf{A}$ vector potential
A additive variable
$\mathcal{A}$ additive variable density
$\mathbf{A}$ four-potential
$\mathbf{B}$ magnetic field vector
B_P poloidal magnetic field
B_T toroidal magnetic field
b impact parameter
$\mathbf{b}$ magnetic field to plasma density ratio ($\mathbf{B}/\rho$)
c speed of light
c_s speed of sound
D diffusion coefficient, distribution function, boundary layer thickness, Stix coefficient D
D_a ambipolar diffusion coefficient
D_k distribution sequence
D_{kl} dynamic pressure tensor
$\mathbf{D}$ electric displacement field
$\mathbf{e}_k$ unit vector in k-th axis direction
$\mathbf{e}_B$ unit vector in $\mathbf{B}$ direction
e elementary charge, internal energy density
$\mathscr{E}$ energy
$\mathbf{E}$ electric field intensity
f function, probability density, number of degrees of freedom
f_1 probability density perturbation
f_{LE} local equilibrium probability density
f_α probability density of species α
$\mathbf{f}$ force density
F force magnitude
$\mathbf{F}_{ext}$ external force field
g statistical weight, relative velocity magnitude, amplification factor, gravitational acceleration
$\mathbf{g}$ gravitational acceleration vector
$\mathbf{g}$ relative velocity $\mathbf{g} = \mathbf{v}_\alpha - \mathbf{v}_\beta$
G gravitational constant
G, $\mathbf{G}$ Green function
$G_{\alpha\beta}$ Second Rosenbluth potential
h distance, height
$\hbar$ Plancka constant
H Hamiltonian
$H_{\alpha\beta}$ first Rosenbluth potential
$\mathcal{H}$ helicity density
$\mathbf{H}$ magnetic field intensity
i linear electric current density
i imaginary unit
I electric current, ionization potential, integral value
I_m modified Bessel function
$\mathbf{j}$ flux, current density
$\mathbf{j}_C$ conduction current
$\mathbf{j}_M$ magnetization current
$\mathbf{j}_N$ particle flux
$\mathbf{j}_m$ mass flux
$\mathbf{j}_Q$ charge flux
$\mathbf{J}$ flux four-vector
J_0, J_1 Bessel functions
J_2 second adiabatic invariant
k_B Boltzmann constant

$\mathbf{k}$ wave vector
$\mathbf{k}_{\alpha\beta}$ unit vector in relative velocity direction
K constant, helicity
K_m modified Bessel function,
l length
L Lagrange function, distance, Stix coefficient L
$\mathscr{L}$ Lagrangian density
L_{kl} kinetic coefficients
L_{elmg} field Lagrangian
L_{int} interaction Lagrangian
L_{part} particle Lagrangian
m mass, instability mode
m_0 rest mass
$\mathbf{M}$ magnetization vector
$\mathscr{M}_{kl}$ angular momentum density
n number density
$\mathbf{n}$ normal vector
N number of particles, refractive index
N_{D} number of particles in Debye sphere
N_{L} Left-handed wave refractive index
N_{O} ordinary wave refractive index]
N_{R} right-handed wave refractive index
N_{X} extraordinary wave refractive index
$\mathscr{N}$ linear particle density
$\mathscr{N}_{klm}$ angular momentum flux
p pressure, momentum magnitude
p_{M} magnetic pressure
$\mathbf{p}$ momentum
$\mathbf{p}_{\mathrm{E}}$ electric dipole moment
$\mathbf{p}_{\mathrm{M}}$ magnetic dipole moment
p_q generalized momentum
P period, power, polynomial function
P_{kl} pressure tensor, transition probability, Legendre polynomial
$\mathscr{P}$ transition probability density, power density
q generalized coordinate, safety factor
$\mathbf{q}$ heat flux
Q charge
r radial distance
$\mathbf{r}$ position vector
$\mathbf{R}$ guiding center position vector
R major radius in tokamak, plasma filament radius, stellar radius, Stix coefficient R
R_{k} radius of curvature
R_{D} drift radius
R_{L} Larmor radius
s lenth parametrization, specific entropy
S area, collision term, entropy, Stix coefficient S
t time
T kinetic energy, period, temperature
T_{kl} momentum flux tensor, Maxwell stress tensor
u rescaled velocity, $u = \gamma v$, velocity field magnitude
$\mathbf{u}$ continuum velocity field
U voltage
$\mathbf{v}$ velocity vector
$\mathbf{v}_{\mathrm{A}}$ Alfvén velocity vector
$\mathbf{v}_{\alpha\beta}$ relative velocity
$\mathbf{v}_{(\alpha\beta)}$ center-of-mass velocity
v velocity magnitude
v_{f} phase velocity
v_{g} group velocity
$v_{\parallel}$ parallel velocity component
$v_{\perp}$ perpendicular velocity component
v_{A} Alfvén velocity
v_{D} drift velocity
v_{T} mean thermal velocity
V potential energy, volume

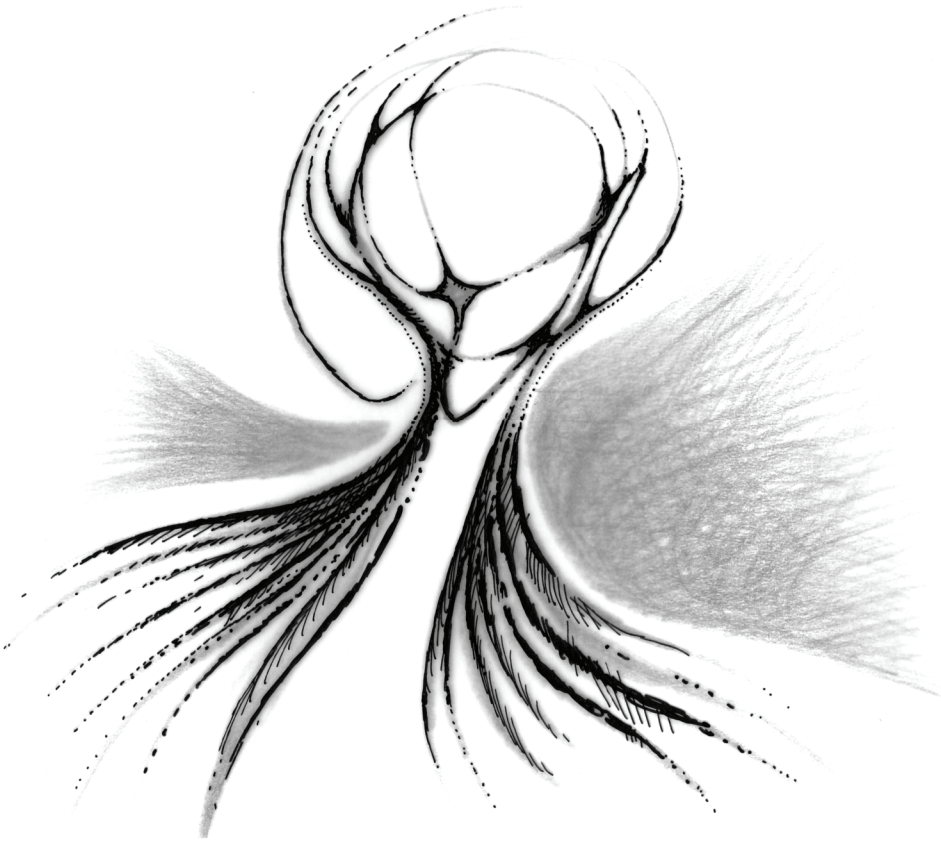
V_G gravitational potential energy
V_E electric potential energy
V_{kl} viscosity tensor
$\mathbf{V}$ vector field
$\mathscr{V}$ Verdet constant
V.P. principal value of integral
w probability, velikost chaotické složky rychlosti
$\mathbf{w}$ chaotic velocity magnitude
$W_\perp$ perpendicular kinetic energy
W_I ionization energy
W_M magnetic energy
$\mathbf{x}$ position
x coordinate x
X generalized force, Stix coefficient X
y coordinate y
Y_m Bessel functions of the second kind
Y_{lm} spherical harmonics
z coordinate z, complex argument
Z ionization degree
α angle, constatnt
β angle, inverse temperature ($1/k_BT$), beta parameter (p/p_M)
$\boldsymbol{\beta}_0$ unit vector in magnetic field direction
γ relativistic coefficient, polytropic index, random number, angle, instability growth rate
$\boldsymbol{\gamma}$ elestromagnetic field momentum density
δ Dirac delta distribution, diffusion region thickness, skin depth
δ_{kl} Kronecker delta
Δ diffusion region length
Δ difference value, Laplacian
ε expansion parameter, quantum state energy, permittivity
ε_0 vacuum permittivity
ε_F Fermi energy
ε_{klm} Levi-Civita tensor
ζ second viscosity coefficient
η first viscosity coefficient, resistivity
η_M magnetic viscosity
κ thermal conductivity coefficient
λ wavelength, multiplicative constant, Lagrange multiplier
λ_D Debye length
Λ Coulomb logarithm argument
θ angle, poloidal angle
μ first adiabatic invariant, magnetic moment, mobility, reduced mass, permeability, KG equation constant
$\boldsymbol{\mu}$ first adiabatic invariant, magnetic moment vector
μ_0 vacuum permeability
ν_c collision frequency
ξ complex coordinate, substituted variable, random variable
$\boldsymbol{\xi}$ displacement vector
Π total pressure
ρ density, tokamak chamber radial distance
$\boldsymbol{\rho}$ gyration radius vector
ρ_Q charge density
ρ_m mass density
ρ_W energy density
σ cross-section, differential conductivity, surface tension
τ gyration time, damping time pre-acceleration time
τ_A Alfvén time
τ_c mean free time
τ_R resistive time
τ_{REC} reconnection time

φ	phase, azimuthal/toroidal angle
ϕ	potential, summation invariant, error function dispersion relation
ϕ_E	electric potential
ϕ_G	gravitational potential
χ	scattering angle
ψ	summation invariant, Chandrasekhar function, wave function, magnetic surface
ψ_k	partial wave
ω	angular frequency
ω_c	cyklotron frequency
ω_d	lower hybrid frequency
ω_h	upper hybrid frequency
ω_L	left cutoff frequency
ω_p	plasma frequency
ω_R	right cutoff frequency
$\boldsymbol{\omega}$	vorticity
Ω	solid angle, shifted frequency spatial integration domain

Subscripts and Superscripts

a	particle index
A, Al	Alfvén
c	cyclotron
dr	driven reconnection
DL	double layer
e	electrons
E	electric
EM	electromagnetic
Ha	Hartman
i	ions
i,j, k	Cartesian axes 1, 2, 3
L	left-handed
Lu	Lundquist
M	Mach magnetic
MA	Mach-Alfvén
O	ordinary
p	plaama
P	Petschek, poloidal particles
R	right-handed
Re	Reynolds
rec	reconnection
s	sound
sp	spontaneous reconnection
T	toroidal
X	extraordinary
α	species α
$\parallel$	parallel
$\perp$	perpendicular

Biographical Index



Plasma Theory



Abraham, Max (1875–1922), a German physicist primarily concerned with electromagnetic field theory. He graduated from Humboldt University and worked at the University of Göttingen, completing his doctorate under Max Planck. Upon invitation from Tullio Levi-Civita, he accepted a mechanics professorship at the Technical University of Milan. Independently of others, he derived the force exerted on a particle by its own radiation emission, known today as the Abraham-Lorentz force. Skeptical of new paradigms, he formulated an alternative framework to general relativity, which violated the equivalence principle. He also proposed an electron theory, conceptualizing it as a rigid sphere with surface-distributed charge. During World War I, he returned to Germany to research military radio communication at the Technical University of Stuttgart. Following his death, Max Born and Max von Laue remarked: "*He loved his absolute ether, his field equations, his rigid electron just as a youth loves his first flame, whose memory no later experience can extinguish.*"



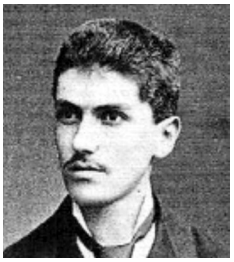
Alfvén, Hannes Olof Gösta (1908–1995), a Swedish physicist and astrophysicist, regarded as a founder of modern plasma physics. He developed initial formulations of magnetohydrodynamics and introduced the frozen-in magnetic field concept. In 1939, he published a theory of magnetic storms and auroras, laying the foundations of Earth's magnetosphere theory. In 1950, he elucidated the formation of auroral vortex structures via diocotron instability. The Alfvén velocity and Alfvén number are named in his honor. Although some conjectures were subsequently disproven – notably his opposition to the Big Bang theory and his belief in a matter-antimatter symmetric universe – he achieved broad recognition. He graduated from Uppsala University. For his work, he received the Lomonosov Gold Medal, the Dirac Medal, the William Bowie Medal, and membership in the Royal Society. He was awarded the Nobel Prize in 1970.



Van Allen, James Alfred (1914–2006), an American space scientist who pioneered the placement of Geiger counters aboard the initial American satellites Explorer I and Explorer III. These satellites discovered tori of high-energy charged particles surrounding Earth, designated today as the Van Allen radiation belts. Consequently, the majority of his active career was dedicated to magnetospheric phenomena. He was a leading figure in American space exploration during the Cold War, contributing to the development of the Pioneer and Mariner probes, as well as the Orbiting Geophysical Observatory (OGO). He graduated from the University of Iowa. For his work, he received numerous accolades, including the Elliott Cresson Medal, the William Bowie Medal, the Gold Medal of the Royal Astronomical Society, the National Medal of Science, the Crafoord Prize, and the Vannevar Bush Award. Both the Van Allen radiation belts and the Van Allen Probes spacecraft mission are named in his honor.



Appleton, sir Edward Victor (1892–1965), an English physicist and astronomer who investigated the atmosphere and demonstrated the existence of the ionosphere. He received the Nobel Prize in Physics in 1947. Named in his honor are the Appleton layer of the ionosphere, which reflects radio waves, the Appleton-Hartree equation for electromagnetic wave propagation in plasma with a homogeneous magnetic field, and the Rutherford Appleton Laboratory (RAL), one of the most prominent British national laboratories. He studied at the University of Edinburgh and later at Cambridge. In addition to the Nobel Prize, he received numerous accolades, including the Hughes Medal, the Faraday Medal, the Royal Medal, the Albert Medal of the Royal Society of Arts, and the Chree Medal (now the Appleton Medal) in 2008.



Beltrami, Eugenio (1835–1899), an Italian mathematician and physicist who investigated non-Euclidean geometry, electricity, and magnetism. Named in his honor are Beltrami theorem regarding curved surface mapping, the Beltrami field (whose curl is proportional to the field itself), and the Laplace-Beltrami operator. In plasma physics, Beltrami fields play a crucial role in describing helical structures. He worked extensively on applying tensor calculus to theoretical physics. He studied at the University of Pavia, but his studies were terminated due to his political views. Nevertheless, he became a professor at the University of Bologna in 1862 and subsequently worked at universities in Bologna, Rome, Pisa, and Pavia. In 1898, the former young rebel became a venerable senator of the Kingdom of Italy.



Bennett, Willard Harrison (1903–1987), an American scientist and inventor born in Findlay, United States. He investigated gas ionization by electric fields and invented radiofrequency mass spectrometry, currently utilized on various space probes. His spectrometer first flew into space aboard the Soviet Sputnik 3 satellite in 1958. In 1934, he derived a mathematical solution for plasma filament (pinch) equilibrium under constant current density, designated today as the Bennett pinch, which is highly significant for thermonuclear fusion. He predicted the existence of Earth's radiation belts six years prior to their actual discovery. He studied at the Carnegie Institute of Technology, Ohio State University, and the University of Michigan.



Bhatnagar, Prabhu Lal (1912–1976), an Indian mathematician and astrophysicist who investigated astrophysics, white dwarfs, and the origin of the Solar System. In plasma physics, he focused on statistical calculations and, together with Eugene Gross and Max Krook, formulated the BGK approximation of the Boltzmann equation in 1954. In later years, he dedicated his research to non-linear hydrodynamics. He studied at the University of Allahabad and Agra University, subsequently receiving a Fulbright scholarship at Harvard University. In 1950, he became a fellow of the Indian National Science Academy, and in 1955, a fellow of the Indian Academy of Sciences. In 1956, he became a professor of applied mathematics at the Indian Institute of Science. For his work, he received the Padma Bhushan order in 1968, presented by the President of India, which constitutes the third-highest civilian honor.



Birkeland, Kristian (1867–1917), a Norwegian physicist and inventor. He manufactured artificial fertilizers, developed an electromagnetic gun, and investigated auroras and charged particle trajectories in magnetic fields. He deduced that specific solar phenomena release charged particle beams into space, which occasionally strike Earth and trigger auroras. In his laboratory, he constructed a *terrella* – a small Earth model – to investigate aurora formation conditions. The Birkeland currents flowing along magnetic field lines are named in his honor. He worked at the University of Oslo. In 1994, his portrait alongside the terrella appeared on the Norwegian 200-kroner banknote, which was, however, replaced by a cod motif in 2017. His research was misunderstood during his lifetime, which contributed to his suicide. Birkeland's legacy was subsequently expanded by Hannes Alfvén. His aurora formation theory was verified much later via satellite measurements.

Boltzmann, Ludwig, see section *Statistical Physics*, "Selected Topics II."

Buneman, Oscar, see section *Numerical Simulations*, this textbook.

Carlqvist, Per (1938), a Swedish physicist who investigated stellar evolution, the solar wind, and double layer theory. Together with Hannes Alfvén, he proposed a solar flare theory where double layers play a fundamental role. He generalized the Bennett pinch equilibrium solution. He graduated from the KTH Royal Institute of Technology in Stockholm, where he continues to work today.

Coulomb, Charles, see section *Electromagnetic Field*, "Selected Topics II."



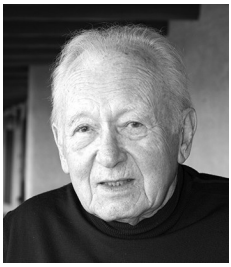
Cowling, Thomas George (1906–1990), an English astronomer who proved in 1934 that stellar and planetary magnetic fields cannot be generated by axisymmetric current ring (Cowling antidynamo theorem). He correctly understood sunspots as manifestations of an internal fluid dynamo. He classified non-radial stellar oscillations, establishing the foundations of helioseismology, and was the first to construct a stellar model with a convective core and radiative envelope (Cowling model). Cowling studied mathematics at Oxford. He worked at universities in Dundee and Manchester, and became a professor at the University of Wales and the University of Leeds. He received the Hughes Medal. From 1965 to 1967, he served as the president of the Royal Astronomical Society.



Davydov, Aleksandr Sergeyevich (1912–1993), a Soviet and Ukrainian physicist who graduated from Moscow State University. For several decades, he served as the director of the Institute for Theoretical Physics of the Ukrainian Academy of Sciences. He primaly investigated molecular crystals and their interaction with light, focusing on scattering, absorption, and diffraction. He discovered Davydov splitting in vibrational spectra and identified soliton solutions for crystal excitations. In 1973, he applied solitons to the propagation of nerve impulses in animal muscles, spanning theoretical physics and biophysics. He also investigated collective excitations in atomic nuclei. For his scientific achievements, he was awarded several prominent state honors, including Shevchenko National Prize, the Lenin Prize and the Order of Lenin.



Debye, Peter Joseph William (1884–1966), a Dutch physicist and chemist. He was the first to describe asymmetric molecular behavior using the dipole moment, investigating them via X-ray diffractometry; molecular dipole moments are still measured in Debye units. His research extended Einstein's specific heat theory with low-frequency phonons, addressed electrolyte electrical conductivity and atomic envelopes, and elucidated the Compton effect. In 1936, he received the Nobel Prize in Chemistry for the study of molecular structures behaviour. Within plasma physics, the Debye shielding length is named in his honor.

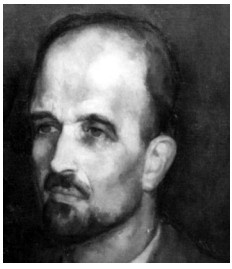


Dreicer, Harry (1927–2025), a German-American plasma physicist focused on controlled thermonuclear fusion. His parents fled the Bolshevik Revolution to Germany, where he was born, later moving to Italy and eventually emigrating to the United States due to Jewish persecution. He graduated from the Massachusetts Institute of Technology (MIT), defending a doctorate on runaway electrons. In his doctoral thesis, he derived the electric field value required for electrons to enter the runaway regime, where acceleration by the field dominates over collisional damping (known today as the Dreicer field). He spent most of his active career (42 years) at the Los Alamos National Laboratory.



Drude, Paul Karl Ludwig (1863–1906), a German physicist. He conducted experiments in electricity and magnetism, verifying Maxwell electromagnetic field theory. He introduced the symbol *c* for the speed of light in vacuum. In 1900, he developed a model to calculate the electrical, thermal, and optical properties of matter. In plasma physics, Drude elementary conduction theory is widely utilized. He linked optics directly to electromagnetic field theory. Drude studied mathematics and physics at the University of Göttingen. His name is borne by a lunar crater and the Paul Drude Institute for Solid State Electronics in Berlin.

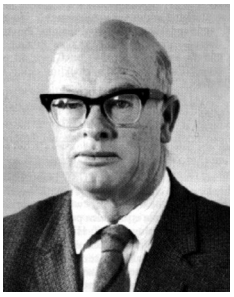
Fick, Adolf Eugen (1821–1901), a German physiologist who develop glass contact lenses. He pioneered the technique for measuring cardiac output (heart blood flow) and formulated the law of material diffusion, known in physics as the Fick law.



Fokker, Adriaan Daniël (1887–1972), a Dutch physicist and musician, cousin of the famous aircraft designer Anthony Fokker. Together with Max Planck, he derived the Fokker-Planck equation in 1913, which remains the standard for the statistical description of plasma during Coulomb collisions. Fokker also published several papers on special and general relativity. Mathematically, he investigated musical scales and successfully designed musical instruments, most notably the 31-ton Fokker organ located at the Teyler Museum in Haarlem.

Fourier, Jean-Baptiste de, see section *Mathematics for Physics*, “Selected Topics I.”

Gibbs, Josiah, see section *Statistical Physic*s, “Selected Topics II.”



Giovanelli, Ronald Gordon (1915–1984), an Australian astronomer and physicist. He investigated solar flares and the electron acceleration mechanism within variable magnetic fields. In 1946, he was the first to propose that magnetic X-line null points could serve as sources for plasma heating and particle acceleration, initiating research into magnetic field line reconnection and predicting the existence of this phenomenon. In 1949, he conducted a detailed analysis of scenarios where electron acceleration by an electric field dominates over collisional damping. This results in a population of runaway electrons, a phenomenon first noted by cloud chamber inventor Charles Wilson in 1925. Giovanelli founded the Fleurs Observatory near Sydney. He graduated from the University of Sydney, where he also obtained his doctorate, and received the Edgeworth David Medal.



Goldreich, Peter (*1939), an American astrophysicist, co-formulator of the magnetohydrodynamic turbulence model (with Seshadri Sridhar) and a pioneer of planetary migration theory. He graduated from Cornell University, obtaining his doctorate under Thomas Gold. In 1969, he became a professor of planetary science at Caltech, and since 2003, he has also served as a professor at Princeton. For his research, he received dozens of medals and accolades, most notably the Chapman Medal, the Gold Medal of the Royal Astronomical Society, the National Medal of Science, the Gerard P. Kuiper Prize, and the Shaw Prize. The asteroid 3805 Goldreich is named in his honor.

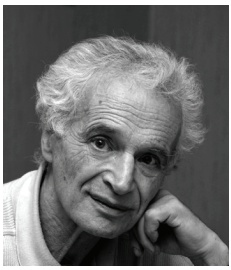


Gould, Roy Walter (1927–2022), an American electrical engineer and physicist specializing in plasma physics. Together with Alvin Trivelpiece, he discovered electrostatic waves in 1959 that propagate as solitons along the surface of a magnetized plasma column, known today as the Trivelpiece-Gould soliton. He investigated microwaves and their propagation in plasma, including solar radio noise, and contributed to rocket engine development at the NASA Jet Propulsion Laboratory. In 1994, he received the James Clerk Maxwell Prize for Plasma Physics. Gould graduated from Caltech (bachelor's) and Stanford University (master's), subsequently returning to Caltech for his doctorate.

Gordon, Walter, see section *Quantum theory*, "Selected Topics I."



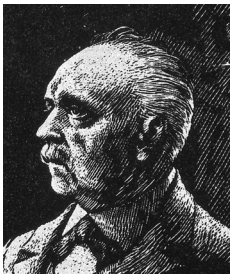
Gross, Eugene (1926–1991), an American theoretical physicist. He investigated boson interactions in quantum field theory, boson condensates, oscillations and waves in plasma, and plasma kinetic theory. Together with Prabhu Lal Bhatnagar and Max Krook, he derived the BGK approximation of the Boltzmann equation in 1954, which serves as a suitable substitution for the collision term. Gross graduated from Princeton University and received a Fulbright scholarship at the University of Rome. He worked as a visiting professor at the Massachusetts Institute of Technology (MIT) and held positions at Syracuse University and Brandeis University.



Gurevich, Aleksandr Viktorovich (1930–2023), a Soviet and Russian physicist who proposed in 1992 that runaway electrons, accelerated either within our atmosphere or by cosmic rays, serve as the triggering mechanism for lightning. Gurevich investigated plasma kinetic theory, ionospheric physics, and in later decades focused on neutron star magnetospheres and dark matter. He graduated from Moscow State University. For his research, he received the Landau Gold Medal, the Appleton Prize, the Mandelstam Prize, and the Friedman Prize.

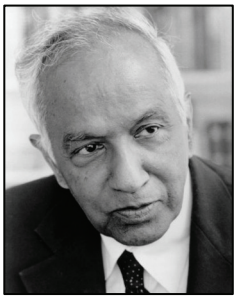
Hartmann, Julian, Frederik (1881–1951), a Danish engineer and physicist who published a mathematical solution for conducting fluid flow within a homogeneous magnetic field in 1937 and designed an electromagnetic conduction pump for molten metals. This device was experimentally verified on mercury by Freimut Lazarus. Within plasma physics, the Hartmann number and the Hartmann layer are named in his honor.

Hartree, Douglas Rayner (1897–1958), an English mathematician and physicist. He focused on numerical analysis and its application within quantum theory and atomic physics. Named in his honor are the Hartree-Fock numerical method and the Appleton-Hartree equation for electromagnetic wave propagation in plasma with a magnetic field.

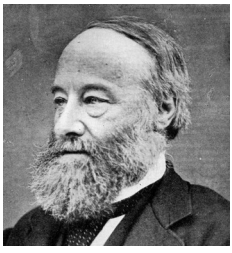


Helmholtz, Hermann Ludwig Ferdinand von (1821–1894), a German physician and physicist of immensely broad scope who investigated electromagnetic theory, thermodynamics, mechanics, color vision theory, and acoustics. In plasma physics, the Helmholtz equation is utilized, which is satisfied by Beltrami helical fields. The Kelvin-Helmholtz instability, occurring at the interface of two media with different velocities, is named in his honor. Electrical engineers recognize the Helmholtz resonator and the Helmholtz coil, both of which he first constructed.

Hugoniot, Henri Pierre (1851–1887), a French engineer and inventor, who co-developed the theory of fluid shock waves. Together with William Rankine, he derived the conditions for parameter discontinuities across a shock wave, known as the Rankine-Hugoniot relations. He also worked for the French Navy, achieving the rank of captain.

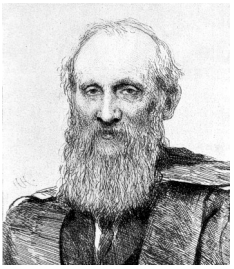


Chandrasekhar, Subrahmanyan (1910–1995), an Indian astrophysicist who worked in England and later in the United States. He primarily investigated stellar structure theory, the mathematical theory of black holes, and general relativity. Utilizing the equation of state, he derived the maximum possible mass of a white dwarf, known as the Chandrasekhar limit. The Chandra X-ray Observatory, launched into space in 1999, was named in his honor. Within statistical and plasma physics, the Chandrasekhar function is widely utilized. In 1983, he received the Nobel Prize in Physics for his contributions to stellar structure and evolution processes.



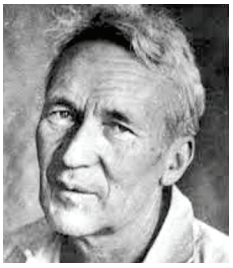
Joule, James Prescott (1818–1889), an English physicist and brewer who investigated the nature of heat and its relationship to mechanical energy. He collaborated with Lord Kelvin to establish the absolute temperature scale, investigated magnetostric-

tion, and derived the relationship for heat generated by electric currents passing through matter. This Joule heating constitutes the primary dissipation process in plasma. The SI unit of energy is named in his honor. Joule constructed highly precise measuring instruments, demonstrating that heat is a form of energy rather than a fluid substance.

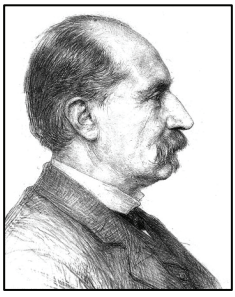


Kelvin, lord (1824–1907), born William Thomson, a prominent Scottish physicist. He investigated heat conduction and calorimetry, and designed instruments for measuring electrical quantities, such as the Kelvin (Thomson) bridge for measuring low resistances. He participated in laying transatlantic telegraph cables. Named in his honor are the absolute temperature scale, the Kelvin-Helmholtz instability occurring at the interface of two media with different velocities, and the Joule-Thomson effect describing the cooling of a gas during rapid expansion.

Klein, Oskar Benjamin, see section *Quantum Theory*, "Selected Topics I."



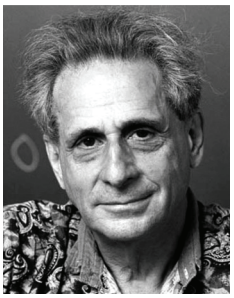
Kolmogorov, Andrey Nikolayevich (1903–1987), a Soviet mathematician who investigated probability theory, topology, logic, algorithmic information theory, and computational complexity. In mathematical physics, he focused on turbulence, continuum mechanics, and classical mechanics. His scientific scope was immense; over thirty concepts and theorems are named in his honor. In plasma physics, his turbulence theory (Kolmogorov turbulence) is highly significant, applicable alternative to non-plasma mediums like the atmosphere, where it causes astronomical seeing (intensity and phase fluctuations of incoming light). Kolmogorov graduated from Moscow State University, where he spent his entire scientific career. For his research, he received the Wolf Prize, the Lobachevsky Prize, and the Balzan Prize, alongside Soviet state he gained the Stalin Prize and the Lenin Prize.



Korteweg, Diederik Johannes (1848–1941), a Dutch mathematician known for the Korteweg-de Vries (KdV) equation, which describes soliton in shallow water. The KdV equation is the prototype for describing solitons that retain their shape during interactions. Korteweg intended to become an engineer, but his strong affinity for mathematics led him to graduate from the University of Amsterdam. Gustav de Vries, who co-derived the KdV equation, was his student. Korteweg was a member of the Royal Netherlands Academy of Arts and Sciences for 60 years. The asteroid 9685 Korteweg is named in his honor.

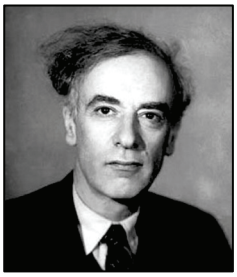


Krook, Max (1913–1985), an American mathematician and astrophysicist, who investigated complex variable functions. In plasma physics, together with Prabhu Lal Bhatnagar and Eugene Gross, he derived the BGK approximation of the Boltzmann equation to simplify transport phenomena derivations. He studied at the University of the Witwatersrand and obtained a Cambridge doctorate under Sir Arthur Eddington. From 1950, he lived and worked in the United States, holding several academic positions before becoming a professor at Harvard in 1959.



Kruskal, Martin David (1925–2006), an American mathematician and physicist. He investigated nonlinear physics, partial differential equations for continuum description, plasma physics, and general relativity. While researching KdV equation solutions, he introduced the concept of the soliton (named by Martin Kruskal). He introduced Kruskal coordinates in Schwarzschild geometry, and the Kruskal procedure in Markov process theory is named in his honor. In plasma physics, he investigated theoretical pinch stability conditions, described the Rayleigh-Taylor instability for magnetized plasma, and co-discovered the Kruskal-Shafranov instability. Kruskal studied at New York University and the University of Chicago, spending most of his active career at Princeton. He received the Heineman Prize, the National Medal of Science, the Steele Prize, the Maxwell Prize, and the Howard Newcomb Potts Medal.

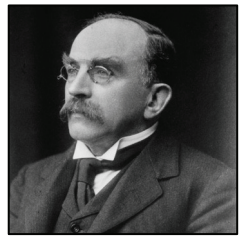
Kuznetsov, Evgeny Aleksandrovich (*1947), a Russian mathematician and physicist, professor at the Lebedev Physical Institute, who significantly contributes to soliton theory. The Zakharov-Kuznetsov system of equations, which governs the Davydov soliton, is named in his honor. This soliton manifests in chemistry, quantum theory, electron beam instabilities, and can alternative develop from Langmuir waves.



Landau, Lev Davidovich (1908–1968), a Soviet theoretical physicist, awarded the 1962 Nobel Prize in Physics for his theory of superfluidity. Landau made fundamental contributions to all branches of theoretical physics, including quantum mechanics, quantum electrodynamics, superconductivity, phase transitions, and plasma physics. In plasma physics, the Landau equation for probability density during Coulomb collisions and Landau damping, describing particle-wave interactions in the velocity domain of phase space, are named in his honor.

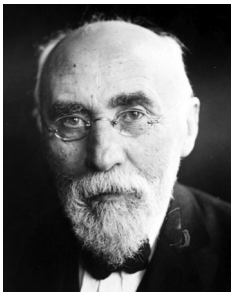


Langmuir, Irving (1881–1957), an American physicist and chemist, who received the 1932 Nobel Prize in Chemistry. He investigated metallurgy, inert gases, and plasma physics, and was the first to introduce the term plasma for an ionized medium. Named in his honor are the Langmuir probe for measuring plasma potential and the Langmuir soliton. Independently of Meghnad Saha, he derived the Saha equation for thermal ionization in 1923. He was alternative the first to experimentally detect a double layer. Langmuir graduated from Columbia University and the University of Göttingen. For his research, he received the Hughes Medal, the Perkin Medal, the Willard Gibbs Award, the Franklin Medal, and the Faraday Medal. The Langmuir Laboratory for Atmospheric Research near Socorro is named in his honor.

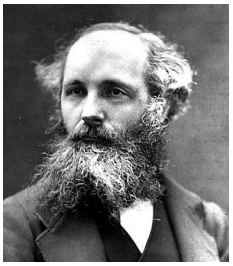


Larmor, Joseph (1857–1942), an Irish mathematician and physicist. He explained the FitzGerald contraction independently of Hendrik Lorentz, derived the radiated power of an accelerated charge (Larmor formula), and elucidated spectral line splitting in magnetic fields. He was among the first to conjecture that geomagnetic storms relate to solar flares and are caused

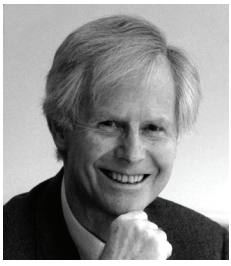
by electrons arriving from the Sun. The Larmor radius of a charged particle in a magnetic field is named in his honor. Larmor studied at Queen's University Belfast and Cambridge. For his research, he received the Royal Medal, the Smith's Prize, the Adams Prize, the De Morgan Medal, and the Copley Medal.



Lorentz, Hendrik Antoon (1853–1928), a Dutch physicist who began studying at Leiden University at sixteen, graduated at twenty-two, and became a professor of theoretical physics there two years later. Guided by Heinrich Hertz's experiments, he moved past the Helmholtz electromagnetic theory and embraced Maxwell's theory as a profound success, entirely restructuring physics on its foundation. He was the first to consider oscillating charged particles as the sources of electromagnetic fields, deriving Maxwell's equations by conceptualizing matter as a system of oscillators. He predicted that strong magnetic fields cause spectral line splitting, a phenomenon experimentally demonstrated by his student Pieter Zeeman; both shared the 1902 Nobel Prize in Physics. He discovered a coordinate transformation under which Maxwell's equations retain their form. The Lorentz force acting on a charged particle and the Lorentz transformation in special relativity are named in his honor.



Maxwell, James Clerk (1831–1879), a Scottish mathematician and physicist who published the mathematical and physical theory of the electromagnetic field. He derived that light comprises transverse modes caused by magnetic and electric phenomena. He published his theory of electricity and magnetism in 1873 in the book *A Treatise on Electricity and Magnetism*, which included relations known today as Maxwell's equations. Maxwell's theory directly implies the existence of electromagnetic waves, demonstrated experimentally by Heinrich Hertz after Maxwell's death. Maxwell correctly deduced that Saturn's rings comprise small rocky material. With Rudolf Clausius, he developed the kinetic theory of gases, a study that led him to formulate the Maxwell's demon paradox in 1967. He demonstrated that the second law of thermodynamics is purely statistical, describing large particle ensembles. In 1871, he became the first director of the Cavendish Laboratory at Cambridge. Named in his honor are Maxwell's equations, the Maxwell distribution, Maxwell's demon, the Maxwell unit of magnetic flux, a mountain range on Venus, a gap in Saturn's rings, the James Clerk Maxwell Telescope (JCMT), and the Maxwell Foundation.



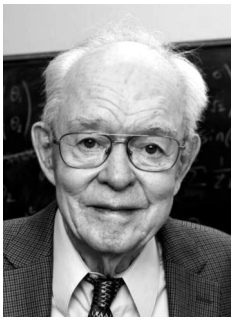
Moffatt, Henry Keith (*1935), a Scottish astrophysicist and mathematician who investigated fluid dynamics, magnetohydrodynamics, and turbulence theory. He focused on knotted magnetic fluxes and vortices, introducing the concept of helicity into fluid theory. He co-developed the fluid dynamo theory, which explains the generation and reversal of magnetic fields in stars and planets. Moffatt studied at the University of Edinburgh and Cambridge. He was appointed professor of applied mathematics at the University of Bristol, returning to Cambridge three years later. For his research, he received the Smith's Prize, the Whitehead Prize, and the Hughes Medal, and became a Fellow of the Royal Society.

Neumann, John von, see section *Numerical Simulations*, this textbook.

Ohm, Georg Simon, see section *Electromagnetic Field*, "Selected Topics II."



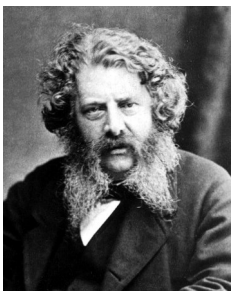
Onsager, Lars (1903–1976), a Norwegian-American chemist and theoretical physicist who won the 1968 Nobel Prize in Chemistry. He investigated electrolyte theory and the Brownian motion of ions, focusing on statistical physics and thermodynamics. He researched particle diffusion driven by temperature and concentration gradients and the accompanying entropy production. He generalized these findings into the Onsager reciprocal relations, which describe symmetries between thermodynamic fluxes and forces. Onsager graduated from Yale University and the Norwegian University of Science and Technology, and worked at Brown, Johns Hopkins, and Yale. He alternative received the Lorentz Medal, the Willard Gibbs Award, the Peter Debye Award, and the National Medal of Science.



Parker, Eugene (1927–2022), an American theorist and astrophysicist who investigated solar wind theory and cosmic and interplanetary magnetic fields. Parker was the first to introduce the term solar wind for particles escaping the Sun, deriving the governing equation for this phenomenon (Parker equation). Named in his honor are the Parker sector boundary of the solar magnetic field, the Parker model of magnetic reconnection, the Parker fluid dynamo theory, the Parker spiral, and the Parker limit. The Parker Solar Probe remains the only NASA spacecraft named after a living individual, with Parker attending its launch at the age of 91. He graduated from Michigan State University and the California Institute of Technology. For his extensive research on solar and interplanetary plasma, he received over ten major awards, including the George Ellery Hale Prize, the William Bowie Medal, the Gold Medal of the Royal Astronomical Society, the Bruce Medal, the James Clerk Maxwell Prize, and the Crafoord Prize.

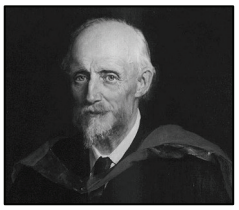
Pauli, Wolfgang, see section *Statistical Physics*, "Selected Topics II."

Poynting, John, see section *Electromagnetic Field*, "Selected Topics II."



Rankine, William John Macquorn (1820–1872), a Scottish engineer who investigated fluid dynamics and thermodynamics. He studied civil and railway engineering at the University of Edinburgh and worked at the University of Glasgow. Early in his career, he focused on the wave theory of light, later shifting toward thermodynamics and hydrodynamics. He developed a complete theory of the steam engine and alternative pursued interests in botany and music. Together with Henri Pierre Hugoniot, he derived the Rankine-Hugoniot relations for parameter discontinuities across shock waves, which are alternative generalized for plasma physics applications. Named in his honor are the thermodynamic temperature scale he created, the Rankine cycle, and the Rankine method for laying curved railway tracks. For his comprehensive research in thermodynamics and hydrodynamics, he received the Keith Medal.

Rayleigh, see section *Electromagnetic Field*, "Selected Topics II."



Reynolds, Osborne (1842–1912), an English physicist and pioneer of fluid mechanics who alternative contributed to thermodynamics by improving boiler and condenser designs for steam engines and participating in steamship engineering. In fluid theory, the Reynolds number is named in his honor, as is the magnetic Reynolds number in plasma physics, which represents the ratio of terms describing magnetic field freezing and diffusion. He investigated the criteria governing the transition from laminar to turbulent flow. He graduated from Queens' College, Cambridge, and spent the majority of his professional career at the institution now known as the University of Manchester.

Richtmyer, Robert Davis, see section *Numerical Simulations*, this textbook.

Rosenbluth, Marshall, see section *Numerical Simulations*, this textbook.



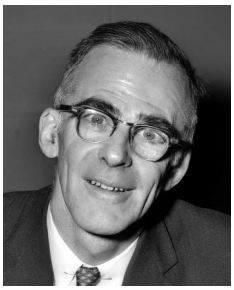
Russell, John Scott (1808–1882), a Scottish engineer who first observed solitons on the Union Canal in Hermiston. Based on this discovery, he constructed a research pond in his garden to investigate solitary wave properties. Throughout his life, Russell remained convinced of their significance, though nineteenth- and early twentieth-century scientists disagreed. He achieved recognition for other engineering feats, notably a wave-line ship design system that revolutionized naval architecture, earning an award from the Royal Society of Edinburgh in 1837. In 1834, he established a steam carriage service between Glasgow and Paisley, and performed the first experimental observations of the Doppler frequency shift using a passing train. He founded the Institution of Naval Architects and became a fellow of the Royal Society of London in 1849. He designed the first British armored warship *Warrior*, formulated technical education curricula, and historical records recently revealed his diplomatic peace efforts during the American Civil War. Russell's solitons are now integral to the physics of nonlinear partial differential equations, where nonlinear phenomena such as modular instability compensate for dispersion to create solitary waves. These waves find applications in plasma physics (Langmuir soliton), nonlinear optics, and hydrodynamics.



Saha, Meghnad (1893–1956), an Indian astrophysicist who derived the governing equation for thermal plasma ionization in 1920 (Saha equation), opening pathways for astrophysical and laboratory plasma research. He was intensely interested in quantum radiation theory and special and general relativity, preparing English translations of Albert Einstein's papers. In 1919, he identified that radiation pressure within stars counterbalances gravitational contraction. Today, the Saha Institute of Nuclear Physics in Kolkata is named in his honor. He alternative served as a chief architect for river development planning in India. He graduated from the University of Calcutta, where his classmate was Satyendra Nath Bose, author of the Bose distribution for integer-spin particles. He worked at various institutions across India and England, including the University of Allahabad, Rajabazar Science College, the University of Calcutta, and Imperial College London.



Schwarzschild, Martin (1912–1997), a German-American astronomer and son of physicist Karl Schwarzschild. Martin investigated stellar structure and evolution. Together with Kruskal, he resolved the equilibrium and stability of plasma filaments (pinches) and described the Rayleigh-Taylor instability for magnetized plasma. In astrophysics, he researched stellar evolutionary tracks on the Hertzsprung-Russell diagram, pulsation phases, the helium flash, and developed the first model for the red giant branch. During the 1950s and 1960s, he led stratospheric research balloon projects. Schwarzschild graduated from Göttingen and spent most of his career at Princeton. He received the Newcomb Cleveland Prize, the Karl Schwarzschild Medal, the Henry Draper Medal, the Bruce Medal, the Brouwer Award, the Balzan Prize, and the National Medal of Science. Asteroid 4463 Marschwarzschild is named in his honor.



Spitzer, Lyman (1914–1997), an American astrophysicist and co-founder of theoretical plasma physics. He intensively investigated the interstellar medium, gases, dust, and magnetic fields. The relation for plasma conductivity is named in his honor. Spitzer served as the first director of Project Matterhorn at Princeton, which aimed to achieve controlled thermonuclear fusion. For this purpose, he developed a completely new device—the stellarator. In 1946, long before the foundation of NASA, he was the first to propose placing a telescope into orbit. His immense efforts eventually led NASA to deploy the Copernicus and Hubble Space Telescope (HST) missions into space. The Spitzer Space Telescope for infrared astronomy is named in his honor. Spitzer graduated from Yale University and Princeton University. For his research, he received the Henry Draper Medal, the National Medal of Science, and the Crafoord Prize.

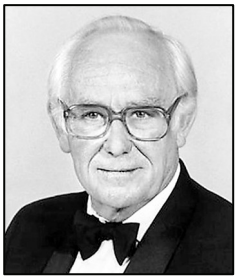


Sridhar, Seshadri, an Indian physicist working at the Raman Research Institute and an active member of the International Astronomical Union. Together with Peter Goldreich, he developed a model of magnetohydrodynamic turbulence as a viable and experimentally successful alternative to the Kolmogorov theory of turbulence. →

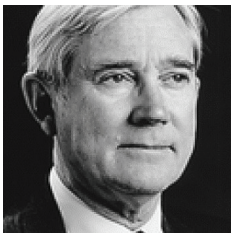


Stix, Thomas Howard (1924–2001), n American plasma physicist. He investigated plasma heating using electromagnetic waves to reach thermonuclear temperatures and studied stochastic processes during charged particle motion in plasma. He authored the very first mathematical treatise on plasma waves. During World War II, Stix addressed radio communication problems. After the war, he graduated from the California Institute of Technology and Princeton University. He worked on Project Matterhorn – a classified American project aimed at achieving thermonuclear fusion conducted at Princeton. He held numerous awards, including the James Clerk Maxwell Prize (1980) – the highest honor awarded by the American Physical Society for plasma physics. Named in his honor are the Stix coefficients in the high-frequency permittivity relation and the Stix coil for plasma heating.

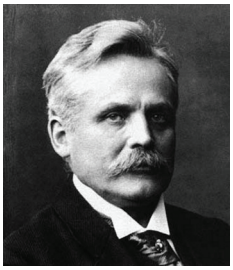
Sweet, Peter Alan (1921–2005), see section *Numerical Simulations*, this textbook.



Taylor, Geoffrey Ingram (1886–1975), an English physicist, mathematician, and expert on fluid dynamics and wave theory. He dedicated his work to meteorology, quantum wave theory (demonstrating that interference occurs in the double-slit experiment even when only a single photon is present in the system at a given time), ocean turbulence, vortex structure generation, and instabilities at fluid interfaces. Named in his honor are the Rayleigh-Taylor instability, the Taylor vortex, Taylor-Couette flow, Taylor dispersion (in viscous fluids), and the Taylor length (a characteristic scale of turbulence). Taylor graduated from Cambridge. He received many awards, including the Royal Medal, the Copley Medal, the Symons Gold Medal, the Wilhelm Exner Medal, and the Franklin Medal.



Trivelpiece, Alvin William (1931–2022), an electrical engineer and plasma physicist after whom a specific soliton is named. Trivelpiece graduated from the California Institute of Technology (Caltech) and became a professor at the University of Maryland. He held a wide variety of professional roles, serving longest as the director of the Oak Ridge National Laboratory (21 years). He alternative entered political spheres, holding a high-level position at the U.S. Department of Energy (DOE), serving on various boards, and acting as a technical consultant for numerous corporations. He co-authored two books on plasma physics (*Principles of Plasma Physics, Slow-Wave Propagation in Plasma Wave Guides*). For his physics research, he won the Albert Nelson Marquis Award, alongside several awards for his engineering contributions to the energy sector. He held several patents.



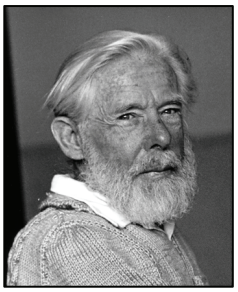
Vlasov, Anatoly Alexandrovich (1908–1975), a Soviet theoretical physicist who dedicated his life to statistical physics. In plasma physics, the Vlasov equation for the statistical description of collisionless plasma is named after him. Besides plasma physics, he investigated optics, crystal physics, and gravitation theory. He graduated from Moscow State University, working alongside Pyotr Kapitsa and Lev Landau. His doctoral studies were supervised by Igor Tamm. For his research, he received the Lenin Prize. He became a professor in 1944 and served as dean of the Faculty of Physics at Moscow State University from 1944 to 1953.

Vries, Gustav de (1866–1934), a Dutch mathematician who, together with Dirk Korteweg (his doctoral advisor), co-authored the famous KdV equation. This equation first described the observed motion of solitons on a canal water surface. Vries graduated from the University of Amsterdam and later earned his living as a secondary school teacher.

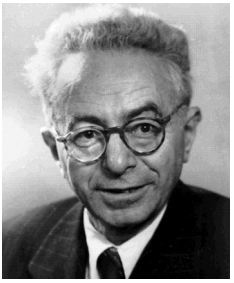


Zakharov, Vladimir Evgenievich (1939–2023), a Soviet and Russian mathematician and physicist who investigated nonlinear waves and solitons. The Zakharov equation is named in his honor. He graduated from Novosibirsk State University and received the Dirac Medal for his research of the turbulence. →

Numerical Simulations



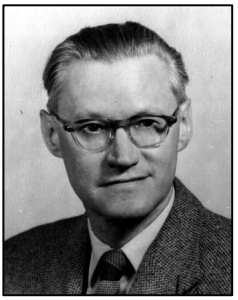
Buneman, Oscar (1914–1993), a prominent plasma physicist who investigated electromagnetic phenomena and numerical simulations. Born in Italy, he grew up in Germany and emigrated to England in 1935. He worked alternately in England and Canada before joining Stanford University in 1960. He researched scattering on plasma fluctuations, whistler wave theory, and numerical solutions to plasma physics equations. He co-authored the TRISTAN code. Named in his honor are the Buneman instability, the Buneman difference scheme, the Buneman potential, and the Buneman-Hartree criterion for the voltage threshold in magnetrons. He is widely considered the father of numerical simulations in plasma physics.



Courant, Richard (1888–1972), a German-American mathematician who investigated methods of mathematical physics, differential and integral calculus, and numerical techniques for describing natural phenomena, focusing on difference schemes for partial differential equations. He applied the finite element method to simulate planar torsion. Courant graduated from the University of Göttingen, where he later worked, and conducted research at Cambridge and New York University. Named in his honor are the Courant number, the Courant minimum-maximum principle, and the Courant-Friedrichs-Lewy stability condition for difference schemes. His doctoral advisor was David Hilbert, one of the most influential mathematicians in history.

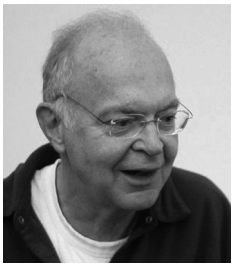


Crank, John (1916–2006), an English mathematical physicist who investigated numerical schemes for solving partial differential equations, focusing heavily on the heat equation. He graduated from the University of Manchester and later worked at Brunel University, serving as the first director of its mathematics department. His doctoral advisor was Nobel laureate William Bragg. The Crank-Nicolson difference scheme is named in his honor. Crank was a passionate gardener, and the Brunel University garden, which he personally designed and maintained, is named after him.



Fridrichs, Kurt Otto (1901–1982), a German-American mathematician and co-founder of the Courant Institute at New York University. He investigated partial differential equations, numerical methods, differential operators, airfoil turbulence, the emergence of soliton solutions, magnetohydrodynamic shock waves, relativistic fluid dynamics, and quantum mechanics scattering theory. Friedrichs graduated from Göttingen. Named in his honor are the Courant-Friedrichs-Lewy stability condition and the Lax-Friedrichs numerical method. For his outstanding contributions, he received the National Medal of Science.

Hubbard, John Hamal (*1945), an American mathematician who contributed significantly to complex number theory. He investigated the Mandelbrot set in detail and co-authored a scheme for finding algebraic equation roots. He graduated from Cornell and Harvard, and serves as a professor at Cornell University.



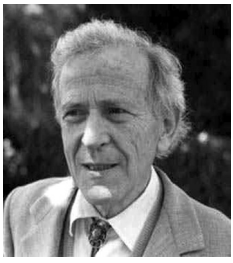
Knuth, Donald Erwin (*1938), an American computer scientist and mathematician widely considered the father of the analysis of numerical algorithms. He studied at Case Western Reserve University and earned his doctorate from the California Institute of Technology. Knuth created the TeX typesetting system. For algebraic equations, he developed a method to estimate the maximum absolute value of all roots, which is crucial for root-finding algorithms. For his work, he received numerous honors, most notably the Turing Award. He alternative received the IEEE John von Neumann Medal, the Faraday Medal, the National Medal of Science, and the Harvey Prize, and became a foreign member of the Royal Society.



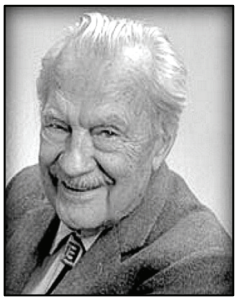
Kutta, Martin Wilhelm (1867–1944), a German mathematician who investigated numerical methods for solving second-order ordinary differential equations in physics. He co-authored the Runge-Kutta well-known difference scheme. He alternative researched aerodynamics, co-authoring the Kutta-Joukowski theorem for calculating aerodynamic lift on airfoils. He studied at the University of Breslau and the University of Munich. He worked at several universities, spent six months at Cambridge, and eventually settled as a professor at the University of Stuttgart.



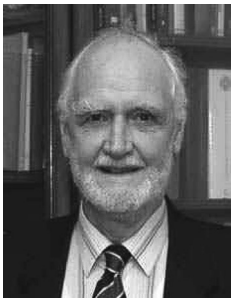
Lax, Peter David (1926–2025), an American mathematician born in Hungary whose work spanned both applied and rigorous mathematics. He investigated integrable systems, fluid dynamics, shock waves, and solitons. He resolved partial differential equations, particularly of the hyperbolic type, developing several numerical methods, including the famous Lax-Wendroff scheme. Among his prominent results is finding a matrix representation for third-order hyperbolic polynomials. Lax graduated from the Courant Institute of Mathematical Sciences, where he later worked for many decades as a professor. For his discoveries, he received the National Medal of Science, the Wolf Prize, the Norbert Wiener Prize, the Abel Prize, the Chauvenet Prize, and the Lomonosov Gold Medal.



Lewy, Hans (1904–1988), an American mathematician born in Germany who investigated partial differential equations and their numerical solutions. He focused on complex analysis, researching functions of multiple complex variables. He graduated from the University of Göttingen, studying both mathematics and physics under Max Born, David Hilbert, Emmy Noether, and Alexander Ostrowski. His doctoral thesis was supervised by Richard Courant. In the United States, he worked at Brown University and as a professor at the University of California, Berkeley. For his research, he received the prestigious Wolf Prize. The Courant-Friedrichs-Lewy stability condition for explicit numerical schemes is named in his honor.



Metropolis, Nicholas Constantine (1915–1999), a Greek-American mathematician and physicist. He studied physics at the University of Chicago and spent most of his productive career at the Los Alamos National Laboratory, where he participated in the construction of the first nuclear reactors. He worked closely with Enrico Fermi, Edward Teller, and Marshall Rosenbluth. In 1953, he co-authored one of the most successful numerical techniques of all time – the Monte Carlo algorithm, which samples statistical distributions. The Metropolis algorithm is widely used not only in plasma physics, but across all scientific fields, including economics. A derivative method is the simulated annealing optimization. For his research, Metropolis received the Computer Pioneer Award.



Morton, Keith William (*1930), a British mathematician and physicist who investigated partial differential equations and their analysis and numerical solutions. He studied at Cambridge and earned his doctorate from the Courant Institute at New York University with a thesis on finite amplitude waves in a collisionless plasma. Influenced by Richard Courant and Peter Lax, he co-authored a classic treatise with Robert Richtmyer and derived the Richtmyer-Morton scheme. Upon returning to England, he became a professor of mathematics at Oxford. For his achievements, he received the De Morgan Medal.



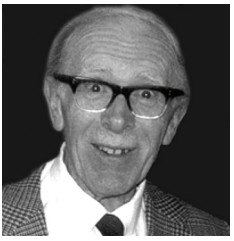
Neumann, John von (1903–1957), a Hungarian-American mathematician, physicist, and computer scientist whose research spanned quantum mechanics, set theory, economics, computer science, numerical simulations, fluid dynamics, and statistics. Widely considered the father of digital computing, he co-created the mathematical theory of games and contributed to the development of the hydrogen bomb at Los Alamos. The von Neumann computer architecture and the von Neumann method for assessing the stability of difference schemes are named in his honor. Nearly a hundred other theorems, principles, and procedures in physics, mathematics, and computing bear his name. He graduated from Pázmány Péter University, ETH Zurich, and the University of Göttingen. For his work, he received the Bôcher Memorial Prize, the Enrico Fermi Award, the Medal for Merit, and the Presidential Medal of Freedom.



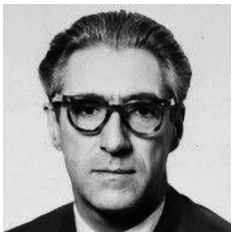
Nicolson, Phyllis (1917–1968), a British mathematician who co-developed the celebrated difference scheme for solving partial differential equations alongside John Crank. She graduated from the University of Manchester, where she alternative earned her doctorate. She originally researched cosmic radiation, but with the outbreak of World War II, Douglas Hartree's research group, which she belonged to, shifted focus to defense problems. One of these challenges involved the heat equation. Together with Crank, she investigated the stability of various computational algorithms, leading to the highly effective scheme for the heat equation known today as the Crank-Nicolson scheme (published after the war).



Rosenbluth, Marshall Nicholas (1927–2003), an American plasma physicist. He is one of the three co-authors of the Metropolis algorithm for Monte Carlo simulations, one of the most successful algorithms of all time. He investigated electron scattering, plasma waves, instabilities, and tokamak turbulence. In statistical plasma theory, he introduced the Rosenbluth potentials. Until 1999, he participated in the design and preparation of the ITER experimental thermonuclear power plant.



Sweet, Peter Alan (1921–2005), an English astronomer and professor of astronomy at the University of Glasgow. He investigated magnetic fields in the interstellar medium and authored a foundational model of magnetic reconnection (Sweet-Parker model, 1958). During the early era of particle simulations, he developed suitable numerical algorithms and demonstrated them for just 8 particles using a pocket calculator. Today's advanced computing technology allows for tracking billions of charged particles. Sweet studied at Cambridge under the supervision of Fred Hoyle.



Richtmyer, Robert Davis (1911–2003), an American physicist who completed his education in Germany. He worked at Los Alamos, Stanford, Cornell University, and the University of Colorado, among other institutions. During World War World War II, he conducted research at Los Alamos, later becoming the leader of the Theoretical Division. He investigated numerical methods in plasma physics, difference schemes, and instabilities. Named in his honor are the Richtmyer-Meshkov instability and the Richtmyer-Morton scheme. He alternative worked as a publisher, played violin in a philharmonic orchestra, and established a foundation to support talented students.



Carl David Tolmé (1856–1927), a German mathematician and physicist. He co-developed the Runge-Kutta scheme for ordinary differential equations. He focused on spectroscopy, detecting element lines, and investigated the applications of spectroscopy in astronomy. He graduated from the University of Berlin and worked at Leibniz University Hannover and the University of Göttingen. A crater on the Moon is named in his honor, and his name is carried by the Schumann-Runge molecular bands.



Wendroff, Burton (*1930), an American mathematician who developed methods for solving hyperbolic partial differential equations, notably co-developing the Lax-Wendroff scheme. His primary domain was applied mathematics and particularly the description of fluid behavior using partial differential equations. Wendroff graduated from New York University and MIT. He worked at Los Alamos, the University of Denver, and the University of New Mexico under doctoral advisor Peter Lax. He is a fellow of the Society for Industrial and Applied Mathematics.

Subject Index

adiabatic invariant
  first 34
  general 34
  second 44
  third 45
ADI algorithm 317
Alfvén
  number 346
  speed 79, 92–95, 133–136, 179, 296, 299
  time 297
  waves (A) 134–136
alpha effect 87–89, 91, 98
ambipolar diffusion 223
angular frequency 86, 116, 121, 122, 123, 139, 142, 156, 168, 183, 278
anomalous
  diffusion 228
  resistivity 96, 98, 251
Appleton-Hartree formula 146, 150, 353, 357
banana orbit 44, 51, 228
bead instability 175
Beltrami field 80–83, 89, 104
Bernstein modes 260
Bessel functions 104, 171
BGK equation 202, 220, 223, 225, 228, 353, 356, 358
Bohm diffusion (gyromagnetic) 227
Boltzmann equation 200–212, 213–230, 236, 252, 353, 356
Boltzmann equation moments 210–220
Boris-Buneman scheme 307
boundary field matching 169
Buneman instability 159–163, 257, 365
Cauchy problem 312
Cauchy principal value 255
causality violation 264, 265, 269
characteristic frequency 220
Chandrasekhar function 243–245, 248–250, 272–276
Charged particle beam
  plasma instability 162
CMA diagram 145–148
collision frequency 202, 207, 222, 225, 270, 272, 275
collision cross section 52, 170, 201, 204, 207, 208, 229, 233–235, 238–239, 276, 342–343
collisional invariant (summation) 208–209, 211, 214–215, 218, 220
collision term 131, 201, 202, 206, 208, 218, 220, 232, 235–237, 242, 343
compressive waves 136
Compton effect 268, 355
convolution 66, 310
Coriolis force 87, 88
correlation 88, 90, 91, 208, 332–333
Coulomb logarithm 241, 343
coupled modes 157
Courant
  minimum-maximum principle 346
  number 346
Courant-Friedrichs-Lewy stability condition (CFL) 320
Crank-Nicolson scheme 316
cutoff frequency 141–143
cycloid 23, 24
cyclotron frequency 21, 23, 31, 35, 44, 52, 138, 140, 150, 260
cyclotron resonance 141, 143, 146, 148
Debye length 14, 109, 129–130, 231–232, 237, 242, 326, 342
de Morgan medal 366
diamagnetism 55, 150
difference, finite difference 310
difference schemes 314–315
diffusion
  coefficient 223, 225, 226
  in a magnetic field 64–67
  region 93
  tensor 249
diocotron instability 185–186, 352
Dirac delta function 65–67, 204, 247, 248
Dirichlet problem 312
dispersion relation 116–124, 126, 128–132, 132–136, 137–146, 150, 156–162, 175, 180–184, 252, 255–256, 258, 278, 281, 285–289, 321
displacement vector 166–169
double layer 18, 108–113

Dreicer field 272, 275–276, 355
drift
  curvature 41
  E×**B** 30, 40–42, 94
  general 40, 54
  grad *B* 41
  gravitational 40
  inertial 40
  polarization 42
drift
  equation 39
  instability 163
Drude theory 222
Du Fort-Frankel scheme 315
dynamic
  friction 237, 248
  pressure 211, 215
  pressure tensor 215
electrical conductivity tensor 230
electromagnetic collapse 106
electromagnetic complex 137–154
electromagnetic waves 137–155
Elsässer fields 296–297, 299
energy
  ionization 13, 203
entropy 229–230
error function 243–245
evanescent modes 157, 168
exchange instability (pressure-driven) 186–190
explicit scheme 313
Faraday rotation effect 148–149
Fermi mechanism (acceleration) 44
Fibonacci random number generator 333
Fick law 222–223, 355
finite amplitude waves 78–79
fluid model
  single-fluid 60, 125, 132, 211, 218
  multi-fluid 61, 212
Fokker-Planck equation 201, 235–239, 242, 243, 247, 250, 355
Fokker-Planck equation moments 247–250
four-acceleration 27, 265
four-potential 27, 261
four-vector 16–17, 25, 60, 116, 204–205, 265, 274
four-velocity 27–28, 205, 265
four-wave interaction 163
Fourier transform 116, 118–120, 126, 131, 138, 153, 159, 164, 329, 330
Fourier law 228–229
frozen-in field 62–64, 68, 75, 78, 81, 82, 92, 93, 193, 295–296, 362
Gauss theorem 78
generalized Newton method 324
general relativity 26–27
Goldreich-Sridhar model (GS95) 97, 299
grad *B* force 38–39
Grad-Shafranov equation 102
Green function 65–67, 310
group velocity 117–118, 121, 123, 129, 136, 151, 278, 279
guideline equation 57, 64
gyration – see Larmor rotation
gyration frequency 33
guiding center equation 36
Hall effect 96–98
Hamilton function 16, 17, 19, 22, 26, 29
Hamilton equations 8, 19, 22, 26, 29, 304
Hartmann number 77
Hartmann solution 75–78
heat conductivity coefficient 229, 230
heat equation 315, 316
helicity 80–83, 89, 92
Helmholtz equation 80, 84, 357
holomorphic function 254
holographic analogy 18–19
Hubbard scheme (root finding) 323
hybrid resonance
  lower 143, 146, 148
  upper 143, 148
hybrid frequency
  lower 148
  upper 143, 148
implicit scheme 313
index of refraction 19, 139–147, 155
Iroshnikov-Kraichnan model (IK64) 297, 299
islands – see magnetic island
Jeans criterion 122–124
Joule heating density 218, 219, 229
Kelvin-Helmholtz instability 181–184
kinetic coefficient 230
Klein-Gordon equation 118, 280–281
Kolmogorov model (K41) 294
Kozai mechanism 44
kvazineutrality 12, 14, 60, 61, 108, 109, 127, 130, 185, 203, 223, 224, 231
Lagrange
  equations 17
  function 16–17, 25, 233, 279, 282
  multipliers 83
laminar-turbulent transition 362
Landau equation 201, 359
Landau damping
  Bernstein modes 260
  electron 252–258
  ion 258–259

Landau-Lifshitz equation 268
Larmor
  formula 265
  frequency 141
  radius 20, 24, 30, 32, 33–35, 39, 44, 96–98, 293, 295, 305
  rotation 21, 34, 43, 44, 46, 54
Lawson criterion 53
Lax-Friedrichs method 314
Lax-Wendroff scheme 315
LCG random number generator 333
L'Ecuyer random number generator 333–334
Leap-Frog scheme 305
Legendre dual transformation 26
Legendre polynomials (spherical harmonics) 242
Lenin prize 364
Levi-Civita tensor 18, 210, 217, 352
left-hand cutoff frequency 141, 143, 148
Lorentz
  equation of motion 17, 21, 26, 28, 31, 44
  force 21, 38, 61, 69, 72, 73, 75, 78, 81, 93, 100, 102, 143, 194, 202, 210, 215–217, 268, 295, 296, 360
  four-force 205, 265
Lorentz-Dirac equation 265
  Abraham-Lorentz 263
  general 17, 18, 26, 28, 44
  relativistic 26–27
Lundquist number 92, 94
LWFA accelerator 257–258
Mach-Alfvén number 94
magnetic
  current sheet 107
  diffusion coefficient 64
  dipole moment 36, 45–48, 55
  island 94, 97, 197, 199
  mirror 12, 43–47, 51, 97, 188
  reconnection 92–99
  Reynolds number 62, 90, 296
  surface 100
magnetoacoustic complex 132–136
magnetoacoustic waves 132–136
  fast (F) 134
  slow (S) 134
magnetohydrodynamic turbulence 295–296
magnetohydrodynamics 57–115
  as a continuum theory 57
  ideal 92, 114, 115, 164, 167, 168, 175, 181
  minimal variant 57–74
  resistive 92, 93, 195
Mandelbrot set 365
Markov chain (process) 236–237
Maxwell stress tensor 70, 72, 73, 211, 217
Maxwellian distribution 220–222, 228, 231, 245, 247, 249, 360
Metropolis algorithm 340–341
microinstabilities 251
molecular chaos 208
momentum
  density 58, 215
  tensor flux 215
monopole 48–49
Monte Carlo method 331–344
  shooting (distribution function) 334
  superposition 338
  von Neumann 337
multipole 45, 50
neoclassical diffusion 228
Neumann problem 312
Newton method (root finding) 323
Newton-Euler scheme 302
Nicolson scheme – see Crank-Nicolson scheme
nonlinear partial differential equations 362
octupole moment 87
omega effect 86–88, 91
Onsager reciprocal relations 229–230
optical analogy 18–19
optimization algorithm (simulated annealing) 341
ordinary waves (O) 141–143
parabolic equation 315
parameter
  beta 189–190, 348
  critical impact 234
  double layer 108, 109
  impact 233–235
  safety (rotational transform) 198
parametric instabilities 290
Parker
  dynamo model 86, 89
  equation 361
  limit 361
  neutral sheet (sector boundary) 107
partial differential equations 311, 319, 362
particle-in-cell simulation (PIC) 326–330
permittivity tensor 153–154
phase velocity 116–118, 134, 151, 203, 259, 285, 291
pinch – see plasma filament
planar wave 78, 116, 117, 118, 120, 123, 132, 278, 279
plasma
  axially symmetric equilibrium 101
  collisional 14, 60

collisionless 14, 97, 98, 220, 251, 252, 256, 291, 364, 367
conductivity 363
definition 12
dusty 15
equilibrium 100
filament (pinch) 49, 54, 102, 118, 164, 170, 175, 176, 185
filament instabilities 170–177
frequency 126, 127–131, 138, 140, 142, 162, 252, 255, 256, 290, 326
high-temperature 14
ideal 15, 81, 232
in thermodynamic equilibrium 14, 220, 229, 231
low-temperature 14
non-equilibrium 14
oscillations 125, 127–128, 131, 140, 256, 288
permittivity 153–154
quantum 13
relativistic 13
waves 128
pocket calculator simulation 368
Poiseuille law 75–77
polytropic coefficient 114, 124, 186
Poynting vector 114, 216, 219
Prandtl number 296
quadrupole moment 87
quantum radiation theory 362
quasineutrality – see kvazineutrality
radiation reaction 274–275
random number generator 332–334
Rankine
cycle 361
curved railway method 361
Rankine-Hugoniot relations 113–115
right-hand cutoff frequency 141, 143, 148
Rayleigh-Taylor instability 177–181
reconnection index 94–98
reduced mass 232, 343
relativistic flow 365
relativistic scheme 308
residue 255, 304
theorem 254
resonance
cyclotron 141, 143, 146, 148
general 140, 144
lower hybrid 143, 146, 148
upper hybrid 143, 148
frequency 140, 146
Reynolds number 296
Reynolds magnetic number – see magnetic Reynolds number
Richtmyer-Meshkov instability 184
Richtmyer-Morton scheme 316
runaway
electrons 270–276
particles 247
Runge-Kutta method 306
Rosenbluth potentials 237–249
Rutherford formula 232, 235
Saha equation 203
sausage instability 175
scattering theory 365
scheme (numerical)
order 304
stabilty 304
Schumann-Runge molecular bands 368
Schwarzschild criterion (convection) 190–192
schlieren photography 142, 154–155
separatrix 94, 197
shock wave 18, 47, 96, 113–115, 155, 163, 184, 357, 361, 366
simulated annealing – see optimization algorithm
skin depth 348
soliton solutions 362, 365
spectroscopy 368
spherical harmonics – see Legendre polynomials
Spitzer formula 251
stability condition
CFL 320
John von Neumann 318
general 304, 318
statistical distribution sampling 367
steam engine theory 361, 362
stellarator 50, 363
stellar equilibrium 124
Stix
coefficients 145–146
coil 363
Stokes theorem 35, 86
substantive derivative 57, 62, 64, 68, 69, 285
Sweet-Parker model 94–98, 368
tearing instability (island) 196–197
tensor
permittivity 153–154
pressure 72, 211, 214–215
thermal
conductivity 230
viscosity 71
thermal conductivity coefficient 229, 230
thermoelectric effect 185, 229
thermo-diffusion effect 229

tokamak 44, 49–53, 85, 93, 143, 198–199, 228, 271, 272, 274–275
  Compass D 52–53, 275
  ITER 52–53, 272, 368
  JET 52–53, 271
  Tore Supra 52
tokamak instabilities 198
torsion simulation 365
transverse waves 136, 360
transport equation (moment) 209
trochoid 23–24
Turing award 365
turbulence
  anisotropic strong 299
  Elsässer fields 296–297, 299
  GS model 97, 299
  IK model 297
  Kolmogorov 294–295
  magnetohydrodynamic 295–296
turbulent cascade 293–294
two-stream instability – see Buneman instability
vector identities 18
velocity
  Alfvén – see Alfvén speed
  group – see group velocity
  light 16, 30, 33, 60, 117, 118, 138, 216, 267, 355
  phase – see phase velocity
  sound 121, 123, 126, 130, 134, 136
viscosity 71, 211, 296
Vlasov equation 202, 220, 252, 364
von Neumann
  architecture 367
  boundary condition 312
  method 318, 337–338
  stability criterion 318
vortex structure generation 362
wave equation 68, 78, 79, 118, 193, 280, 287, 288, 290, 311, 319
wave packet 78, 117, 118, 278–281, 289
wave vector 132–133, 142, 149, 151, 156, 158, 163, 260, 318
wavefront 116, 134, 135, 146, 147, 278
waves
  Alfvén – see Alfvén waves
  electromagnetic – see electromagnetic waves
  extraordinary (X) 141–143
  left-hand polarized (L) 140–141
  longitudinal 121, 125, 131, 136, 252, 256
  magnetoacoustic – see magnetoacoustic waves
  ordinary (O) 141–143
  plasma – see plasma waves
  right-hand polarized (R) 140–141
Weibel instability 198
Weyl algorithm 321
whistlers 150–153
Zakharov equation 362



References

Lecture Recordings

www.aldebaran.cz, section Study;
www.vsprednasky.cz;
www.youtube.com/watch?v=9lUe9I5ERbk

Other Volumes of this Textbook

[1] P. Kulhánek: *Selected Topics in Theoretical Physics I (Theoretical Mechanics, Quantum Theory, Mathematics for Physics)*; AGA 2020, ISBN: 978-80-906638-2-4, online version (2026): https://www.aldebaran.cz/studium/TF1_en.pdf

[2] P. Kulhánek: *Selected Topics in Theoretical Physics II* (*Statistical Physics, Electromagnetic Field, Relativity*); AGA 2020, ISBN: 978-80-906638-3-1, online version (2026): https://www.aldebaran.cz/studium/TF2_en.pdf

Textbooks on Plasma Physics

[3] B. J. Rye, J. C. Taylor (editors): *Physics of hot plasmas*; Scottish Summer School; Oliver & Boyd, Edinburgh, 1968.

[4] G. B. Rybicki, A. P. Lightman: *Radiative Processes in Astrophysics*; John Wiley & Sons, 1979.

[5] D. R. Nicholson: *Introduction to Plasma Theory*, John Wiley & Sons Inc, 1983, ISBN: 047109045X.

[6] R. A. Cairns: *Plasma Physics*; Blackie, Glasgow, 1985.

[7] J. P. Freidberg: *Ideal Magnetohydrodynamics* (2nd Edition); Cambridge University Press, 2024, ISBN: 978-1009424752.

[8] A. L. Peratt: *Physics of the Plasma Universe* (2nd Edition); Springer, 2015, ISBN: 978-1461478188.

[9] S. P. Gary: *Theory of Space Plasma Microinstabilities*; Cambridge University Press, 1993.

[10] R. Dendy (editor): *Plasma Physics – An Introductory Course*; Cambridge University Press, 1995, ISBN: 978-0521484527.

[11] S. D. Pinches: *Nonlinear Interaction of Fast Particles with Alfvén Waves in Tokamaks*, University of Nottingham, 1996, online http://www.ipp.mpg.de/~Simon.Pinches/thesis/.

[12] T. E. Cravens: *Physics of Solar System Plasmas*, Cambridge Atmospheric and Space Science Series, Cambridge University Press, 1997, ISBN: 0-52161194-6

[13] T. J. Dolan: *Fusion Research; Principles, Experiments and Technology*; Pergamon Press, 1982, 2000.

[14] E. Infeld, G. Rowlands: *Nonlinear waves, solitons, and chaos*; Cambridge University Press, 2000.

[15] E. Priest, T. Forbes: *Magnetic Reconnection – MHD Theory and Applications*; Cambridge University Press, 2000, ISBN: 0-52148179-1.

[16] T. J. M. Boyd, J. J. Sanderson: *The Physics of Plasmas*, Cambridge University Press, 2005, ISBN: 0521459125.

[17] A. A. Fridman, L. A. Kennedy: *Plasma Physics and Engineering*; Taylor & Francis Routledge, 2004.

[18] F. F. Chen: *Introduction to Plasma Physics and Controlled Fusion* (3rd Edition); Springer, 2016, ISBN: 978-3319223087.

[19] H. Goedbloed, R. Keppens, S. Poedts: *Magnetohydrodynamics of Laboratory and Astrophysical Plasmas*; Cambridge University Press, 2019, ISBN: 978-1107123922.

[20] K. Miyamoto: *Plasma Physics for Controlled Fusion* (2nd Edition); Springer, 2016, ISBN: 978-3662512166.

[21] T. H. Stix: *Waves in Plasmas,* Springer, 2006, ISBN: 0883188597.

[22] M. De Bock: *Understanding and controlling plasma rotation in tokamaks*; Technische Universiteit Eindhoven, 2007.

[23] J. P. Freidberg: *Plasma Physics and Fusion Energy*, Cambridge University Press, 2007.

[24] P. M. Bellan: *Fundamentals of Plasma Physics*; Cambridge University Press, 2008, ISBN: 978-0521528009.

[25] K. S. Thorne, Roger D. Blandford: *Modern Classical Physics: Optics, Fluids, Plasmas, Elasticity, Relativity, and Statistical Physics*; Princeton University Press, 2021, ISBN: 978-0691159027.

[26] J. D. Huba: *NRL Plasma Formulary*; Naval Research Laboratory, Plasma Physics Division, 2024, https://www.nrl.navy.mil/News-Media/Publications/nrl-plasma-formulary/.

[27] M. Karlický: *Plasma Astrophysics*; Matfyz Press 2014

[28] A. Piel: *Plasma Physics: An Introduction to Laboratory, Space, and Fusion Plasmas* (2nd Edition); Springer, 2022, ISBN: 978-3031046162.

[29] P. M. Bellan: *Waves and Oscillations in Plasmas*; CRC Press, 2022, ISBN: 978-1032049182.

[30] N. A. Krall, A. W. Trivelpiece: *Principles of Plasma Physics* (Classic Reprint); Decel Press, 2021.

Numerical Simulations

[31] A. Ralston, P. Rabinowitz: A First Course in Numerical Analysis (2nd Edition); Dover Publications, 2001, ISBN: 978-0486414546.

[32] R. Y. Rubinstein, D. P. Kroese: *Simulation and the Monte Carlo Method* (3rd Edition); John Wiley & Sons, 2016, ISBN: 978-1118632161.

[33] R. L. Burden, J. D. Faires, A. M. Burden: *Numerical Analysis* (10th Edition); Cengage Learning, 2016, ISBN: 978-1305253667.

[34] J. Hubbard, D. Schleicher, S. Sutherland: *How to Find All Roots of Complex Polynomials With Newton's Method*; Inventiones Mathematicae 146 (2001).

[35] G. W. Collins, II: *Fundamental Numerical Methods and Data Analysis*; 2003, ADS Digital Library for Physics and Astronomy, online: http://ads.harvard.edu/books/1990fnmd.book/.

[36] C. K. Birdsall, A. B. Langdon: *Plasma Physics via Computer Simulation*; IoP, Series in Plasma Physics, 2004 (Reprint 2018).

[37] P. Blanchard, R. L. Devaney, G. R. Hall: *Differential Equations* (4th Edition); Cengage Learning, 2012, ISBN: 978-1133109037.

[38] S. J. Chapman: *Fortran for Scientists &* Engineers (4th Edition); McGraw-Hill Education, 2018, ISBN: 978-0073385891.

[39] A. J. Chorin, O. H. Hald: *Stochastic Tools in Mathematics and Science*; Vol. 1, (3rd Edition); Surveys and Tutorials in the Applied Mathematical Sciences, Springer, 2013, ISBN: 978-1461470748.

[40] A. Quarteroni: *Numerical Model for Differential Problems*; (3rd Edition); Springer, 2017, ISBN: 978-3319493152.

[41] A. K. Jaiswall, A. Khandelwall: *A Textbook of Computer Based Numerical and Statistical Techniques*; New Age International Publishers, 2010.

[42] W. H. Press, S. A. Teukolsky, W. T. Vetterling, B. P. Flannery: *Numerical Recipes 3rd Edition: The Art of Scientific Computing*; Cambridge Unniversity Press 2007

[43] P. O. J. Scherer: *Computational Physics I: Numerical Methods* (4th Edition); Graduate Texts in Physics, Springer Nature, 2026, ISBN: 978-3032078551.

[44] P. O. J. Scherer: *Computational Physics II: Simulation of Classical and Quantum Systems* (4th Edition); Graduate Texts in Physics, Springer Nature, 2026, ISBN: 978-3032078513.

[45] T. Sauer: *Numerical Analysis* (3rd Edition); Pearson, 2018, ISBN: 978-0134696454.

[46] M. T. Heath: *Scientific Computing*: An Introductory Survey (Revised 2nd Edition); SIAM – Society for Industrial and Applied Mathematics, 2018, ISBN: 978-1611975574.

Papers and Books – Derivations of Important Relations

[47] G. M. Kremer: *Theory and applications of the relativistic Boltzmann equation*; International Journal of Geometrical Methods in Modern Physics, Vol. 11, 1460005 (2014); arXiv:1404.7083 [cond-mat.stat-mech]

[48] M. Abraham: *Theorie der Elektrizität: Elektromagnetische Theorie der Strahlung; Teubner*, Leipzig (1905)

[49] P. A. M. Dirac: *Classical Theory of Radiating Electrons*; Proc. Roy. Soc. London **A167**, 148 (1938)

[50] W. Pauli: *Theory of Relativity*; Pergamon Press 1958

[51] E. Poisson: *An introduction to the Lorentz-Dirac equation*; arXiv:gr-qc/9912045v1 (1999)

[52] M. Ibison, H. E Puthoff: *Relativistic integro-differential form of the Lorentz–Dirac equation in 3D without runaways*; J. Phys. A: Math. Gen. 34, 3421–3428 (2001)

[53] A. C. M. de Oca, N. G. C. Bizet: *Newton-like equations for a radiating particle*; Physical Review D91, 016001 (2015)

[54] M. Jirka: *Ultra-intense laser-matter interaction*; Doctoral thesis, FNSPE CTU, 2018

[55] M. C. Williams: *Solitons – Interactions, Theoretical and Experimental Challenges and Perspectives*; Nova Science Publishers 2013

[56] S. Vongehr: *Solitons*; Nanjing University 1997, online: aldebaran.cz/studium/tpla/docs/Vongehr-solitons.pdf

[57] R. Grimshaw: *Korteweg-de Vries Equation*; Loughborough University (UK) 2008. online: aldebaran.cz/studium/tpla/docs/KdV_Grimshaw.pdf

[58] E. M. de Jager: *On the Origin of the Korteweg-de Vries Equation*; arXiv:math/0602661v2 [math.HO] 8 Dec 2011

[59] K. Banks: *Solitons and the Korteweg de Vries Equation: Starting with Shallow-Water Waves*; Semantic Scholar 2012; online: aldebaran.cz/studium/tpla/docs/KdV_Banks.pdf

[60] N. N. Rao, R. K. Varma: *A theory for Langmuir solitons*; J. Plasma Physics (1982), vol. 27, part 1, pp. 95–120

[61] P. Kulhánek: *3D PIC Model of the Helical Current Filament*; Inaugural Dissertation (prof), 2004, Collection of 3D PIC package papers, FEE CTU (2004), online: https://www.aldebaran.cz/~kulhanek/texts/2004_PIC.pdf

[62] V. Delong, R. Beňo, D. Břeň, Petr Kulhánek: *Notes on the relativistic movement of runaway electrons in parallel electric and magnetic fields*; Physics of Plasmas 23, 094504 (2016)

[63] L. Šubr: *Lecture notes NAST008: Cosmic electrodynamics*; MFF UK 2017; online: https://astro.mff.cuni.cz/vyuka/AST008/NAST008_notes.pdf

[64] E. R. Tracy, A. J. Brizard, A. S. Richardson, A. N. Kaufman: *Ray Tracing and Beyond: Phase Space Methods in Plasma Wave Theory*; Cambridge University Press (2014)

[65] B. A. Hnat: *Plasma Turbulence*; University of Warwick, 2016. Online: http://sp2rc.group.shef.ac.uk/assssp16/lectures/L12Hnat.pdf

[66] S. S. Cerri, D. Grošelj, L. Franci: *Kinetic plasma turbulence: recent insights and open questions from 3D3V simulations*; Front. Astron. Space Sci., 11 Oct 2019

[67] A. N. Kolmogorov: *The local structure of turbulence in incompressible viscous fluid for very large Reynolds numbers*; Proceedings of the USSR Academy of Sciences, 1941, 299–303. Online anglický překlad: https://courses.physics.ucsd.edu/2014/Spring/physics281/kolmogorov41.pdf

[68] H. Knoepfel, D. A. Spong: *Runaway Electrons in Toroidal Discharges*; Nuclear Fusion **19**/6 (1979)

[69] H. Dreicer: *Electron and Ion Runaway in a Fully Ionized Gas. I*. Phys. Rev. 115 (1959), 238–249

[70] A. V. Gurevich, G. M. Milikh, R. A. Roussel-Dupre: *Runaway electron mechanism of air breakdown and preconditioning during a thunderstorm.* Physics Letters A 165 (1992), 463–468

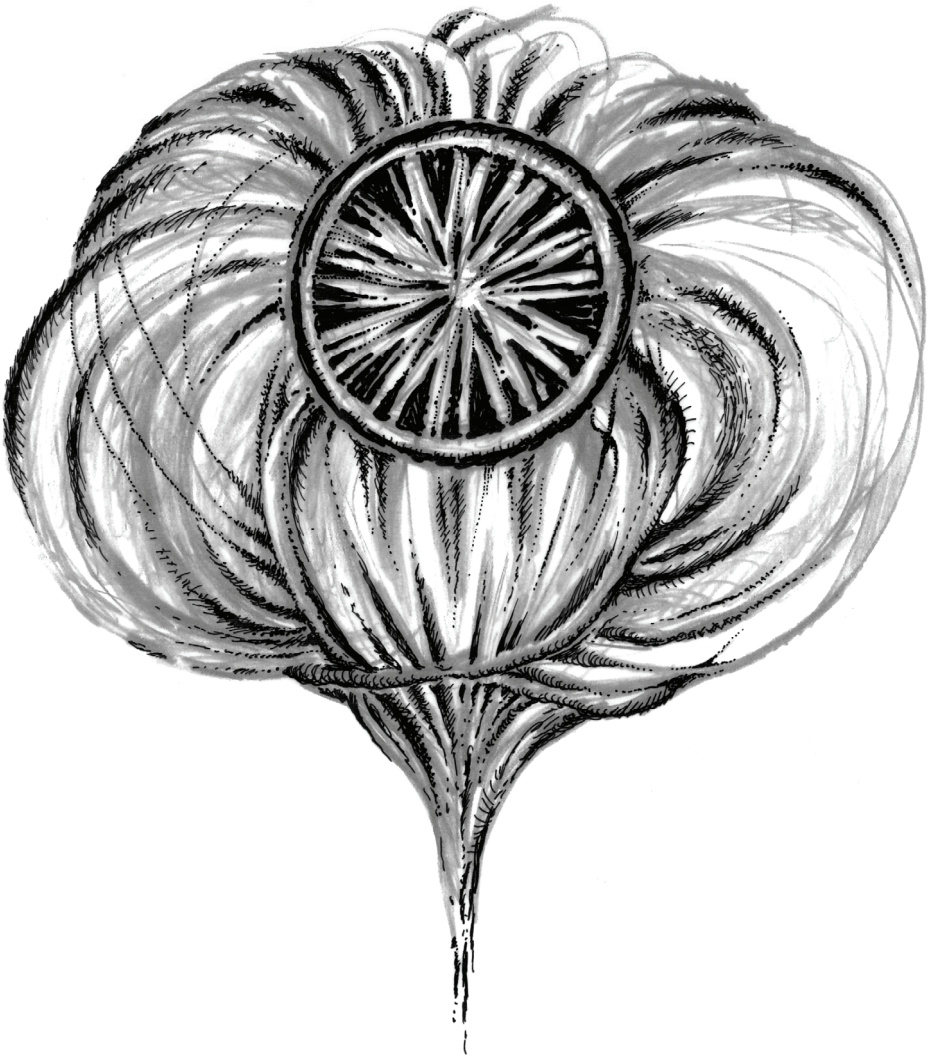
[71] R. G. Giovanelli: *Electron Energies Resulting from an Electric Field in a Highly Ionized Gas*. Phil. Mag. 40 (1949), 206–214

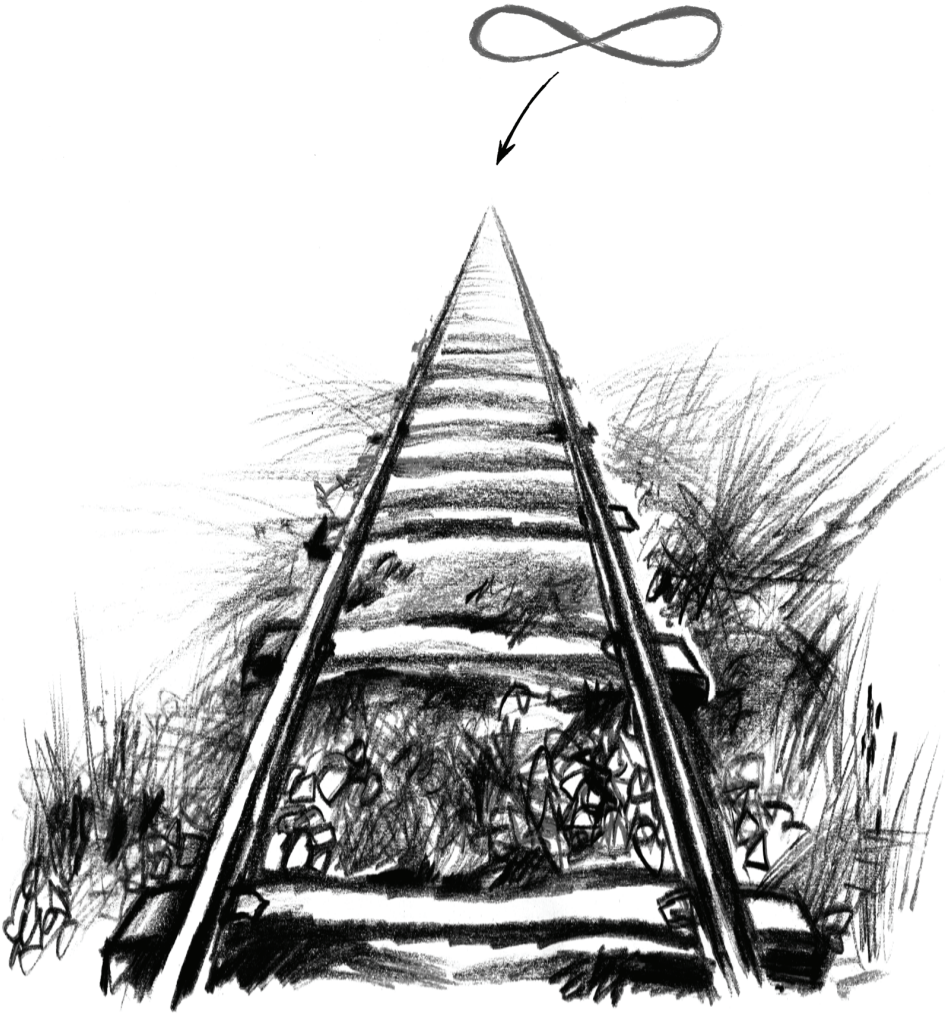
[72] R. Jaspers: *Relativistic runaway electrons in tokamak plasmas*. PhD thesis, TU Eindhoven, 1995, [online] https://pure.tue.nl/ws/files/1475618/431410.pdf

[73] C. T. R. Wilson: *The acceleration of β-particles in strong electric fields such as those of thunderclouds. Proc. Cambridge Philos. Soc.* 22 (1925), 534–538

[74] J. R. Dwyer: *A fundamental limit on electric fields in air*. Geophysical Research Letters 30/20 (2003), 2055-2059

Inside Other Volumes





Selected Topics in Theoretical Physics I

The first volume of “Selected Topics” serves as an introductory textbook for the entire series. It begins with the fundamental concepts of theoretical mechanics. The reader will become familiar with the elegance of describing mechanical and other phenomena using the Lagrangian and Hamiltonian equations, as well as Poisson brackets. The second part is dedicated to quantum theory. Relatively standard topics concerning the structure and interpretation of quantum theory are followed by problems related to the boundary between the quantum and classical worlds, the disproof of the existence of hidden variables, the EPR paradox, and Bell's inequalities. The final part of the first volume is devoted to the mathematical foundations necessary for studying physical phenomena. The reader may refer to this section of the textbook whenever they encounter mathematical tools required for reading the physics chapters.

THEORETICAL MECHANICS

- Integral principles of mechanics
- Conservation laws in nature
- Hamilton's canonical equations
- Selected problems in theoretical mechanics
- Nonlinear dynamical systems
- Lagrangian equations for field problems

QUANTUM THEORY

- Micro-world and macro-world
- Fundamental principles of quantum theory
- Harmonic oscillator
- Simple one-dimensional systems
- Spherically symmetric potential
- Time evolution
- Relativistic quantum theory, spin
- Fermions and bosons
- Quantum theory and hidden variables

MATHEMATICS FOR PHYSICS

- Einstein summation convention
- Complex numbers and functions
- Vectors and tensors
- Dirac notation and operators in quantum theory
- From gradient to helicity
- Multidimensional integrals
- Some special functions
- Generalized functions
- Conic sections, trigonometry, and more



Selected Topics in Theoretical Physics II

The next volume of “Selected Topics” builds upon the introductory textbook you are currently holding in your hands. The necessary mathematical foundations for both the second and third volumes are included in the first volume of the trilogy. The second volume is dedicated to statistical physics, the electromagnetic field, and relativity. To understand statistical physics, at least a basic knowledge of theoretical mechanics and quantum theory is required. The theory of the electromagnetic field demonstrates the elegance of Maxwell's equations and derives individual physical phenomena from them, leading up to various types of electromagnetic radiation. The final part of the second volume is devoted to relativity, which completely transformed our understanding of how the world around us functions. It begins with special relativity and continues with the foundations of general relativity, the current theory of gravitational interaction.

STATISTICAL PHYSICS

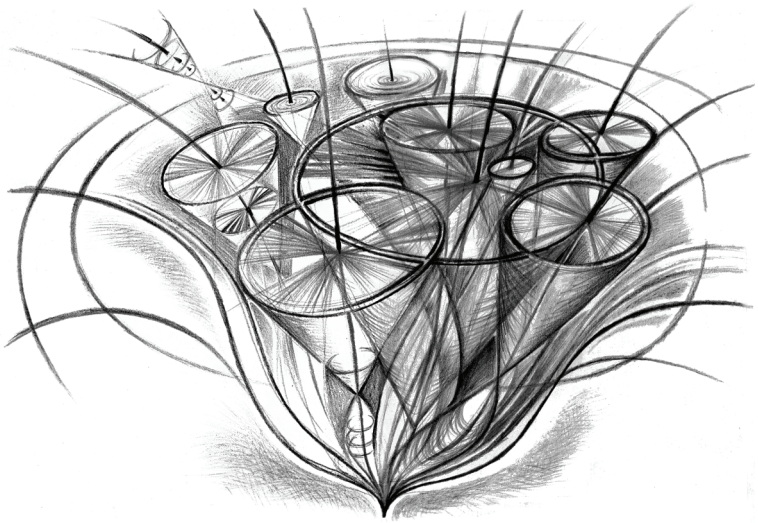
- Selected topics in thermodynamics
- Fundamental concepts of statistical physics
- Gibbs canonical ensemble
- Simple examples
- Advanced examples
- Grand canonical ensemble
- Fermions and bosons
- Fluctuations and entropy
- Magnetically active systems

ELECTROMAGNETIC FIELD

- Maxwell equations
- Electrostatics
- Magnetostatics
- Conservation laws
- Electromagnetic waves
- Electromagnetic potentials
- Electromagnetic radiation
- Cavity resonators

RELATIVITY

- From special relativity to the equivalence principle
- Metric, covariant derivative
- Geodetic equation
- Time dilation and gravitational redshift
- Riemann curvature tensor and Einstein's field equations
- Gravitational waves
- Schwarzschild solution and motion in Schwarzschild geometry
- Frame-dragging by a rotating body
- Introduction to cosmology



Petr Kulhánek
Selected Topics in Theoretical Physics III
(1. Plasma Theory, 2. Numerical Simulations)

No part of this publication may be published, reproduced, or distributed in any manner or by any means without the express written permission of the author and the AGA publisher.

Author: Prof. RNDr. Petr Kulhánek, Ph.D.
Graphics and Cover: Ing. arch. Ivan Havlíček
Format: 165×235 mm, 384 pages, 228 illustrations
Publisher: AGA (Aldebaran Group for Astrophysics)
Lecture Recordings: aldebaran.cz (Daniel Handl, FEE CTU)
Front Cover Image: Twin Jet Nebula M2-9, NASA/HST/ESA
Back Cover Image: Twin Jet Nebula (Minkowski) M2-9, HST
Edition: Reprint of the 2nd edition, December 2024, Prague
Electronic Version Update: October 11, 2026
Printed by: TISK CENTRUM s.r.o.

ISBN 978-80-906638-4-8